**UNIVERSITÀ DEGLI STUDI DI MILANO**

DOTTORATO DI RICERCA IN SCIENZE DELLA TERRA

*Ciclo XXXIII*

DIPARTIMENTO DI SCIENZE DELLA TERRA

# Post-genetic Evolution of Ophiolite-hosted Cr-PGE Ores: Lithospheric and Economic Significance

GEO/09

Ph.D. Thesis

Micol Bussolesi
I.D. R11847

Tutor:
Prof. Giovanni Grieco

Coordinator:
Prof. Fernando Camara Artigas

Academic Year 2019-2020

# Abstract

Chromitite layers, pods and lenses within ophiolite ultramafic rocks are major industrial chromium sources and contain sub-economic Platinum Group Elements (PGE) enrichments. PGE and chromium are considered Critical Raw Materials (CRM) by the European Union, due to their employment in a wide range of sectors. The criticality of CRM is related to their importance for the economy, and to the risk associated with their supply. The study of altered chromitites can give us important insights on their evolution, as well as on the behavior of precious metals in contact with altering fluids. In the present work, the three main post-magmatic processes affecting podiform chromitites have been addressed: high-T subsolidus re-equilibration of olivine and spinel, low-T circulation of fluids at high (chloritization) and low (serpentinization) $fS_2$ and $fO_2$ respectively.

Olivine and chromite diffusivity patterns, developed during subsolidus re-equilibration due to Mg-Fe exchange reactions, are useful tools for the reconstruction of the thermal history down to 650 °C. In the present work we developed a new approach using an exponential function to model XMg variations with the distance from the grain boundary. The new approach produced reliable primary and re-equilibrated XMg values, then used to infer re-equilibrated and primary temperatures, as well as to estimate the cooling rates of the olivine- chromite-bearing rocks. The approach, developed starting from the case study of Finero subcontinental mantle, has been employed with good results also for two partially serpentinized ophiolite chromitites, Iballe and Nea Roda.

Low-T circulating fluids at high $fS_2$ and $fO_2$ conditions can alter primary mineralogical assemblages and induce crystallization of secondary minerals. The high sulfur and oxygen fugacities favor the replacement of primary silicates by chlorite, and the formation of ferrian chromite. Chloritized chromitites from Gomati and Nea Roda (Greece) have been selected to study the remobilization of elements during the circulation of such fluids. Primary Base Metal Minerals (BMM) are altered and replaced by secondary ones, but no alloys are generated, as they are not stable under these conditions. Platinum Group Minerals (PGM) are not affected by the circulating fluids, and retain their magmatic imprint, as also confirmed by primary mantle-normalized PGE patterns, with a Ru peak.

Low-T circulating fluids at low $fS_2$ and $fO_2$ conditions are the most common within ophiolite chromitites, and are responsible for the major altering process of this kind of deposit: serpentinization. Serpentinized chromitites from Skyros (Greece) and Abdasht-Soghan (Iran) have been selected to study the remobilization of elements during the circulation of such fluids. The low sulfur and oxygen fugacities favor the replacement of primary silicates by serpentine, and the formation of magnetite. A distinctive feature of serpentinization is the replacement of primary BMM with base metal alloys, as well as with secondary sulfides. PGM are also highly affected by the serpentinizing conditions, and

tend to lose sulfur and be transformed into alloys. This generates a remobilization of PGE into the circulating fluids. The remobilization, estimated within the Abdasht-Soghan complex through a mass balance calculation on a partially desulfurized laurite grain, occurred at two different scales. Os was the first element to exit laurite lattice to form Os-rich alloys. However, the mass balance calculation showed that the PGM mostly lost Ru. This implies a second, larger scale, remobilization where Ru acted as the most soluble PGE in the desulfurizing fluids. The mobility of PGE into the fluids hence follows the order: Ru>>Os>>Ir. This is confirmed by PGE patterns, which present a double peak, for Ru and Os.

Post-magmatic processes affect the economic assessment of chromite ore deposits. In this study we focused on the quality parameters of a chromite sand for the foundry industry. Foundry chromite sands are the most valuable chromite commodity, and are currently not produced within the EU. The best chromite foundry sands are from layered intrusions, with South Africa as the main producer. In order to find alternative sources of this commodity, we tested the behavior of two industrial ophiolite chromite sands from Iran and Greece, enriched through shaking tables and spirals.

Ophiolite chromite sands do not meet the most critical quality parameter, the Acid Demand value, that depends on the reactivity of the silicate impurities in an acid environment. The presence of serpentine, a highly reactive mineral widespread in ophiolite chromitites, lowers the performance of the sand. On the other hand, olivine, the second most common silicate mineral in podiform chromitites, shows low reactivity. The production of chromite foundry sands starting from ophiolite chromites is possible, but only for those where the silicate impurities assemblage is dominated by olivine, with very low or negligible amounts of serpentine. Two examples of ophiolite chromitites with a low degree of serpentinization within the EU are Aetoraches and Rizo deposits, in Greece. Their chromite sands exceed the Acid Demand thresholds by a low amount, and an affordable degree of purification could lower the ADT values and make them suitable for the foundry market.

# CHAPTER 1: Introduction

The European Commission classifies as Critical Raw Materials (CRM) those materials deemed crucial to European economy, due to their employment in a wide range of applications (Deloitte Sustainability et al., 2017a). Among the sectors employing CRM, some examples are defense, automotive, metals, medical devices, consumer electronics and green technology. The criticality of CRM is related to their importance for the economy, and to the risk associated with their supply. The first list of CRM was compiled by EU in 2011, and was revised and updated in 2014 and in 2017 (Tab. 1.1), with the prospective of updating it every 3 years based on production, market and technology development.

Tab. 1.1 List of CRM for the EU updated to 2017.

| **2017 CRM** | | | |
|---|---|---|---|
| Antimony | Fluorspar | LREE | Scandium |
| Baryte | Gallium | Magnesium | Silicon metal |
| Beryllium | Germanium | Natural graphite | Tantalum |
| Bismuth | Hafnium | Natural rubber | Tungsten |
| Borate | Helium | Niobium | Vanadium |
| Cobalt | HREE | PGM | |
| Coking coal | Indium | Phosphate rock | |

Of the 61 candidates, 26 raw materials were identified as critical. The assessment and identification of CRM is fruit of an accurate analysis of the economic importance and the supply risk, that considers factors such as governance performance and trade aspects of raw material producing countries (Fig. 1.1). Three materials identified as CRM in 2014 were not included in the 2017 list: chromium, coking coal and magnesite.

The main world suppliers of CRM are reported in Fig. 1.2. China is the leader supplier of CRM, and makes up 70% of the global supplies, providing 15 of the 26 CRM listed in the 2017 EU report (including all REE). Other countries producing important critical raw materials are USA (Beryllum and Helium), Brazil (Niobium), South Africa (Iridium, Platinum, Rhodium, Ruthenium) and Russia (Palladium). The only CRM produced in Europe is Hafnium, of which France is a global supplier.

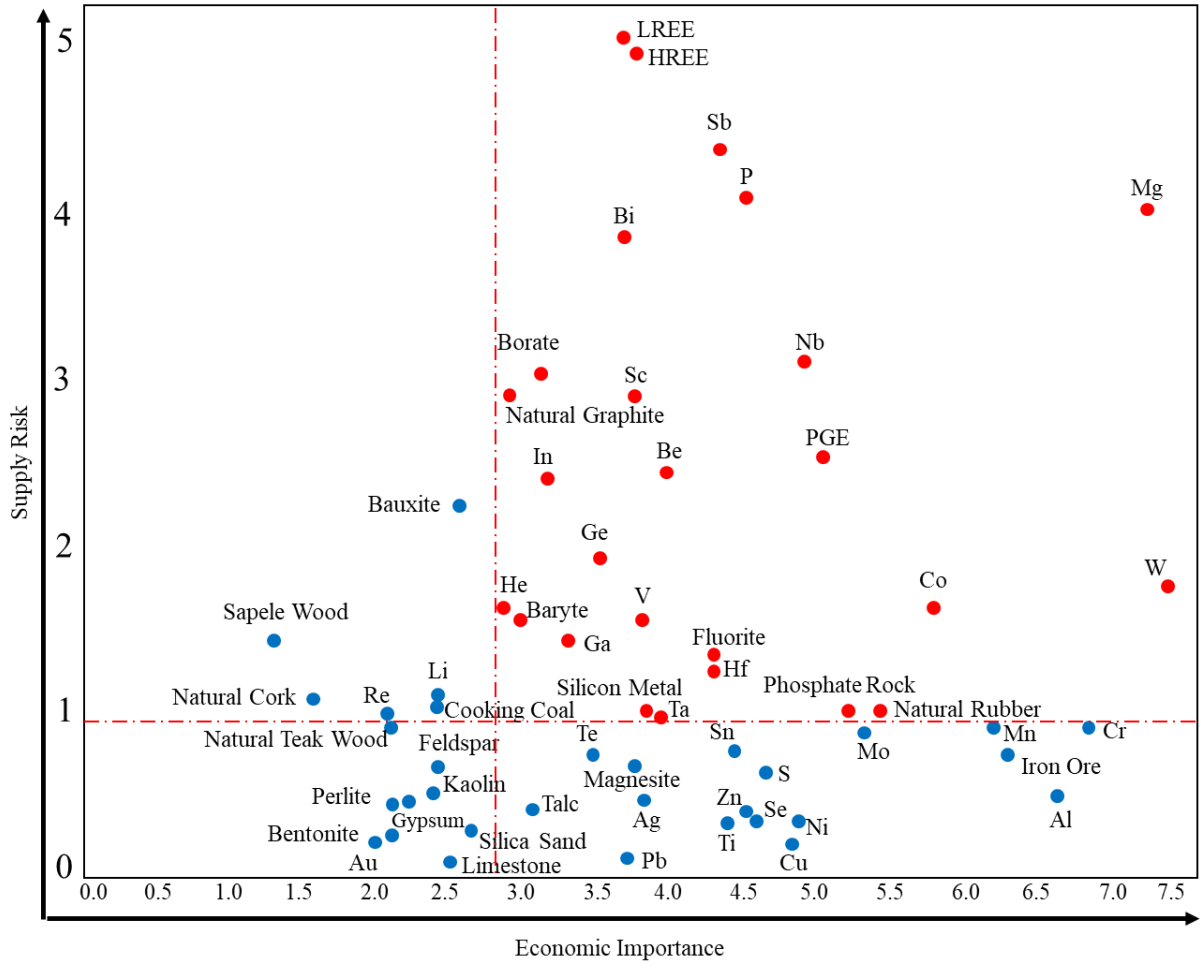


Fig. 1.1 List of critical (red) and non-critical (blue) raw materials important for the EU economy (Deloitte Sustainability et al., 2017a).

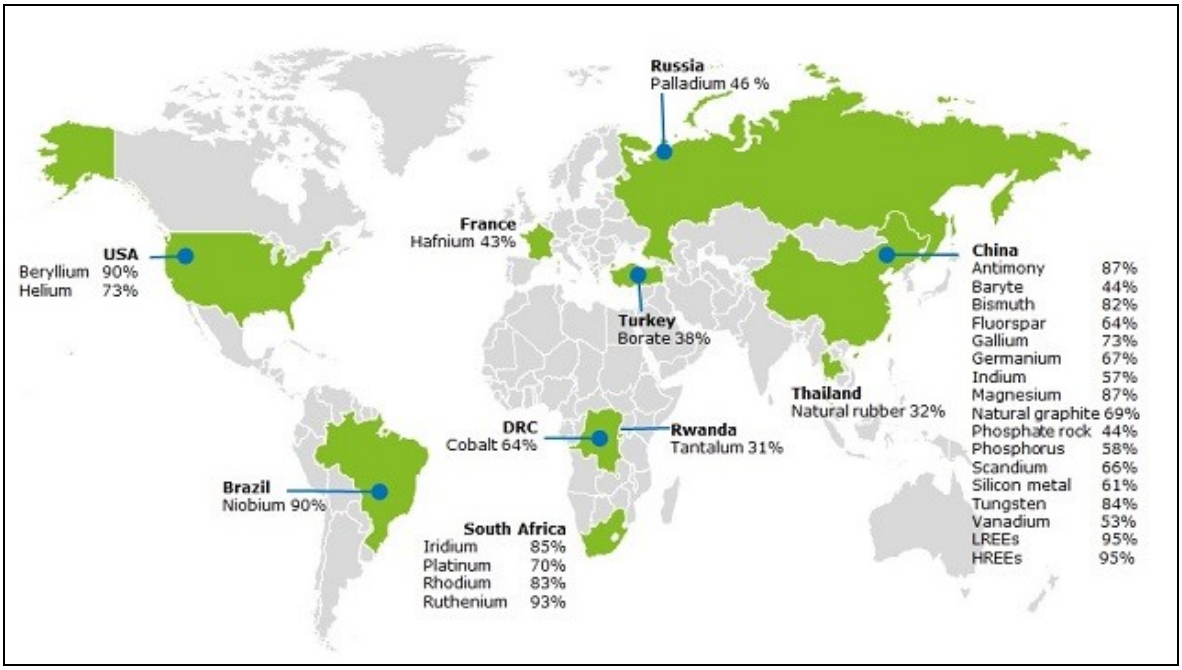


Fig. 1.2 Countries accounting for the largest share of CRM global supply (Deloitte Sustainability et al., 2017a).

*Platinum Group Elements*

On the specific matter of PGE, which are one of the focus of the present work, there is a concern over their security and supply within the EU (Deloitte Sustainability et al., 2017b). A measure taken by some countries to ensure supply and mitigate impacts of shortage are metal stockpiles. However, it is becoming important to fund researches aimed to find new resources and possibly extract PGE from different ores (Deloitte Sustainability et al., 2017b). Although new mines have opened in some PGE producing countries (e.g. South Africa), ensuring huge resources for many years, EU concerns resides in the social, environmental, political and economic situation of such countries. Other concerns are related to the nature of some PGE deposits. For example, Pd extracted in Noril'sk is a by-product of Ni production, so that it is difficult to assess long-term availability of PGE from these mines (Deloitte Sustainability et al., 2017b; Johnson Matthey, 2020). Supplies of PGE from secondary materials saw a reduction in 2016, due to opening of new mines with low PGE price, resulting in a reduction of collection and processing of autocatalysts. Recycling of primary materials, however, rose in 2018 and 2019, and is expected to reach a plateau in the future (Johnson Matthey, 2020).

*Chromium*

Chromium in the EU is employed mainly for the production of stainless steel (74%) and secondarily for alloy steel materials (19%). As a result of the criticality assessment, it was deemed not critical in 2011, critical in 2014 and not critical in 2017. However, despite the fact that Cr is not considered a CRM, it should be noted that it is very close to the threshold established by the EU, and that the chromium processing industry is highly strategic for Europe (Deloitte Sustainability et al., 2017a; European Commission, 2017).

Overall, chromium market is unpredictable, considering the major suppliers (South Africa, Kazakhstan, China), and the fact that the demand of chrome ore has been on the rise in the past 10 years. Moreover, China in 2016 has put a 20% export tax on ferrochromium and bought South Africa and Zimbabwe mines, which could result in a domination of the chromium market by this country (European Commission, 2017).

## 1.1. Aim of the work

The aim of this work is to propose a comprehensive study of the effects of post-magmatic processes on chromite mineralization, and to assess the implications on the economic value of the ore. Three main post-magmatic processes are considered in this study: olivine-spinel subsolidus re-equilibration, circulation of serpentinizing fluids and circulation of chloritizing fluids. Moreover, the economic implications of post-magmatic alteration of ophiolite chromitites on the production of chromite sands for the foundry industry will be assessed.

Olivine-spinel subsolidus exchange is a post-magmatic process affecting chromitites down to at least 650 °C. It involves a Mg-Fe exchange between olivine and spinel that is temperature dependent. For this reason, olivine spinel couples have been used for geothermometry and geospeedometry. The aim of this work is to develop a new methodology to assess accurate primary and re-equilibrated XMg values within partially serpentinized chromitites, through the study of diffusivity curves. These values will be used to assess the thermal history of chromitite massifs and to infer their cooling rates.

The circulation of fluids is a well-known process affecting primary mineralogical assemblages and mobility of precious metals within chromitites. Circulation of fluids at low-T can result in chloritization (high $fS_2$ and $fO_2$) or serpentinization (low $fS_2$ and $fO_2$) of the rocks. The aim of this work is to study the remobilization of precious metals in contact with fluids at different conditions, and their potential reconcentration. For this purpose, we selected two localities showing widespread chlorite alteration and two more showing serpentine alteration. In order to assess precious metal remobilization, we will study primary and secondary Base Metal Minerals and Platinum Group Minerals assemblages, as well as the normalized whole rock PGE patterns.

Chromite sands for the foundry industry are a valuable commodity, employed for high-demanding casting of steel. The market is currently dominated by stratiform chromite ores from South Africa, which produces the top-quality foundry sands due to the low reactivity of silicate impurities. The aim of this work is to assess the reactivity of ophiolite chromitite silicate impurities, depending on the degree and type of alteration due to the post-magmatic processes.

The following chromite deposits have been studied:

Tab. 1.2 List of chromite deposits considered in the present work.

| **Deposit** | **Country** | **Type** | **Study** |
|---|---|---|---|
| Finero | Italy | Subcontinental mantle | Olivine-Spinel re-equilibration |
| Iballe | Albania | Ophiolite | Olivine-Spinel re-equilibration |
| Nea Roda | Greece | Ophiolite | Olivine-Spinel re-equilibration<br>PGE remobilization (chloritization) |
| Gomati | Greece | Ophiolite | PGE remobilization (chloritization) |
| Abdasht-Soghan | Iran | Ophiolite | PGE remobilization (serpentinization) |
| Skyros | Greece | Ophiolite | PGE remobilization (serpentinization) |
| Neyriz | Iran | Ophiolite | Chromite foundry sands |
| Aetoraches and Rizo | Greece | Ophiolite | Chromite foundry sands |

# 1.2. Chromite

## 1.2.1. Properties and Industrial Applications

Chromium (Cr) is a transition metal with atomic number 24, standard atomic weight 51.996 u and density 7.19 g/cm$^3$. It exists in nature mainly in three valence states, 2+, 3+ (the most stable) and 6+. Rarely it assumes valence states 4+ or 5+. Cr is the 22$^{nd}$ element in order of abundance in the upper crust, with an average concentration of 92 ppm (Rudnick and Gao, 2003), while in the rocks of the upper mantle (peridotites), concentrations of Cr rich up to 3000 ppm.

There are several minerals containing Cr in traces or as a minor element, and only in few minerals this metal is present in economic amounts. The most widespread of these minerals is chromite. Chromite is a mineral belonging to the Spinel Group, a family of oxides with general formula $X^{2+}Y^{3+}{}_2O_4$ that crystallizes in the cubic system. Site X is occupied by divalent cations ($Fe^{2+}$, Mg, Zn, Ni, Co), while site Y is occupied by trivalent cations ($Fe^{3+}$, Al, Cr, V, Mn) or tetravalent ones (Ti). By definition, chromite has the mineralogical formula $FeCr_2O_4$, but in ore deposits it is commonly considered chromite any spinel with $Cr_2O_3$ content higher than 37% (Papp and Lipin, 2001). Chromite forms a solid solution with hercynite ($FeAl_2O_4$), magnesiochromite ($MgCr_2O4$) and magnetite ($FeFe_2O_4$) (Fig. 1.3).

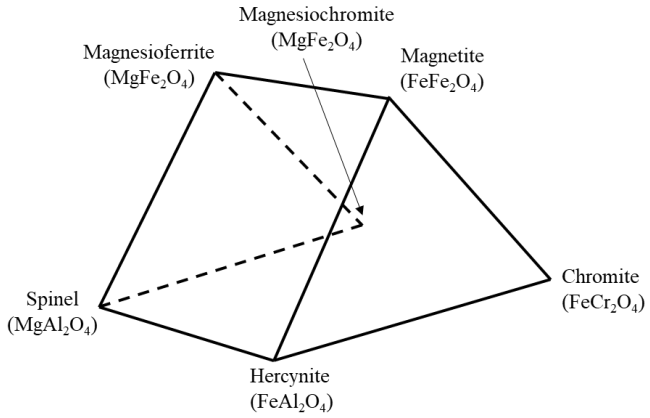


Fig. 1.3 Spinel group end-members.

Chromite is the only source of chrome, a metal used for a wide variety of applications. After extraction of the ore, chromite is beneficiated and separated in 4 grades: metallurgical (42-46% $Cr_2O_3$), refractory grade (30-40% $Cr_2O_3$), foundry sand (44-46.5% $Cr_2O_3$) and chemical (40-46.5% $Cr_2O_3$) (European Commission, 2017). The metallurgical industry is the major consumer of chromite, mainly for the production of stainless steel. Other consumers are the chemical (2.1%) and foundry (1.7%) industries, while the refractory use makes up only 0.2% (Fig. 1.4).

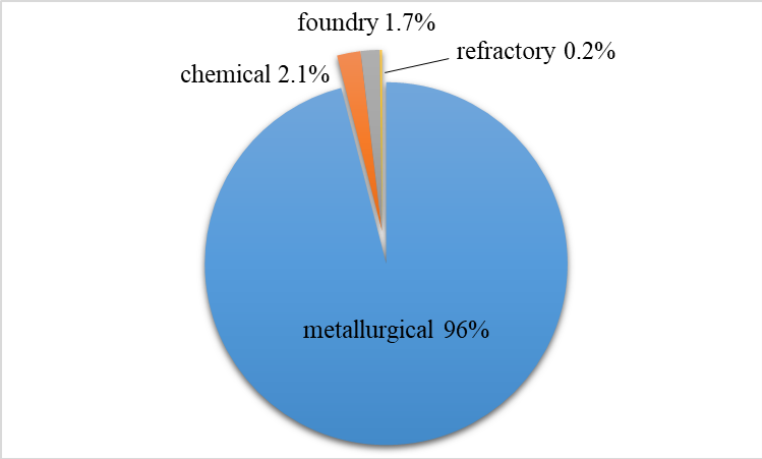


Fig. 1.4 Industrial uses of chromite.

- Metallurgical Industry: chromium is employed for steel and non-ferrous alloys production, to give final products resistance to corrosion, oxidation and better mechanical and thermal properties. Generally, Cr-rich ores are melted to form ferrochromium alloys (containing 50 to 70% of Cr) and Cr metal, which are then used to produce steels (Fig. 1.5 A).
- Foundry and Refractory Industries: in the foundry industry, chromite is employed in bricks to cover the walls of furnaces, or as foundry sands to form casting moulds. Chromite foundry sands have special properties, such as high melting point (2180 °C), low thermal expansion and neutral chemical behavior (Pedrotti, 2012). Foundry sands are generally mixed with binding resins to produce moulds (Fig. 1.5 B), and thus require a very low silica content in order to avoid reaction between sands and resins, causing a decrease in the sand performance.
- Chemical Industry: chromium is used to produce colored pigments, for leather tanning or as a corrosion control agent, applied to metallic surfaces.

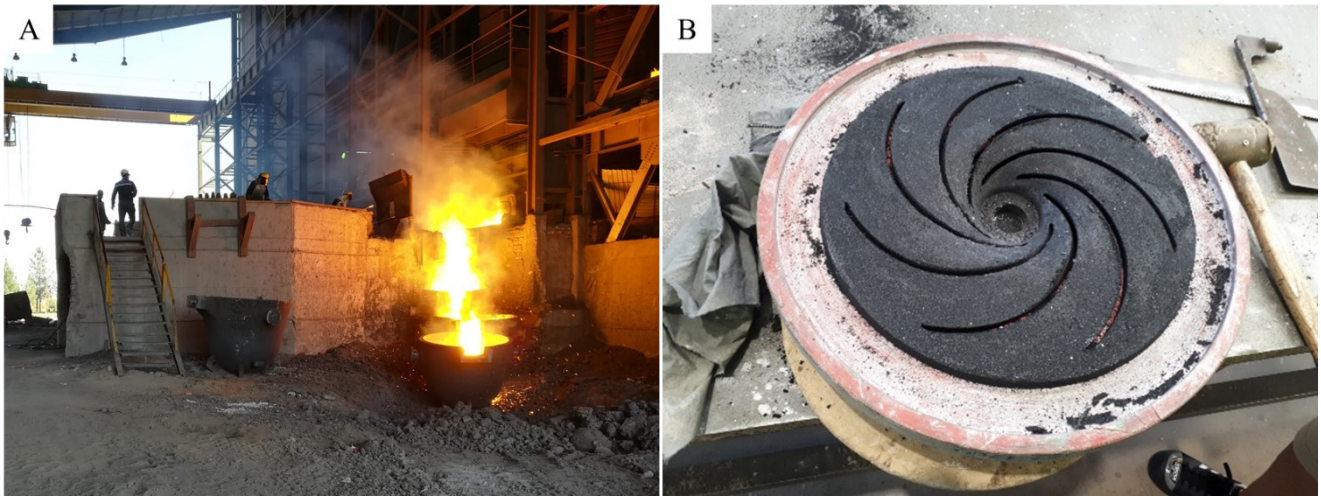


Fig. 1.5 (A) Iranian plant for ferrochromium production (Joghatay ferrochrome plant, Khorassan Razavi Province, Iran); (B) chromite foundry sand mould for refractory use (Flowserve Foudry, Desio, Italy).

## 1.2.2. Market and Prices

Commercial chromite deposits are mainly stratiform and podiform ores (see paragraph 1.2.3). The Bushveld stratiform deposits in South Africa and those in the Great Dyke in Zimbabwe contain most of the world chromite reserves (European Commission, 2017 and references therein). Podiform deposits are generally smaller than stratiform ones, but with higher Cr:Fe ratios, and for this reason they are better suited for metallurgical purposes.

Current global resources of chromium are estimated to be at 12 billion tonnes (shipping grade chromite, 45% $Cr_2O_3$), with 95% of resources located in South Africa and Kazakhstan (USGS, 2020a). Reserves are estimated at 480 Mt (shipping grade chromite). Within the EU, chromium resources are located mainly in Finland, with an amount of 148.6 Mt of ore (corresponding to 19.6 Mt of Cr) (Bio Intelligence Service, 2015), and reserves are about 50 Mt of ore (~13 Mt Cr). Other minor chromium resources are located in Sweden (38.6 Mt), Greece (2 Mt), and in the European continent in Albania (48.4 Mt) and Serbia (0.089 Mt) (Minerals4EU, 2014).

According to USGS (2020), in 2019 the top producers of chromite ore were South Africa, Turkey, Kazakhstan, and India (Tab. 1.2).

Tab. 1.3 World mine production and reserves in the years 2018 and 2019 (USGS, 2020a).

| | **Mine Production (thousand tons)** | | **Reserves (thousand tons)** |
|---|---|---|---|
| | 2016 | 2017 | |
| USA | - | - | 620 |
| Finland | 2,210 | 2,200 | 13,000 |
| India | 4,300 | 4,100 | 100,000 |
| Kazakhstan | 6,690 | 6,700 | 230,000 |
| South Africa | 17,600 | 17,000 | 200,000 |
| Turkey | 8,000 | 10,000 | 26,000 |
| Other Countries | 4,250 | 4,000 | - |
| World Total | 43,100 | 44,000 | 570,000 |

Mine production is thousands of tons, gross weight, of marketable chromite ore

Reserves are expressed in thousand tons of shipping-grade chromite (normalized to 45% $Cr_2O_3$)

The world production of ferrochromium is dominated by China, South Africa, Kazakhstan and India, with other countries producing less than 5% of ferrochromium (Fig. 1.6) (European Commission, 2017). Recycling of secondary materials (stainless steel) is well established, and reaches recycling rates between 70% and 92%. End-of-life recycling input in the EU is 21% (European Commission, 2017).

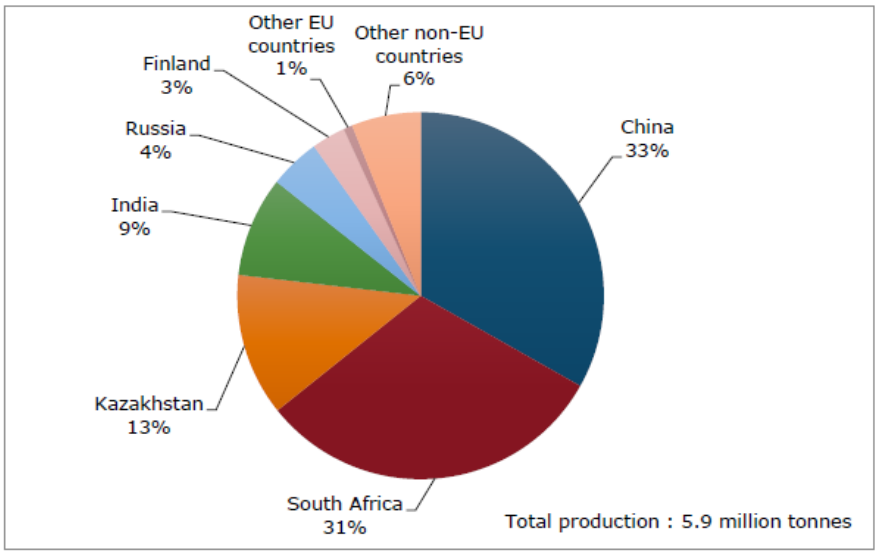


Fig. 1.6 Global production of ferrochromium, average 2010-2014 (British Geological Survey, 2016).

In the EU three countries produce about 220kt of ferrochromium (Finland, Sweden and Germany), while 720kt of ferrochromium are imported every year. European industries use semi-finished stainless steel and alloy steel products to manufacture finished products, mainly refractory bricks, casting moulds and chemicals. These are strategic products due to their use in aviation and in the nuclear sector (European Commission, 2017).

Chromite prices follow positive and negative trends depending on the period and the demand. After a collapse due to the economic crisis of 2008, chromite price is now following a positive trend, with cost increasing every year. Chromite foundry sands, in particular, showed an increase from 400-500 $/ton at the beginning of 2018 to 545-565 $/ton in June 2018, following an increase in the demand. With a price of over 500 $/ton, foundry quality is the most valuable chromite commodity on the market, followed by chemical grade (300 $/ton) and metallurgical grade (150 $/ton). The rise in prices has some important consequences, such as the reopening of abandoned mines and the introduction of minor companies in the market.

### 1.2.3. Chromitites

Chromite can be found as an accessory phase in many lithologies, but the only economically important deposits are chromitites, which are lithologies where chromite is a major mineralogical phase (Papp and Lipin, 2001). Chromitites can be found in two main geologic settings, layered intrusions and ophiolites. Chromitites in layered intrusions form continuous beds, and are called stratiform deposits, while chromitites in ophiolites form lenses and pods, and are called podiform deposits (Papp and Lipin, 2001). Minor sources of chromitite are constituted by laterites, products of peridotites

weathering (Fig. 1.7) and chromitites associated to Alaskan-type intrusions, which are not exploited for chromite but can be associated to economic PGE deposits.

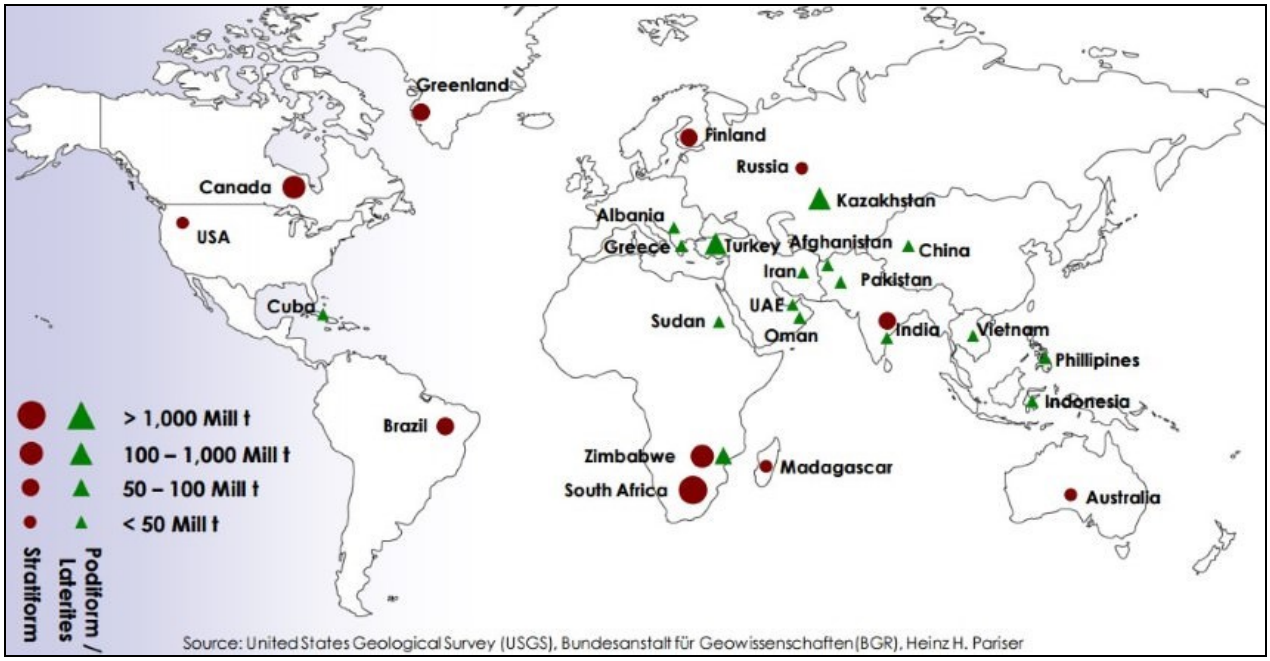


Fig. 1.7 Global distribution of major chromite ore deposits (from USGS).

*Stratiform Deposits*

Stratiform chromitites are associated to layered magmatic intrusions, and are constituted by large continuous bodies slowly cooled down within a magmatic chamber. All the economic stratiform deposits are all of Precambrian age, and the youngest of them is the Bushveld Complex, South Africa (1.9 billion years). Chromite ores in ultramafic layered complexes are usually localized in thin but continuous layers, with a lateral extension of dozens of km. Massive or disseminated chromite ores show a cumulate texture, and the silicate matrix is constituted by pyroxenes and sometimes plagioclase. Chromite beds in general are alternated with norite, anorthosite and pyroxenite beds (Papp and Lipin, 2001). However, in the Bushveld complex, chromitite layers can be found associated to harzburgites and pyroxenites (LG), to pyroxenite, norite and anorthosite (MG) and to orthopyroxenite, harzburgite, norite and anorthosite (UG), within the Lower and the Upper Critical Zones. Ni-Fe-Cu-PGE sulfides can be found associated to stratiform deposits, mainly enclosed within chromite grains. PGM in stratiform deposits mainly consist of Pt, Pd and Rh sulfides.

The genesis of chromitite layers within stratiform deposits is related to magma mixing (Irvine, 1977). The mixing of a fractionated magma with a more primitive one can shift the crystallization into the chromite stability field and result in the formation of massive chromite layers. This model requires repeated introduction of primitive magma in the system, in order to produce the peridotite-chromite layers typical of stratiform layered intrusions.

*Podiform Deposits*

Podiform chromitites are associated to dunites or more rarely to pyroxenites, harzburgites and lherzolites within the mantle sections of ophiolites, large portions of oceanic lithosphere obducted onto continental margins during tectonic processes, where they are usually localized close to the Moho. Less frequent are the ores hosted within the cumulate section of the ophiolite, where they form lens-shaped bodies of different dimensions. Within the peridotite bodies, chromitite is almost always associated with dunite or serpentinite (Thayer, 1961). In particular, a common feature of many podiform chromitites is a characteristic dunite envelope (or dunite halo), which can have different thickness. Close to the mantle-crust transition, they can also be found in association to gabbros and pyroxenites. The deposits are often associated to shear zones, and can be displaced and intensely deformed (Thayer, 1961). Podiform chromitites display a wide variety of textures. The main ones are massive, schlieren, nodular and disseminated (Fig. 1.8). All can grade into each other, and can be found within the same deposit. Nodular and anti-nodular textures are a peculiar feature of podiform chromitites, as they are absent within stratiform deposits (González-Jiménez et al., 2014b).

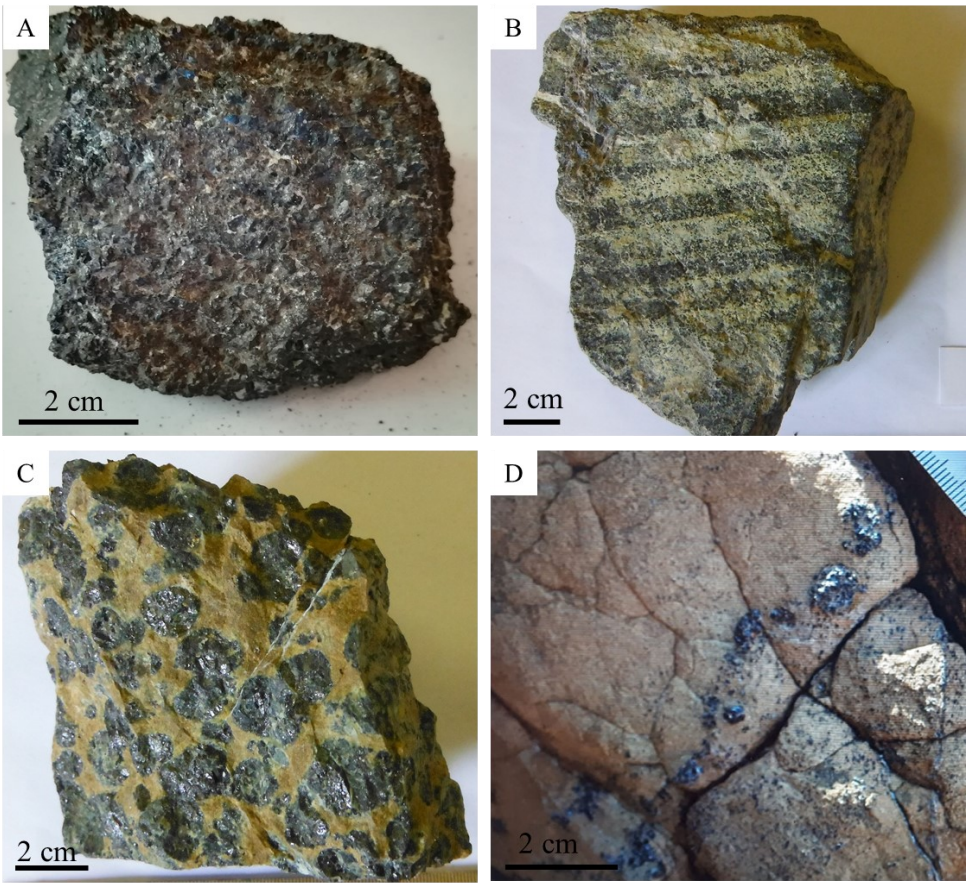


Fig. 1.8 Examples of chromitite textures from the Abdasht-Soghan complex, Iran (A-C) and Nea Roda, Greece (D). (A) massive; (B) schlieren; (C) nodular and (D) disseminated.

The composition of chromites in ophiolites has a strong affinity with the one of spinels in boninites, suggesting that boninites may be the main parent magma for podiform deposits (Barnes and Roeder, 2001). Usually, the composition of spinels in podiform deposits is intermediate between boninite and MORB, with a very low (<0.2 wt%) $TiO_2$ content. The main point of debate about the formation of chromitites is the process that can lead to a high concentration of chromite in a silicate magma containing relatively low amounts of Cr (between 600 and 1200 ppm) (Zhou et al., 2001). The genetic models proposed during the years can be grouped into three categories (González-Jiménez et al., 2014b):

- Fractional crystallization: crystallization of chromite within magma chambers, in open conduits where there is a flow of basaltic melt, or in the upper mantle under spreading ridges (Lago et al., 1982; Leblanc and Nicolas, 1992). Chromite, the first phase to crystallize, forms aggregates kept in suspension until the flow slows down and the nodules settle at the base of the conduit. This model can explain the presence of disseminated chromite, but not the formation of massive chromitites. A variant of the model suggests that the composition of the melt could be changed by melt-rock reactions (Zhou et al., 1994), or assimilation of pre-existing rocks (Bédard and Hébert, 1998). Different assimilated rocks could explain the formation of high-Cr or high-Al chromites.
- Mixing and mingling of melts in dunite channels: chromitites enveloped in dunites are the product of mantle-melt interaction (Arai, 1997; Arai and Yurimoto, 1994; Zhou et al., 1994). The proposed mechanism is similar to the one suggested for chromitites in layered intrusions. Mantle-melt interactions produce a secondary melt enriched in Si and Cr by dissolution of orthopyroxenes (Arai and Yurimoto, 1994). Further mixing of Si and Cr-rich secondary melt with a new pulse of primitive magma can result in spinel oversaturation and therefore precipitation of chromite (Zhou et al., 1994). This process results in a zonation from chromitite to dunite and finally harzburgite and lherzolite, as observed in several ophiolite bodies (Zhou et al., 1996, 1994).
- Fluid related models: chromite ore formation involves the separation of volatile-rich fluid phases from small fractions of evolving hydrous silicate melts. Major and minor element composition of several ophiolite chromitites do not have MORB affinity but a boninitic one. These melts are believed to have been formed by remelting of previously depleted peridotites in forearc suprasubduction setting where volatiles can produce hydrous silicate melts (Gonzalez-Jimenez et al., 2011a). During the last years, experimental studies have tried to simulate the genetic conditions of chromitites in suprasubduction settings. Ballhaus (1998) simulated the

crystallization of chromite between siliceous and fayalitic melts, and observed that chromite nucleates only in the least siliceous melts, forming nodular textures. Later, Matveev and Ballhaus (2002) oversaturated the system with water, and demonstrated how chromite grains tend to collect in the fluid phase while olivine resides in the melt. This is an effective mechanism for the accumulation of chromitites accompanied by lower amounts of olivine.

- Integrated model: a new integrated model was developed taking into account geochemical data coupled with petrologic, field and microstructural observations (González-Jiménez et al., 2014b). In order to form massive chromitite bodies, it is necessary to have a very large volume of mantle peridotite (Leblanc and Ceuleneer, 1991). This suggests that to form a chromitite body, a continuous flow of melt is required, leaving behind highly-depleted peridotites, with thickness proportional to the volume crossed. However, the thickness of dunite envelops appears to be unrelated to the size of the chromitite body, suggesting that these two lithologies may not be coeval, but that dunite could be a pathway for the transport and emplacement of the chromite parental melt (González-Jiménez et al., 2014b). Big dunite channels (up to a few hundred meters) can form beneath spreading centers through dissolution of pyroxenes, becoming high-porosity and high-permeability patterns for the ascent of melts (Cocomazzi et al., 2020; Kelemen, 1990; Kelemen et al., 2000, 1999, 1997, 1995; Kelemen and Dick, 1995). The channels finally tend to coalesce (Braun and Kelemen, 2002) and to form a single dunite body. The network of channels is, according to some Authors, the ideal environment for the formation of chromitite bodies through mixing of different melts (Spiegelman and Kelemen, 2003). Two dunite channels can carry melts with different $SiO_2$ contents. The coalescence of these channels leads to mixing of different magmas, triggering chromite precipitation, which would result in a disseminated texture (González-Jiménez et al., 2014b). Different melts can also mix at the intersection of big melt-filled channels, and chromite can precipitate as nodules (Ballhaus, 1998) and later aggregate to produce massive chromitite bodies, obstructing the channel. Finally, in the peripheral part of the bodies, chromite forms stockworks and fills breccias (González-Jiménez et al., 2014b), suggesting the presence of chromite-bearing fluids inside cracks.

Podiform chromitites can be related to two geologic environments (Fig. 1.9): island arcs and nascent spreading centers (back-arc basins) (Zhou and Robinson, 1997). Island arcs provide a huge input of volatiles, leading to high degrees of partial melting and formation of high-Cr chromitites. In nascent spreading centers, the volatile input would be lower, generating lower degrees of partial melting and

high-Al chromites (Zhou et al., 1994). The residual peridotites formed in the last scenario will be moderately depleted lherzolites, and cpx-bearing harzburgites.

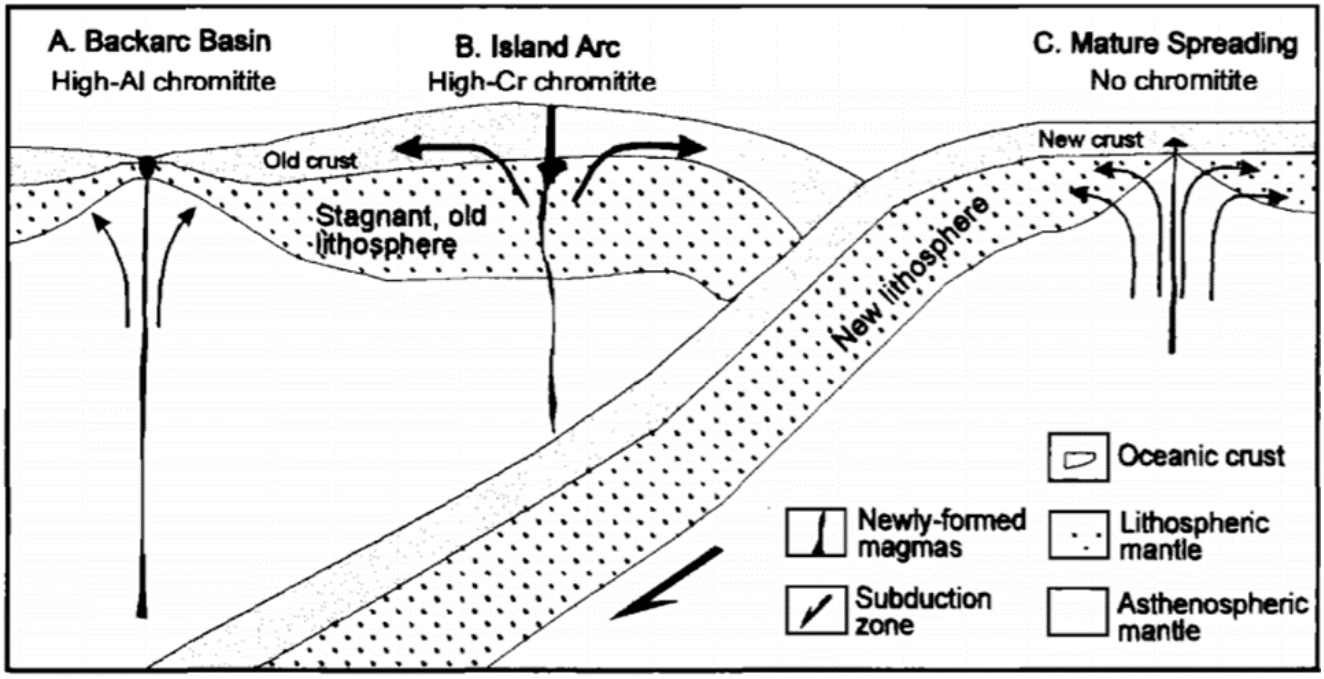


Fig. 1.9 Simplified scheme showing two possible tectonic environments for the formation of podiform chromites (from Zhou and Robinson, 1997).

*Supra-Moho chromitites*

Chromitite deposits are usually included within the mantle sequence, but can be found also within supra-Moho mafic-ultramafic cumulates, where morphology and ore grades are comparable with stratiform deposits more than with podiform ones. This supra-Moho level of magmatic exchange between astenospheric mantle and the constructing oceanic crust is called Moho Transition Zone (MTZ) (Boudier and Nicolas, 1995).

Within the Oman ophiolite, the MTZ presents a variable thickness, up to hundreds of meters, and it is mainly composed of dunites, gabbros, pyroxenites and chromitites.

The MTZ in the Nurali ophiolite is a dunite-wehrlite-pyroxenite-chromitite layered section that overlays a peridotite sequence (Grieco et al., 2007; Pertsev et al., 1997; Zaccarini et al., 2004a), much like the Oman MTZ. This zone is interpreted as the product of multistage magmatic crystallization in narrow chambers (Pertsev et al., 1997). Chemical trends across the Transition Zone show a gradual increase of Mg# and depletion in compatible elements upsection, and the occurrence of high-Mg enstatite-olivine cumulates at the top (Pertsev et al., 1997).

Malitch et al. (2003) reports supra-Moho chromitites occurring closely above the mantle section of the Kraubath ophiolite (Austria), suggesting a possible formation in the cumulate section above the Moho.

Supra-Moho chromitites usually have distinct geochemical features from the underlying mantle chromitite. The composition of spinels in the supra-Moho chromitites is quite unusual, more similar to ophiolitic cumulates and layered intrusions than to podiform bodies. Spinel Cr# [Cr/(Cr+Al)] in supra-Moho chromitites of Nurali (Grieco et al., 2007; Zaccarini et al., 2004a) and Oman (Boudier and Nicolas, 1995) is lower than the one of below-Moho chromitites (generally below 0.62). Supra-Moho chromitites of the Kraubath ophiolite, on the other hand, show Cr# between 0.73 and 0.77, higher than values reported for Nurali and Oman supra-Moho chromitites, but lower than the underlying podiform bodies, whose spinel Cr# varies between 0.81 and 0.86.

Differences between mantle and supra-Moho chromitites have also been detected in their PGE content. MTZ chromitites are usually richer in PPGE with respect to IPGE, and their PGE total content was repeatedly reported as higher than in the corresponding chromitites below the Moho (Economou-Eliopoulos, 1996), with values reaching 750ppb in Kraubath (Malitch et al., 2003a), and up to 26700 ppb in Nurali (Grieco et al., 2007).

*Classification of chromitites in ophiolites*

González-Jiménez et al. (2014b) suggest a classification based on structural criteria, geochemistry and PGE content:

- Type-I chromitites are the most common within ophiolite sequences. Type-I deposits are present as lenses and pods, with massive, schlieren, nodular or disseminated textures. As most relevant feature, they present enrichment in IPGE (Os, Ir, Ru), relative to PPGE (Rh, Pt, Pd). Cr# is highly variable, while Mg# does not present a wide variation (Barnes and Roeder, 2001; Irvine, 1967; Leblanc and Nicolas, 1992). There is a distinction in Type-I chromitites between below-Moho (Cr# > 0.6) and those located in the crust-mantle transition zone (Cr # <0.6).
- Type-II chromitites are less abundant than Type-I and are characterized by an enrichment in PPGE relative to IPGE. The deposits are commonly constituted by layers within the lower crust, crust-mantle transition zone (Prichard et al., 1996; Tarkian et al., 1996), arc roots (Moreno et al., 2001) or crustal cumulate rocks (Grieco et al., 2007). Their PGE whole rock content is generally higher than in Type-I chromitites. The group can be further divided into Type-IIA (Cr# and Mg# overlapping Type-I chromitites) and Type-IIB (overlapping compositional range of layered intrusions).

### 1.2.4. Petrogenetic Applications

Spinels crystallize in a wide range of solid solutions, at different PT conditions. They are refractory and resistant to alteration, and in the case of chromite, among the first phases to crystallize. Due to

these properties, they are often used as petrogenetic indicators (Irvine, 1965; O'Neill and Wall, 1987; Sack and Ghiorso, 1991). Some compositional trends have been recognized within spinels belonging to different environments (Barnes and Roeder, 2001):

- Cr-Al trend: particularly evident in various mantle and lower crust spinels (ophiolite peridotites, basalts, mantle xenoliths), it is characterized by an increasing Cr/(Cr+Al) at increasing $Fe^{2+}/(Fe^{2+}+Mg)$. This variation in the spinel composition has been interpreted as a subsolidus re-equilibration with olivine, and is the basis of spinel-olivine geothermometers (Ballhaus et al., 1991; Irvine, 1967; Sack and Ghiorso, 1991).
- Fe-Ti trend: present in most differentiated mafic-ultramafic bodies, it shows an increasing $Fe^{3+}$ and $Fe^{2+}/(Fe^{2+}+Mg)$ accompanied by increasing $TiO_2$. This trend is attributed to the evolution of spinel compositions during fractional crystallization of olivine and pyroxene, which produces an increase of Fe/Mg and Ti in the melt (Henderson, 1976; Henderson and Wood, 1982; Roeder and Campbell, 1985). The $Fe^{2+}/(Fe^{2+}+Mg)$ increase in this case is due both to fractional crystallization and subsolidus re-equilibration with coexisting silicates.
- Kimberlite trend: similar to the Fe-Ti trend, it differs in maintaining a nearly constant $Fe^{2+}/(Fe^{2+}+Mg)$ over a wide range of varying $Fe^{3+}$ and $TiO_2$. This trend is a result of the enrichment in $Fe^{3+}$ with respect to $Fe^{2+}$ in some magmas, and is evident in kimberlites and alkali basalts.
- Rum trend: restricted to chromites occurring within gabbroic rocks in some layered intrusions, involves an increase in Al at the expense of Cr, and a decrease in $Fe^{3+}$ and $Fe^{2+}/(Fe^{2+}+Mg)$ (Henderson, 1976; Henderson and Wood, 1982).

*Geothermometry and Geospeedometry*

The crystal structure of spinels allows a certain number of cation substitutions both in tetrahedral and in octahedral sites. In particular, the Mg-$Fe^{2+}$ exchange between olivine and chromite is important because it is temperature-dependent. This cation exchange was first studied by Irvine (1965), who linked spinel and olivine compositions to temperature, calibrating the first olivine-spinel geothermometer. Cr-spinel typically occurs in close association with olivine and/or pyroxene. Thus, the main reactions occurring in the system can be summarized as follows (Irvine, 1965):

(a) $\frac{1}{2}Fe_2SiO_4 + MgCr_2O_4 \rightleftarrows \frac{1}{2}Mg_2SiO_4 + FeCr_2O_4$

(b) $\frac{1}{2}Fe_2SiO_4 + MgAl_2O_4 \rightleftarrows \frac{1}{2}Mg_2SiO_4 + FeAl_2O_4$

(c) $\frac{1}{2}Fe_2SiO_4 + MgFe_2O_4 \rightleftarrows \frac{1}{2}Mg_2SiO_4 + Fe_3O_4$

Irvine (1965) linked the chemical composition of these phases to the equilibrium constant of the exchange reaction (Kd), and used its temperature dependence to estimate coexisting olivine and spinel equilibrium temperatures. This geothermometer was later implemented by several Authors (e.g. Ballhaus et al., 1991; Engi, 1983; O'Neill and Wall, 1987).

The olivine-spinel geothermometer potentially works over a wide range of temperatures, from high-T conditions down to at least 650°C, until the cessation of the elemental exchange (Fabriès, 1979; Freer, 1981; Greenfield et al., 2013; Grieco et al., 2018; Lehmann, 1983). One of the factors that affects the possibility to reach equilibrium is the "r" factor (olivine to chromite volume ratio), first mentioned by Engi (1983) and later studied by (Grieco et al., 2018). Chromitites and surrounding dunites show a wide range of r values, from high (≈ 1) in dunites with accessory spinel, to the lowest values in massive chromitites (≈ 0), where there is spinel predominance over olivine. Given the high variability of chromitite textures, there is a wide range of intermediate values dependent on the texturally controlled modal proportions of olivine *vs* spinel. During re-equilibration at high r values (peridotites with accessory spinel), olivine composition is almost unaffected, while spinel can change considerably its composition. On the contrary, when the re-equilibration occurs at low r values, it is the chromite composition that results unaffected by olivine-spinel exchange (Grieco et al., 2018).

At high temperature subsolidus conditions, diffusivity is sufficiently efficient to ensure a homogeneous spinel that is in equilibrium with surrounding olivine. With decreasing temperature, the diffusion profile reflects lower diffusivity to the point where elemental exchange can no longer proceed (Ozawa, 1983). This critical temperature is relatively low compared to other exchange reactions used as geothermometers in peridotites. Ca-Mg partitioning in pyroxenes or Mg-$Fe^{2+}$ exchange between orthopyroxene and spinel, are stopped at higher temperatures (Fabriès, 1979; Freer, 1981; Greenfield et al., 2013; Lehmann, 1983; Ozawa, 1983). This implies that Fe-Mg distribution for olivine-spinel exchange is more sensitive to cooling, and records lower temperatures.

Geothermometry of olivine-spinel exchange applied to rim-rim analyses has been repeatedly used to estimate the thermometric cessation of elemental exchange conditions. Core-core analyses are cited in the literature as a means to determine the original chemical compositions of olivine-chromite pairs (Greenfield et al., 2013). The assumption that core compositions retain their primary imprint, however, is not always true. In fact, it is dependent on chromite modal content (Grieco et al., 2018), and spinel grain size (Ozawa, 1984, 1983). Incomplete exchanges can result in compositional heterogeneities within olivine-spinel couples, due to their interdiffusivity coefficients and temperature. This heterogeneity is shown in typical olivine-spinel diffusivity patterns developed during cooling (Ozawa, 1983). Olivine is more magnesian close to the spinel, while spinel shows the opposite trend close to

olivine. Mg-$Fe^{2+}$ zoning can thus also be used to estimate a cooling rate in ultramafic rocks (Ozawa, 1984, 1983). In particular, spinel XMg appears to be more sensitive to cooling rate differences than olivine XMg, especially at low rates within the range of ~850 – ~650 °C. Ozawa (1984) calculated cooling rate profiles for several types of natural rocks at different initial temperatures of the system, numerically solving the differential equations that describe the Mg-$Fe^{2+}$ exchange system of a spherical spinel surrounded by olivine. His solution reveals a relationship between temperature and spinel grain size (diameter). Temperatures in his model are neither primary nor re-equilibrated, but calculated using spinel and olivine XMg core analyses. In these estimates, olivine XMg coincides with the primary value but not in chromite: this equivalence it is valid only for grains with a radius larger than diffusion distance.

# 1.3. Platinum Group Elements

## 1.3.1. Properties and Industrial Applications

Platinum Group Elements (PGE) are six transition metals clustered together in the periodic table (Fig. 1.10): ruthenium (Ru), rhodium (Rh), palladium (Pd), osmium (Os), iridium (Ir) and platinum (Pt).

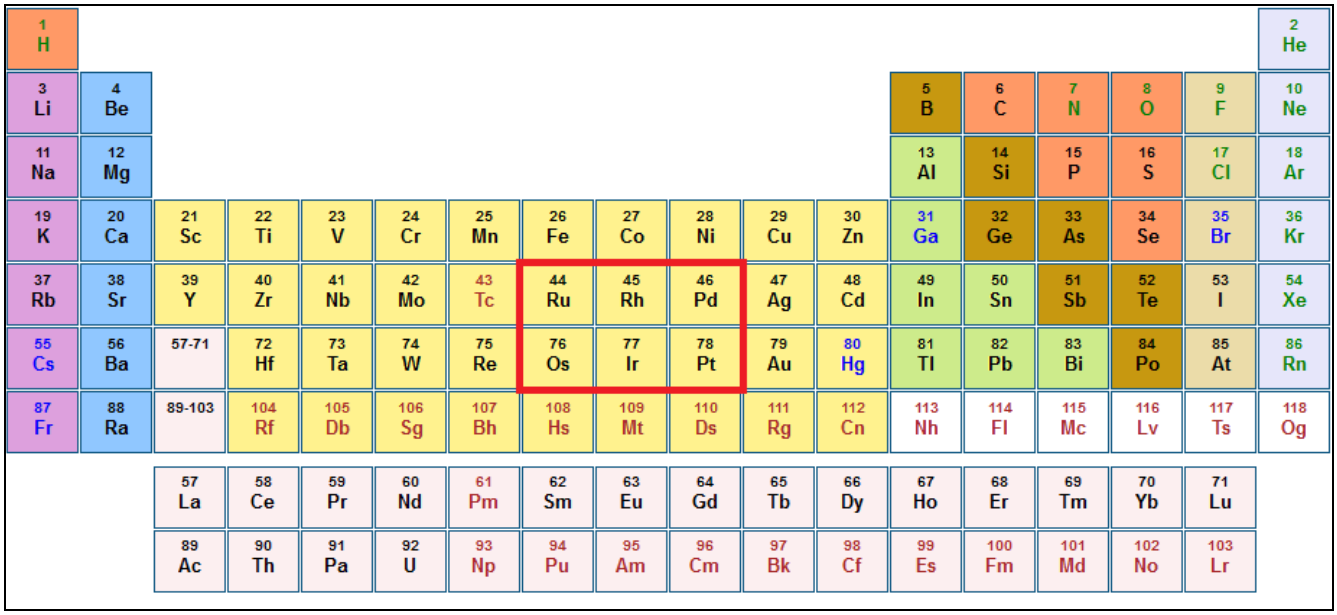


Fig. 1.10 PGE position in the periodic table.

They have similar properties, such as high melting point and corrosion resistance, and they are widely employed as catalysts, to accelerate or control the rate of many oxidation, reduction or hydrogenation reactions. The most used metals in catalytic converters are Pt, Pd and Rh, indispensable to decrease hydrocarbon, carbon monoxide and nitrous oxide emissions in automobile exhaust. Specifically, Pt is mainly used in light duty diesel engines, Pd for light duty petrol engines, and Rh for three-way catalytic converters (Johnson Matthey, 2020). Pt and Pd are interchangeable to some degrees, but not fully substitutable (Deloitte Sustainability et al., 2017b).

In the industry, almost all PGE are used as catalysts in chemical manufacture and petroleum refining. In particular, Pt is used for the production of nitric oxide and high-octane gasoline. Pd and Rh are used for the production of several plastics and polymer precursors. Ru is used in the production of ammonia, and, together with Ir, in electrochemical processes (Deloitte Sustainability et al., 2017b). Other applications are in the jewelry, electronic (Pt and Pd are used in the construction of printed circuit board, or as thermocouples), glass production and medical industry.

A supply chain for PGE used as catalysts in the automotive industry is shown in Fig. 1.11 (European Commission, 2014). The first step is mining and processing. As PGE are present in the ore at very low

concentrations, typical processing steps are crushing and milling, froth flotation and magnetic separation (or dense media separation) (British Geological Survey, 2009). After being processed close to the extraction site, the concentrate undergoes a smelting process to separate PGE from other Base Metals (BM) present. This and further stages may take place in other countries and by several companies. The separation of each metal is achieved through hydrometallurgy, forming metal salts, that can be further refined into metals (through a heating treatment) or other forms. For the automotive industry, PGE are supplied as salts. Salts are then used to produce catalytic converters, which are installed on vehicles and used. At the end of the vehicle life, PGE can be partially recovered and re-processed.

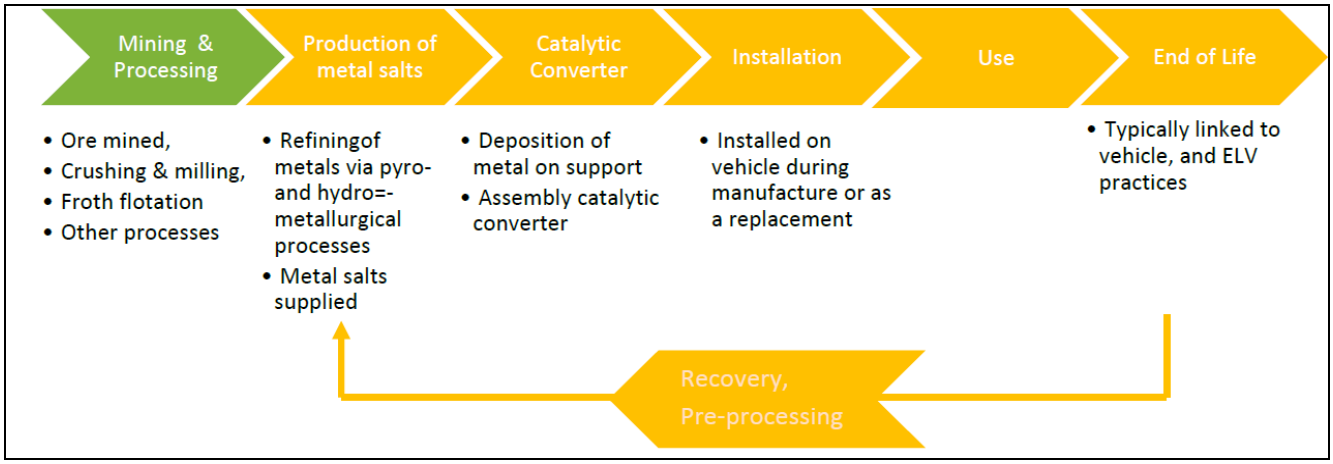


Fig. 1.11 Supply chain for PGE automotive catalysts; in orange are highlighted the stages occurring in Europe.

### 1.3.2. Market and Prices

The largest primary PGE suppliers of Europe are South Africa and Russia, with Pt-Pd rich and Ni-Cu rich deposits respectively, where PGE are recovered as by-products. The supply of the other PGE is related to the production of Pt and Pd. PGE recycling also contributes to the supply of these metals. Global PGE reserves are estimated at 66,000 tonnes by USGS, and over 95% is located in the Bushveld Complex, South Africa (Tab. 1.3) (Deloitte Sustainability et al., 2017b). Noril'sk proven and probable reserves, however, are at 2,400 tonnes, exceeding USGS estimates (Norilsk Nickel, 2015). Other studies estimate global PGE reserves at 90,700 tonnes, 70% of which in South Africa (Mudd, 2012).

Tab. 1.4 World Supply and Reserves of Platinum Group Elements in 2016 (USGS, 2020b); n.a. (not available).

| Country | Total Supply (tonnes) | Total % | Reserves |
|---|---|---|---|
| South Africa | 264 | 61 | 63,000 |
| Russia | 117 | 27 | 1,100 |

| | | | |
|---|---|---|---|
| Zimbabwe | 22 | 5 | n.a. |
| Canada | 11.9 | 3 | 310 |
| US | 7.5 | 2 | 900 |
| Other Countries | 8 | 2 | 800 |
| World Total | 430 | | 66,110 |
| **Other Supply** | | | |
| Recycling | 134 | | |
| Stock Sales Russia | 8 | | |
| Total Supply | 572 | | |

Some studies also report data regarding PGE production in Europe (Tab. 1.4), but there is not a comprehensive study summarizing the whole production, so data are only partial (Minerals4EU, 2014).

Tab. 1.5 Europe PGE resources (Minerals4EU, 2014).

| Country | Code | PGM | Quantity (Mt) | Grade (g/t) | Resource |
|---|---|---|---|---|---|
| Greenland | JORC | Pt | 5.08 | 0.06 | Indicated |
| Sweden | Historic | Pd | 0.2 | 0.4 | Historic Resource Estimate |
| Finland | NI 43-101 | Pd | 145 | 0.47 | Measured |
| | JORC | Pd | 15 | 1.3 | Indicated |
| | NI 43-101 | Pt | 145 | 0.22 | Measured |
| | JORC | Pt | 15 | 0.39 | Indicated |
| | None | Rh | 8.5 | 0.092 | Historic Resource Estimate |

Individual PGE world mine production is reported in Tab. 1.5. South Africa is the dominant supplier of Pt, Rh, Ru, Ir and Os, and shares the dominion of the Pd production with Russia. The main companies mining and refining PGM in South Africa are Anglo American Platinum, Impala Platinum and Lonmin. The majority of Pd supplied by Russia comes from the Noril'sk-Talnakh district (Deloitte Sustainability et al., 2017b).

Tab. 1.6 World mine production of PGE (British Geological Survey et al., 2018; Deloitte Sustainability et al., 2017b); recycling data excluding closed loop recycling.

| Country | Platinum | | Palladium | | Other PGE | |
|---|---|---|---|---|---|---|
| | Tonnes | % | Tonnes | % | Tonnes | % |
| South Africa | 93.99 | 64.13 | 58.41 | 31.95 | 36.04 | 81.96 |
| Russia | 22.00 | 15.01 | 81.30 | 44.46 | 2.80 | 6.37 |
| Zimbabwe | 12.48 | 8.52 | 10.14 | 5.54 | 2.80 | 6.37 |

| | | | | | | |
|---|---|---|---|---|---|---|
| Canada | 10.70 | 7.30 | 18.70 | 10.23 | 1.20 | 2.73 |
| USA | 3.65 | 2.49 | 12.20 | 6.67 | 0.00 | 0.00 |
| China | 1.40 | 0.96 | 0.70 | 0.38 | 0.00 | 0.00 |
| Colombia | 1.13 | 0.77 | 0.00 | 0.00 | 0.00 | 0.00 |
| Finland | 1.06 | 0.72 | 0.81 | 0.44 | 0.00 | 0.00 |
| Botswana | 0.09 | 0.06 | 0.56 | 0.31 | 0.00 | 0.00 |
| Poland | 0.06 | 0.04 | 0.03 | 0.02 | 0.00 | 0.00 |
| **World tot** (mine production) | **146.57** | | **182.8** | | **43.98** | |
| **Recycling** | **64.4** | | **85.6** | | **9.6** | |
| **Total Supply** | **210.97** | | **268.4** | | **53.58** | |

The supply of PGE from secondary materials is well established and growing, especially in Europe. Recycling of automotive catalysts is the major contributor (Deloitte Sustainability et al., 2017b), especially as 95% of PGE of spent catalysts can be reconverted. Aside from the automotive, other sources of secondary materials are jewelry, electronic material and industrial by-products of non-ferrous mining.

*Europe trades*

In the years, trade flows in and out of Europe have considerably changed. Until 2011, imports of PGE outweighed exports. In 2012 there was a drop in the imports, transforming EU in a net exporter of PGE, and roughly maintaining the trend until 2014 (Eurostat, 2016). Major suppliers to Europe are Switzerland (traditionally a point of PGE storage), South Africa and USA (Fig. 1.12 A). Destinations of PGE exports (Fig. 1.12 B) are mainly USA, Macedonia, Hong Kong and China.

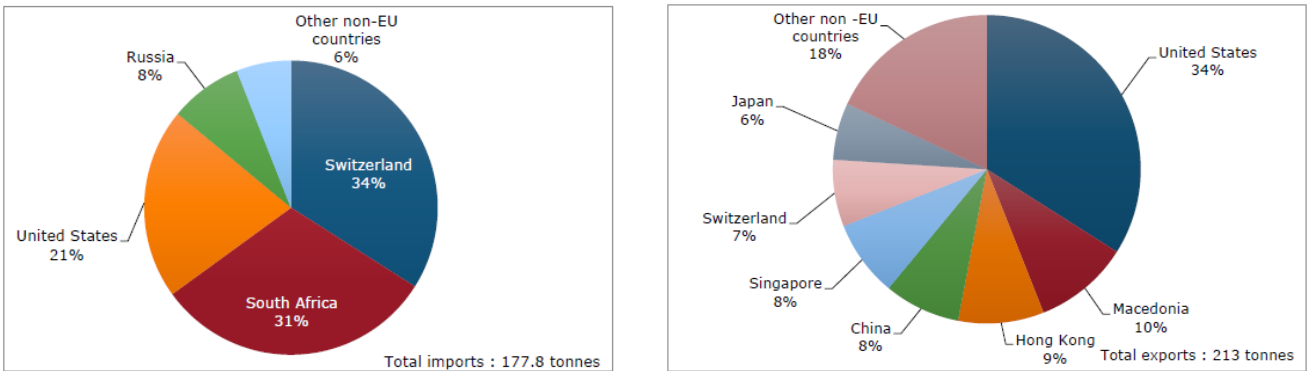


Fig. 1.12 A) Sources of EU PGE imports in 2014; B) Destinations of EU PGE exports in 2014 (Eurostat, 2016).

PGE are bought and sold in various forms. Prices typically refer to metals with minimum purities of 99.9%. Changes in PGE prices are not strictly related to investments, but on the variations in output or consumer demand ("Price pressures on metals," 2019). The price of Pt has been quite volatile in the last 14 years (Fig. 1.13 A). In particular, in 2008 there was a sharp fall, following the global financial

crisis. The price recovered in 2009-2010, but suffered a smooth downward trend since then, due to the economic recession (Deloitte Sustainability et al., 2017b). The price of Pd also shows a high degree of volatility (Fig. 1.13 B), but with a general positive trend that sharply increased since January 2018. Rh prices during the last 14 years had two sharp spikes (Fig. 1.13 C). The first one was at the beginning of 2008, the second one at the beginning of 2020. Pd and Rh price increase in 2020 is probably due to the increasingly tightening emission restrictions which have led to an increase in the demand of these metals for the automotive sector (Johnson Matthey, 2020). Iridium has more than doubled in price over the last three years (Fig. 1.13 D, due to its employment in industrial catalysts (e.g. production of acetic acid), and given the scarcity of this metal, even small increases in industrial use are quickly reflected on the market price. Ruthenium prices saw the maximum price spike in 2007 (Fig. 1.13 E), after it was suggested to use a Ru-based catalyst instead of using a much costlier Pd one (Heraeus Precious Metals, 2018). Os prices tend to be stable over time (~400 $/oz), due to its limited industrial use and difficulty in working it. A summary of the price variability from 2006 to 2020 is reported in Fig. 1.13 F.

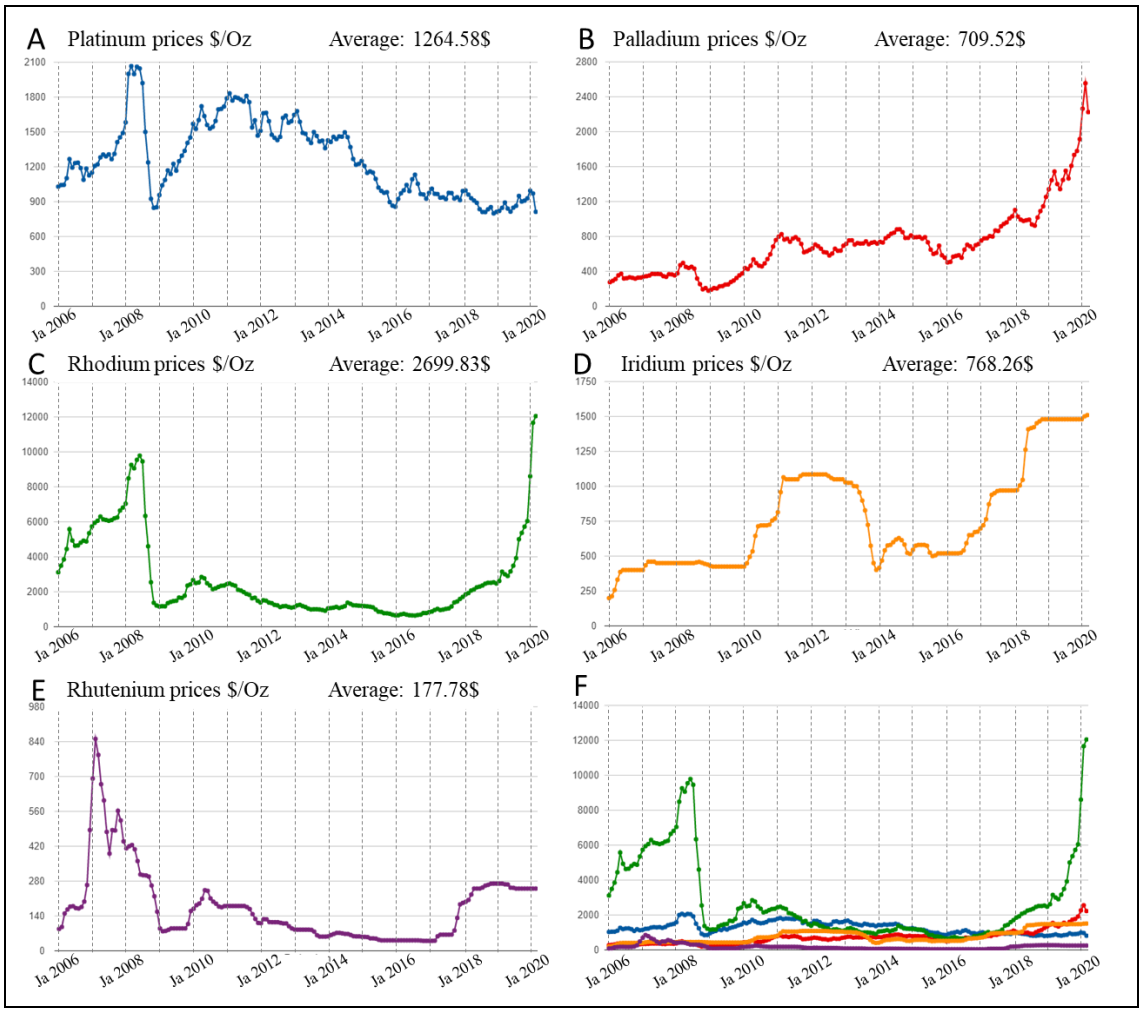


Fig. 1.13 Price of Pt (A), Pd (B), Rh (C), Ir (D), Ru (E) and a summary of PGE prices (F) expressed as $ per ounce in the period between January 2006 and March 2020 (http://www.platinum.matthey.com).

The demand of these metals has been booming, and the supply is struggling to keep up with it, leading to search for alternatives (e.g., Pt, now used mainly for diesel catalytic converters, instead of Pd, which is used in gasoline engines). On the other hand, for some metals, such as Rhodium, there is not a cheaper alternative, so that exploration for new sources is becoming imperative. Gold is another possible substitute for PGE, but its price limited this use (Deloitte Sustainability et al., 2017b).

### 1.3.3. Geochemical behavior

Many of the chemical properties that are of industrial interest also result in distinct geochemical behavior. PGE, gold and rhenium are highly siderophile and chalcophile elements, and as such they partition into the metallic phase rather than into the oxide one (Brenan, 2008). This low capacity to bond with oxygen is the primary cause of scarcity of PGE in the crust. Moreover, due to their high metal-silicate partition coefficient ($D > 10^4$), it is believed that they were sequestered into the core during the core-mantle separation (Lorand et al., 2008). The average concentration of Pt and Pd in the crust is 0.005 g/ton. Ir, Rh and Ru have a concentration of 0.001 g/ton (British Geological Survey, 2009). The concentration of PGE in the mantle is estimated $10^5$ times lower than in the CI chondrites, but still $10^2$ higher than in the continental crust (McDonough and Sun, 1995; Wedepohl, 1995), thus explaining why they are enriched in igneous rocks derived from early crystallization of primary mantle melts. Their siderophile/chalcophile behavior can be used as a tracer in order to understand differentiation processes that involve metal or sulfide phases. Although PGE abundance in the mantle is lower than in CI chondrites, the relative abundances are too close to chondrite ratios to be a result of core-mantle segregation. A possible explanation could be a continuous influx of chondritic material to the Earth once the core was already formed (Chou, 1978), but possible bombardment records have already been destroyed by geodynamic activity.

Based on their behavior in geological systems, PGE are divided in two sub-groups: IPGE (iridium sub-group, including Os, Ir and Ru) and PPGE (platinum-palladium sub-group, including Pt, Pd and Rh).

Due to PGE affinity to sulfides, magmas in equilibrium with sulfides remaining in the residual mantle will be PGE-poor while at higher degrees of partial melting, able to consume all the sulfides, magmas will be PGE-rich, with values approaching those of the primitive mantle (Fig. 1.14). This explanation is valid for the whole PGE content, but does not explain the fractionated PGE chondrite patterns, because experimental data show that all PGE have affinity for sulfide melts (Alard et al., 2000). Ballhaus et al. (2006) confirmed that 90% of the PGE in the mantle are in base-metal sulfides, and identified two sulfide populations. The first population consists of Os-Ir-Ru rich and Rh-rich sulfides in the form of Fe-Ni mss (monosulfide solid solution) inclusions in olivine, showing the same negative

PGE pattern as residual mantle. The second population is a Pd- Pt-rich Ni-sulfide or Cu-sulfide, representing the crystallization product of Cu-Ni-rich sulfide melt with a positive slope in PGE patterns (basalt-like).

During partial melting, the second population fractionates into the magma, resulting in the depletion of Pt and Pd in the residual mantle. The depletion factor increases with the degree of melting (and so with the amount of magma extracted from the mantle). However, the silicate melt dissolves thousands of ppm of sulfur, so at sufficiently high degrees of partial melting (30-50%), similar to those needed to generate komatiite in the Archean, all the mss (carrying Os, Ir, Ru and Rh) is expected to be consumed by the magma. At this stage, the mss liberates micrometer-scale Ru-Os-Ir sulfides/alloys and Pt-Ir alloys, which retain the PGE inside the residual peridotite (Luguet et al., 2007). Mantle-derived magmas show a trend opposite to that of residual peridotites: MORBs are depleted in IPGE relative to the mantle composition, because their mantle source still contains base-metal sulfides (Lorand et al., 2008 and references therein).

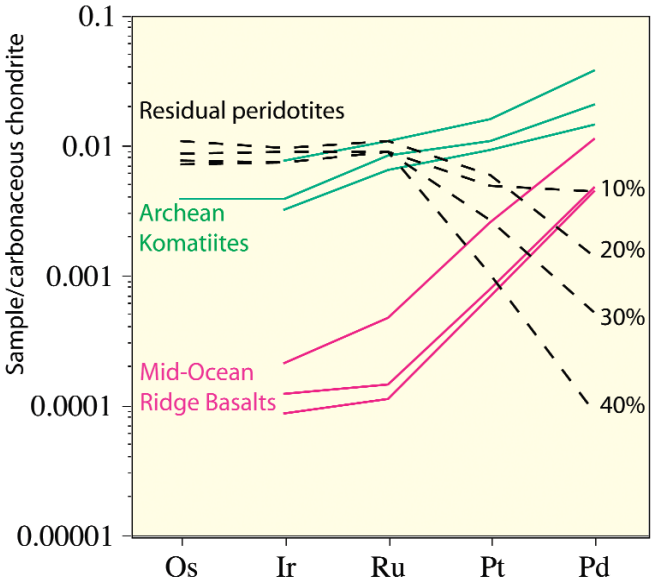


Fig. 1.14 Chondrite-normalized PGE abundances in residual peridotites and mantle-derived magmas (from Lorand et al., 2008).

In ophiolites, arc-related melts formed above subduction zones are generated by relatively high degrees of partial melting (20%), which almost completely dissolve mantle sulfides, producing basaltic melts enriched in PGE. As a consequence, chromitites formed from this type of melt will be PGE-rich. On the contrary, basalts formed beneath spreading centers form at lower degrees of partial melting, and will therefore be PGE-poor. At higher degrees of partial melting (>25 %), the volatile PGE (Pt, Pd) would be diluted in the melts, producing PGE-rich chromitites barren of these two elements (Gonzalez-Jimenez et al., 2011a).

### 1.3.4. PGE deposits

The upper crust contains about 0.5 ppb of platinum, and the average grade of mined ores ranges from 5 to 15 ppm (Zientek and Loferski, 2014). Therefore, the formation of an ore deposit requires a process able to raise PGE concentration of at least four orders of magnitude above their typical abundance in the crust.

As stated in the previous paragraph, PGE are more abundant within sulfide melts than in coexisting silicate melts, due to preferential bonding with sulfide ions than with oxygen. In mantle magmas, sulfur is present as $S^{-2}$ ions, which dissolve into silicate magma by forming FeS species (Mungall and Naldrett, 2008). The potential to form deposits is thus strictly related with sulfur geochemistry, degree of partial melting and possibility to trap immiscible sulfide liquid within a magmatic system (Mungall and Naldrett, 2008).

Sulfur solubility in mafic melts formed by mantle melting ranges between 500 and 1000 ppm (Mavrogenes and O'Neill, 1999). Since the upper mantle contains an average of 250 ppm of S, low degrees of melting cannot dissolve all the S present (Keays, 1995). This is the reason why basaltic magmas have low PGE content and are not economically viable sources of these precious metals. On the contrary, at high degrees of partial melting, such as those achieved by Archean komatiites magmas, all the sulfur is dissolved into the silicate melt, and the concentration of PGE is dictated by mineral-melt partitioning; IPGE are slightly compatible with the restitic peridotite, while PPGE go into the silicate melt (Mungall and Naldrett, 2008). Alternatively, if the oxygen fugacity is high enough to convert sulfide to sulfate, the net solubility of sulfur is increased by a factor 10, and any degree of melting may permit a mafic magma to form in the absence of a sulfide phase (Jugo, 2004). These magmas have the potential to form PGE deposits.

To form a deposit, a fertile magma needs to become saturated with sulfide melt in a place within the crust where it can be trapped. Magmas are generated under sulfide-undersaturated conditions, and only later mechanisms provoke sulfide saturation (Mungall and Naldrett, 2008). In particular, as sulphur does not enter into the solid phases forming in a cooling silicate magma, its concentration increases during cooling, until sulfide saturation is reached. When the evolved magma reaches sulfide saturation, droplets of sulfide nucleate and grow, settling in the magma body. The first sulfides to form will contain the most strongly chalcophile elements, in this case the PGE (e.g. Main Sulfide Zone of the Great Dyke, Merensky Reef of the Bushveld) (Mungall, 2002). The second mechanism involves crustal assimilation by the primitive sulfide undersaturated magma. Contamination of mantle-derived magmas by cooler siliceous crustal rocks can provoke sulfide saturation by increasing silica concentration and decreasing the temperature, two factors that lower the sulfur content needed to attain

sulfide saturation (Mungall and Naldrett, 2008; Ripley and Li, 2013). The sulfur geochemistry plays an important role in the attainment of the right conditions to form a PGE-rich deposit. If the magma is barely above sulfide saturation, the amount of PGE partitioning into the sulfide phase is small compared to the total amount of PGE in the system. At the same time, if the amount of sulfide melt is too high, the PGE partition into the sulfide diminishes the concentration of PGE in the silicate magma and hence the concertation in the sulfide phase (Mungall and Naldrett, 2008). At high degrees of sulfide supersaturation correspond high volumes of PGE-poor sulfides, generating PGE-poor Ni-Cu deposits. Campbell and Naldrett (1979) describe this relation with an equation:

$$C_{sul} = C_0 D^{sul/sil} \frac{R+1}{R+D^{sul/sil}}$$

where $C_{sul}$ is the concentration of a PGE in the melt, $C_0$ is the concentration of a PGE in the entire system, R is silicate/sulfide mass ratio and $D^{sul/sil}$ is the partition coefficient.

Once formed, the sulfide droplets settle at the base of the magmatic body, as happens in layered intrusions. At some point, the sulfide melt will reach its liquidus temperature and begin to form crystals of monosulfide solid solution (mss) or magnetite, or both. With proceeding cooling, they will be joined by intermediate solid solution phases, and in the last stages there will be crystallization of pentlandite, millerite, bornite and copper-sulfides (Mungall and Naldrett, 2008). Pt, Pd and gold are not hosted in these phases (with the exception of pentlandite), so that fractionated sulfide melts result highly enriched in these elements compared to the sulfide that initially equilibrated with the magma. The result is that economic PGE mineralization can spawn from non-economic sulfide (e.g. Ni) deposits (case of Sudbury mineralization). In the ultimate stages (200-700 °C), sulfide melts evolve into high mobile liquid solutions composed of PGE, Au, Ag, S, Te, Bi, Sb, As and Cl, producing PGE sulfides, intermetallic compounds and sulfosalts (Mungall and Naldrett, 2008).

PGE deposits are typically classified as follows (Mungall and Naldrett, 2008):

- *Peripheral to or within accumulations of sulfide liquid*: formed by crystallization of a sulfide liquid that has already been concentrated from mafic/ultramafic silicate magma. Rich in Cu, Pt, Pd and Au and poor in Rh, Ru, Ir and Os. Examples: Noril'sk (Siberia), Sudbury (Canada). In this type of deposits, PGE are usually by-products of primary products. In Noril'sk, the revenue is 25% from PGM, 43% from Ni and 27% from Cu (Willis et al., 2012).
- *Layers of very high-PGE-tenor sulfides within a layered intrusion*: stratiform accumulations of sparsely disseminated PGE-rich sulfides, such as the ones in the Merensky Reef (Bushveld). The metals show a vertical zoning, and Pt, Pd and Rh concentrations are higher at the base of the sulfide zone, and decrease upwards (Naldrett and Wilson, 1990). They can be associated

with chromitite horizons (UG-2, UG-1, MG-3, MG-2 chromitites of the Bushveld Complex). The grade of mined ores from the Bushveld complex is typically 4-8 g/t of Pt+Pd.

- *Development of PGE-rich immiscible sulfides prior to or during emplacement into their present location*: gives rise to weak marginal accumulations of sulfides (Finland, Kola Peninsula or Ontario, Canada). From this ore type, as for Noril'sk and Sudbury, PGE are by-products or co-products of primary products.
- *Delayed separation of sulfide during the crystallization of a layered intrusion:* this mechanism generates deposits rich in Cu, Pt, Pd and Au, and poor in Ru, Ir and Os. Examples include Rio Jacaré intrusion of Bahia (Brazil) and Platinova Reef (Skaergaard Intrusion).
- *Chromite crystallization without the development of sulfide immiscibility:* these deposits, found mostly in ophiolite complexes, are enriched in Ru, Ir and Os and poor in Ni, Cu, Pt, Pd and Au. They do not constitute economic deposits, but can give rise to placer deposits (for example in the Urals).
- *Hydrothermal redistribution of PGE*: their genesis, not yet fully understood, is probably the result of Cl-rich aqueous fluids concentrating PGE. Deposition is controlled by changes in pH or redox state. Under certain conditions, NaCl brines can dissolve high concentrations of Pt. Examples of these deposits are New Rambler Mine (Wyoming), Waterberg deposit (Transvaal, South Africa) and Coronation Hill (Australia).
- *Secondary concentration of PGE associated with schlieren chromitites in zoned dunite-pyroxenite intrusions*: these deposits, commonly referred to as "Alaskan-type" usually concentrate Pt. Examples include deposits in the Urals.

After extraction, the ore is concentrated through crushing, milling, froth flotation and/or magnetic separation (European Commission, 2014). Following flotation, the final concentrate is dried and smelted at temperatures >1300°C, to remove silicon, iron and sulphur (Deloitte Sustainability et al., 2017b), resulting in ingots constituted for the 60% by mixed PGE. Base metals are then removed with different techniques depending on the composition. The full details of refinement are not known to the public, but involve several hydrometallurgical steps to further purify PGE from the remaining base metals. Within the EU, PGE refinement takes place in Belgium, Germany, Norway (and UK). Europe based companies are, among others, Anglo American, Glencore Xstrata and Johnson Matthey.

## 1.4 PGM and BMM in ophiolite chromitites

### 1.4.1 Platinum Group Minerals

Although trace amounts of PGE can reside in the structure of some silicate and oxide minerals (olivine, chromite), the dominant hosts for these elements are Platinum Group Minerals (PGM) and, in minor amount, Base Metal Minerals (BMM) (Ahmed, 2007; González-Jiménez et al., 2014a; Stockman and Hlava, 1984). There are more than 100 PGM species, either composed only by PGE or in combination with other elements, such as Fe, Cu, Ni or bonded to ligands such as S, As, Sb or Te (Cabri, 2002).

Within ophiolite chromitites, PGE can reach concentrations up to $10^3$ ppb (Economou-Eliopoulos, 1996; Gervilla et al., 2005; Prichard and Lord, 1988; Zaccarini et al., 2016). Based on their PGE content, chromitites are divided in two groups (González-Jiménez et al., 2014a): Type I chromitites are enriched in Os, Ir and Ru (IPGE). Type II chromitites are enriched in Rh, Pt and Pd (PPGE) relative to IPGE, and PPGM are often found interstitial to chromite grains. Chondrite-normalized PGE patterns in ophiolite chromitites usually show an enrichment in IPGE relative to PPGE.

PGM in chromitites may form single or composite grains (with BMM and/or silicates) dispersed in chromites or, more rarely, within the silicate matrix. They can be found in four microstructural position (González-Jiménez et al., 2014a):

1) Chromite unaltered zones
2) Open fractures
3) Chromite altered rims or edges (ferrian-chromite)
4) Inclusion trails (may correspond to former grain boundaries or healed fractures)

Within Type I chromitites, PGM are preferentially located in unaltered zones, rather than in open fractures or along the edges. The most common minerals are Os-Ir-Ru ones, such as laurite ($RuS_2$)-erlichmanite ($OsS_2$), irarsite (IrAsS), and Os-Ir-Ru alloys. Some Pt-Pd-Rh-rich minerals can be found, such as sperrylite ($PtAs_2$) and Pt-Pd-Rh alloys. PGE-oxides (e.g. Ru-Os-Ir-(Fe) oxides) can be found in altered zones, typically along the rim of laurite or erlichmanite. This association is probably due to destabilization of the primary sulfide to yield secondary PGE alloys or oxides (Auge and Legendre, 1994; Garuti and Zaccarini, 1997; Gonzalez-Jimenez et al., 2011b; González-Jiménez et al., 2011, 2010; Proenza et al., 2007; Stockman and Hlava, 1984; Uysal et al., 2009).

Type II chromitites are enriched in PPGE with respect to IPGE, resulting in abundance of PPGM. The most common minerals are sperrylite, stibiopalladinite ($Pd_5Sb_2$), isoferroplatinum ($Pt_3Fe$) and members of cooperite (PtS)- braggite (PdS) solid solution. Primary euhedral minerals are mainly

located in unaltered chromite crystals, while secondary PGM are located in altered zones, where they are transformed into alloys or oxides (González-Jiménez et al., 2014a).

The dominant PGE in ophiolite are Os, Ir and Ru (Augé, 1985; Legendre and Augé, 1986), however, Pt and Pd enrichments have been detected within sulfide-bearing chromitites from ophiolites (Auge et al., 1999; Prichard et al., 2008a). Typical Pt-Pd minerals found within ophiolite chromitites are isoferruplatinum ($Pt_3Fe$), cooperate (PtS), sperrylite ($PtAs_2$), geversite ($PtSb_2$), hongshiite (PtCu), stibiopalladinite ($Pd_5Sb_2$) and PGE-enriched base metal sulfides (Auge et al., 1998).

*Genetic Models*

In sulfide-saturated rocks, PGM are likely to form either by exsolution from primary base metal sulfides during cooling, or differentiation of magmatic sulfide liquid. Commonly, PGM are found as inclusions within chromites. Their presence as inclusions can be explained either by formation at high temperatures and later entrapment at the time of chromite crystallization, or alternatively as deposition from hydromagmatic fluid or as the result of desulfidation of pre-existing base-metal sulfides (Brenan, 2008).

In ophiolite chromitites, PGM have been, for a long time, interpreted as having crystallized before or at the same time of the chromite and then been incorporated as solid inclusion (Augé, 1985; Augé and Johan, 1988; Gervilla et al., 2005; Prichard et al., 2008a; Tarkian et al., 1991). Here follows a brief description of the genetic theories:

- Exsolution of platinum-group elements from chromite: PGE could have been hosted into the chromite lattice at high temperature and later exsolved during cooling (Naldrett and Cabri, 1976). Later studies (Locmelis et al., 2011; Pagé et al., 2012) ruled out this hypothesis by demonstrating that PGE are not contained in chromite lattice, but form microinclusions.
- Crystallization from melts/fluids and physical trapping by growing chromite: Augé (1985) and Stockman and Hlava (1984) suggested that the euhedral shape of many primary PGM could reflect direct crystallization from melts/fluids, before or at the same time as chromite. Tredoux et al. (1995) suggested the formation of nanoclusters of PGE in suspension within the melt which are stabilized by some ligands (S, As, Sb, Te, Se) until they coalesce to form alloys. Later experiments by Ballhaus et al. (2006), Bockrath et al. (2004) and Matveev and Ballhaus (2002) confirmed that during the crystallization of chromite from a basaltic melt, between 900 and 1400 °C and 0.4-1.5 GPa, Os, Ir and Ru alloys may form, nucleate, and be incorporated into chromite crystals, or react with S in the melt to produce sulfides. Pt and Pd tend to form fewer and larger metallic phases suspended in the silicate matrix. This explains the fractionation of IPGE and PPGE, and the fact that IPGE are more abundant in Type I

chromitites. The abundance of PPGE in Type II chromitites could indicate precipitation from melts that are already depleted in IPGE, and were more likely to be saturated in S or other ligands (González-Jiménez et al., 2014a).

- Crystallization of platinum-group minerals in a dynamic regime: laurite in equilibrium with Os-Ir alloys can precipitate from basaltic melts at 1200-1300 °C at log$fS_2$ of -2 to -3 (Andrews and Brenan, 2002; Bockrath et al., 2004). Moreover, the solubility of Os in laurite increases with decreasing T, and/or increasing $fS_2$. Three magmatic zoning can be commonly found: i) Os-poor laurite cores with Os-rich rims (normal zoning); ii) Os-rich cores and Os-poor rims (reverse zoning); iii) complex intergrowths of laurite/erlichmanite (oscillatory zoning). Normal zoning can be explained with different stages of fractional crystallization during cooling, but to explain reverse and oscillatory zoning a mechanism that creates $fS_2$ gradients is needed. Gervilla et al. (2005) and González-Jiménez et al. (2009) suggested that short term variations of T-$fO_2$-$fS_2$ can occur in an open system. The proposed model is the following (González-Jiménez et al., 2014a, 2010):
  i. A local decrease in $fO_2$ at the chromite grain boundary, caused by the partitioning of $Cr^{3+}$ and $Fe^{3+}$ in chromite, causes saturation of the most oxidized PGE species (Os, Ru, maybe Ir) in the melt/fluid (Ballhaus et al., 2006), and the formation of clusters of metallic PGE and PGM at the grain boundaries of chromite (Ballhaus et al., 2006; Finnigan et al., 2008).
  ii. Once formed, these micrograins remain attached to chromite surface.
  iii. Laurite crystallizes either from the melt or by reaction of already formed Os-Ir-Ru alloys with the melt, due to increase in $fS_2$. Local variations of T-$fO_2$-$fS_2$ would promote laurite crystallization with different Ru/(Ru+Os) ratios, and would explain the coexistence in the same sample of laurite, irarsite, Os, Ir and Ir-sulfides, but also the presence of Ni-sulfides as inclusions in unaltered chromites. If they are PGE-free they were probably not crystallized from an immiscible sulfide melt but were crystallized directly from the melt when $fS_2$ rose above the values necessary to form erlichmanite, (log$fS_2$= -1 - 0.5 at 1100-1200°C; Barin, 1995). The presence of pentlandite inclusions remains dubious, as this sulfide forms by decomposition of a mss crystallising in equilibrium with a sulfide melt above 850°C and in equilibrium with high-temperature heazlewoodite below 850°C (González-Jiménez et al., 2010; Karup-Møller and Makovicky, 1995).

- Assimilation of pre-existing platinum-group minerals from country host rocks: previous models assume that PGE at the beginning are dissolved into the basaltic melt. However some authors argued that at the P-T-$fO_2$-$fS_2$ conditions at which chromitites form in the mantle, the silicate melts have little ability to dissolve PGE (Bockrath et al., 2004; Fonseca et al., 2012). Bockrath et al. (2004) suggest that PGE form and then are transported as immiscible sulfide droplets. These droplets remain trapped in the silicate melt until P decreases and they dissolve into the melt. Fonseca et al. (2012) added that during extractions of melt, the concentration of S and FeO might promote desulfurization and formation of PGM (in particular Os-Ir alloys). Small events of melt extraction in series could produce a decreasing $fS_2$, promoting the breakdown of PGE-bearing sulfides into residual laurites and Os-Ir alloys.
- Mantle veining: crack propagations in the mantle lead to pathways for the transport of metasomatic fluids and melts over significant distances. This model could explain the arrays of PGM along healed fractures.
- Subsolidus recrystallization: Gervilla et al. (2012) suggested that between 550 and 700 °C, infiltration of water in chromitites may promote reactions and lead to formation of chlorite and ferrian-chromite, with a loss of about 43% of the chromite mass, compensated by formation of a spongy texture. These pores network allows the easy circulation of fluids, favoring the reaction of PGM with hydrothermal fluids. As the formation of ferrian-chromite occurs under reducing conditions (Gervilla et al., 2012), it is expected that magmatic sulfides would be destabilized via desulfurization, consistent with S-deficiency shown by many laurites found in altered parts of chromites. However, in some sites it was found that laurite overgrows secondary Ru-Ir-Os alloys or irarsite, suggesting that laurite can also crystallize at lower temperatures. Ru-Os-Ir metal nuggets may have formed after desulfurization of laurite-erlichmanite, and later reacted with S-bearing fluids to produce secondary laurite. It could also happen that a big enough increase in T could re-homogenize the newly formed PGM, eliminating any record of its previous history and making it indistinguishable from primary PGM.

*Alteration of PGM and PGE re-mobilization*

PGM are commonly altered during post-genetic processes, and their PGE content can be remobilized at different scales. PGM alteration commonly starts with corrosion along the grain boundaries, with possible reprecipitation of some components as alloys or oxides. Secondary grains may coexist with secondary silicates (e.g., chlorite) within pores in chromites. PGM found in the silicate matrix, exhibit subhedral morphologies and are often located close to altered chromite grains (González-Jiménez et

al., 2010). A common alteration feature is the presence of PGE alloys. While Os-Ir alloys are sometimes ascribed to a magmatic environment (Brenan and Andrews, 2001), they can also be the product of alteration of primary laurites due to pervasive percolation of low $fS_2$ fluids, during metamorphic events (Garuti and Zaccarini, 1997; González-Jiménez et al., 2014a; Prichard et al., 2008a; Proenza et al., 2007; Zaccarini et al., 2005). The presence of native Ru is also attributed to alteration stages, as primary Ru has never been reported (Garuti and Zaccarini, 1997; Proenza et al., 2007).

This is due to an inversion of the $fS_2$ magmatic trend, leading to formation of native PGE rather than sulfides (Kieser, 1994; McElduff and Stumpfl, 1990; Nilsson, 1990; Prichard et al., 1994; Prichard and Tarkian, 1988). The general desulfurization trend involves initial loss of S, sometimes counterbalanced by an uptake of Ni, Fe or Cu, followed by complete replacement of the primary PGM by a new alloy or sulfide. Prichard et al. (1994) suggest that Pt- and Pd-bearing alloys in chromitites from Shetland ophiolite derived by alteration of magmatic PGM during serpentinization with a mobility of PGE of just few microns. Garuti and Zaccarini (1997) argued that a secondary awaruite-PGE alloy assemblage in Vourinos chromitite was due to desulfurization of the primary BMM-PGM assemblage during serpentinization. González-Jiménez et al. (2010) ascribe the formation of a secondary BMM-PGM assemblage along fractures and cracks of chromite grains in the Dobromirtsi chromitites to the percolation of altering fluids, with a combination of reducing and oxidizing events, related to regional metamorphism. Auge and Legendre (1994) studied PGE enrichment in chromitites and laterites in New Caledonia. In the mineralization and in the alluvium the following PGM are present: Pt-Fe oxides, Ir-Fe-Pt-Rh oxides and Ru-Mn-Fe oxide-hydroxide. They were formed through oxidation of Pt-Fe precursors (alloy or sulfide), due to the circulation of low-temperature oxidizing fluids.

During PGM alteration, PGE are remobilized to some extent. Zaccarini et al. (2005) suggested that alteration of laurites produces a release of Ir and Os and formation of native Ru. Moreover, the presence of native Os in altered chromite, but not in the silicate matrix, suggests that some Os can be lost during alteration (González-Jiménez et al., 2010; Zaccarini et al., 2005). Rh, Pt and Pd, which are usually present in low amounts in ophiolite chromitites, have nonetheless been detected within sulfarsenides and other alteration phases, proving they were remobilized during post magmatic processes (González-Jiménez et al., 2010). Ru-rich pentlandite has been detected in several ophiolite complexes (Dobromirtsi, Shetland, Vourinos among others), suggesting that this mineral is formed during alteration of chromitites, by the partial desulfurization of laurites.

### 1.4.2 Base Metal Minerals

Base metals are common and inexpensive metals, distinguished from precious metals for their tendency to oxidize and be easily corroded. The most abundant base metals are Fe, Ni, Pb, Zn and Cu. Small amounts of base metals (e.g., Ni, Fe, Cu) can be found in ophiolite chromitites, contained in base metal minerals (mainly sulfides).

The formation of base metal sulfides is related to the immiscibility of sulfide melts in silicate ones. The crystallization of sulfides at magmatic conditions in ophiolite complexes is controlled by $fS_2$ and temperature (Andrews and Brenan, 2002; Bockrath et al., 2004; Brenan and Andrews, 2001). As the sulfide component within the mantle has a low-melting character (Kullerud, 1969; Naldrett, 1973), restitic harzburgites are usually very poor in sulfur, impeding the formation of large sulfide masses (Prichard et al., 2008a).

Primitive sulfides in ophiolite chromitites are mainly Ni-rich pentlandite, coexisting with pyrrhotite and chalcopyrite (Lorand, 1987). Experiments by Kullerud (1969) indicate that at temperatures between 610 and 860 °C a monosulfide solid solution coexists with a $Ni_{3\pm x}S_2$ phase, along with a low amount of copper sulfide solid solution. During cooling, at about 610 °C, reactions between mss and $Ni_{3\pm x}S_2$ produce pentlandite and Ni-poor mss. Primary and secondary base metal minerals are often located in the silicate gangue of chromitites, and only rare primary BMM can be found in unaltered chromite grains (González-Jiménez et al., 2010; Zhu et al., 2016).

*Alteration of BMM and BM remobilization*

During post-magmatic processes, primary sulfides are often altered by circulating fluids, forming secondary Fe-Ni-Cu assemblages dependent on the fluid chemistry and conditions. Eckstrand (1975) and Frost (1985) and Frost and Beard (2007) argue that the presence of native metals and alloys in serpentinites (e.g. awaruite) is indicative of extremely low oxygen fugacity (eight orders of magnitude below PPM -pyrite-pyrrhotite-magnetite buffer- at 300 °C), coupled with low sulfur fugacity (10 orders of magnitude below PPM) (Chamberlain, 1966; Frost, 1985; Frost and Beard, 2007; Kanehira et al., 1975; Klein et al., 2009). Primary sulfides in peridotites (pentlandite, pyrrothite, bornite and sometimes chalcopyrite) are partially replaced by secondary phases during serpentinization. Typical assemblages that can be found in partially serpentinized peridotites are pentlandite, awaruite and magnetite or pentlandite, heazlewoodite and magnetite (Klein et al., 2009). Desulfurization of pentlandite to form awaruite and magnetite is indicative of low oxygen and sulfur fugacities in the system. Breakdown of pentlandite into heazlewoodite and magnetite, on the other hand, is indicative of higher oxygen fugacities than the ones needed for the breakdown into awaruite and magnetite (Klein et al., 2009). The breakdown of pentlandite usually begins at temperatures below 550 °C (Kullerud,

1963). Heazlewoodite can co-occur also with millerite and godlevskite. Godlevskite is thought to replace heazlewoodite during later stages of serpentinization, while millerite grows at the expense of both heazlewoodite and godlevskite (Klein et al., 2009).

While Ni-Fe sulfides and alloys form during magmatic stages or during serpentinization by replacement of other phases, Ni-Fe arsenides, sulfarsenides and antimonides, on the contrary, crystallize during alteration of chromite, with As and Sb supplied by circulating hydrothermal fluids during metamorphism, and Ni released from olivine and primary sulfides (González-Jiménez et al., 2010; Malitch et al., 2003a; Proenza et al., 2008). Ni arsenides and antimonides have been reported in association with Ni-Fe sulfides within chromitites (Nixon et al., 1990; Oen et al., 1980; Tredoux et al., 2016; Zaccarini et al., 2006). The most common antimonides are nisbite and breithauptite, but in some localities other unknown antimonides have been detected (Tredoux et al., 2016). Antimonides are usually closely associated to arsenides, sometimes forming solid solutions, with As and Sb partially replacing one another (Tredoux et al., 2016). Typical accessory arsenides within chromitites are maucherite, orcelite and nickeline. The assemblage of maucherite, orcelite and heazlewoodite is stable at 450 °C (Kullerud and Yund, 1962), while heazlewoodite at lower temperatures is replaced by millerite, and maucherite by orcelite. Phase relations in the Ni-As-S system indicate that maucherite-$Ni_{3\pm x}S_2$ is stable above 556 °C, while at lower temperatures (below 450 °C), maucherite is stable with heazlewoodite (Kullerud and Yund, 1962). Reactions with serpentinizing fluids lead to partial replacement of maucherite by orcelite, and of heazlewoodite and pentlandite by millerite, as observed by Oen et al. (1980). Maucherite and millerite may also form through hydrothermal modification of ultramafic rocks, by replacement of Ni-Cu sulfides or by precipitation in metasomatic conditions. Antimonides stability fields reported by Okamoto (2009) on synthetic compounds reveal that antimonides are stable over a wide range of temperatures, up to 1100 °C. However, natural antimonides occurring within chromitites appear to be stable below 600 °C.

# CHAPTER 2: Geological setting of the investigated complexes

## 2.1 Finero

The Ivrea-Verbano Zone (Fig. 2.1) is a geodynamic domain of the Southern Alps (Northern Italy) that represents a complete cross-section through deep continental crust (Mehnert, 1975) and is characterized by the presence of lower crustal rocks (Sinigoi et al., 1994). It consists of amphibolite-to-granulite facies paragneiss (Kinzigitic Formation) intruded by huge volumes of mafic to intermediate plutonic rocks (Mafic Complex). The Mafic Complex, probably deformed in an extensional environment, is an arcuate structure with an axis roughly corresponding to the Sesia Valley (Quick et al., 1994). At its base, three peridotite bodies outcrop along the Canavese line that separates the Ivrea-Verbano Zone from the Alpine domains. They are, from South to North, Baldissero, Balmuccia and Finero. These mantle tectonites are considered to be obducted fragments of subcontinental mantle, showing variable degrees of metasomatism as well as different degrees of partial melting (Hartmann and Wedepohl, 1993).

The Finero ultramafic body is the largest of the three massifs exposed in the Ivrea-Verbano Zone. It forms an antiformal structure consisting of concentric units (Fig. 2.2), that comprise from rim to core, four main units: External Gabbro, Amphibole Peridotite, Layered Internal Zone and Phlogopite-Peridotite (Coltorti and Siena, 1984). The External Gabbro consists of garnet–amphibole bearing gabbros with rare pyroxenitic and anorthositic layers. The Amphibole Peridotite comprises dunites, wherlites and lherzolites enriched in pargasitic amphibole. The Layered Internal Zone consists of cm-thick lithologic layers of amphibole–peridotite, amphibole–websterite, garnet–amphibole gabbros and anorthosite. The Phlogopite–Peridotite unit, mainly harzburgite, shows some peculiar features that differentiate it from the other peridotite bodies of the area. The first one is the presence of chromitite-bearing metasomatic dunites within harzburgites, cut by clinopyroxenite dykes. The second one is a pervasive re-fertilization of the primary mantle assemblage witnessed by phlogopite and pargasitic-to-edenitic amphibole (Coltorti and Siena, 1984; Exley et al., 1982; Garuti et al., 2001; Grieco et al., 2001; Zanetti et al., 1999).

Within the Finero Phlogopite Peridotite, stratiform and podiform chromitite bodies occur in contact with dunites, usually in the marginal zone of the unit (Garuti et al., 1995; Grieco et al., 2004, 2001). Chromitites form irregular pods, schlieren, lenses and discontinuous layers up to 100m long and 0.5m thick (Grieco et al., 2001). Most chromitites contain olivine and/or clinopyroxene and amphiboles as minor phases, and locally Fe-Ni-Cu sulfides as accessory phases. Chromite crystals are typically coarse and show high-Mg and high-Cr. They also sometimes display peculiar zonings in contact with

olivine crystals, with a $Cr_2O_3$ depletion up to 7% close to the grain boundary (Grieco et al., 2001). The origin of chromitites and associated dunites is attributed to a pervasive metasomatism that affected the Finero Phlogopite Peridotite (Grieco et al., 2001; Zaccarini et al., 2004b).

The Finero Peridotite Massif underwent at least two metasomatic events that resulted in the development of amphibole, phlogopite, apatite and dolomite. Geochemical studies argue for a crustal origin of the metasomatic agent of the first event, which derived from a subducting slab (Hartmann and Wedepohl, 1993). Zanetti et al. (1999) suggest a formation model where a subducting plate produces $H_2O$-undersaturated, silica-rich melts that infiltrate the harzburgites and react with pyroxenes to form chromitite pods and associated dunites, as well as secondary clinopyroxene and amphibole in the harzburgite (Grieco et al., 2001). Zanetti et al. (2016), on the basis of field relationship, major and trace element compositions of spinels and associated minerals, suggest that chromitite layers were segregated from hybrid melts derived from the mantle, contaminated by a continental crustal component. The ages inferred for the first metasomatic event by some Authors are 208 ± 2 my (Grieco et al., 2001) and ~290 Ma or earlier (Zanetti et al., 2016). Another interpretation of the provenance of metasomatic fluids is that the Phlogopite-Peridotite of Finero may represent variously depleted and re-enriched parts of a mantle plume emplaced at the base of the subcontinental crust due to extension and thinning of the lithosphere (Garuti et al., 2001; Zaccarini et al., 2004b). Chromitites would then be the result of the interaction of uprising alkaline-carbonatitic fluids with the host peridotite (Zaccarini et al., 2004b).

The second metasomatic event is related to a later intrusion of clinopyroxenitic dykes, when water-rich fluids penetrated the harzburgites along cracks and fractures at a relatively shallow crustal level, forming phlogopite (Grieco et al., 2001).

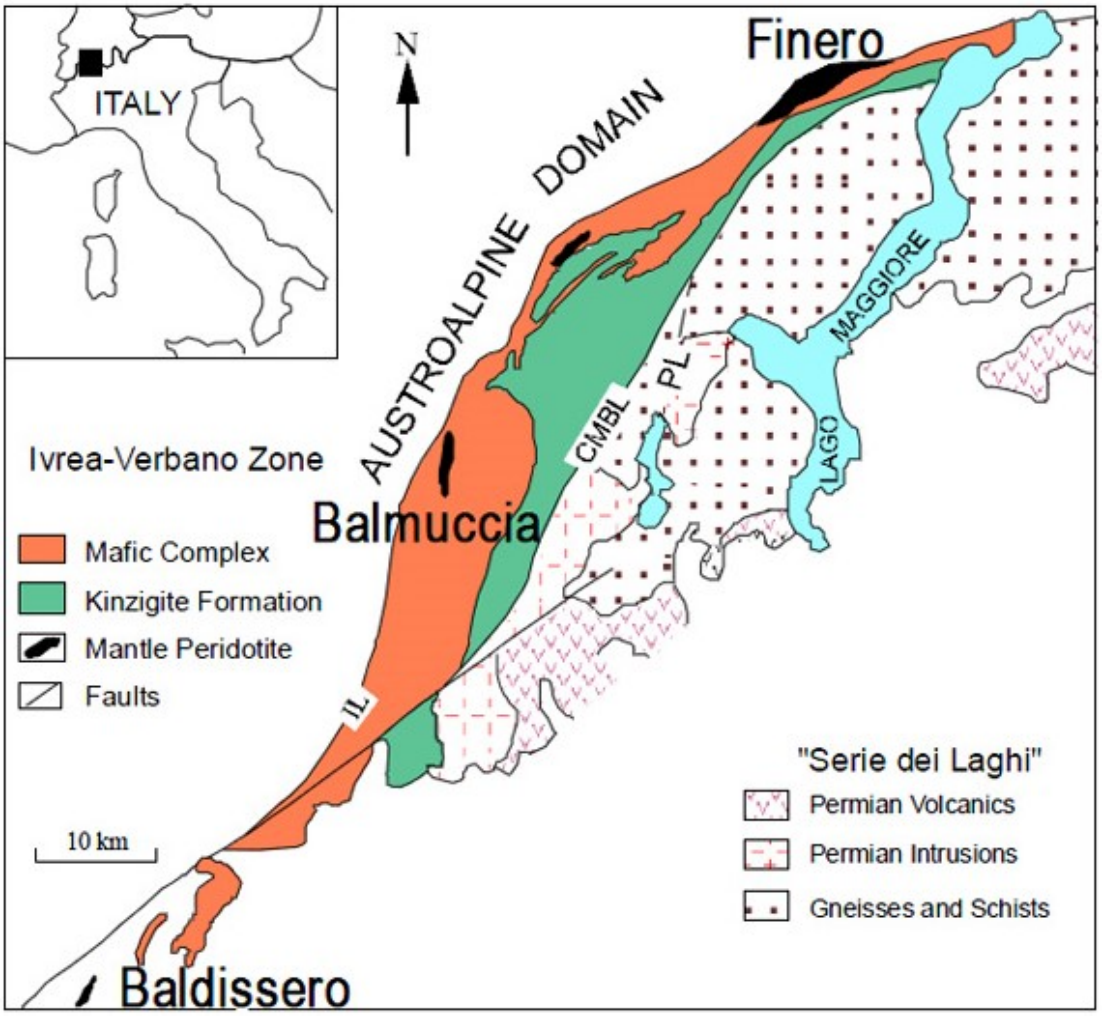


Fig. 2.1 Geological sketch map of the Ivrea Verbano Zone (from Zanetti et al., 1999).

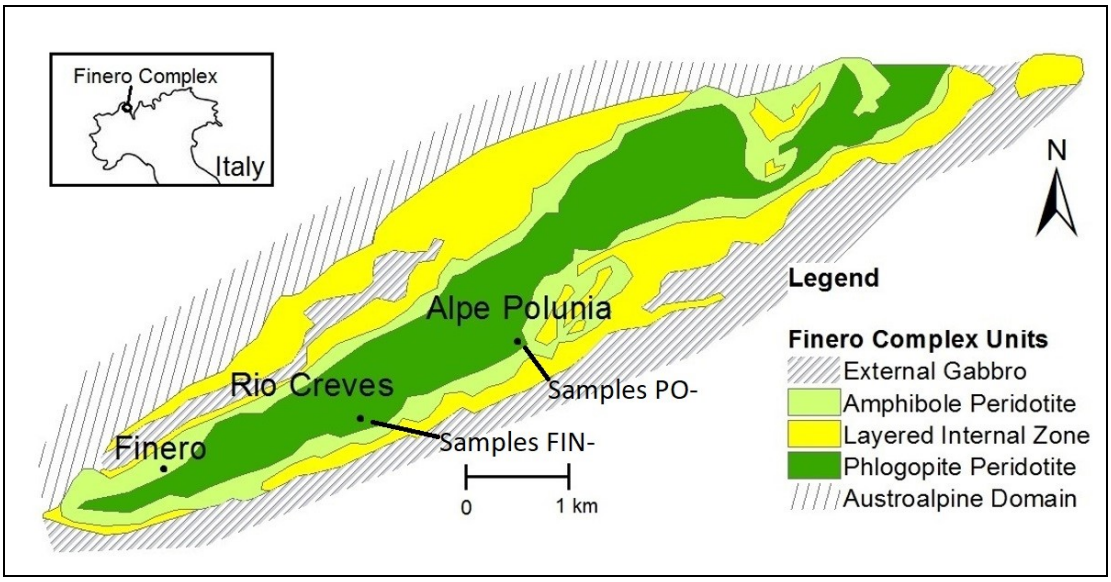


Fig. 2.2 Simplified geological map of the Finero Complex, Ivrea-Verbano Zone, Northern Italy (from Bussolesi et al., 2019).

## 2.2 Gomati and Nea Roda

Gomati and Nea Roda are two ophiolite bodies geographically located in the Chalkidiki Peninsula, Northern Greece, ~80 km SE of the city of Thessaloniki. Small chromite deposits exploited in the past can be found in different localities in the complexes. Christodoulou (1980) reports the peak of the exploitation activity of these bodies during World War II, by German occupants.

The Chalkidiki Peninsula is a geologically complex region, which comprises several geotectonic zones belonging to the Hellenides belt, tectonically emplaced during a Mesozoic to Cenozoic evolution of subduction and collision. The Hellenides are part of the Alpine-Himalayan orogenic belt, and were formed by the collision of Africa and Europe in the late Cretaceous. They are separated into two tectonic groups: the External Hellenides and the Internal Hellenides. The Internal Hellenides are further divided in tectonic zones. The main ones are, from west to east: Pelagonian Zone (PZ), Vardar Zone, Serbo-Macedonian Massif (SMM) and Rhodope Massif (RM), all roughly oriented NNW-SSE (Fig. 2.3) (Anders et al., 2006 and references therein). Gomati and Nea Roda ophiolites are comprised into the SMM, which is divided from the Pelagonian Zone to the west by a suture zone, the Vardar Zone, hosting several Jurassic ophiolite bodies. To the east, the SMM borders the Rhodope Massif.

*Pelagonian Zone*

The Pelagonian Zone is formed by a an assemblage of tectonic units mainly consisting of a Paleozoic metamorphic basement (Mountrakis, 1986; Papanikolaou, 1997). It consists of a Neoproterozoic (713-699 Ma) and Variscan (320–280 Ma) crystalline basement (Anders et al., 2007, 2006) superimposed by Late Jurassic ophiolites and Upper Paleozoic and Mesozoic sedimentary sequences.

*Vardar Zone*

Between the Pelagonian Zone and the Serbo-Macedonian Massif lies the Vardar Suture Zone, which includes numerous ophiolitic bodies, and is regarded as a main Tethyan suture (Bortolotti et al., 2005; Saccani et al., 2008). The Vardar Zone is divided into three units: Peonias, Paikon and Almopias subzones (Mercier, 1966). The Almopias subzone is interpreted as the relic of a former ocean basin (referred to in the literature either as Almopias, Vardar, Maliac, Axios or Eastern Neotethys) subducted eastwards under the Serbo-Macedonian Massif in the Mid to Late Jurassic. During Late Jurassic, ophiolites from the Almopias ocean obducted westward onto the Pelagonian Zone (Mercier et al., 1975). A small ocean basin, however, still existed through the Cretaceous, and finally closed during the Tertiary, when the ophiolites were thrusted onto the Paikon subzone (Sharp and Robertson, 1994). The Late Jurassic-Early Cretaceous ophiolite emplacement onto the Pelagonian zone affected the Vardar zone units and was followed by the terminal closure of the Vardar Ocean and the

subsequent oblique continental collision in the early Tertiary (Koukouvelas and Aydin, 2002; Tranos et al., 1999).

*Serbo-Macedonian Massif and Rhodope Massif*

The Serbo-Macedonian Massif (SMM) and the Rhodope Massif (RM), extending through Serbia, North Macedonia, Greece and Bulgaria, consist of amphibolite-facies metamorphic rocks forming the basement of the Alpine orogenic belt (Bonev et al., 2018, 2013; Bonev and Dilek, 2010; Dixon and Dimitriadis, 1984; Himmerikus et al., 2009; Ricou et al., 1998). A later Cenozoic extension is recorded by Late Cretaceous to Miocene granitoid intrusions outcropping in both massifs (Bonev et al., 2012; Ricou et al., 1998). Mafic-ultramafic bodies are present in nearly all the crystalline basement of SMM and RM, overlying Middle to Late Paleozoic-Triassic platform carbonate rocks (Papanikolaou, 2013). Mafic rocks are locally associated to lherzolite-clinopyroxenite cumulates (Bazylev et al., 2013). The comparable tectono-metamorphic fabrics of SMM and RM indicate a similar evolution at least since later Cretaceous, however the igneous history of both complexes is still poorly constrained. Two models have been proposed, considering them either as Tethyan ophiolitic allochthonous sheets, remnant of the Permian Paleothetys suture (Şengör et al., 1984), or as Mesozoic rift-related igneous complexes (Bonev et al., 2012; Dixon and Dimitriadis, 1984; Himmerikus et al., 2009; Robertson et al., 1996).

In Northern Greece, the SMM is divided into a lower unit, the Kerdyllion Unit, and an upper one, the Vertiskos Unit, separated by a SW-dipping thrust (Fig. 2.4) (Kockel, 1977; Kockel et al., 1971). The Kerdyllion unit, cropping out in the eastern part, is composed of migmatized gneiss and schist intruded by Triassic to Cenozoic granitoid rocks (Himmerikus et al., 2009). The Vertiskos unit, cropping out in the central part of the SMM, consists of an alternation of gneiss and schist hosting mafic-ultramafic bodies known as the Therma-Volvi-Gomati (TGV) complex (Dixon and Dimitriadis, 1984; Kockel, 1977). Rb–Sr ages in the range 280–300 Ma (Borsi et al., 1965) of the Vertiskos series were used to infer a Variscan or older age for the Serbo-Macedonian Massif. U–Pb zircon dating of the Vertiskos series gneisses has shown the presence of heterogeneous Neoproterozoic and Silurian (428–433 Ma) igneous basement units, which were intruded by Middle-Late Triassic A-type Arnea granites.

The Vertiskos Unit is overlain by a Permian-Early Triassic clastic and volcanic succession, that may represent the sedimentary cover related to the Triassic rifting (Dimitriadis and Asvesta, 1993; Ferrière and Stais, 1995).


Fig. 2.3 Major structural elements of the Aegean Sea region. The red circles represent the area of study (Gomati, Nea Roda and Skyros); modified after Zachariadis (2007) and Cornelius (2008).

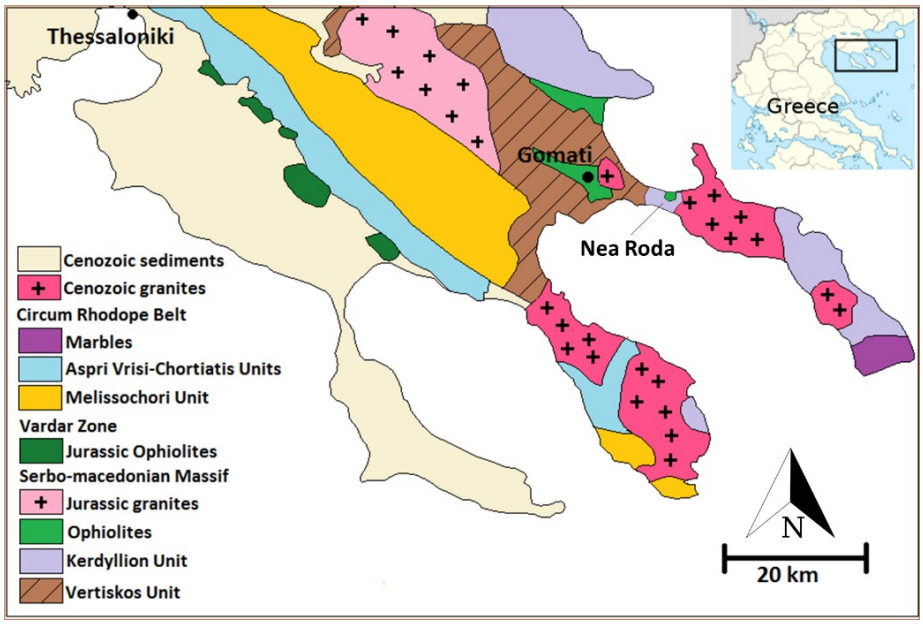


Fig. 2.4 Simplified geological map of the Chalkidiki peninsula of Greece (modified from Bussolesi et al., 2020).

The TVG tectonic evolution involves an extensional tectonic setting in the Middle to Late Permian induced by the breakup of the continental crust of Neoproterozoic and Paleozoic PZ, SMM and RM (Bonev et al., 2018). In the Middle to Late Triassic the Maliac ocean begun to spread, continuing until Middle Jurassic, leading to widening of the Neotethys (Ferriere et al., 2016). At this point, the TGV and associated A-type metagranitoids intruded the thinned rift, filling the SMM part of the rift system, accompanied by volcanic rocks (Asvesta and Dimitriadis, 2010). Based on geochemical features, the TGV complex has MORB and IAT supra-subduction affinities (Bonev et al., 2018). The enriched petrographic signature of the metamorphic rocks is interpreted as the result of upwelling of fertile magma, coinciding with a Late Triassic rifting phase. The subduction-related component, on the other hand, was probably inherited by the Paleotethys subduction, which produced arc-related magmatism (Bonev and Dilek, 2010). The Thermo-Volvi-Gomati proto-ophiolitic complex has been interpreted as the result of intra-continental rifting within the Serbo-Macedonian and Rhodope continental margin. It thus represents a precursor of the Neotethyan crust formation along the Eurasian plate boundary following Paleotethys closure (Bonev and Dilek, 2010).

Thermi, the northernmost body of the complex, consists of metabasalts, rare peridotite and metagabbro. The Volvi body occupies the central part of the Vertiskos unit and consists of metagabbroes and metabasaltic dykes. The Gomati ophiolite consists of serpentinized peridotites with scattered chromitite occurrences presenting massive, schlieren and disseminated textures. Several ophiolite outcrops have been found into the Vertiskos unit, close to the Gomati village (Fig. 2.5 A), in Paivouni, Tripes, Moutsares and Limonadika (Christodoulou, 1980; Economou, 1984), and close to the Nea Roda village. The bodies are generally concordant to the foliation of the Vertiskos unit hosting them (Fig. 2.5 B), and form small pods, less than 10m thick. Chromitites and related rocks are heavily altered and show intense chloritization and ferritchromitization. Preserved primary silicates consist mainly of olivines and clinopyroxenes. The Nea Roda ultramafic body contains magnesite bodies of hydrothermal origin developing parallel to the peridotite layering (Bonev et al., 2018; Michailidis et al., 1995), and is rimmed to the east by an amphibolite body. Michailidis et al. (1995) reported a high-Fe composition of the preserved olivines, and high Cr# of chromite, compatible with advanced degrees of partial melting (passive margin or subduction zone). Nea Roda chromitites have some compositional affinity to the chromite bodies found in western Chalkidiki, while Gomati chromitites are very different (e.g., lower Cr content). Michailidis et al. (1995) propose different times of emplacement for the two bodies, with a younger age of emplacement for Nea Roda (post-Triassic). An additional mafic-ultramafic body crops out to the North of Gomati, close to the Stratoni village. The southern part of the Stratoni body consists of massive to banded amphibolites, which are underlain by

peridotite to the north (Bonev et al., 2018; Siron et al., 2018). The amphibolite preserves the texture of its gabbroic protolith, which could be similar to the Volvi fine grained metagabbro. The underlying peridotite and mostly pyroxenite, on the contrary, preserve primary features, documenting a low degree of metamorphism (Bonev et al., 2018). U-Pb zircon geochronology on Volvi bodies indicate a crystallization age during Middle Triassic. In contrast, the Stratoni dating has Ordovician, Silurian, Devonian and Carboniferous zircons, attributed to the Vertiskos crystalline basement of pre-Mesozoic age.

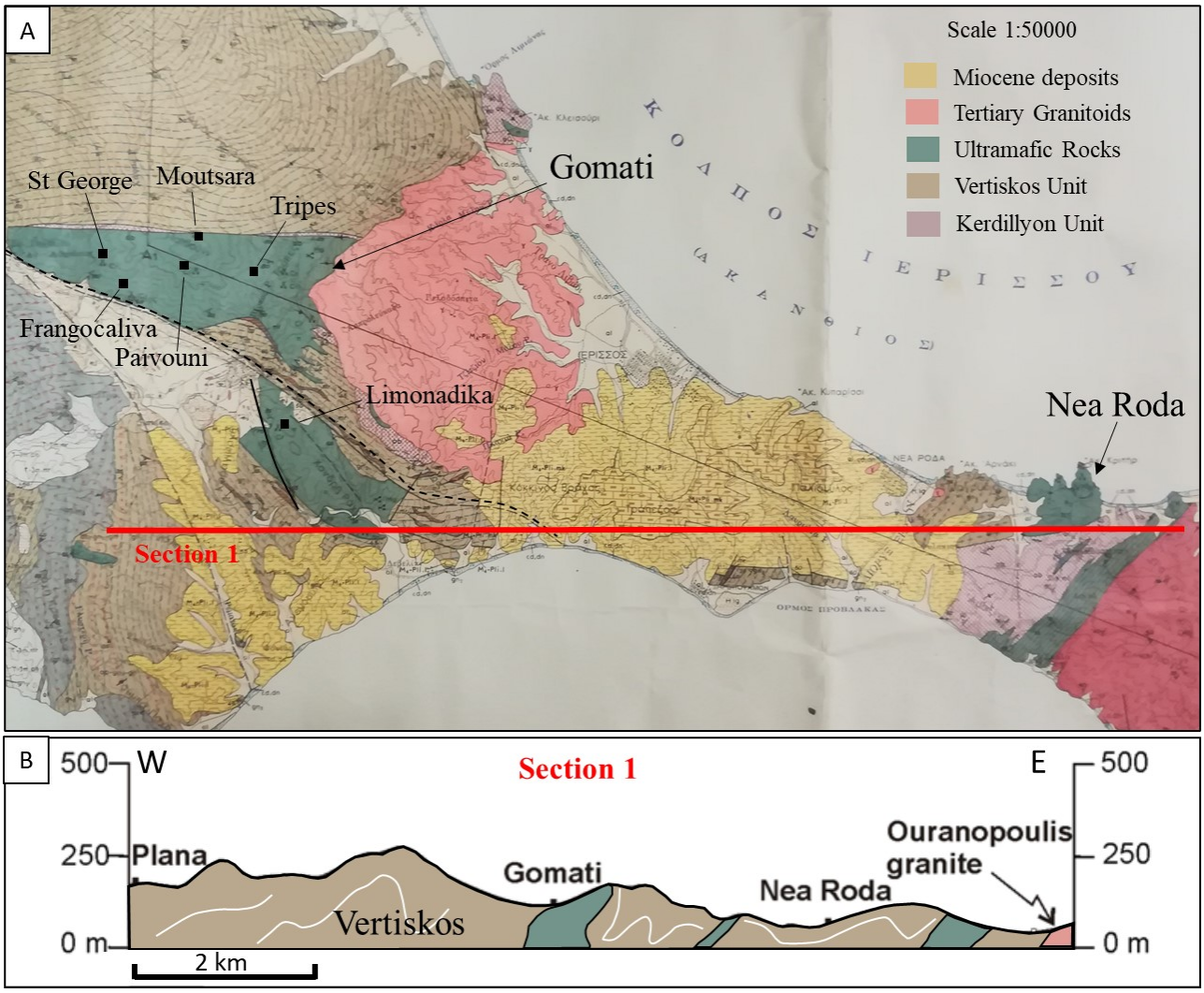


Fig. 2.5 A) Part of the 1:50000 scale geological map of the Ierissos sheet, with location of old chromitite mines (Christodoulou, 1980; IGME, 1978); B) geologic section through Gomati and Nea Roda body (modified after Bonev et al., 2018).

## 2.3 Skyros

Skyros island is the largest (209 square km) and easternmost of the northern Sporades, a group of Greek islands in the Aegean Sea. It is geologically located in the Internal Hellenides (see paragraph 2.1.2), and is comprised in the tectonic terrane of the Pelagonian Zone, (Fig. 2.3), bordered to the west by the External Hellenides and to the east by the Vardar suture zone.

The Pelagonian Zone is regarded either as a microcontinent between the Vardar (E) and Pindos (W) oceans (Nirta et al., 2015), or as the eastern continental margin of the Adria Plate separated from the European plate by a single oceanic basin (i.e., the Vardar Ocean). The Pelagonian Zone of Greece is a Permo-Carboniferous continental margin (Vavassis et al., 2000; Yarwood and Aftalion, 1976) covered with Mesozoic carbonates deposited on a Neoproterozoic and older continental basement that was separated from southern Eurasia during the breakoff of Pangea (Anders et al., 2007) and subsequently reunited to Eurasia during the Alpine accretion (Ricou et al., 1998). Several phases of deformation, intrusion, sedimentation and obduction related to continent-ocean and later continent-continent convergence are recorded, and can be summarized as follows:

1. Late Paleozoic – Early Triassic: the breakup of Pangea triggers a rifting phase, with consequent formation of the Pelagonian passive margin, consisting of Variscan crystalline basement formed by schists, orthogneisses, paragneiss, amphibolites and granites of the upper Carboniferous (De Bono et al., 2001). Between Permian and Early Triassic, the Pelagonian basement is intruded by Permo-Triassic granitoids, and a sedimentation phase settles on top of the Variscan basement (Anders et al., 2007; Schenker et al., 2014).
2. Middle Triassic – Lower Jurassic: deposition of shallow-water limestone and intra-platform and marginal carbonate sequences (Papanikolaou, 1997).
3. Late Jurassic – Early Cretaceous: south-westward obduction of ophiolitic segments, carbonates, metavolcanites and Triassic–Jurassic marbles of the Vardar passive margin (a branch of Neotethys) onto Pelagonia. At the same time, sheets of the Pindos paleo basin, including flysch and ophiolitic fragments, are obducted north-eastward.
4. Late Cretaceous – Paleogene: the obduction phase is followed by the subduction of Pelagonia under the micro-continent Rhodopia and by a collision phase associated with exhumation and deformation stages (orogenesis) (Faupl and Wagreich, 2000).
5. Upper Paleocene – Upper Eocene: a second orogenic stage (Mesohellenic phase) definitely closes the Paleo-Tethys ocean.

The ophiolite complexes of the Pelagonian Zone are regarded either as part of the Vardar ocean (where the Pelagonian Zone constitutes the easternmost rim of the Adria continental margin) (Jacobshagen

and Matarangas, 1972; Kilias et al., 2010; Schmid et al., 2008), or as slices of two different oceans (Pindos and Vardar) (Beccaluva et al., 1994; Hynes et al., 1972; Rassios and Dilek, 2009; Robertson, 2012; Robertson et al., 1996).

The geology of Skyros is quite complex. The three main geologic units of the area are: Pelagonian Zone, Eohellenic Nappe and Skyros Unit (Karkalis et al., 2017) (Fig. 2.6). The Skyros ophiolite is comprised mainly into the Eohellenic nappe ophiolitic mélange, and is constituted by highly deformed serpentinite and massive gabbroic rocks (Fig. 2.7). Ophiolites are mostly located in the central and eastern parts of the island and to a lesser extent in the western part. The Eohellenic Nappe was emplaced during Late Jurassic to Early Cretaceous, and tectonically overthrusts the Pelagonian zone rocks (Harder et al., 1983; Katsikatsos, 1992; Pe-Piper et al., 2004). The ultramafic bodies consist of serpentinized dunites and harzburgites with small, non-economic chromitite bodies, generally less than 10m thick, sometimes cut by rodingite dykes and massive gabbros and diabases (Karkalis et al., 2017). The whole rock assemblage is intensely mylonitized and altered. Serpentinized harzburgites constitute the main lithology. They contain orthopyroxene and olivine relicts, altered Cr-spinel and secondary magnetite, and they are crosscut by magnesite veinlets. Associated gabbros, cut by secondary quartz veins, are medium-grained, formed by plagioclase and two generations of hornblende amphiboles (primary and metamorphic) (Koutsovitis, 2012). Accessory minerals include epidote, zoisite, Fe-Ti oxides and hematite. The basaltic lava is highly altered, and is formed mainly by clinopyroxene relicts, secondary albite, chlorite epidote, titanite and pumpellyte (Karkalis et al., 2017). A carbonation event is testified by the presence of rodingite dykes, rich in hydrogarnets, vesuvianite, chlorite, diopside and clinopyroxene. The high levels of serpentinization and rodingitization reflect alteration processes that affected the Skyros ultramafic massif during exhumation, due to circulation of hydrothermal fluids, possibly generated during subduction. Based on geochemical data, Karkalis et al. (2017) suggest alteration and deformation of the massifs due to subduction-related processes. Trace elements patterns show island arc affinity. Spinel chemistry in serpentinites have affinity to back-arc basin ones (Karkalis et al., 2017). Chromitites from the Agios Alexandria locality are enriched in PGE up to 3 ppm (Agiorgitis and Wolf, 1978; Economou et al., 1986), and in the Achladones locality show an enrichment up to 1 ppm (Tarkian et al., 1992). Main PGM-BMM assemblage consist of Ni-Fe sulfides and Os-rich laurite.

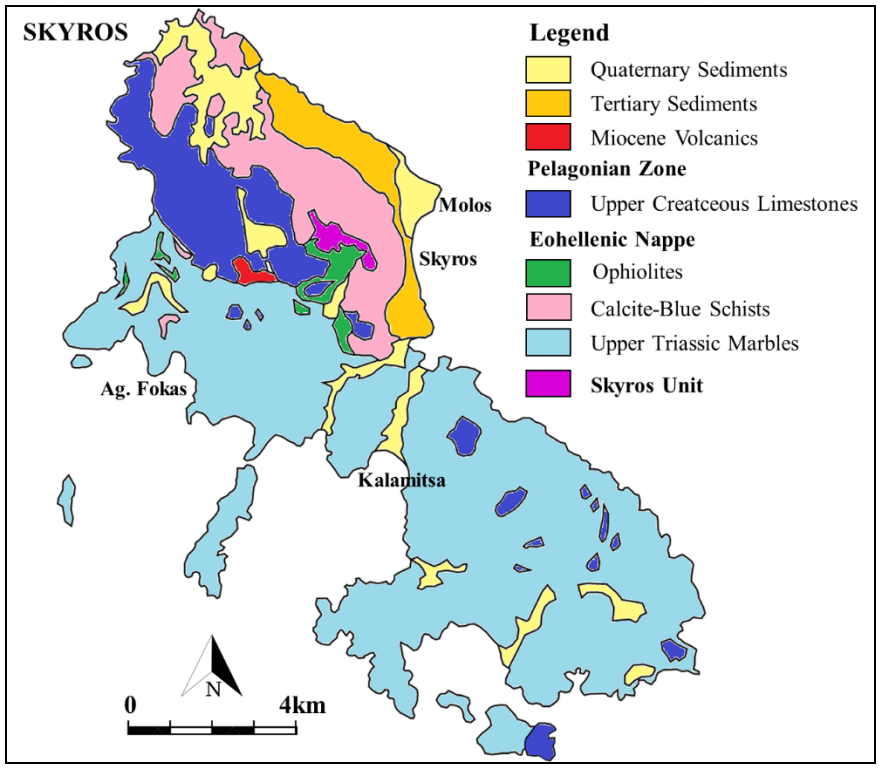


Fig. 2.6 Schematic geological map of the Skyros Island (modified after Papantoniou, 2015)

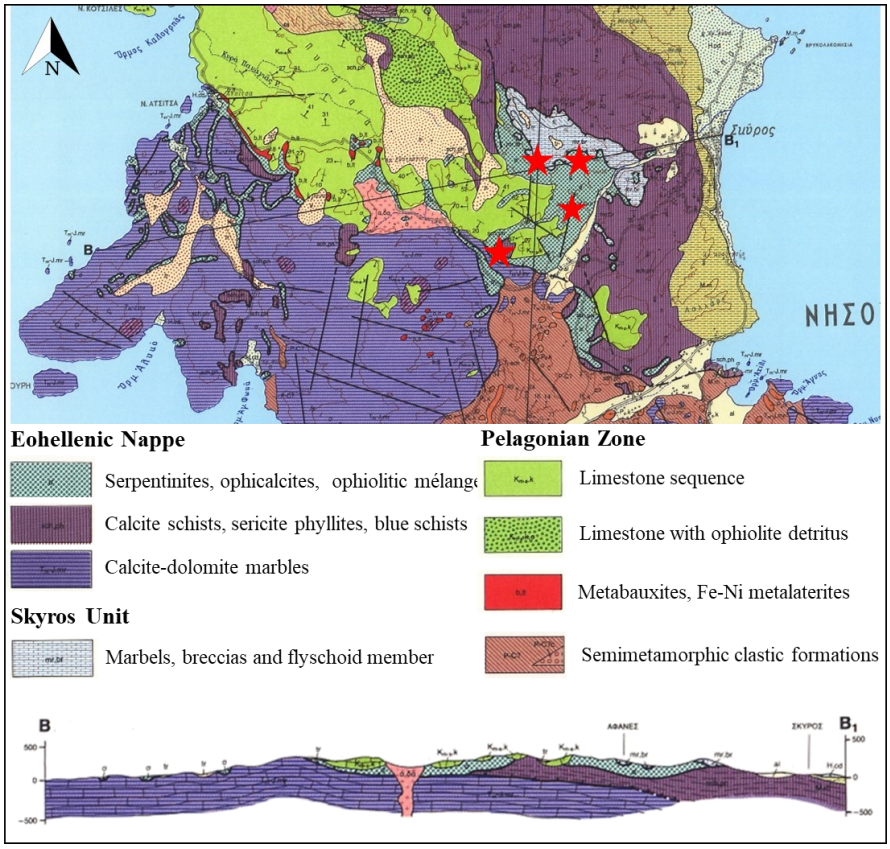


Fig. 2.7 Detail of the Skyros 1:50,000 geological map and geological section through the ophiolitic mélange of Skyros (Jacobshagen and Matarangas, 1972); red stars represent sampling locations.

## 2.4 Iballe

Albanian ophiolites stretch from North to South along the whole country. According to geological reconstructions, these bodies are remnants of oceanic lithosphere derived from the Mesozoic Tethyan ocean, located between Eurasia and Adria (Bortolotti et al., 1996). Iballe ophiolite belongs to a well exposed ophiolite sequence cropping out in the northern part of the country, within the Mirdita ophiolite.

Albanian Alps (referred to as Dinarides or Albanides) are characterized by continental and oceanic tectonic units testifying the evolution of the Jurassic Tethys ocean (Bortolotti et al., 1996; Robertson and Dixon, 1984). Like for the Hellenides, which are the Dinarides continuation to the south, the Dinarides geodynamic evolution begins with the break-up of Gondwana during Middle-Late Triassic, leading to the development of the Jurassic Tethys ocean. From Middle Jurassic to Early Cretaceous, a new geodynamic regime led to Tethys subduction and successive obduction onto continental margins. Ophiolites outcropping along the territory represent the suture zones formed during the closure of the oceanic basin (Bortolotti et al., 1996) (Fig. 2.8).

Based on petrological and geochemical data, ophiolites are divided into two different belts: western and eastern-type ophiolites (Dilek et al., 2007; Shallo et al., 1987) (Fig. 2.8). Despite their differences, the two belts do not present sharp contacts, but gradual lateral changes. The western ophiolites consist of clinopyroxene-bearing harzburgites with rare chromitite occurrences, plagioclase lherzolites, rare dunites and amphibole peridotites. The volcanic sequence is mainly represented by MOR-type basalts (Shallo et al., 2010). The eastern ophiolites consist of depleted harzburgites and dunites with abundant chromitite bodies, covered by a pyroxenite layer, a plutonic sequence (gabbronorite, gabbro, diorite, plagiogranite) and a sheeted dyke complex (Shallo et al., 2010). Iballe ophiolite is comprised into the western ophiolites (Dilek et al., 2005), and in particular within the Krabbi massif, and is mainly constituted by lherzolites and minor plagioclase-bearing peridotite (Dilek et al., 2007) (Fig. 2.9). However, some Authors report the location of the Krabbi massif within the eastern-type ophiolites (Saccani and Tassinari, 2015), as the limit between the two types is yet not well defined. Chromitite occurrences within Iballe are small bodies. In particular, the sampled one is a lens of 30m x 2m, hosted within fresh dunite. The genesis of the two ophiolite belts is debated. Some models argue for the formation of western ophiolites by seafloor spreading and of eastern ophiolite by intraoceanic subduction (Beccaluva et al., 1994; Shallo, 1994). Bortolotti et al. (2005) argue for a formation in the same oceanic basin which records a first MOR spreading center event subsequently evolving into a supra-subduction setting. (Beccaluva et al., 2005) propose a formation of eastern ophiolite through ascending mantle diapirs in an incipient arc, while western ophiolites are formed in a supra-subduction

setting. Dilek et al. (2007) argue that all Albanian ophiolites were formed in a supra-subduction setting. Albanian ophiolites are characterized by a high metallogenic potential (Ibrahim, 2015), with important Cr, Cu, Ni and Fe ores. Olivine and magnesite are also a potentially interesting raw material. High chromite-bearing deposits in the western ophiolites are hosted into the harzburgitic-dunitic mantle, while low potential chromite deposits are hosted into lherzolite sections of the belt.

Chromite ores are mainly of metallurgical grade, with minor refractory grade deposits. Three chromitite groups have been defined: high-$Cr_2O_3$ chromitites (most abundant), high-$Al_2O_3$ chromitites and high-FeO chromitites. Reserves have been estimated at 32.8 million tonnes (Ibrahim, 2015). Copper deposits are located into volcanics of the eastern belt, and are characterized by a pyrite-chalcopyrite-sphalerite paragenesis. The ore deposits are associated to the basaltic sequences and in minor amounts to the sheeted dyke complexes. Iron and Nickel are mainly associated to laterite deposits, formed by lateritization of ultrabasic rocks of the eastern belt during Late Jurassic (Ibrahim, 2015). PGE deposits are mainly related to mantle chromitites (IPGE-rich), low grade disseminated BMS in transitional dunite (Pd-rich) and transition dunite-pyroxenite zone (Pt-rich) (Ibrahim, 2015).

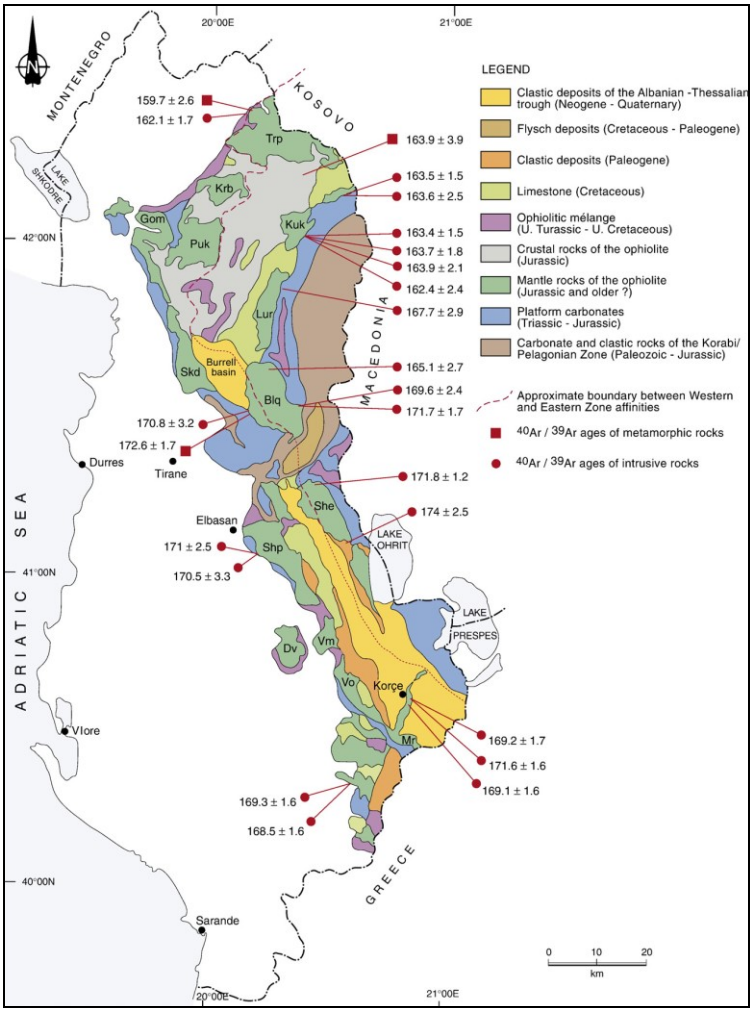


Fig. 2.8 Geological map of the Albanian ophiolites and the associated tectonic units (Dilek et al., 2007).

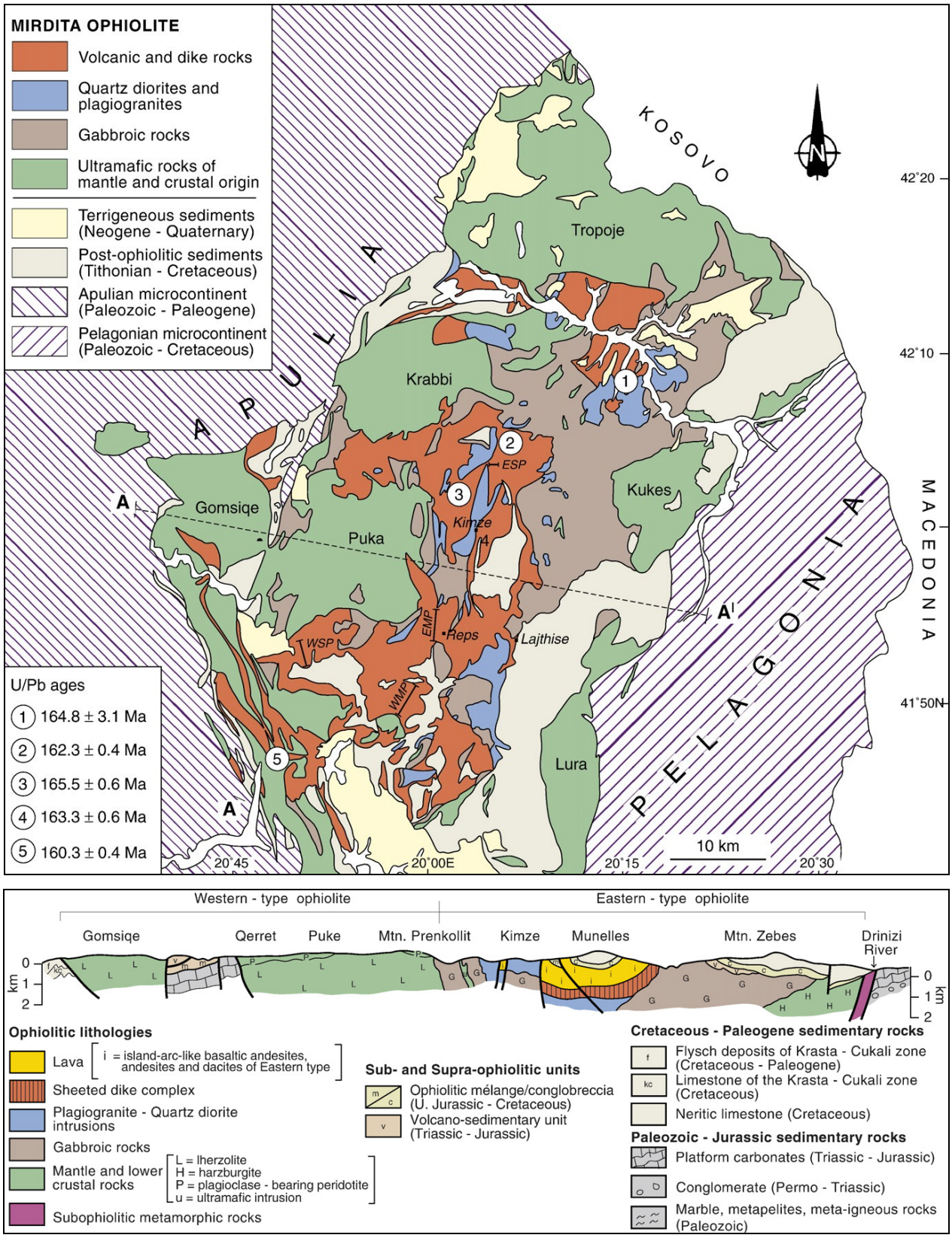


Fig. 2.9 A) Geological map of the Mirdita ophiolite in Northen Albania; B) Cross-section from A to A' (modified adter Dilek et al., 2007).

## 2.5 Abdasht-Soghan

Abdasht and Soghan mafic-ultramafic complexes are located in a 60 km long and 5-10 km wide E-W trending area in the Haji Abad-Esfandagheh district of the Kerman province, Southern Iran, within the Zagros belt (Jannessary et al., 2012; Najafzadeh and Ahmadipour, 2016). The Haji-Abad-Esfandagheh complexes are the second largest chromite producers in Iran after the Faryab chromitite deposits.

The Zagros orogen formed during the Late Eocene-Oligocene collision between Eurasia and Arabia after complete subduction of the Neotethys ocean. The Eurasia-Arabia suture zone, called Main Zagros Thrust (MTZ), is marked by the presence of several ophiolite bodies (Ricou, 1977, 1971). The Iranian crust is divided into four geotectonic units: the Sanandaj-Sirjan Zone, the Zagros Fold and Thrust Belt, Central Iran and the Urmia-Dokhtar Magmatic Assemblage (UDMA) (Alavi, 1994; Berberian and King, 1981; Ghazi and Moazzen, 2015; Mohajjel and Fergusson, 2000; Stöcklin, 1968) (Fig. 2.10). The Sanandaj-Sirjan Zone consists of Late Proterozoic-Mesozoic metamorphic rocks (metacarbonates, schists, gneisses and amphibolites), overlain by Phanerozoic shallow-water sediments and intruded by Mesozoic plutons (Ghazi and Moazzen, 2015; Jamali et al., 2010). The Zagros Fold and Thrust Belt forms the external part of the orogen. It consists of folded and faulted Paleozoic and Mesozoic successions overlain by Cenozoic clastic rocks, and resting on highly metamorphosed Proterozoic Pan-African basement (Ghazi and Moazzen, 2015). The Central Iran zone, located between the Arabian and Eurasian plates, consists of two crustal domains: the North West Iranian Plate (NWIP) and the Central Iranian Microcontinent (CIM). The NWIP comprises the region north of the Darouneh Fault and south of the Alborz Mountains, and the CIM comprises a terrain limited by the Sistan, Nain-Baft, Makran and Sabzevar ophiolites (Şengör, 1990). The UDMA is a magmatic arc of the active Iranian margin during Tertiary (Arvin et al., 2007; Omrani et al., 2008). It is composed of tholeiitic, calc-alkaline, adakitic, and K-rich alkaline intrusive and extrusive rocks and comprises gabbros, diorites, granodiorites, and granite bodies. It also contains widely distributed basaltic lava flows, trachybasalts, ignimbrites, and pyroclastic rocks (Alavi, 1994).

In Iran two major ophiolite belts are preserved: less abundant Paleozoic Ophiolites, mainly spread in the north and linked to the subduction of the Paleotethys (Weber-Diefenbach et al., 1986) and more abundant Mesozoic Ophiolites (Alavi, 1994), linked to the subduction of the Neotethys ocean.

Abdasht and Soghan are considered part of the inner belt of the Zagros Mesozoic ophiolites, with an age spanning from Late Triassic to Cretaceous. They were probably formed in a fore-arc setting within a suprasubduction geodynamic environment, from a magma with boninitic affinity (Najafzadeh and Ahmadipour, 2016, 2014).

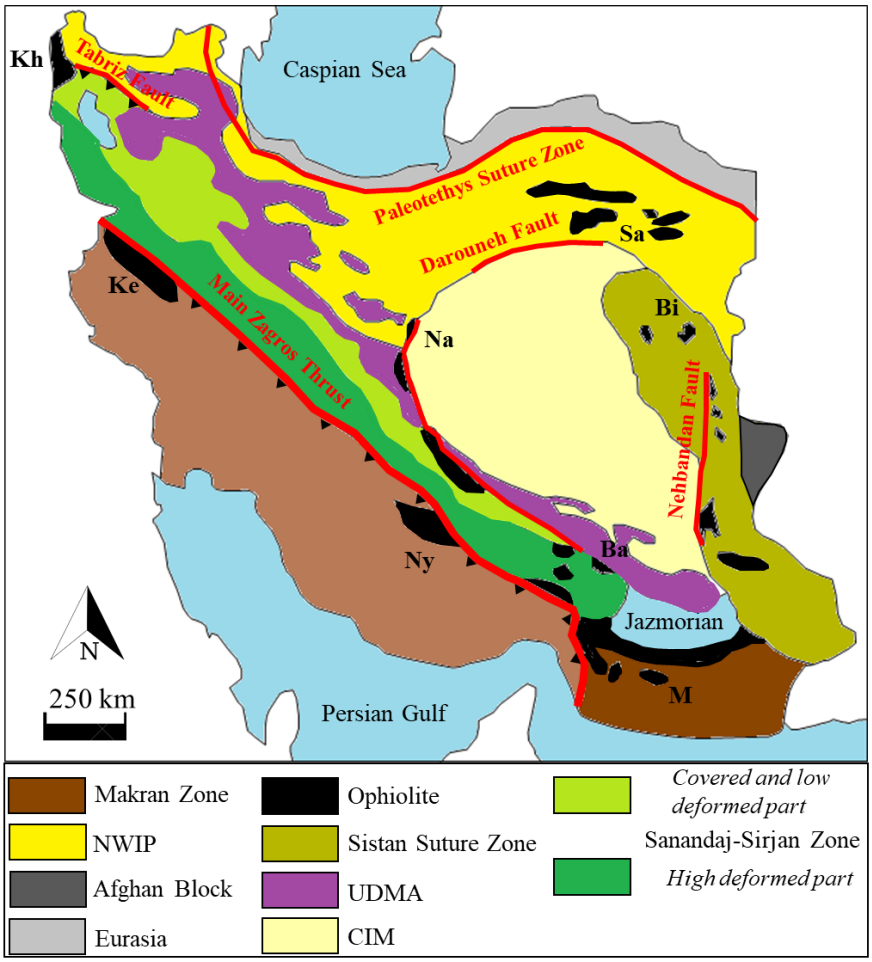


Fig. 2.10 Main tectonic elements of Iran (modified after Stocklin, 1968). Na – Nain, Ba – Baft, Kh – Khoy, Ny – Neyriz, Ke – Kermanshah, Sa – Sabzevar, M – Makran, and Bi – Birjand ophiolites (modified after Ghazi and Moazzen, 2015).

*Soghan complex*

The Soghan complex is about 8 and 5 km in N–S and E–W directions respectively and is composed of five main units (Fig. 2.11): Gechin unit, Main Soghan unit, Transition Zone and Layered Gabbros, overlain by the Sargaz-Abshur metamorphic unit.

Gechin unit is located in the northern portion of the complex, and presents fault contacts both with the mélange and with the Main Soghan Unit (Fig. 2.11 A). The main lithologies are dunite and harzburgites, both affected by strong serpentinization. Minor chromitite bodies are present and were exploited in the past. The Main Soghan unit is composed of alternating dunite, harzburgite, and chromitite, which are highly faulted and metamorphosed. This unit is the main host for exploited chromitite bodies, which present textures varying from massive to schlieren, banded and disseminated. Several diabasic dykes up to few meters thick cross-cut it (Ahmadipour et al., 2003). The Transition Zone, characterized by lherzolite, dunite, pyroxenite and wherlite (Ahmadipour et al., 2003) crops out

south-east of the Main Soghan unit. The Layered Gabbro forms the southeastern part of the Soghan complex and is intruded into the Sargaz-Abshur metamorphic unit. It consists of plagioclase-peridotites, gabbroes, norites and ferrogabbros (Ahmadipour et al., 2003).

*Abdasht complex*

The Abdasht complex, extended for 7×5 km in N–S and E–W directions respectively, is located 3 km west of Soghan. It is mainly composed of variably serpentinized dunite, harzburgite, websterite and minor wherlite and lherzolite (Fig. 2.11 B) (Najafzadeh and Ahmadipour, 2016). Dunites occur as small pods enveloped by harzburgites, which are the most abundant lithology. Contacts between the two lithologies is always sharp. Several chromitite bodies crop out in the Abdasht complex, following three distinct pseudo-stratigraphic levels (Jannessary et al., 2012). These chromitite bodies are included in mantle tectonite (dunites and harzburgites) and have different textures including schlieren/disseminated in the basal level, tabular/disseminated in the intermediate level and layered/massive in the highest level. The bodies have different sizes, up to 3 km long and 25 m thick, and some of them are actively mined. They are all concordant with the host rock layering and present sharp contacts with surrounding lithologies (Najafzadeh and Ahmadipour, 2016).

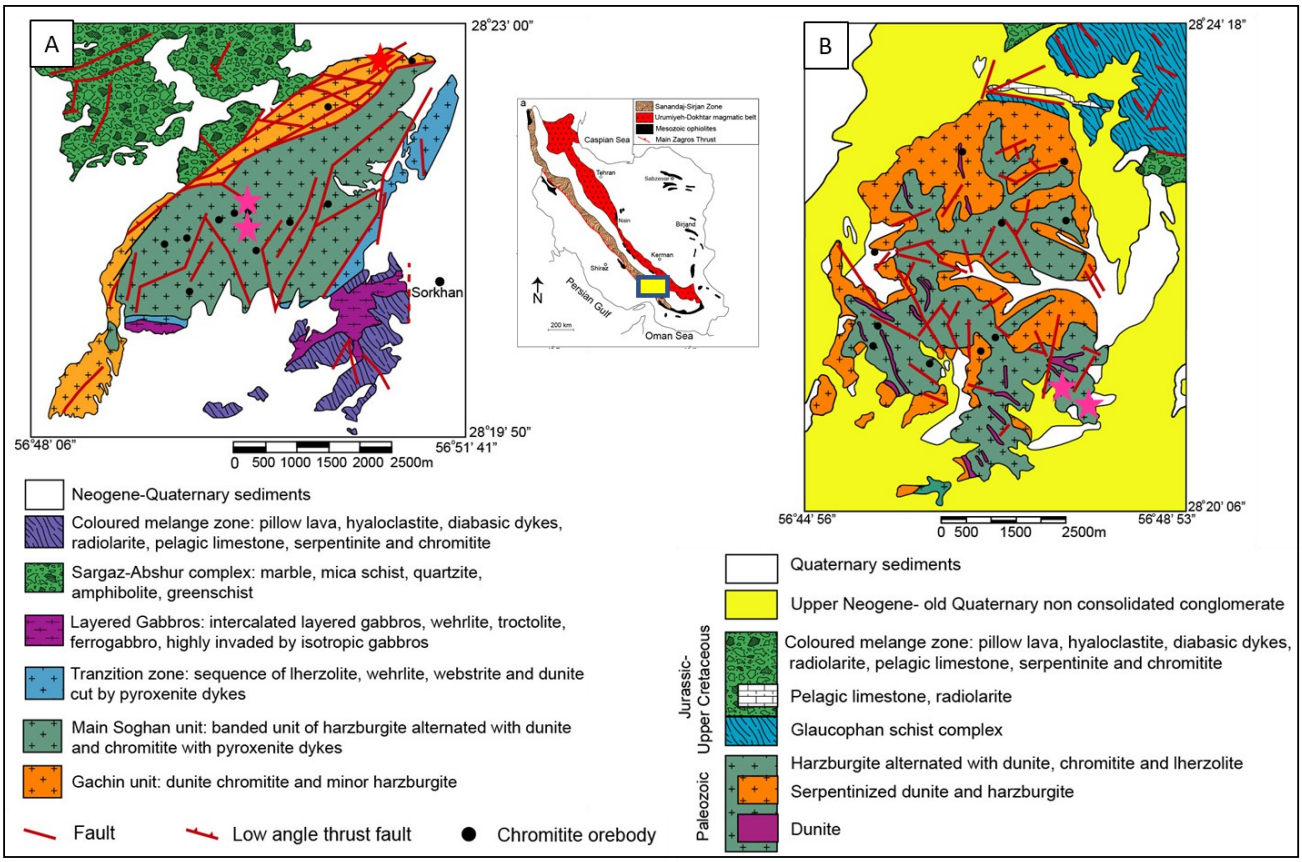


Fig. 2.11 A) Simplified geological map of the Soghan ultramafic complex; B) Simplified geological map of the Abdasht ultramafic complex (from Grieco et al., 2020); pink stars represent sample locations.

# CHAPTER 3: Olivine-spinel re-equilibration

For the present study, chromitite and dunite samples from three localities (Finero, Nea Roda and Iballe) have been analyzed. In order to study the Mg-$Fe^{2+}$ exchange between olivine and spinel, small (~100x100 μm) regions of selected fresh samples were chosen for a detailed investigation involving a high density of point analyses arranged in grids and traverses, with an increasing number of points close to the intergranular limit. Some of the data and discussion have been already published:

- Bussolesi, M., Grieco, G., Tzamos, E. (2019). Olivine–spinel diffusivity patterns in chromitites and dunites from the Finero Phlogopite-Peridotite (Ivrea-Verbano Zone, Southern Alps): implications for the thermal history of the massif. Minerals. Vol. 9(2), 75.

## 3.1 Analytical methods

### 3.1.1. EMPA

Mineral chemistry of chromites and olivines was determined through a JEOL 8200 electron microprobe equipped with a wavelength dispersive system (SEM-WDS) at the Earth Sciences Department (University of Milan). The system was operated using an accelerating voltage of 15 kV, a sample current on brass of 15nA, a counting time of 20s on the peaks and 10s on the background. A series of natural minerals was used as standards: wollastonite for Si, forsterite for Mg, ilmenite for Ti, fayalite for Fe, anorthite for Al and Ca, chromite for Cr, niccolite for Ni, rhodonite for Mn and Zn, and metallic V for that element. The approximate detection limit is 0.01 wt% for each element. $Fe^{3+}$ was recalculated from microprobe analyses assuming perfect stoichiometry, based on 8-oxygen formula.
Part of the samples was analyzed through a JEOL 8200 electron microprobe at the University of Leoben, Austria. The system was operated with an accelerating voltage of 15 kV and beam current of 10 nA, a counting time of 20s on the peaks and 10s on the background. The elements were analyzed using the Kα line. Specimens of chromite, rhodonite, ilmenite, albite, pentlandite, wollastonite, kaersutite, sphalerite, and metallic vanadium were used as standards. The following diffracting crystals were used: TAP for Na, Mg, and Al; PETJ for K, Si, and Ca; LIFH for Ti, V, Cr, Zn, Mn, Fe, and Ni.

### 3.1.2. Diffusivity Curve Determination

Diffusivity profile modeling was achieved through OriginLab software, by modelling the distribution of chromites and olivines XMg *vs* their distance from the intergranular limit with an exponential curve (Bussolesi et al., 2019). Temperature recalculations were performed following Ballhaus et al. (1991) and Fabriès (1979) calibrations. Cooling rates are after Ozawa (1984).

# 3.2 Finero

## 3.2.1. Mineralogy and texture

Sampled chromitites crop out within dunite bodies of the Phlogopite-Peridotite zone in two localities: Rio Creves and Alpe Polunia (Fig. 3.1). A list of the samples is reported in Tab. 3.1.

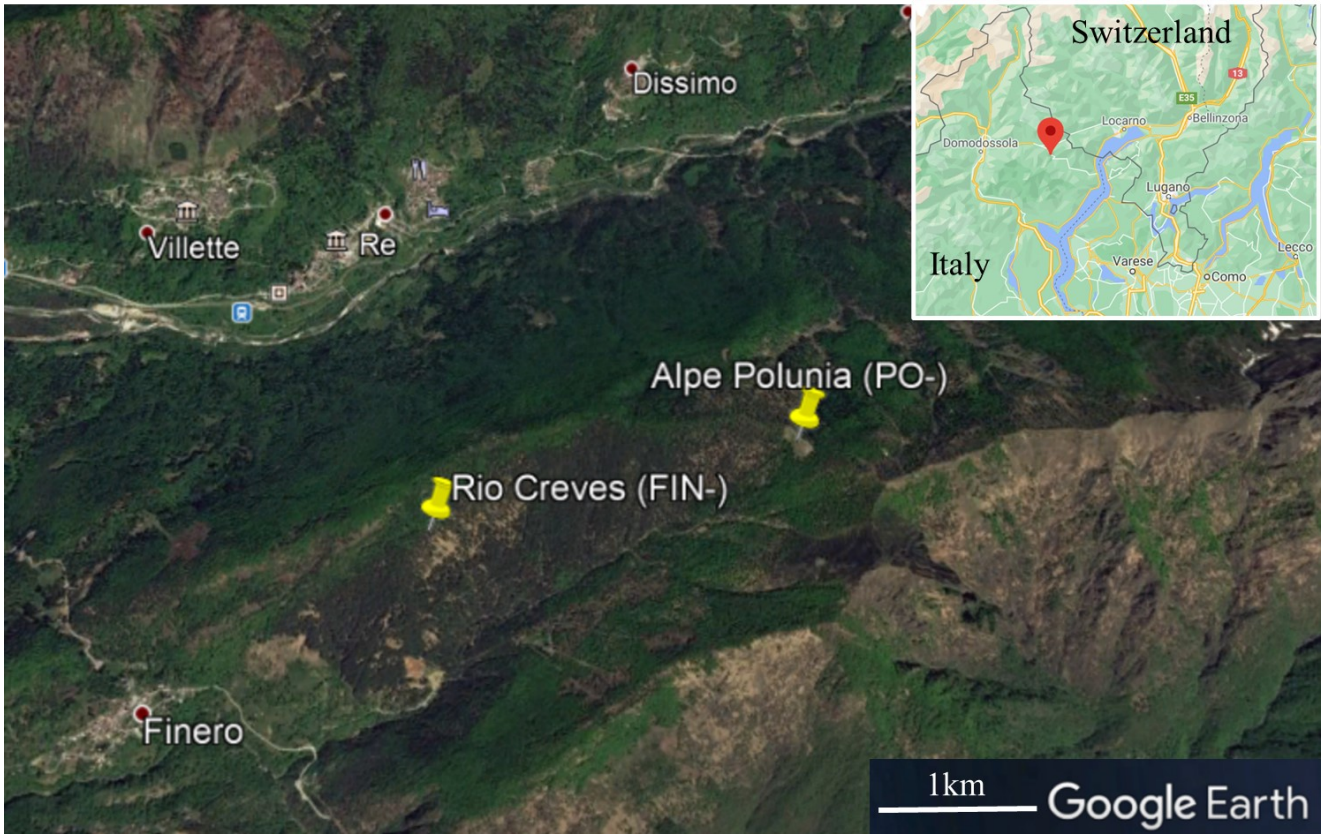


Fig. 3.1 Finero sample locations.

Tab. 3.1 Finero sampling and analyses (**bold**: EMPA).

| Zone | Coordinates | Sample | Lithology |
|---|---|---|---|
| Rio Creves | N 46°6'51.05"<br>E 8°33'9.74" | **FIN01A,** FIN01B, FIN02A, **FIN02B,** FIN02C, FIN02D, FIN03A, FIN05A, FIN07A, FIN08A, FIN08B**, DUN-FIN** | chromitite, dunite |
| Alpe Polunia | N 46° 7'4.51"<br>E 8°34'27.40" | **PO4A**, PO4B, PO2A, PO2B, PO3 | chromitite |

The chromitite bodies occur as irregular pods, lenses, layers and schlieren, up to several meters long and half a meter thick (Fig. 3.2). Analyzed samples include chromitites, host dunites (CHD, chromitite-hosting dunites) and dunites that are not spatially related to chromitites (CFD, chromitite-free dunites). Contacts between chromitites and host dunites are characterized by a sharp transition from high chromite modal contents to dispersed spinel.

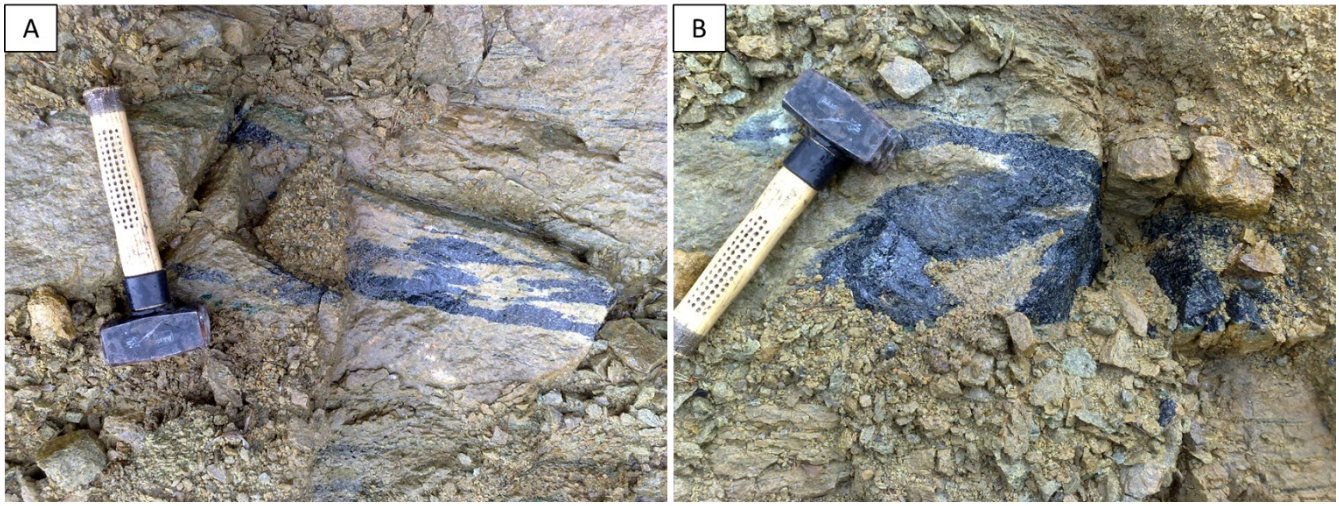


Fig. 3.2 A) and B): chromitite occurrences in Rio Creves locality.

Chromites in chromitites have polygonal and more rarely irregular shapes, with grain size ranging from sub-millimetric to millimetric. Massive chromitites consist of coarse-grained chromite with interstitial silicate gangue, mainly composed of olivine with subordinate orthopyroxene and clinopyroxene (Fig. 3.3A). Chromite grains rarely present fractures (Fig. 3.3B), and alteration into ferrian chromite was never detected. Chromite disseminated in dunite is often found in euhedral crystals with grain size lower than 1 mm, dispersed in a silicate matrix (Fig. 3.3C, D).

Olivine is the major silicate constituent in all considered lithologies, and is present in polygonal to irregular crystals in dunite, and in polygonal to anhedral crystals in massive chromitites, where it can also be an interstitial phase (Fig. 3.3A to D). Minor constituents of the silicate matrix are in order: orthopyroxenes (Fig. 3.3E, F), clinopyroxenes and pargasitic amphibole (present mainly in CFD).

Serpentinization was not detected in our samples, even though some portions of the Finero massif are partially serpentinized, mainly in association with major fracture zones.

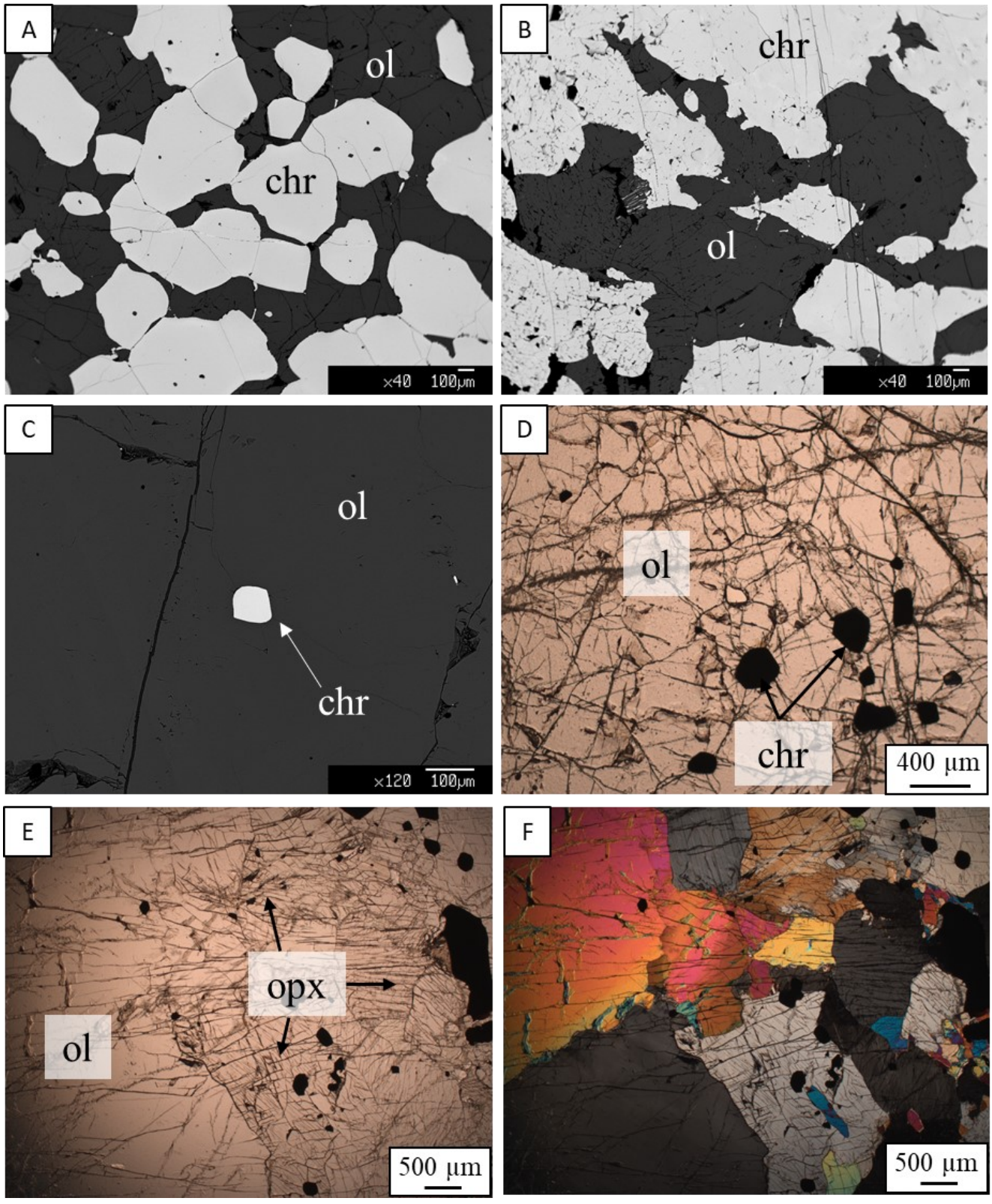


Fig. 3.3 BSE images of massive chromitites from Polunia (A) and Rio Creves (B); BSE images of disseminated chromite in CHD from Rio Creves (C); PPL (D, E) and XPL (F) images of olivine and pyroxene crystals in CHD from Rio Creves.

### 3.2.2. Mineral chemistry

*Chromite*

Chromite average compositions (Tab. 3.2) are based on core analyses, in order to avoid any zonation of the mineral. Complete microprobe analyses are reported in the Appendix (Tab. A3.1 to Tab. A3.7). Mineral chemistry of Cr-spinel depends on the host rock: chromitite, chromitite-hosting dunite (CHD), and chromitite-free dunite (CFD). Spinels within massive chromitites have the highest MgO content, ranging between 10.74 and 11.74 wt%, and the lowest FeO content (16.95 - 18.61 wt%). $Fe_2O_3$ content is between 3.40 and 6.28 wt%. $Cr_2O_3$ content ranges between 50.06 and 53.92 wt%, and $Al_2O_3$ content ranges between 13.49 and 16.34 wt%. Chromites in CHD are characterized by a slightly lower $Cr_2O_3$ content (48.60 - 51.32 wt%, with an average of 50.25 wt%), lower MgO (between 6.89 and 9.56 wt%) and higher FeO (20.34 - 24.34 wt%). $Al_2O_3$ contents are comparable to the ones in the mineralization, with a variability between 13.00 and 16.42 wt%, and $Fe_2O_3$ content ranges between 4.42 and 8.04 wt%. Within CFD, chromite shows lower MgO (4.41 – 4.68 wt%) and higher FeO (24.97 – 25.42 wt%) contents. $Al_2O_3$ and $Fe_2O_3$ contents range respectively between 5.78 - 5.98, and 6.64 - 7.57 wt%, and $Cr_2O_3$ concentrations are high, ranging between 56.03 and 56.83 wt%.

The diversity among chromites in the three different lithologies extend to chromite trace element contents. Spinels within chromitites and CHD have high Ti (between 2617 and 4967 ppm), Zn (400 – 3173 ppm) and Mn (339 – 2820, with an average of 1492 ppm) contents, and low Ni (67 -1560, with an average of 706 ppm) and V (0 - 779 ppm). Trace elements in CFD spinels show significant differences in Ti concentration (294 – 883 ppm), Ni (95 – 852, with an average of 389 ppm) and Zn (3343 – 5863 ppm), while Mn and V concentrations are respectively 2786 – 3739 and 30 - 470 ppm.

Variation in XMg [=Mg/(Mg+$Fe^{2+}$)] and XCr [=Cr/(Cr+Al)] in chromites is dependent on the host rock lithology (Fig. 3.4). Chromitite Cr-spinels have the highest XMg, with averages of 0.523 for Rio Creves and 0.531 for Polunia, and average XCr of 0.711 (Rio Creves) and 0.699 (Polunia). CHD Cr-spinels have average XMg variable between 0.382 (Rio Creves) and 0.443 (Polunia), and average XCr of 0.714 (Rio Creves) and 0.688 (Polunia). CFD Cr-spinels have considerably lower XMg (0.244 average), and high XCr (0.866).

Tab. 3.2 Major and trace elements average composition and standard deviation of chromite cores from Rio Creves and Alpe Polunia, for: chromitite, CHD and CFD. XCr [=Cr/(Cr+Al)]. XMg [=(Mg/(Mg+$Fe^{2+}$)].

| | **CHROMITITE** | | | | **CHD** | | | | **CFD** | |
|---|---|---|---|---|---|---|---|---|---|---|
| Sample | FIN01A | | PO4A | | FIN02B | | PO4A | | DUN-FIN | |
| Elem. | **Avg** | St.Dev | **Avg** | St.Dev | **Avg** | St.Dev | **Avg** | St.Dev | **Avg** | St.Dev |
| $TiO_2$ | **0.62** | 0.05 | **0.58** | 0.04 | **0.67** | 0.09 | **0.56** | 0.02 | **0.09** | 0.03 |
| $Al_2O_3$ | **14.02** | 0.43 | **15.01** | 0.38 | **13.47** | 0.28 | **15.37** | 0.73 | **5.89** | 0.07 |

| | | | | | | | | | | |
|---|---|---|---|---|---|---|---|---|---|---|
| $Cr_2O_3$ | **51.32** | 0.58 | **51.89** | 0.54 | **50.04** | 0.44 | **50.47** | 1.27 | **56.49** | 0.33 |
| $V_2O_3$ | **0.05** | 0.03 | **0.10** | 0.04 | **0.16** | 0.03 | **0.06** | 0.04 | **0.07** | 0.04 |
| $Fe_2O_3$ | **5.91** | 0.22 | **4.47** | 0.36 | **7.25** | 0.41 | **4.64** | 0.21 | **7.18** | 0.29 |
| FeO | **17.97** | 0.35 | **17.77** | 0.38 | **23.01** | 0.81 | **20.74** | 0.36 | **25.21** | 0.18 |
| MnO | **0.15** | 0.03 | **0.15** | 0.05 | **0.26** | 0.05 | **0.18** | 0.04 | **0.41** | 0.04 |
| MgO | **11.06** | 0.26 | **11.27** | 0.23 | **7.98** | 0.53 | **9.37** | 0.22 | **4.57** | 0.08 |
| NiO | **0.10** | 0.03 | **0.09** | 0.04 | **0.08** | 0.04 | **0.13** | 0.02 | **0.05** | 0.02 |
| CaO | **0.01** | 0.01 | **0.01** | 0.01 | **0.01** | 0.01 | **0.01** | 0.01 | **0.02** | 0.01 |
| ZnO | **0.12** | 0.08 | **0.15** | 0.11 | **0.20** | 0.07 | **0.15** | 0.10 | **0.53** | 0.11 |
| TOT | **101.39** | 0.36 | **101.51** | 0.37 | **101.60** | 0.40 | **101.71** | 0.59 | **100.52** | 0.32 |
| Ti | **0.01** | 0.00 | **0.01** | 0.00 | **0.02** | 0.00 | **0.01** | 0.00 | **0.00** | 0.00 |
| Al | **0.53** | 0.01 | **0.56** | 0.01 | **0.52** | 0.01 | **0.58** | 0.03 | **0.24** | 0.00 |
| Cr | **1.30** | 0.02 | **1.30** | 0.02 | **1.28** | 0.01 | **1.28** | 0.03 | **1.56** | 0.01 |
| V | **0.00** | 0.00 | **0.00** | 0.00 | **0.00** | 0.00 | **0.00** | 0.00 | **0.00** | 0.00 |
| $Fe^{3+}$ | **0.14** | 0.01 | **0.11** | 0.01 | **0.18** | 0.01 | **0.11** | 0.01 | **0.19** | 0.01 |
| $Fe^{2+}$ | **0.48** | 0.01 | **0.47** | 0.01 | **0.62** | 0.02 | **0.56** | 0.01 | **0.74** | 0.01 |
| Mn | **0.00** | 0.00 | **0.00** | 0.00 | **0.01** | 0.00 | **0.00** | 0.00 | **0.01** | 0.00 |
| Mg | **0.53** | 0.01 | **0.53** | 0.01 | **0.39** | 0.02 | **0.45** | 0.01 | **0.24** | 0.00 |
| Ni | **0.00** | 0.00 | **0.00** | 0.00 | **0.00** | 0.00 | **0.00** | 0.00 | **0.00** | 0.00 |
| Ca | **0.00** | 0.00 | **0.00** | 0.00 | **0.00** | 0.00 | **0.00** | 0.00 | **0.00** | 0.00 |
| Zn | **0.00** | 0.00 | **0.00** | 0.00 | **0.00** | 0.00 | **0.00** | 0.00 | **0.01** | 0.00 |
| XCr | **0.71** | 0.01 | **0.70** | 0.01 | **0.71** | 0.00 | **0.69** | 0.02 | **0.87** | 0.00 |
| XMg | **0.52** | 0.01 | **0.53** | 0.01 | **0.38** | 0.02 | **0.45** | 0.01 | **0.24** | 0.00 |

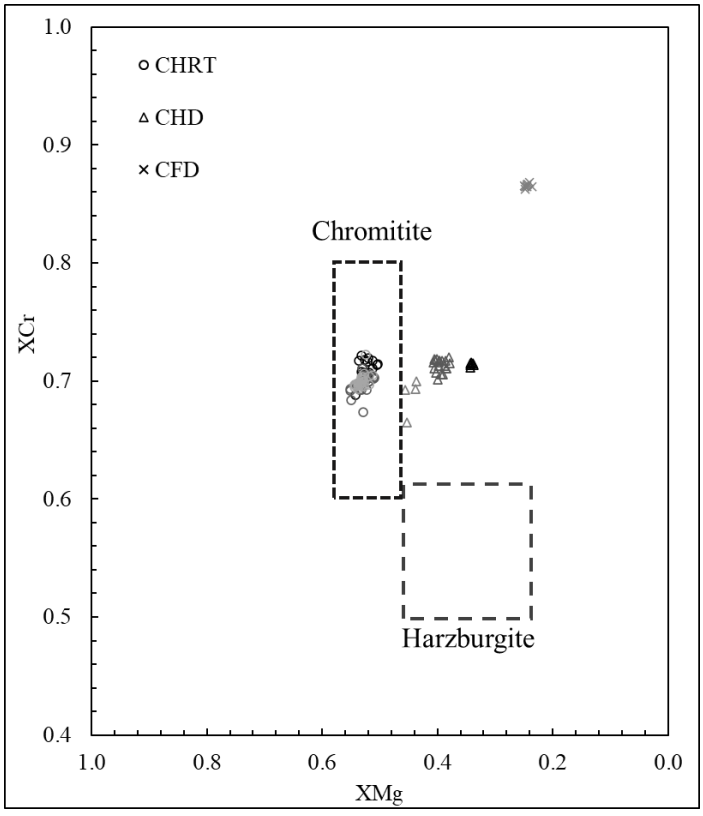


Fig. 3.4 XMg [=Mg/(Mg+Fe2+)] vs XCr [=Cr/(Cr+Al)] values of spinels in three lithologies (CHRT: chromitite; CHD: chromitite-hosting dunite; CFD: chromitite-free dunite) compared to Finero harzburgite and chromitite compositional fields (modified after Bussolesi et al., 2019). Harzburgite data are from Grieco et al. (2001); chromitite data are from Zanetti et al. (2016).

*Olivine*

Olivine mineral chemistry, reported as core analyses average composition, is dependent on the host rock (Tab. 3.3). In chromitites, olivine is strongly forsteritic, with a high MgO content (50.59 – 54.78 wt%) and low FeO (4.70 – 6.40 wt%). Average XMg is 0.942 for both localities. Olivines in CHD show slightly lower MgO content (49.50 – 51.50 wt%) and higher FeO (6.90 – 8.60 wt%), resulting in a lower XMg, with an average of 0.917 for Rio Creves and 0.926 for Polunia. Within CFD, MgO content is even lower (48.48 – 49.67 wt%) and FeO is the highest (8.26 – 8.70 wt%). The average XMg is 0.912.

Chromitites, CHD and CFD also show a variability in olivine trace element composition, in particular concerning Mn and Ni. Ni is the most abundant trace element in olivines, and is variable between 2079 and 4626 ppm in chromitites, 1807 and 4207 ppm in CHD and 1959 and 3352 ppm in CFD. Mn has low concentration in chromitites (154 – 1170 ppm), increasing abundance in CHD (380 – 1425 ppm) and the highest concentration in CFD (638 – 1556 ppm). For the other trace elements, standard deviation is too high to infer any reliable pattern.

Tab. 3.3 Major and trace elements average content and standard deviation of olivine cores from Rio Creves and Alpe Polunia, for the three host rocks: chromitite, CHD, CFD. XMg [=(Mg/(Mg+$Fe^{2+}$)].

| | **CHROMITITE** | | | | **CHD** | | | | **CFD** | |
|---|---|---|---|---|---|---|---|---|---|---|
| Sample | FIN01A | | PO4A | | FIN02B | | PO4A | | DUN-FIN | |
| Elem. | **Avg** | St.Dev | **Avg** | St.Dev | **Avg** | St.Dev | **Avg** | St.Dev | **Avg** | St.Dev |
| $SiO_2$ | **40.88** | 0.25 | **41.57** | 0.36 | **41.16** | 0.46 | **41.29** | 0.18 | **40.81** | 0.20 |
| $TiO_2$ | **0.01** | 0.02 | **0.01** | 0.02 | **0.01** | 0.02 | **0.02** | 0.03 | **0.02** | 0.02 |
| $Al_2O_3$ | **0.00** | 0.01 | **0.01** | 0.01 | **0.01** | 0.01 | **0.01** | 0.01 | **0.01** | 0.01 |
| $Cr_2O_3$ | **0.02** | 0.02 | **0.01** | 0.02 | **0.02** | 0.03 | **0.02** | 0.02 | **0.03** | 0.03 |
| $V_2O_3$ | **0.01** | 0.02 | **0.01** | 0.01 | **0.01** | 0.02 | **0.01** | 0.01 | **0.01** | 0.01 |
| FeO | **5.68** | 0.35 | **5.69** | 0.39 | **8.17** | 0.24 | **7.26** | 0.13 | **8.47** | 0.16 |
| MnO | **0.08** | 0.03 | **0.08** | 0.03 | **0.13** | 0.03 | **0.12** | 0.03 | **0.16** | 0.03 |
| MgO | **51.34** | 0.43 | **52.12** | 0.64 | **50.41** | 0.35 | **50.86** | 0.27 | **48.99** | 0.33 |
| NiO | **0.35** | 0.05 | **0.46** | 0.05 | **0.32** | 0.04 | **0.45** | 0.04 | **0.37** | 0.05 |
| ZnO | **0.05** | 0.04 | **0.02** | 0.04 | **0.04** | 0.05 | **0.03** | 0.05 | **0.04** | 0.04 |
| TOT | **98.42** | 0.53 | **100.01** | 0.55 | **100.30** | 0.48 | **100.08** | 0.31 | **98.92** | 0.30 |
| Si | **1.00** | 0.00 | **1.00** | 0.01 | **1.00** | 0.01 | **1.00** | 0.00 | **1.01** | 0.01 |
| Ti | **0.00** | 0.00 | **0.00** | 0.00 | **0.00** | 0.00 | **0.00** | 0.00 | **0.00** | 0.00 |
| Al | **0.00** | 0.00 | **0.00** | 0.00 | **0.00** | 0.00 | **0.00** | 0.00 | **0.00** | 0.00 |
| Cr | **0.00** | 0.00 | **0.00** | 0.00 | **0.00** | 0.00 | **0.00** | 0.00 | **0.00** | 0.00 |
| V | **0.00** | 0.00 | **0.00** | 0.00 | **0.00** | 0.00 | **0.00** | 0.00 | **0.00** | 0.00 |
| $Fe^{2+}$ | **0.12** | 0.01 | **0.11** | 0.01 | **0.17** | 0.00 | **0.15** | 0.00 | **0.18** | 0.00 |
| Mn | **0.00** | 0.00 | **0.00** | 0.00 | **0.00** | 0.00 | **0.00** | 0.00 | **0.00** | 0.00 |
| Mg | **1.87** | 0.01 | **1.87** | 0.01 | **1.82** | 0.01 | **1.84** | 0.01 | **1.80** | 0.01 |
| Ni | **0.01** | 0.00 | **0.01** | 0.00 | **0.01** | 0.00 | **0.01** | 0.00 | **0.01** | 0.00 |
| Zn | **0.00** | 0.00 | **0.00** | 0.00 | **0.00** | 0.00 | **0.00** | 0.00 | **0.00** | 0.00 |
| XMg | **0.94** | 0.00 | **0.94** | 0.00 | **0.92** | 0.00 | **0.93** | 0.00 | **0.91** | 0.00 |

*Mg-$Fe^{2+}$ zoning in olivine and spinel*

Data show a correlation of olivine and chromite XMg with distance from the intergranular limit (Fig. 3.5), varying among different lithologies.

Olivines in chromitites always show a zonation approaching the chromite rim, with an increase in XMg of about 0.020. The zonation usually extends as far as 0.1 mm from the intergranular limit (Fig. 3.6A). Chromites in chromitites show a zonation with ΔXMg always 2-3 times larger than the one in olivines, but data appear more dispersed. This is probably due to $Fe^{2+}$-$Fe^{3+}$ repartitioning (Fig. 3.6B). The zonation extent, lower than in olivines, is < 0.1 mm.

Olivines in CHD always show a zonation approaching the chromite rim, with an increase in XMg of about 0.020, as in chromitites. The zonation extends as far as 0.2 mm from the intergranular limit (Fig. 3.7A). Chromites dispersed in CHD do not show a zonation pattern, but are homogeneous. The only exception is a micro-area within a sample from Polunia (PO4A-GRID3) that shows a trend in chromite-XMg (Fig. 3.7B), although dispersion of data is high.

Olivines in CFD show a zonation approaching the chromite rim, with an increase in XMg of about 0.020. The zonation is limited to the first microns from the rim (Fig. 3.8A). Chromites in CFD do not show any trend (Fig. 3.8B).

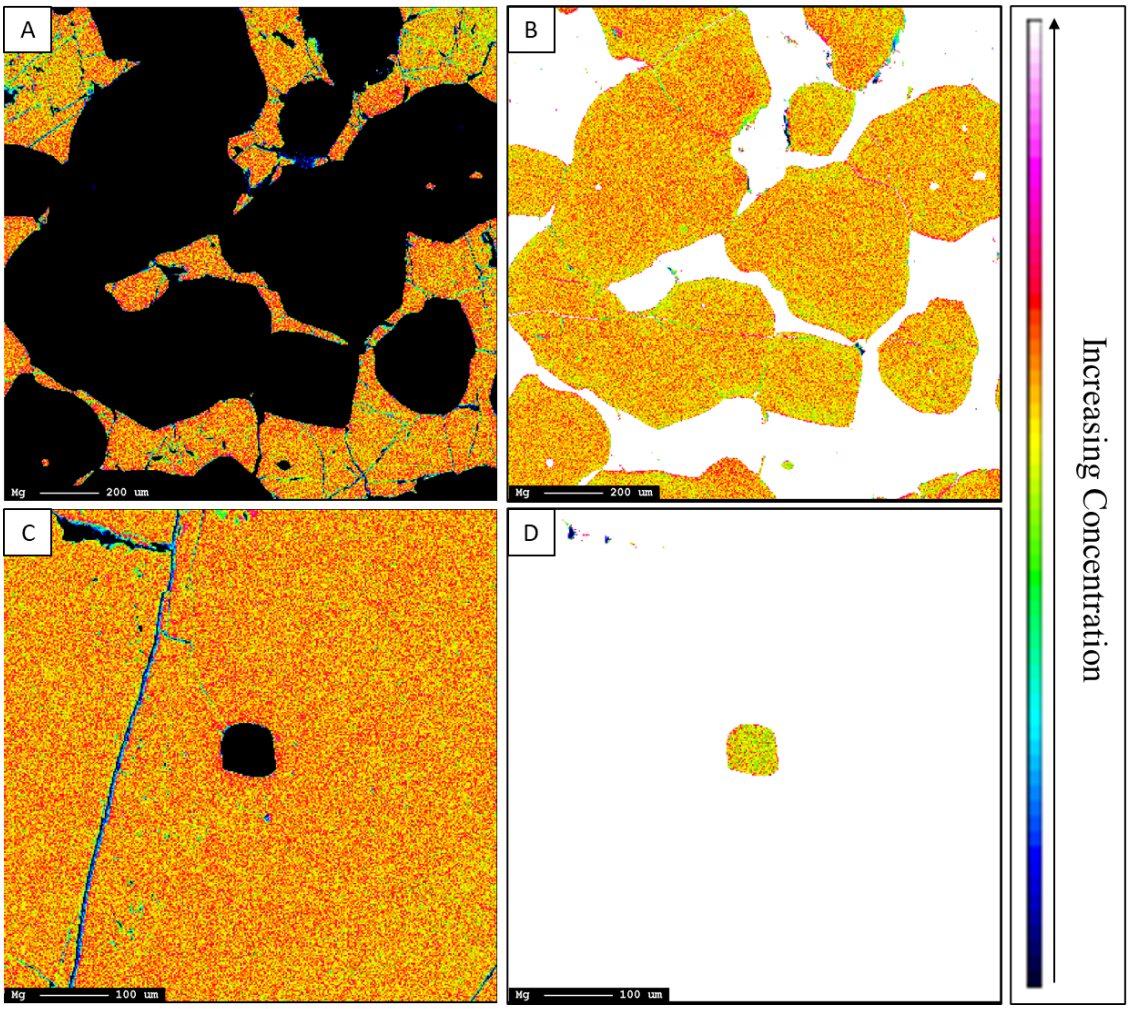


Fig. 3.5 Mg atomic maps of two micro-areas within chromitites (A, B) and CHD (C, D), highlighting the concentration of Mg within olivines (A, C) and chromites (B, D).

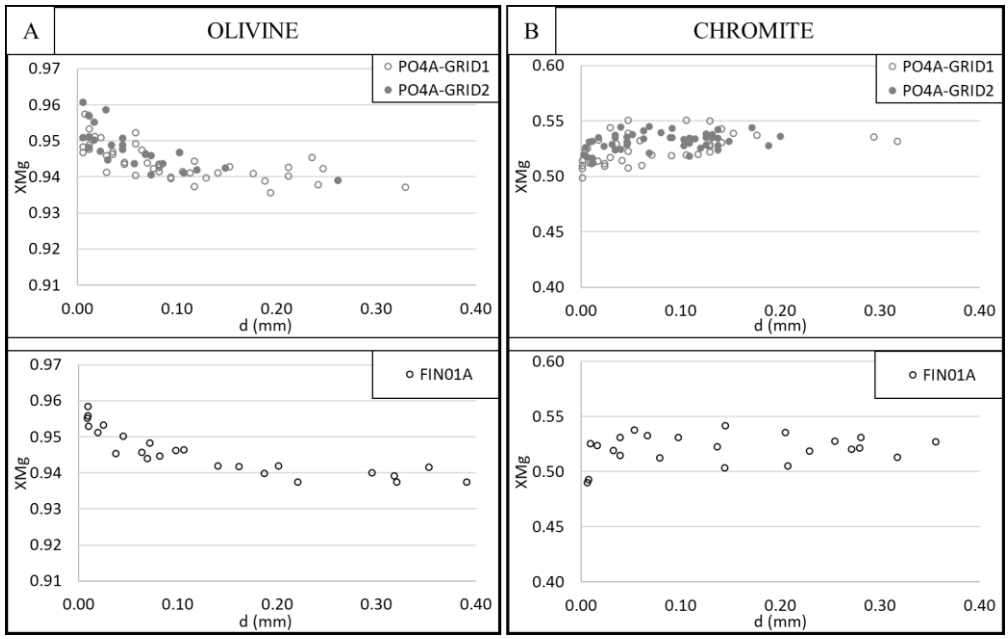


Fig. 3.6 XMg *vs* distance from the grain boundary in olivines (A) and chromites (B) within chromitites.

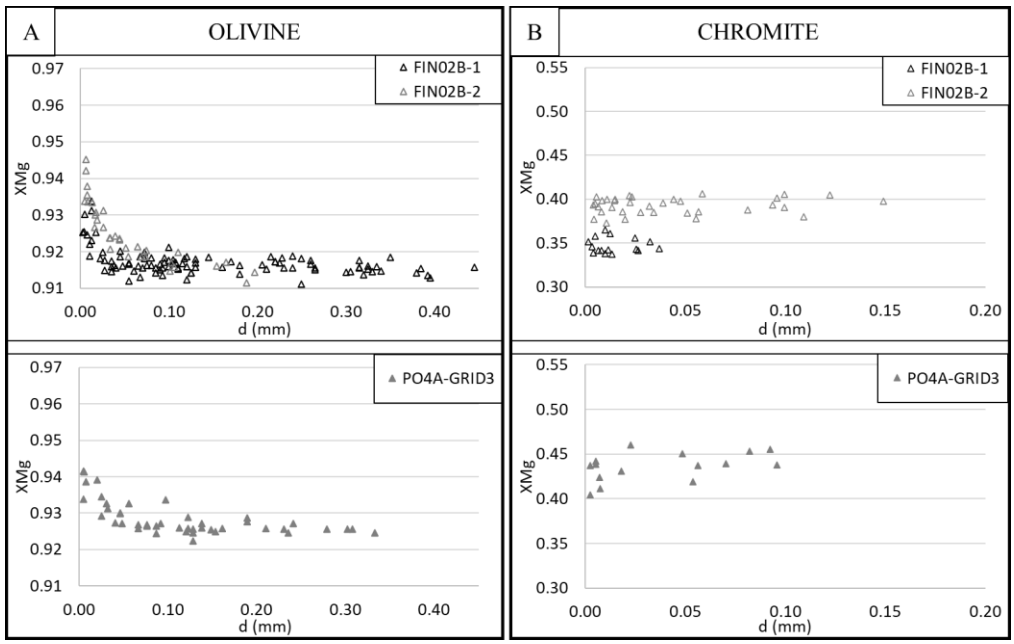


Fig. 3.7 XMg *vs* distance from the grain boundary in A) olivines in CHD and B) chromites in CHD.

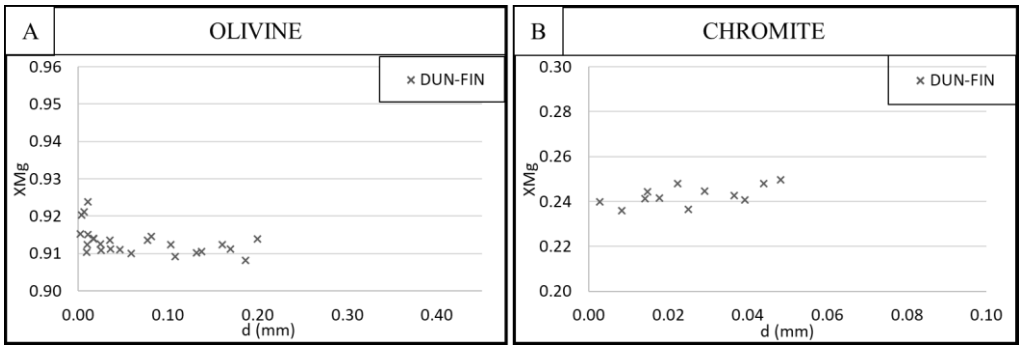


Fig. 3.8 XMg *vs* distance from the grain boundary in A) olivines in CHD and B) chromites in CHD.

## 3.2.3. Discussion

### 3.2.3.1. Olivine-spinel re-equilibration

Numerous mineralogical and experimental data have proven the high Mg-$Fe^{2+}$ diffusivity between olivine and spinel (Freer and O'reilly, 1980; Greenfield et al., 2013), which causes Mg-$Fe^{2+}$ exchange between olivine and spinel down to relatively low temperatures. Recent studies report low-temperature diffusivity experimental data down to 750 °C (Dohmen and Chakraborty, 2007; Vogt et al., 2015), however Méducin et al. (2004) report that Mg and $Fe^{2+}$ are still significantly disordered down to temperatures as low as 600 °C. Incomplete Mg and $Fe^{2+}$ exchange, which is dependent on interdiffusivity coefficients and temperature (Irvine, 1967; Medaris, 1975; Ozawa, 1983), causes compositional heterogeneities within olivine and spinel. In order to evaluate the extent of this exchange, olivine and spinels in unaltered (serpentine-free) chromitites, chromitite-hosting dunites and chromitite-free dunites were analyzed.

The correlation between the Kd of the exchange reaction and temperature (Ballhaus et al., 1991; Fabriès, 1979; Irvine, 1967, 1965), which was first studied by Irvine (1967, 1965), results in the typical olivine and spinel diffusion profiles developed during cooling (Ozawa, 1983). These profiles show that olivine is more magnesian close to the grain boundary, whereas magnesium in chromite grains decreases close to the rim. $Fe^{2+}$ has the opposite trend, and hence XMg ratio was used to reveals diffusivity patterns.

At high temperature subsolidus conditions, diffusivity is sufficiently efficient to ensure a homogeneous spinel that is in equilibrium with surrounding olivine. With decreasing temperature, the diffusion profile reflects lower diffusivity to the point where elemental exchange can no longer proceed (Ozawa, 1983). This critical temperature is relatively low compared to other exchange reactions used as geothermometers in peridotites. Ca-Mg partitioning in pyroxenes or Mg-$Fe^{2+}$ exchange between orthopyroxene and spinel, are blocked at higher temperatures (Fabriès, 1979; Freer, 1981; Greenfield et al., 2013; Lehmann, 1983). This implies that Fe-Mg distribution between olivine and spinel is more sensitive to cooling, and records lower temperatures.

### 3.2.3.2. Diffusivity curve analyses (primary and re-equilibration compositions)

Olivine and spinel compositions at grain boundaries reflect the critical temperature below which subsolidus exchange cannot proceed. Within the cores of mineral grains, in particular in the cores of larger-sized grains, minerals appear to retain their primary composition, which can be used to estimate their primary crystallization temperature.

The composition of mineral rims is usually determined through arithmetic mean of several coupled analyses, within 10-20 microns from the grain boundary. As calculated XMg diffusion pattern follows an exponential trend (Ozawa, 1984, 1983), also confirmed for Finero, estimates of the true rim compositions are very sensitive to the distance from the grain boundary. XMg diffusivity patterns in the Finero samples are restricted to distances of less than 100 microns from the rim: the highest variability is observed within the initial few tens of microns from the grain rims. The use of a simple arithmetic mean as a composition leads to XMg overestimation for spinel rim compositions and underestimation for olivine, hence producing equilibrium temperature assessments higher than actual rim equilibrium conditions.

Our approach is based on the determination of a "best-fit" correlation curve, then used to calculate rim and core XMg values. Assumptions for this approach are an initial homogeneous composition of both olivine and chromite (primary composition) at the point of their original crystallization, and a finite value of XMg at the rim imparted during re-equilibration. XMg value as a function of distance from the grain boundary is modelled to fit the dataset following two boundary conditions. Setting x = 0 at the chromite-olivine grain boundary and XMg = f(x), these conditions are:

$$\lim_{x\to\infty} f(x) = XMg_{pr}$$

$$\lim_{x\to 0} f(x) = XMg_{eq}$$

The curve must approach an asymptote corresponding to $XMg_{pr}$, the primary XMg, and must have an intercept corresponding to $XMg_{eq}$, the re-equilibrated XMg.

The diffusivity curve was fitted with an exponential function using OriginLab software as follows:

$$y = a - bc^x$$

with:

$$XMg = y$$

$$XMg_{pr} = a$$

$$XMg_{eq} = (a - b)$$

Diffusivity curves were modelled for spinel and olivine datasets (Tab. 3.4, Fig. 3.9). Diffusivity patterns always appear well delineated for olivine, while dispersion of data is higher for spinels. The higher uncertainty for chromites is probably due to $Fe^{2+}$-$Fe^{3+}$ partitioning. The computation of primary and re-equilibrated XMg values of olivine is always possible since its original composition is dependent on the crystal grain size; olivine grain sizes in the sample set are sufficiently large even in massive chromitites. The original XMg within chromites was computed in all our chromitite samples,

but was possible only for one dunite sample. In dunites, small, disseminated chromite grains within the olivine matrix are always completely re-equilibrated and only one grain was large enough to allow $XMg_{pr}$ computation. The exponential curves thus modelled provide also an estimate of a diffusion distance beyond which there is no more subsolidus exchange. For olivines, curves are smooth and the diffusion distance is comprised between 0.08 and 0.20 mm, with the highest values in chromitites. Chromite curves are more abrupt, and the diffusion distance ranges between 0.04 and 0.20 mm in chromitite samples. The only diffusion distance value of chromite in dunites is 0.06 mm. Diffusion distances confirm that a simple arithmetic mean approach cannot be applied in Finero.

Tab. 3.4 Parameters a, b, c and associated standard error of calculated curves and primary (pr) and re-equilibrated (eq) XMg atomic ratios of chromites and olivines for three host rocks.

**Chromite**

| Sample | Locality | Host rock | a | St.Er. | b | St.Er. | c | St.Er. | $XMg_{pr}$ | $XMg_{eq}$ |
|---|---|---|---|---|---|---|---|---|---|---|
| FIN01A | Rio Creves | Chromitite | 0.525 | 0.0023 | 0.052 | 0.0553 | 1.62E-53 | 2.2E-51 | 0.525 | 0.472 |
| PO4A-GR1 | Polunia | Chromitite | 0.534 | 0.0053 | 0.022 | 0.0059 | 4.71E-09 | 6.6E-08 | 0.534 | 0.512 |
| PO4A-GR2 | Polunia | Chromitite | 0.534 | 0.0015 | 0.011 | 0.0041 | 7.39E-21 | 2.8E-18 | 0.534 | 0.523 |
| FIN02B-1 | Rio Creves | CHD | n.c. | n.c. | n.c. | n.c. | n.c. | n.c. | n.c. | 0.347* |
| FIN02B-2 | Rio Creves | CHD | n.c. | n.c. | n.c. | n.c. | n.c. | n.c. | n.c. | 0.393* |
| PO4A-GR3 | Polunia | CHD | 0.443 | 0.0084 | 0.029 | 0.0274 | 1.31E-45 | 2.5E-43 | 0.443 | 0.413 |
| DUN-FIN | Rio Creves | CFD | n.c. | n.c. | n.c. | n.c. | n.c. | n.c. | n.c. | 0.240* |

**Olivine**

| Sample | Locality | Host rock | a | St.Er. | b | St.Er. | c | St.Er. | $XMg_{pr}$ | $XMg_{eq}$ |
|---|---|---|---|---|---|---|---|---|---|---|
| FIN01A | Rio Creves | Chromitite | 0.938 | 0.0009 | -0.018 | 0.0013 | 8.13E-06 | 1.9E-05 | 0.938 | 0.957 |
| PO4A-GR1 | Polunia | Chromitite | 0.940 | 0.0012 | -0.013 | 0.0020 | 1.54E-10 | 1.3E-09 | 0.940 | 0.953 |
| PO4A-GR2 | Polunia | Chromitite | 0.939 | 0.0043 | -0.016 | 0.0039 | 8.66E-06 | 5.9E-05 | 0.939 | 0.955 |
| FIN02B-1 | Rio Creves | CHD | 0.916 | 0.0003 | -0.015 | 0.0018 | 4.42E-25 | 5.1E-24 | 0.916 | 0.931 |
| FIN02B-2 | Rio Creves | CHD | 0.916 | 0.0010 | -0.027 | 0.0017 | 4.06E-15 | 2.0E-14 | 0.916 | 0.943 |
| PO4A-GR3 | Polunia | CHD | 0.926 | 0.0005 | -0.016 | 0.0016 | 2.11E-14 | 1.3E-13 | 0.926 | 0.942 |
| DUN-FIN | Rio Creves | CFD | 0.911 | 0.0009 | -0.008 | 0.0027 | 1.76E-26 | 6.8E-25 | 0.911 | 0.919 |

* Calculated as average XMg value; n.c. not computable

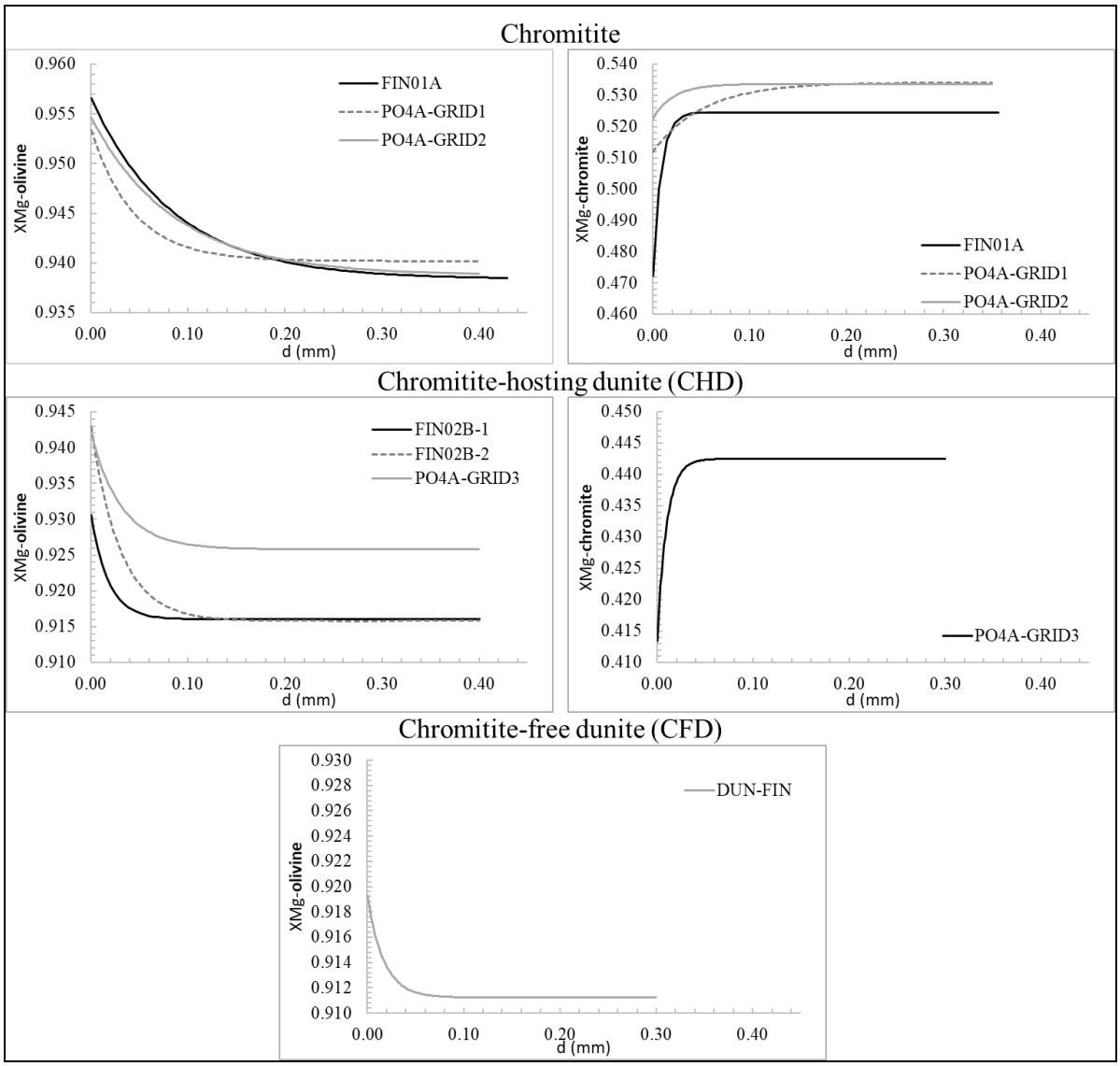


Fig. 3.9 Diffusivity curve of olivines and chromites in three host rocks through OriginLab software; XMg [=Mg/(Mg+$Fe^{2+}$)]; d (mm): distance from the grain boundary (modified from Bussolesi et al. 2019).

### 3.2.3.3. Geothermometry

Geothermometry of olivine-spinel exchange applied to rim-rim analyses has been repeatedly used to estimate the thermometric cessation of elemental exchange conditions. Core-core analyses are cited in the literature as a means to determine the original mineralogic compositions of olivine-chromite pairs (Greenfield et al., 2013). The assumption that core compositions retain their primary imprint, however, is not always true. In fact, it is dependent on chromite modal content (Grieco et al., 2018), and spinel grain size (Ozawa, 1984, 1983).

Temperature estimates were applied to re-equilibrated and primary XMg values following Ballhaus et al. (1991) calibration (Tab. 3.5). The olivine-spinel re-equilibrated temperatures range between 694 and 715 °C within chromitites, with an average of 707 °C, between 657 and 675 °C in CHD (average

value 666 °C) and only a single re-equilibration temperature of 656 °C could be estimated from the CFD sample. The Rio Creves locality shows an average re-equilibration temperature of 667 °C, while Polunia has a slightly higher average temperature (694 °C). Primary temperatures in chromitites range between 812 and 849 °C, with an average of 826 °C. Within CHD from Polunia, the only computed primary temperature is 753 °C. The Rio Creves locality has the highest primary temperature value (849 °C), while Polunia shows an average primary temperature of 794 °C.

Tab. 3.5 Primary and re-equilibrated temperatures ($T_{pr}$ and $T_{eq}$ respectively); n.c.: not computable.

| Sample | Locality | Lithology | $T_{pr}$(°C) | $T_{eq}$(°C) |
|---|---|---|---|---|
| FIN01A | Rio Creves | chromitite | 849 | 694 |
| PO4A-GR1 | Polunia | chromitite | 812 | 713 |
| PO4A-GR2 | Polunia | chromitite | 817 | 715 |
| FIN02B-1 | Rio Creves | CHD | n.c. | 657 |
| FIN02B-2 | Rio Creves | CHD | n.c. | 675 |
| PO4A-GR3 | Polunia | CHD | 753 | 662 |
| DUN-FIN | Rio Creves | CFD | n.c. | 656 |

Re-equilibration temperatures record the closing temperatures of the subsolidus mineral exchange system. Within peridotites, olivine-spinel is the system that "freezes" last with decreasing temperatures, allowing a determination of the thermal history of the rocks down to ~650 °C.

Primary temperatures represent the threshold temperatures below which diffusivity cannot maintain compositional homogeneity within the crystals (Fabriès, 1979; Freer, 1981; Greenfield et al., 2013; Irvine, 1965).

### 3.2.3.4. Cooling rates

Mg-$Fe^{2+}$ zoning used to infer primary and re-equilibrated compositions and temperatures can also be used to estimate a cooling rate in ultramafic rocks (Ozawa, 1984, 1983). In particular, spinel XMg appears to be more sensitive to cooling rate differences than olivine XMg, especially at low rates within the range of ~850 – ~650 °C. Ozawa (1984) calculated cooling rate profiles for several types of natural rocks at different initial temperatures of the system, numerically solving the differential equations that describe the Mg-$Fe^{2+}$ exchange system of a spherical spinel surrounded by olivine. His solution reveals a relationship between temperature and spinel grain diameter. Temperatures in his model are neither primary nor re-equilibrated, but calculated using spinel and olivine XMg core analyses. In these estimates, olivine XMg coincides with the primary value but the same is not true for chromite: the equivalence is valid only for grains with a radius larger than diffusion distance.

Fig. 3.10 is a semi-logarithmic plot of grain diameter vs T(°C): it results in a function with two knees and two asymptotes. The asymptote at higher temperatures reflects the presence of non re-equilibrated

core areas for larger grains that apparently preserve the primary composition. The asymptote at lower temperatures is a mathematical construct that reflects the re-equilibrated areas approaching the grain boundary (d→0). The steeper portion of the curve is ascribed to the cooling rates of the rocks. These trends follow constant cooling rate curves or, when they deviate from these patterns, imply a variable cooling rate. Thus, a deviation within the dataset plot indicates a change in cooling rate conditions, as often happens for natural systems. Smooth, near horizontal trends can be explained both by a low initial temperature and a change in cooling conditions from lower to higher cooling rates with decreasing temperature. Published studies demonstrate cooling rates for the Iwanaidake peridotites to be on the order of $10^{-4}$ - $10^{-1}$ °C/yr, while for extrusive rocks such as picrites, cooling rates are estimated at $10^{3}$ to $10^{4}$ °C/yr (Ozawa, 1984).

Finero diffusion curves derived within our study were redrawn assuming that the diameter of spinel grains (as considered by Ozawa, 1984), is equivalent to two times the distance from the grain boundary (d). These were then compared to constant cooling rate profiles compatible with presumed Finero conditions (initial temperature <900 °C, pressure 0.9 - 1.1 GPa, Fig. 3.10).

Our results indicate that Finero cooling rates are between $10^{-4}$ °C/yr and $10^{-2}$ °C/yr, corresponding to the steeper portion of the S-shaped curves of Fig. 3.10. Only one curve suggests slower cooling rates (FIN01A, $10^{-3}$-$10^{-2}$ °C/yr). These rates are within the range established for Japanese peridotites, but with a different slope. Peridotites of the Iwanaidake ophiolite have steep slopes, almost along constant cooling rate curves; Finero peridotites show gentle slopes, indicative of a rapid increase in cooling rate conditions between ~850 and ~650 °C.

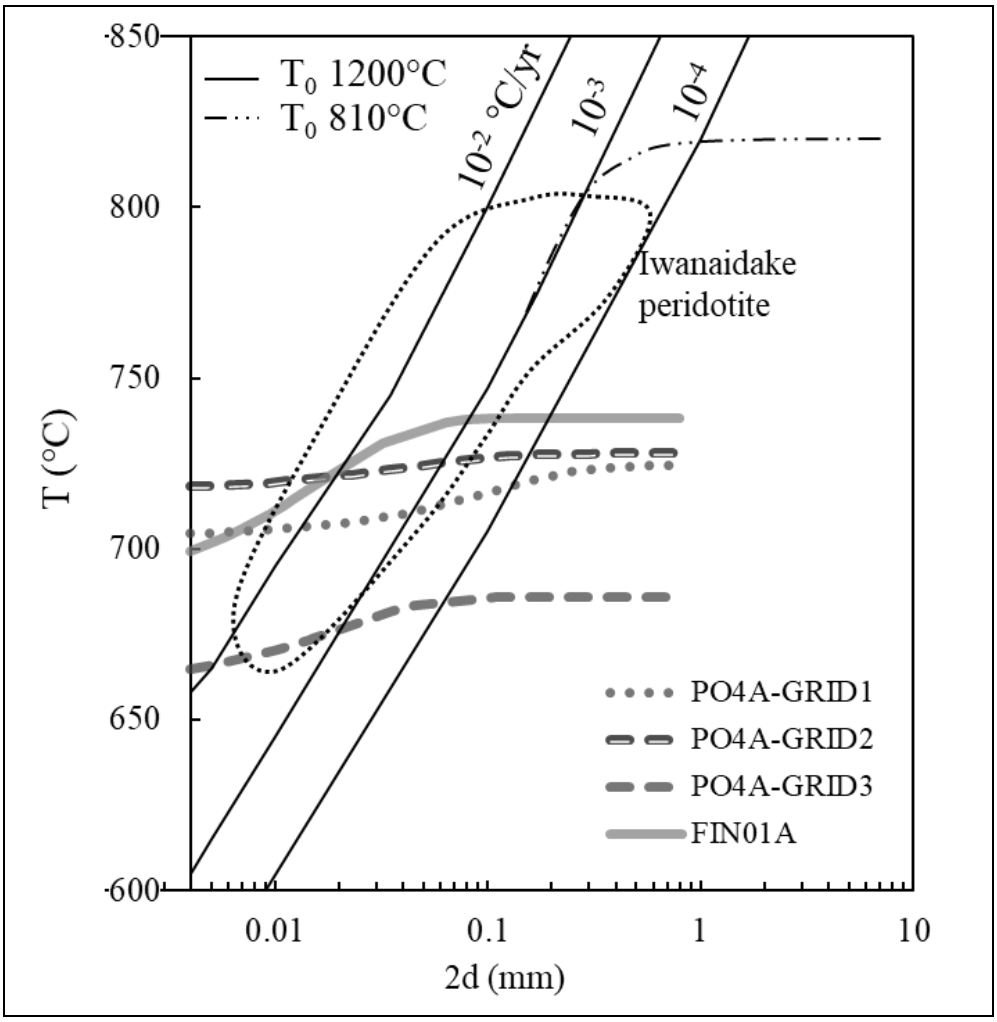


Fig. 3.10 2d vs T (°C) plot of Finero diffusion curves. Temperatures are calculated according to Fabriès (1979), constant cooling rate curves and Iwanaidake peridotite field are from Ozawa (1984). $T_0$: initial temperature for the calculation of constant cooling rate curves (modified after Bussolesi et al., 2019).

### 3.2.3.5. Finero thermal history

The thermal history of Finero massif has been established by various researcher datasets based on U-Pb zircon ages (Badanina et al., 2013; Grieco et al., 2001; Zanetti et al., 2016), diffusion of Pb and Zr in rutile (Smye and Stockli, 2014), geodynamical data (Wolff et al., 2012), and petrographic-mineralogic data (Giovanardi et al., 2013). Diffusivity profiles can add an important contribution to the reconstruction of the thermal history of the massif. Petrographic and chemical data suggest that at least two metasomatic events affected the Finero massif at different times (Grieco et al., 2004, 2001). During the first event, estimated in the Permian, reactions between a mafic melt and surrounding harzburgites produced chromitite pods and associated dunites, as well as a suite of secondary mineralogical phases such as clinopyroxenes and amphiboles in the harzburgite. The second metasomatic event was characterized by the intrusion of clinopyroxenite dykes, followed by the

infiltration in the harzburgite, along fractures, of a hydrous phase. The reaction between the water-rich fluid and the host rock produced phlogopite, the distinguishing feature of this second event.

The main metasomatic event that led to re-enrichment of the Finero body is still under debate. The volatile-rich fluids could have been derived from a crustal slab in a subduction setting (Hartmann and Wedepohl, 1993; Zanetti et al., 1999). A second possibility theorizes that fluids were derived from a mantle plume emplaced at the base of the subcontinental crust, in an extensional tectonic setting (Exley et al., 1982; Garuti et al., 2001). Chromitites and their dunite host bodies are generally accepted to have formed by metasomatic interaction of basic melts with surrounding harzburgite (Grieco et al., 2001), during an early Permian underplating event (288 ± 7 Ma) (Badanina et al., 2013). Following the Permian event, peculiar P-T conditions caused a re-heating that re-equilibrated the U-Pb system (Smye and Stockli, 2014): this resulted in a large time span documented by zircon ages within the matrix of chromitites dating from Late Triassic to Early Jurassic (Badanina et al., 2013; Grieco et al., 2001; Zanetti et al., 2016). The absence of melting in this time span suggests an upper limit to the maximum temperature of this re-heating event at 965 °C, that is, the solidus estimated for Finero harzburgites (Giovanardi et al., 2013).

The continuous cooling profile shown by our diffusivity data, without evidence of re-heating patterns suggests that there was no re-heating condition of the rocks, and is in agreement with a model requiring simple cooling from the high Permian temperatures. However, recent studies support the hypothesis of a long permanence, at least till Mesozoic time, of the Finero body at great depths, corresponding to ~1 GPa (Siena and Coltorti, 1989), or 0.9-1.1 GPa (Christy, 1989; Sills et al., 1983), based mainly on the reaction involving the formation of metamorphic sapphirine in gabbros of the Lower Internal Zone. Obtained cooling profiles can be better interpreted as due to complete re-setting of the olivine-spinel geothermometer. A long residence of the olivine-spinel system at temperatures just below the subsolidus completely re-homogenized olivine and spinel compositions. In this case, primary temperatures record the peak of the re-heating event at 849 °C, the highest primary temperature recorded. The Late Triassic chromitites zircon ages (208 Ma) (Grieco et al., 2001) thus date the time of the second thermal peak.

Exhumation of the Finero Complex initiated during the Early Jurassic (Giovanardi et al., 2013; Wolff et al., 2012; Zanetti et al., 2016). The exhumation event was rapid, bringing the complex to a shallow to mid-crustal position. The extensional activity is concurrent to the opening of the Piedmont Ocean. Exhumation was controlled by two major boundary faults, the Insubric Line and the Pogallo Line (Wolff et al., 2012).

Finero olivine and spinel diffusion curves show that their re-equilibration is very limited. This limited re-equilibration could have been influenced by a low initial temperature and/or reflects the rapid, increasing with time, cooling rate. Cooling rates of $10^{-4}$-$10^{-2}$ °C/yr, recorded at Finero agree with a rapid rate of exhumation to a shallow to mid-crustal position. This is a result similar to the one modelled for the Iwanaidake ophiolite of Japan (Ozawa, 1984).

The Ivrea Verbano Zone geotherm, estimated from geothermometric and geobarometric data determined for the amphibolite to granulite facies of rocks along the Strona Valley (Henk et al., 1997; Wolff et al., 2012) is 22 °C/km in the Permian. From the Permian onward, Finero cooling rates yield an initial exhumation velocity, in thermal equilibrium with the 22 °C/km geotherm, of 0.45 cm/yr, that, with time, increased up to 45 cm/yr. The initial velocity is lower than the regional 2 cm/yr tectonic uplift velocity (Wogelius and Bishop, 1989) suggesting that initial uplift of Finero massif did not occur in equilibrium with the geothermal gradient. If the ascent occurred at the estimated 2 cm/yr velocity and with a $10^{-4}$ °C/yr cooling rate, the uplift was almost adiabatic. Such exhumation conditions would provide supporting evidence for the Late Triassic thermal plume as a cause of the re-heating event. The increase of cooling rate up to $10^{-2}$ °C/yr results in an unrealistic 45 cm/yr uplift. As such an exhumation ascent occurred after the thermal peak, the fast final cooling rate could be due to the combination of rapid uplift with decreasing geothermal gradient following the Late Triassic re-heating.

### 3.2.4. Conclusion

Olivine and chromite diffusivity patterns are useful tools for the reconstruction of the thermal history of chromitites and associated dunites rocks down to at least 650 °C. The use of an exponential function to model XMg with distance from grain boundary minimizes potential error in the calculation of re-equilibrated and primary mineral compositions, producing more reliable temperature assessments.

An initial Early Permian metasomatic event was responsible for the formation of chromitite bodies and their host dunite within the Finero massif. This event is not recorded in chromite and olivine compositions as they were completely re-equilibrated during the Late-Triassic. Re-equilibration was caused by re-heating at temperatures up to 849 °C, just below the estimated 965 °C solidus temperature. This thermal peak can be dated at 208 Ma, the age recorded by zircons in chromitite, as it completely reset the zircon U-Pb system. A subsequent exhumational uplift of Finero to a mid-crustal position occurred during the Early Jurassic rifting event at increasing cooling rates, demonstrated by re-equilibration temperatures. Rapid final cooling rates follow the cessation of the Jurassic thermal peak as the geothermal gradient was decreasing.

# 3.3 Nea Roda

## 3.3.1. Mineralogy and texture

Small chromitite bodies occur to the East of the Nea Roda village (Fig. 3.11). Part of the samples (Tab. 3.6) was collected from a peridotite outcrop on the coast, where rare dunite dykes are enclosed within host harzburgite (Fig. 3.12A). Dunites are mostly fresh, and host small chromitite lenses up to 10 cm thick (Fig. 3.12B). Chromitites have a disseminated texture with rare chromite nodules marking some of the mineralized layer. Close to the peridotite outcrop, chromitite occurrences were found in a highly altered soil where altered massive chromitite samples were collected. Mineralogy and texture of altered chromitites will be discussed in Chapter 4.

Tab. 3.6 Nea Roda sampling and analyses (**bold**: EMPA; underlined: whole rock PGE content)

| Zone | Coordinates | Sample | Lithology |
|---|---|---|---|
| Dunite dyke | 40°22'45.8'' – 23°57'37.9'' | **GR58, GR62, GR63B** | Fresh dunite and chromitite |
| | 40°22'41.3'' – 23°57'50.5'' | NRO1, NRO3, | amphibolite |
| Dump | 40°22'56.832 – 23°57'36.404 | NRO4, NRO5, **NRO6, NRO9** | Altered chromitite |


Fig. 3.11 Nea Roda sample locations.

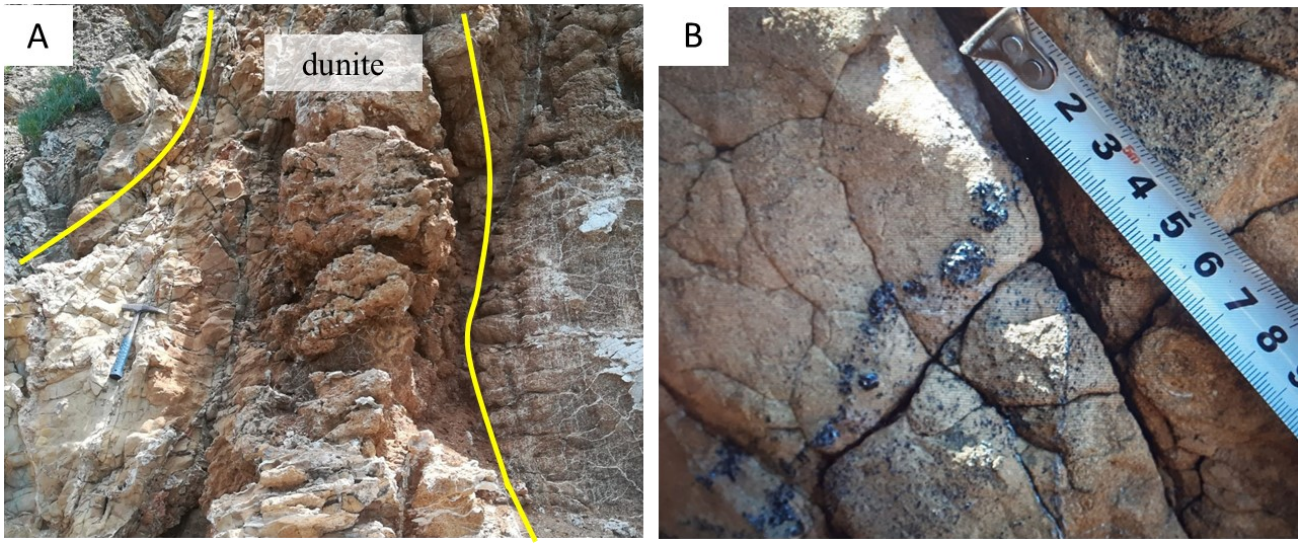


Fig. 3.12 Dunite dyke (A) hosting chromitite layers (B) in Nea Roda, Greece.

Chromite crystals within dunite-hosted chromitites have polygonal to irregular shape, with grain size ranging from submillimetric to millimetric (Fig. 3.13A, B), and show rare alteration into ferrian chromite (Fig. 3.13A). The silicate gangue is constituted by olivine grains partially replaced by serpentine, forming a typical mesh texture. Some chlorite crystal was detected close to ferrian chromite alteration. BMM and PGM were not detected in the samples.

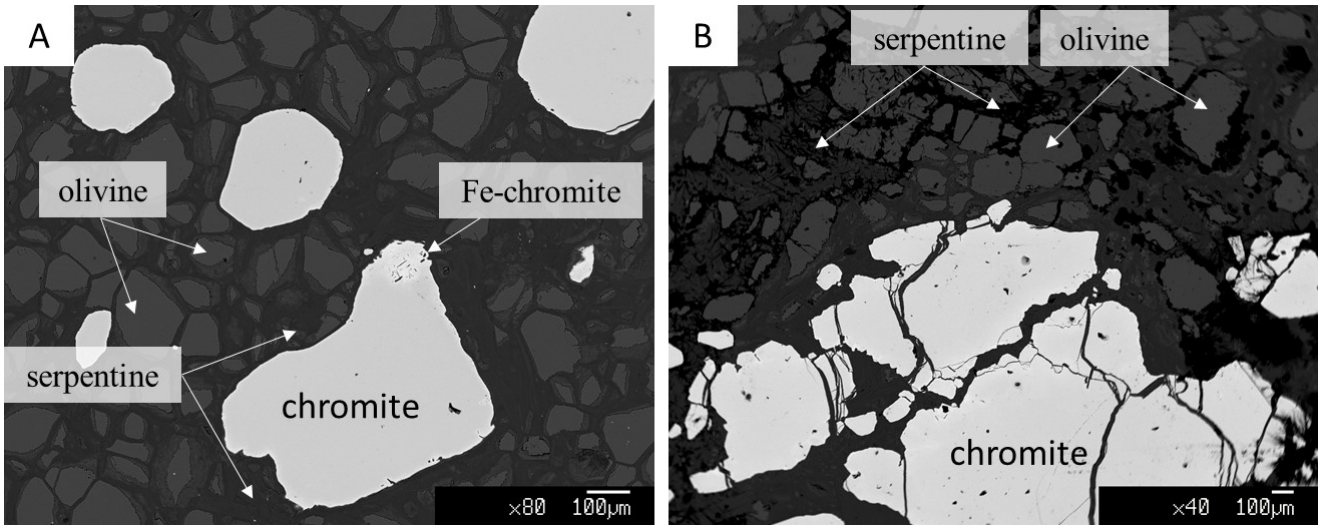


Fig. 3.13 A) and B) BSE images of chromitites from Nea Roda.

## 3.3.2. Mineral chemistry

*Chromite*

Chromite average compositions (Tab. 3.7) are based on core analyses of fresh chromitite samples, in order to avoid any zonation of the mineral. Complete microprobe analyses are reported in the Appendix (Tab. A3.8 to Tab. A3.11). All analyzed samples are chromitites with disseminated texture,

and their mineralogical composition is rather homogeneous. MgO content ranges between 5.28 and 10.22 wt%, with lower values in samples GR62 and GR63 and higher values in sample GR58. FeO content ranges between 18.05 and 25.69 wt%, and $Fe_2O_3$ content is lower than 5.01 wt%. $Cr_2O_3$ content ranges between 53.32 and 60.48 wt%, higher in sample GR58 than in samples GR62 and GR63, and $Al_2O_3$ content ranges between 8.84 and 13.83 wt%.

Spinels of sample GR58 are generally characterized by slightly higher $Cr_2O_3$ and MgO and lower $Al_2O_3$ and FeOtot with respect to samples GR62 and GR63. These slight differences reflect in a higher XMg [=Mg/(Mg+$Fe^{2+}$)] of sample GR58 (0.808 average) with respect to GR62 and GR63 (0.732 and 0.733 averages respectively), and also in a higher XCr [=Cr/(Cr+Al)].

Tab. 3.7 Major and trace elements average composition and standard deviation of chromite cores from Nea Roda disseminated chromitites. XCr [=Cr/(Cr+Al)]; XMg [=(Mg/(Mg+$Fe^{2+}$)]; bdl: below detection limit.

| Sample | GR58 | | GR63 | | GR62 | |
|---|---|---|---|---|---|---|
| Elem. | Avg | St.Dev | Avg | St.Dev | Avg | St.Dev |
| $TiO_2$ | **0.10** | 0.01 | **0.21** | 0.06 | **0.17** | 0.03 |
| $Al_2O_3$ | **9.58** | 0.39 | **12.89** | 0.61 | **13.47** | 0.35 |
| $Cr_2O_3$ | **60.21** | 0.19 | **54.21** | 0.45 | **55.24** | 0.79 |
| $V_2O_3$ | **0.06** | 0.02 | **0.10** | 0.03 | **bdl** | bdl |
| $Fe_2O_3$ | **1.85** | 0.22 | **3.77** | 0.63 | **0.89** | 0.66 |
| FeO | **19.63** | 1.04 | **22.11** | 0.64 | **23.91** | 0.98 |
| MnO | **0.19** | 0.06 | **0.25** | 0.05 | **0.24** | 0.07 |
| MgO | **9.15** | 0.71 | **8.03** | 0.48 | **6.80** | 0.63 |
| NiO | **0.03** | 0.04 | **0.06** | 0.05 | **0.03** | 0.03 |
| CaO | **0.01** | 0.01 | **0.01** | 0.01 | **0.01** | 0.01 |
| ZnO | **0.10** | 0.08 | **0.17** | 0.11 | **0.04** | 0.03 |
| TOT | **100.91** | 0.28 | **101.75** | 0.39 | **100.83** | 0.54 |
| Ti | **0.00** | 0.00 | **0.01** | 0.00 | **0.00** | 0.00 |
| Al | **0.37** | 0.01 | **0.50** | 0.02 | **0.52** | 0.01 |
| Cr | **1.57** | 0.01 | **1.40** | 0.01 | **1.44** | 0.01 |
| V | **0.00** | 0.00 | **0.00** | 0.00 | **0.00** | 0.00 |
| $Fe^{3+}$ | **0.05** | 0.01 | **0.09** | 0.02 | **0.02** | 0.02 |
| $Fe^{2+}$ | **0.54** | 0.03 | **0.60** | 0.02 | **0.66** | 0.03 |
| Mn | **0.01** | 0.00 | **0.01** | 0.00 | **0.01** | 0.00 |
| Mg | **0.45** | 0.03 | **0.39** | 0.02 | **0.34** | 0.03 |
| Ni | **0.00** | 0.00 | **0.00** | 0.00 | **0.00** | 0.00 |
| Ca | **0.00** | 0.00 | **0.00** | 0.00 | **0.00** | 0.00 |
| Zn | **0.00** | 0.00 | **0.00** | 0.00 | **0.00** | 0.00 |
| XCr | **0.808** | 0.007 | **0.732** | 0.003 | **0.733** | 0.006 |
| XMg | **0.454** | 0.032 | **0.393** | 0.021 | **0.336** | 0.030 |

*Olivine*

Olivine mineral chemistry is based on core analyses of olivine crystals (Tab. 3.8). Olivine composition is strongly forsteritic and rather homogeneous in all the samples. MgO content varies between 50.1 and 55.0 wt% and FeO ranges between 4.6 and 8.3 wt%. XMg ratio varies between 0.916 and 0.953. Olivines also show a Ni enrichment, varying between 0.32 and 0.54 wt%.

Tab. 3.8 Major and trace elements average composition and standard deviation of olivine cores from Nea Roda disseminated chromitites. XMg [=(Mg/(Mg+$Fe^{2+}$)].

| Sample | GR-58 | | GR63 | | GR62 | |
|---|---|---|---|---|---|---|
| Elem. | Avg | St.Dev | Avg | St.Dev | Avg | St.Dev |
| $SiO_2$ | **41.19** | 0.28 | **39.63** | 0.98 | **42.29** | 0.41 |
| $TiO_2$ | **0.02** | 0.02 | **0.01** | 0.01 | **0.01** | 0.01 |
| $Al_2O_3$ | **0.00** | 0.01 | **0.00** | 0.01 | **0.01** | 0.01 |
| $Cr_2O_3$ | **0.04** | 0.05 | **0.11** | 0.08 | **0.07** | 0.07 |
| FeO | **4.81** | 0.18 | **6.70** | 0.15 | **7.30** | 0.35 |
| MnO | **0.08** | 0.02 | **0.10** | 0.03 | **0.10** | 0.06 |
| MgO | **51.86** | 0.19 | **51.28** | 0.85 | **51.43** | 0.51 |
| NiO | **0.43** | 0.05 | **0.43** | 0.04 | **0.37** | 0.03 |
| CaO | **0.01** | 0.01 | **0.01** | 0.01 | **0.01** | 0.01 |
| ZnO | **0.03** | 0.03 | **0.03** | 0.04 | **0.01** | 0.02 |
| TOT | **98.49** | 0.38 | **98.30** | 0.87 | **101.60** | 0.62 |
| Si | **1.00** | 0.00 | **0.97** | 0.02 | **1.01** | 0.01 |
| Ti | **0.00** | 0.00 | **0.00** | 0.00 | **0.00** | 0.00 |
| Al | **0.00** | 0.00 | **0.00** | 0.00 | **0.00** | 0.00 |
| Cr | **0.00** | 0.00 | **0.00** | 0.00 | **0.00** | 0.00 |
| $Fe^{2+}$ | **0.10** | 0.00 | **0.14** | 0.00 | **0.15** | 0.01 |
| Mn | **0.00** | 0.00 | **0.00** | 0.00 | **0.00** | 0.00 |
| Mg | **1.89** | 0.01 | **1.88** | 0.02 | **1.83** | 0.01 |
| Ni | **0.01** | 0.00 | **0.01** | 0.00 | **0.01** | 0.00 |
| Ca | **0.00** | 0.00 | **0.00** | 0.00 | **0.00** | 0.00 |
| Zn | **0.00** | 0.00 | **0.00** | 0.00 | **0.00** | 0.00 |
| XMg | **0.951** | 0.002 | **0.932** | 0.001 | **0.926** | 0.003 |

*Serpentine and chlorite*

Nea Roda samples are partially serpentinized, and minerals of the antigorite/chrysotile/lizardite subgroup replace olivine crystals along the rims (Tab. 3.9). Chlorite minerals of the chlinochlore species were also detected (Tab. 3.9), associated to partially ferrian chromitized rims.

Tab. 3.9 Major and trace elements average composition and standard deviation of serpentine and chlorite crystals from Nea Roda disseminated chromitites; bdl: below detection limit

| Mineral | Serpentine | | Chlorite | |
|---|---|---|---|---|
| Variety | **antigorite/chrysotile/lizardite** | | **chlinochlore** | |
| Elem. | Avg | St.Dev | Avg | St.Dev |
| $SiO_2$ | **40.65** | 1.71 | **31.75** | 1.10 |
| $TiO_2$ | **0.01** | 0.01 | **0.01** | 0.02 |
| $Al_2O_3$ | **0.07** | 0.19 | **14.57** | 1.84 |
| $Cr_2O_3$ | **0.10** | 0.17 | **3.38** | 0.98 |
| FeO | **4.27** | 1.28 | **2.03** | 0.29 |
| MnO | **0.07** | 0.05 | **0.03** | 0.04 |
| MgO | **38.02** | 2.36 | **32.68** | 1.22 |
| NiO | **0.27** | 0.33 | **bdl** | |
| CaO | **0.08** | 0.08 | **0.07** | 0.07 |
| ZnO | **0.03** | 0.05 | **0.03** | 0.04 |
| TOT | **83.61** | 1.38 | **84.61** | 2.00 |

*Mg-$Fe^{2+}$ zoning in olivine and spinel*

In Nea Roda, data do not show a correlation between olivine XMg and distance from the grain boundary (Fig. 3.14A). The only correlation between XMg and distance from the grain boundary was found for chromites (Fig. 3.14B). Olivines XMg show a wide dispersion of data, and do not present the increase in XMg values close to the grain boundary typical of olivine-chromite re-equilibration. Chromites show a zonation with ΔXMg up to 0.20. The zonation extends as far as 0.3 mm from the grain boundary (Fig. 3.14 B).

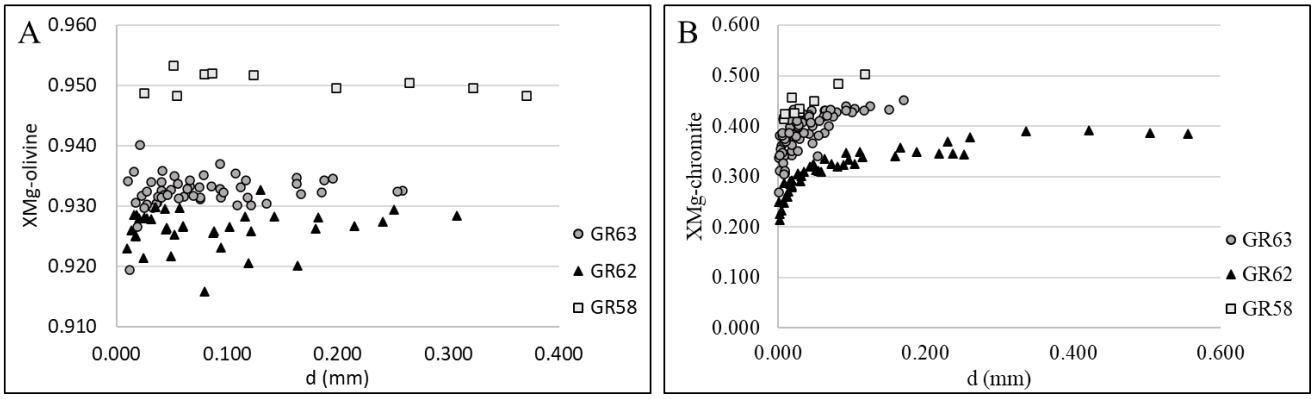


Fig. 3.14 XMg variation vs distance from the grain boundary in A) olivines in chromitites and B) chromites in chromitites.

## 3.3.3. Discussion

### 3.3.3.1. Diffusivity curve analyses (primary and re-equilibration compositions)

Olivine and spinel compositions at grain boundaries reflect the critical temperature below which subsolidus exchange cannot proceed. Within the cores of mineral grains, in particular of larger-sized grains, minerals appear to retain their primary composition, which can be used to estimate their primary crystallization temperature. As XMg diffusion curves follow an exponential trend, rim compositions are sensitive to the distance from the grain boundary. Bussolesi et al. (2019) propose an exponential modeling for XMg diffusion curves, and proceed to calculate primary ($XMg_{pr}$) and re-equilibrated ($XMg_{eq}$) XMg values for olivine and chromite crystals.

Nea Roda diffusivity curves, however, present peculiar patterns (Fig. 3.14A, B). XMg variation with the distance from the grain boundary is absent within olivines, while chromites apparently present a "normal" trend (e.g. XMg decreases close to the grain boundary). A possible explanation would be the lack of subsolidus re-equilibration in the Nea Roda samples, that would explain the absence of a diffusivity pattern in olivine crystals. The presence of diffusivity patterns in chromites could therefore be an artefact explained either by incipient ferrian-chromitization or by a magmatic zoning.

### 3.3.3.2. Geothermometry

The lack of diffusion patterns in olivine crystals, and the possibility that the XMg variation in chromites could be due either to magmatic zoning or to incipient ferrian chromitization, allows only the calculation of a temperature using core analyses (hence allowing calculation of primary temperatures). In Tab. 3.10 are reported the average core values and temperature estimates using Ballhaus et al. (1991) geothermometer.

Tab. 3.10 Parameters for the calculation of primary temperatures using Ballhaus et al. (1991) calibration.

| Sample | GR58 | GR63 | GR62 |
|---|---|---|---|
| XMg-ol | 0.950 | 0.932 | 0.926 |
| XMg-sp | 0.454 | 0.393 | 0.332 |
| XCr*-sp[1] | 0.790 | 0.704 | 0.726 |
| $XFe^{3+}$-sp[2] | 0.078 | 0.132 | 0.036 |
| XTi-sp[3] | 0.002 | 0.005 | 0.004 |
| KD | 23.058 | 21.106 | 25.259 |
| P (Gpa) | 0.3 | 0.3 | 0.3 |
| R | 8.3145 | 8.3145 | 8.3145 |
| **T(°C)** | **633** | **656** | **551** |

[1] $Cr/(Cr+Al+Fe^{3+})$ [2] $Fe^{3+}/(Fetot)$ [3] mol Ti

Estimated temperatures for disseminated chromitite range from 550°C to 656°C. Olivine-spinel thermometry on Nea Roda chromitites was performed by Michailidis et al. (1995) following Roeder et al. (1979) and Fabriès (1979) calibrations, with temperature estimates of 530-620°C and 640-745°C respectively. These low temperatures have been interpreted as re-equilibration temperatures (Michailidis et al., 1995). However, the lack of diffusion patterns in olivine seems more in agreement with a limited or absent Mg-$Fe^{2+}$ exchange. This could be achieved through rapid cooling and consequent freeze of the exchange reaction.

## 3.3.4. Conclusion

Nea Roda ophiolite hosts small disseminated chromitite bodies enclosed within dunite dykes. Mineral chemistry analyses of spinel and olivine along traverses highlighted the absence of diffusivity patterns in olivines, and the presence of "fake" patterns within spinels, probably due to magmatic zoning or ferrian chromitization. This allowed only the calculation of a primary temperature, using only core data. Resulting temperatures are comprised between 550°C to 656°C in accordance with data from the same locality. These low temperatures, coupled with the absence of diffusion patterns, can be explained by a genesis in a relatively surficial environment, followed by rapid cooling. Genetic and post-genetic features of Nea Roda will be discussed in more detail in Chapter 4.

# 3.4 Iballe

## 3.4.1. Mineralogy and texture

Chromitite and dunite samples (Tab. 3.11) were collected from the Iballe mine, in Northern Albania (Fig. 3.15) and are part of the rock samples collection of the University of Milan.

Tab. 3.11 Iballe sampling and analyses (**bold**: EMPA).

| Zone | Coordinates | Sample | Lithology |
|---|---|---|---|
| Iballe | 42° 11’ 00” N, 49° 57’ 14” E | PUKA1, **PUKA2, PUKA3** | Chromitite + dunite |
| | 42°11’ 32.5” N, 19° 77’ 44” E | **OLPU1**, OLPU2, **OLPU3** | dunite |


Fig. 3.15 Iballe samples location.

Chromitites and dunites are mostly fresh, with little to absent serpentinization. Chromitites present a massive texture, with subhedral chromite crystals rarely showing alteration into ferrian chromite. Olivine, the primary silicate associated to chromite, is an interstitial phase. Serpentine is not widespread, but when present partially replaces olivine grains along the rim (Fig. 3.16A). Dunites present a mineralogical assemblage constituted by olivine, minor clinopyroxene and dispersed chromite crystals. Olivine crystals are fractured and partially replaced by serpentine along the rim.

Anhedral clinopyroxene crystals are found in abundance within the samples. Chromites show polygonal shape, with rounded edges, and are partially fractured. No ferrian chromite alteration was detected (Fig. 3.16B).

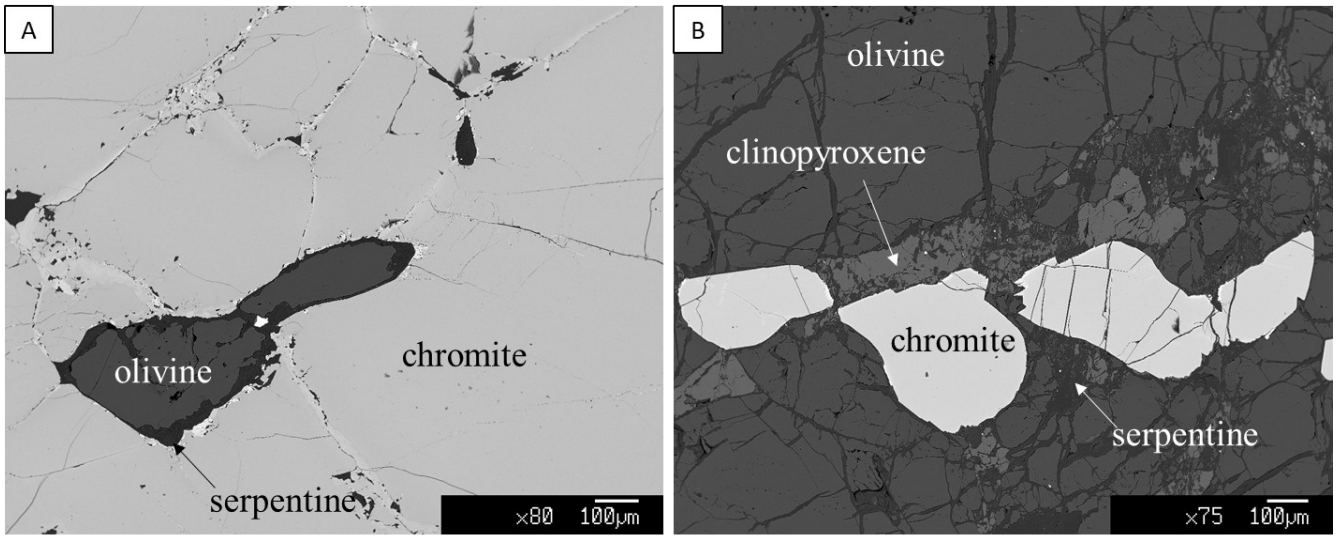


Fig. 3.16 BSE images of A) massive chromitite and B) dunite with dispersed spinel within Iballe.

## 3.4.2. Mineral chemistry

*Chromite*

Chromite average compositions (Tab. 3.12) are based on core analyses of fresh chromitite samples, in order to avoid any zonation of the mineral. Complete microprobe analyses are reported in the Appendix (Tab. A3.12 to Tab. A3.16). Analyzed samples consist of dunites with dispersed spinels (OLPU-) and massive chromitites (PUKA-), which show a wide variability.

Chromite in dunites is characterized by MgO content ranging between 4.18 and 11.54 wt% and FeO content between 16.10 and 22.50 wt%. $Cr_2O_3$ and $Al_2O_3$ contents vary between 61.33 and 63.85 wt% and between 7.23 and 9.22 wt% respectively. XMg ranges between 0.363 and 0.561, and XCr ranges between 0.817 and 0.855.

Chromite in massive chromitites is characterized by higher MgO contents, ranging between 15.52 and 16.38 wt%, and lower FeO contents, ranging between 11.25 and 12.66 wt%. $Cr_2O_3$ contents are lower than in dunite spinels, and range between 42.87 and 46.76 wt%, while $Al_2O_3$ contents are higher, ranging from 22.64 to 26.69 wt%. These compositional differences result in a higher XMg (0.689-0.717) and lower XCr (0.521-0.581) with respect to dispersed spinels in dunites.

Tab. 3.12 Major and trace elements average content and standard deviation of chromite cores from Iballe.

| | DUNITE | | | | MASSIVE CHROMITITE | | | |
|---|---|---|---|---|---|---|---|---|
| | OLPU1 | | OLPU3 | | PUKA2 | | PUKA3 | |
| | **Avg** | St.Dev | **Avg** | St.Dev | **Avg** | St.Dev | **Avg** | St.Dev |

| | | | | | | | | |
|---|---|---|---|---|---|---|---|---|
| $TiO_2$ | **0.06** | 0.04 | **0.08** | 0.02 | **0.12** | 0.02 | **0.06** | 0.03 |
| $Al_2O_3$ | **8.88** | 0.26 | **8.11** | 0.27 | **26.39** | 0.16 | **24.06** | 0.64 |
| $Cr_2O_3$ | **61.92** | 0.40 | **63.00** | 0.52 | **43.35** | 0.31 | **46.07** | 0.39 |
| $V_2O_3$ | **0.17** | 0.02 | **0.00** | 0.00 | **0.00** | 0.00 | **0.20** | 0.04 |
| $Fe_2O_3$ | **1.90** | 0.28 | **0.06** | 0.09 | **3.36** | 0.28 | **2.90** | 0.49 |
| FeO | **16.99** | 0.89 | **20.24** | 0.71 | **12.20** | 0.27 | **11.73** | 0.24 |
| MnO | **0.15** | 0.03 | **0.14** | 0.06 | **0.07** | 0.05 | **0.04** | 0.02 |
| MgO | **10.84** | 0.66 | **8.36** | 0.38 | **15.93** | 0.20 | **15.84** | 0.17 |
| NiO | **0.04** | 0.04 | **0.03** | 0.04 | **0.16** | 0.03 | **0.20** | 0.04 |
| CaO | **0.01** | 0.01 | **0.01** | 0.01 | **0.01** | 0.01 | **0.01** | 0.01 |
| ZnO | **0.19** | 0.12 | **0.04** | 0.04 | **0.02** | 0.03 | **0.06** | 0.06 |
| TOT | **101.19** | 0.42 | **100.09** | 0.63 | **101.61** | 0.57 | **101.19** | 0.48 |
| Ti | **0.00** | 0.00 | **0.00** | 0.00 | **0.00** | 0.00 | **0.00** | 0.00 |
| Al | **0.34** | 0.01 | **0.32** | 0.01 | **0.91** | 0.01 | **0.84** | 0.02 |
| Cr | **1.60** | 0.01 | **1.68** | 0.01 | **1.01** | 0.01 | **1.08** | 0.01 |
| V | **0.00** | 0.00 | **0.00** | 0.00 | **0.00** | 0.00 | **0.00** | 0.00 |
| $Fe^{3+}$ | **0.05** | 0.01 | **0.00** | 0.00 | **0.07** | 0.01 | **0.06** | 0.01 |
| $Fe^{2+}$ | **0.46** | 0.03 | **0.57** | 0.02 | **0.30** | 0.01 | **0.29** | 0.01 |
| Mn | **0.00** | 0.00 | **0.00** | 0.00 | **0.00** | 0.00 | **0.00** | 0.00 |
| Mg | **0.53** | 0.03 | **0.42** | 0.02 | **0.70** | 0.01 | **0.70** | 0.01 |
| Ni | **0.00** | 0.00 | **0.00** | 0.00 | **0.00** | 0.00 | **0.00** | 0.00 |
| Ca | **0.00** | 0.00 | **0.00** | 0.00 | **0.00** | 0.00 | **0.00** | 0.00 |
| Zn | **0.00** | 0.00 | **0.00** | 0.00 | **0.00** | 0.00 | **0.00** | 0.00 |
| XCr | **0.824** | 0.004 | **0.839** | 0.005 | **0.524** | 0.002 | **0.562** | 0.008 |
| XMg | **0.532** | 0.028 | **0.424** | 0.019 | **0.699** | 0.007 | **0.706** | 0.006 |

*Olivine*

Olivine average compositions and standard deviations of dunites and massive chromitites are reported in Tab. 3.13. Olivine crystals in dunites are characterized by MgO content ranging between 49.34 and 54.64 wt% and FeO content between 5.56 and 6.90 wt%. XMg varies between 0.930 and 0.943. NiO content varies between 0.38 and 0.53 wt%.

Olivines in massive chromitites are characterized by MgO content ranging between 50.34 and 53.80 wt%, FeO content ranging between 3.74 and 6.08 wt% and XMg varying between 0.939 and 0.962. NiO content varies between 0.68 and 0.96 wt%.

Tab. 3.13 Major and trace elements average content and standard deviation of olivine cores from Iballe.

| | DUNITE | | | | MASSIVE CHROMITITE | | | |
|---|---|---|---|---|---|---|---|---|
| | OLPU1 | | OLPU3 | | PUKA2 | | PUKA3 | |
| | **Avg** | St.Dev | **Avg** | St.Dev | **Avg** | St.Dev | **Avg** | St.Dev |
| $SiO_2$ | **41.28** | 0.73 | **40.56** | 0.58 | **41.70** | 0.76 | **41.43** | 0.32 |
| $TiO_2$ | **0.01** | 0.02 | **0.01** | 0.02 | **0.01** | 0.01 | **0.01** | 0.01 |
| $Al_2O_3$ | **0.01** | 0.01 | **0.01** | 0.01 | **0.03** | 0.10 | **0.01** | 0.02 |
| $Cr_2O_3$ | **0.01** | 0.01 | **0.01** | 0.02 | **0.03** | 0.09 | **0.16** | 0.11 |
| FeO | **5.90** | 0.14 | **6.49** | 0.28 | **5.36** | 0.46 | **4.21** | 0.16 |
| MnO | **0.08** | 0.03 | **0.08** | 0.05 | **0.07** | 0.04 | **0.07** | 0.02 |

| | | | | | | | | |
|---|---|---|---|---|---|---|---|---|
| MgO | **52.16** | 0.78 | **52.20** | 0.53 | **52.63** | 0.85 | **52.33** | 0.73 |
| NiO | **0.44** | 0.05 | **0.38** | 0.03 | **0.56** | 0.05 | **0.840** | 0.10 |
| CaO | **0.03** | 0.02 | **0.04** | 0.02 | **0.02** | 0.02 | **0.02** | 0.01 |
| ZnO | **0.03** | 0.04 | **0.01** | 0.02 | **0.01** | 0.02 | **0.02** | 0.04 |
| TOT | **99.95** | 0.91 | **99.79** | 0.82 | **100.42** | 0.89 | **99.09** | 0.95 |
| Si | **0.99** | 0.02 | **0.98** | 0.01 | **1.00** | 0.02 | **1.00** | 0.01 |
| Ti | **0.00** | 0.00 | **0.00** | 0.00 | **0.00** | 0.00 | **0.00** | 0.00 |
| Al | **0.00** | 0.00 | **0.00** | 0.00 | **0.00** | 0.00 | **0.00** | 0.00 |
| Cr | **0.00** | 0.00 | **0.00** | 0.00 | **0.00** | 0.00 | **0.00** | 0.00 |
| $Fe^{2+}$ | **0.12** | 0.00 | **0.13** | 0.01 | **0.11** | 0.01 | **0.09** | 0.00 |
| Mn | **0.00** | 0.00 | **0.00** | 0.00 | **0.00** | 0.00 | **0.00** | 0.00 |
| Mg | **1.87** | 0.02 | **1.88** | 0.01 | **1.88** | 0.02 | **1.89** | 0.01 |
| Ni | **0.01** | 0.00 | **0.01** | 0.00 | **0.01** | 0.00 | **0.02** | 0.00 |
| Ca | **0.00** | 0.00 | **0.00** | 0.00 | **0.00** | 0.00 | **0.00** | 0.00 |
| Zn | **0.00** | 0.00 | **0.00** | 0.00 | **0.00** | 0.00 | **0.00** | 0.00 |
| XMg | **0.940** | 0.002 | **0.935** | 0.003 | **0.945** | 0.004 | **0.957** | 0.002 |

*Mg-$Fe^{2+}$ zoning in olivine and spinel*

Data show a correlation of olivine and chromite XMg with distance from the grain boundary (Fig. 3.17), varying between chromitites and dunites.

Olivines in dunite always show a zonation approaching the olivine-chromite boundary, with an increase in XMg up to 0.020. The zonation usually extends as far as 150 μm from the intergranular limit (Fig. 3.17A). Chromites in dunites show a zonation with a ΔXMg about 2 times larger than the one in olivines, and the extent of the zonation is lower than 0.1 mm (Fig. 3.17B).

Olivines in chromitite show a zonation only in one of the two cases, due to limited grain size of some olivine crystals which prevented gaining data at a distance from the grain boundary > 100 μm. The increase in XMg close to the grain boundary is about 0.020, and the zonation extends as far as 350 μm (Fig. 3.17A). Chromites in chromitites show a decrease in XMg close to the grain boundary. The decrease is limited to the first microns (<200 μm) and the maximum ΔXMg is 0.05 (Fig. 3.17B).

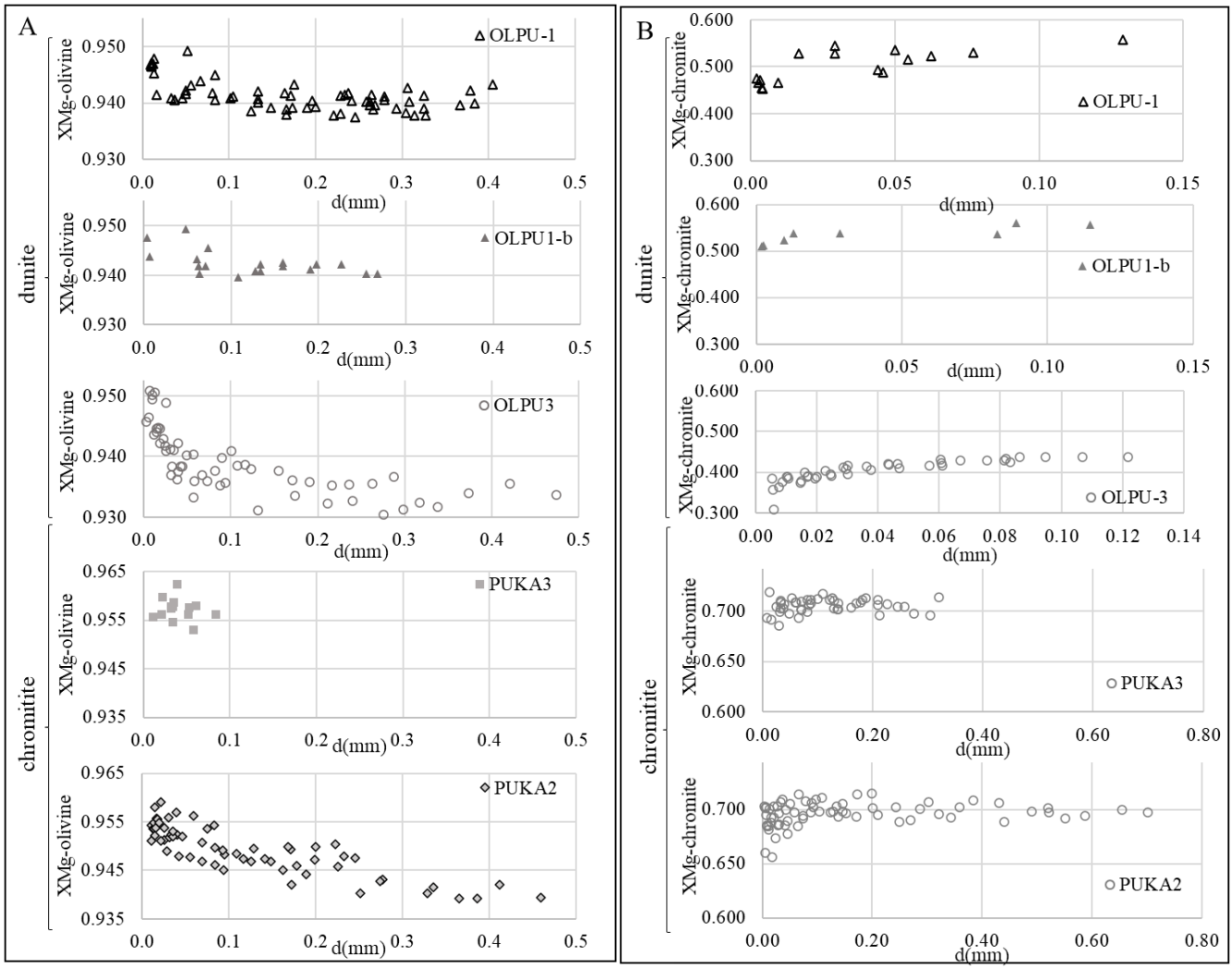


Fig. 3.17 XMg variation vs distance from the intergranular limit within A) olivines in dunites and chromitites and B) chromites in dunites and chromitites.

## 3.4.3. Discussion

### 3.4.3.1. Diffusivity curve analyses (primary and re-equilibration compositions)

Diffusivity curves were modelled for spinel and olivine datasets (Tab. 3.14, Fig. 3.18). The computation of primary and re-equilibrated XMg values of olivine was always possible in dunite, while it was possible for only one chromitite sample (PUKA2). Within sample PUKA3 the computation was not possible, due to the small crystal size of olivines, which are completely re-equilibrated. Chromite XMg, on the contrary, was computed in all the analyzed samples.

The exponential curves thus modelled provide also an estimate of a diffusion distance beyond which there is no more subsolidus exchange. Diffusion patterns for olivine and chromite crystals are different in the two lithologies. In massive chromitites, the only olivine pattern extends for quite a distance,

reaching the asymptote between 0.5 and 1 mm. Olivine patterns within dunites, on the contrary, show a diffusion distance comprised between 80 and 150 µm.

Chromite patterns within massive chromitites are quite smooth, different from the more abrupt ones found in the Finero complex. Diffusion distance ranges between 40 and 50 µm from the grain boundary. Within dunites, chromites show even smoother patterns, and the diffusion distance is below 100 µm.

Tab. 3.14 Parameters a, b, c and associated standard error of calculated curves and primary (pr) and re-equilibrated (eq) XMg atomic ratios of chromites and olivines for three host rocks.

| **Chromite** | | | | | | | | | |
|---|---|---|---|---|---|---|---|---|---|
| Sample | Host rock | a | St.Er. | b | St.Er. | c | St.Er. | $XMg_{pr}$ | $XMg_{eq}$ |
| OLPU-1 | Dunite | 0.527 | 0.010 | 0.081 | 0.019 | 3.87E-35 | 2.21E-33 | 0.527 | 0.446 |
| OLPU1-b | Dunite | 0.551 | 0.006 | 0.045 | 0.010 | 6.49E-27 | 2.23E-25 | 0.551 | 0.506 |
| OLPU-3 | Dunite | 0.443 | 0.007 | 0.078 | 0.005 | 6.42E-11 | 3.47E-10 | 0.443 | 0.364 |
| PUKA2 | Chromitite | 0.697 | 0.003 | 0.053 | 0.017 | 1.43E-24 | 3.63E-23 | 0.697 | 0.644 |
| PUKA3 | Chromitie | 0.707 | 0.001 | 0.024 | 0.012 | 1.64E-24 | 4.45E-23 | 0.707 | 0.683 |
| **Olivine** | | | | | | | | | |
| Sample | Host rock | a | St.Er. | b | St.Er. | c | St.Er. | $XMg_{pr}$ | $XMg_{eq}$ |
| OLPU-1 | Dunite | 0.940 | 0.000 | -0.008 | 0.001 | 4.28E-09 | 2.44E-08 | 0.940 | 0.948 |
| OLPU1-b | Dunite | 0.941 | 0.001 | -0.005 | 0.001 | 7.78E-13 | 1.26E-11 | 0.941 | 0.947 |
| OLPU-3 | Dunite | 0.934 | 0.001 | -0.015 | 0.002 | 8.52E-12 | 4.45E-11 | 0.934 | 0.950 |
| PUKA2 | Chromitite | 0.934 | 0.006 | -0.020 | 0.006 | 5.14E-02 | 7.81E-02 | 0.934 | 0.955 |
| PUKA3 | Chromitie | n.c. | n.c. | n.c. | n.c. | n.c. | n.c. | 0.957* | 0.957* |
| * Calculated as average XMg value; n.c. not computable | | | | | | | | | |

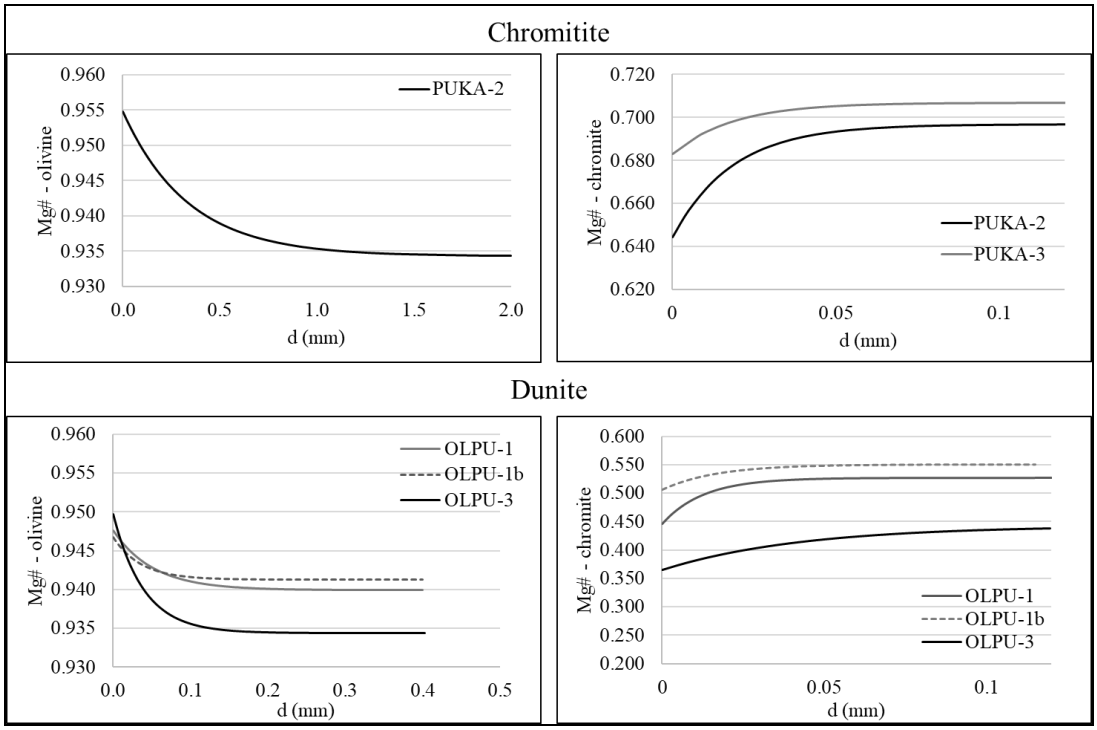

Fig. 3.18 Diffusivity curve of olivines and chromites in chromitites and dunites from the Iballe mine; Mg# [=Mg/(Mg+$Fe^{2+}$)]; d (mm): distance from the grain boundary.

### 3.4.3.2. Geothermometry

Temperature estimates were applied to re-equilibrated and primary XMg values following Ballhaus et al. (1991) calibration (Table 3.15). The olivine-spinel re-equilibrated temperatures are 626 and 783 °C within chromitites, and range between 533 and 723 °C in dunite. Primary temperatures in chromitites are 803 and 992°C. Temperatures recorded within dunites are lower, ranging between 658 and 804 °C.

Tab. 3.15 Primary and re-equilibrated temperatures ($T_{pr}$ and $T_{eq}$ respectively); n.c.: not computable.

| Sample | Lithology | $T_{pr}$(°C) | $T_{eq}$(°C) |
|---|---|---|---|
| OLPU-1 | dunite | 778 | 658 |
| OLPU-1b | dunite | 804 | 723 |
| OLPU-3 | dunite | 658 | 533 |
| PUKA2 | chromitite | 992 | 626 |
| PUKA3 | chromitite | 803* | 783* |

* values are based on averages, and are underestimated (Tpr) and overestimated (Teq)

Re-equilibration temperatures record the closing temperatures of the subsolidus mineral exchange system. Within peridotites, olivine-spinel is the system that "freezes" last with decreasing temperatures, allowing a determination of the thermal history of the rocks down to ~650 °C. Primary temperatures represent the threshold temperatures below which diffusivity cannot maintain compositional homogeneity within the crystals (Fabriès, 1979; Freer, 1981; Greenfield et al., 2013; Irvine, 1965).

Iballe temperatures are in agreement with geothermometry data obtained by (Saccani and Tassinari, 2015) for Eastern and Western Mirdita Ophiolites, which vary between 725 and 810°C within mafic-ultramafic cumulates.

### 3.4.3.3. Cooling rates

Mg-$Fe^{2+}$ zoning used to infer primary and re-equilibrated compositions and temperatures can also be used to estimate a cooling rate in ultramafic rocks (Ozawa, 1984, 1983). Cooling rates for the Krabbi massif were assessed through comparison with cooling rate profiles calculated by Ozawa (1984) for the Iwanaidake peridotites. Fig. 3.19 is a semi-logarithmic plot of grain diameter vs T(°C): it results in a function with two knees and two asymptotes. The asymptote at higher temperatures reflects the presence of non re-equilibrated core areas for larger grains that apparently preserve the primary composition. The asymptote at lower temperatures is a mathematical construct that reflects the re-equilibrated areas approaching the grain boundary (d→0). The steeper portion of the curve is ascribed

to the cooling rates of the rocks. These trends follow constant cooling rate curves or, when they deviate from these patterns, imply a variable cooling rate. Thus, a deviation within the dataset plot indicates a change in cooling rate conditions, as often happens for natural systems. Smooth, near horizontal trends can be explained both by a low initial temperature and a change in cooling conditions from lower to higher cooling rates with decreasing temperature. In Fig. 3.19 are reported constant cooling rate curves for peridotite spinels with XCr = 0.78 (similar to spinels in OLPU samples) and for peridotite spinels with XCr = 0.50), similar to spinels in PUKA samples.

Iballe diffusion curves have been calculated for samples PUKA2, OLPU-3 and an average between OLPU-1 and OLPU-1b. Sample PUKA 3 was not considered due to the lack of diffusion patterns. Iballe diffusion curves derived within our study were redrawn assuming that the diameter of spinel grains (as considered by Ozawa (1984), is equivalent to two times the distance from the grain boundary (d).

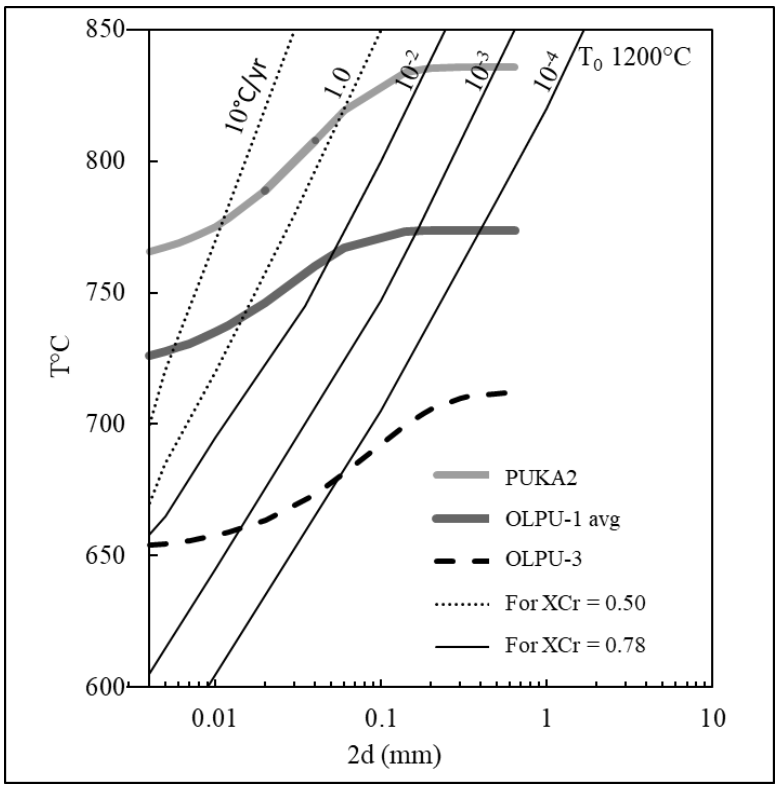


Fig. 3.19 2d *vs* T (°C) plot of Iballe diffusion curves. Temperatures are calculated according to Fabriès (1979), constant cooling rate curves for XCr 0.50 and 0.78 are from Ozawa (1984). $T_0$: initial temperature for the calculation of constant cooling rate curves.

Our results indicate that Iballe cooling rates are highly variable between the different samples. OLPU-3 presents the lowest temperature (Tab. 3.15), and also the lowest cooling rate, varying from < $10^{-4}$ to $10^{-4}$ °C/yr. The other dunite sample, OLPU-1 (which is an average between two curves obtained within the same sample), shows higher temperature and cooling rate (> $10^{-2}$ °C/yr). Massive chromitites

present a curve with steeper inclines, implying almost a constant cooling rate, with values comprised between 1 and 10 °C/yr. These different rates can be explained with a different genetic history of chromitites and dunites, as suggested also by the differences in spinel mineral chemistry.

### 3.4.3.4. Iballe genetic history

Chromitites in ophiolites are generally divided into high-Cr chromitites, which are widespread and interpreted as generated from boninitic magmas in suprasubduction settings, and high-Al chromitites, more rare, and interpreted as generated from less refractory magmas at mid-ocean ridge settings (Ballhaus, 1998; Miura et al., 2012; Zhou et al., 1994). There are numerous cases in which an ophiolite massif contains both types of chromitites (Gervilla et al., 2005; González-Jiménez et al., 2011; Qiu et al., 2018; Zhou et al., 2014), with high-Cr chromitites stratigraphically positioned in the mantle and high-Al chromitites within the Moho Transition Zone (Ahmed and Arai, 2002; Rollinson, 2008).

Qiu et al. (2018) analyzed spinels from high-Al and high-Cr chromitites, mantle dunites and MTZ dunites from the Bulqiza ultamafic massif, located in central Albania. The Authors report similar XCr from spinels in high-Cr chromitites and mantle dunites (~0.80), but different XMg, higher in high-Cr chromitites than in mantle dunites. MTZ dunites have XCr similar to high-Al chromitites and slightly lower XMg (Fig. 3.20A). A comparison between our samples and the samples from Bulqiza massif reveals that Iballe dunites are similar to mantle dunites, while massive chromitites fit into the field of high-Al chromitites. High-Cr spinels in dunites show a boninitic affinity (Fig. 3.20B), while high-Al spinels within chromitites are more similar to MORB spinels.

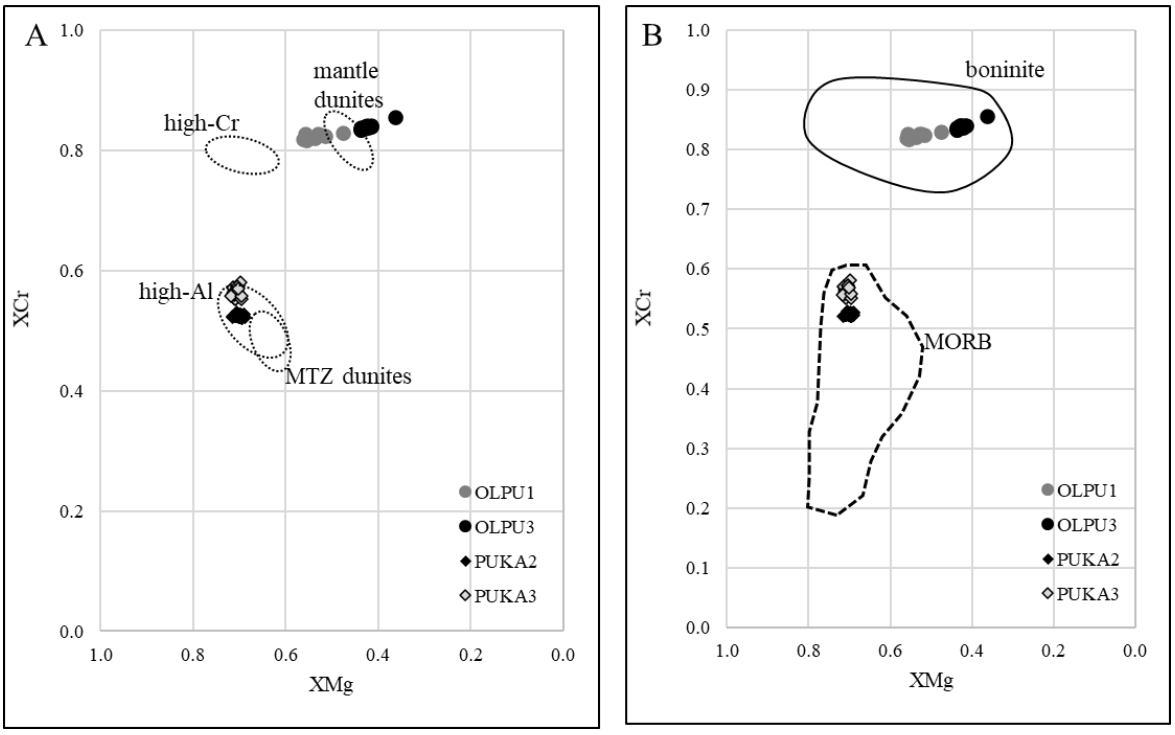

Fig. 3.20 XCr vs XMg of massive chromitite and dunite spinels; A) compositional fields for mantle dunites, high-Cr chromitites, high-Al chromitites and MTZ dunites are referred to the Bulqiza ultramafic massifs in Albania (Qiu et al., 2018); B) compositional fields of boninites and MORB are from Barnes and Roeder (2001).

Numerous studies highlighted positive correlations between $Al_2O_3$ and $TiO_2$ contents in spinels and in coexisting melts (Ghosh and Bhatta, 2014; Kamenetsky et al., 2001; Rollinson, 2008; Zaccarini et al., 2011). Hence, $Al_2O_3$ and $TiO_2$ contents of a parental melt can be recovered from the spinel composition. From the positive correlation found by Kamenetsky et al. (2001), the $Al_2O_3$ content in a parental magma is calculated as:

$$Al_2O_{3\ melt} = 5.2253 * \ln(Al_2O_{3\ spinel}) + 1.12$$

The correlations between $TiO_2$ in spinels and in a coexisting melt, on the other hand, differ between MORB and arc settings:

$$TiO_{2\ melt-MORB} = 1.5907 * TiO_{2\ spinel}^{0.6322}$$

$$TiO_{2\ melt-arc} = 1.0963 * TiO_{2\ spinel}^{0.7863}$$

From the parental melt analyses, it appears that high-Cr spinels within dunites have an arc signature (Fig. 3.21A), similar to the one found for high-Cr chromitites (Qiu et al., 2018), while high-Al spinels within massive chromitites retain a MORB-like signature. However, as observed also by Qiu et al. (2018) (Fig. 3.21B), high-Al chromitites spinels have $TiO_2$ content lower than typical MORB spinels (Kamenetsky et al., 2001), probably because they are derived from partial melting of a residual mantle which had already experienced a low degree of melt extraction (Qiu et al., 2018).

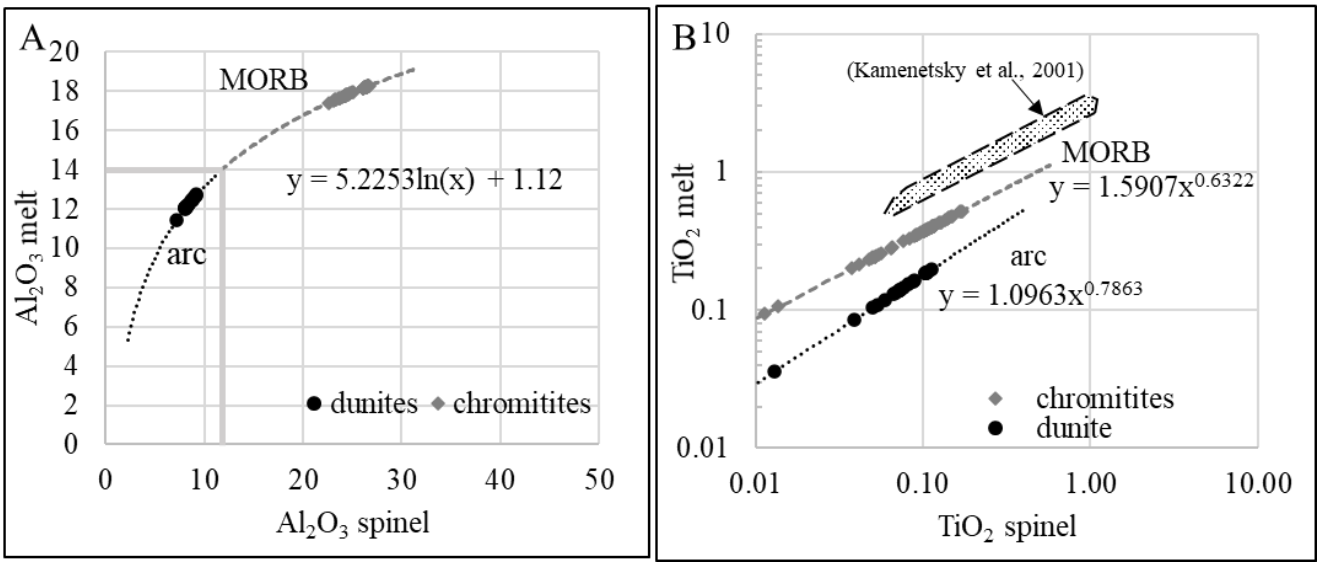


Fig. 3.21 Plots of calculated $Al_2O_3$ (A) and $TiO_2$ (B) composition of melts in equilibrium with Iballe spinels within dunites and massive chromitites; dotted field represents MORB data from Kamenetsky et al. (2001).

The difference in $TiO_2$ content between high-Al chromitites and MORB spinels could suggest that the origin of Iballe chromitites is not in a MORB setting, despite the similar XMg and XCr values. In fact, many known supra-Moho chromitites show MORB-like signatures. Qiu et al. (2018) reports an enrichment in PPGE with respect to IPGE in Bulqiza high-Al chromitites, which strongly suggests a supra-Moho origin for those rocks.

Low-Cr and Al-rich podiform chromitites from the Moho Transition Zone are also believed to have derived from tholeiitic basalts formed at mid-ocean ridge, ocean island or island arc settings. Pertsev et al. (1997) suggest that the source of the magma generating supra-Moho chromitites and associated rocks should be localized in a residual zone undergoing high degrees of partial melting. The trends observed in Nurali massif are in agreement with a multistage crystallization of magma portions, gradually depleting the mantle source (Pertsev et al., 1997).

Saccani and Tassinari (2015) suggest that the low-Ti and high-Al contents of spinels in the Krabbi massif, in which Iballe is located, could indicate an origin from low-Ti tholeiites. A model that explains the coexistence of MORB and SSZ-type melts suggests the establishment of a subduction zone close to an active mid-ocean ridge, at high thermal regimes. In this model, Western Mirdita Ophiolites are located very close to the subduction zone, and the proximity of both MORB and SSZ-type sources allowed minor, late MORB-type melt to be generated at the same time as boninitic melt in the Eastern Mirdita Ophiolites (Bébien et al., 2000; Dilek et al., 2008; Saccani et al., 2011).

Both the models fit with an origin of high-Al chromitites from tholeiitic magmas at a mid-ocean ridge setting.

The different cooling rates inferred for the Iballe dunites and chromitites could be explained by genesis of dunites in a supra-subduction setting, and later cooling at relatively low cooling rates, while the higher temperatures inferred for the chromitites fit better with a formation in a MORB setting, with consequent cooling at fast cooling rates. This supports the model by Saccani et al. (2015) of coexistence of MORB and SSZ environments in adjacent setting.

Another model proposes an evolution from MORB to boninitic magmas within the same SSZ environment (Dilek et al., 2008), but for the model to work the ophiolites need to have formed in a small marginal basin (such as Mirdita-Pindos one). However, the extent of the Pindos basin (or even its existence) are still debated (Saccani and Tassinari, 2015).

A discriminating factor to locate Iballe chromitites above or under the Moho would be the PGE content of Iballe massive chromitites, as supra-Moho chromitites typically show an enrichment in PPGE with respect to IPGE, as reported by Qiu et al. (2018).

### 3.4.4. Conclusion

The Iballe massif is located into the Krabbi Zone of the Mirdita ophiolite, straddling the Eastern and Western type ophiolites. Samples collected at the Iballe mine are divided into high-Cr spinel bearing dunites and high-Al spinel chromitites. The geothermometry and geospeedometry assessments on the two sets of samples reveal that chromitites were formed at relatively high temperatures and suffered a fast cooling at nearly constant cooling rate. Dunites reveal lower temperatures of formation and lower cooling rates than chromitites. This remarkable difference in cooling and genetic conditions is also reflected in the spinel chemistry. Chromitite spinels have low Cr and high Al contents, quite similar to MORB spinels, while dunite spinels are high-Cr, and show a boninitic affinity. A comparison with other massifs of the Mirdita ophiolites reveals that high-Al chromitites are not uncommon, and are either explained as formed in a supra-Moho setting or in a MORB setting, from low-Ti tholeiitic magmas.

The coexistence in the same massif of MORB and SSZ signatures supports the model proposed by Saccani and Tassinari (2015) about the establishment of a subduction zone close to an active mid-ocean ridge, with a tectonic evolution that brought both signatures to overlap within the same portion of ophiolite. The very high cooling rate of Iballe chromitites could be indicative also of a shallow origin of these rocks, within or above the Moho Transition Zone. Iballe dunites, on the other hand, show a boninitic signature, and were formed in a supra-subduction geodynamic setting.

# CHAPTER 4: PGE and BME remobilization

In this chapter, we assess Platinum Group Elements and Base Metal Elements remobilization during post-magmatic processes in different localities. In particular, we analyzed chloritized samples from Gomati and Nea Roda (Greece), and serpentinized samples from Abdasht-Soghan (Iran) and Skyros (Greece). Some of the data and discussion have been already published:

- Grieco, G., Bussolesi, M., Eslami, A., Gentile, A., Cavallo, A., Lian, D., Yang., J., Ghaseminejad, F. (2020). Differential platinum group elements (PGE) re-mobilization at low $fS_2$ in Abdasht and Soghan mafic-ultramafic complexes (Southern Iran). Lithos, Vol. 366-367.
- Bussolesi, M., Zaccarini F., Grieco G., Tzamos E. (2020). Rare and new minerals in the Ni-Cu-Sb-As system: first finding in the Gomati ophiolite, Greece. Period. Miner. Vol. 89.

## 4.1 Analytical methods

### 4.1.1 EMPA

Mineral chemistry of chromites and silicates was determined through a JEOL 8200 electron microprobe equipped with a wavelength dispersive system (SEM-WDS) at the Earth Sciences Department of the University of Milan. The system was operated using an accelerating voltage of 15 kV, a sample current on brass of 15nA, a counting time of 20s on the peaks and 10s on the background. Ka lines were used for major elements, and Ma lines for PGM analyses. A series of natural minerals was used as standards: wollastonite for Si, forsterite for Mg, ilmenite for Ti, fayalite for Fe, anorthite for Al and Ca, chromite for Cr, niccolite for Ni, rhodonite for Mn and Zn, and metallic V for that element. The approximate detection limit is 0.01 wt% for each element. $Fe^{3+}$ was recalculated from microprobe analyses assuming perfect stoichiometry, based on 8-oxygen formula. For the analyses of PGM and BMM, PGM standards used are niccolite for As and Ni, chalcopyrite for S, Fe, Cu and pure metals for Sb, Os, Ir, Rh, Pt, Pd, and Ru.

Part of the samples (from Gomati and Nea Roda) was analyzed through a Jeol JXA 8200 electron microprobe at the Eugen F. Stumpfl Laboratory at the University of Leoben, Austria. The system was operated with an accelerating voltage of 15 kV and beam current of 10 nA, a counting time of 20s on the peaks and 10s on the background. The elements were analyzed using the Kα line. Specimens of chromite, rhodonite, ilmenite, albite, pentlandite, wollastonite, kaersutite, sphalerite, and metallic vanadium were used as standards. The following diffracting crystals were used: TAP for Na, Mg, and Al; PETJ for K, Si, and Ca; and LIFH for Ti, V, Cr, Zn, Mn, Fe, and Ni. For the analyses of BMM and PGM were analyzed with 20 kV accelerating voltage, 10 nA beam current, and beam diameter of

about 1 micron. The peak and background counting times were 20 and 10s, respectively. The following lines were selected: Kα for S, Ni, Fe and Cu, Mα for Pb and Os and Lα for As, Sb, Ir, Ru, Rh, Pd, and Pt. The standards employed were: galena (Pb), chalcopyrite (Cu), pyrite (Fe,S), stibnite (Sb), synthetic GaAs (As), and millerite (Ni). The reference materials were pure metals for the six PGE (Ru, Rh, Pd, Os, Ir and Pt). Automatic correction was performed for the Ru-Rh and Rh-Pd interferences.

### 4.1.2 PGE

Samples of Gomati, Skyros and Nea Roda have been sent to Actlabs laboratory in Canada for PGE analyses. Samples up to 25 g in size were fire assayed using a nickel sulphide (NiS) fire assay procedure. The nickel sulphide button was dissolved in concentrated HCl and the resulting residue which contains all the PGE and Au was collected on a filter paper. One batch of 34 samples includes 2 blanks, 3 certified standards and 3 duplicates. The residue underwent 2 irradiations and 3 separate counts to measure all the PGE and Au. Instrumental Neutron Activation Analysis (INAA) is an analytical technique which is dependent on measuring gamma radiation induced in the sample by irradiation with neutrons. The primary source of neutrons for irradiation is a nuclear reactor. Each element which is activated emits a "fingerprint" of gamma radiation which can be measured and quantified. Multi-element analyses of practically any material, from the smallest sample which can be weighed accurately to very large samples, have been analyzed routinely by INAA. Detection limits for each element are: 2 ppb (Os), 0.1 ppb (Ir), 5 ppb (Ru), 0.2 ppb (Rh), 5 ppb (Pt), 2 ppb (Pd), 0.5ppb (Au).

Platinum-group elements of Abdasht-Soghan were analyzed at the National Research Center for Geoanalysis, Chinese Academy of Geological Sciences, Beijing. PGE were concentrated using the nickel sulfide fire assay and Te-coprecipitation method (Jackson et al., 1990), and were analyzed using ICP-MS. PGE reference material GBW07290 was measured to ensure consistency of the analytical results for PGE. Analytical processes have been described in detail by Dai et al. (2011).

# 4.2 Remobilization in chloritized chromitites

## 4.2.1 Mineralogy and texture

### 4.2.1.1. Gomati

Chromitites and their host rocks were sampled from three localities within the Gomati complex (Tab. 4.1), all three corresponding to small abandoned mines exploited by Germans during the second world war. The localities (Fig. 4.1) are St. George, Tripes and Limonadika.

Tab. 4.1 Gomati sampling and analyses (**bold**: EMPA; underlined: whole rock PGE content; *italics*: whole rock LA-ICP-MS)

| Zone | Coordinates | Sample | Lithology |
|---|---|---|---|
| St. George | 40°24.3260' – 23°46.4250' | GO1, **GO2**, **GO3** | chromitite, pyroxenite |
| | 40°24.1250' – 23°48.6690' | GO4 | serpentinite |
| | 40°24.3150' – 23°48.4390' | GO5 | serpentinite |
| | 40°24.5560' – 23°45.9380' | STG1, STG2 | serpentinite |
| | 40°24.6180' – 23°45.9870' | STG3 | serpentinite |
| | 40°24.7590' – 23°46.1080' | STG4, STG5 | serpentinite |
| | 40°23.9030' – 23°47.7890' | GON1, GON2, GON3 | chromitite |
| | 40°24.1230' – 23°47.7500' | GON4 | chromitite |
| | 40°24.0530' – 23°47.7730' | GON5, GON6 | amphibolite |
| | 40°24'26.6'' – 23°46'00.7'' | ***GOM1A***, *GOM1B* | serpentinite, chromitite, pyroxenite |
| | 40°24'17.0'' – 23°46'24.7'' | ***GOM2A***, **GOM2B/1/2**, **GOM2C** | chromitite |
| | 40°24'20.9'' – 23°46'25.3'' | ***GR54A*, GR54C, GR54D, *GR55***, *GR56* | chromitite |
| Tripes | 40°24.7680' – 23°48.6120' | TRI1, TRI2, TRI3 | serpentinite |
| | 40°25.0090' – 23°48.5660' | TRI4, TRI5, TRI6, TRI7, TRI8 | serpentinite |
| | 40°24.9800' – 23°48.4410' | TRI9 | serpentinite |
| | 40°24.9630' – 23°48.3000' | **TRI10/A/B** | chromitite |
| | 40°24.8620' – 23°48.2170' | TRI11 | serpentinite |
| | 40°24.8030' – 23°48.1260' | TRI12 | serpentinite |
| | 40°24.6930' – 23°48.1510' | TRI13, TRI14, TRI15 | serpentinite |
| Limonadika | 40°23.2590' – 23°48.2840' | **LIM1**, LIM2 | chromitite |
| | 40°23.2740' – 23°48.1900' | **LIM3** | chromitite |
| | 40°23.3280' – 23°48.1950' | LIM4 | serpentinite |
| | 40°23.3890' – 23°48.3330' | LIM5 | amphibolite |
| | 40°22.3510' – 23°49.3060' | SUD1, SUD2 | serpentinite |
| | 40°22.5220' – 23°49.3190' | SUD3 | serpentinite |
| | 40°22.5750' – 23°49.1710' | SUD4, SUD5 | serpentinite |

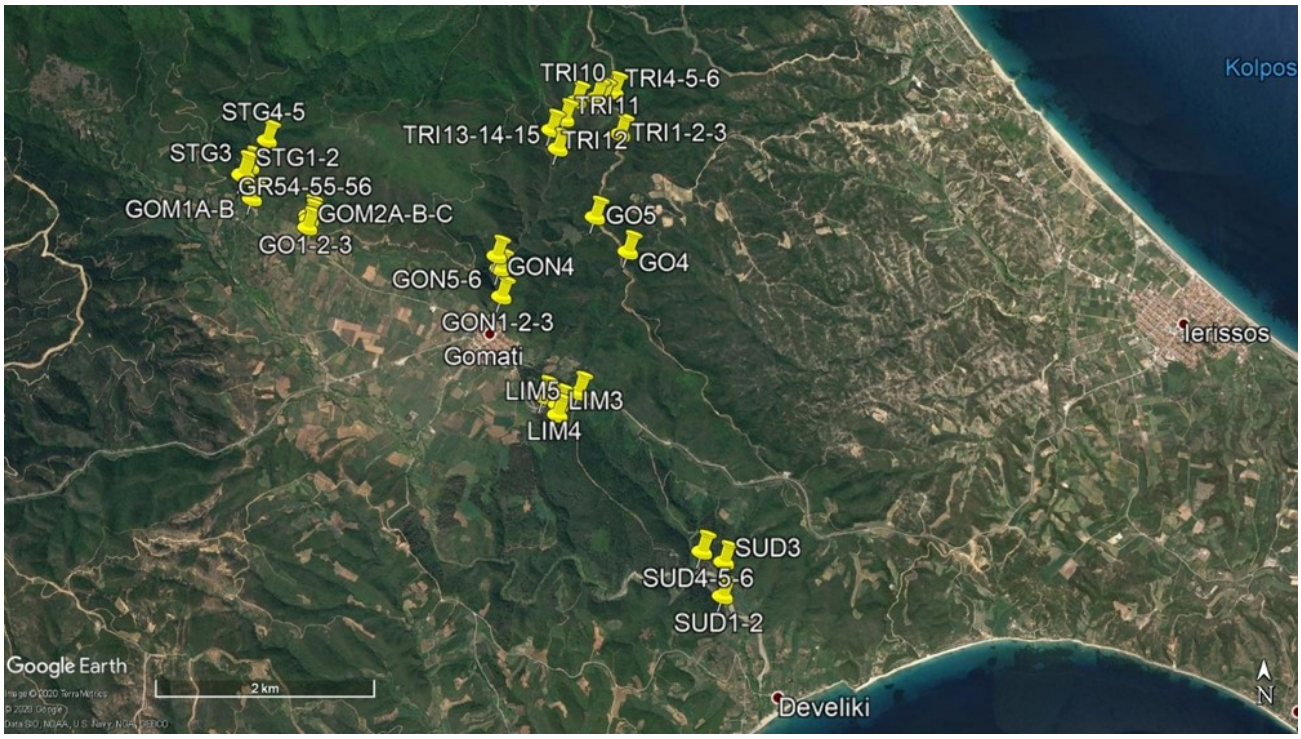


Fig. 4.1 Gomati sample locations.

***St. George***

The St. George chapel is located just north of the Gomati village. Samples collected in this area consist of serpentinite, pyroxenite, disseminated and layered chromitites (Fig. 4.2A, B). In the St. George area, small chromitite bodies, typically deformed, with massive and disseminated textures occur in pods and lenses in sharp contact with pyroxenite host rocks.

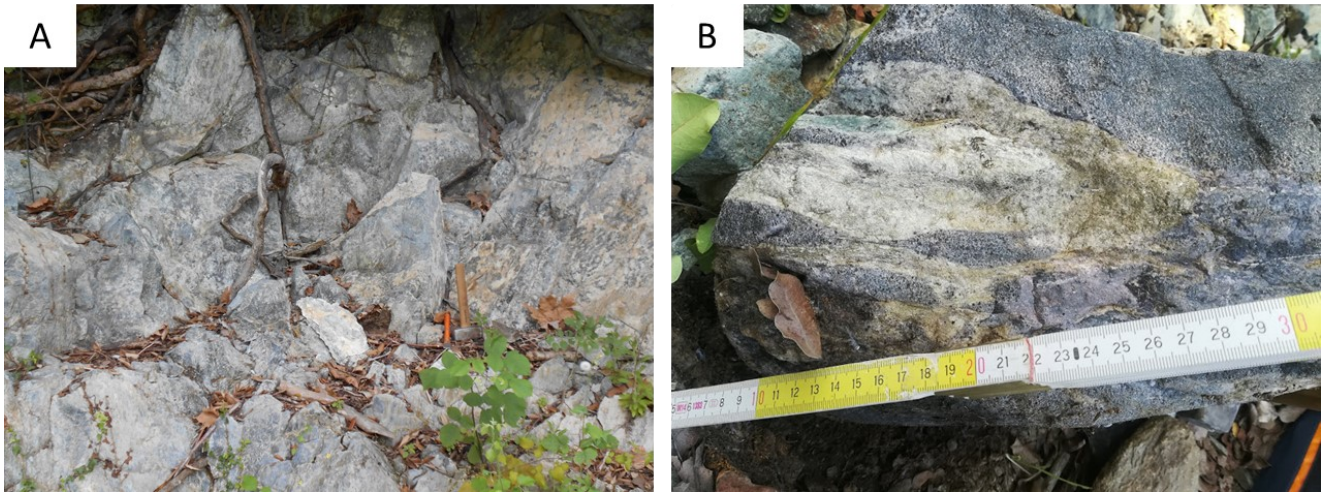


Fig. 4.2 Serpentinite (A) and chromitite lenses (B) from St. George outcrops.

Chromitites are composed of subhedral to anhedral crystals of chromian spinel in a chloritic groundmass (Fig. 4.3A). Chromian spinels show a peculiar texture, characterized by polygonal and rounded grains that contain abundant inclusions of chlorite generally oriented along the crystal planes

of the host chromite, and filling pores caused by ferrian chromite alteration. Primary silicates are mostly replaced by Cr-chlorite, and the only preserved relicts are pyroxene crystals. Ferrian chromitization is widespread and concentrates along rims and cracks. Only cores of big crystals are unaltered (Fig. 4.3B), while smaller ones are completely altered.

The associated pyroxenites and minor dunites are heavily altered. In particular, clinopyroxenes are partially replaced by Cr-chlorite (Fig. 4.3C). The groundmass is constituted by fine-grained aggregates of chlorite and serpentine (Fig. 4.3D). Dispersed Cr-spinels are mainly subhedral and completely altered into ferrian-chromite. No primary inclusion was detected in the silicate phases.

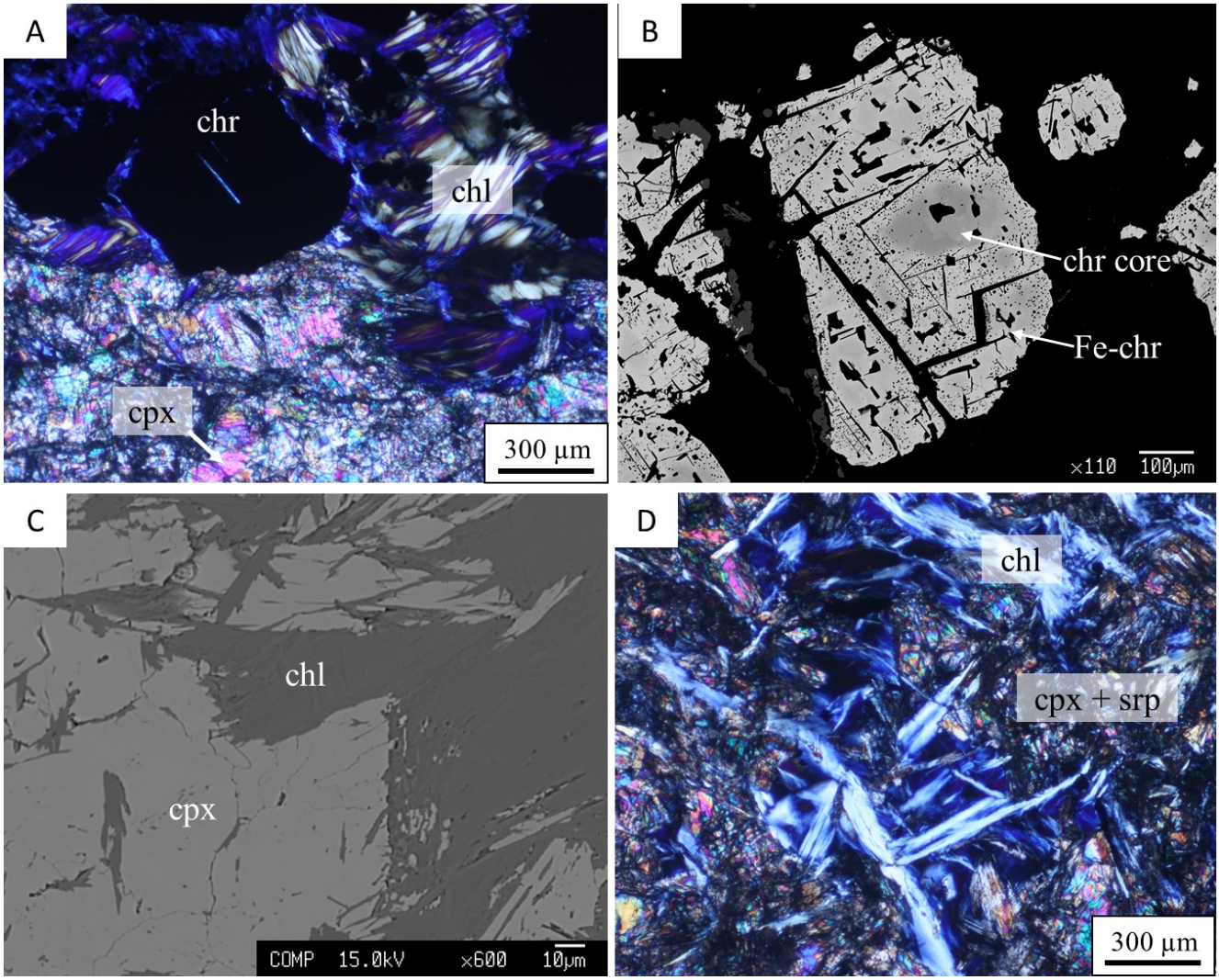


Fig. 4.3 XPL (A and D) and BSE (B and C) images of St. George samples, Gomati.

*PGM and BMM*

PGM are abundant within chromitites at St. George, but none were found in the silicate host rocks. They are found mainly within unaltered chromite (Fig. 4.4A-D), and rarely within altered chromite or fractured zones (Fig. 4.4E-F). PGM in unaltered chromite are generally euhedral to subhedral, and

they are present both as single (Fig. 4.4A, B, F) or polyphase inclusions (Fig. 4.4C-E). Laurite, the most abundant PGM, is usually homogeneous, and rarely crystals display some zonation (Fig. 4.4B). PGM grains are often associated to silicates (amphibole or chlorite), sulfides (Fig. 4.4C), or other PGE-bearing phases, such as irarsite, or Ir-Sb-As sulfides (Fig. 4.4D). Within the silicate matrix no PGM was detected. In the altered portion of chromites (Fe-chromite rim, cracks or rims in contact with the matrix), PGM are mostly subhedral to anhedral (Fig. 4.4E, F), and can display corroded boundaries, suggesting dissolution processes.

BMM are abundant both in chromitites and their associated pyroxenites. The assemblage comprises Ni-Fe sulfides, arsenides and antimonides, plus some rare copper phase, such as chalcocite. Primary sulfides are rare and mostly enclosed within chromites, and they consist of pentlandite grains (Fig. 4.4D). The sulfide phases are, in order of abundance, heazlewoodite, millerite, pentlandite and Cu-sulfides. Heazlewoodite is distributed primarily within the silicate matrix and associated to altered chromite, where it fills up pores generated through alteration of chromite into ferrian chromite. Within the silicate matrix, heazlewoodite is found either as a single phase or in association with other mineralogical phases, such as arsenides or antimonides (Fig. 4.5A-C). Millerite is found mainly in altered chromite or in the silicate matrix, usually in association with other BMM (sulfides, arsenides, antimonides) (Fig. 4.5D-E). Copper sulfides are rare, and are found within the silicate matrix or associated to fractured and altered chromites, either as single or polyphasic grains (Fig. 4.5F).

Arsenides and antimonides are abundant, especially within the silicate matrix and in pyroxenites. While arsenides were found both in altered chromite and within the silicate matrix, antimonides were found only within the silicate matrix. The most abundant arsenide is orcelite, found both in altered chromite and within the silicate gangue (Fig. 4.6A). A mineral with formula approaching dienerite ($Ni_3As$) was found associated to other phases, mostly antimonides (Fig. 4.6B-F). Of the antimonides, the only identified mineral is breithauptite (Fig. 4.6D), while the other Sb-phases are unknown minerals (Fig. 4.6B-F, Fig. 4.7) (Bussolesi et al., 2020b).

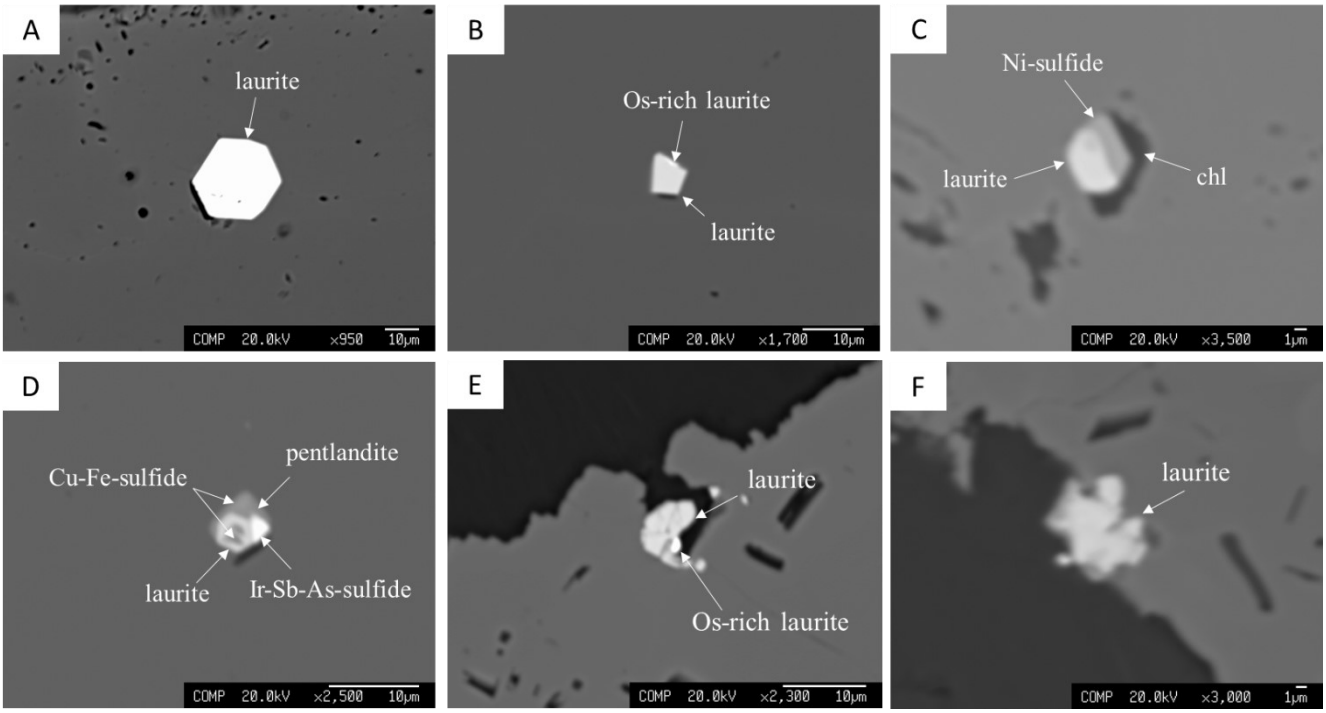


Fig. 4.4 BSE images of Platinum group minerals within St. George chromitites.

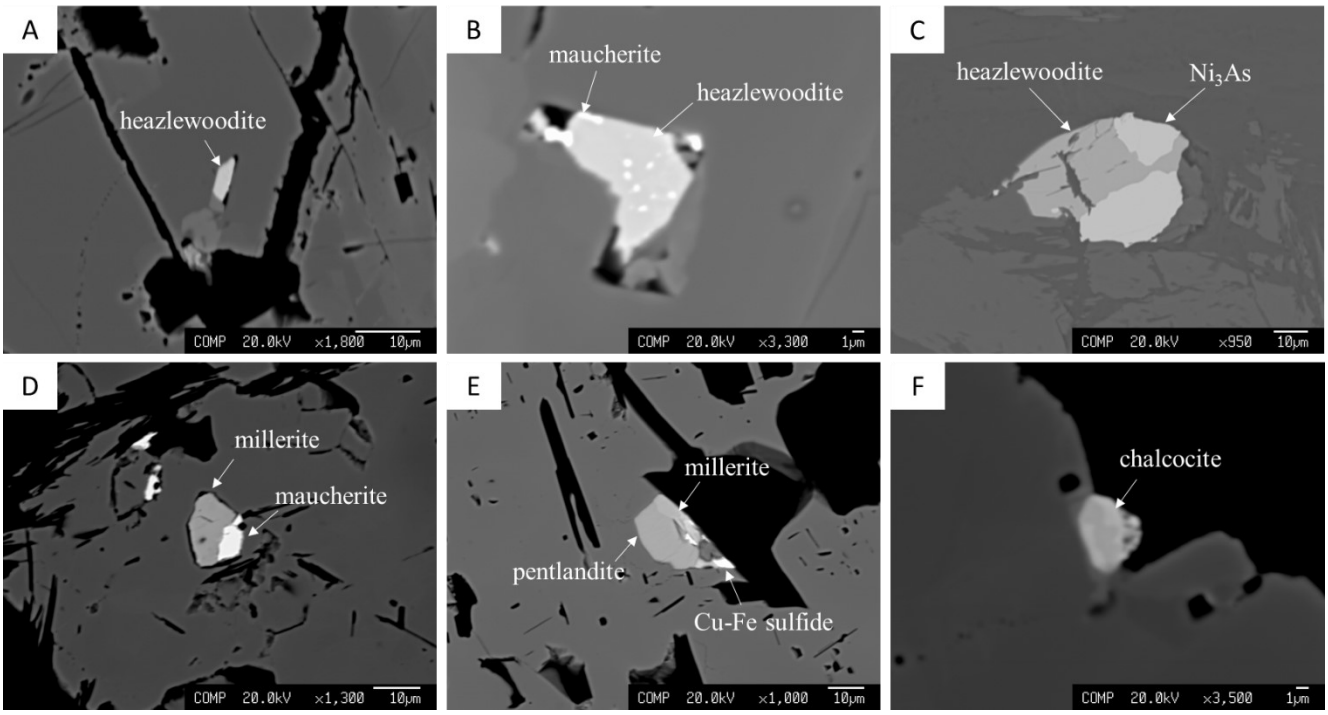


Fig. 4.5 BSE images of Ni-Fe-Cu sulfides within St. George chromitites.

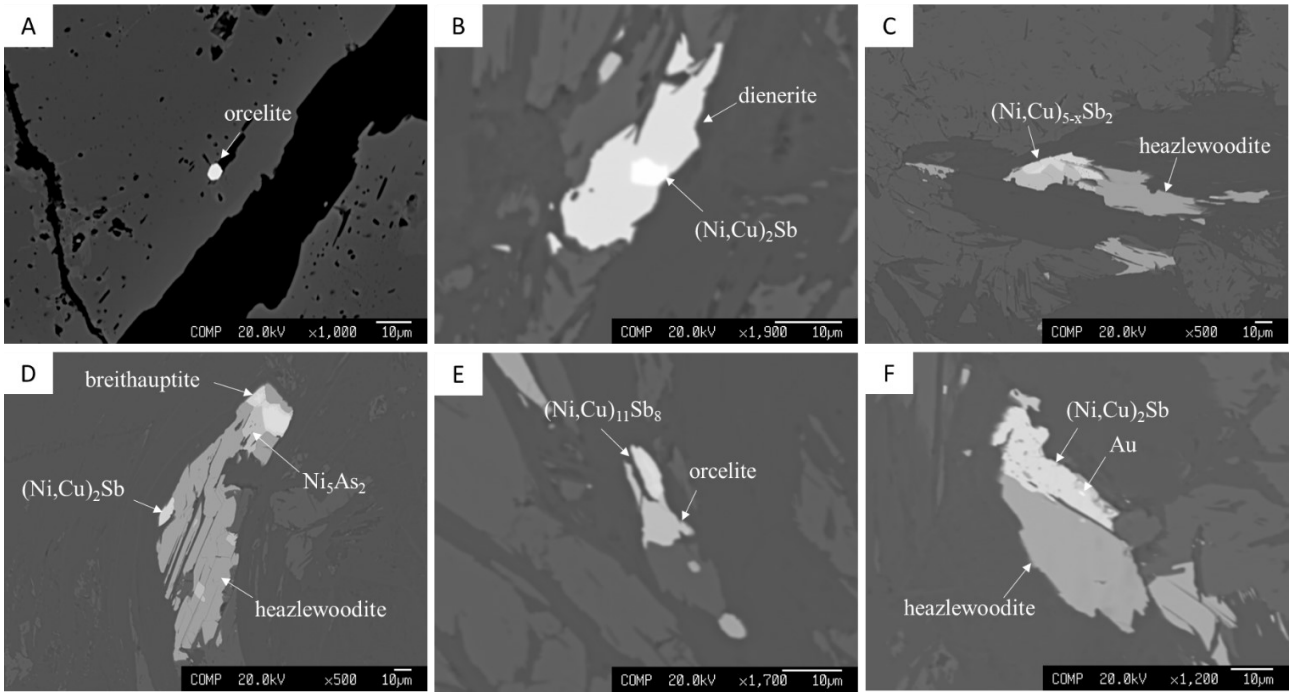


Fig. 4.6 BSE images of Ni-arsenides and Ni-Cu antimonides within St. George pyroxenites.

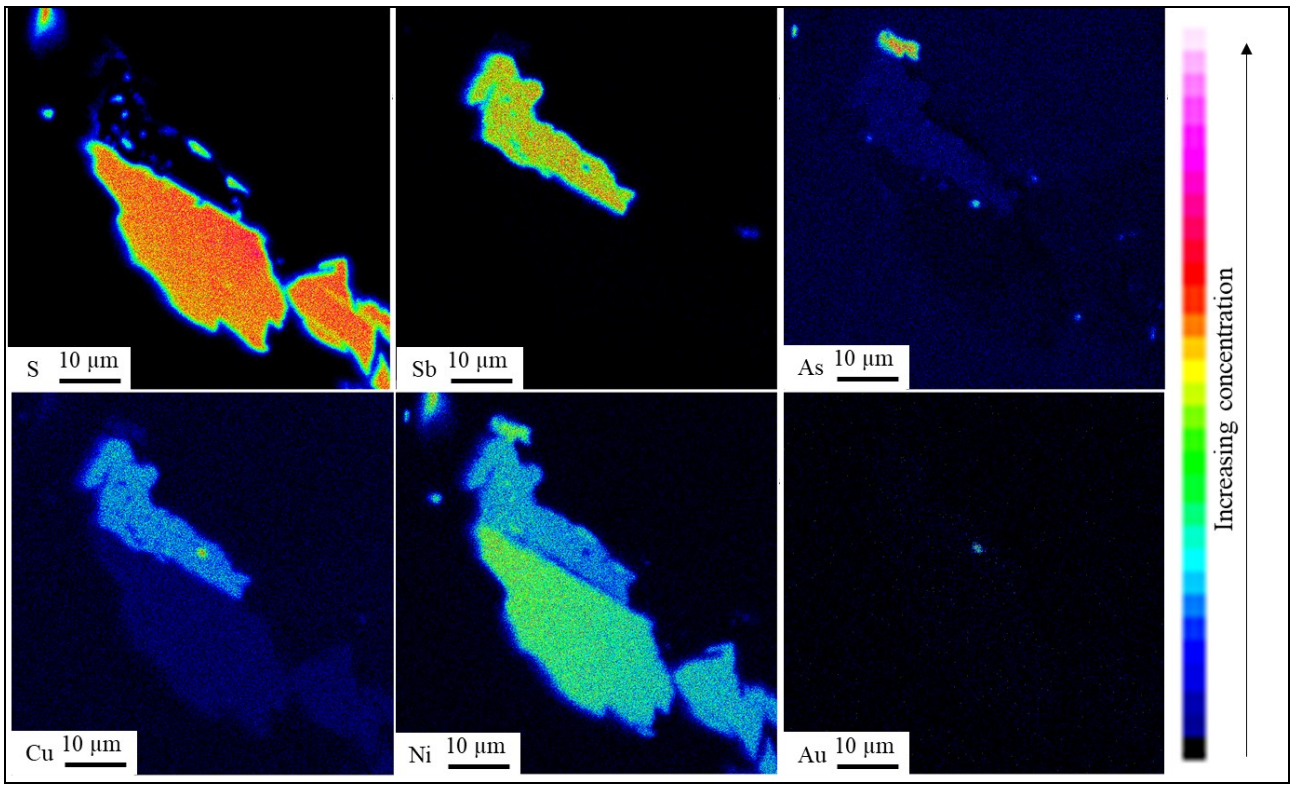


Fig. 4.7 Atomic maps of the mineral assemblage of Fig. 4.6F.

***Tripes***

Tripes locality is nowadays a quite inaccessible area, due to vegetation overgrown, but it was possible to collect serpentinite host rocks and massive chromitites from small outcrops, less than 1m thick (Fig. 4.8).

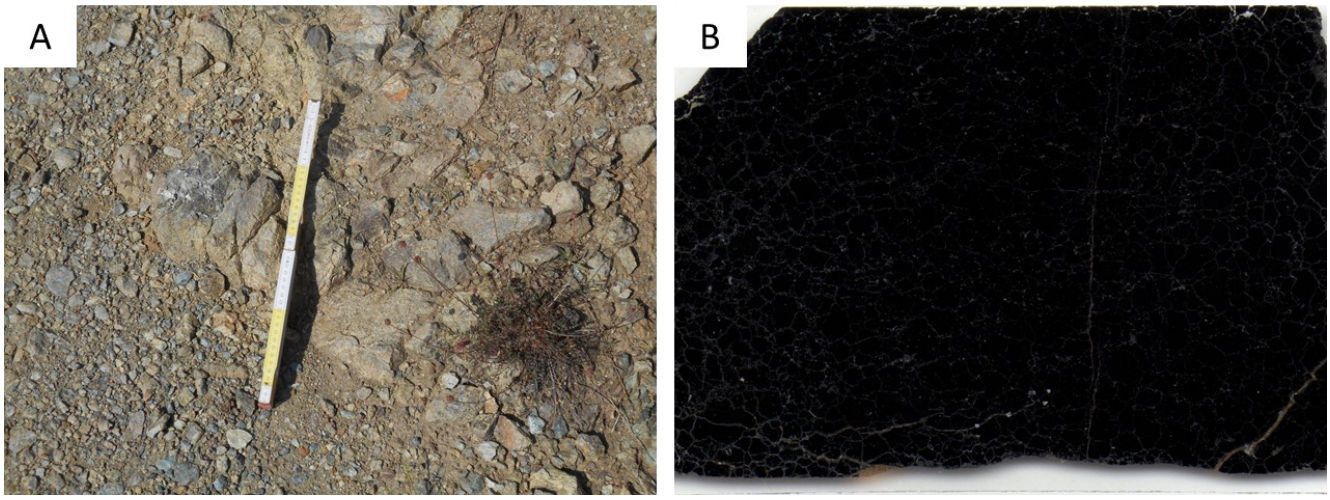


Fig. 4.8 A) Serpentinite (from Storni, 2020) and B) massive chromitite thin section from Tripes, Gomati.

Massive chromitites from the Tripes area are characterized by > 90% chromite modal content. Chromite crystals have euhedral to subhedral shape and show fractures and ferrian chromite rims. Primary silicates have been completely replaced by Cr-chlorite (Fig. 4.9A, B). Associated serpentinites are highly altered and the only relicts of primary silicates are olivine and clinopyroxene.

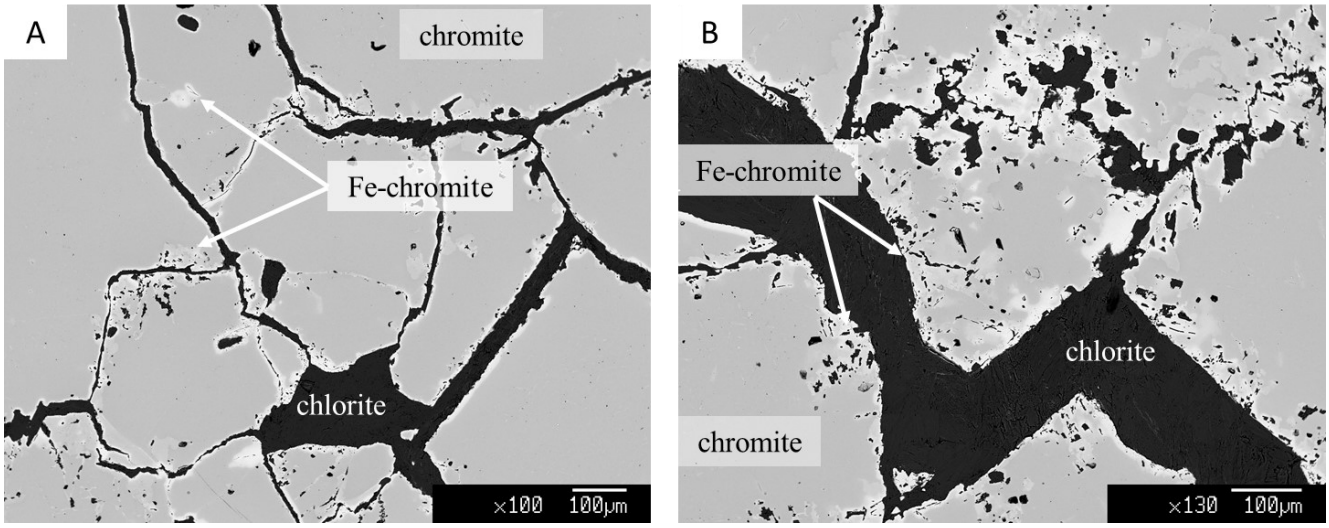


Fig. 4.9 BSE images of massive chromitites from Tripes, Gomati.

*PGM and BMM*

PGM, which are particularly abundant in Tripes, are mostly euhedral grains eclosed in unaltered chromite. Only in one case the PGM grain has anhedral shape. The majority of the PGM belong to the laurite-erlichmanite series, usually present as single grains (Fig. 4.10A, B) and sometimes associated to other sulfides (Fig. 4.10C). Five unknown PGM have been also found in the samples. They are four Ir-Rh-Ni-Fe-Cu sulfides with similar compositions (Fig. 4.10D, E, Fig. 4.11) and one Ru-Os-Ir-Ni-Fe sulfide (Fig. 4.10F).

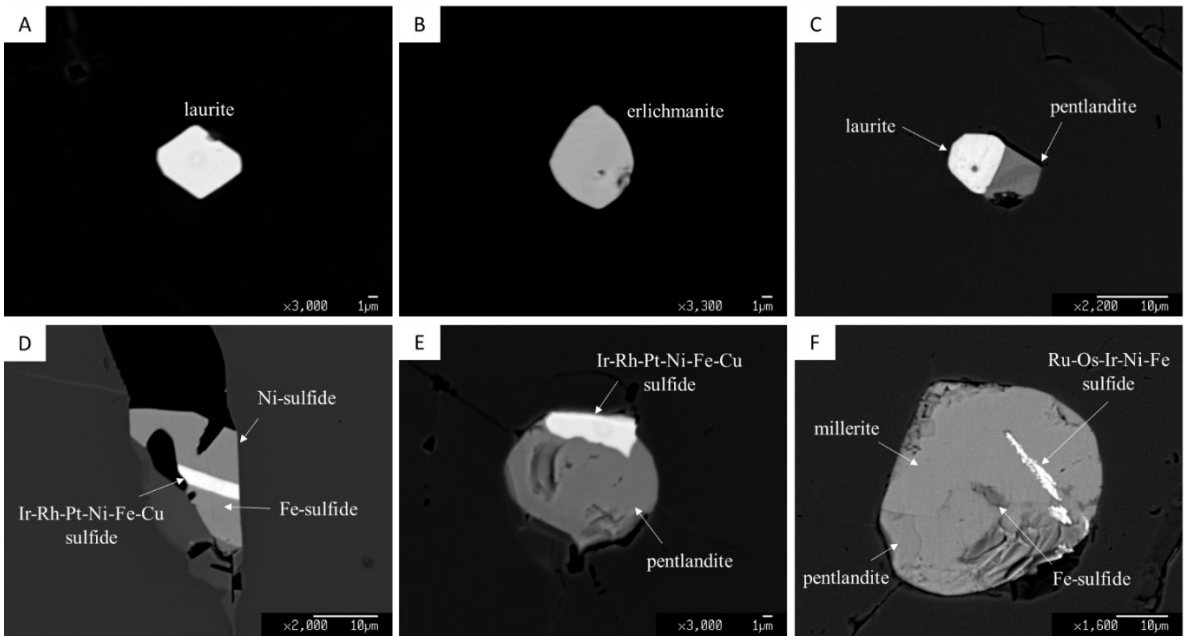


Fig. 4.10 BSE images of Platinum group minerals from Tripes, Gomati.

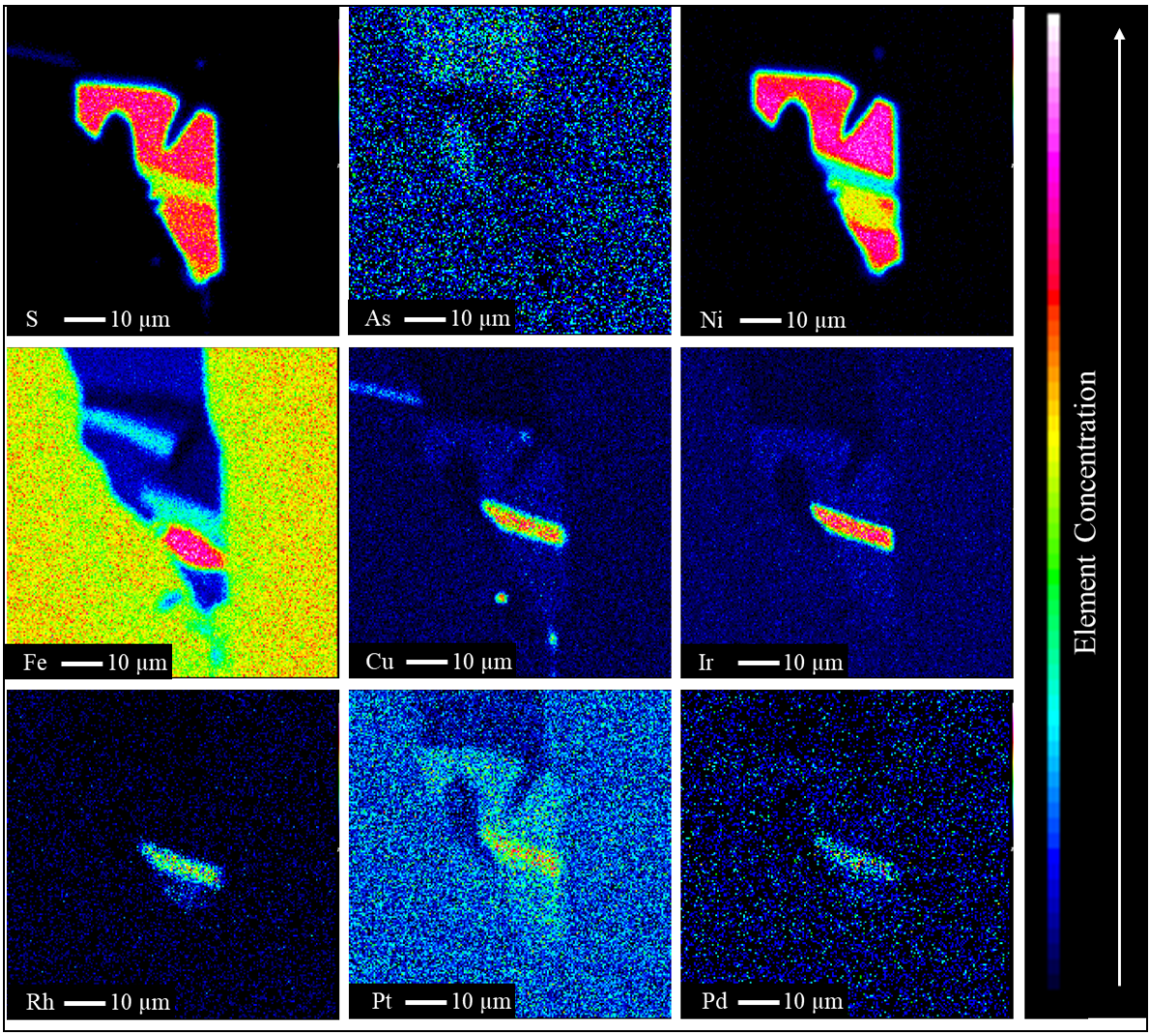


Fig. 4.11 Atomic maps of the mineral assemblage of Fig. 4.10D.

The BMM assemblage is quite poor, and comprises Ni-Fe sulfides, rare copper phases (e.g. pyrite) and rare arsenides. Primary sulfides consist of pentlandites mostly found enclosed in chromite grains, in association with other sulfides (Fig. 4.10C, E, F) or more rarely as single phase. Secondary sulfides are rare and consist mostly of rare millerite and one arsenide (nickeline).

***Limonadika***

The area of Limonadika was the most inaccessible due to dense vegetation. In the north side of this area (southern unit of Gomati complex), samples of altered disseminated chromitite and serpentinite were collected (Fig. 4.12). In the southernmost part of the complex large magnesite veins were present, crosscutting serpentinites and amphibolites.

Chromitites from the Limonadika area are disseminated, characterized by coarse chromite grains in a chloritic silicate matrix. Chromite crystals have euhedral to subhedral shape and show fractures and ferrian chromite rims. Primary silicates have been completely replaced by Cr-chlorite (Fig. 4.13A, B).

*PGM and BMM*

Among all Gomati localities, Limonadika is the poorest in BMM, and no PGM were detected. BMM are found mainly as inclusions in unaltered chromites or in the pores in the ferrian chromite rims. The only primary BMM are rare pentlandite grains, while secondary BMM are millerite, nickeline and an unknown Cu-sulfide (Fig. 4.14A, B).

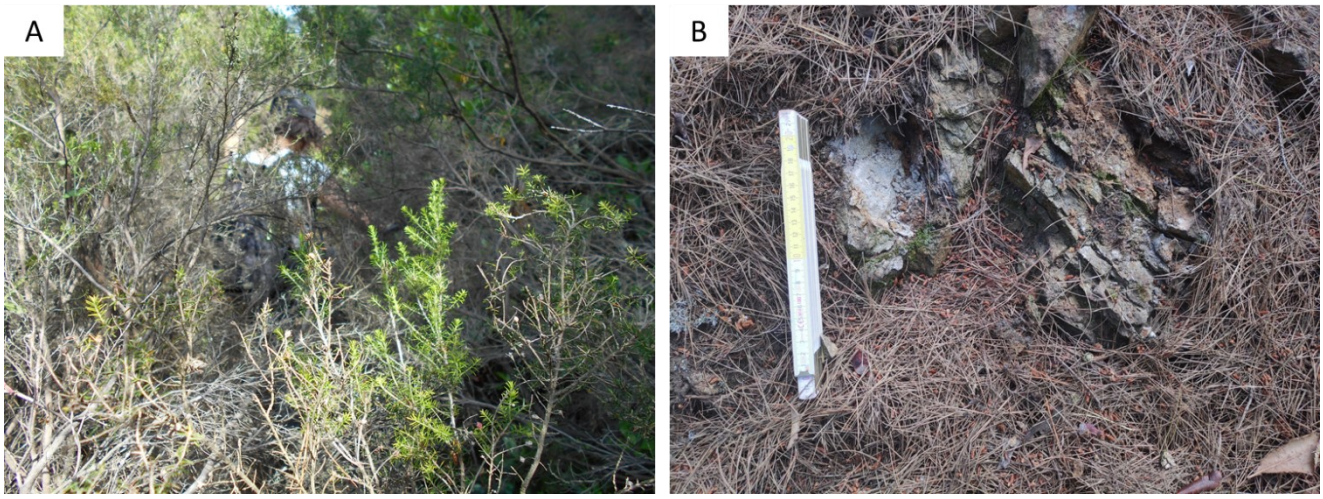


Fig. 4.12 A) and B) Limonadika sample location (from Storni, 2020).

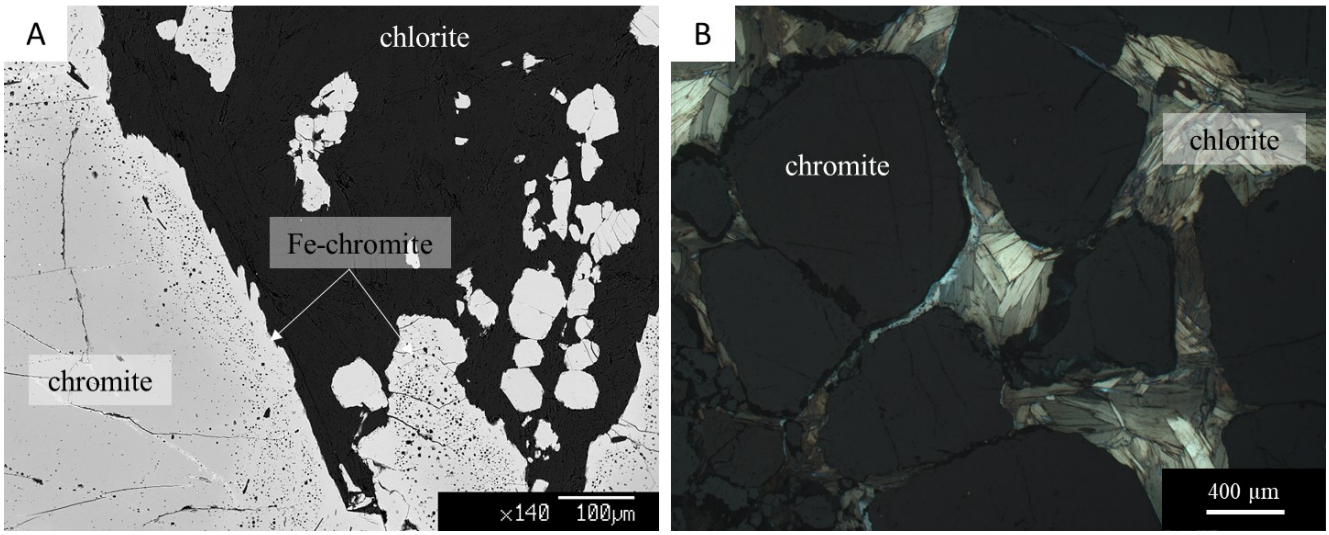


Fig. 4.13 A) BSE and B) XPL images (transmitted light) of a chromitite sample from Limonadika.

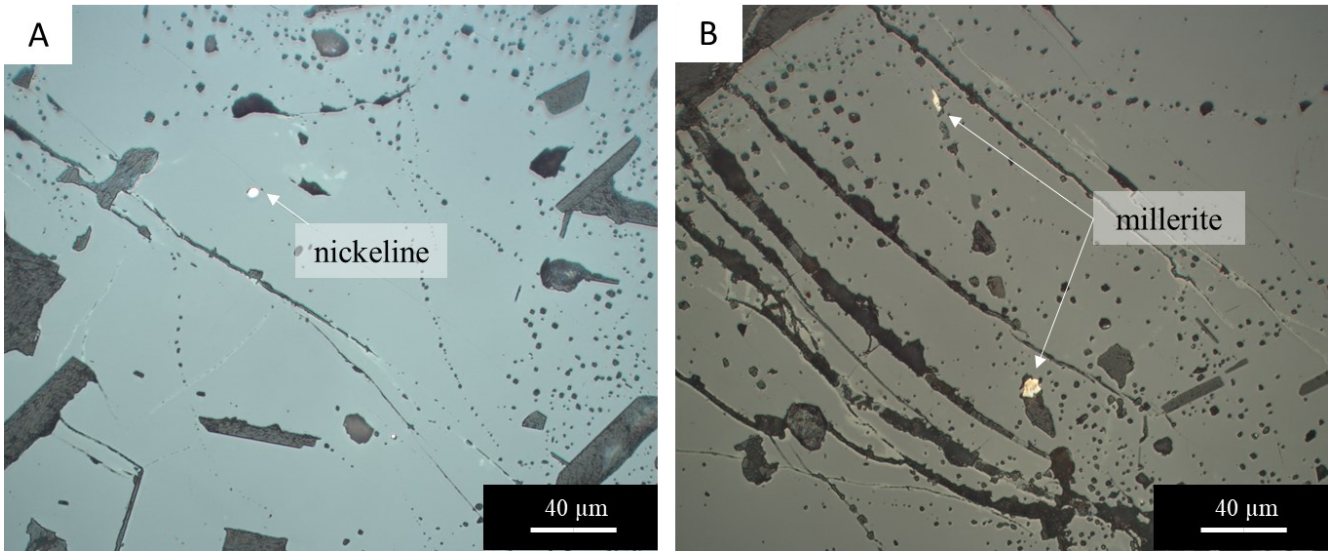


Fig. 4.14 A) PPL and B) XPL images in reflected light of rare sulfides within Limonadika chromitites.

#### 4.2.1.2. Nea Roda

Sampling locations of Nea Roda are reported in Chapter 3 (Tab. 3.5, Fig. 3.11). For the study of PGE and BME remobilization during post-magmatic processes, only altered chromitites have been considered, as BMM and PGM were not found in fresh chromitites. Chromitites have a disseminated texture with rare chromite nodules marking some of the mineralized layer. Close to the peridotite outcrop, chromitite occurrences were found in a highly altered soil (Fig. 4.15A), where massive chromitite samples were collected (Fig. 4.15B).

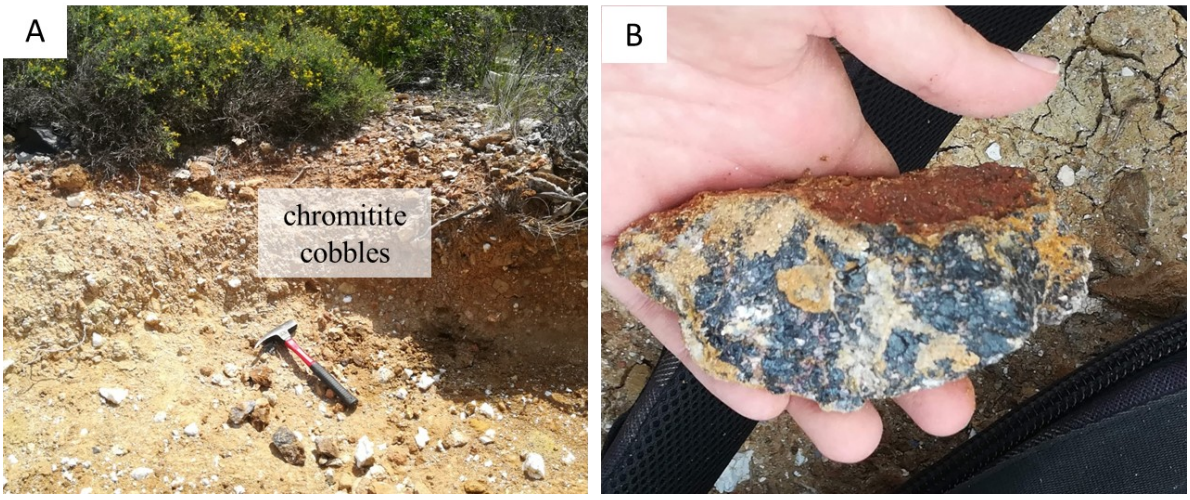


Fig. 4.15 Nea Roda sample location (A) and hand specimen (B).

Massive chromitites are composed mostly of subhedral chromite crystals in a chlorite groundmass (Fig. 4.16A, B). Chromite is frequently altered into ferrian chromite, and all primary silicates have been replaced by Cr-chlorite. The BMM assemblage is poor, and constituted by rare sulfides (millerite, godlevskite) and arsenides (maucherite), all found as inclusions within chromite or ferrian chromite. The only PGM found at Nea Roda is a laurite crystal (Fig. 4.17).

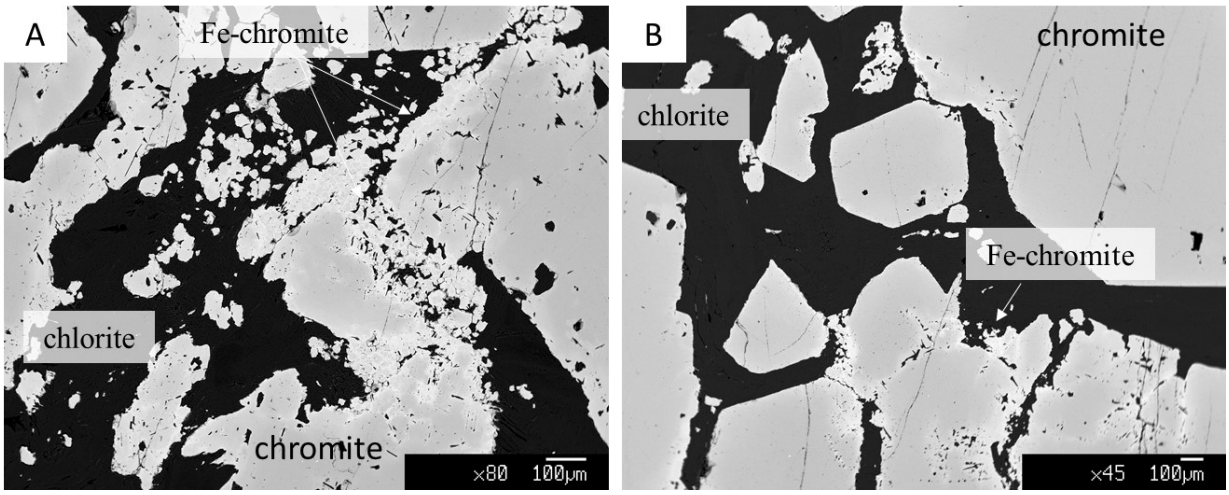


Fig. 4.16 A) and B) BSE images of Nea Roda chromitites.

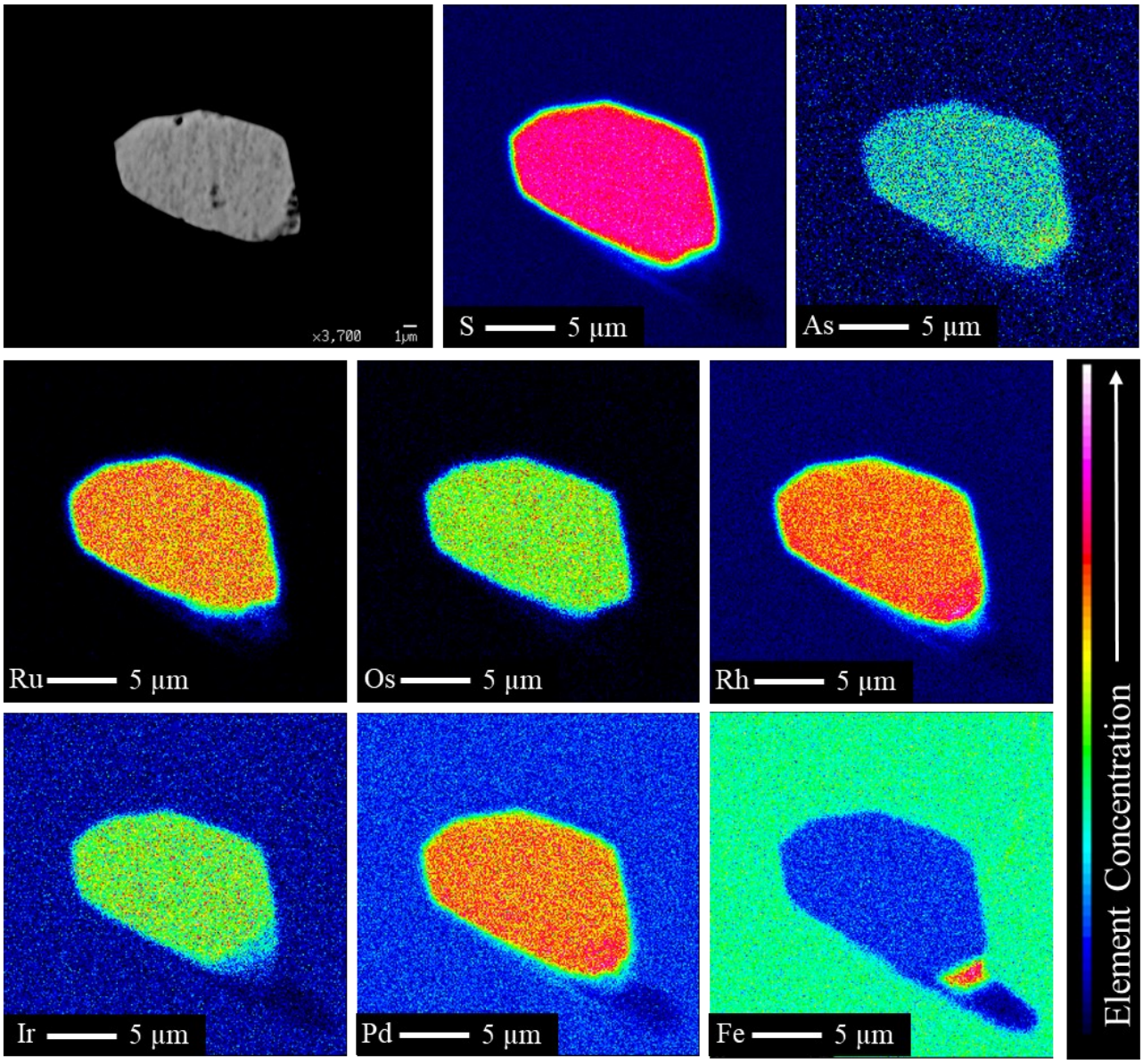


Fig. 4.17 Atomic maps of the only PGM detected within Nea Roda.

### 4.2.2 Mineral and whole rock chemistry

Complete microprobe analyses of Gomati and Nea Roda are reported in the Appendix (Tab. A4.1 to Tab. A4.9).

#### 4.2.2.1. Gomati

*Chromite*

Chromite average compositions (Tab. 4.2) are based on core analyses. The composition of the spinels is rather heterogeneous among the different localities (St. George, Tripes and Limonadika). MgO content ranges between 4.18 and 9.85 wt% in St. George, between 8.37 and 11.92 wt% in Tripes and between 7.19 and 10.49 wt% in Limonadika. FeO content ranges between 14.03 and 26.80 wt% in St.

George, between 20.33 and 25.29 wt% in Tripes and between 19.30 and 23.04 wt% in Limonadika. $Cr_2O_3$ contents are more variable between the three areas. St. George and Limonadika have similar contents, ranging between 51.13 and 65.54 wt% and between 57.69 and 68.38 wt% respectively. Tripes shows lower $Cr_2O_3$ contents, comprised between 43.54 and 45.22 wt%. $Al_2O_3$ contents, on the contrary, are lower in St. George and Limonadika (6.08-12.44 and 2.04-11.66 wt% respectively) with respect to Tripes, where they range between 18.99 and 19.73 wt%.

Tab. 4.2 Chromite cores average composition (wt%) and standard deviation from Gomati chromitites.

| | GOM2A | | GOM2B | | GOM2C | | GR54A | | GR54C | | GR54D | | GR55 | | TRI10 | | LIM3 | |
|---|---|---|---|---|---|---|---|---|---|---|---|---|---|---|---|---|---|---|
| wt% | **Avg** | StDev | **Avg** | StDev | **Avg** | StDev | **Avg** | StDev | **Avg** | StDev | **Avg** | StDev | **Avg** | StDev | **Avg** | StDev | **Avg** | StDev |
| $TiO_2$ | **0.28** | 0.07 | **0.46** | 0.08 | **0.30** | 0.06 | **0.31** | 0.05 | **0.30** | 0.06 | **0.25** | 0.04 | **0.17** | 0.04 | **0.28** | 0.03 | **0.12** | 0.04 |
| $Al_2O_3$ | **10.89** | 1.62 | **9.79** | 2.19 | **10.87** | 1.59 | **10.71** | 2.08 | **10.98** | 1.42 | **9.68** | 1.70 | **10.91** | 0.58 | **19.37** | 0.32 | **5.25** | 4.51 |
| $Cr_2O_3$ | **56.94** | 2.13 | **53.17** | 1.52 | **55.87** | 1.68 | **55.28** | 1.88 | **56.18** | 1.75 | **57.51** | 1.69 | **60.58** | 1.32 | **44.31** | 0.80 | **64.52** | 5.01 |
| $Fe_2O_3$ | **2.01** | 0.63 | **5.13** | 1.03 | **1.73** | 0.61 | **2.36** | 0.95 | **2.71** | 0.87 | **1.91** | 0.79 | **0.00** | 0.00 | **3.20** | 0.06 | **1.22** | 0.24 |
| FeO | **21.55** | 0.62 | **25.83** | 0.61 | **21.05** | 0.96 | **21.64** | 1.01 | **22.50** | 0.53 | **20.70** | 1.07 | **17.05** | 0.97 | **22.86** | 2.75 | **21.88** | 1.73 |
| MnO | **0.14** | 0.08 | **0.33** | 0.06 | **0.17** | 0.07 | **0.17** | 0.07 | **0.17** | 0.07 | **0.15** | 0.07 | **0.11** | 0.06 | **0.43** | 0.23 | **0.36** | 0.02 |
| MgO | **8.01** | 0.51 | **5.07** | 0.55 | **7.96** | 0.73 | **7.60** | 0.83 | **7.49** | 0.41 | **8.12** | 0.76 | **9.30** | 0.32 | **10.20** | 1.97 | **8.13** | 1.58 |
| NiO | **0.08** | 0.03 | **0.06** | 0.02 | **0.05** | 0.03 | **0.05** | 0.03 | **0.04** | 0.03 | **0.04** | 0.04 | **0.06** | 0.04 | **0.15** | 0.06 | **0.07** | 0.03 |
| ZnO | **0.04** | 0.04 | **0.04** | 0.05 | **0.03** | 0.03 | **0.03** | 0.02 | **0.04** | 0.03 | **0.03** | 0.03 | **0.03** | 0.03 | **na** | na | **na** | na |
| Total | **99.96** | 0.74 | **100.08** | 0.49 | **98.16** | 0.75 | **98.29** | 0.62 | **100.55** | 0.43 | **98.50** | 1.02 | **98.46** | 1.01 | **100.86** | 0.51 | **101.64** | 0.29 |
| Ti | **0.01** | 0.00 | **0.01** | 0.00 | **0.01** | 0.00 | **0.01** | 0.00 | **0.01** | 0.00 | **0.01** | 0.00 | **0.00** | 0.00 | **0.01** | 0.00 | **0.00** | 0.00 |
| Al | **0.43** | 0.06 | **0.40** | 0.08 | **0.43** | 0.06 | **0.43** | 0.08 | **0.43** | 0.05 | **0.39** | 0.07 | **0.43** | 0.02 | **0.72** | 0.00 | **0.20** | 0.17 |
| Cr | **1.50** | 0.07 | **1.44** | 0.06 | **1.50** | 0.05 | **1.49** | 0.07 | **1.48** | 0.06 | **1.55** | 0.05 | **1.61** | 0.03 | **1.10** | 0.00 | **1.72** | 0.18 |
| $Fe^{3+}$ | **0.05** | 0.02 | **0.13** | 0.03 | **0.04** | 0.02 | **0.06** | 0.02 | **0.07** | 0.02 | **0.05** | 0.02 | **0.00** | 0.00 | **0.08** | 0.00 | **0.03** | 0.01 |
| $Fe^{2+}$ | **0.60** | 0.02 | **0.74** | 0.03 | **0.60** | 0.03 | **0.62** | 0.04 | **0.63** | 0.02 | **0.59** | 0.03 | **0.48** | 0.03 | **0.60** | 0.08 | **0.62** | 0.06 |
| Mn | **0.00** | 0.00 | **0.01** | 0.00 | **0.01** | 0.00 | **0.00** | 0.00 | **0.00** | 0.00 | **0.00** | 0.00 | **0.00** | 0.00 | **0.01** | 0.01 | **0.01** | 0.00 |
| Mg | **0.40** | 0.02 | **0.26** | 0.03 | **0.40** | 0.03 | **0.39** | 0.04 | **0.37** | 0.02 | **0.41** | 0.04 | **0.47** | 0.01 | **0.48** | 0.08 | **0.41** | 0.07 |
| Ni | **0.00** | 0.00 | **0.00** | 0.00 | **0.00** | 0.00 | **0.00** | 0.00 | **0.00** | 0.00 | **0.00** | 0.00 | **0.00** | 0.00 | **0.00** | 0.00 | **0.00** | 0.00 |
| Zn | **0.00** | 0.00 | **0.00** | 0.00 | **0.00** | 0.00 | **0.00** | 0.00 | **0.00** | 0.00 | **0.00** | 0.00 | **0.00** | 0.00 | **na** | na | **na** | na |
| XMg | **0.40** | 0.02 | **0.26** | 0.03 | **0.40** | 0.03 | **0.38** | 0.04 | **0.37** | 0.02 | **0.41** | 0.04 | **0.49** | 0.02 | **0.44** | 0.08 | **0.40** | 0.06 |
| XCr | **0.78** | 0.03 | **0.79** | 0.04 | **0.78** | 0.03 | **0.78** | 0.04 | **0.77** | 0.03 | **0.80** | 0.03 | **0.79** | 0.01 | **0.61** | 0.00 | **0.89** | 0.09 |

*Pyroxene and olivine*

Silicate minerals within chromitites are almost completely replaced by chlorite. The only relicts found are clinopyroxene crystals (Tab. 4.3), of the same composition as those found in pyroxenites associated with chromitites. Average values of wollastonite%, enstatite% and ferrosilite% in pyroxenes from chromitite are 51.39, 47.92 and 0.39 respectively, while pyroxenes within the host rock have wollastonite%, enstatite% and ferrosilite% of 48.05, 51.10 and 0.21. Clinopyroxenes are Ca and Mg-rich and Al-free, and can be classified as diopsides and augites. In one section Mg-rich olivine crystals were found in the silicate rocks associated to the chromitites.

Tab. 4.3 Pyroxene and olivine average composition (wt%) and standard deviation from Gomati.

| | GOM2B-cpx | | GR54C-cpx | | GR54A-ol | |
|---|---|---|---|---|---|---|
| | **Avg** | St Dev | **Avg** | St Dev | **Avg** | St Dev |
| $SiO_2$ | **53.67** | 1.02 | **54.57** | 0.84 | **41.16** | 0.45 |
| $TiO_2$ | **0.03** | 0.03 | **0.04** | 0.03 | **0.01** | 0.02 |
| $Al_2O_3$ | **0.12** | 0.18 | **0.21** | 0.13 | **0.00** | 0.01 |
| $Cr_2O_3$ | **0.11** | 0.11 | **0.10** | 0.12 | **0.01** | 0.02 |
| $Fe_2O_3$ | **0.59** | 0.31 | **0.33** | 0.21 | **0.00** | 0.00 |
| FeO | **0.15** | 0.25 | **0.12** | 0.20 | **6.67** | 0.26 |
| MnO | **0.01** | 0.02 | **0.01** | 0.02 | **0.08** | 0.02 |
| NiO | **0.00** | 0.00 | **0.00** | 0.00 | **0.00** | 0.00 |
| ZnO | **0.01** | 0.01 | **0.01** | 0.02 | **0.01** | 0.02 |
| MgO | **18.70** | 1.23 | **18.79** | 0.45 | **52.86** | 0.58 |
| CaO | **24.47** | 1.31 | **24.81** | 0.83 | **0.00** | 0.01 |
| $Na_2O$ | **0.04** | 0.03 | **0.08** | 0.05 | **na** | na |
| Total | **97.92** | 1.05 | **99.09** | 1.06 | **100.82** | 0.75 |
| Si | **1.97** | 0.03 | **1.98** | 0.02 | **0.98** | 0.01 |
| Ti | **0.00** | 0.00 | **0.00** | 0.00 | **0.00** | 0.00 |
| Al | **0.01** | 0.01 | **0.01** | 0.01 | **0.00** | 0.00 |
| Cr | **0.00** | 0.00 | **0.00** | 0.00 | **0.00** | 0.00 |
| $Fe^3$ | **0.02** | 0.01 | **0.01** | 0.01 | **0.00** | 0.00 |
| $Fe^2$ | **0.00** | 0.01 | **0.00** | 0.01 | **0.13** | 0.01 |
| Mn | **0.00** | 0.00 | **0.00** | 0.00 | **0.00** | 0.00 |
| Ni | **0.00** | 0.00 | **0.00** | 0.00 | **0.00** | 0.00 |
| Zn | **0.00** | 0.00 | **0.00** | 0.00 | **0.00** | 0.00 |
| Mg | **1.03** | 0.07 | **1.02** | 0.03 | **1.88** | 0.01 |
| Ca | **0.97** | 0.05 | **0.97** | 0.03 | **0.00** | 0.00 |
| Na | **0.00** | 0.00 | **0.01** | 0.00 | **na** | na |

*Chlorite and serpentine*

Within the pyroxenites, chlorite and serpentine crystals partially replace primary silicates (pyroxene and minor olivine). Chlorite composition within chromitites and pyroxenites is homogeneous. Average cation content of Si is 6.38 in St. Georges, 5.85 in Tripes and 7.17 in Limonadika (Tab. 4.4). The analyzed chlorites are all clinochlore and penninite crystals, with some grains of talc-chlorite and a single sheridanite found in Tripes. However, due to the presence of abundant $Cr_2O_3$ (up to 5 wt%), the term chromian chlorite to define Gomati chlorites is more appropriate. Serpentine was found exclusively within chromitite host rocks, where it forms part of the silicate matrix. It is characterized by MgO content varying between 36.46 and 42.78 wt% and FeO content varying between 1.07 and 7.03 wt% (Tab. 4.5).

Tab. 4.4 Chlorite average composition (wt%) and standard deviation from Gomati.

| | GOM1A | | GOM2A | | GOM2B | | GOM2C | | GR54A | | GR54C | | GR54D | | GR55 | | TRI10 | | LIM3 | |
|---|---|---|---|---|---|---|---|---|---|---|---|---|---|---|---|---|---|---|---|---|
| wt% | **Avg** | StDev | **Avg** | StDev | **Avg** | StDev | **Avg** | StDev | **Avg** | StDev | **Avg** | StDev | **Avg** | StDev | **Avg** | StDev | **Avg** | StDev | **Avg** | StDev |
| $SiO_2$ | **32.31** | 1.96 | **31.51** | 0.67 | **33.92** | 3.19 | **32.25** | 1.13 | **34.64** | 3.37 | **34.98** | 3.18 | **33.23** | 1.91 | **31.88** | 0.43 | **30.39** | 1.94 | **37.91** | 5.12 |
| $TiO_2$ | **0.03** | 0.03 | **0.02** | 0.02 | **0.02** | 0.01 | **0.02** | 0.03 | **0.04** | 0.02 | **0.02** | 0.02 | **0.03** | 0.02 | **0.02** | 0.02 | **0.04** | 0.02 | **0.02** | 0.03 |
| $Al_2O_3$ | **12.88** | 2.36 | **15.37** | 0.75 | **10.03** | 3.43 | **13.00** | 1.57 | **9.69** | 4.48 | **10.26** | 3.76 | **12.09** | 3.13 | **14.65** | 0.78 | **17.37** | 3.73 | **7.36** | 5.09 |
| $Cr_2O_3$ | **1.40** | 0.76 | **4.36** | 1.03 | **2.72** | 1.40 | **4.12** | 0.68 | **3.47** | 1.20 | **3.54** | 1.43 | **4.35** | 1.06 | **4.35** | 0.37 | **2.90** | 0.71 | **3.26** | 1.69 |
| $Fe_2O_3$ | **1.53** | 1.64 | **0.00** | 0.00 | **0.19** | 0.49 | **0.09** | 0.25 | **0.04** | 0.10 | **0.05** | 0.21 | **0.00** | 0.00 | **0.00** | 0.00 | **0.00** | 0.00 | **0.00** | 0.00 |
| FeO | **6.08** | 0.95 | **1.51** | 0.33 | **2.04** | 0.41 | **1.63** | 0.28 | **1.64** | 0.33 | **1.30** | 0.42 | **1.52** | 0.20 | **1.19** | 0.09 | **2.22** | 0.57 | **1.48** | 0.20 |
| MnO | **0.03** | 0.04 | **0.01** | 0.03 | **0.01** | 0.01 | **0.02** | 0.03 | **0.01** | 0.02 | **0.03** | 0.03 | **0.02** | 0.02 | **0.02** | 0.02 | **0.02** | 0.01 | **0.01** | 0.01 |
| NiO | **0.12** | 0.02 | **0.31** | 0.04 | **0.00** | 0.00 | **0.18** | 0.05 | **0.21** | 0.10 | **0.09** | 0.10 | **0.22** | 0.05 | **0.39** | 0.04 | **0.23** | 0.04 | **0.27** | 0.06 |
| ZnO | **0.01** | 0.02 | **0.01** | 0.02 | **0.01** | 0.01 | **0.01** | 0.01 | **0.01** | 0.01 | **0.01** | 0.01 | **0.00** | 0.01 | **0.01** | 0.01 | **na** | na | **na** | na |

| | | | | | | | | | | | | | | | | | | | |
|---|---|---|---|---|---|---|---|---|---|---|---|---|---|---|---|---|---|---|---|
| MgO | **31.86** | 1.23 | **32.94** | 0.72 | **34.46** | 1.54 | **33.70** | 0.34 | **35.21** | 1.95 | **35.02** | 1.77 | **34.03** | 1.26 | **32.78** | 0.50 | **32.48** | 0.95 | **35.89** | 1.71 |
| CaO | **0.04** | 0.02 | **0.01** | 0.01 | **0.06** | 0.06 | **0.02** | 0.01 | **0.01** | 0.01 | **0.04** | 0.06 | **0.01** | 0.01 | **0.03** | 0.02 | **0.03** | 0.02 | **0.10** | 0.09 |
| $Na_2O$ | **0.01** | 0.01 | **0.01** | 0.01 | **0.00** | 0.01 | **0.02** | 0.02 | **0.01** | 0.02 | **0.00** | 0.01 | **0.00** | 0.01 | **0.02** | 0.01 | **0.02** | 0.02 | **0.02** | 0.02 |
| $K_2O$ | **0.01** | 0.01 | **0.01** | 0.01 | **0.00** | 0.00 | **0.03** | 0.03 | **0.01** | 0.01 | **0.00** | 0.01 | **0.01** | 0.01 | **0.02** | 0.06 | **0.03** | 0.03 | **0.03** | 0.01 |
| $H_2O$ | **12.30** | 0.19 | **12.44** | 0.10 | **12.14** | 0.14 | **12.33** | 0.10 | **12.35** | 0.12 | **12.40** | 0.14 | **12.37** | 0.18 | **12.34** | 0.09 | **12.47** | 0.06 | **12.67** | 0.19 |
| Total | **98.61** | 1.89 | **98.49** | 0.73 | **95.61** | 0.97 | **97.41** | 0.91 | **97.33** | 0.95 | **97.76** | 1.39 | **97.88** | 1.28 | **97.71** | 0.79 | **98.20** | 0.49 | **99.01** | 0.92 |
| Si | **6.30** | 0.36 | **6.07** | 0.10 | **6.70** | 0.61 | **6.28** | 0.21 | **6.73** | 0.63 | **6.77** | 0.60 | **6.44** | 0.35 | **6.20** | 0.07 | **5.85** | 0.39 | **7.17** | 0.88 |
| Ti | **0.00** | 0.00 | **0.00** | 0.00 | **0.00** | 0.00 | **0.00** | 0.00 | **0.01** | 0.00 | **0.00** | 0.00 | **0.00** | 0.00 | **0.00** | 0.00 | **0.01** | 0.00 | **0.00** | 0.00 |
| Al | **2.96** | 0.54 | **3.49** | 0.18 | **2.34** | 0.80 | **2.98** | 0.35 | **2.22** | 1.03 | **2.34** | 0.86 | **2.76** | 0.71 | **3.36** | 0.18 | **3.94** | 0.83 | **1.65** | 1.15 |
| Cr | **0.22** | 0.12 | **0.66** | 0.16 | **0.43** | 0.22 | **0.63** | 0.11 | **0.53** | 0.18 | **0.54** | 0.22 | **0.67** | 0.17 | **0.67** | 0.06 | **0.44** | 0.11 | **0.49** | 0.26 |
| $Fe^3$ | **0.22** | 0.24 | **0.00** | 0.00 | **0.03** | 0.07 | **0.01** | 0.04 | **0.01** | 0.01 | **0.01** | 0.03 | **0.00** | 0.00 | **0.00** | 0.00 | **0.00** | 0.00 | **0.00** | 0.00 |
| $Fe^2$ | **0.99** | 0.15 | **0.24** | 0.05 | **0.34** | 0.07 | **0.27** | 0.04 | **0.27** | 0.05 | **0.21** | 0.07 | **0.25** | 0.03 | **0.19** | 0.01 | **0.36** | 0.09 | **0.23** | 0.03 |
| Mn | **0.01** | 0.01 | **0.00** | 0.00 | **0.00** | 0.00 | **0.00** | 0.00 | **0.00** | 0.00 | **0.00** | 0.01 | **0.00** | 0.00 | **0.00** | 0.00 | **0.00** | 0.00 | **0.00** | 0.00 |
| Ni | **0.02** | 0.00 | **0.05** | 0.01 | **0.00** | 0.00 | **0.03** | 0.01 | **0.03** | 0.02 | **0.01** | 0.02 | **0.03** | 0.01 | **0.06** | 0.01 | **0.04** | 0.01 | **0.04** | 0.01 |
| Zn | **0.00** | 0.00 | **0.00** | 0.00 | **0.00** | 0.00 | **0.00** | 0.00 | **0.00** | 0.00 | **0.00** | 0.00 | **0.00** | 0.00 | **0.00** | 0.00 | **na** | na | **na** | na |
| Mg | **9.26** | 0.35 | **9.46** | 0.15 | **10.15** | 0.40 | **9.78** | 0.11 | **10.19** | 0.53 | **10.10** | 0.51 | **9.83** | 0.33 | **9.50** | 0.14 | **9.32** | 0.30 | **10.13** | 0.34 |
| Ca | **0.01** | 0.00 | **0.00** | 0.00 | **0.01** | 0.01 | **0.00** | 0.00 | **0.00** | 0.00 | **0.01** | 0.01 | **0.00** | 0.00 | **0.01** | 0.00 | **0.01** | 0.00 | **0.02** | 0.02 |
| Na | **0.01** | 0.01 | **0.00** | 0.00 | **0.00** | 0.00 | **0.01** | 0.01 | **0.01** | 0.01 | **0.00** | 0.00 | **0.00** | 0.00 | **0.01** | 0.01 | **0.01** | 0.01 | **0.01** | 0.01 |
| K | **0.00** | 0.00 | **0.00** | 0.00 | **0.00** | 0.00 | **0.01** | 0.01 | **0.00** | 0.00 | **0.00** | 0.00 | **0.00** | 0.00 | **0.01** | 0.01 | **0.01** | 0.01 | **0.01** | 0.00 |
| H | **16.00** | 0.00 | **16.00** | 0.00 | **16.00** | 0.00 | **16.00** | 0.00 | **16.00** | 0.00 | **16.00** | 0.00 | **16.00** | 0.00 | **16.00** | 0.00 | **16.00** | 0.00 | **16.00** | 0.00 |

Tab. 4.5 Selected microprobe analyses of serpentine crystals from Gomati; bdl: below detection limit.

| **Wt%** | **GOM1A 17** | **GOM1A 18** | **GOM1A 26** | **GOM1A 27** | **GOM1A 28** | **GOM2C 10** | **GOM2C 11** | **GOM2C 12** | **GOM2C 15** | **GOM2C 21** | **GR54A 21** | **GR54A 24** |
|---|---|---|---|---|---|---|---|---|---|---|---|---|
| MgO | 36.46 | 36.83 | 36.58 | 36.63 | 37.31 | 39.81 | 40.29 | 40.82 | 40.08 | 38.95 | 42.78 | 39.59 |
| $Al_2O_3$ | 0.60 | 0.40 | 0.85 | 0.66 | 0.69 | 0.21 | 0.08 | 0.16 | 0.31 | 0.11 | 0.66 | 0.24 |
| $SiO_2$ | 43.15 | 43.04 | 42.17 | 42.32 | 42.32 | 41.77 | 41.39 | 42.78 | 42.05 | 41.77 | 41.91 | 42.69 |
| $Cr_2O_3$ | 0.00 | 0.05 | 0.22 | 0.08 | 0.07 | 0.36 | 0.17 | 0.24 | 0.25 | 0.18 | 0.86 | 0.37 |
| FeO | 6.54 | 6.70 | 6.99 | 6.76 | 7.03 | 1.19 | 1.25 | 1.09 | 1.24 | 1.07 | 2.29 | 1.23 |
| $Na_2O$ | 0.02 | bdl | 0.01 | bdl | bdl | bdl | bdl | bdl | bdl | 0.01 | 0.01 | bdl |
| CaO | 0.02 | bdl | 0.01 | bdl | 0.05 | 0.03 | 0.03 | 0.02 | 0.02 | 0.02 | bdl | 0.01 |
| $TiO_2$ | bdl | 0.02 | 0.01 | bdl | 0.02 | bdl | 0.03 | 0.04 | 0.04 | 0.04 | 0.01 | bdl |
| MnO | 0.07 | 0.04 | 0.09 | 0.10 | 0.09 | 0.09 | bdl | bdl | 0.06 | 0.06 | 0.04 | 0.01 |
| $K_2O$ | 0.03 | bdl | bdl | 0.01 | bdl | 0.02 | bdl | bdl | 0.01 | bdl | 0.02 | bdl |
| ZnO | 0.04 | 0.01 | bdl | bdl | bdl | bdl | bdl | bdl | bdl | 0.01 | 0.01 | bdl |
| $H_2O$ | 12.62 | 12.62 | 12.54 | 12.52 | 12.64 | 12.37 | 12.34 | 12.65 | 12.47 | 12.24 | 12.91 | 12.50 |
| Tot | 99.49 | 99.69 | 99.47 | 99.10 | 100.21 | 95.84 | 95.58 | 97.78 | 96.52 | 94.45 | 101.49 | 96.65 |
| Mg | 5.17 | 5.22 | 5.22 | 5.23 | 5.28 | 5.75 | 5.83 | 5.77 | 5.75 | 5.69 | 5.92 | 5.66 |
| Al tot | 0.07 | 0.04 | 0.10 | 0.07 | 0.08 | 0.02 | 0.01 | 0.02 | 0.03 | 0.01 | 0.07 | 0.03 |
| Si | 4.10 | 4.09 | 4.03 | 4.05 | 4.02 | 4.05 | 4.02 | 4.06 | 4.04 | 4.09 | 3.89 | 4.10 |
| Cr | 0.00 | 0.01 | 0.03 | 0.01 | 0.01 | 0.04 | 0.02 | 0.03 | 0.03 | 0.02 | 0.09 | 0.04 |
| Fe tot | 0.52 | 0.53 | 0.56 | 0.54 | 0.56 | 0.10 | 0.10 | 0.09 | 0.10 | 0.09 | 0.18 | 0.10 |
| Na | 0.00 | 0.00 | 0.00 | 0.00 | 0.00 | 0.00 | 0.00 | 0.00 | 0.00 | 0.00 | 0.00 | 0.00 |
| Ca | 0.00 | 0.00 | 0.00 | 0.00 | 0.00 | 0.00 | 0.00 | 0.00 | 0.00 | 0.00 | 0.00 | 0.00 |
| Ti | 0.00 | 0.00 | 0.00 | 0.00 | 0.00 | 0.00 | 0.00 | 0.00 | 0.00 | 0.00 | 0.00 | 0.00 |
| Mn | 0.01 | 0.00 | 0.01 | 0.01 | 0.01 | 0.01 | 0.00 | 0.00 | 0.00 | 0.01 | 0.00 | 0.00 |
| K | 0.00 | 0.00 | 0.00 | 0.00 | 0.00 | 0.00 | 0.00 | 0.00 | 0.00 | 0.00 | 0.00 | 0.00 |
| Zn | 0.00 | 0.00 | 0.00 | 0.00 | 0.00 | 0.00 | 0.00 | 0.00 | 0.00 | 0.00 | 0.00 | 0.00 |
| OH * | 8.00 | 8.00 | 8.00 | 8.00 | 8.00 | 8.00 | 8.00 | 8.00 | 8.00 | 8.00 | 8.00 | 8.00 |

*Base Metal Minerals*

Base Metal Minerals detected in the Gomati massif are sulfides (Tab. 4.6), arsenides (Tab. 4.7) and antimonides (Tab. 4.8). Heazlewoodite and millerite are the most abundant sulfides, followed by pentlandite, chalcocite and some unknown Cu-Ni-Fe sulfide. A pyrite grain was also detected. The major element composition of sulfides is quite homogeneous, but some minerals show enrichments in As, Ir, Os, Pt and Pd, generally between 0.1 and 0.6 wt%. Heazlewoodite and millerite have residual

Fe contents up to 2.23 wt%. Two grains of an unknown sulfide have been detected in two different areas (Limonadika and St. George). Both show similar S and Fe contents, (31.46 and 5.57 wt% in Limonadika, 32.74 and 4.23 wt% in St. George), but different Ni and Cu contents (26.67 and 33.65 wt% within Limonadika, 33.95 and 23.73 wt% within St. George).

Arsenides within Gomati are quite abundant, and have been detected both within massive chromitites and associated pyroxenites. Only Ni-arsenides are present. Maucherite is the most abundant, followed by nickeline and orcelite. Two analyzed minerals are unknown species. Their recalculated mineral formulas are $Ni_3As$ and $Ni_5As_2$. The minerals with formula $Ni_3As$ may correspond to the mineral dienerite, formerly discredited by the IMA and only recently under revalidation. The minerals with formula $Ni_5(As,Sb)_2$ may correspond to new compounds (Bussolesi et al., 2020b).

Four antimonide species have been detected in St. George locality. The minerals are abundant within pyroxenites associated to massive chromitites, and rare within massive chromitites, where they are found within the silicate gangue. The only known antimonide is the mineral breithauptite (NiSb), while the other three unnamed species are Ni-Cu antimonides that cluster around the following compositions: $(Ni,Cu)_{5-x}Sb_2$, $(Ni,Cu)_2Sb$ and $(Ni,Cu)_{11}Sb_8$. As-Sb substitution, which was observed in similar mineralogical assemblages (Tredoux et al., 2016) is not present in Gomati.

Tab. 4.6 Selected microprobe analyses of sulfides in Gomati; na: not analyzed; bdl: below detection limit.

| Sample | S | Ir | Os | As | Rh | Pt | Ru | Pd | Fe | Ni | Cu | Totale |
|---|---|---|---|---|---|---|---|---|---|---|---|---|
| ***wt%*** | | | | | | ***Pentlandite ($(Ni,Fe)_9S_8$)*** | | | | | | |
| GO3-3 | 33.08 | bdl | bdl | 0.13 | 0.04 | 0.48 | bdl | bdl | 22.78 | 41.45 | 0.48 | 98.44 |
| LIM1-8 | 33.19 | 0.14 | 0.11 | 0.03 | bdl | 0.19 | bdl | bdl | 23.91 | 39.50 | bdl | 97.08 |
| TRI10A-19 | 32.26 | 0.24 | bdl | 0.06 | 0.01 | bdl | bdl | bdl | 27.81 | 38.25 | bdl | 98.63 |
| GOM2A-SU-9 | 31.93 | na | na | bdl | na | na | na | na | 22.16 | 43.61 | bdl | 98.02 |
| | | | | | | ***Heazlewoodite ($Ni_3S_2$)*** | | | | | | |
| GO2-3b | 27.01 | 0.15 | 0.02 | 0.06 | bdl | bdl | bdl | bdl | 0.36 | 73.46 | bdl | 101.07 |
| GOM2BSULF65 | 26.51 | na | na | na | na | na | na | na | 0.09 | 72.59 | 0.04 | 99.23 |
| GOM2C-SU-2 | 25.50 | na | na | bdl | na | na | na | na | 1.19 | 72.64 | 0.04 | 99.48 |
| GR54A-SULF-6 | 25.94 | na | na | bdl | na | na | na | na | 0.61 | 71.56 | 0.04 | 98.17 |
| GR54D-SULF-1 | 26.82 | na | na | bdl | na | na | na | na | 1.20 | 73.41 | bdl | 101.43 |
| | | | | | | ***Millerite (NiS)*** | | | | | | |
| LIM3-7 | 34.96 | bdl | bdl | 0.23 | 0.08 | bdl | bdl | bdl | 0.83 | 63.05 | bdl | 99.14 |
| TRI10A-29c | 35.04 | 0.25 | 0.02 | bdl | bdl | 0.62 | bdl | 0.03 | 2.18 | 62.55 | bdl | 100.68 |
| GOM2A-SU-12 | 33.83 | na | na | bdl | na | na | na | na | 1.34 | 62.58 | 0.01 | 97.76 |
| GOM2B-SU-7 | 33.73 | na | na | bdl | na | na | na | na | 2.23 | 63.90 | 0.44 | 100.38 |
| GOM2C-SU-5 | 33.48 | na | na | bdl | na | na | na | na | 1.12 | 62.15 | 0.03 | 96.77 |
| GR54D-SU-6 | 32.28 | na | na | bdl | na | na | na | na | 0.36 | 61.15 | 0.11 | 93.98 |
| GR55-SU-2 | 34.30 | na | na | 0.35 | na | na | na | na | 1.19 | 60.60 | 1.15 | 97.65 |
| | | | | | | ***Chalcocite ($Cu_2S$)*** | | | | | | |
| GO3-3b | 21.09 | bdl | bdl | bdl | bdl | bdl | bdl | 0.02 | 1.65 | 0.26 | 76.77 | 99.78 |
| GOM2A-SU-14 | 21.41 | na | na | 0.00 | na | na | na | na | 1.20 | 1.88 | 72.03 | 96.52 |
| GOM2B-SU-62 | 20.66 | na | na | 0.00 | na | na | na | na | 1.07 | 0.00 | 79.58 | 101.33 |
| | | | | | | ***Unknown Cu-Ni-Fe sulfide*** | | | | | | |
| LIM3-9 | 31.46 | bdl | bdl | 1.17 | bdl | bdl | 0.01 | 0.01 | 5.57 | 26.67 | 33.65 | 98.53 |
| GOM2C-SU-1 | 32.74 | na | na | bdl | na | na | na | na | 4.23 | 33.95 | 23.73 | 95.14 |
| | | | | | | ***Pyrite ($FeS_2$)*** | | | | | | |
| TRI10A-29b | 51.77 | bdl | bdl | 0.08 | 0.06 | bdl | bdl | bdl | 44.67 | 2.08 | bdl | 98.65 |
| ***apfu*** | | | | | | ***Pentlandite ($(Ni,Fe)_9S_8$)*** | | | | | | |
| GO3-3 | 8.13 | 0.00 | 0.00 | 0.01 | 0.00 | 0.02 | 0.00 | 0.00 | 3.21 | 5.56 | 0.06 | 17.00 |
| LIM1-8 | 8.23 | 0.01 | 0.00 | 0.00 | 0.00 | 0.01 | 0.00 | 0.00 | 3.40 | 5.35 | 0.00 | 17.00 |
| TRI10A-19 | 7.93 | 0.01 | 0.00 | 0.01 | 0.00 | 0.00 | 0.00 | 0.00 | 3.92 | 5.13 | 0.00 | 17.00 |
| GOM2A-SU-9 | 7.93 | na | na | 0.00 | na | na | na | na | 3.16 | 5.92 | 0.00 | 17.00 |
| | | | | | | ***Heazlewoodite ($Ni_3S_2$)*** | | | | | | |
| GO2-3b | 2.00 | 0.00 | 0.00 | 0.00 | 0.00 | 0.00 | 0.00 | 0.00 | 0.02 | 2.98 | 0.00 | 5.00 |

| | | | | | | | | | | | | |
|---|---|---|---|---|---|---|---|---|---|---|---|---|
| GOM2BSULF65 | 2.00 | na | na | na | na | na | na | na | 0.00 | 2.99 | 0.00 | 5.00 |
| GOM2C-SU-2 | 1.94 | na | na | 0.00 | na | na | na | na | 0.05 | 3.01 | 0.00 | 5.00 |
| GR54A-SU-6 | 1.98 | na | na | 0.00 | na | na | na | na | 0.03 | 2.99 | 0.00 | 5.00 |
| GR54D-SU-1 | 1.98 | na | na | 0.00 | na | na | na | na | 0.05 | 2.97 | 0.00 | 5.00 |
| | | | | | | ***Millerite (NiS)*** | | | | | | |
| LIM3-7 | 1.00 | 0.00 | 0.00 | 0.00 | 0.00 | 0.00 | 0.00 | 0.00 | 0.01 | 0.98 | 0.00 | 2.00 |
| TRI10A-29c | 0.99 | 0.00 | 0.00 | 0.00 | 0.00 | 0.00 | 0.00 | 0.00 | 0.04 | 0.97 | 0.00 | 2.00 |
| GOM2A-SU-12 | 0.98 | na | na | 0.00 | na | na | na | na | 0.02 | 0.99 | 0.00 | 2.00 |
| GOM2B-SU-7 | 0.96 | na | na | 0.00 | na | na | na | na | 0.04 | 1.00 | 0.01 | 2.00 |
| GOM2C-SU-5 | 0.98 | na | na | 0.00 | na | na | na | na | 0.02 | 1.00 | 0.00 | 2.00 |
| GR54D-SU-6 | 0.98 | na | na | 0.00 | na | na | na | na | 0.01 | 1.01 | 0.00 | 2.00 |
| GR55-SU-2 | 1.00 | na | na | 0.00 | na | na | na | na | 0.02 | 0.96 | 0.02 | 2.00 |
| | | | | | | ***Chalcocite ($Cu_2S$)*** | | | | | | |
| GO3-3b | 1.04 | 0.00 | 0.00 | 0.00 | 0.00 | 0.00 | 0.00 | 0.00 | 0.05 | 0.01 | 1.91 | 3.00 |
| GOM2A-SU-14 | 1.08 | na | na | 0.00 | na | na | na | na | 0.03 | 0.05 | 1.83 | 3.00 |
| GOM2B-SU-62 | 1.01 | na | na | 0.00 | na | na | na | na | 0.03 | 0.00 | 1.96 | 3.00 |
| | | | | | | ***Unknown Cu-Ni-Fe sulfide*** | | | | | | |
| LIM3-9 | - | - | - | - | - | - | - | - | - | - | - | - |
| GOM2C-SU-1 | - | - | - | - | - | - | - | - | - | - | - | - |
| | | | | | | ***Pyrite ($FeS_2$)*** | | | | | | |
| TRI10A-29b | 1.98 | 0.00 | 0.00 | 0.00 | 0.00 | 0.00 | 0.00 | 0.00 | 0.98 | 0.04 | 0.00 | 3.00 |

Tab. 4.7 Selected microprobe analyses of arsenides in Gomati; na: not analyzed; bdl: below detection limit.

| Sample | As | S | Ir | Pt | Ni | Fe | Cu | Sb | Total |
|---|---|---|---|---|---|---|---|---|---|
| ***wt%*** | | | | | ***Maucherite ($Ni_{11}As_8$)*** | | | | |
| GOM2A-SULF-1 | 44.76 | 0.51 | na | na | 49.16 | 1.80 | 0.03 | 1.01 | 97.28 |
| GOM2C-SULF-10 | 46.24 | 0.14 | na | na | 51.28 | 1.33 | 0.06 | 1.56 | 100.61 |
| GR54C-SULF-2 | 45.54 | 0.15 | na | na | 54.39 | 0.29 | 0.05 | 2.72 | 103.21 |
| | | | | | ***Nickeline (NiAs)*** | | | | |
| GOM2A-SULF-4 | 50.60 | 0.41 | na | na | 41.56 | 1.89 | 0.01 | 3.16 | 97.64 |
| GR55-SULF-1 | 54.57 | 0.16 | na | na | 41.30 | 1.09 | bdl | 0.30 | 97.42 |
| LIM1-9 | 55.03 | 0.74 | bdl | 0.69 | 42.26 | 1.35 | bdl | n.a. | 100.07 |
| TRI10-10d | 56.46 | 0.43 | 0.14 | bdl | 42.34 | 1.22 | bdl | n.a. | 100.59 |
| | | | | | ***Dinerite* ($Ni_3(As,Sb)$)*** | | | | |
| GOM2BSULF60 | 31.71 | bdl | na | na | 68.59 | 0.16 | 0.17 | 0.91 | 101.55 |
| GOM2B-SULF-13 | 31.52 | bdl | na | na | 67.41 | 0.13 | 0.10 | 0.78 | 99.93 |
| GOM2B-SULF-10 | 31.91 | 0.02 | na | na | 67.70 | 0.09 | 0.17 | 0.88 | 100.76 |
| | | | | | ***$Ni_5(As,Sb)_2$*** | | | | |
| GOM2B-SULF-27 | 32.90 | 0.01 | na | na | 66.38 | 0.10 | 0.22 | 1.17 | 100.79 |
| GOM2B-SULF-53 | 33.86 | 0.03 | na | na | 65.64 | 0.12 | 0.12 | 0.69 | 100.47 |
| GOM2B-SULF-52 | 34.19 | 0.01 | na | na | 65.15 | 0.11 | 0.20 | 0.71 | 100.36 |
| GOM2BSULF69 | 32.85 | 0.03 | na | na | 64.77 | 0.17 | 0.14 | 1.80 | 99.78 |
| | | | | | ***Orcelite ($Ni_{5-x}(As,Sb)_2$), x = 0.23*** | | | | |
| GOM2B-SULF-38 | 35.71 | 0.03 | na | na | 64.91 | 0.20 | 0.04 | 0.75 | 101.63 |
| GOM2B-SULF-45 | 34.70 | 0.01 | na | na | 64.71 | 0.23 | 0.14 | 0.71 | 100.49 |
| GOM2A-SULF-2 | 34.52 | 0.02 | na | na | 62.25 | 1.36 | 0.96 | 1.19 | 100.28 |
| GOM2A-SULF-3 | 34.50 | bdl | na | na | 61.91 | 1.31 | 0.99 | 1.19 | 99.91 |
| ***apfu*** | | | | | ***Maucherite ($Ni_{11}As_8$)*** | | | | |
| GOM2A-SULF-1 | 7.61 | 0.20 | 0.00 | 0.00 | 10.67 | 0.41 | 0.01 | 0.11 | 19.00 |
| GOM2C-SULF-10 | 7.65 | 0.05 | 0.00 | 0.00 | 10.83 | 0.29 | 0.01 | 0.16 | 19.00 |
| GR54C-SULF-2 | 7.37 | 0.06 | 0.00 | 0.00 | 11.23 | 0.06 | 0.01 | 0.27 | 19.00 |
| | | | | | ***Nickeline (NiAs)*** | | | | |
| GOM2A-SULF-4 | 0.93 | 0.02 | 0.00 | 0.00 | 0.97 | 0.05 | 0.00 | 0.04 | 2.00 |
| GR55-SULF-1 | 1.00 | 0.01 | 0.00 | 0.00 | 0.96 | 0.03 | 0.00 | 0.00 | 2.00 |
| LIM1-9 | 0.98 | 0.03 | 0.00 | 0.00 | 0.96 | 0.03 | 0.00 | 0.00 | 2.00 |
| TRI10-10d | 1.00 | 0.02 | 0.00 | 0.00 | 0.95 | 0.03 | 0.00 | 0.00 | 2.00 |
| | | | | | ***Dinerite* ($Ni_3(As,Sb)$)*** | | | | |
| GOM2BSULF60 | 1.05 | 0.00 | 0.00 | 0.00 | 2.91 | 0.01 | 0.01 | 0.02 | 4.00 |
| GOM2B-SULF-13 | 1.07 | 0.00 | 0.00 | 0.00 | 2.91 | 0.01 | 0.00 | 0.02 | 4.00 |
| GOM2B-SULF-10 | 1.07 | 0.00 | 0.00 | 0.00 | 2.90 | 0.00 | 0.01 | 0.02 | 4.00 |
| | | | | | ***$Ni_5(As,Sb)_2$*** | | | | |
| GOM2B-SULF-27 | 1.94 | 0.00 | 0.00 | 0.00 | 4.99 | 0.01 | 0.02 | 0.04 | 7.00 |
| GOM2B-SULF-53 | 2.00 | 0.00 | 0.00 | 0.00 | 4.95 | 0.01 | 0.01 | 0.02 | 7.00 |
| GOM2B-SULF-52 | 2.02 | 0.00 | 0.00 | 0.00 | 4.93 | 0.01 | 0.01 | 0.03 | 7.00 |
| GOM2BSULF69 | 1.96 | 0.00 | 0.00 | 0.00 | 4.94 | 0.01 | 0.01 | 0.07 | 7.00 |
| | | | | | ***Orcelite ($Ni_{5-x}(As,Sb)_2$), x = 0.23*** | | | | |
| GOM2B-SULF-38 | 2.02 | 0.00 | 0.00 | 0.00 | 4.70 | 0.01 | 0.00 | 0.03 | 6.77 |
| GOM2B-SULF-45 | 1.99 | 0.00 | 0.00 | 0.00 | 4.73 | 0.02 | 0.01 | 0.02 | 6.77 |

| | | | | | | | | | |
|---|---|---|---|---|---|---|---|---|---|
| GOM2A-SULF-2 | 1.99 | 0.00 | 0.00 | 0.00 | 4.57 | 0.10 | 0.06 | 0.04 | 6.77 |
| GOM2A-SULF-3 | 1.99 | 0.00 | 0.00 | 0.00 | 4.56 | 0.10 | 0.07 | 0.04 | 6.77 |

* The mineral dinerite was discredited by the IMA

Tab. 4.8 Selected microprobe analyses of antimonides in Gomati; na: not analyzed; bdl: below detection limit

| | As | S | Ni | Fe | Cu | Sb | Total |
|---|---|---|---|---|---|---|---|
| ***wt%*** | | | | $(Ni,Cu)_{5-x}(Sb,As)_2$ | | | |
| GOM2B-SULF-1 | 1.19 | bdl | 41.07 | 0.08 | 12.44 | 46.23 | 101.02 |
| GOM2B-SULF-16 | 0.98 | 0.03 | 40.91 | 0.08 | 12.55 | 47.15 | 101.70 |
| GOM2B-SULF-21 | 1.06 | bdl | 39.87 | 0.13 | 12.60 | 46.44 | 100.10 |
| | | | | $(Ni,Cu)_2(Sb,As)$ | | | |
| GOM2B-SULF-20 | 1.21 | bdl | 38.97 | 0.13 | 12.76 | 47.59 | 100.67 |
| GOM2B-SULF-22 | 1.15 | bdl | 39.51 | 0.11 | 12.92 | 47.92 | 101.62 |
| GOM2B-SULF-15 | 1.08 | 0.22 | 36.71 | 0.09 | 13.88 | 48.61 | 100.60 |
| GOM2B-SULF-23 | 1.25 | 0.02 | 37.61 | 0.11 | 12.96 | 48.39 | 100.33 |
| GOM2B-SULF-29 | 1.16 | 0.03 | 37.74 | 0.13 | 13.16 | 48.48 | 100.73 |
| GOM2B-SULF-30 | 1.13 | 0.01 | 37.57 | 0.11 | 13.08 | 48.88 | 100.78 |
| GOM2B-SULF-35 | 1.46 | 0.03 | 38.62 | 0.10 | 11.35 | 49.99 | 101.55 |
| GOM2B-SULF-44 | 1.22 | bdl | 33.62 | 0.23 | 13.50 | 50.59 | 99.15 |
| GOM2B-SULF-50 | 1.16 | 0.01 | 37.72 | 0.12 | 13.11 | 47.32 | 99.46 |
| GOM2BSULF70 | 1.36 | bdl | 37.41 | 0.08 | 13.03 | 48.69 | 100.56 |
| | | | | $(Ni,Cu)_{11}(Sb,As)_8$ | | | |
| GOM2B-SULF-40 | 1.61 | 0.06 | 34.62 | 0.24 | 6.81 | 58.53 | 101.86 |
| | | | | ***breithauptite - NiSb*** | | | |
| GOM2B-SULF-3 | 2.10 | bdl | 31.28 | 0.55 | 0.02 | 65.67 | 99.65 |
| GOM2B-SULF-5 | 1.97 | 0.02 | 31.55 | 0.09 | 0.10 | 65.36 | 99.09 |
| GOM2B-SULF-6 | 2.00 | 0.02 | 32.13 | 0.06 | 0.10 | 67.05 | 101.35 |
| GOM2B-SULF-7 | 1.89 | bdl | 32.14 | 0.08 | 0.06 | 65.85 | 100.04 |
| GOM2B-SULF-8 | 1.76 | 0.01 | 32.75 | 0.03 | 0.06 | 65.37 | 99.98 |
| GOM2B-SULF-14 | 1.78 | bdl | 32.10 | 0.08 | 0.08 | 65.77 | 99.81 |
| GOM2B-SULF-26 | 1.73 | 0.02 | 32.97 | 0.06 | 0.07 | 65.21 | 100.06 |
| GOM2B-SULF-31 | 1.79 | bdl | 34.92 | 0.08 | 0.03 | 64.58 | 101.41 |
| GOM2B-SULF-34 | 1.39 | 0.02 | 34.12 | 0.10 | 0.95 | 63.56 | 100.14 |
| GOM2B-SULF-37 | 1.58 | bdl | 32.63 | 0.10 | 0.18 | 65.70 | 100.19 |
| ***apfu*** | | | | $(Ni,Cu)_{5-x}(Sb,As)_2$ | | | |
| GOM2B-SULF-1 | 0.08 | 0.00 | 3.66 | 0.01 | 1.03 | 1.99 | 6.77 |
| GOM2B-SULF-16 | 0.07 | 0.00 | 3.64 | 0.01 | 1.03 | 2.02 | 6.77 |
| GOM2B-SULF-21 | 0.07 | 0.00 | 3.61 | 0.01 | 1.05 | 2.02 | 6.77 |
| | | | | $(Ni,Cu)_2(Sb,As)$ | | | |
| GOM2B-SULF-20 | 0.04 | 0.00 | 1.56 | 0.01 | 0.47 | 0.92 | 3.00 |
| GOM2B-SULF-22 | 0.04 | 0.00 | 1.57 | 0.00 | 0.47 | 0.92 | 3.00 |
| GOM2B-SULF-15 | 0.03 | 0.02 | 1.48 | 0.00 | 0.52 | 0.95 | 3.00 |
| GOM2B-SULF-23 | 0.04 | 0.00 | 1.52 | 0.00 | 0.49 | 0.95 | 3.00 |
| GOM2B-SULF-29 | 0.04 | 0.00 | 1.52 | 0.01 | 0.49 | 0.94 | 3.00 |
| GOM2B-SULF-30 | 0.04 | 0.00 | 1.52 | 0.00 | 0.49 | 0.95 | 3.00 |
| GOM2B-SULF-35 | 0.05 | 0.00 | 1.56 | 0.00 | 0.42 | 0.97 | 3.00 |
| GOM2B-SULF-44 | 0.04 | 0.00 | 1.41 | 0.01 | 0.52 | 1.02 | 3.00 |
| GOM2B-SULF-50 | 0.04 | 0.00 | 1.54 | 0.01 | 0.49 | 0.93 | 3.00 |
| GOM2BSULF70 | 0.04 | 0.00 | 1.52 | 0.00 | 0.49 | 0.95 | 3.00 |
| | | | | $(Ni,Cu)_{11}(Sb,As)_8$ | | | |
| GOM2B-SULF-40 | 0.34 | 0.03 | 9.30 | 0.07 | 1.69 | 7.58 | 19.00 |
| | | | | ***breithauptite - NiSb*** | | | |
| GOM2B-SULF-3 | 0.05 | 0.00 | 0.96 | 0.02 | 0.00 | 0.97 | 2.00 |
| GOM2B-SULF-5 | 0.05 | 0.00 | 0.97 | 0.00 | 0.00 | 0.97 | 2.00 |
| GOM2B-SULF-6 | 0.05 | 0.00 | 0.97 | 0.00 | 0.00 | 0.98 | 2.00 |
| GOM2B-SULF-7 | 0.05 | 0.00 | 0.98 | 0.00 | 0.00 | 0.97 | 2.00 |
| GOM2B-SULF-8 | 0.04 | 0.00 | 1.00 | 0.00 | 0.00 | 0.96 | 2.00 |
| GOM2B-SULF-14 | 0.04 | 0.00 | 0.98 | 0.00 | 0.00 | 0.97 | 2.00 |
| GOM2B-SULF-26 | 0.04 | 0.00 | 1.00 | 0.00 | 0.00 | 0.95 | 2.00 |
| GOM2B-SULF-31 | 0.04 | 0.00 | 1.03 | 0.00 | 0.00 | 0.92 | 2.00 |
| GOM2B-SULF-34 | 0.03 | 0.00 | 1.02 | 0.00 | 0.03 | 0.92 | 2.00 |
| GOM2B-SULF-37 | 0.04 | 0.00 | 0.99 | 0.00 | 0.00 | 0.96 | 2.00 |

*Platinum Group Minerals*

PGM within Gomati are widespread, and were found in St. George and Tripes localities (Tab. 4.9). The highest number of PGM was detected in Tripes, where minerals of the laurite-erlichmanite series are the most widespread. This locality also contains two unknown PGE-sulfides. One of them is a Ni-

Ir-Fe-Cu-Rh sulfide (Fig. 4.11), while the other is a Ru-Ir-Fe sulfide. Within Gomati, all the analyzed crystals belong to the laurite-erlichmanite series. No PGM was detected in Limonadika.

Tab. 4.9 Selected microprobe analyses of PGM in Gomati; na: not analyzed; bdl: below detection limit.

| | S | Ir | Os | As | Rh | Pt | Ru | Pd | Fe | Ni | Cu | Totale |
|---|---|---|---|---|---|---|---|---|---|---|---|---|
| ***wt%*** | | | | | ***laurite ($RuS_2$) - erlichmanite ($OsS_2$)*** | | | | | | | |
| GO2-4 | 34.35 | 3.05 | 16.11 | 3.12 | 0.00 | 0.00 | 42.97 | 0.00 | 0.95 | 0.24 | 0.00 | 100.79 |
| TRI10-9 | 28.64 | 0.00 | 55.59 | 0.27 | 0.00 | 0.00 | 11.43 | 0.00 | 1.07 | 0.00 | 0.00 | 97.00 |
| TRI10-11b | 36.01 | 0.74 | 17.28 | 1.02 | 0.00 | 0.00 | 43.60 | 0.00 | 1.13 | 0.13 | 0.02 | 99.93 |
| GOM2B2-11 | 32.17 | 2.88 | 19.87 | 3.37 | 0.00 | 0.00 | 40.47 | 0.00 | 0.75 | 0.11 | 0.00 | 99.61 |
| TRI10A-14 | 33.49 | 4.25 | 22.30 | 1.28 | 0.00 | 0.00 | 35.90 | 0.00 | 0.86 | 0.08 | 0.00 | 98.16 |
| GOM2A-PGM-1 | 33.67 | 6.03 | 11.60 | 1.48 | 0.41 | 0.00 | 40.35 | 1.46 | n.a. | n.a. | n.a. | 95.00 |
| GOM2A-PGM-6 | 33.98 | 2.17 | 23.90 | 1.20 | 0.82 | 0.00 | 37.71 | 1.28 | n.a. | n.a. | n.a. | 101.06 |
| GOM2C-PGM-2 | 33.75 | 5.72 | 23.96 | 1.08 | 1.04 | 0.00 | 34.00 | 1.02 | n.a. | n.a. | n.a. | 100.57 |
| GR54A-PGM-2 | 33.02 | 7.18 | 21.64 | 1.39 | 1.29 | 0.00 | 34.36 | 1.07 | n.a. | n.a. | n.a. | 99.95 |
| GR54C-PGM-2 | 34.91 | 6.64 | 17.72 | 1.30 | 1.09 | 0.00 | 37.77 | 1.52 | n.a. | n.a. | n.a. | 100.95 |
| GR54D-PGM-4 | 32.32 | 6.82 | 15.61 | 1.04 | 1.79 | 0.00 | 35.48 | 1.30 | n.a. | n.a. | n.a. | 94.36 |
| | | | | | ***unknown (Ni,Ir,Fe,Cu,Rh)S*** | | | | | | | |
| TRI10-5 | 26.36 | 38.85 | 0.00 | 0.00 | 2.05 | 0.69 | 0.00 | 0.00 | 7.98 | 17.41 | 6.12 | 99.46 |
| TRI10-6b | 26.47 | 37.43 | 0.00 | 0.00 | 2.45 | 0.87 | 0.00 | 0.00 | 8.69 | 17.88 | 5.97 | 99.76 |
| TRI10-12 | 26.90 | 33.62 | 0.00 | 0.00 | 4.06 | 2.02 | 0.00 | 0.11 | 8.00 | 18.13 | 6.26 | 99.10 |
| TRI10A-22 | 24.88 | 33.94 | 0.06 | 0.00 | 0.93 | 8.11 | 0.00 | 0.00 | 7.92 | 16.11 | 5.88 | 97.84 |
| | | | | | ***unknown - $(Ru,Ir,Fe,Ni,Cu)S_2$*** | | | | | | | |
| TRI10A-29 | 35.93 | 22.09 | 4.55 | 1.07 | 0.00 | 0.00 | 29.09 | 0.00 | 4.66 | 3.33 | 1.48 | 102.20 |
| ***apfu*** | | | | | ***laurite ($RuS_2$) - erlichmanite ($OsS_2$)*** | | | | | | | |
| GO2-4 | 1.94 | 0.03 | 0.15 | 0.08 | 0.00 | 0.00 | 0.77 | 0.00 | 0.03 | 0.01 | 0.00 | 3.00 |
| TRI10-9 | 2.03 | 0.00 | 0.66 | 0.01 | 0.00 | 0.00 | 0.26 | 0.00 | 0.04 | 0.00 | 0.00 | 3.00 |
| TRI10-11b | 2.00 | 0.01 | 0.16 | 0.02 | 0.00 | 0.00 | 0.77 | 0.00 | 0.04 | 0.00 | 0.00 | 3.00 |
| GOM2B2-11 | 1.90 | 0.03 | 0.20 | 0.09 | 0.00 | 0.00 | 0.76 | 0.00 | 0.03 | 0.00 | 0.00 | 3.00 |
| TRI10A-14 | 1.99 | 0.04 | 0.22 | 0.03 | 0.00 | 0.00 | 0.68 | 0.00 | 0.03 | 0.00 | 0.00 | 3.00 |
| GOM2A-PGM-1 | 1.99 | 0.06 | 0.12 | 0.04 | 0.01 | 0.00 | 0.76 | 0.03 | 0.00 | 0.00 | 0.00 | 3.00 |
| GOM2A-PGM-6 | 1.98 | 0.02 | 0.23 | 0.03 | 0.01 | 0.00 | 0.70 | 0.02 | 0.00 | 0.00 | 0.00 | 3.00 |
| GOM2C-PGM-2 | 2.00 | 0.06 | 0.24 | 0.03 | 0.02 | 0.00 | 0.64 | 0.02 | 0.00 | 0.00 | 0.00 | 3.00 |
| GR54A-PGM-2 | 1.98 | 0.07 | 0.22 | 0.04 | 0.02 | 0.00 | 0.65 | 0.02 | 0.00 | 0.00 | 0.00 | 3.00 |
| GR54C-PGM-2 | 2.00 | 0.06 | 0.17 | 0.03 | 0.02 | 0.00 | 0.69 | 0.03 | 0.00 | 0.00 | 0.00 | 3.00 |
| GR54D-PGM-4 | 1.99 | 0.07 | 0.16 | 0.03 | 0.03 | 0.00 | 0.69 | 0.02 | 0.00 | 0.00 | 0.00 | 3.00 |
| | | | | | ***unknown (Ni,Ir,Fe,Cu,Rh)S*** | | | | | | | |
| TRI10-5 | 1.04 | 0.26 | 0.00 | 0.00 | 0.03 | 0.00 | 0.00 | 0.00 | 0.18 | 0.37 | 0.12 | 2.00 |
| TRI10-6b | 1.03 | 0.24 | 0.00 | 0.00 | 0.03 | 0.01 | 0.00 | 0.00 | 0.19 | 0.38 | 0.12 | 2.00 |
| TRI10-12 | 1.04 | 0.22 | 0.00 | 0.00 | 0.05 | 0.01 | 0.00 | 0.00 | 0.18 | 0.38 | 0.12 | 2.00 |
| TRI10A-22 | 1.03 | 0.23 | 0.00 | 0.00 | 0.01 | 0.05 | 0.00 | 0.00 | 0.19 | 0.36 | 0.12 | 2.00 |
| | | | | | ***unknown (Ru,Ir,Fe,Ni,Cu)$S_2$*** | | | | | | | |
| TRI10A-29 | 1.95 | 0.20 | 0.04 | 0.02 | 0.00 | 0.00 | 0.50 | 0.00 | 0.15 | 0.10 | 0.04 | 3.00 |

*Platinum Group Elements*

Whole rock PGE content was analyzed for 6 chromitite samples from St. George, Tripes and Limonadika (Tab. 4.10). Total PGE content ranges between 175 and 3516 ppb. The chromitite sample from Limonadika (LIM-) is the poorest in PGE, and it is more enriched in IPGE than PPGE. St. George chromitites (GR- and GOM-) are 1.9 to 2.3 times richer in PGE with respect to Limonadika, and they too show an enrichment in IPGE with respect to PPGE. On the contrary, Tripes chromitite (TRI-) shows an anomalous high PGE content, 9 times higher than St. George one and 20 times higher

than Limonadika one. IPGE are more abundant than PPGE, following St. George and Limonadika trends, but the IPGE/PPGE ratios is the lowest, suggesting a slight PPGE enrichment.

Tab. 4.10 Whole rock PGE concentration (ppb) in Gomati.

| Sample | Os | Ir | Ru | Rh | Pt | Pd | Total | IPGE | PPGE | IPGE/PPGE |
|---|---|---|---|---|---|---|---|---|---|---|
| GOM2A | 41 | 70 | 282 | 14 | 8 | 4 | 419 | 393 | 26 | 15 |
| GOM2B | 59 | 63 | 220 | 11 | 7 | 3 | 363 | 342 | 21 | 16 |
| GR54A | 51 | 48 | 213 | 12 | 5 | 3 | 332 | 312 | 20 | 15 |
| GR54D | 61 | 70 | 264 | 11 | 5 | 5 | 416 | 395 | 21 | 19 |
| TRI10 | 481 | 1080 | 1560 | 220 | 168 | 7 | 3516 | 3121 | 395 | 8 |
| LIM1 | 22 | 41 | 94 | 10 | 6 | 2 | 175 | 157 | 18 | 9 |

### 4.2.2.2. Nea Roda

*Chromite*

Chromite average compositions (Tab. 4.11) in massive chromitites are based on core analyses of chromitite samples. Chromite compositions within disseminated chromitite and dunites of Nea Roda are reported in Tab. 3.7 (Chapter 3). The average MgO content of chromite within massive chromitites is 13.49 wt%, higher than in disseminated chromitites and dunites (8.0 wt% on average), while average FeO and $Fe_2O_3$ contents are lower (15.47 and 1.10 wt% in massive chromitites *vs* 22.0 and 2.17 wt% in disseminated chromitites and dunites). Average $Cr_2O_3$ content in massive chromitites is 54.45 wt%, similar to the one in disseminated chromitites and dunites, while the average $Al_2O_3$ content is higher, with a value of 16.05 wt% vs a value of 12.0 wt%. These differences are reflected in a higher XMg ratio (0.608) and slightly lower XCr ratio (0.695) than in disseminated chromitites and dunites.

Tab. 4.11 Selected microprobe analyses of chromite cores from Nea Roda massive chromitites.

| wt % | NRO9-4 | NRO9-5 | NRO9-10 | NRO9-12 | NRO9-14 |
|---|---|---|---|---|---|
| $TiO_2$ | 0.20 | 0.17 | 0.17 | 0.25 | 0.20 |
| $Al_2O_3$ | 16.85 | 17.68 | 16.40 | 16.52 | 12.80 |
| $Cr_2O_3$ | 53.41 | 52.68 | 53.93 | 54.27 | 57.97 |
| $Fe_2O_3$ | 1.06 | 1.23 | 1.10 | 1.06 | 1.06 |
| FeO | 15.39 | 14.72 | 15.11 | 15.38 | 16.76 |
| MnO | 0.07 | 0.10 | 0.11 | 0.05 | 0.12 |
| MgO | 13.49 | 14.22 | 13.66 | 13.73 | 12.37 |
| NiO | 0.08 | 0.07 | 0.11 | 0.08 | 0.01 |
| TOT | 100.59 | 100.91 | 100.67 | 101.40 | 101.34 |
| Ti | 0.01 | 0.00 | 0.00 | 0.01 | 0.01 |
| Al | 0.62 | 0.64 | 0.60 | 0.60 | 0.48 |
| Cr | 1.32 | 1.28 | 1.33 | 1.33 | 1.45 |
| $Fe^{3+}$ | 0.03 | 0.03 | 0.03 | 0.03 | 0.03 |
| $Fe^{2+}$ | 0.40 | 0.38 | 0.39 | 0.40 | 0.44 |
| Mn | 0.00 | 0.00 | 0.00 | 0.00 | 0.00 |
| Mg | 0.63 | 0.65 | 0.63 | 0.63 | 0.59 |

| | | | | | |
|---|---|---|---|---|---|
| Ni | 0.00 | 0.00 | 0.00 | 0.00 | 0.00 |
| XCr | 0.680 | 0.667 | 0.688 | 0.688 | 0.752 |
| XMg | 0.610 | 0.633 | 0.617 | 0.614 | 0.568 |

*Chlorite*

No primary silicates were detected in massive chromitites. All secondary silicates detected are interstitial chlorite grains (Tab. 4.12). Following chlorite classification of Hey (1954), the analyzed chlorites fit into the chlinochlore compositional field.

Tab. 4.12 Selected microprobe analyses of chlorites from Nea Roda massive chromitites.

| **wt%** | **NRO9-1** | **NRO9-2** | **NRO9-8** | **NRO9-15** |
|---|---|---|---|---|
| $SiO_2$ | 31.35 | 31.74 | 32.17 | 31.04 |
| $TiO_2$ | 0.02 | 0.04 | 0.00 | 0.07 |
| $Al_2O_3$ | 15.34 | 15.35 | 14.42 | 15.17 |
| $Cr_2O_3$ | 3.54 | 3.53 | 3.85 | 3.65 |
| $Fe_2O_3$ | 0.00 | 0.00 | 0.00 | 0.00 |
| FeO | 1.25 | 1.22 | 0.97 | 0.34 |
| MnO | 0.01 | 0.00 | 0.00 | 0.01 |
| NiO | 0.41 | 0.38 | 0.35 | 0.36 |
| MgO | 33.77 | 32.92 | 34.69 | 34.52 |
| CaO | 0.02 | 0.04 | 0.01 | 0.00 |
| $Na_2O$ | bdl | 0.01 | 0.02 | 0.02 |
| $K_2O$ | bdl | bdl | bdl | bdl |
| $H_2O$ | 12.49 | 12.45 | 12.61 | 12.55 |
| Total | 98.20 | 97.68 | 99.09 | 98.68 |
| Si | 6.02 | 6.12 | 6.12 | 5.93 |
| Ti | 0.00 | 0.01 | 0.00 | 0.01 |
| Al | 3.47 | 3.49 | 3.23 | 3.42 |
| Cr | 0.54 | 0.54 | 0.58 | 0.55 |
| $Fe^3$ | 0.00 | 0.00 | 0.00 | 0.14 |
| $Fe^2$ | 0.20 | 0.20 | 0.15 | 0.05 |
| Mn | 0.00 | 0.00 | 0.00 | 0.00 |
| Ni | 0.06 | 0.06 | 0.05 | 0.05 |
| Mg | 9.67 | 9.46 | 9.83 | 9.84 |
| Ca | 0.00 | 0.01 | 0.00 | 0.00 |
| Na | 0.00 | 0.00 | 0.01 | 0.01 |
| K | 0.00 | 0.00 | 0.00 | 0.00 |
| H | 16.00 | 16.00 | 16.00 | 16.00 |

*Base Metal Minerals*

Base metal minerals are not abundant within massive chromitites, and were not detected within disseminated chromitites and dunites. The analyzed mineralogical species are sulfides (millerite and

godlevskite) and arsenides (maucherite) (Tab. 4.13). Major element compositions are rather homogeneous, but it should be noted that some BMM grains show Pt enrichments (up to 0.68 wt%).

Tab. 4.13 Selected microprobe analyses of BMM in Nea Roda; bdl: below detection limit.

| Sample | S | Ir | Os | As | Rh | Pt | Ru | Pd | Fe | Ni | Cu | Totale |
|---|---|---|---|---|---|---|---|---|---|---|---|---|
| ***wt%*** | | | | | | ***Millerite - NiS*** | | | | | | |
| NR09-16 | 36.03 | bdl | 0.01 | 0.27 | bdl | bdl | bdl | bdl | 1.01 | 63.04 | 0.00 | 100.37 |
| NR09-18 | 36.74 | bdl | bdl | 0.29 | bdl | bdl | bdl | 0.03 | 1.44 | 61.92 | 0.00 | 100.42 |
| | | | | | | ***Godlevskite - $(Ni,Fe)_9S_8$*** | | | | | | |
| NR06-12 | 32.31 | 0.40 | 0.02 | 0.38 | 0.04 | 0.11 | bdl | bdl | 8.60 | 56.12 | 0.00 | 97.97 |
| NR06-15 | 36.91 | bdl | bdl | 0.26 | 0.04 | 0.68 | bdl | bdl | 13.36 | 48.31 | 0.41 | 99.97 |
| | | | | | | ***Maucherite - $Ni_{11}As_8$*** | | | | | | |
| NR06-1 | 0.61 | 0.14 | 0.01 | 45.51 | 0.10 | 0.02 | 0.03 | 0.00 | 1.37 | 51.29 | 0.04 | 99.11 |
| ***a.p.f.u.*** | | | | | | ***Millerite - NiS*** | | | | | | |
| NR09-16 | 1.01 | 0.00 | 0.00 | 0.00 | 0.00 | 0.00 | 0.00 | 0.00 | 0.02 | 0.97 | 0.00 | 2.00 |
| NR09-18 | 1.03 | 0.00 | 0.00 | 0.00 | 0.00 | 0.00 | 0.00 | 0.00 | 0.02 | 0.95 | 0.00 | 2.00 |
| | | | | | | ***Godlevskite - $(Ni,Fe)_9S_8$*** | | | | | | |
| NR06-12 | 8.06 | 0.02 | 0.00 | 0.04 | 0.00 | 0.00 | 0.00 | 0.00 | 1.23 | 7.65 | 0.00 | 17.00 |
| NR06-15 | 8.79 | 0.00 | 0.00 | 0.03 | 0.00 | 0.03 | 0.00 | 0.00 | 1.83 | 6.28 | 0.05 | 17.00 |
| | | | | | | ***Maucherite - $Ni_{11}As_8$*** | | | | | | |
| NR06-15 | 0.24 | 0.01 | 0.00 | 7.56 | 0.01 | 0.00 | 0.00 | 0.00 | 0.31 | 10.87 | 0.01 | 19.00 |

*Platinum Group Minerals*

PGM are rare within Nea Roda, and only one laurite grain was detected (Fig. 4.17). The crystal is homogeneous and has the empirical formula $(Os_{0.16}Ru_{0.73}Ir_{0.07}As_{0.03}Fe_{0.02})S_{1.99}$.

*Platinum Group Elements*

Whole rock PGE content was analyzed for 3 chromitite samples and one host rock (NRO1) (Tab. 4.14). Total PGE content ranges between 108.4 and 146.7 ppb. All chromitite samples are enriched in Ru, Os and Ir. The IPGE/PPGE ratio is high, between 6.9 and 18.6.

Tab. 4.14 Whole rock PGE concentration (ppb) in Nea Roda.

| Sample | Os | Ir | Ru | Rh | Pt | Pd | Total | IPGE | PPGE | IPGE/PPGE |
|---|---|---|---|---|---|---|---|---|---|---|
| NRO1 | bdl | 15.6 | 79 | 9.8 | bdl | 4 | 108.4 | 94.6 | 13.8 | 6.86 |
| NRO4 | 13 | 20.9 | 90 | 9.2 | bdl | bdl | 133.1 | 123.9 | 9.2 | 13.47 |
| NRO6 | 25 | 20.2 | 94 | 7.5 | bdl | bdl | 146.7 | 139.2 | 7.5 | 18.56 |
| NRO9 | 22 | 16.3 | 80 | 7.3 | bdl | bdl | 125.6 | 118.3 | 7.3 | 16.21 |

## 4.2.3 Discussion

### 4.2.3.1. Chromite composition

Spinels from Gomati localities show similar XMg values, but very different XCr values (Fig. 4.18A). Limonadika chromites have the highest XCr values, ranging between 0.77 and 0.96. St. George chromites have slightly lowest XCr, from 0.74 to 0.87, partially overlapping the Limonadika field. Tripes shows the most different XCr values, ranging between 0.60 and 0.61. Chromite compositions of the three localities fit with data obtained by Christodoulou (1980) on spinels from both massive and disseminated chromitites of northern Gomati (Fig. 4.18A).

Nea Roda spinels show both different XMg and XCr values depending on the lithology of the host rock. Spinels within fresh disseminated chromitites are clustered in two separate compositional fields. For this reason, Michailidis et al. (1995) define the group with higher XCr values as "disseminated chromitites" and the group with lower XCr values as "dunite". However, samples GR62, GR63 and GR58 are not distinguishable based on rock texture and have been therefore defined as "fresh disseminated chromitite". Sample GR58 has the highest XCr values, around 0.80, and XMg between 0.48 and 0.52, while samples GR62 and GR63 have lower XCr (0.72 – 0.78) and lower XMg (0.30 - 0.48). Spinels within chloritized massive chromitites display the lowest XCr values, from 0.67 to 0.75. Chromite composition fits well with data obtained by Michailidis et al. (1995) on spinels from massive chromitites, disseminated chromite, dunite and harzburgite of the same area (Fig. 4.18B).

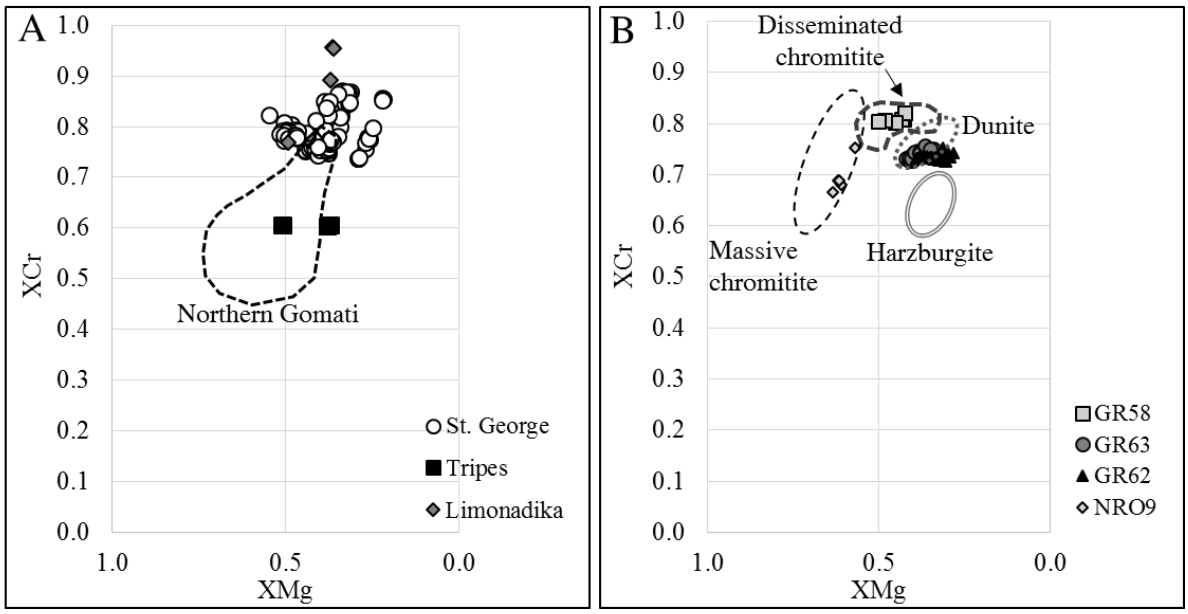


Fig. 4.18 XMg vs XCr values of Gomati (A) and Nea Roda (B); compositional fields: Northern Gomati from Christodoulou (1980), massive chromitite, harzburgite, dunite, disseminated chromite from Michailidis et al. (1995).

Spinels from Gomati and Nea Roda display variable compositions also on the Cr-Al-$Fe^{3+}$ ternary plot (Fig. 4.19). Spinels from St. George and Limonadika and from Nea Roda disseminated chromitites fall into the compositional field of chromite. Spinels from Tripes and Nea Roda massive chromitites, on the other hand, are enriched in $Al_2O_3$ and plot into the compositional field of Al-chromites. A comparison with data from the same localities reveals that Tripes has the same Al-rich mineralogical composition of chromites from northern Gomati (Christodoulou, 1980). Fresh disseminated chromitites and massive chromitites from Nea Roda also have a composition similar to chromitiferous dunites and chromitites of the same area analyzed and described by Michailidis et al. (1995).

High-Al chromitites from Nea Roda and Gomati also show a high $TiO_2$ content, more similar to chromites in stratiform chromitites than to those of podiform ones (Fig. 4.20A). High $Al_2O_3$ and $TiO_2$ contents in podiform chromitite spinels can be associated to a stratigraphic position within or above the Moho Transition Zone (Grieco et al., 2007; Zaccarini et al., 2004a). Massive chromitites from Tripes have a composition similar to Nurali CHR-II chromites (Zaccarini et al., 2004a) (Fig. 4.20B). Spinels of Nea Roda massive chromitites, on the other hand, have a composition similar to Nurali Level 1 and Level 3 (Grieco et al., 2007), while chromites from St. George and Nea Roda disseminated chromitites partially overlap with Kraubath supra-Moho compositional field (Malitch et al., 2003a).

Ophiolite chromitite deposits are distinguished into high-Cr chromitites and high-Al chromitites, based on the differences in chromian spinel composition. High-Cr chromitites are thought to have been crystallized out of boninitic magmas in the deeper parts of the mantle sequence, whereas, high-Al chromitites by MORB-type magmas in shallower parts of the mantle section near the petrological Moho (Ahmed and Arai, 2002; Gonzalez-Jimenez et al., 2011b; Uysal et al., 2007; Zaccarini et al., 2011).

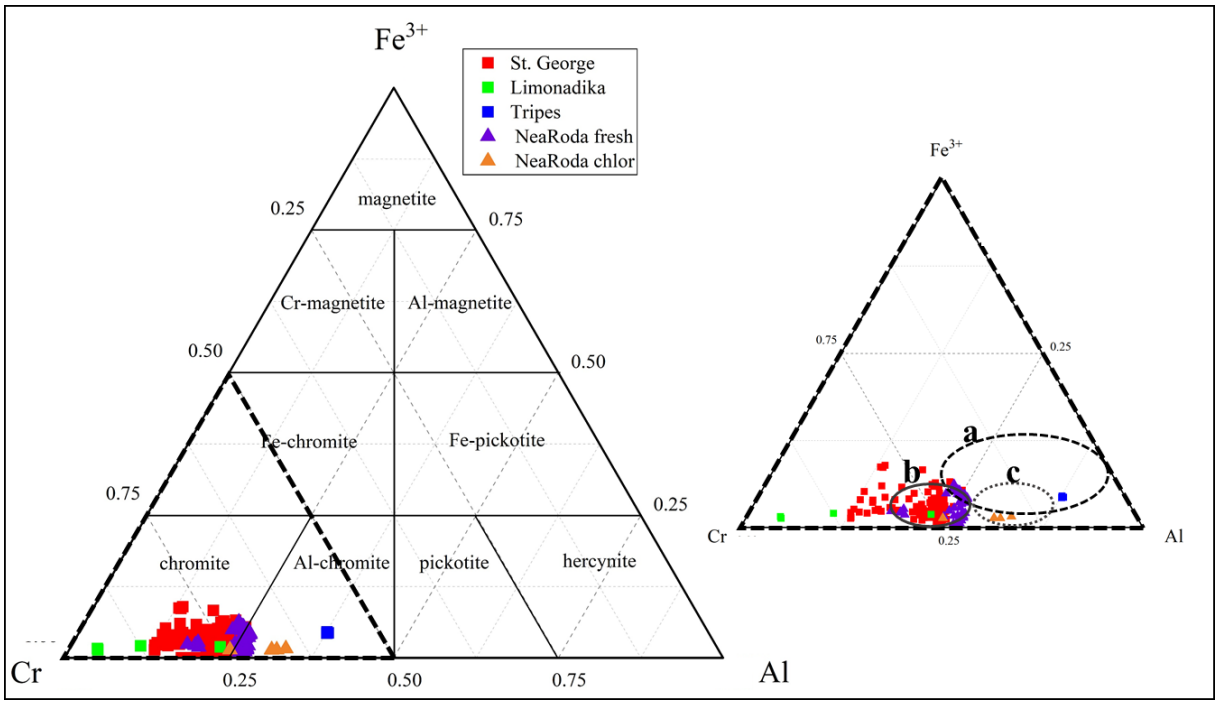


Fig. 4.19 Classification diagram of Gomati and Nea Roda chromites; field "a" refers to chromite compositions from northern Gomati (Christodoulou, 1980), field "b" and "c" refer respectively to chromitiferous dunite and chromitite from Nea Roda (Michailidis et al., 1995).

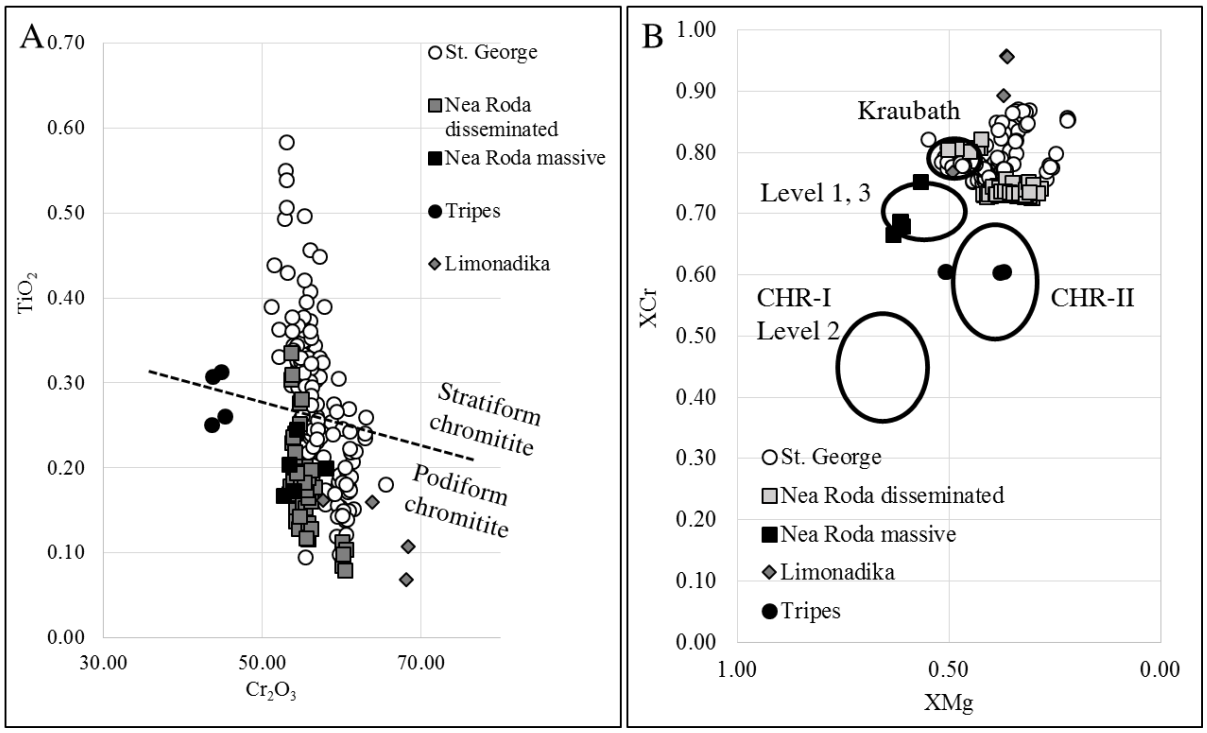


Fig. 4.20 A) $Cr_2O_3$ vs $TiO_2$ content of Nea Roda and Gomati chromites; stratiform and podiform chromitite division is from Arai et al. (2004). B) XMg vs XC of Nea Roda and Gomati chromites; compositional fields of Nurali CHRI and CHRII are from Zaccarini et al. (2004a), of Nurali Level 1, 2 and 3 are from Grieco et al. (2007)) and of Kraubath are from Malitch et al. (2003).

$Al_2O_3$ and $TiO_2$ contents of a parental melt can be derived from the spinel composition. From the positive correlation found by Kamenetsky et al. (2001), the $Al_2O_3$ content in a parental magma is calculated as:

$$Al_2O_{3melt} = 5.2181 * \ln(Al_2O_{3spinel}) - 1.0505$$

The correlations between $TiO_2$ in spinels and in a coexisting melt, on the other hand, differ between MORB and arc settings (Rollinson, 2008), and are calculated as:

$$TiO_{2melt-MORB} = 1.5907 * TiO_{2spinel}^{0.6322}$$

$$TiO_{2melt-arc} = 1.0963 * TiO_{2spinel}^{0.7863}$$

Maurel and Maurel (1982) calculated the FeO/MgO ratio in the melt starting from the composition of the spinel:

$$\ln\frac{FeO}{MgO}spinel = 0.47 - 1.07 * Y^{Al} + 0.64 * Y^{FeIII} + \ln\frac{FeO}{MgO}melt$$

where: $Y^{Al} = Al/(Al+Cr+Fe^{III})$ and $Y^{FeIII} = Fe^{III}/(Fe^{III}+Al+Cr)$

Parental melt analysis (Fig. 4.21) results show that disseminated chromitites from Nea Roda and chromitites from St. George and Limonadika have an arc signature, while massive chromitites from Nea Roda and Gomati fit better the MORB signature field (Fig. 4.21A). The $TiO_2$ content of spinels, moreover, is very similar to the one of MORB spinels (4.21B). However, a comparison of the calculated parental magma with primitive magmas from different tectonic settings reveals that the overlap with primitive melt fields is very limited. This is due to a very high FeO/MgO ratio within the parent melt. This high ratio, coupled with low primary temperatures obtained for Nea Roda disseminated chromitites (Chapter 3), suggests a genesis from a highly differentiated product. In the case of Nea Roda disseminated chromitites, moreover, the melt was generated at shallow levels and underwent rapid cooling in small dunite dykes, as suggested by the lack of Fe-Mg subsolidus exchange, probably frozen before its onset (Chapter 3, paragraph 3.3).

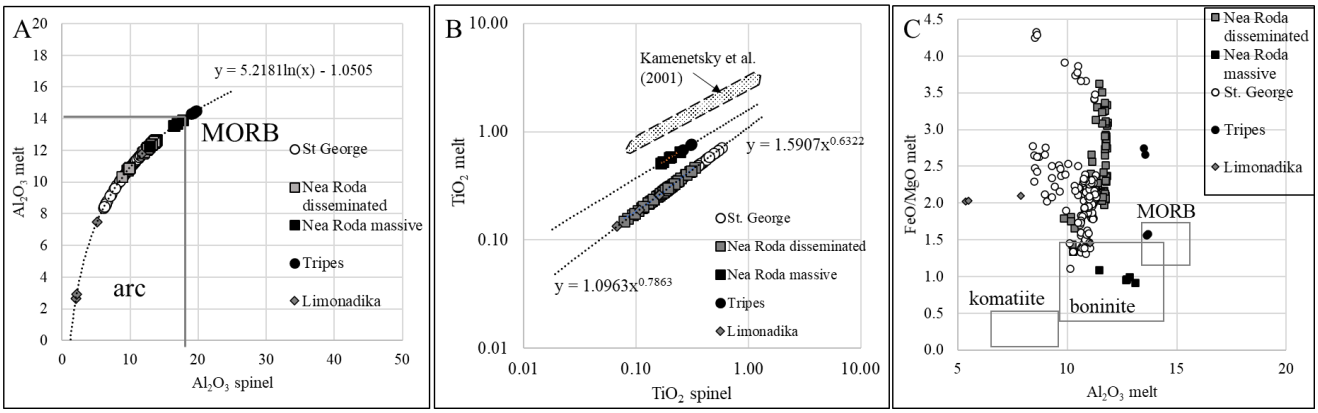

Fig. 4.21 A) $Al_2O_3$ spinel vs $Al_2O_3$ melt (wt%) for Gomati and Nea Roda spinels B) $TiO_2$ spinel vs $TiO_2$ melt (wt%) for Gomati and Nea Roda spinels C) FeO/MgO melt vs $Al_2O_3$ melt (wt%) calculated on the basis of the chemical composition of Gomati and Nea Roda chromites; tectonic discrimination fields from Barnes and Roeder (2001).

#### 4.2.3.2. Secondary silicates composition

Massive chromitites from Gomati and Nea Roda, and associated pyroxenites show widespread alteration. Rare pyroxenes are the only relicts of primary silicates within chromitites, scattered in a chlorite silicate matrix. Associated pyroxenites are made up by variably fractured clinopyroxenes partially replaced by chlorite, and by a fine-grained matrix of serpentine and chlorite crystals.

Chloritization of massive chromitites is a well-known process which was detected in several mafic ultramafic massifs. Many studies report the formation of Cr-chlorite and ferrian chromite during low-T hydrothermal alteration (e.g. Colás et al., 2019; Kapsiotis, 2015). Colás et al. (2017) and Gervilla et al. (2012) describe the reaction between primary chromite and olivine in the presence of $SiO_2$-rich fluids, producing clinochlore and Fe-rich chromite. This reaction involves chromite loss, resulting in the development of a porous texture (Gervilla et al., 2012). According to Gervilla et al. (2012) this stage takes place under water-saturated and reducing conditions. A further alteration stage results from the exhaustion of olivine and subsequent increase of $fO_2$ in the fluid. The interaction of Fe-rich chromite from the first alteration stage with these oxidizing fluids produces ferrian chromite with a non-porous texture (Gervilla et al., 2012; Mukherjee et al., 2010).

González-Jiménez et al. (2009) and Kimball (1990) propose the formation of chlorite and ferrian chromite through the reaction of chromite with MgO- and $SiO_2$-rich fluids:

$(Mg,Fe)(Al,Cr)_2O_4$ + MgO-$SiO_2$-rich fluid = $Mg_5AlSi_3AlO_{10}(OH)_8$ + $(Fe,Mg)(Cr,Al)_2O_4$

Kimball (1990) proposes temperatures up to 400 °C for this process, however, González-Jiménez et al. (2009) suggest that lower temperatures (up to 300 °C) could favor the serpentinization of olivine and pyroxenes, and create the MgO- $SiO_2$-rich environment necessary for the reaction. González-Jiménez et al. (2009) propose three alteration stages for the Dobromirtsi chromitites (SE Bulgaria). The first stage is the replacement of olivine by serpentine, with chromite remaining unaltered. The second stage involves the reaction of chromite with MgO and $SiO_2$-rich fluids to form chlorite and ferrian chromite. The third stage involves the reaction of serpentine and chromite to form chlorite and ferrian chromite, under oxidizing conditions, as also proposed by Mellini et al. (2005) and Merlini et al. (2009).

Chromite + Serpentine + Water + Oxygen = Fe-chromite + Chlorite

This reaction was found to affect serpentine mesh structures, transforming them into a disordered chlorite-serpentine intergrowth (Mellini et al., 2005), very similar to the one observed within St.

George clinopyroxenites. Massive chromitites from Gomati and Nea Roda do not show olivine or serpentine relicts. On the contrary, the only primary silicates are clinopyroxene relicts.

Several studies report replacement of clinopyroxene by chlorite, a process that takes place at low T and P (Centrella et al., 2018; Good et al., 1997; Helgadóttir et al., 2015). This suggests that chlorite and ferrian chromite in massive chromitites could have been formed at the expense of primary clinopyroxene and chromite. An alternative could be the transformation of clinopyroxene into serpentine and subsequent reaction of serpentine with chromite to form chlorite and ferrian chromite, with complete obliteration of serpentine during the reaction.

#### 4.2.3.3. PGM and BMM assemblage

Many base metal minerals were found within Gomati and Nea Roda, mainly associated with the silicate gangue and rarely enclosed within chromite crystals. The assemblage is dominated by sulfides and arsenides within chromitites, and by sulfides, arsenides and antimonides within associated pyroxenites. Platinum Group Minerals are widespread in Gomati and rare in Nea Roda. They were found exclusively within chromitites, mainly as inclusions within chromites.

*Ni-Fe-Cu sulfide assemblage*

Primary BMM within ophiolite chromitites are generally Ni-Fe sulfides, such as pentlandite, which are sometimes associated to Cu-sulfides. Kullerud (1963) studied the thermal stability of pentlandite. At temperatures above 610 °C, an assemblage of pyrrhotite + $Ni_{3\pm x}S_2$ is stable. Below this temperature, the stable Ni-Fe sulfides are pentlandite + pyrrhotite (450 – 610 °C) or pentlandite + $Ni_{3\pm x}S_2$ (550 – 610 °C) or pentlandite + heazlewoodite (450 – 550 °C), depending on the metal-to-sulfur ratio. If some copper is present in the system, also primary minerals in the Ni-Fe-Cu system can be found, such as chalcopyrite, chalcocite or bornite (Proenza et al., 2001). Heazlewoodite, millerite and Ni-Fe alloys are the most common secondary base metal minerals within ophiolite chromitites (Klein and Bach, 2009). The alteration of pentlandite into heazlewoodite occurs below 550°C, while the formation of Ni-Fe alloys has been estimated at 360-445 °C (Tzamos et al., 2016). Godlevskite is another common secondary BMM within serpentinized massifs. From its textural and chemical characteristics, it is thought to be the result of a solid-state re-equilibration from high-temperature MSS, stable between 577 and 436 °C, followed by annealing below 379 °C (Kerestedjian et al., 2007). Heazlewoodite and godlevskite, moreover, can be replaced by millerite if $fO_2$ and $fS_2$ increase, like during steatitization of ultramafic rocks (Klein and Bach, 2009). However, it should be noted that droplets of millerite and chalcocite have been found within primary laurites in the Caridad chromitites (González-Jiménez et al., 2012), so in some cases millerite can be formed during crystallization of laurite, at magmatic temperatures.

Based on mineralogy and textural relations, the only primary sulfide in Gomati and Nea Roda is pentlandite, found predominantly as euhedral grains within unaltered chromites. Secondary sulfides are godlevskite, heazlewoodite, millerite and chalcocite, displaying euhedral to anhedral shape and detected within the silicate gangue. No alloy was detected in neither of the two complexes (Fig. 4.22). This suggests that the $fO_2$ and $fS_2$ conditions allowed the formation of S-rich secondary sulfides, and only limited desulfurization (e.g. replacement of pentlandite by heazlewoodite) took place. Such conditions can also be responsible for the chloritization affecting the massif, as in hydrothermal systems, Mg-chlorite forms between 200 and 300 °C (Beaufort et al., 2015), and at different sulfur and oxygen fugacities (Walshe, 1986).

The sulfide assemblage is variable among the localities. Tripes is dominated by pentlandite, and no millerite and heazlewoodite have been detected. This could be due to the high chromite modal content, which favors the preservation of primary sulfides within unaltered chromite grains. A single pyrite crystal was also found associated to a Fe-Ni sulfide, a Ni sulfide and a PGM too small to be analyzed. St. George chromitites are dominated by heazlewoodite and millerite, with few primary pentlandites preserved. Moreover, chalcocite was detected only within this locality. Ni-Pb sulfides, probably corresponding to the mineral shandite, were also found within St. George locality. Limonadika is poor in sulfides, and only millerite, pentlandite and an unknown Cu-Ni sulfide have been detected. Nea Roda massive chromitites also show a poor sulfide assemblage, made up entirely of Ni-Fe sulfides, with no copper phases.

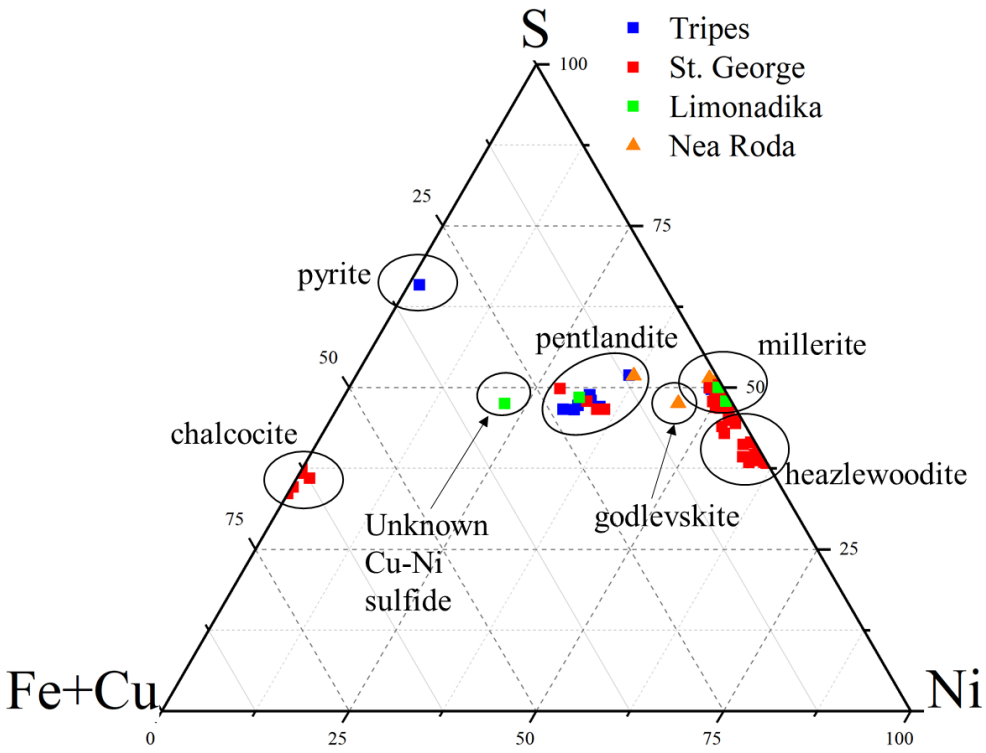


Fig. 4.22 Ternary diagram (at. %) of Ni-Fe-Cu sulfides in Gomati and Nea Roda.

*Arsenide and antimonide assemblage*

The composition of arsenides and antimonides found in St. George has been plotted as atomic proportions in the ternary diagram of Fig. 4.23, and compared with minerals from the Bon Accord complex in South Africa (Tredoux et al., 2016). The only known mineralogical species detected in Gomati are nickeline, maucherite, orcelite and breithauptite, while several other crystals belong to unknown phases. Minerals with a similar composition were detected in the Bon Accord oxide body of South Africa (Tredoux et al., 2016) and in the Alaskan-type Tulameen complex of Canada (Nixon et al., 1990). However, the partial Sb-As substitution described in the Bon Accord minerals (Fig. 4.23) is not present in the analysed grains. Moreover, Gomati antimonides are enriched in Cu up to 13.59 wt%, while Bon Accord antimonides are Cu-free. Two unknown antimonides with ideal formula $(Ni,Cu)_2Sb$ and $Ni_3Sb$ were also detected in the Tulameen complex. The unknown mineralogical species analyzed in Gomati correspond to the following mineral formulae: $Ni_3As$, $Ni_5As_2$, $(Ni,Cu)_{5-x}Sb_2$, $(Ni,Cu)_2Sb$ and $(Ni,Cu)_{11}Sb8$. None of these phases is listed in the approved minerals compilation of the International Mineralogical Association as of July 2020 (http://cnmnc.main.jp/). The analyses that approach the stoichiometry $(Ni,Cu)_{5-x}Sb_2$ may correspond to a Sb-analogue of orcelite and the $(Ni,Cu)_{11}Sb_8$ compound probably represents the Cu-rich Sb-analogue of the mineral maucherite ($Ni_{11}As_8$), also found in the Bon Accord body (Tredoux et al., 2016). The $(Ni,Cu)_2Sb$ phase has a composition similar to the one reported by Nixon et al. (1990) in the chromitite from Tulameen complex. About As-dominant compositions, $Ni_3As$ may correspond to the mineral dienerite, formerly discredited by the IMA and only recently under revalidation (Bonazzi and Bindi, 2019), while the species $Ni_5As_2$ could represent a new arsenide. Taking into consideration the small size of some of the analyzed grains and their mode of occurrence, i.e. associated with heazlewoodite, we cannot exclude that a small amount of the detected Ni may be a contribution from the Ni-sulfide. For this reason, some of the calculated stoichiometries may show a slight enrichment in Ni due to the influence of the associated minerals.

Experimental studies (Hewitt, 1948) prove that nikeline and breithauptite form solid solutions in artificial melts. However, natural observations reveal that they also can occur together. The coexistence of NiSb and NiAs is explained by Hewitt (1948) either with replacement of breithauptite by nickeline or with crystallization at low temperatures, in the presence of aqueous fluids, which would prevent the formation of solid solutions. Ni-As and Ni-Sb phase diagrams (Fig. 4.24A, B) (Okamoto, 2009; Raghavan, 2004; Yund, 1961) show that maucherite, nickeline, orcelite, breithauptite and other antimonides are stable over a wide range of temperatures, up to 1000°C. However, the assemblages maucherite + orcelite and maucherite + nickeline are stable at temperatures below 800 °C, and the mineral $Ni_5Sb_2$ occurs at temperatures above 556°C. This last phase has not been observed

in the Gomati chromitite, thus implying that the crystallization of the antimonides in the studied sample may have occurred at temperatures lower than 600 °C, or even less if we consider that the presence of impurities within the antimonides in Gomati could have further lowered the temperature. The genesis of arsenides and antimonides at low-T is also supported by the presence of other accessory minerals such as heazlewoodite and shandite, whose upper thermal stability is respectively 556 °C (Tzamos et al., 2016) and 500 °C (Zhmodik and Agafonov, 2000).

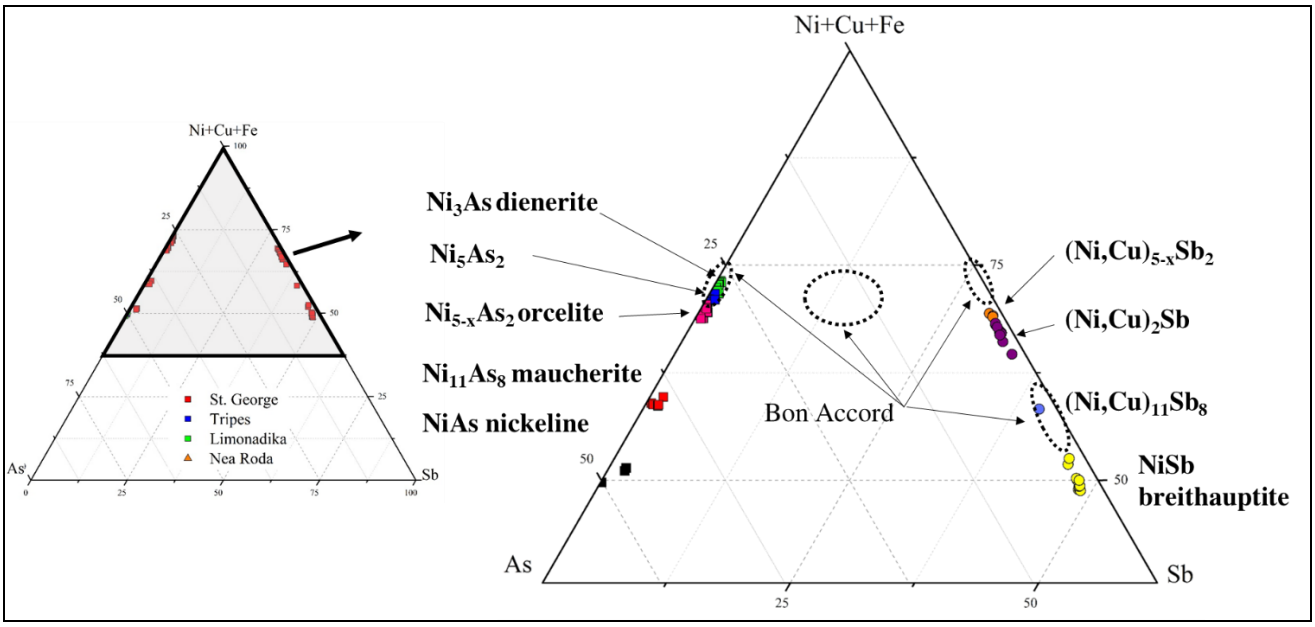


Fig. 4.23 Ternary diagram (at. %) of Ni-Fe-Cu arsenides and antimonides in Gomati and Nea Roda.

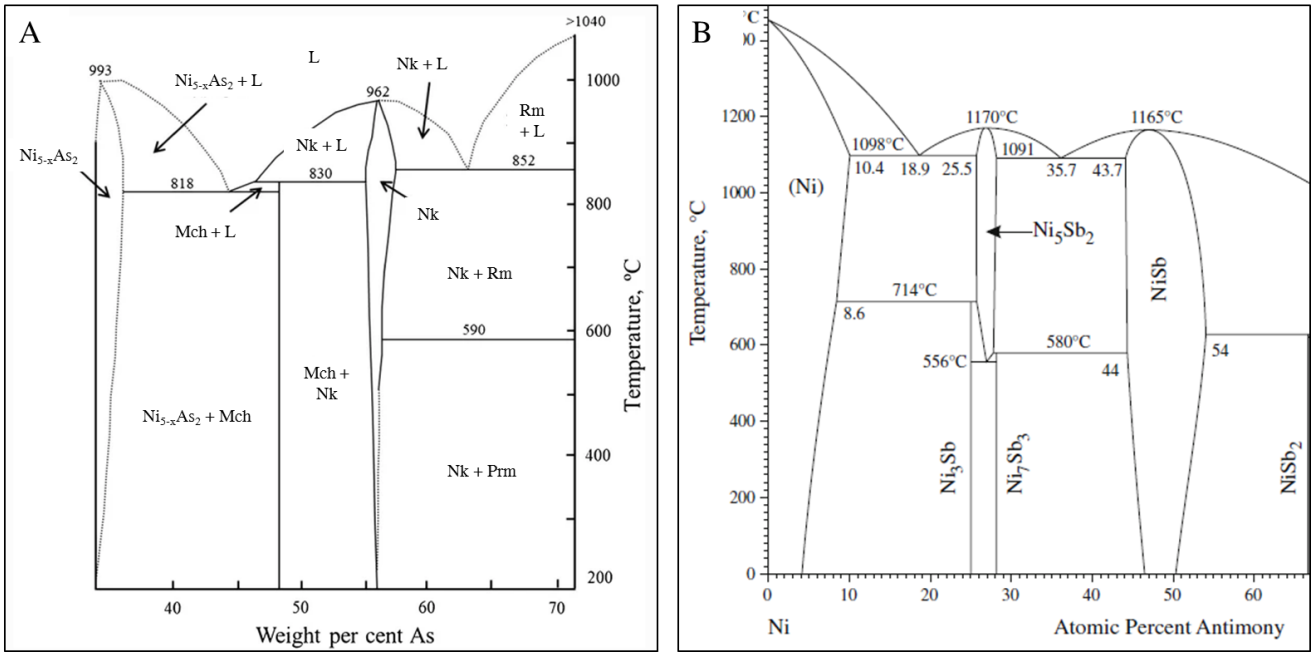


Fig. 4.24 A) Partial phase diagram of the Ni-As system (modified after Piña et al., 2015; Yund, 1961); abbreviations are Mch, maucherite; Nk, nickeline, Rm, rammelsbergite; Prm, pararammelsbergite. B) partial phase diagram of the Ni-Sb system (modified after Okamoto, 2009).

The source of the metals in the Ni-As-Cu-Sb system is currently unknown. Minerals in the Ni-As-Sb-Ag-Au-Cu have also been found within other ultramafic complexes, like the Ognit Complex (Barkov et al., 2019; Shvedov and Barkov, 2017), where Authors suggest that the formation of these phases may be related to cooling in a fluid-enriched system. Ultramafic rocks contain nickel and arsenic that may have a magmatic origin or be related with the alteration of their host rocks during serpentinization (Kapsiotis et al., 2011; Prichard et al., 2008a). However, the presence in Gomati of abundant minerals containing Sb, together with shandite and chalcocite, described in the present work, as well as native silver (Economou, 1984), supports the hypothesis that Sb, Pb, Cu, Au and Ag were metasomatically added during cooling. The occurrence of a metasomatic event in the Gomati chromitite was reported by Scarpelis and Economou (1978), confirming the activity of a fluid phase that can be considered responsible for the crystallization of the rare and accessory phases described in this contribution. Sb-rich porphyry mineralizations occurring in the area (Tzamos et al., 2019) are probably the source of the metals, which could have been transported through migrating fluids within fault zones. The Kassandra mining district contains porphyry Au-Cu mineralization and Au-Ag-Pb-Zn-Cu carbonate replacement deposits associated with Oligocene-Miocene intrusions emplaced in the metamorphic basement of the Serbo-Macedonian Massif. The genesis of these deposits is related to the onset of an extensional regime in the middle Eocene, responsible for the development of widespread normal and transtensional faults (Siron et al., 2018). The fault system in the area is the probable conduit for metasomatic fluids affecting Gomati and generating the low-T mineralogical assemblage.

Although their small size makes it very difficult to obtain X-ray diffraction data, we can argue, based on electron microprobe analyses only, that the following four minerals in the Ni-Cu-Sb-As system have been found in the Gomati chromitite and could represent new mineral species: $Ni_5As_2$, $(Ni,Cu)_{5-x}Sb_2$, $(Ni,Cu)_2Sb$, and $(Ni,Cu)_{11}Sb_8$. Moreover, $Ni_3As$ could correspond to the formerly discredited mineral dienerite, therefore supporting its revalidation.

*Platinum Group Mineral assemblage*

PGM in Gomati and Nea Roda were found only enclosed within chromites. The assemblage is quite homogeneous, made up mainly by minerals of the laurite-erlichmanite series (Fig. 4.25A). Euhedral PGM enclosed in chromite probably have a magmatic origin, and were formed at the same time or slightly prior to chromite crystallization. Experimental studies (Bockrath et al., 2004; Brenan and Andrews, 2001) show how Os-free laurite can crystallize in equilibrium with Os-Ir alloys at 1200-1300 °C, at log$fS_2$ ranging from -2 to -1.3, and that Os solubility in laurite increases with decreasing temperature and/or increasing $fS_2$. González-Jiménez et al. (2009a, 2010) suggest that different Os contents within laurites could reflect the crystallization of laurites in a dynamic regime, with

increasing $fS_2$ conditions, which can occur during cooling. The absence of PGE alloys within unaltered chromite and the presence of Os within laurite suggests that in Gomati and Nea Roda $fS_2$ conditions were higher than those necessary to stabilize metal alloys. Secondary PGM were not detected neither in Gomati nor in Nea Roda.

The unknown Ni-Ir-Fe-Cu sulfides found in Tripes have stoichiometry approaching Me/S 1:1 (Fig. 4.25B). Minerals with a similar composition were detected within the Ojen lherzolite massif in Spain (Torres-Ruiz et al., 1996) and within mantle tectonites of the Tiebaghi massif of New Caledonia (Legendre and Augé, 1986) and the Finero complex (Garuti et al., 1990). These minerals have been classified by Garuti et al. (1995) as PGE-rich sulfides. In particular, they could represent a PGE-rich variety of pyrrothite (Garuti et al., 1995), especially considering that Ir and Rh have a preferential solubility within this mineral (Cabri and Laflamme, 1981). However, the possibility that they could represent a new mineralogical species cannot be excluded.

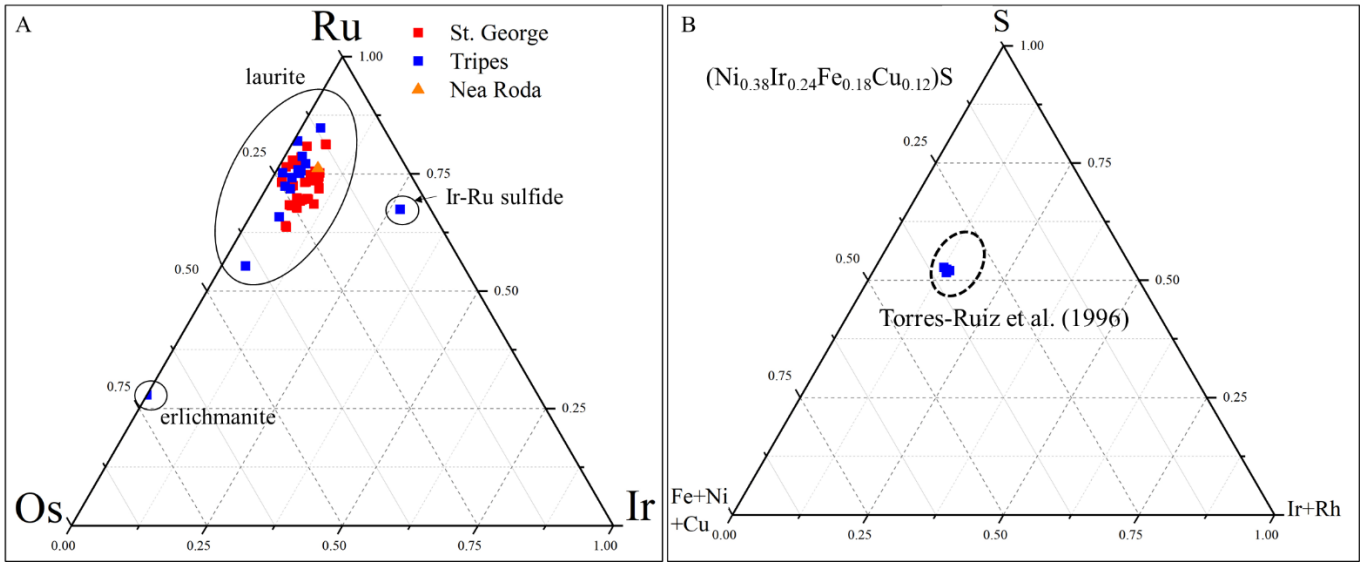


Fig. 4.25 Ternary compositional diagram (atm. %) of A) PGM of the laurite-erlichmanite series and B) unknown Ni-Ir-Fe-Cu sulfide found in Tripes.

### 4.2.3.4. PGE remobilization

PGE in the primitive mantle are hosted within a monosulfide solid solution (mss) (Lorand and Alard, 2001). The PGE content of a melt is therefore dependent on the degree of partial melting of the primitive mantle, and on the dissolution of the mss within the melt. Chromitites enriched in PGE crystallize in equilibrium with melts formed in a critical melting interval, which was identified by Prichard et al. (2008) at 20-25% melt. Lower degrees of melting would produce PGE-poor chromitites (e.g. basaltic melts formed beneath spreading centers) (Ahmed and Arai, 2002; Economou-Eliopoulos, 1996; Gervilla et al., 2005; Gonzalez-Jimenez et al., 2011a). On the contrary, higher degrees of melting would dilute the PGE content, especially in Pt and Pd, the two PGE that fractionate into the

melt (Brenan and Andrews, 2001). Arc-related melts forming above subduction slabs are usually generated by degrees of partial melting >20%, and are therefore rich in PGE (Ahmed and Arai, 2002; Economou-Eliopoulos, 1996; Gervilla et al., 2005; Gonzalez-Jimenez et al., 2011a). Small batches of melt produced within the critical melting interval will have higher PGE content than melts formed by successive increments of melt that reacted and mixed in their way upwards in the mantle (Jannessary et al., 2012; O'Hara et al., 2001).

Ophiolite chromitites, enriched in IPGE with respect to PPGE, are the result of this fractionating process (Economou-Eliopoulos, 1996; Grieco et al., 2020, 2004; Proenza et al., 2007). PPGE-enriched patterns in ophiolite chromitites are rare, and attributed for the most part to hydrothermal alteration (Malitch et al., 2003a, 2003b; Yang and Seccombe, 1993).

Chromitites in the Moho Transition Zone, on the contrary, show highly variable IPGE/PPGE ratios (Grieco et al., 2007; Malitch et al., 2003b; Zaccarini et al., 2004a). Nurali CHR-II and Level 1 chromitites (Grieco et al., 2007; Zaccarini et al., 2004a), enriched in PPGE, are the result of the first stages of partial melting of the primitive mantle, when sulfur saturated melts rich in Pt and Pd are produced (Grieco et al., 2007; Zhou et al., 1998). Kraubath banded chromitites, formed in the transition zone at the base of the cumulate sequence above the Moho (Malitch et al., 2003b), also show a PPGE enrichment similar to Nurali Level 1 and CHR-II, although with a lower PGE total content. Remelting of the residual mantle causes the dissolution of the Ru- Os- Ir- and Rh-rich mss, generating melts enriched in IPGE, like those corresponding to Nurali CHR-I and Level 2 chromitites.

Chromitites from Gomati and Nea Roda show high concentration of IPGE (Ir, Os, Ru) compared with PPGE (Pt, Pd, Rh). Nea Roda, St. George and Limonadika show patterns similar to typical ophiolite chromitites (Fig. 4.26A), enriched in IPGE with respect to PPGE. Of the three localitites, St. George has the highest PGE content, while Limonadika and Nea Roda are the most depleted. Tripes chromitite is decidedly different from the others, and shows Os- Ir- Ru and Rh enrichments similar to those found in Nurali Level 2 and CHR-I chromitites (Grieco et al., 2007; Zaccarini et al., 2004a) (Fig. 4.26B).

The high PGE content in Tripes reflects a higher melting degree with respect to Nea Roda, St. Geoge and Limonadika, and could be related to a differentiation process within a magma chamber, as suggested by Malitch et al. (2003b) for Kraubath supra-Moho chromitites and by Grieco et al. (2007) for Nurali chromitites. The high Ir content could indicate that the crystallization of chromite continued to temperatures lower than 1000 °C, and to high $fS_2$ conditions (Andrews and Brenan, 2002).

The primary nature of PGE-bearing phases and the PGE patterns of chromitites suggest that PGE were not remobilized during post-magmatic processes within Gomati and Nea Roda. Primary PGM are found mostly enclosed within unaltered chromite or within ferrian chromite rims, in contact with

secondary silicates. The euhedral shape of PGM and their lack of zoning or corroded rims suggest that alteration fluids did not affect these minerals. From the base metal sulfide assemblage, we can infer that only limited alteration took place under relatively high $fS_2$ conditions, as testified by replacement of primary sulfides by secondary sulfides and not by base metal alloys.

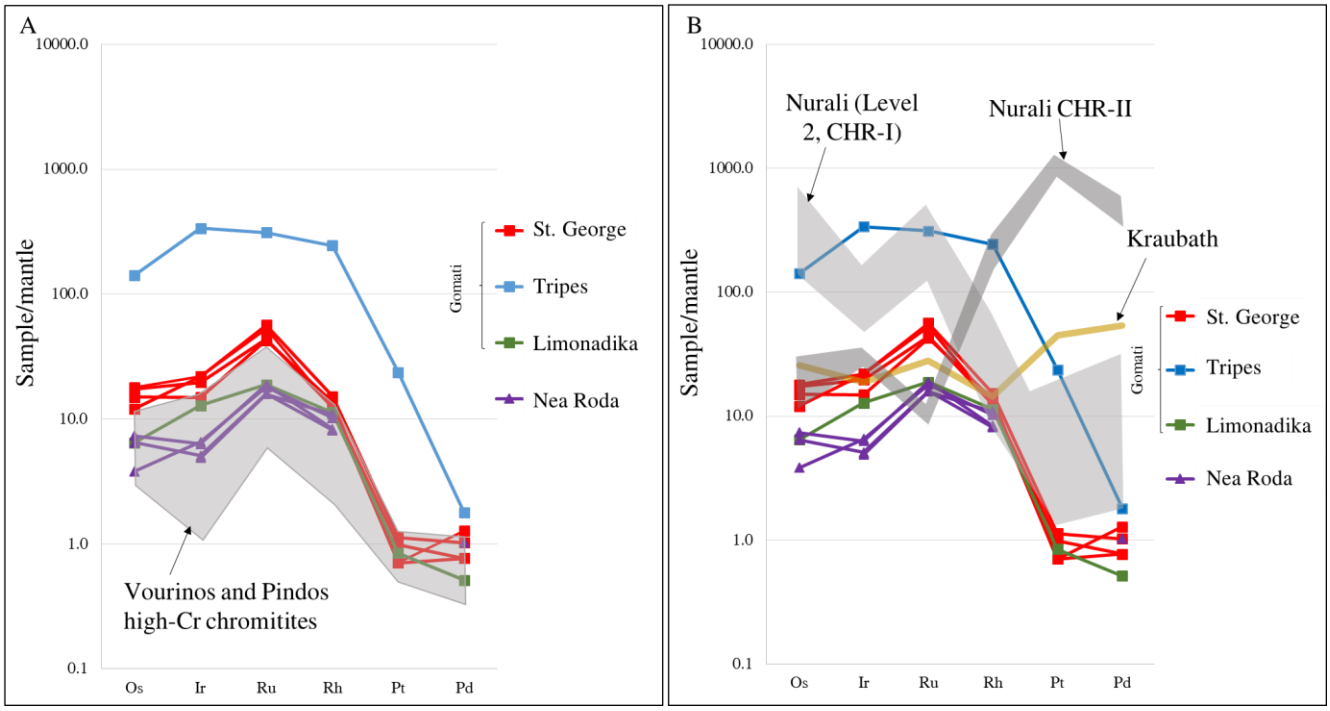


Fig. 4.26 Mantle normalized (McDonough and Sun, 1995) patterns of Gomati and Nea Roda chromitites compared to A) Vourinos and Pindos high-Cr ophiolite chromitites (Economou-Eliopoulos, 1996) and B) Supra-Moho chromitites from Nurali (Grieco et al., 2007; Zaccarini et al., 2004a) and Kraubath (Malitch et al., 2003b).

### 4.2.3.5. Gomati and Nea Roda evolution

The coexistence of high-Al and high-Cr chromitites both in Gomati and Nea Roda suggests a genesis from different parental melts, varying in composition from MORB-like melts formed at back-arc setting for the high-Al chromitites (Tripes) to boninites related to a supra-subduction zone melting for the high-Cr chromitites (Limonadika) (Ahmed and Arai, 2002; González-Jiménez et al., 2011; Uysal et al., 2007; Zaccarini et al., 2011). Spinel mineral chemistry and parent melt compositions, moreover, coupled with the association of chromitites with clinopyroxenites and the presence of clinopyroxene relicts interstitial to chromites, typical of supra-Moho chromitites, suggests a supra-Moho genesis for Tripes and Nea Roda massive chromitites. St. George and Nea Roda disseminated chromitites display intermediate compositions, more similar to Kraubath chromitites, which were generated closely above the upper mantle boundary within the Moho transition zone (Malitch et al., 2003a). The interpretation of Nea Roda disseminated chromitites as generated within the Moho Transition Zone is also in

agreement with data from Michailidis et al. (1995), which interprets the exposed massif as a thrust block of a section through the Transition Zone, which is a zone of dunite, chromitite, pyroxenite and wherlite bands overlying the peridotites and underlying the cumulate rocks.

PGE patterns of Gomati and Nea Roda chromitites fit well with the above-mentioned model. Limonadika, St. George and Nea Roda show low PGE contents, typical of podiform chromitites, with a peak on Ru due to the presence of abundant laurite. Tripes chromitite shows very high PGE contents, comparable to those of Nurali supra-Moho chromitites. The pattern shows enrichments in Os, Ru, Ir and Rh, and depletion in Pt and Pd. This suggests that these chromitites formed from batches of magma deriving from later stages of partial melting, similar to Nurali Level 2 and CHR-I chromitites, in opposition to Nurali Level 1 and CHR-II chromitites which formed from melts generated during the first stages of partial melting of the mantle and hence rich in Pt and Pd. The enrichment in Os, Ir, Ru and Rh indicates that the degree of partial melting was high enough to dissolve all the PGE-hosting sulfides, and give rise to melts which can in turn generate PGE-rich chromitites. However, this level of enrichment can be achieved only by small batches of melt that did not dilute through mixing with other melts.

Another explanation for the high PGE content is through enrichment processes in a magma chamber, after the emplacement in the cumulate section above the Moho Transition Zone. However, the mechanisms responsible for the PGE enrichments within layered intrusions (e.g. within the Merensky Reef, Bushveld or the J-M Reef, Stillwater), do not seem to have played a role in the genesis of Tripes chromitites. There are two main schools of thinking about the genesis of the Merensky and J-M Reef. One group believes that the PGE have been concentrated from below, when Cl-brines are released from consolidated cumulates and, while ascending into the overlying magma chamber, they dissolve PGE, Ni and Cu, which subsequently crystallize (Naldrett et al., 2008). The second group argues for a mixing of new and old magmas in the magma chamber which causes sulfide immiscibility. Immiscible sulfides settle along with pyroxene to produce PGE-enriched pyroxene cumulates (Naldrett et al., 2008).

Barnes et al. (2006), Cabri and Laflamme (1976) and Prichard et al. (2004) suggest that Pt, Pd, Au, Bi, Te, As and Sb are concentrated in a late-stage residual melt. Crystallization of this liquid forms PGM around the margins of sulfide blebs, and in veins interstitial to the surrounding silicates, as observed in the Platreef (Holwell and McDonald, 2007). The few PGM included in chromite are IPGE-sulfides, formed during early magmatic stages in sulfide-undersaturated conditions. If sulfur-saturation occurs concurrently with, or prior to, the earliest crystallizing phases, laurite and Ru–Ir–Os alloy will not form and the IPGE will partition into mss (Brenan and Andrews, 2001; Holwell and McDonald, 2007).

The high PPGE/IPGE ratio within layered intrusions suggest a late stage enrichment of PPGE within the magma chamber. On the contrary, the low IPGE/PPGE ratio within Gomati and Nea Roda chromitites suggest that the IPGE enrichment is related to early magmatic processes within the mantle. Moreover, PGE mineralization within layered intrusions are not hosted within chromitites, and these metals are either hosted within base metal sulfides or form PGM interstitial to the silicate assemblage. Within Gomati and Nea Roda, on the contrary, PGM are included within chromites, and the ones found within the silicate matrix are rare.

Both Gomati and Nea Roda underwent pervasive alteration during their post magmatic evolution. The circulation of post-magmatic fluids caused the replacement of primary silicates by chlorite, the breakdown of primary sulfides into secondary ones and the crystallization of secondary arsenides and antmonides. Arsenides and antimonides in the area probably crystallized at temperatures below 600 °C due to the circulation of hydrothermal fluids rich in Sb, Pb, Cu, Au and Ag, originating from the porphyry Cu-Au of the Kassandra district. Secondary Ni-Fe sulfides also crystallized or replaced primary sulfides at temperatures below 556°C (Tzamos et al., 2016). The absence of alloys suggests that the circulating fluids had relatively high $fS_2$, and only limited desulfurization of primary sulfides took place. High $fS_2$ fluids could have also been responsible for the formation of widespread chlorite and ferrian chromite. Experimental studies showed that Mg-rch chlorite forms at temperatures between 200 and 300 °C, at different sulfur and oxygen fugacities (Beaufort et al., 2015).

The circulating fluids altering the silicate and Ni-Fe sulfide assemblage, however, did not affect the primary PGM assemblage. As primary PGM are mainly early magmatic phases which were included in chromite crystals, they were generally not touched by altering fluids. In the few cases where PGM came in contact with circulating fluids, however, they were not altered, suggesting that fluids had high $fS_2$.

PGE patterns also suggest that no PGE remobilization took place. Ophiolite chromitites which suffered hydrothermal alteration show enrichments in PPGE (due to the mobility of Pd and Pt under hydrothermal conditions) (Yang and Seccombe, 1993), and serpentinization affects the pattern by remobilizing at least partially Ru and Rh, and creating a characteristic PGE pattern with double peaks at Os and Ru (Grieco et al., 2020).

### 4.2.4 Conclusion

Chromitites from Gomati and Nea Roda are associated to different stratigraphic positions. Limonadika chromitites show spinel mineral chemistry, parent melt composition and PGE contents similar to typical ophiolite chromitites, formed under the Moho. St. George and Nea Roda chromitites show spinel chemistry intermediate between ophiolite chromitite spinels (high-Cr) and supra-Moho spinels (high-Al), and PGE contents comparable to those of Limonadika. Their composition is similar to Kraubath spinels, and suggests a formation in the Moho Transition Zone, at the base of the cumulate sequence. Tripes chromitites show spinel mineral chemistry similar to those of Nurali supra-Moho chromitites, and enrichments in PGE up to 3 ppm. The high IPGE/PPGE ratio of Tripes chromitites suggests that the PGE enrichment is related to primary processes in the mantle, and not to secondary ones in the magma chamber, as is the case for PGE-rich deposits within layered intrusions. Tripes chromitites crystallized from magmas generated in the critical melting interval (20-25%), which is the most favorable to dissolve all the PGE-hosting sulfides in the mantle and produce a PGE-rich melt.

The post-magmatic evolution of Gomati and Nea Roda was dominated by a strong alteration event related to the circulation of high $fO_2$ and $fS_2$ fluids, responsible for the alteration of chromite into ferrian chromite and the replacement of primary silicates by chlorite. The BMM assemblage was affected by the alteration event. Primary sulfides were replaced by secondary ones, but the high $fS_2$ conditions prevented the formation of secondary BM-alloys. Moreover, the introduction of Cu, Sb and As in the system, transported from the Kassandra porphyry deposits through faults, led to the crystallization of low-T antimonides and arsenides. The circulating fluids, however, did not alter the PGM assemblage, and PGE were not remobilized, as confirmed also by the Ru peak in the PGE mantle-normalized patterns.

# 4.3. Remobilization in serpentinized chromitites

## 4.3.1 Mineralogy and texture

### 4.3.1.1. Skyros

Sampling in the Skyros island took place between Agio Iohannis and Agio Alexandria localities, where small chromitite bodies occur within hosting serpentinites (Fig. 4.27, Tab.4.15).

Tab. 4.15 Skyros samples and analyses (**bold**: EMPA; underlined: whole rock PGE content).

| Zone | Coordinates | Sample | Lithology |
|---|---|---|---|
| Agio Iohannis | 38°54'05.45'' – 24°32'48.21'' | **SKY8A**, **SKY8B**, SKY8C | chromitites |
| | 38°53'44.98– 24°31'40.23'' | SKY1 | serpentinite |
| | | SKY2A, SKY3 | magnetite, serpentinite |
| | | SKY4, SKY6 | serpentinite, magnetite |
| Northern Agio Iohannis | 38°54'15.39'' – 24°32'38.05'' | **SK3A**, SK3E, **SK3H**, **SK3I** | chromitites |
| | 38°54'10.68'' – 24°32'3.41'' | **SK4A,** SK5A | chromitite, serpentinite |
| Agio Alexandria | 38°53'30.22'' – 24°31'21.22'' | SKY9, **SKY10** | serpentinite, chromitite |
| | 38°53'29.90'' – 24°31'21.23'' | **SKY11A,** SKY13 | chromitites |
| | | SKY12 | epidosite |
| | 38°53'21.46'' – 24°31'27.12'' | **SKY14A**, **SKY14B-A**, B | chromitites |
| | 38°53'21.11'' – 24°31'27.49'' | **SK13** | magnetite |

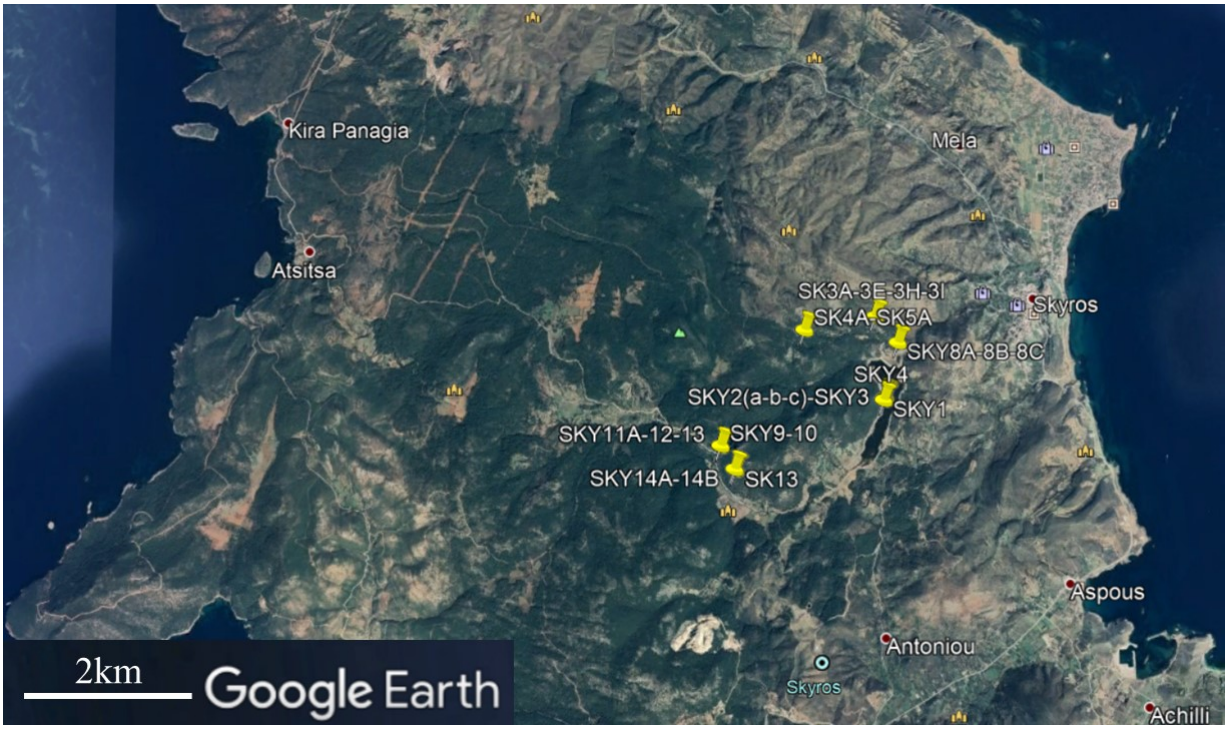


Fig. 4.27 Skyros sample locations.

Chromitite samples from the Agio Iohannis area were found mainly within a debris (Fig. 4.28A) on a dirt road (samples SKY8A to SKY 8C). Chromitite samples from Agio Alexandria were collected from serpentinite outcrops along a dirt road (Fig. 4.28B) and from debris in a small wood (Fig. 4.28C). In the area between Agio Iohannis and Agio Alexandria, serpentinite and magnetite samples were taken from a 50m long and 5m high outcrop (Fig. 4.28D).

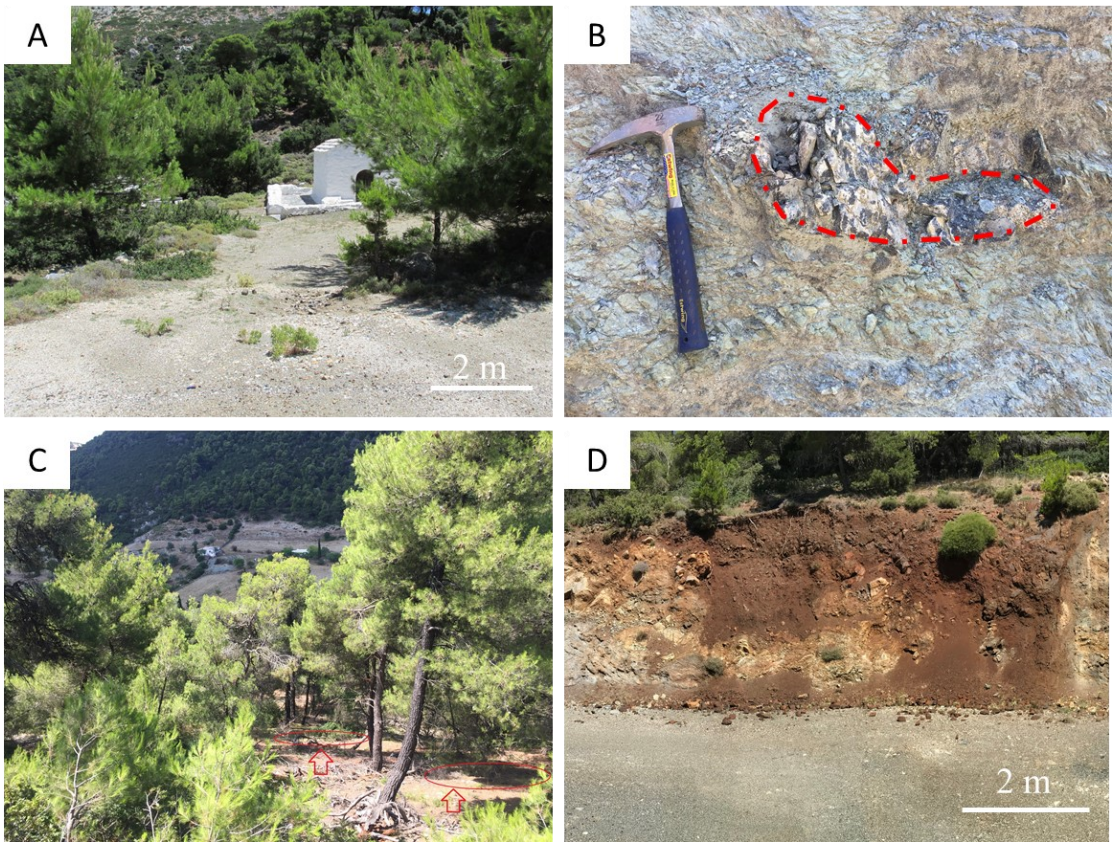


Fig. 4.28 Sampling localities of Skyros island. A) Agio Iohannis; B) and C) Agio Alexandria; D) between Agio Iohannis and Agio Alexandria.

In the Agio Iohannis and Northern Agio Iohannis areas, chromitite with massive and nodular textures occur either in debris or within serpentinized outcrops. Chromitites are composed by subhedral to anhedral crystals of chromian spinel, variably fractured and immersed in a serpentinitic groundmass (Fig. 4.29A). Chromite rims and fracture zones are commonly altered into ferrian chromite. Chlorite is present in some samples but is not widespread. A distinctive feature of many Skyros samples is the presence of thick Cr-garnet crowns surrounding chromite crystals and occasionally developing inside fractures. Uvarovitic garnets are euhedral crystals with bright green colors in PPL (Parallel Polarized Light) (Fig. 4.29B, Fig. 4.30). Primary silicate relicts are rare and constituted by pyroxene crystals. BMM and PGM assemblage is quite poor, and constituted mainly by Fe-Ni-sulfides (heazlewoodite, millerite, and pentlandite) and Fe-Ni alloys (e.g. awaruite). Two PGM were found in the area, a highly altered laurite and a Ni-Ir-Fe alloy (garutiite) (Fig. 4.29C, D).

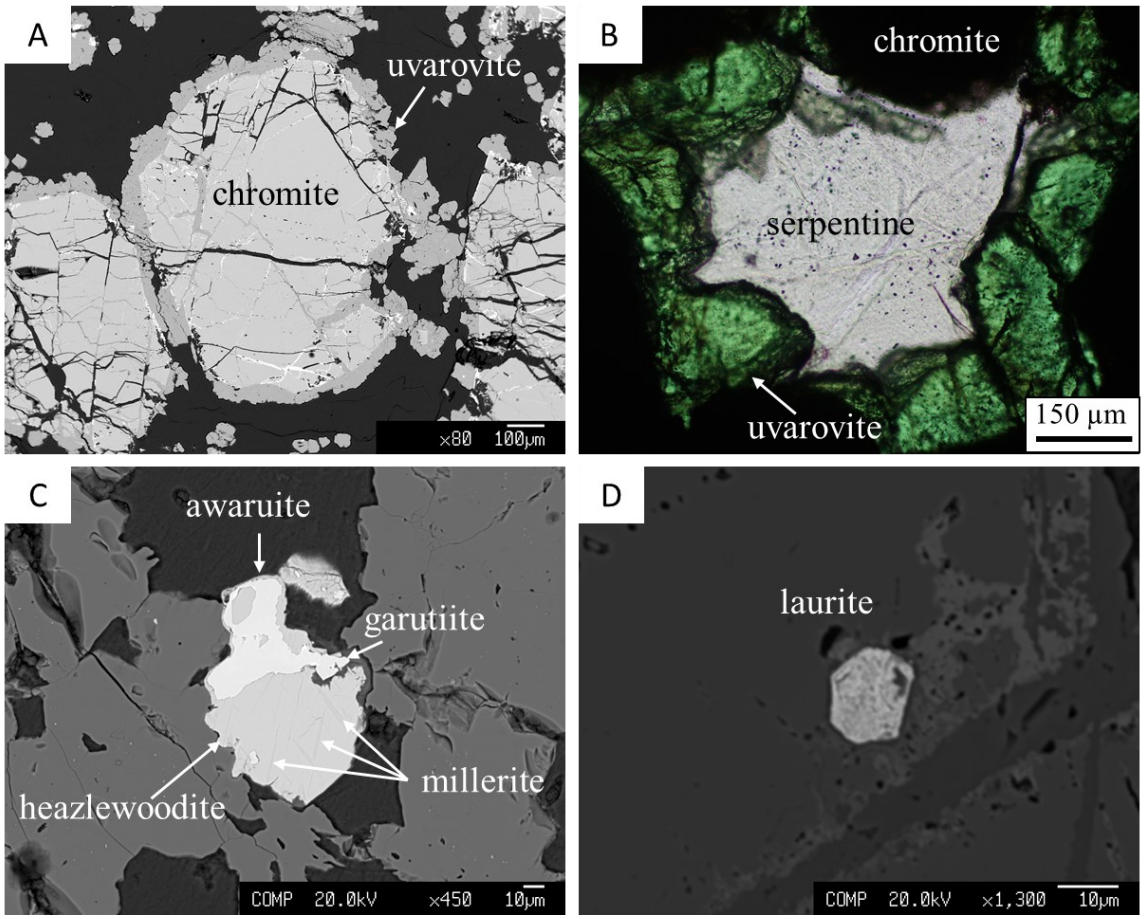


Fig. 4.29 A) BSE image of chromite grains surrounded by Cr-garnet; B) PPL image of Cr-garnet crystals; C) and D) BSE images of two PGM grains found in Skyros.

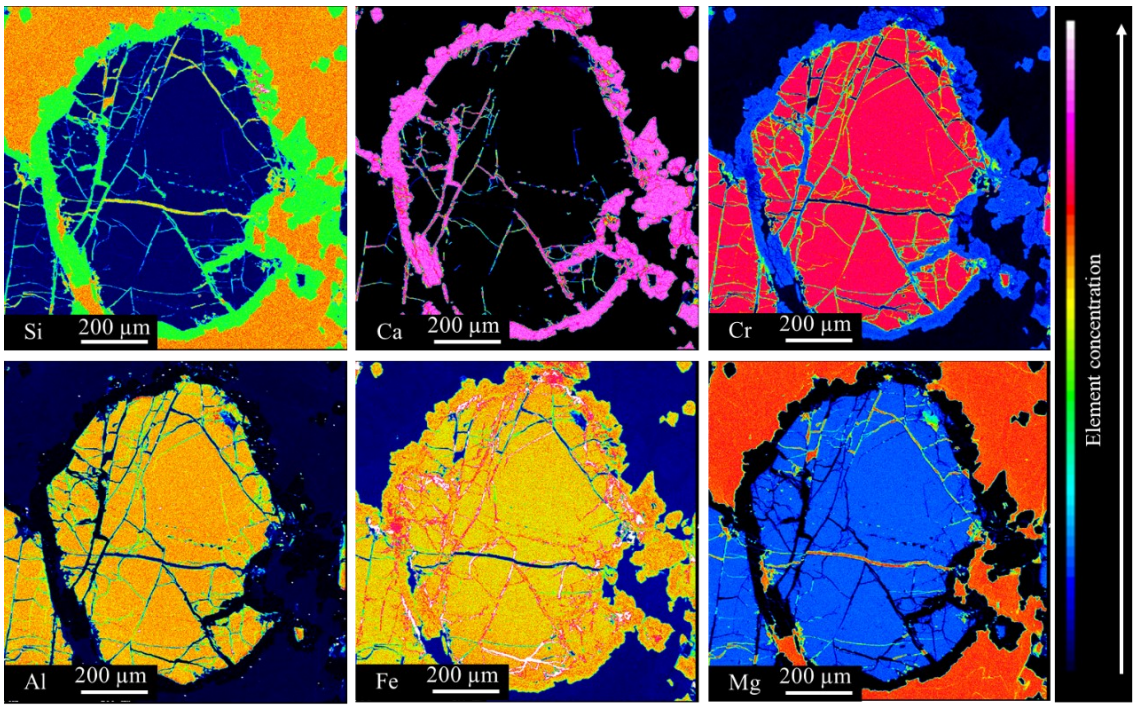


Fig. 4.30 Elemental atomic maps on the same area as Fig. 4.29 A.

Agios Alexandria chromitites were found in pods in highly serpentinized outcrops. Chromite crystals present euhedral to subhedral shape, and are highly altered into ferrian chromite (Fig. 4.31A). Chlorite is sometimes found associated to Fe-chromitized grains, but the silicate matrix is constituted mainly by serpentine. Uvarovite is not present. The most common BMM are Ni-sulfides (heazlewoodite, millerite) and Fe-Ni alloys (awaruite). A Ni-Fe-Cu alloy was also found. The PGM assemblage is poor, and only one Rh-rich PGM was found. In the area massive magnetite rocks are also present (Fig. 4.31B). Accessory phases in massive magnetites are Cu-sulfides and Cu-carbonates (malachite).

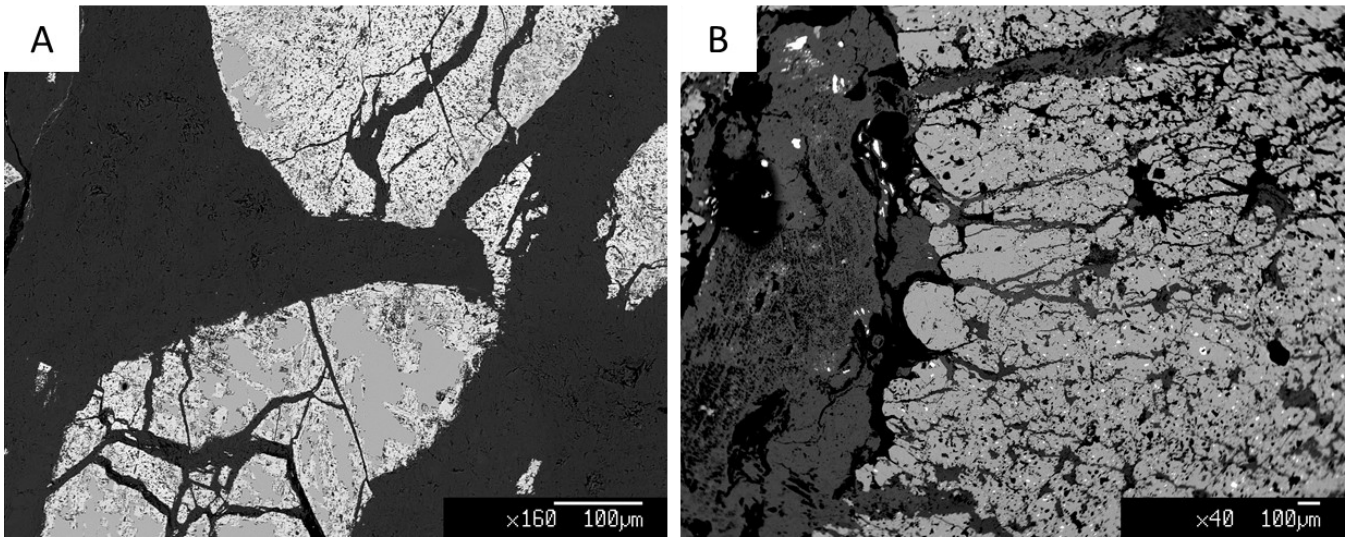


Fig. 4.31 BSE images of A) alteration of chromite into ferrian chromite and B) massive magnetite sample (light gray) in a serpentinitic groundmass (dark gray).

#### 4.3.1.2. Abdasht-Soghan

Sampling in Abdasht and Soghan mafic-ultramafic complexes were collected from surface outcrops, stocks of ore and underground galleries (Gentile, 2015), and include disseminated, banded, nodular and massive chromitites, as well as some host rocks (Fig. 4.32, Tab. 4.16).

Tab. 4.16 Abdasht-Soghan sampling and analyses (**bold**: EMPA; underlined: whole rock PGE content).

| Zone | Coordinates | Sample | Lithology |
|---|---|---|---|
| Soghan – Panjah Metri | 28°20'57.10'' – 56°50'10.10'' | **IRSOA01**, **IRSOA02**, **IRSOA03**, **IRSOA04**, **IRSOA06**, IRSOA07, **IRSOA08**, **IRSOA09** | chromitite |
| | 28°20'57.10'' – 56°50'10.10'' | IRSOA10, IRSOA11 | host rock |
| | 28°20'58.64'' – 56°50'08.57'' | **IRSOB01** | chromitite |
| | 28°20'58.64'' – 56°50'08.57'' | IRSOB02, **IRSOB03** | host rock |
| Soghan – Omid Bekhoda | 28°21'21.32'' – 56°50'08.77'' | **IRSOC01**, **IRSOC02** | chromitite |
| Soghan - Gechin | 28°22'36.42'' – 56°51'28.29'' | **IRSOD03** | chromitite |
| Abdasht | 28°21'01.76'' – 56°46'41.45'' | **IRABA01**, **IRABA02**, **IRABA03** | chromitite |
| | 28°21'08.76'' – 56°46'30.07'' | **IRABB01**, **IRABB03**, **IRABB04**, **IRABB05**, **IRABB06** | chromitite |

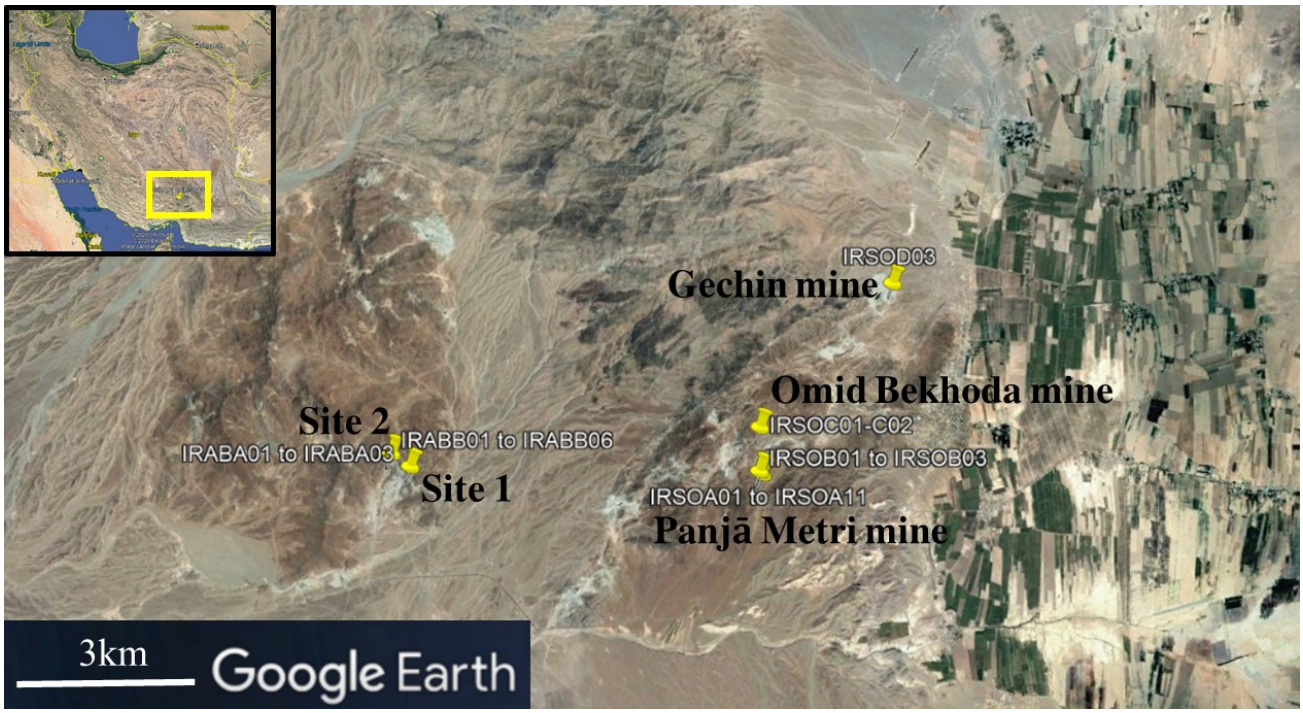


Fig. 4.32 Abdasht-Soghan sample locations.

Three mining areas were sampled in Soghan: Panjā Metri, Omid Bekhoda and Gechin. Two mining areas were sampled in Abdasht: Site 1 and Site 2 (Fig. 4.33).

In the Panjā Metri mine are conveyed the run of mine of different ore bodies (Fig. 4.33A). Ore samples were collected from the stock and from an underground gallery (Fig. 4.33B). The chromitite bodies are enclosed within highly serpentinized dunites.

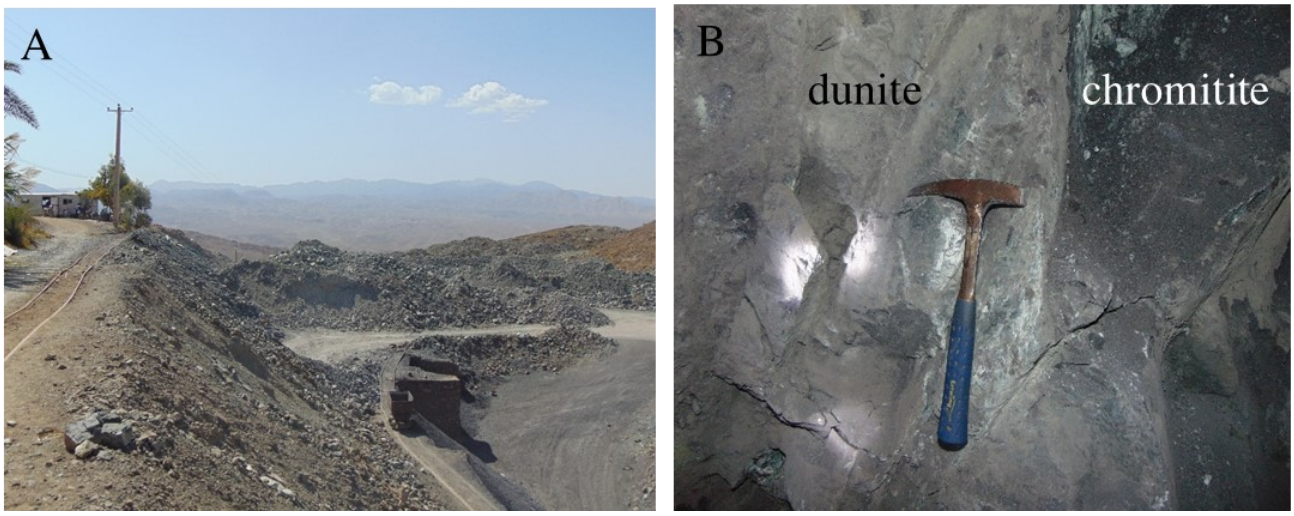


Fig. 4.33 A) External part of the Panjā Metri mine B) contact between chromitite and dunite in an underground tunnel; pictures are from Gentile (2015).

The Omid Bekhoda mining area contains several ore bodies, all exploited and then worked and collected in a single stock. The main ore body is a sub-vertical high-grade chromitite lens enclosed in serpentinized dunite (Fig. 4.34A). Late magnesite veins (Fig. 4.34B) cut the outcrops.

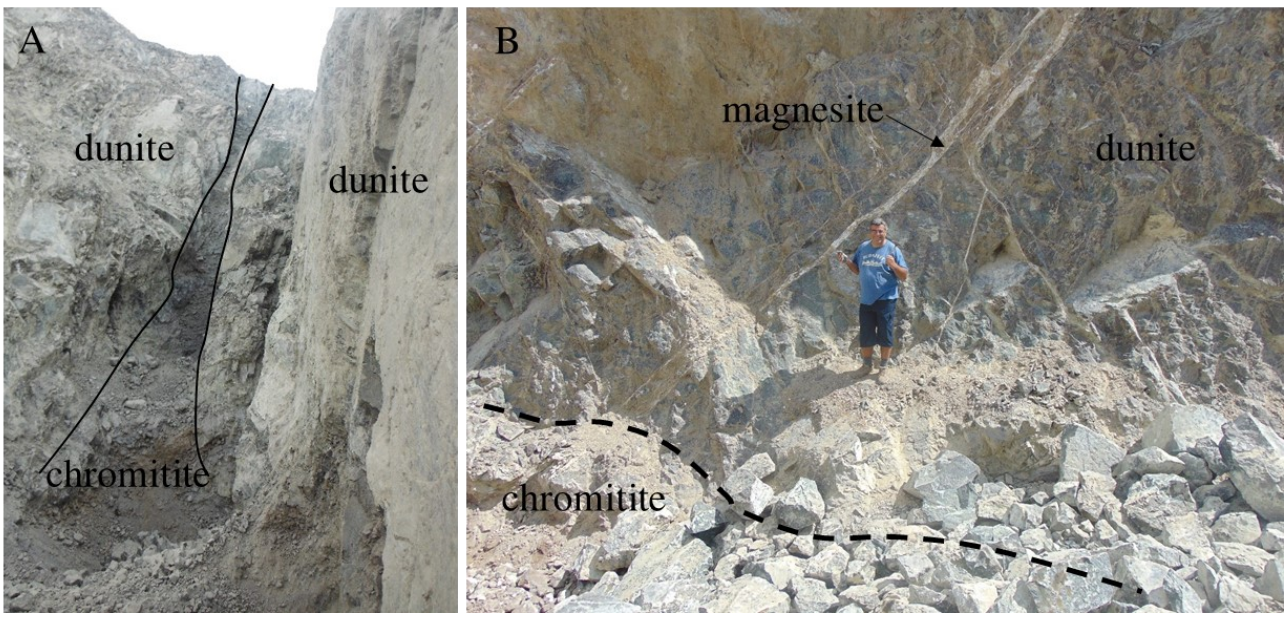


Fig. 4.34 A) Lenticular ore body mined in the Omid Bekhoda area; B) top of the chromitite lens; pictures are from Gentile (2015).

Gechin, located in the northeastern part of the Soghan complex, is a dismissed mine. Huge, highly serpentinized chromitite bodies were exploited over the years, and only few samples can be collected from the area. Chromitite and associated host rocks are highly fractured and show pervasive alteration, highlighted by the presence of serpentine, brucite and magnesite.

Within Abdasht, two mining sites have been sampled: Site 1 and Site 2. Site 1 collects the run of mine of several bodies (Fig. 4.35A), which consist of massive chromitites enveloped in serpentinized dunite. This site also hosts a small enrichment plant, working with jig concentrators. Site 2 consists of an underground tunnel from which massive chromitite and host rock samples were collected (Fig. 4.35B).


Fig. 4.35 A) Massive chromitite stock from Site 1; B) Service area of the mining area of Site 2; pictures are from Gentile (2015).

*Main Assemblage*

Chromitites from the Abdasht-Soghan complex are mostly composed of subhedral to anhedral crystals of chromite in an olivine-serpentine-chlorite matrix. The grain size is highly variable, with small (few micrometers) crystals in dunites and disseminated chromitite and big crystals (up to 10 mm) within massive chromitites. Almost all samples are fractured, testifying that the rocks underwent a strong deformation process (Fig. 4.36A).

The most common textures are fine to coarse-grained massive and banded chromitites, while nodular texture is less common. Disseminated chromitites are also widespread, and can be found mainly surrounding the massive and banded ore bodies.

Ferrian chromite alteration is present but not widespread, and affects chromite rims at different degrees. The extent of ferrian chromitization is outlined by the porosity of the ferrian chromite compared to the non-porous texture of primary chromite, and can reach up to 60% in massive and banded ores and 100% in disseminated ores (Fig. 4.36B).

Primary phases in the silicate matrix are rare, and limited to few olivine relicts. Only few samples of dunites from the Soghan massif show lower degrees of serpentinization and abundant olivine (Fig.

4.36C). Olivine is commonly altered into serpentine, which replaces the primary mineral starting from fractures. Small magnetite crystals are systematically associated to serpentine. Cr-chlorite is present but not widespread, and always grows from serpentine. The presence of Cr-chlorite is associated to the presence of ferrian chromite rims. Brucite and Mg-Fe-hydroxides are sometimes present and can be abundant in some samples (Fig. 4.36D). Dolomite was also detected as a minor phase at the Omid Bekhoda mine, and uvarovite was found in the Gechin mine.

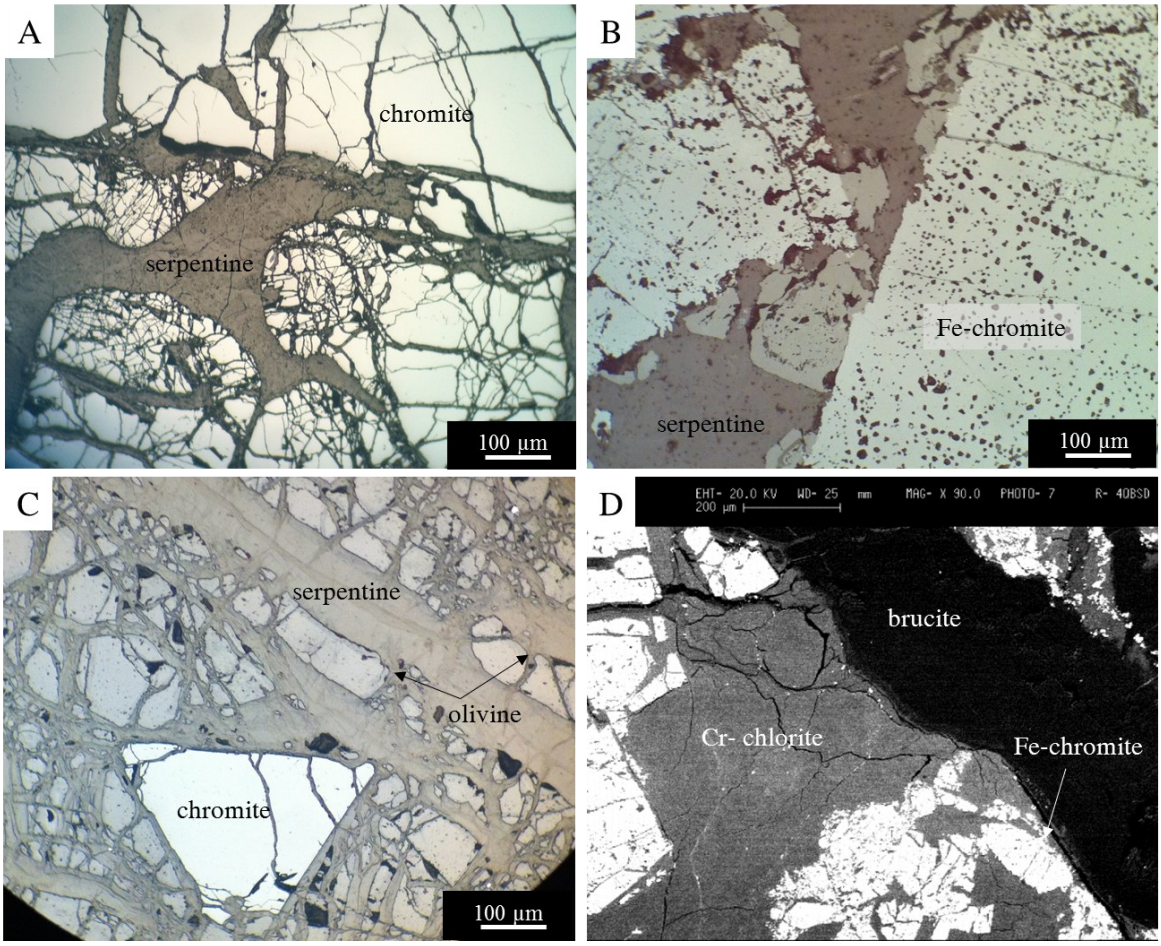


Fig. 4.36 PPL images (reflected light) of A) highly fractured massive chromitite; B) ferrian chromite alteration producing a typical porous texture; C) disseminated chromitite with low degree of serpentinization; D) BSE image of a deeply Fe-chromitized sample, with a late brucite vein.

*Sulfides*

Grains, blebs and aggregates of BMM were found mainly in the silicate matrix and more rarely as inclusions within chromite. BMM are abundant within Abdasht, while Soghan is characterized by a lower amount and diversity.

Within Soghan, the BMM assemblage is dominated by awaruite and heazlewoodite, with the first one replacing the second one in many cases (Fig. 4.37A). The only primary sulfide detected is a single

pentlandite grain rimmed by bornite. Native copper blebs were also found associated to ferrian chromite and chlorite (Fig. 4.37B).

Abdasht shows a more diversified BMM assemblage. As in Soghan, the only primary sulfides detected are rare pentlandite grains. The most abundant secondary sulfides are heazlewoodite (Fig. 4.37C), followed by millerite. Ni-arsenides are present in the form of maucherites (Fig. 4.37D). Alloys in the Abdasht complex are mainly Ni- and Ni-Cu alloys.

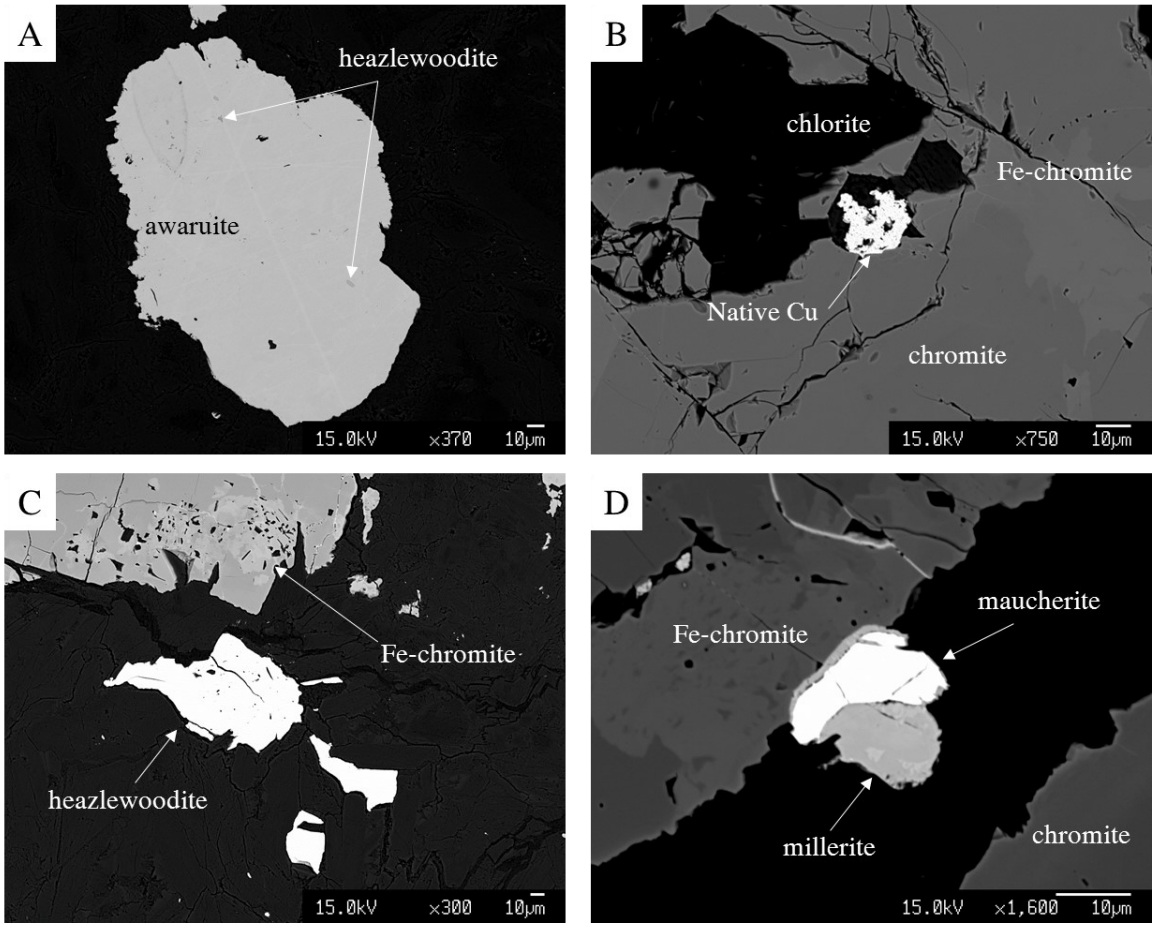


Fig. 4.37 BSE images of A) awaruite bleb with tiny heazlewoodite relicts from Panjah Metri mine, Soghan; B) native Cu bleb between ferrian chromite and chlorite in Soghan; C) heazlewoodite aggregates within olivine matrix in Abdasht; D) millerite and maucherite within the Abdasht complex.

*Platinum Group Minerals*

A total of twenty PGM were found in the studied sections, but some of them could not be analyzed due to their small size. Laurite is the most common PGM, and is always found enclosed within unaltered chromite. It usually forms euhedral crystals (Fig. 4.38A), and can be associated to silicates (Fig. 4.38B) or form polyphasic PGM/BMM aggregates (Fig. 4.38C, D).

PGE alloys are also common within Abdasht-Soghan. They are systematically associated to ferrian chromite pores or fracture zone, and can form single grain inclusions (Fig. 4.38E), or reaction zones around laurites (Fig. 4.38F).

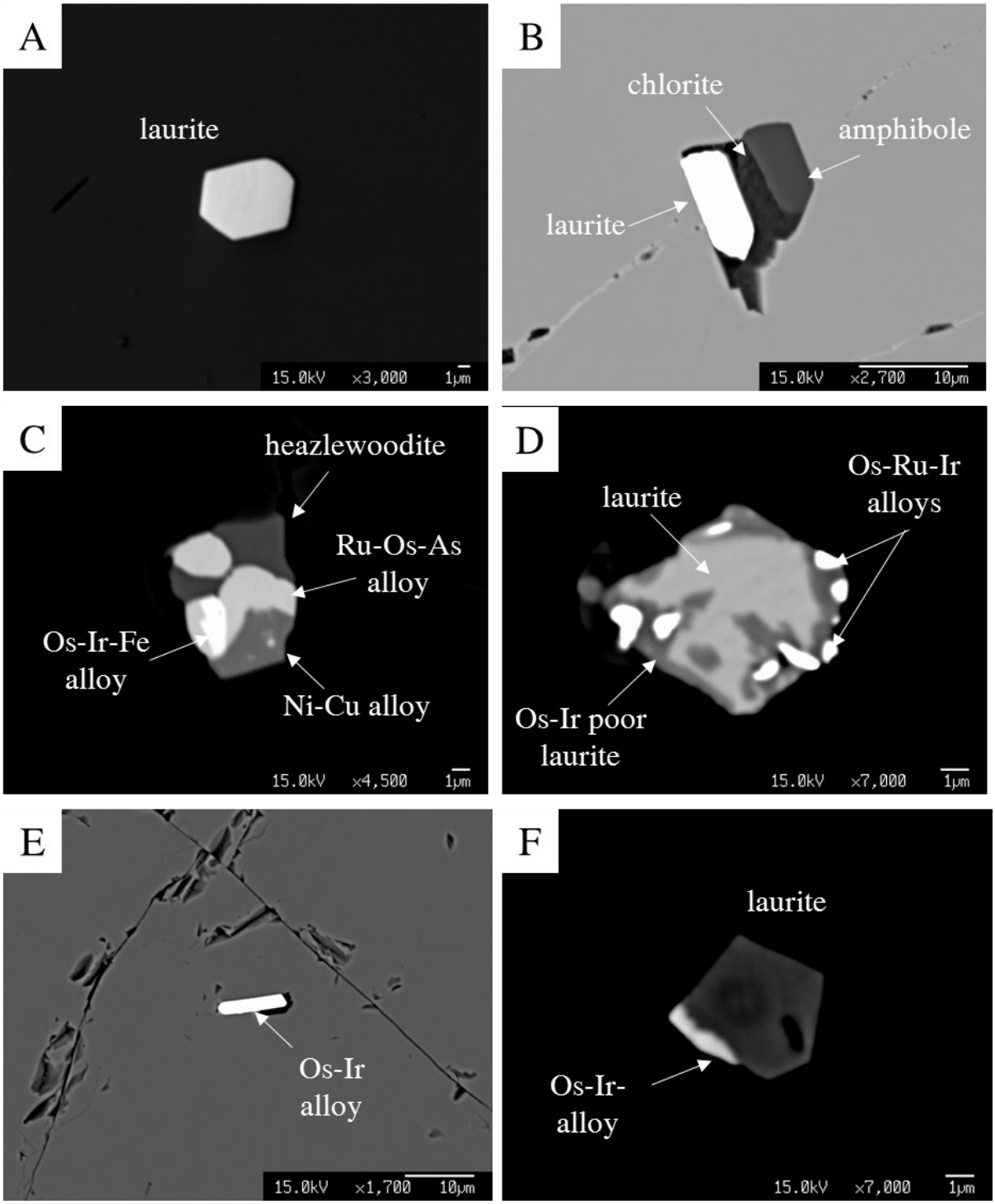


Fig. 4.38 BSE images of A) euhedral laurite inclusion within chromite; B) polyphasic inclusion in chromite containing laurite, chlorite and amphibole from Soghan; C) polyphasic PGM-BMM assemblage from Abdasht; D) polyphasic PGE sulfide and alloy assemblage in Abdasht; E) Os-Ir alloy inclusion in chromite from Soghan; F) laurite crystal rimmed by a Os-Ir alloy in Soghan.

### 4.3.2 Mineral and whole rock chemistry

Complete microprobe analyses of Skyros and Abdasht-Soghan are reported in the Appendix (Tab. A4.10 to Tab. A4.17).

#### 4.3.2.1. Skyros

*Chromite*

Chromite average compositions (Tab. 4.17) are based on core analyses. The composition of the spinels is rather heterogeneous among the different areas, Northern Agio Iohannis, Agio Iohannis and Agio Alexandria.

MgO content ranges between 6.81 and 12.07 wt% in Northern Agio Iohannis, between 14.12 and 15.00 wt% in Agio Iohannis and between 14.74 and 15.81 wt% in Agio Alexandria. FeO content ranges between 14.51 and 17.08 wt% in Northern Agio Iohannis, between 11.81 and 14.15 wt% in Agio Iohannis and between 11.87 and 13.03 wt% in Agio Alexandria. $Cr_2O_3$ contents are higher within Northern Agio Iohannis, with values comprised between 46.24 and 58.03 wt%, than in Agio Iohannis (52.98 – 54.57 wt%) and Agio Alexandria (51.39 – 52.75 wt%). $Al_2O_3$ contents, on the contrary, are higher in Agio Alexandria (18.19 – 20.07 wt%) than in Agio Iohannis (16.18 – 17.92 wt%) and Northern Agio Iohannis (11.37 – 19.00 wt%).

Chromite rims are often altered into ferrian chromite, and show an enrichment in $Cr_2O_3$ and $Fe_2O_3$ and a depletion in $Al_2O_3$ content. Magnetite and Cr-magnetite were also detected in samples from Northern Agio Iohannis and Agio Iohannis. These minerals are characterized by low $Cr_2O_3$ and $Al_2O_3$ contents, and high $FeO_{tot}$ contents.

Tab. 4.17 Major elements average content (wt%) and standard deviation of chromite cores from Skyros.

| | Northern Agio Iohannis | | | | | | | | Agio Iohannis | | | | Agio Alexandria | |
|---|---|---|---|---|---|---|---|---|---|---|---|---|---|---|
| | SK3A | | SK3E | | SK3H | | SK3I | | SKY8A | | SKY8B | | SKY10 | |
| | **Avg** | St.Dev. | **Avg** | St.Dev. | **Avg** | St.Dev. | **Avg** | St.Dev. | **Avg** | St.Dev. | **Avg** | St.Dev. | **Avg** | St.Dev. |
| $SiO_2$ | **0.11** | 0.22 | **0.39** | 0.90 | **0.09** | 0.35 | **0.02** | 0.02 | **0.03** | 0.02 | **0.03** | 0.01 | **0.03** | 0.02 |
| $TiO_2$ | **0.25** | 0.03 | **0.29** | 0.02 | **0.24** | 0.03 | **0.21** | 0.02 | **0.20** | 0.03 | **0.22** | 0.03 | **0.24** | 0.05 |
| $Al_2O_3$ | **12.53** | 1.22 | **18.26** | 0.38 | **13.78** | 0.74 | **11.91** | 0.27 | **17.61** | 0.16 | **16.80** | 0.26 | **19.23** | 0.61 |
| $Cr_2O_3$ | **55.42** | 0.66 | **45.91** | 1.59 | **55.14** | 1.11 | **55.84** | 0.45 | **53.81** | 0.43 | **53.90** | 0.39 | **52.10** | 0.40 |
| $Fe_2O_3$ | **0.73** | 1.34 | **2.21** | 1.10 | **0.03** | 0.18 | **1.55** | 0.42 | **2.43** | 0.33 | **2.13** | 0.29 | **2.73** | 0.46 |
| FeO | **15.94** | 1.01 | **21.56** | 1.41 | **16.28** | 0.50 | **18.69** | 0.64 | **13.43** | 0.41 | **12.36** | 0.31 | **12.47** | 0.40 |
| MnO | **0.12** | 0.26 | **0.17** | 0.06 | **0.10** | 0.09 | **0.12** | 0.08 | **0.07** | 0.04 | **0.05** | 0.03 | **0.07** | 0.04 |
| MgO | **11.18** | 0.76 | **8.33** | 0.75 | **10.79** | 0.29 | **9.59** | 0.44 | **14.52** | 0.23 | **14.77** | 0.19 | **15.35** | 0.31 |
| TOTAL | **96.28** | 0.54 | **97.11** | 0.77 | **96.44** | 0.63 | **97.93** | 0.45 | **102.09** | 0.34 | **100.25** | 0.33 | **102.22** | 0.47 |
| Si | **0.00** | 0.01 | **0.01** | 0.03 | **0.00** | 0.01 | **0.00** | 0.00 | **0.00** | 0.00 | **0.00** | 0.00 | **0.00** | 0.00 |
| Ti | **0.01** | 0.00 | **0.01** | 0.00 | **0.01** | 0.00 | **0.01** | 0.00 | **0.00** | 0.00 | **0.01** | 0.00 | **0.01** | 0.00 |
| Al | **0.49** | 0.05 | **0.71** | 0.02 | **0.54** | 0.03 | **0.47** | 0.01 | **0.63** | 0.01 | **0.61** | 0.01 | **0.68** | 0.02 |
| Cr | **1.47** | 0.01 | **1.20** | 0.03 | **1.45** | 0.03 | **1.48** | 0.01 | **1.30** | 0.01 | **1.32** | 0.01 | **1.24** | 0.02 |
| $Fe^3$ | **0.02** | 0.04 | **0.05** | 0.03 | **0.00** | 0.00 | **0.04** | 0.01 | **0.06** | 0.01 | **0.05** | 0.01 | **0.06** | 0.01 |
| $Fe^2$ | **0.45** | 0.03 | **0.60** | 0.04 | **0.45** | 0.01 | **0.52** | 0.02 | **0.34** | 0.01 | **0.32** | 0.01 | **0.31** | 0.01 |
| Mn | **0.00** | 0.01 | **0.00** | 0.00 | **0.00** | 0.00 | **0.00** | 0.00 | **0.00** | 0.00 | **0.00** | 0.00 | **0.00** | 0.00 |
| Mg | **0.56** | 0.03 | **0.41** | 0.03 | **0.54** | 0.01 | **0.48** | 0.02 | **0.66** | 0.01 | **0.68** | 0.01 | **0.69** | 0.01 |

| | | | | | | | | | | | | | | |
|---|---|---|---|---|---|---|---|---|---|---|---|---|---|---|
| XMg | **0.56** | 0.03 | **0.41** | 0.04 | **0.54** | 0.01 | **0.48** | 0.02 | **0.66** | 0.01 | **0.68** | 0.01 | **0.69** | 0.01 |
| XCr | **0.75** | 0.02 | **0.63** | 0.01 | **0.73** | 0.01 | **0.76** | 0.00 | **0.67** | 0.00 | **0.68** | 0.00 | **0.65** | 0.01 |

*Silicates*

The silicate assemblage is quite heterogeneous, both between different localities and among the samples. Within Northern Agios Iohannis chromitites, the silicate assemblage is made up primarily of serpentine, with less abundant or absent chlorite. Chlorite, when present, is always associated to ferrian chromitized rims, and is enriched in $Cr_2O_3$ up to 4.63 wt%. Chromite crystals within Northern Agio Iohannis, moreover, are surrounded by Cr-garnets with a composition comprised between the uvarovite and andradite endmembers (Tab. 4.18). $Cr_2O_3$ and $Fe_2O_3$ contents within Cr-garnets vary between 8.82 and 20.83 wt% and 14.54 and 30.04 wt% respectively.

Samples SKY8A and SKY8B from Agio Iohannis show completely different silicate assemblages. Sample SKY8A is highly serpentinized, and chromite crystals are rimmed by Cr-garnets with $Cr_2O_3$ contents up to 12.95 wt% and $Fe_2O_3$ contents up to 23.56 wt%. Sample SKY8B, on the contrary, is chloritized and primary silicate relicts are constituted by pyroxene crystals, both orthopyroxenes (enstatite) and clinopyroxenes (diopside) (Tab. 4.18). Diopsides are enriched in $Cr_2O_3$ up to 1.58 wt%, while chlorites show $Cr_2O_3$ enrichments up to 4.94 wt%.

Chromitite sample SK10 from Agio Alexandria shows a silicate matrix dominated by Cr-chlorite. No primary silicate relicts were detected (Tab. 4.18).

Tab. 4.18 EMPA representative analyses of silicate minerals in Skyros.

| | Northern Agio Iohannis | | | | | Agio Iohannis | | | | | | Agio Alexandria | |
|---|---|---|---|---|---|---|---|---|---|---|---|---|---|
| | serp | chlorite | | garnet | | Serp | garnet | chlorite | | diopside | enstatite | chlorite | |
| | SK3H | SK3H | SK3H | SK3A | SK3H | SKY8A | SKY8A | SKY8B | SKY8B | SKY8B | SKY8B | SKY10 | SKY10 |
| $SiO_2$ | 40.87 | 34.13 | 32.98 | 31.78 | 35.68 | 43.24 | 36.25 | 33.57 | 32.06 | 55.54 | 58.83 | 28.60 | 29.26 |
| $TiO_2$ | nd | 0.01 | 0.02 | 0.29 | 0.08 | 0.09 | 0.09 | nd | nd | 0.10 | 0.01 | 0.01 | 0.03 |
| $Al_2O_3$ | 0.83 | 11.75 | 10.83 | 0.59 | 0.09 | 0.71 | 0.26 | 15.26 | 14.44 | 0.97 | 0.52 | 17.79 | 17.61 |
| FeO | 1.59 | 0.89 | 0.91 | nd | 2.96 | 1.93 | nd | 0.69 | 0.52 | 1.72 | 3.52 | 0.70 | 0.57 |
| $Fe_2O_3$ | nd | nd | nd | 15.98 | 19.46 | nd | 17.04 | nd | nd | nd | nd | nd | nd |
| MnO | 0.01 | 0.01 | 0.02 | nd | nd | 0.05 | 0.02 | nd | 0.03 | 0.03 | 0.09 | nd | 0.01 |
| MgO | 40.12 | 35.08 | 34.58 | 0.48 | 0.04 | 38.84 | 0.05 | 34.60 | 33.35 | 18.10 | 36.85 | 33.34 | 33.33 |
| CaO | 0.06 | 0.01 | 0.03 | 30.43 | 30.99 | 0.07 | 34.58 | 0.01 | 0.00 | 23.09 | 0.48 | 0.02 | 0.01 |
| $Na_2O$ | nd | nd | 0.01 | nd | nd | nd | nd | nd | 0.01 | 0.35 | nd | nd | 0.01 |
| $K_2O$ | nd | nd | nd | nd | nd | 0.01 | nd | 0.01 | nd | nd | nd | 0.02 | nd |
| $Cr_2O_3$ | 0.90 | 2.40 | 4.63 | 20.83 | 12.92 | 0.92 | 12.33 | 0.73 | 4.23 | 1.72 | 0.91 | 5.04 | 4.45 |
| $H_2O$* | 12.37 | 12.17 | 11.78 | 0.00 | 0.00 | 12.38 | nd | 12.53 | 11.98 | 0.00 | 0.00 | 11.91 | 11.98 |
| Tot | 96.76 | 96.45 | 95.80 | 100.38 | 102.22 | 98.31 | 100.62 | 96.67 | 96.62 | 101.62 | 101.20 | 97.43 | 97.26 |

*Base Metal Minerals*

Base Metal Minerals are not abundant within Skyros chromitites, and only few grains were detected (Tab. 4.19). Secondary Ni sulfides commonly show enrichments in PGE. Agio Iohannis chromitites contain rare pentlandite, millerite and heazlewoodite grains. Heazlewoodite crystals show enrichments

in PGE content up to 1.01 wt%. One millerite crystal shows enrichments in Pt (0.54 wt%) and Os (0.11 wt%).

Northern Agio Iohannis chromitites display the most heterogeneous BMM assemblage, with awaruites pentlandite, millerite, heazlewoodite, Cu-Ni alloys and Ni-arsenides (orcelite and a mineral approaching the stoichiometry of dienerite). Major element compositions are rather homogeneous, but some of the minerals show enrichments in Co. Ni-Fe alloys contain Co up to 1.41 wt%, and pentlandite up to 0.99 wt%. Millerite and heazlewoodite are sometimes enriched in Co up to 0.63 wt%.

Agio Alexandria chromitites show a BMM assemblage constituted by Ni-Fe alloys, millerite, heazlewoodite and a Cu-alloy. Ni-Fe alloys show enrichments in PGE up to 0.53 wt% (Pt up to 0.46 wt%), heazlewoodite crystals are enriched in PGE up to 1.09 wt% (Pt up to 0.69 wt% and Ir up to 0.46 wt%).

Tab. 4.19 Selcted EMPA analyses of Base Metal Minerals within Skyros.

| | As | S | Ni | Fe | Cu | Sb | Ir | Co | Os | Pt | Rh | Tot |
|---|---|---|---|---|---|---|---|---|---|---|---|---|
| **wt%** | | | | | | **awaruites and alloys** | | | | | | |
| SK3H-5 | bdl | bdl | 76.23 | 22.96 | 0.80 | bdl | bdl | 1.41 | bdl | bdl | bdl | 101.40 |
| SK3I- 6 | bdl | 2.30 | 73.98 | 19.82 | 0.56 | bdl | bdl | 0.56 | bdl | bdl | bdl | 97.22 |
| SKY14BA-H1 | 0.03 | 2.02 | 83.12 | 5.25 | 3.68 | bdl | bdl | bdl | bdl | 0.46 | 0.01 | 94.63 |
| | | | | | | **pentlandite** | | | | | | |
| SK3A- 6 | bdl | 31.88 | 41.14 | 24.26 | 0.05 | bdl | bdl | 0.71 | bdl | bdl | bdl | 98.03 |
| SKY8B-D1 | 0.03 | 33.42 | 43.18 | 22.61 | 0.00 | bdl | bdl | bdl | 0.02 | 0.05 | 0.04 | 99.35 |
| | | | | | | **millerite** | | | | | | |
| SK3H- 10 | bdl | 32.94 | 66.75 | 0.09 | 0.07 | bdl | 0.14 | bdl | 0.00 | bdl | bdl | 100.00 |
| SK3A- 5 | 0.11 | 32.22 | 65.81 | 1.04 | 0.07 | bdl | bdl | 0.02 | 0.00 | bdl | bdl | 99.26 |
| SKY8B-D8 | 0.00 | 35.78 | 63.39 | 0.82 | 0.00 | bdl | 0.05 | bdl | 0.11 | 0.54 | 0.05 | 100.74 |
| | | | | | | **heazlewoodite** | | | | | | |
| SK3A- 8 | bdl | 25.25 | 74.40 | 0.73 | 0.10 | bdl | bdl | bdl | bdl | bdl | bdl | 100.47 |
| SK3I- 4 | bdl | 25.35 | 72.52 | 2.00 | 0.01 | bdl | bdl | 0.18 | bdl | bdl | bdl | 100.07 |
| SKY14B-F5 | 0.01 | 27.43 | 70.40 | 1.45 | bdl | bdl | 0.36 | bdl | bdl | 0.69 | bdl | 100.34 |
| SKY10-I12 | 0.02 | 27.04 | 71.70 | 1.65 | bdl | bdl | 0.13 | bdl | bdl | 0.09 | 0.06 | 100.69 |
| | | | | | | **Cu alloys** | | | | | | |
| SK3H- 15 | 0.01 | 0.03 | 15.62 | 1.89 | 84.83 | bdl | bdl | 0.08 | bdl | bdl | bdl | 102.46 |
| SKY14A-G2 | 0.00 | 0.03 | 0.11 | 0.98 | 56.25 | bdl | bdl | bdl | bdl | bdl | bdl | 57.38 |
| | | | | | | **Ni arsenides** | | | | | | |
| SK3A- 9 | 33.51 | 0.00 | 70.26 | 0.41 | 0.04 | 0.73 | bdl | bdl | bdl | bdl | bdl | 104.95 |
| SK3A- 10 | 36.00 | 0.01 | 67.33 | 0.33 | 0.05 | 0.95 | bdl | bdl | bdl | bdl | bdl | 104.66 |
| **apfu** | | | | | | **awaruites and alloys** | | | | | | |
| SK3H-5 | 0.00 | 0.00 | 3.16 | 1.00 | 0.03 | 0.00 | 0.00 | 0.06 | 0.00 | 0.00 | 0.00 | 4.25 |
| SK3I- 6 | 0.00 | 0.20 | 3.55 | 1.00 | 0.02 | 0.00 | 0.00 | 0.03 | 0.00 | 0.00 | 0.00 | 4.81 |
| SKY14BA-H1 | 0.00 | 0.67 | 15.06 | 1.00 | 0.62 | 0.00 | 0.00 | 0.00 | 0.00 | 0.03 | 0.00 | 17.38 |
| | | | | | | **pentlandite** | | | | | | |
| SK3A- 6 | 0.00 | 7.89 | 5.56 | 3.45 | 0.01 | 0.00 | 0.00 | 0.10 | 0.00 | 0.00 | 0.00 | 17.00 |
| SKY8B-D1 | 0.00 | 8.11 | 5.73 | 3.15 | 0.00 | 0.00 | 0.00 | 0.00 | 0.00 | 0.00 | 0.00 | 17.00 |
| | | | | | | **millerite** | | | | | | |
| SK3H- 10 | 0.00 | 0.95 | 1.05 | 0.00 | 0.00 | 0.00 | 0.00 | 0.00 | 0.00 | 0.00 | 0.00 | 2.00 |
| SK3A- 5 | 0.00 | 0.94 | 1.04 | 0.02 | 0.00 | 0.00 | 0.00 | 0.00 | 0.00 | 0.00 | 0.00 | 2.00 |
| SKY8B-D8 | 0.00 | 1.01 | 0.98 | 0.01 | 0.00 | 0.00 | 0.00 | 0.00 | 0.00 | 0.00 | 0.00 | 2.00 |
| | | | | | | **heazlewoodite** | | | | | | |
| SK3A- 8 | 0.00 | 1.90 | 3.06 | 0.03 | 0.00 | 0.00 | 0.00 | 0.00 | 0.00 | 0.00 | 0.00 | 5.00 |
| SK3I- 4 | 0.00 | 1.91 | 2.99 | 0.09 | 0.00 | 0.00 | 0.00 | 0.01 | 0.00 | 0.00 | 0.00 | 5.00 |
| SKY14B-F5 | 0.00 | 2.05 | 2.87 | 0.06 | 0.00 | 0.00 | 0.00 | 0.00 | 0.00 | 0.01 | 0.00 | 5.00 |
| SKY10-I12 | 0.00 | 2.01 | 2.91 | 0.07 | 0.00 | 0.00 | 0.00 | 0.00 | 0.00 | 0.00 | 0.00 | 5.00 |
| | | | | | | **Cu alloys** | | | | | | |
| SK3H- 15 | 0.00 | 0.00 | 0.20 | 0.03 | 1.00 | 0.00 | 0.00 | 0.00 | 0.00 | 0.00 | 0.00 | 1.23 |
| SKY14A- | 0.00 | 0.00 | 0.00 | 0.02 | 1.00 | 0.00 | 0.00 | 0.00 | 0.00 | 0.00 | 0.00 | 1.02 |

| G2 | | | | | | | | | | | | |
|---|---|---|---|---|---|---|---|---|---|---|---|---|
| | | | | | | **Ni arsenides** | | | | | | |
| SK3A- 9 | 1.08 | 0.00 | 2.89 | 0.02 | 0.00 | 0.01 | 0.00 | 0.00 | 0.00 | 0.00 | 0.00 | 4.00 |
| SK3A- 10 | 1.98 | 0.00 | 4.73 | 0.02 | 0.00 | 0.03 | 0.00 | 0.00 | 0.00 | 0.00 | 0.00 | 6.77 |

*Platinum Group Minerals*

Only three PGM were detected at Skyros. Two of them were detected in the same thin section (SK3H) from Northern Agios Iohannis. These two PGM are an altered laurite and a garutiite (Ni-Fe-Ir alloy) crystal. The last PGM was found in sample SKY10 (Agio Alexandria) and it consists in a Rh-Ni-Cu-Fe sulfide (Tab. 4.20). Other studies in the same areas report the presence of laurite included within chromite (Tarkian et al., 1992), and of Ru-Ir-Os sulfides and alloys within the silicate matrix, interstitial to chromite grains (Economou-Eliopoulos, 2007).

Tab. 4.20 EMPA analyses of PGM crystals detected in Skyros.

| **wt%** | **As** | **S** | **Ru** | **Ir** | **Os** | **Pd** | **Pt** | **Rh** | **Ni** | **Fe** | **Cu** | **Co** | **Total** |
|---|---|---|---|---|---|---|---|---|---|---|---|---|---|
| SK3H-1 | 4.86 | 20.21 | 54.34 | 6.76 | 11.36 | 1.43 | bdl | 1.05 | bdl | bdl | bdl | bdl | 100.00 |
| SK3H- 4 | 0.68 | 1.40 | bdl | 10.13 | bdl | bdl | bdl | bdl | 69.01 | 10.14 | 2.94 | 0.89 | 95.17 |
| SKY10-I11 | 0.00 | 9.84 | bdl | bdl | 0.09 | 0.93 | 0.36 | 24.31 | 24.91 | 2.72 | 8.59 | bdl | 71.75 |
| **apfu** | | | | | | | | | | | | | |
| SK3H-1 | 0.14 | 1.40 | 1.19 | 0.08 | 0.13 | 0.03 | 0.00 | 0.02 | 0.00 | 0.00 | 0.00 | 0.00 | 3.00 |
| SK3H- 4 | 0.02 | 0.09 | 0.00 | 0.10 | 0.00 | 0.00 | 0.00 | 0.00 | 2.31 | 0.36 | 0.09 | 0.03 | 3.00 |
| SKY10-I11 | 0.00 | 0.72 | 0.00 | 0.00 | 0.00 | 0.02 | 0.00 | 0.56 | 1.00 | 0.11 | 0.32 | 0.00 | 2.74 |

*Platinum Group Elements*

Whole rock PGE content was determined for 5 chromitite 2 massive magnetite samples from Agio Iohannis (SKY8A, SKY8B, SKY6), Northern Agio Iohannis (SKY4A) and Agio Alexandria (SKY10, SKY11A, SK113) (Tab. 4.21). Total PGE content for chromitites ranges between 94.05 and 246.93 ppb. Chromitite sample (SK4A) from Northern Agio Iohannis has the highest PGE content (246.93 ppb). All chromitites are enriched in IPGE with respect to PPGE, with IPGE/PPGE ratios varying between 6.55 and 14.49. The two magnetite-rich samples have very different PGE contents. Sample SK-13 has a total PGE content of 17.22 ppb, while sample Sky6 of 173.80. Moreover, they have low IPGE/PPGE ratios, suggesting an enrichment in PPGE with respect to chromitites.

Tab. 4.21 PGE whole rock content (ppb) in Skyros chromitites and magnetite-rich samples.

| Sample | | Os | Ir | Ru | Rh | Pt | Pd | Total PGE | IPGE | PPGE | IPGE/PPGE |
|---|---|---|---|---|---|---|---|---|---|---|---|
| Sky-8a | Chromitite | 32.50 | 24.70 | 53.50 | 3.91 | 1.99 | 1.74 | 118.34 | 110.70 | 7.64 | 14.49 |
| Sky-8b | Chromitite | 4.99 | 12.00 | 45.40 | 6.07 | 2.60 | 0.85 | 71.91 | 62.39 | 9.52 | 6.55 |
| Sky-6 | Magnetite | 10.70 | 28.10 | 55.90 | 10.00 | 40.30 | 28.80 | 173.80 | 94.70 | 79.10 | 1.20 |
| Sky-10 | Chromitite | 14.90 | 16.30 | 52.40 | 7.16 | 1.49 | 1.80 | 94.05 | 83.60 | 10.45 | 8.00 |
| Sky-11a | Chromitite | 27.70 | 19.40 | 67.00 | 5.96 | 1.00 | 2.31 | 123.37 | 114.10 | 9.27 | 12.31 |

| | | | | | | | | | | | |
|---|---|---|---|---|---|---|---|---|---|---|---|
| SK-13 | Magnetite | 1.48 | 1.91 | 4.01 | 5.43 | 2.74 | 1.65 | 17.22 | 7.40 | 9.82 | 0.75 |
| SK-4a | Chromitite | 68.90 | 49.30 | 98.40 | 10.30 | 16.00 | 4.03 | 246.93 | 216.60 | 30.33 | 7.14 |

### 4.3.2.2. Abdasht-Soghan

*Chromite*

Chromite composition is homogeneous between the two massifs (Tab. 4.22). Compositional variations are present only between unaltered and altered chromite, and in different chromite textures.

Unaltered chromites show an average Cr# [Cr/(Cr+Al)] of 0.77, an average Mg# [Mg/(Mg+$Fe^{2+}$)] of 0.66 and an average $Fe^{3+}$# [$Fe^{3+}$/($Fe^{2+}$+Mg+Al)] of 0.07. $TiO_2$ values are low, averaging 0.14 wt%, and $Al_2O_3$ average content is 11.60 wt%.

Some differences occur in chromite mineral chemistry depending on the rock texture. In fine- and coarse-grained massive chromitites chromite Cr# ranges from 0.67 to 0.83 (with average of 0.78), Mg# from 0.61 to 0.75 (with average of 0.68) and $Fe^{3+}$# is lower than 0.10 (with average of 0.06). Banded chromitites have Cr# ranging from 0.77 to 0.83 (with average of 0.80), Mg# from 0.58 to 0.72 (with average of 0.66) and $Fe^{3+}$# from 0.04 to 0.09 (with average of 0.08). Disseminated chromites Cr# ranges from 0.63 to 0.65 (with average of 0.64), Mg# from 0.53 to 0.56 (with average of 0.55) and $Fe^{3+}$# from 0.04 to 0.05 (with average of 0.04). In nodular chromitite, chromites Cr# ranges from 0.73 to 0.80 (with average of 0.77), Mg# from 0.63 to 0.73 (with average of 0.68) and $Fe^{3+}$# from 0.02 to 0.09 (with average of 0.06). Ferrian chromites have Cr# average values of 0.88, average Mg# of 0.40 and an average $Fe^{3+}$# of 0.25. MgO is strongly depleted as well as $Al_2O_3$, whose average content is as low as 4.66 wt%.

Tab. 4.22 representative microprobe analyses of chromite and ferrian chromite from Abdasht and Soghan.

| **Analysis** | **IRAB-A01** | **IRSO-A02** | **IRAB-A01** | **IRSO-B03** | **IRSO-B03** | **IRAB-A03** | **IRAB-BO3** | **IRSO-A04** | **IRAB-BO5** | **IRAB-B06** | **IRSO-B01** |
|---|---|---|---|---|---|---|---|---|---|---|---|
| Texture | massive | massive | massive | dissemin. | dissemin. | dissemin. | banded | banded | banded | nodular | nodular |
| Wt% | Chr | Chr | Fe-Chr | Chr | Chr | Fe-Chr | Chr | Chr | Fe-Chr | Chr | Chr |
| $TiO_2$ | 0.15 | 0.11 | 0.15 | 0.07 | 0.03 | 0.10 | 0.08 | 0.11 | 0.14 | 0.13 | 0.15 |
| $Al_2O_3$ | 10.26 | 9.70 | 7.65 | 19.17 | 18.52 | 6.56 | 11.59 | 9.99 | 7.26 | 13.56 | 10.55 |
| $Cr_2O_3$ | 59.87 | 60.95 | 61.90 | 50.30 | 50.66 | 58.46 | 58.08 | 60.79 | 56.53 | 56.81 | 60.21 |
| $Fe_2O_3$ | 4.20 | 3.65 | 3.19 | 2.05 | 2.34 | 6.33 | 3.83 | 3.65 | 9.14 | 2.01 | 3.62 |
| FeO | 12.18 | 10.69 | 16.38 | 17.94 | 17.14 | 22.11 | 13.06 | 11.22 | 16.47 | 12.82 | 11.12 |
| MgO | 14.47 | 14.94 | 11.16 | 11.44 | 11.72 | 7.39 | 13.63 | 14.79 | 11.06 | 13.87 | 14.88 |
| NiO | 0.11 | 0.17 | 0.08 | 0.01 | 0.07 | 0.00 | 0.14 | 0.04 | 0.01 | 0.00 | 0.15 |
| Total | 100.63 | 99.85 | 100.19 | 100.78 | 100.24 | 100.44 | 100.04 | 100.27 | 99.70 | 99.00 | 100.33 |
| Atoms | | | | | | | | | | | |
| Ti | 0.00 | 0.00 | 0.00 | 0.00 | 0.00 | 0.00 | 0.00 | 0.00 | 0.00 | 0.00 | 0.00 |
| Al | 0.39 | 0.37 | 0.30 | 0.71 | 0.69 | 0.26 | 0.44 | 0.38 | 0.28 | 0.51 | 0.39 |
| Cr | 1.51 | 1.54 | 1.62 | 1.24 | 1.26 | 1.57 | 1.47 | 1.53 | 1.48 | 1.43 | 1.51 |
| $Fe^{3+}$ | 0.10 | 0.09 | 0.08 | 0.05 | 0.06 | 0.16 | 0.09 | 0.09 | 0.23 | 0.05 | 0.09 |
| $Fe^{2+}$ | 0.31 | 0.29 | 0.45 | 0.47 | 0.45 | 0.63 | 0.35 | 0.30 | 0.46 | 0.34 | 0.30 |

| | | | | | | | | | | | |
|---|---|---|---|---|---|---|---|---|---|---|---|
| Mg | 0.69 | 0.71 | 0.55 | 0.53 | 0.55 | 0.37 | 0.65 | 0.70 | 0.55 | 0.66 | 0.70 |
| Ni | 0.00 | 0.00 | 0.00 | 0.00 | 0.00 | 0.00 | 0.00 | 0.00 | 0.00 | 0.00 | 0.00 |
| Mg# | 0.69 | 0.71 | 0.55 | 0.53 | 0.55 | 0.37 | 0.65 | 0.70 | 0.54 | 0.66 | 0.70 |
| Cr# | 0.80 | 0.81 | 0.84 | 0.64 | 0.65 | 0.86 | 0.77 | 0.80 | 0.84 | 0.74 | 0.79 |
| $Fe^{3+}$# | 0.08 | 0.08 | 0.09 | 0.04 | 0.04 | 0.20 | 0.08 | 0.08 | 0.22 | 0.04 | 0.07 |

*Base Metal Minerals*

Base Metal Mineral compositions are reported in Tab. 4.23. Awaruite, other Ni-Fe alloys and heazlewoodite are the most abundant phases among BMM. Awaruite has variable Ni and Fe contents, with the former ranging between 70.20 and 79.57 wt% and the latter between 20.55 and 25.51 wt%. One awaruite has 4.06 wt% residual S content. Some Ni-Fe alloys show too high Ni contents to be classified as awaruites. Their Ni content ranges between 81.42 and 83.48 wt%. One Ni-rich alloy contains 7.58 wt% Ir, 3.85 wt% Cu, 2.18 wt% Ru, 1.70 wt% Rh, 0.77 wt% Os, 0.42 wt% As and 0.19 wt% Pt. Awaruites contain up to 1.03 wt% Cu while Cu content of Ni-Fe alloys is higher, up to 3.85 wt% and never below 3 wt%. Awaruites can contain up to 0.10 wt% Os, 0.57 wt% Ir, 0.36 wt% Pt and 0.26 wt% Pd. Ni-Fe alloys show lower PGE contents, with only Ir up to 0.18 wt%.

Heazlewoodite Ni content ranges between 70.81 and 75.81 wt%, with S ranging between 26.50 and 28.69 wt%. Some residual Fe is always present in heazlewoodite, reaching up to 3.25 wt%. PGE content is low but quite different from that of alloys. The highest PGE contents were found for Pt, Ir, Os and Rh, with peak values respectively at 0.86, 0.76, 0.30 and 0.11 wt%.

The few pentlandite grains detected show incipient alteration at different degrees of Ni-enrichment. Ni ranges between 37.81 and 44.01 wt%. Rh, is the most abundant PGE in pentlandite, up to 0.29 wt% followed by Ir, up to 0.16 wt%.

Maucherite is the only As phase detected. Its Ni and As contents range respectively between 51.33 and 53.82 wt% and 45.67 and 49.09 wt%. Maucherites are systematically enriched in Pt, up to 0.71 wt%. Other PGE contents are low with the exception of one grain with 0.45 wt% Ir. One grain is strongly altered into Ni alloy, with just 14.31 wt% As remaining.

Millerite composition ranges between 64.46 and 68.97 wt% for Ni and between 32.73 and 36.32 wt% for S. it can contain up to 0.95 wt% Cu and 0.12 wt% As. PGE content is low, with the exceptions of Pt, up to 0.45 wt% and Ir, up to 0.26 wt%.

Elemental atomic maps (Fig. 4.39) were acquired on a heazlewoodite grain partially altered into millerite. Heazlewoodite substitution by millerite occurs starting from the fractures, from where it extends into the heazlewoodite crystal. Millerite is depleted in Ni, Cu and Pd compared to heazlewoodite, while Rh and Ir contents are about the same in the two phases.

Tab. 4.23 Selected microprobe analyses of BMM in Abdasht and Soghan. Pn: pentlandite; Bn: bornite; Mlr: millerite; Hzl: heazlewoodite; Mcr: maucherite; Awr: awaruite.

| Wt% | IRSO-B03 Pn | IRSO-B03 Bn | IRAB-A01 Mlr | IRAB-A01 Mlr | IRAB-A03 Hzl | IRSO-A04 Hzl | IRAB-A01 Mcr | IRAB-B01 Awr | IRSO-A1 Awr | IRAB-B01 Ni-As alloy | IRSO-A2 Ni-Fe alloy |
|---|---|---|---|---|---|---|---|---|---|---|---|
| As | 0.01 | 0.07 | 0.12 | 0.10 | 0.03 | 0.00 | 48.27 | 0.14 | 0.05 | 14.31 | 1.98 |
| Os | 0.00 | 0.04 | 0.00 | 0.00 | 0.00 | 0.13 | 0.03 | 0.10 | 0.00 | 0.10 | 0.00 |
| Fe | 31.21 | 11.26 | 0.30 | 0.07 | 0.22 | 2.32 | 0.87 | 23.64 | 24.22 | 0.00 | 10.32 |
| Ir | 0.34 | 0.00 | 0.00 | 0.04 | 0.38 | 0.00 | 0.12 | 0.00 | 0.57 | 0.00 | 0.18 |
| S | 34.39 | 26.57 | 34.93 | 35.67 | 27.33 | 26.50 | 0.00 | 0.00 | 0.00 | 1.37 | 0.02 |
| Ni | 34.38 | 0.18 | 65.03 | 65.58 | 73.86 | 74.06 | 51.33 | 75.68 | 74.55 | 84.11 | 83.28 |
| Pt | 0.00 | 0.00 | 0.00 | 0.10 | 0.00 | 0.00 | 0.21 | 0.26 | 0.00 | 0.00 | 0.28 |
| Ru | 0.00 | 0.01 | 0.00 | 0.00 | 0.00 | 0.00 | 0.00 | 0.02 | 0.01 | 0.00 | 0.07 |
| Cu | 0.37 | 61.99 | 0.95 | 0.16 | 0.00 | 0.00 | 0.00 | 0.60 | 0.00 | 0.04 | 3.28 |
| Rh | 0.00 | 0.02 | 0.03 | 0.03 | 0.00 | 0.00 | 0.00 | 0.00 | 0.00 | 0.06 | 0.00 |
| Pd | 0.00 | 0.01 | 0.00 | 0.01 | 0.01 | 0.00 | 0.00 | 0.10 | 0.01 | 0.00 | 0.00 |
| Total | 100.69 | 100.16 | 101.36 | 101.76 | 101.82 | 103.01 | 100.83 | 100.53 | 99.41 | 100.00 | 99.41 |
| **Atoms** | | | | | | | | | | | |
| As | 0.00 | 0.00 | 0.00 | 0.00 | 0.00 | 0.00 | 8.00 | 0.00 | 0.00 | 0.13 | 0.00 |
| Os | 0.00 | 0.00 | 0.00 | 0.00 | 0.00 | 0.00 | 0.00 | 0.00 | 0.00 | 0.00 | 0.00 |
| Fe | 4.17 | 0.97 | 0.00 | 0.00 | 0.01 | 0.10 | 0.19 | 1.00 | 1.00 | 0.00 | 0.96 |
| Ir | 0.01 | 0.00 | 0.00 | 0.00 | 0.00 | 0.00 | 0.01 | 0.00 | 0.01 | 0.00 | 0.00 |
| S | 8.00 | 4.00 | 1.00 | 1.00 | 2.00 | 2.00 | 0.00 | 0.00 | 0.00 | 0.03 | 0.00 |
| Ni | 4.37 | 0.01 | 1.02 | 1.00 | 2.95 | 3.05 | 10.86 | 3.05 | 2.93 | 1.00 | 3.18 |
| Pt | 0.00 | 0.00 | 0.00 | 0.00 | 0.00 | 0.00 | 0.01 | 0.00 | 0.00 | 0.00 | 0.00 |
| Ru | 0.00 | 0.00 | 0.00 | 0.00 | 0.00 | 0.00 | 0.00 | 0.00 | 0.00 | 0.00 | 0.00 |
| Cu | 0.04 | 4.71 | 0.01 | 0.00 | 0.00 | 0.00 | 0.00 | 0.02 | 0.00 | 0.00 | 0.04 |
| Rh | 0.00 | 0.00 | 0.00 | 0.00 | 0.00 | 0.00 | 0.00 | 0.00 | 0.00 | 0.00 | 0.00 |
| Pd | 0.00 | 0.00 | 0.00 | 0.00 | 0.00 | 0.00 | 0.00 | 0.00 | 0.00 | 0.00 | 0.00 |
| Σ cations | 8.59 | 5.70 | 1.04 | 1.01 | 2.97 | 3.16 | 11.08 | 4.08 | 3.94 | 1.13 | 4.19 |

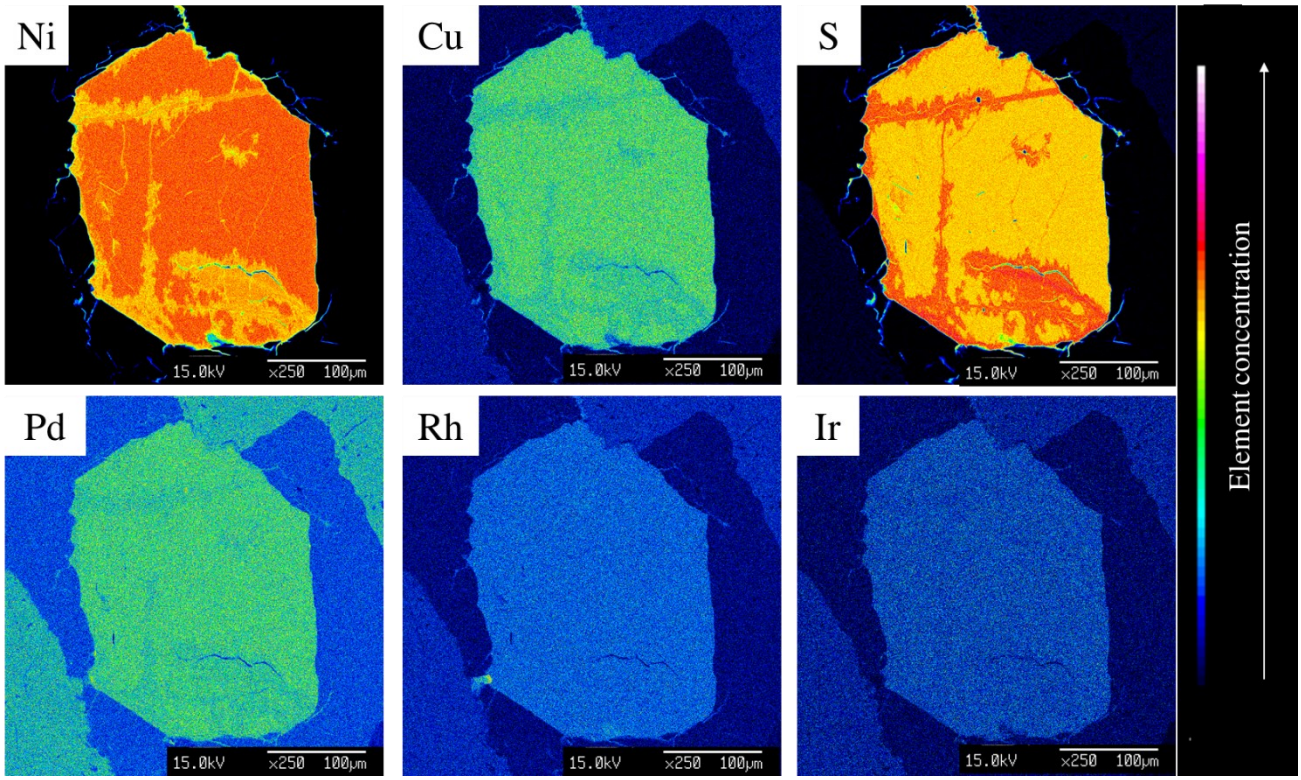


Fig. 4.39 X-ray elemental distribution maps of a heazlewoodite grain partially replaced by millerite along fractures (from Grieco et al., 2020).

*Platinum Group Minerals*

PGM compositions are reported in Tab. 4.24. The overall compositional range of laurite-erlichmanite is very wide, spanning from 0.17 to 0.97 Ru# (Ru/(Os+Ru) atomic proportion). Ir ranges from 0.51 to 9.73 wt% and As from 1.33 to 3.45 wt%. Primary euhedral laurites are Ru-rich and show a restricted range of Ru# (0.78-0.94). Laurite-erlichmanite in polyphasic grains, associated to other PGM (mainly PGE alloys) or BMM are often zoned and display a much wider compositional variability.

PGE alloys are mostly found in polyphase aggregates and show variable relationships with laurite-erlichmanite and BMM. They are mainly Os-Ir-Ru alloys, with very variable proportions among these three PGE. Rh contents are low, up to 1.70 wt%, while Pt and Pd are virtually absent. Base metals content in these alloys is very low, less than 1 wt% and is limited to Ni, Fe and minor Cu. Only one PGE sulfide not belonging to the laurite-erlichmanite series was detected. Its composition is that of a cuproiridsite where Ir is partially replaced by Rh and Cu is partially replaced by Fe.

Pt and Pd are very rare in PGM. The former was found only in an Ir-Fe alloy, probably a chengdeite, which contains 4.10 wt% Pt, the latter is present in laurites, but never exceeds 0.40 wt%.

Elemental atomic maps (Fig. 4.40) were acquired on the laurite partially replaced by Os-Ir alloy of Fig. 4.38D. In spite of the relatively low quality of the maps, due to the very tiny size of the grain some patterns can be identified. Os, Ir and Cu are enriched in the PGE alloy at the rim, while Ru is enriched in the reaction zone.

Tab. 4.24 Selected microprobe analyses of PGM from Abdasht and Soghan.

| **Wt%** | **IRSO-A03** | **IRSO-C01** | **IRAB-B05** | **IRAB-B01** | **IRAB-B01** | **IRAB-B05** | **IRAB-B01** | **IRAB-B01** | **IRSO-B01** | **IRAB-B05** |
|---|---|---|---|---|---|---|---|---|---|---|
| | **Laurite** | **Laurite** | **Laurite** | **Laurite** | **Laurite** | **Cuproididsite** | **Ru-Os-Ir alloy** | **Ni-Cu-Ir alloy** | **Os-Ir alloy** | **Chengdeite** |
| As | 1.46 | 2.35 | 2.32 | 2.04 | 2.30 | 0.03 | 1.00 | 0.42 | 0.06 | 0.02 |
| Os | 17.09 | 8.26 | 11.53 | 13.77 | 3.30 | 0.00 | 44.08 | 0.77 | 66.25 | 0.00 |
| Fe | 0.00 | 0.00 | 0.00 | 0.00 | 0.00 | 3.27 | 0.00 | 2.14 | 0.68 | 7.28 |
| Ir | 9.73 | 9.19 | 7.75 | 6.67 | 0.51 | 45.87 | 25.34 | 7.58 | 31.28 | 87.49 |
| S | 33.79 | 34.38 | 34.66 | 35.76 | 38.74 | 25.20 | 0.00 | 0.00 | 0.01 | 0.00 |
| Ni | 0.00 | 0.00 | 0.05 | 0.01 | 0.02 | 0.00 | 0.19 | 81.42 | 0.00 | 0.17 |
| Pt | 0.00 | 0.00 | 0.00 | 0.00 | 0.00 | 0.00 | 0.00 | 0.19 | 0.00 | 4.10 |
| Ru | 36.27 | 42.64 | 42.38 | 40.21 | 55.14 | 0.05 | 26.93 | 2.18 | 0.74 | 0.00 |
| Cu | 0.19 | 0.07 | 0.00 | 0.15 | 0.08 | 8.78 | 2.41 | 3.85 | 0.07 | 0.83 |
| Rh | 0.43 | 1.53 | 1.43 | 3.38 | 1.93 | 13.80 | 2.24 | 1.70 | 0.31 | 0.07 |
| Pd | 0.37 | 0.48 | 0.00 | 0.02 | 0.24 | 0.00 | 0.00 | 0.00 | 0.00 | 0.06 |
| Total | 99.33 | 98.89 | 100.12 | 102.01 | 102.26 | 97.00 | 102.19 | 100.24 | 99.41 | 100.00 |
| **Atoms** | | | | | | | | | | |
| As | 0.04 | 0.06 | 0.06 | 0.05 | 0.05 | 0.00 | 0.05 | 0.00 | 0.00 | 0.00 |
| Os | 0.17 | 0.08 | 0.11 | 0.13 | 0.03 | 0.00 | 0.87 | 0.00 | 1.00 | 0.00 |
| Fe | 0.00 | 0.00 | 0.00 | 0.00 | 0.00 | 0.30 | 0.00 | 0.03 | 0.04 | 0.29 |
| Ir | 0.10 | 0.09 | 0.07 | 0.06 | 0.00 | 1.21 | 0.49 | 0.03 | 0.47 | 1.00 |
| S | 2.00 | 2.00 | 2.00 | 2.00 | 2.00 | 4.00 | 0.00 | 0.00 | 0.00 | 0.00 |
| Ni | 0.00 | 0.00 | 0.00 | 0.00 | 0.00 | 0.00 | 0.01 | 1.00 | 0.00 | 0.01 |
| Pt | 0.00 | 0.00 | 0.00 | 0.00 | 0.00 | 0.00 | 0.00 | 0.00 | 0.00 | 0.05 |
| Ru | 0.68 | 0.79 | 0.78 | 0.71 | 0.90 | 0.00 | 1.00 | 0.02 | 0.02 | 0.00 |
| Cu | 0.01 | 0.00 | 0.00 | 0.00 | 0.00 | 0.70 | 0.14 | 0.04 | 0.00 | 0.03 |

| | | | | | | | | | | |
|---|---|---|---|---|---|---|---|---|---|---|
| Rh | 0.01 | 0.03 | 0.03 | 0.06 | 0.03 | 0.68 | 0.08 | 0.01 | 0.01 | 0.00 |
| Pd | 0.01 | 0.01 | 0.00 | 0.00 | 0.00 | 0.00 | 0.00 | 0.00 | 0.00 | 0.00 |
| Σ cations | 1.00 | 1.05 | 1.05 | 1.02 | 1.02 | 2.90 | 2.65 | 1.13 | 1.54 | 1.37 |

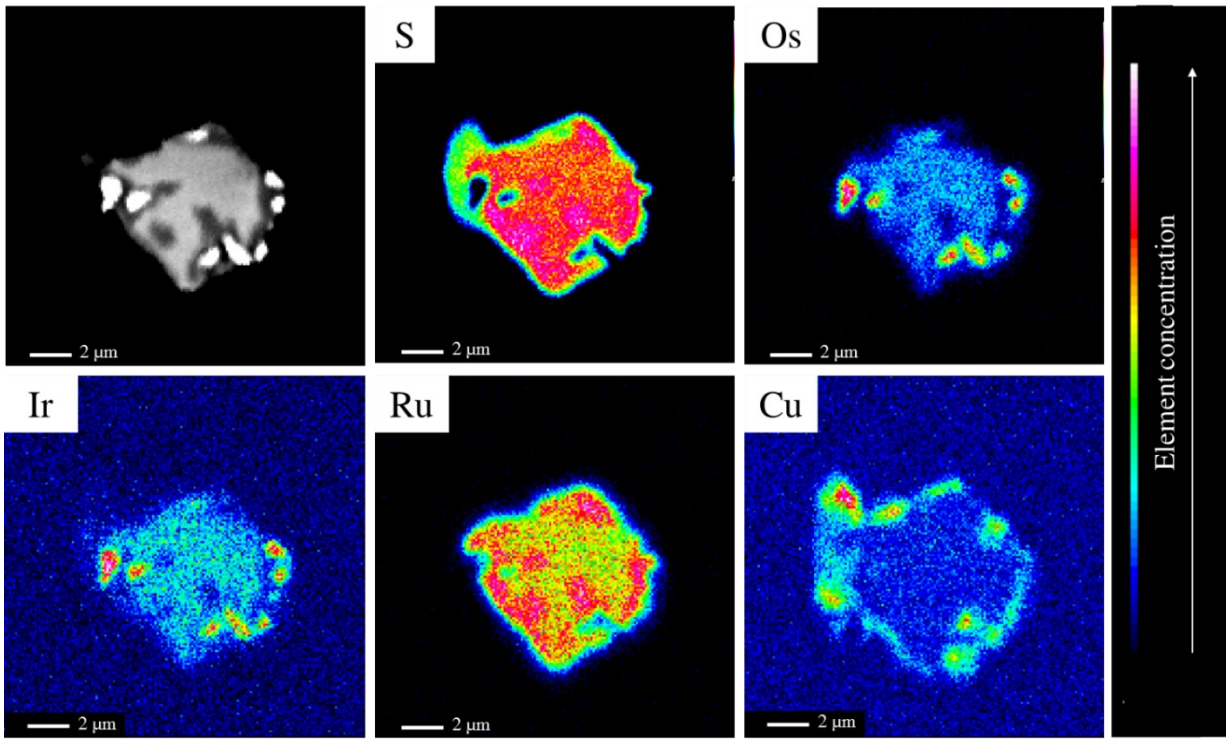


Fig. 4.40 X-ray elemental distribution maps of a PGM polyphasic aggregate.

*Platinum Group Elements*

Whole rock PGE content was analysed for 8 chromitite samples. Chromitite texture, sample location and PGE contents are reported in Tab. 4.25.

Total PGE content ranges between 16.6 and 420.9 ppb. Massive chromitites show a much higher average PGE content (163.62 ppb) than banded ones (43.53 ppb), with the only nodular chromitite analysis in an intermediate situation (109.1 ppb).

All samples are enriched in Os and Ru, one of which is invariably the most abundant PGE. The IPGE/PPGE ratio is high, between 4.81 and 19.86, with the exception of the nodular sample from Soghan, with a ratio of 2.14.

Tab. 4.25 Whole rock PGE contents (ppb) in Abdasht and Soghan.

| | **Texture** | **Os** | **Ir** | **Ru** | **Rh** | **Pt** | **Pd** | **Total PGE** | **IPGE** | **PPGE** | **IPGE/PPGE** |
|---|---|---|---|---|---|---|---|---|---|---|---|
| IRAB-A02 | massive | 46.50 | 27.40 | 77.10 | 7.00 | 5.68 | 2.05 | 165.73 | 151.00 | 14.73 | 10.25 |
| IRAB-B01 | massive | 149.00 | 62.80 | 177.00 | 12.30 | 4.23 | 15.60 | 420.93 | 388.80 | 32.13 | 12.10 |
| IRAB-B03 | banded | 6.91 | 2.59 | 4.58 | 0.63 | 1.16 | 0.70 | 16.57 | 14.08 | 2.49 | 5.65 |
| IRAB-B04 | banded | 33.90 | 13.00 | 38.70 | 2.16 | 1.18 | 0.97 | 89.91 | 85.60 | 4.31 | 19.86 |
| IRSO-A01 | massive | 29.00 | 14.30 | 42.70 | 2.48 | 1.85 | 2.22 | 92.55 | 86.00 | 6.55 | 13.13 |

| | | | | | | | | | | | |
|---|---|---|---|---|---|---|---|---|---|---|---|
| IRSO-A03 | banded | 5.81 | 3.91 | 6.71 | 1.07 | 4.91 | 1.69 | 24.10 | 16.43 | 7.67 | 2.14 |
| IRSO-B01 | nodular | 27.70 | 15.30 | 47.30 | 3.09 | 6.47 | 9.21 | 109.07 | 90.30 | 18.77 | 4.81 |
| IRSO-C02 | massive | 52.90 | 26.70 | 74.20 | 5.96 | 2.20 | 1.66 | 163.62 | 153.80 | 9.82 | 15.66 |

## 4.3.3 Discussion

### 4.3.3.1. Chromite composition

Spinels from Skyros show different compositions among the three localities (Fig. 4.41A). Chromites from Agio Iohannis and Agio Alexandria have XCr and XMg comprised between 0.6 and 0.7. Chromites from Northern Agio Iohannis display very different compositions, with higher XCr (between 0.7 and 0.8) and lower XMg values (between 0.6 and 0.4). Spinels from Agio Iohannis and Agio Alexandria have a composition similar to the ones reported by (Economou-Eliopoulos, 1996) for spinels of the same area, while Northern Agio Iohannis chromites have compositions more similar to the ones from Vavdos and Gerakini deposits, located in the Vardar Zone of the Chalkidiki peninsula (Eastern Ophiolite Belt) (Economou, 1984). The similarities between Skyros chromitites and those of the Vardar Zone suggest that Skyros ophiolite may be related to the Eastern Ophiolite Belt, linked to the closure of the Vardar Ocean. Some Authors (Gartzos et al., 1990; Zachariadis, 2007) suggest that Skyros may be geologically related to the Western Hellenic Ophiolites (e.g. Pindos, Vourinos and Othrys massifs), however Skyros chromites do not present similarities with spinels from the Vourinos and Othrys complexes (Fig. 4.41A).

Spinels from the Abdasht-Soghan complex have slightly different compositions depending on the rock texture. Massive and nodular chromitites have the highest XCr and XMg, comprised between 0.65–0.80 and 0.55–0.75 respectively. Disseminated chromitites have lower XCr (~0.60) and XMg (~0.50). The composition of spinels from massive and disseminated chromitites is in accordance with the results of (Najafzadeh and Ahmadipour, 2016, 2014) (Fig. 4.41B), and is similar to the composition of ophiolite chromitites.

Chromites from Abdasht-Soghan and Skyros display variable composition (Fig. 4.42). Primary spinels plot in the fields of chromite and Al-chromite. Spinels from Abdasht-Soghan plot mainly in the chromite field, with some crystals falling into the Al-chromite field. Spinels from Skyros are more scattered. Northern Agio Iohannis chromites plot between the chromite and Al-chromite fields, while Agio Alexandria and Agio Iohannis spinels plot into the Al-chromite field.

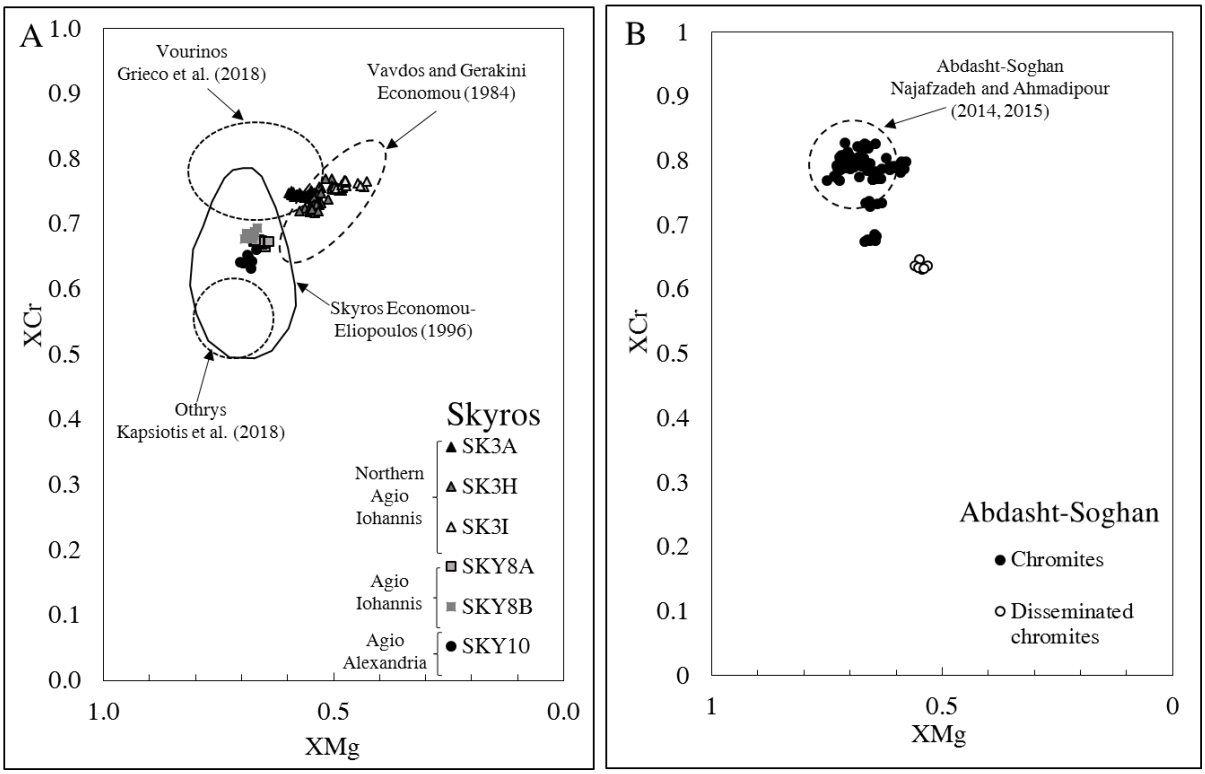


Fig. 4.41 XMg vs XCr values of Skyros (A) and Abdasht-Soghan (B); compositional fields of Vourinos (Grieco et al., 2018), Vavdos and Gerakini (Economou, 1984), Skyros (Economou-Eliopoulos, 1996), Othrys (Kapsiotis et al., 2018) and Abdasht-Soghan (Najafzadeh and Ahmadipour, 2016, 2014) are used for comparison.

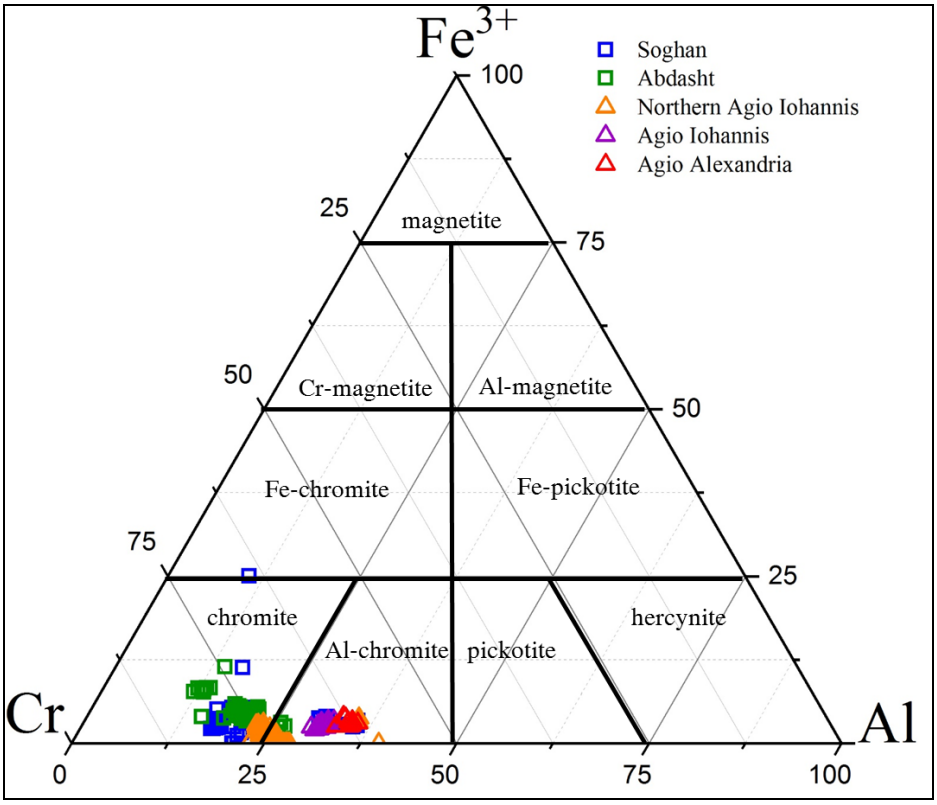


Fig. 4.42 Ternary compositional diagram of Skyros and Soghan-Abdasht spinels.

Al-chromites from Skyros also show relatively high $TiO_2$ content, and plot between the stratiform and podiform chromitite fields (Fig. 4.43A). High $Al_2O_3$ and $TiO_2$ contents can be associated to a stratigraphic position within or above the Moho Transition Zone (Grieco et al., 2007; Zaccarini et al., 2004a), and Al-chromites are thought to derive by MORB-type magmas in shallower parts of the mantle section near the petrological Moho (Ahmed and Arai, 2002; González-Jiménez et al., 2011; Uysal et al., 2007; Zaccarini et al., 2011). Skyros spinels do not have the typical composition of supra-Moho chromitites, however they could have been formed within the Transition Zone, close to the contact between upper mantle peridotites and lower crust gabbros and cumulates.

High-Cr chromitites from Abdasht, on the other hand, show the typical feature of mantle chromitites (Fig. 4.43B), crystallized out of boninitic magmas in the deeper parts of the mantle sequence (Ahmed and Arai, 2002).

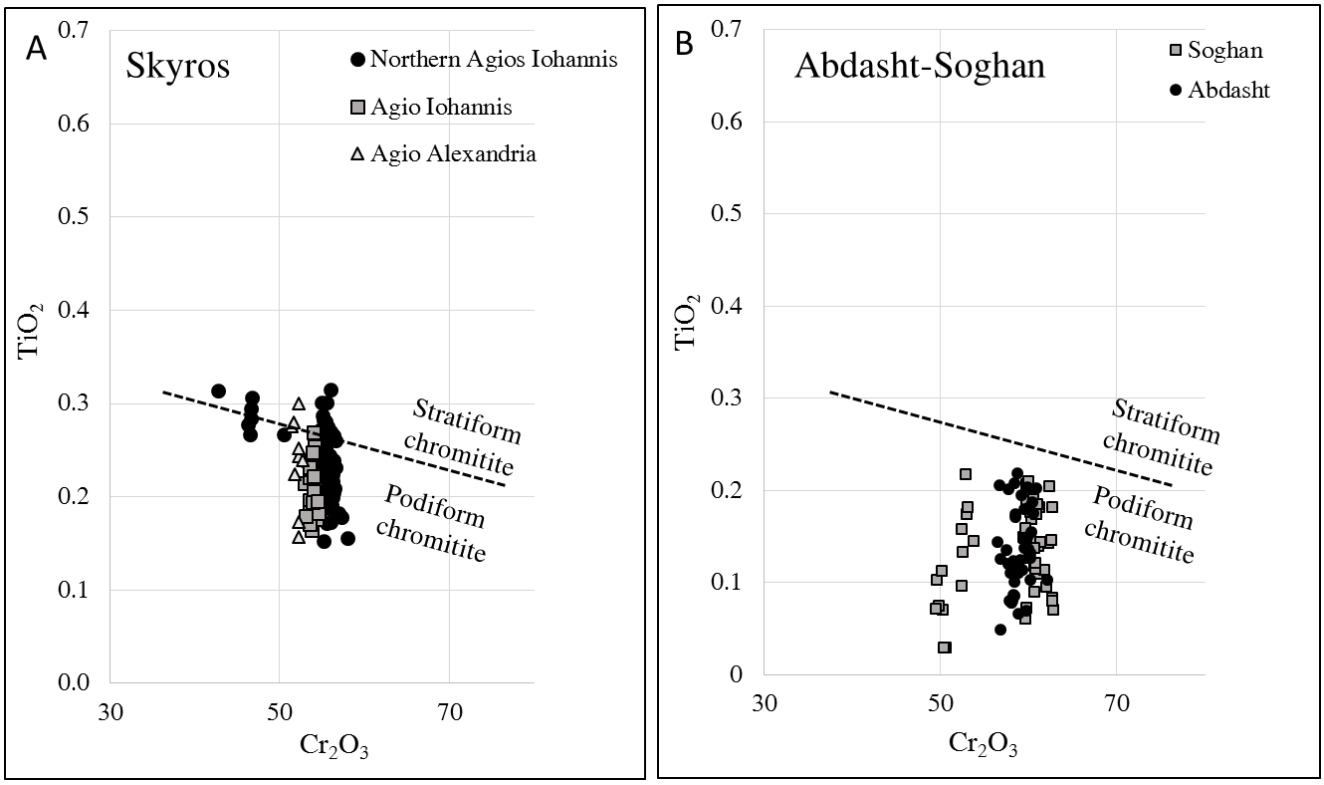


Fig. 4.43 $Cr_2O_3$ vs $TiO_2$ contents of Skyros (A) and Abdasht-Soghan (B) chromites; stratiform and podiform chromitite division is from Arai et al. (2004).

*Parent Melt composition*

Chromites from Northern Agio Iohannis (Skyros) and from the Abdasht-Soghan complex show relatively high $Cr_2O_3$ contents and low $Al_2O_3$ contents (below 14.0 wt%), overlapping the compositional range of spinels formed in an arc environment (Fig. 4.44A). Chromites from Agio Iohannis and Agio Alexandria (Skyros) have slightly lower $Cr_2O_3$ contents and higher $Al_2O_3$ compared to Northern Agio Iohannis, and plot in the compositional field of MORB spinels (Fig. 4.44A).

$Al_2O_3$ and $TiO_2$ contents of a parental melt can be derived from the spinel composition. From the positive correlation found by Kamenetsky et al. (2001), the $Al_2O_3$ content in a parental magma is calculated as:

$$Al_2O_{3melt} = 5.2181 * \ln(Al_2O_{3spinel}) - 1.0505$$

The correlations between $TiO_2$ in spinels and in a coexisting melt, on the other hand, differ between MORB and arc settings (Rollinson, 2008), and are calculated as:

$$TiO_{2melt-MORB} = 1.5907 * TiO_{2spinel}^{0.6322}$$

$$TiO_{2melt-arc} = 1.0963 * TiO_{2spinel}^{0.7863}$$

Maurel and Maurel (1982) calculated the FeO/MgO ratio in the melt starting from the composition of the spinel:

$$\ln \frac{FeO}{MgO} spinel = 0.47 - 1.07 * Y^{Al} + 0.64 * Y^{FeIII} + \ln \frac{FeO}{MgO} melt$$

where:

$Y^{Al} = Al/(Al+Cr+Fe^{III})$

$Y^{FeIII} = Fe^{III}/(Fe^{III}+Al+Cr)$

The parental melt analysis indicates that chromites from Northern Agio Iohannis and Abdasht-Soghan were generated by a parental melt with a composition similar to boninites, with 8 – 14 wt% $Al_2O_3$ and low $TiO_2$ (between 0.15 and 0.40 wt%). The parental melts of Agio Iohannis and Agio Alexandria chromites, on the contrary, have a composition more similar to MORB, with higher $TiO_2$ contents (0.50 – 0.75 wt%) (Fig. 4.44B). The results are confirmed also by the analysis of the FeO/MgO ratio within the parental melt. Northern Agio Iohannis, Abdasht and Soghan mostly plot in the boninitic field, while Agio Alexandria and Agio Iohannis in the MORB one (Fig. 4.44C).

These results furtherly support the hypothesis of the generation of Agio Iohannis and Agio Alexandria chromitites in a MORB setting, probably related to a back-arc basin, as also suggested by Economou-Eliopoulos (1996). Moreover, geochemical data on dispersed spinels in serpentinized rocks from the area, and MORB-normalized trace element patterns of Skyros rodingites, harzburgites, ophicalcites and gabbros (Karkalis et al., 2017), confirm that Skyros ophiolites formed in the supra-subduction environment of the Jurassic- Lower Cretaceous Vardar Ocean.

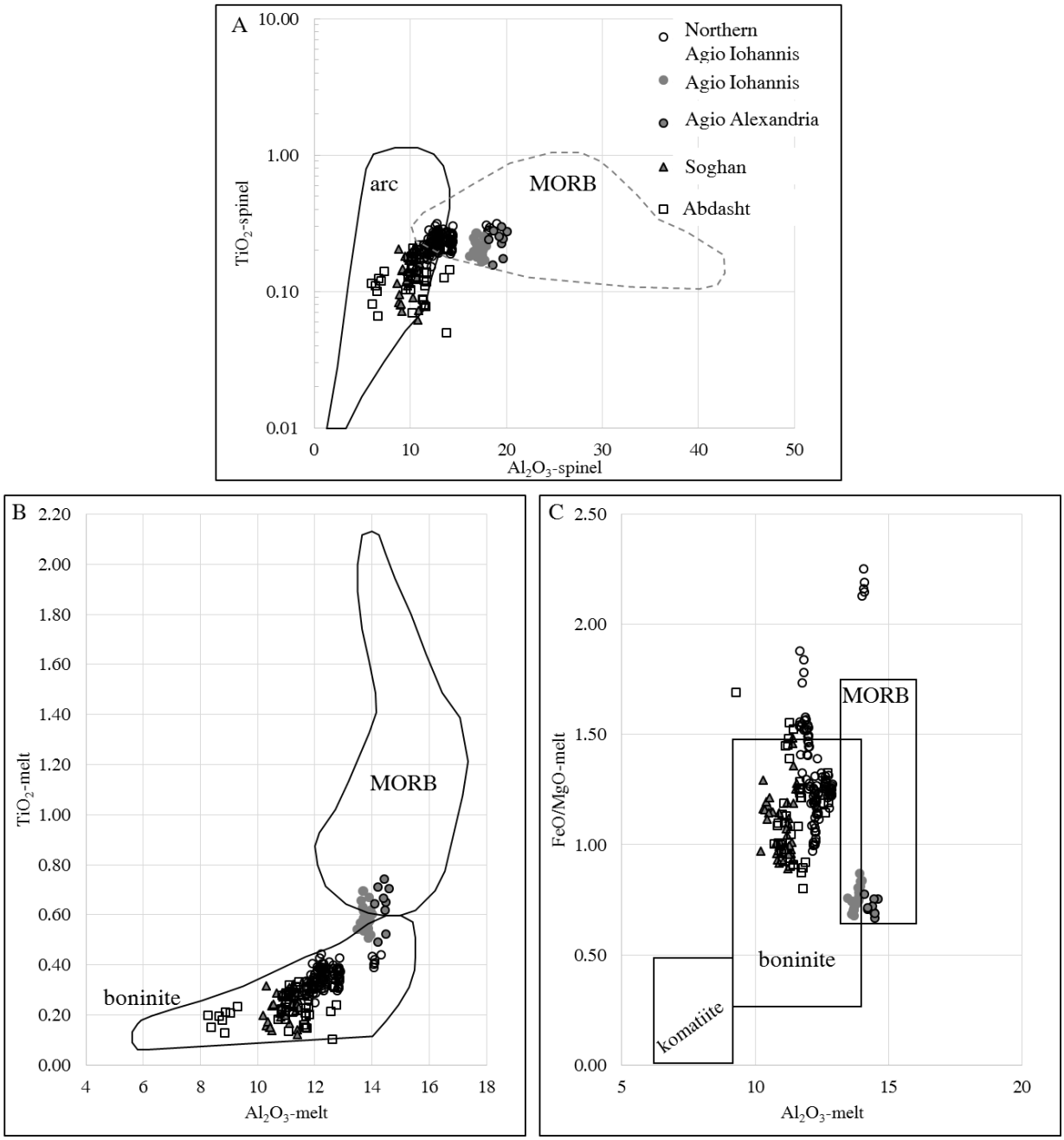


Fig. 4.44 Composition of Skyros and Abdasht-Soghan spinels in terms of A) $TiO_2$ vs $Al_2O_3$ (wt%); B) $TiO_2$ vs $Al_2O_3$ (parent melt): C) FeO/MgO (melt) vs $Al_2O_3$ (melt). Compositional fields are from (González-Jiménez et al., 2020; Kamenetsky et al., 2001; Pagé and Barnes, 2009; Proenza et al., 2007).

### 4.3.3.2. Secondary silicates

Chromitites from Skyros and Abdasht-Soghan are heavily altered. Primary silicates are rare olivine and pyroxene relicts immersed in a silicate matrix composed of serpentine and/or chlorite. Several samples in Skyros, moreover, show widespread crystallization of Cr-garnets associated to chromite rims.

The first alteration stage of Skyros and Abdasht-Soghan chromitites involved the circulation of serpentinizing fluids. Serpentine commonly replaces olivine following the reaction (Frost and Beard, 2007):

$$Mg_2SiO_4 + 2SiO_2 + 4H_2O = Mg_3Si_2O_5(OH)_4 + Mg(OH)_2$$

One of the most distinctive features of serpentinized rocks are the extremely low oxygen fugacities, as indicated by the presence of Ni-Fe alloys (Frost, 1985). The occurrence of Ni-Fe alloys instead of sulfides suggests that serpentinization occurs at low $fS_2$ as well as low $fO_2$. Oxygen and sulfur fugacities are closely related (Frost, 1985). The replacement of olivine by serpentine releases some $H_2$ (Bach et al., 2006; Klein et al., 2009), which can combine with $1/2O_2$ to form $H_2O$ and/or with S to form $H_2S$, lowering $fO_2$ and $fS_2$ (González-Jiménez et al., 2010). As oxygen fugacity falls, sulfides in equilibrium with magnetite become poor in sulfur, forming millerite, heazlewoodite and metal alloys (Frost and Beard, 2007). Serpentinization typically takes place at temperatures below 350 °C (Bach et al., 2004).

Chloritization and alteration of chromite into ferrian chromite within massive chromitites is a well-known process which was detected in several mafic ultramafic massifs. Many studies report the formation of Cr-chlorite and ferrian chromite during low-T hydrothermal alteration (e.g. Colás et al., 2017; Kapsiotis, 2014). According to Mellini et al. (2005) and Merlini et al. (2009), relatively high $fO_2$ conditions favor the reaction of spinel with serpentine, in presence of aqueous fluids, to produce chlorite and ferrian chromite. Proenza et al. (2004) and Mellini et al. (2005) suggest the formation of ferrian chromite and chlorite during low-P low-T retrograde metamorphism, at hydrous, oxidizing conditions. Mukherjee et al. (2010) reports formation of ferrian chromite during low-T hydrothermal events.

The fact that chlorite is only sometimes present in the samples, suggests that a late chloritization event at relatively high $fO_2$ conditions occurred in both complexes, but was limited and not as widespread as the serpentinization one, at least in Abdasht-Soghan and Northern Agio Iohannis. Within Agio Iohannis and Agio Alexandria, chloritization was more pervasive, and chlorite replaced almost all the serpentine, producing a fine-grained chlorite matrix and Cr-magnetite rims (Fig. 4.45A, B).

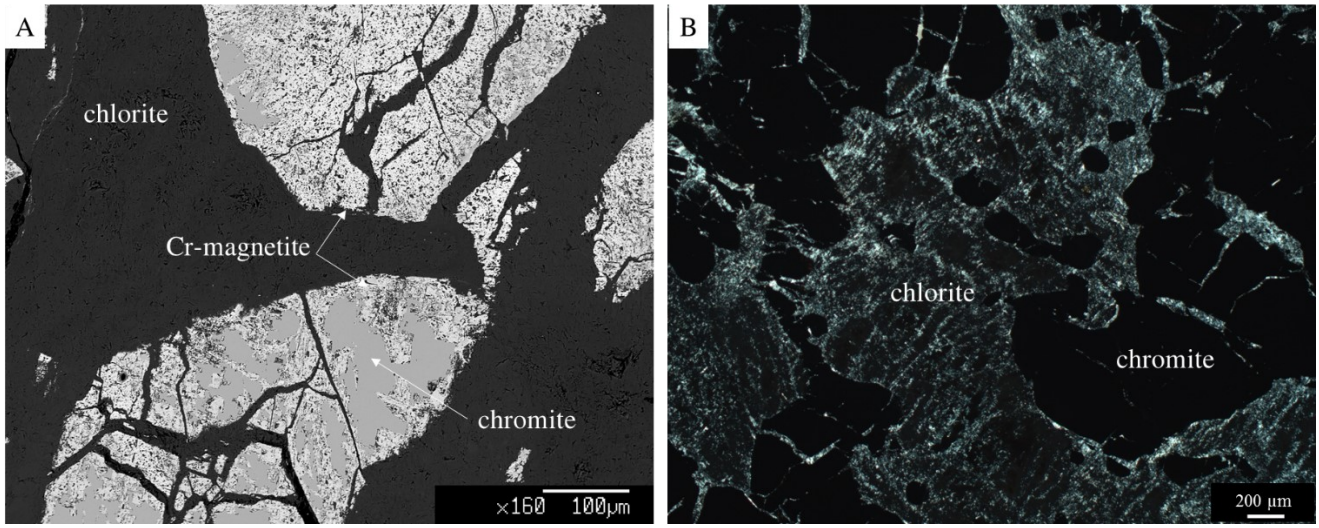


Fig. 4.45 A) BSE and B) XPL images showing Cr-magnetite rims and fine-grained chlorite matrix within Agio Alexandria.

Skyros chromitites show a third alteration process, which involves the crystallization of Cr-garnets. These garnets are a solid solution among the end-members andradite and uvarovite. Pure uvarovite does not exist in nature, so that uvarovitic garnet typically contains amounts of andradite and/or grossular. Uvarovitic garnet has been found in several chromitite deposits (Chakraborty, 1968; Melcher et al., 1997; Proenza et al., 1999). It is usually associated to hydrothermal alteration of chromite-bearing rocks, but details of its formation are still largely unknown (Arai et al., 1999; Klemme et al., 2005; Proenza et al., 1999). Proenza et al. (1999) report Cr-garnets within open fractures in the Moa-Baracoa chromitites, indicating that they formed from a hydrothermal fluid circulating in open spaces. The source of Ca-rich fluids in ophiolites is controversial. Proenza et al. (1999) point at gabbros surrounding the Moa-Baracoa chromitites as the principal source. As in some localities Cr-garnet bearing chromitites are not associated to gabbros, another possible source could be clinopyroxene, which liberates Ca during serpentinization or chloritization (Ghosh and Morishita, 2011; Mittwede and Schandl, 1992; Pal and Das, 2010). Skyros chromitites are associated to an ophiolitic mélange, and are closely related to serpentinites and ophicalcites, that are the probable source of Ca for Cr-garnets.

#### 4.3.3.3. PGM and BMM assemblage

Many base metal minerals were found within Skyros and Abdasht-Soghan, mainly associated with the silicate gangue and rarely enclosed within chromite crystals. The assemblage is dominated by sulfides and Ni-Fe alloys, with minor arsenides. Platinum Group Minerals are rare within Skyros and relatively abundant in Abdasht-Soghan.

*Ni-Fe-Cu base metal minerals*

Primary BMM commonly found in chromitites are Ni-Fe sulfides, namely pentlandite and pyrrhotite, stable at T above 550 °C, below which the assemblage breaks up forming millerite, heazlewoodite or awaruite (Kullerud, 1963). If some copper is present in the system, also primary minerals in the Ni-Fe-Cu system can be found, such as chalcopyrite or bornite (Proenza et al., 2001). Heazlewoodite, millerite and Ni-Fe alloys are the most common secondary base metal minerals within ophiolite chromitites, and they are the result of desulfurization processes (Klein and Bach, 2009). The alteration of pentlandite into heazlewoodite occurs below 550 °C, while the formation of Ni-Fe alloys has been estimated below 445 °C, at low $fO_2$ and $fS_2$ (Tzamos et al., 2016). Heazlewoodite can be replaced by millerite if $fO_2$ and $fS_2$ increase, like during steatitization of ultramafic rocks (Klein and Bach, 2009). Droplets of millerite and chalcocite have been found within primary laurites in the Caridad chromitites (González-Jiménez et al., 2012), so in some cases millerite can be formed during crystallization of laurite, at magmatic temperatures.

Within Skyros and Abdasht-Soghan, the primary BMM detected are all pentlandite grains and one bornite crystal, all found included within unaltered chromites. Secondary BMM, much more abundant in both complexes, are heazlewoodite, millerite, awaruite and Ni-Fe alloys (Fig. 4.46A). Rare Ni-Cu alloys have been detected within Skyros ophiolite. Ni-arsenides are present in both complexes, but are not widespread.

The alteration of pentlandite into heazlewoodite and finally awaruite and the occurrence of millerite and native metals are common features in serpentinized dunites and chromitites (Frost, 1985; Melcher et al., 1997; Prichard et al., 1994; Tzamos et al., 2016), and they can be linked to desulfurization events. Desulfurization within Abdasht-Soghan complex followed two possible patterns: a one-step transformation into awaruites, or a two-step alteration: first into heazlewoodites and then into Ni-rich alloys (Fig. 4.46A).

Primary and secondary BMM in Skyros and Abdasht-Soghan show slight enrichments in Pt and Ir. The few pentlandite crystals found in both complexes are enriched in PGE up to 0.12 wt%. Secondary sulfides and Ni-Fe alloys, however, show enrichments up to 1.09 wt%. Auge et al. (1999) and Lawley et al. (2020) suggest a crystallization of PGE-enriched primary sulfides and a later remobilization and reconcentration of PGE during serpentinization. In these conditions, Pt (a highly siderophile element) partitions into secondary sulfides and alloys. However, pentlandites in Skyros and Abdasht-Soghan do not show a PGE enrichment as high as the one of secondary BMM. This suggests that the PGE enrichment of secondary BMM may derive from circulating PGE-rich fluids, but that the primary source of these PGE, in particular Ir and Pt, may not be primary sulfides. Further investigations on

trace element contents of primary and secondary BMM are necessary in order to understand where PGE are stored and how they are remobilized within these phases.

*Platinum Group Minerals*

Platinum Group Minerals are abundant within Abdasht-Soghan and rare within Skyros. Primary PGM are usually more easily preserved than primary BMM as they are mainly hosted within chromite. Laurites are the most abundant primary PGM found within ophiolite chromitites (González-Jiménez et al., 2014a and references therein), and they directly crystallize from the melt (Augé, 1985; Legendre and Augé, 1986; Stockman and Hlava, 1984). Stoichiometric laurite can precipitate in equilibrium with Os-Ir alloys at 1200–1300 °C and log$fS_2$ between −1.2 and − 2 (Andrews and Brenan, 2002; Bockrath et al., 2004; Brenan and Andrews, 2001). Os becomes more soluble in laurite with decreasing temperature and/or increasing $fS_2$, producing minerals with compositions within the laurite-erlichmanite endmembers (Brenan and Andrews, 2001).

Both at Skyros and Abdasht-Soghan, primary PGM are laurites with variable Os content (Fig. 4.46B). The variability of Os and Ru content of Abdasht-Soghan laurites can be related to slightly different degrees of evolution of the melt, with Ru content decreasing with cooling and/or increasing $fS_2$.

Secondary PGM in Abdasht-Soghan are mainly PGE alloys and partially desulfurized laurites, while in Skyros a partially desulfurized unknown Rh-Cu-Ni sulfide and a small grain of garutiite have been detected.

*Desulfurization*

Primary PGM and BMM can be affected by the circulation of altering fluids. While Os-Ir alloys are sometimes ascribed to a magmatic environment (Brenan and Andrews, 2001), they can also be the product of alteration of primary laurites due to pervasive percolation of low $fS_2$ fluids, during metamorphic events (Garuti and Zaccarini, 1997; González-Jiménez et al., 2014a; Prichard et al., 2008a; Proenza et al., 2007; Zaccarini et al., 2005). Textural evidences in Skyros and Abdasht-Soghan argue for a secondary formation of the PGE alloys. They are almost invariably found as reaction rim zones of primary laurites, and only rarely they are not related to primary PGM. The association with partially or completely desulfurized BMM, moreover, argues for a secondary origin of PGE alloys as completely desulfurized laurites. Only the origin of isolated PGE alloy grains can be doubtful: they could be either primary PGE alloys in equilibrium with a low $fS_2$ melt or again laurites completely desulfurized during percolation of low $fS_2$ fluids. The high Os content of the only grain large enough to be analyzed, together with the ubiquitous textural position, associated to pores or fractures within chromites, anyway, strongly argues for their origin as completely altered laurites (Grieco et al., 2020).

Some PGM grains show intermediate alteration stages where primary laurite rims are S depleted and Os enriched. The best-preserved evidence is a polyphasic grain constituted by a laurite core, an Os-poor laurite reaction zone and an Os-rich alloy rim found in the Abdasht-Soghan complex (Fig. 4.38D).

The composition of secondary BMM and PGM, and the general tendency to lose sulfur, changing primary sulfide into alloys, seem to be the result of desulfurization events, occurred in highly reduced environments (Frost, 1985). Such conditions can be achieved during the early stages of serpentinization, (Garuti and Zaccarini, 1997; Gonzalez-Jimenez et al., 2011a; Prichard et al., 1994), that affected not only primary sulfides (e.g. pentlandites), but also the PGM reached by the fluids.

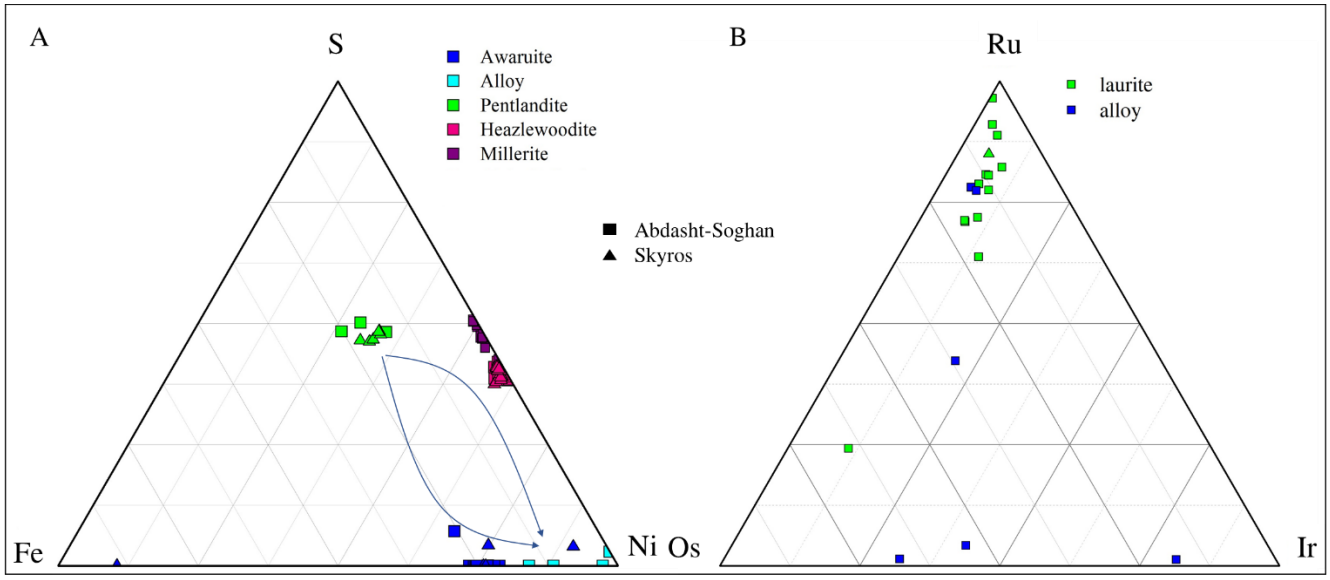


Fig. 4.46 Ternary compositional diagrams (atm%) of A) BMM in Skyros and Abdasht-Soghan and B) PGM in Skyros and Abdahst-Soghan.

### 4.3.3.4. PGE remobilization

PGE remobilization is described by several Authors (e.g. Proenza et al., 2007; Tsoupas and Economou-Eliopoulos, 2008; Uysal et al., 2009; Zaccarini et al., 2009, 2008, 2005), but only few works relate it to serpentinization. Prichard et al. (1994) suggest that Pt- and Pd- bearing alloys from Shetland ophiolite derived from alteration of magmatic PGM during serpentinization with a mobility of PGE of just few microns. Garuti and Zaccarini (1997) argued that a secondary awaruite-PGE alloys assemblage in Vourinos chromitite was due to desulfurization of the primary BMM-PGM assemblage during serpentinization. González-Jiménez et al. (2010) ascribe the formation of a secondary BMM-PGM assemblage along fractures and cracks of chromite grains in the Dobromirtsi chromitites to the percolation of altering fluids, with a combination of reducing and oxidizing events, related to regional metamorphism. More recently, Jiménez–Franco et al. (2020) relate the desulfurization of laurite

crystals within the chromitites of Monte Bueno (Cuba) to fluids circulating during a serpentinization event.

Textural evidence suggests a partial and selective mobility of PGE during serpentinization of Abdasht-Soghan chromitites. Serpentinizing low-$fS_2$ fluids reacted with primary laurites to form PGE alloys whose composition is determined by the differential behavior of PGE. Mineralogy and texture of alloy-laurite composite grains suggests that PGE alloy is the phase in equilibrium with serpentinizing fluids and that the reaction progresses from the rim towards the core.

Zaccarini et al. (2005) studied PGE mobility in eclogite facies metamorphosed chromitite-bearing serpentinites, observing that Os-rich magmatic laurites are partially altered into Ru-rich laurites, often associated to secondary Os-rich alloy. This evidence argues for a mobilization of Os and minor Ir during metamorphism at relatively high temperatures and decreasing $fS_2$. Low $fS_2$ and formation of Os-rich or Ru-rich alloys is a common feature of secondary PGM assemblages (Proenza et al., 2007; Uysal et al., 2009; Zaccarini et al., 2009, 2008, 2005).

Within Abdasht-Soghan textural evidence argues for a local (micrometric) remobilization where Os is the most mobile PGE, thus forming Os-rich alloy, while Ru is retained in laurite, resulting in the Ru-rich laurite of the reaction zone of Fig. 4.38D. The subsolidus diffusion of PGE in order to attain the mineralogical assemblage stable at the new conditions, mainly a low $fS_2$, could also be accompanied by larger scale mobility of PGE due to their solubility in the desulfurizing fluids. This possibility is supported by the evidence that Os-rich alloy grains, derived from complete alteration of primary laurites, have PGE contents different from those of laurite itself. Grieco et al. (2020) exploited the opportunity offered by a partially altered laurite grain, where a primary laurite core is preserved, together with secondary Os-rich alloy and Ru-rich laurite reaction zone, in order to calculate a PGE mass balance. This offers an insight on long range PGE mobility, due to solubility in desulfurizing fluids that pervasively percolated the rock assemblage during serpentinization.

Lawley et al. (2020) also report that precious metal remobilization within ultramafic rocks from British Columbia was limited to the microscale during the early stages of serpentinization. Only progressive serpentinization, characterized by complete replacement of olivine and destabilization of primary BMM to form reduced, low-$fS_2$ secondary minerals, represents an important process to liberate, transport and concentrate these metals within more oxidized and/or sulfur-bearing fluids in surficial and deep subduction environments.

*Desulfurization reaction mass balance*

Grieco et al. (2020) used a former primary euhedral laurite crystal which suffered partial desulfurization to perform an element mass balance. The former rims are enough preserved to show

the euhedral shape of the primary laurite but anyway each grain side is not straight but shows minor irregularities and embayments, suggesting that the present assemblage occupies a volume smaller than the primary one, in agreement with a mass loss from the grain due to loss of sulfur and PGE.

Primary laurite and secondary alloy show very different compositions. The former has a composition that well fits the one of all primary laurites detected, Ru-rich and low in Ir. The latter is depleted in Ru and enriched both in Os and Ir. Rh is a minor constituent of both phases and is depleted in the alloy. Pt and Pd are always too low to show meaningful trends. Finally, alloy shows a depletion in As and an enrichment in Cu compared to laurite.

The mass balance aims to quantify the amount of each element lost or gained at the intermediate and final stages of desulfurization. The desulfurization parameter used is the S content of the whole assemblage and the elements considered are Os, Ir, Ru, Rh, Cu and As.

For the mass balance calculation, it is assumed that laurite is the primary PGM, as also suggested by textural evidences. The secondary alloy is the phase in equilibrium with the serpentinizing fluids circulating within the rock. The present multiphasic assemblage is a transitory stage that was frozen at some point during the ongoing desulfurization process and provides information on the elements flow, in or out of the PGM at an intermediate stage of desulfurization.

Calculations of element losses and gains are based on the measurement of areas occupied by the different phases (Tab. 4.26). The problem of transforming 2D areal data into 3D volume data has been long debated (e.g. Schumaker, 1990), and finds several applications in the reconstruction of crystal sizes and crystal size distribution (e.g. Berger et al., 2011; Jerram et al., 2009). The availability of only one randomly oriented section of the object anyway does not preclude the possibility to get a reliable estimate of the volumes of the three phases.

Due to the concentric disposal of the three phases and the roughly equidimensional shape of primary euhedral laurite, the simple model chosen is that of three concentric spheres. The inner sphere has a radius equivalent to that of a circle having the area of the primary laurite. The intermediate and outer sphere volumes were calculated adding the areas of the reaction zone and alloy respectively.

The volume occupied by the primary laurite corresponds to that of the inner sphere and the volumes occupied by the reaction zone and alloy are calculated as differences respectively between the intermediate and inner sphere and between the outer and intermediate sphere. Finally, the total area was normalized to 100. The volume of phase *n* is calculated as:

$$V_n = \frac{4}{3}\pi^{-\frac{1}{2}}\left(\sum A_n^{\frac{3}{2}} - \sum A_{n-1}^{\frac{3}{2}}\right)$$

Where $A_n$ = measured area of phase *n*, $A_0 = 0$ as primary laurite is modeled as the innermost sphere, and n = 1, 2 and 3 respectively for primary laurite, the reaction zone and the alloy.

The mass of phase *n* is then calculated assuming the most reliable density ($d_n$) value for each phase. For laurite-erlichmanite solid solution, a weighted average density between the two end members was used. For alloys, a weighted average between the pure metals was used.

$$m_n = d_n * V_n$$

The initial mass of primary laurite is unknown. As we do not know what would be the size of final alloy after complete desulfurization, we cannot calculate an absolute value for the amount of each element gained or lost except for sulfur that is completely lost, but it is still possible to calculate the balance of the elements relative to each other. Grieco et al. (2020) chose as reference element Os to which mass balances of other elements are calculated. This choice is based on the fact that Os is the least mobile of all PGE and in the samples, it is only enriched in the residual phases. In order to normalize to constant Os, the initial mass of a laurite containing the whole amount of Os of the PGM assemblage was calculated.

$$m_0 = 100 * \frac{m_{Os}}{C_{Os,lau}}$$

Where $C_{Os,lau}$ is the concentration of Os in laurite, and $m_{Os}$ is calculated as:

$$m_{Os} = \sum n \left[\frac{m_n * C_{Os,n}}{100}\right]$$

The initial mass of each element is then calculated as:

$$m_{i,0} = \frac{m_0 * C_{i,lau}}{100}$$

Where $C_{i,lau}$ is the concentration of element *i* in primary laurite. The mass of each element after partial desulfurization (which is the current mass) is:

$$m_i = \sum n \left[\frac{m_n * C_{i,n}}{100}\right]$$

Where $m_i$ is the current mass of element *i*, $C_{i,n}$ is the concentration of element *i* within phase *n* (in wt%). In order to calculate the final mass of each element we first calculated the final mass of the alloy that is necessary to accommodate all the Os content (which is the mass of the alloy at complete desulfurization):

$$m_f = 100 * \frac{m_{Os}}{C_{Os,alloy}}$$

The final mass of each element is therefore calculated as:

$$m_{i,f} = \frac{m_f * C_{i,alloy}}{100}$$

Where $C_{i,alloy}$ is the concentration of element *i* in the alloy (in wt%). Finally, the loss or gain of each element is calculated as the difference between its final and initial mass, normalized to the initial mass and expressed as %. Mass variation after partial desulfurization (e.g. the current situation of partial desulfurized laurite) will be:

$$\Delta m_{i,pd} = 100 * \frac{(m_i - m_{i,0})}{m_{i,0}}$$

And the mass variation after complete desulfurization will be:

$$\Delta m_{i,cd} = 100 * \frac{(m_{i,f} - m_{i,0})}{m_{i,0}}$$

The parameters used for the calculations are reported in Tab. 4.26, and the finals results of losses and gains are reported in Tab. 4.27 and Fig. 4.47, except for Cu that has a gain too high to be shown in the figure.

Tab. 4.26 Parameters used for the calculation and value of input data.

| **Parameter** | **Description** | **Value** |
|---|---|---|
| $A_n$ laurite | Normalized area of laurite | 49.182 |
| $A_n$ reaction zone | Normalized area of reaction zone | 43.126 |
| $A_n$ alloy | Normalized area of alloy | 7.692 |
| d laurite | Density of laurite | 7.390 |
| d reaction zone | Density of reaction zone | 7.070 |
| d alloy | Density of alloy | 17.193 |
| $V_n$ laurite | Normalized volume of laurite | |
| $V_n$ reaction zone | Normalized volume of reaction zone | |
| $V_n$ alloy | Normalized volume of alloy | |
| $m_0$ | Initial mass of laurite | |
| $m_{Os}$ | Total mass of Os | |
| $m_n$ | Mass of phase *n* | |
| $C_{Os,lau}$ | Concentration of Os in laurite | |
| $m_{i,0}$ | Initial mass of element *i* | |
| $C_{i,lau}$ | Concentration of elelement *i* in laurite | |
| $m_i$ | Current mass of element *i* | |
| $C_{i,n}$ | Concentration of elelement *i* in phase *n* | |
| $m_f$ | Final mass of alloy | |
| $C_{Os,alloy}$ | Concentration of Os in alloy | |
| $m_{i,f}$ | Final mass of element *i* | |

| | |
|---|---|
| $C_{i,alloy}$ | Concentration of elelement *i* in laurite |
| $m_{i,pd}$ | Mass of element *i* after partial desulfurization |
| $\Delta m_i$ | Variation of mass of element *i* after complete desulfurization |
| $\Delta m_{i,cp}$ | Variation of mass of element *i* after partial desulfurization |

Tab. 4.27 Results of the mass balance calculations

| Element | $\Delta m_{i,pd}$ (wt%) | $\Delta m_{i,cd}$ (wt%) |
|---|---|---|
| Os | 0.00 | 0.00 |
| Ru | -6.05 | -79.08 |
| Ir | 5.52 | 18.62 |
| Rh | -37.85 | -79.30 |
| Cu | 260.88 | 388.46 |
| As | -19.21 | -84.69 |
| S | -30.88 | -100.00 |

Data show a correlation between the parameters that is clearly not linear and hence the mobility trend is shown in figure through a parabolic curve. Two elements, Cu and Ir, show a positive Os normalized trend and are added to the system during interaction with fluids. Cu content is very low in the primary laurite and its relatively high content in the alloy is almost completely due to addition from fluids. Cu input during percolation of fluids has been already observed in ultramafic rocks, mainly as native copper within later dykes (Eslami et al., 2018), suggesting that copper is brought into the system by low $fS_2$ fluids. Such evidence was also found in an Abdasht sample where native copper was detected. Iridium is the only PGE showing a mass increase during the desulfurization, up to 18.6%. This Iridium input in the alloy can be due to low partition coefficient between fluid and alloy accompanied by a relatively high concentration in the fluid. Such high concentration could be explained by a release of Ir from olivine during serpentinization that increases its concentration in fluid.

Most of the PGE loss is due to release of Ru from primary laurite. Its final content is reduced to about one fifth of the initial one. The mobility of Ru suggests that this element has a partition coefficient between fluid and alloy much higher than both Ir and Os and can be easily released to the fluids. On the other hand, the high Ru content of the reaction zone, higher than that of both reacting phases, suggests that Ru diffusivity is low. The reaction zone releases Os but not Ru to the alloy, hence inducing the Ru high content of the reaction zone. The low subsolidus diffusivity of Ru could also explain the convex shape of the Ru release curve, as sulfur is remobilized earlier than Ru.

Rh is the most mobile PGE. Its content decreases quickly with desulfurization, tracing a concave desulfurization curve. This suggests that Rh diffusivity and its fluid to alloy partition coefficient are

both high. In spite of its fast release Rh mobility effect on total mass balance is very limited due to low Rh
content of primary laurite.

Finally, As, as expected, shows a mobility similar to that of sulfur, with the low curvature of the desulfurization trend that could be indicative of a linear correlation between the depletion of these two elements.

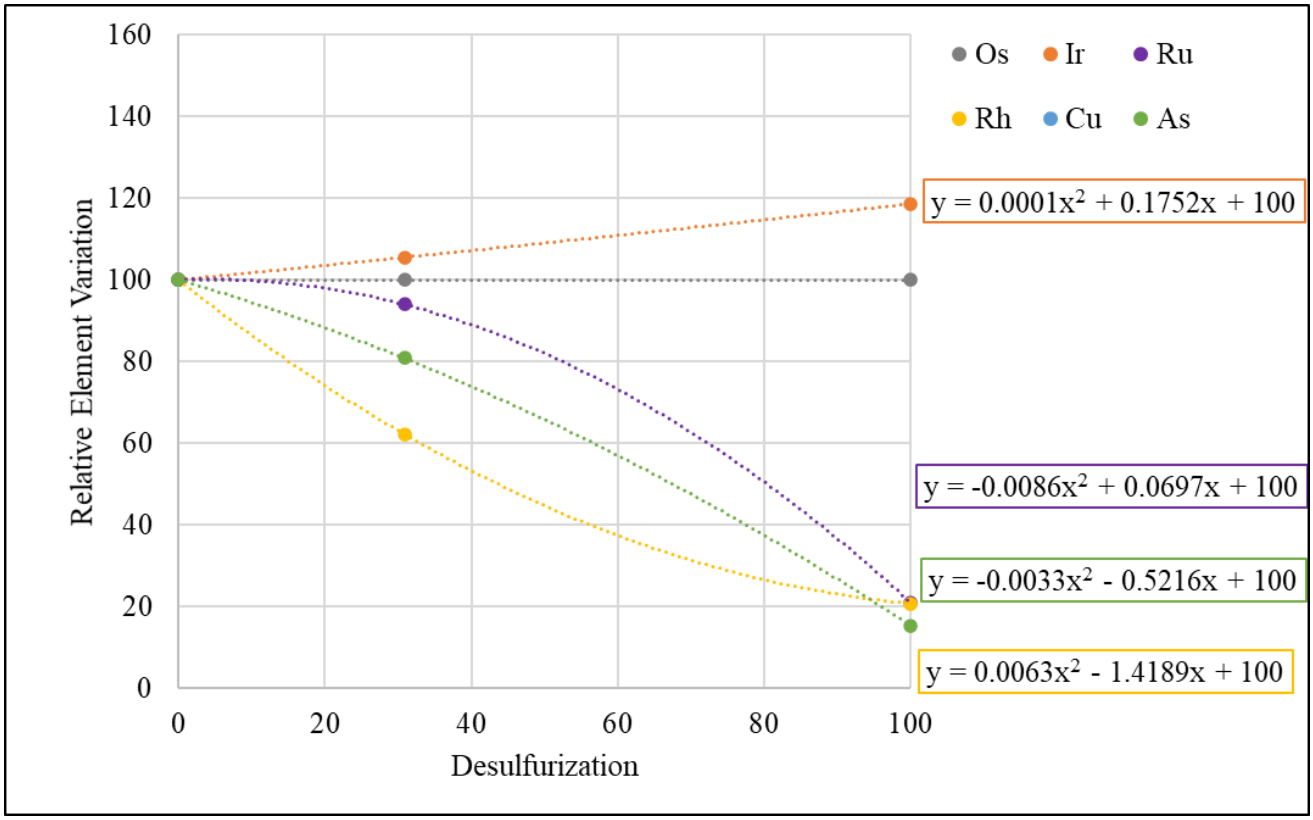


Fig. 4.47 Patterns of Os-normalized PGE losses or gains during desulfurization. On the y-axis are reported losses and gains of Ir, Ru, Rh and As normalized to immobile Os, at three desulfurization steps: 0%, 30% and 100% (modified after Grieco et al., 2020).

*PGE patterns*

PGE in the primitive mantle are hosted within a monosulfide solid solution (mss) (Lorand and Alard, 2001). The PGE content of a melt is therefore dependent on the degree of partial melting of the primitive mantle, and on the dissolution of the mss. Chromitites enriched in PGE crystallize in equilibrium with melts formed in a critical melt interval, which was identified by Prichard et al. (2008) at 20-25%. Lower degrees of melting would produce PGE-poor chromitites (e.g. basaltic melts formed beneath spreading centers) (Ahmed and Arai, 2002; Economou-Eliopoulos, 1996; Gervilla et al., 2005; Gonzalez-Jimenez et al., 2011b), while higher degrees of melting would dilute the PGE content, especially in Pt and Pd, the two PGE that fractionate into the melt (Brenan and Andrews, 2001).

Ophiolite chromitites, enriched in IPGE with respect to PPGE, are the result of this fractionating process (Economou-Eliopoulos, 1996; Grieco et al., 2020, 2004; Proenza et al., 2007). PPGE-enriched patterns in ophiolite chromitites are rare, and attributed mostly to hydrothermal alteration (Malitch et al., 2003b, 2003a; Yang and Seccombe, 1993). However, recent studies highlighted the small-scale remobilization of PGE within chromitites due to low temperature processes, suggesting that the PPGE enrichment may be achieved at the magmatic stage. As IPGM are typically found enclosed within chromite and PPGM are more common as interstitial phases, Prichard et al. (2008b) suggest that crystallization of IPGE occurs prior or during crystallization of chromite, together with the crystallization of minor Pt and Rh. The remaining Pt and Pd, on the other hand, crystallize during sulfur saturation in chromitite formed from a more evolved magma. Prichard et al. (2008b) propose that this crystallization was from a magma that was enriched in PGE because the degree of mantle melting was just sufficient to extract the PGE, but not dilute them in a melt that includes further mantle melting.

Mantle normalized patterns of Skyros and Abdasht-Soghan are reported in Fig. 4.48. In both localities, the patterns are characterized by a general negative slope, from IPGE to PPGE, with a marked drop between Rh and Pt. The low Pt and Pd contents depicted by the sharp drop in the pattern between Rh and Pt is a common feature of ophiolite chromitites (e.g. Economou-Eliopoulos, 1996; Grieco et al., 2004; Proenza et al., 2007; Uysal et al., 2009; Zhou et al., 1998). Such sharp drop pattern was also previously found in other chromitites from Greece (Economou-Eliopoulos, 1996) and Southern Iran (Jannessary et al., 2012; Najafzadeh and Ahmadipour, 2014). Both Skyros and Abdasht-Soghan PGE patterns, however, show some peculiarities. While podiform chromitites patterns usually show a peak for Ru (Fig. 4.48A and B), Skyros and Abdasht-Soghan samples show two peaks, corresponding to Os and Ru. For Abdasht-Soghan and one Skyros sample, Os mantle normalized content results higher or equal to the Ru one. The only exception are chloritized samples from Skyros (SKY8B and SKY10) which show a pattern more similar to the one of typical ophiolite chromitites.

The PGE patterns suggest a loss of Ru compared to Ir and Os that produces a double peak pattern or, in the most altered samples, a flat pattern with lower total PGE content. This kind of feature in whole rock PGE patterns is not observed in all desulfurized chromitites. The patterns in chromitites from the Loma Peguera chromitites in the Dominican Republic (Proenza et al., 2007), Veria ophiolite complex in Northern Greece (Tsoupas and Economou-Eliopoulos, 2008) and Kluchevskoy ophiolite complex in Russia (Zaccarini et al., 2008), among others, do not show such kind of trends. This can be either due to absence of PGE mobility in the samples they studied or to short range mobility, with incorporation of PGE in secondary phases. This latter process could also have been occurred in Skyros and Abdasht-

Soghan chromitites, as many secondary BMM show enrichments in some PGE, mostly Pt, Ir and Pd. On the other hand, some PGE patterns enriched in Os are reported by Uysal et al. (2009) in chromitites from Mugla, Turkey, also hosting altered PGM assemblages. Grieco et al. (2007) also report double peak patterns in chromitites with altered PGM assemblages from Nurali ophiolite. Here the most widespread features of PGM are an irregular core to rim zoning of laurite, where rims are systematically Os-rich, and the abundance of Os-rich alloys.

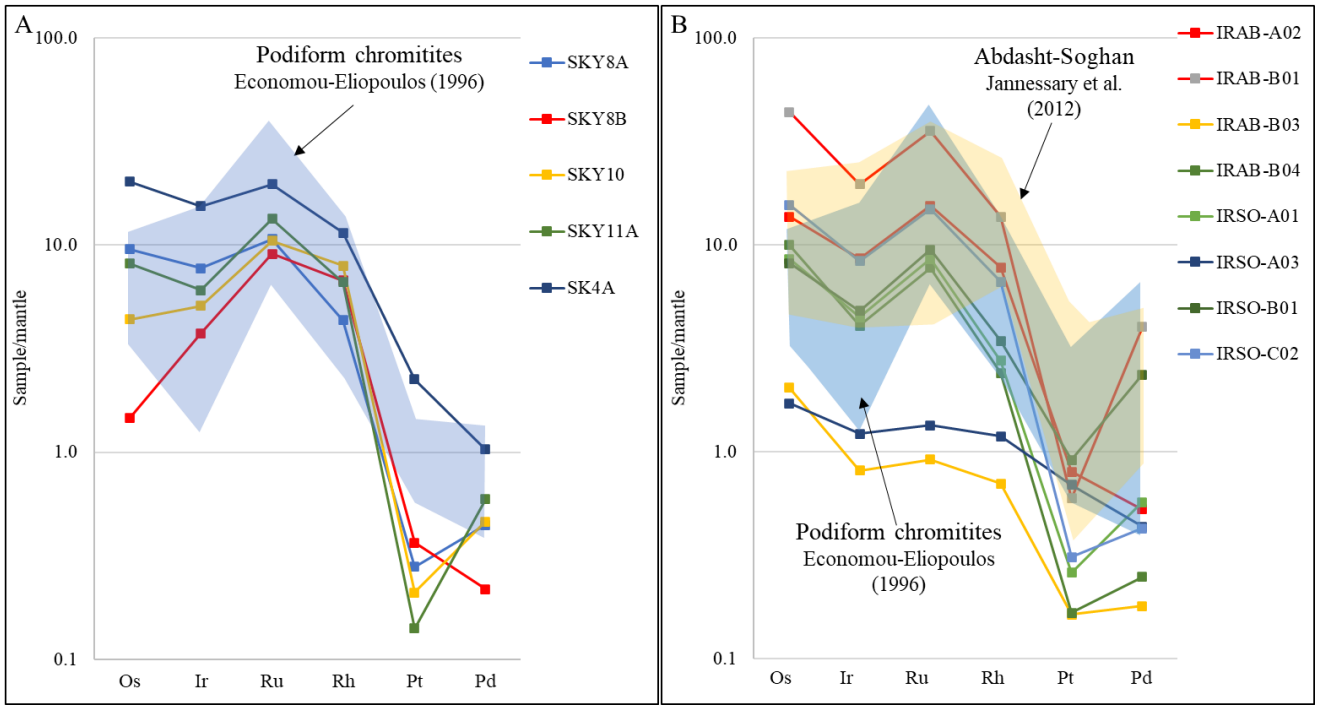


Fig. 4.48 Mantle-normalized (McDonough and Sun, 1995) PGE patterns of A) Skyros and B) Abdasht-Soghan; podiform chromite fields are from Economou-Eliopoulos (1996); Abdasht-Soghan field is from Jannessary et al. (2012).

In order to check if the Os peak and the low total PGE flat patterns can be related to the desulfurization process we compared the relative abundance of Os, Ru and Ir in the whole rock with the effect of desulfurization on PGM composition (Fig. 4.49). The desulfurization curves of Os, Ir and Ru for Abdasht-Soghan (Fig. 4.47), were used to plot a desulfurization trend in the Os-Ru-Ir diagram. This can be compared to the relative abundance of Ru, Os and Ir in whole rock.

The full set of samples from Abdasht and Soghan, comprising those from Jannessary et al. (2012) plot close to the desulfurization line, showing that desulfurization of laurite is the main post-magmatic process that affected PGM. Samples from Jannessary et al. (2012) were probably collected from a less serpentinized part of the ore, as also suggested by their host rock analysis of a dunite. They show a desulfurization degree between 0 and 75%, that, due to the downward convexity of the Ru remobilization curve (Fig. 4.49) results in a little change of the IPGE relative ratios and hence in PGE

normalized patterns similar to those of average ophiolite chromitites, showing a single Ru peak. The samples used for this work, on the other hand, were collected from strongly serpentinized portions of the ore and were affected by 75 to 100% desulfurization (Grieco et al., 2020). In these conditions most of the Ru is remobilized, causing a relative increase of Os that results in the double peak pattern.

The situation is similar for Skyros samples. One sample presents a desulfurization degree slightly higher than 50%, and it corresponds to a sample that shows a single Ru peak (Fig. 4.48). The other samples all show desulfurization degrees between 75 and 100%.

Grieco et al. (2004) observed similar changes of PGE contents and chondritic patterns shapes in Finero chromitites. The patterns change from negative to positive slopes in the IPGE portion of the pattern, with decreasing total PGE content. The Authors ascribed this effect to the percolation of metasomatizing fluids that were responsible for the re-hydration of harzburgite due to crystallization of secondary amphibole. These fluids selectively leached PGE giving, as a result, the inversion of slope in the IPGE portion of the patterns.

It is not possible, due to their low content, to provide reliable information on the behavior of PPGE. According to mass balance Rh is very mobile and this is reflected in its lower content in the most desulfurized samples. PGE whole rock data suggest that Pt and Pd are not depleted in desulfurized samples and a possible clue of this behavior is the presence of an Ir alloy (chengdeite) with 4.10 wt% Pt, and of slight PPGE enrichments within secondary BMM.

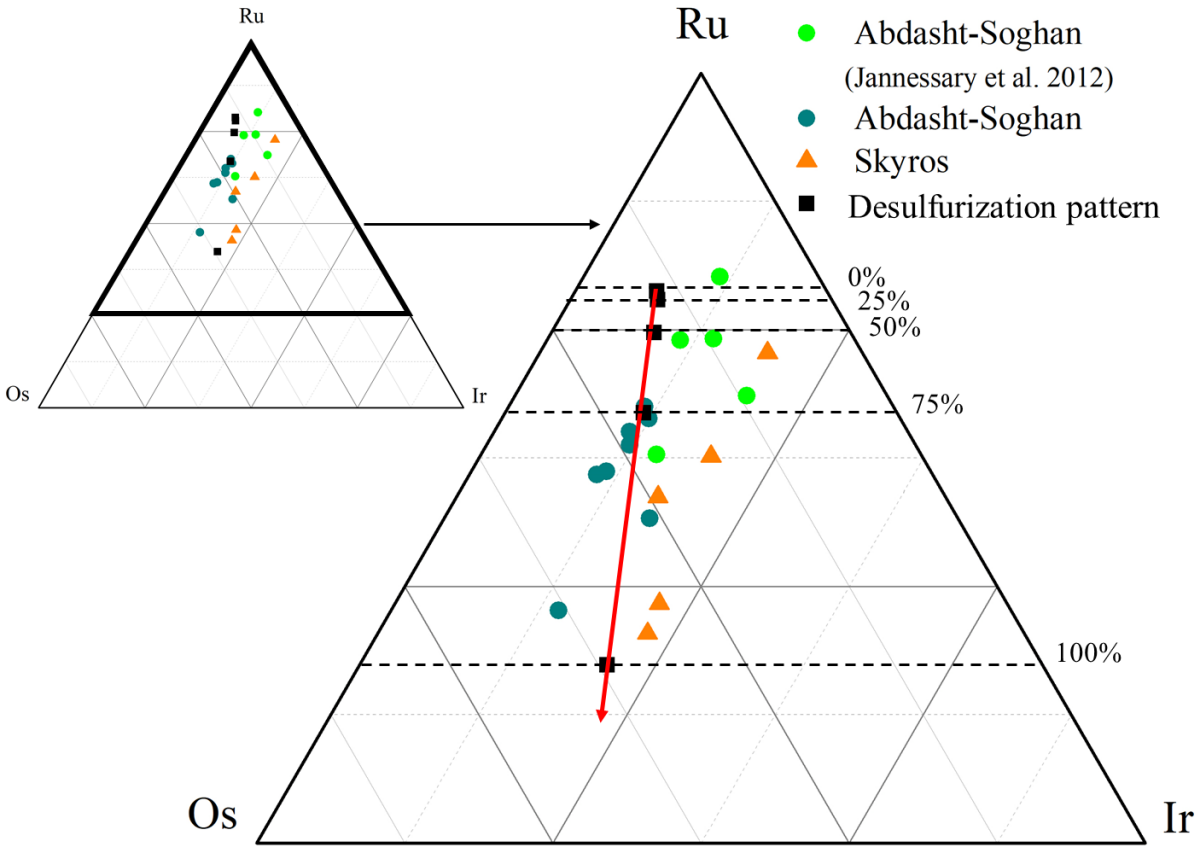

Fig. 4.49 Ternary Ru-Os-Ir diagram of PGE concentration in Abdasht-Soghan and Skyros; black squares represent different desulfurization stages, from 0 % (not desulfurized) to 100 % (completely desulfurized), obtained from Abdasht-Soghan desulfurization curves. Abdasht-Soghan PGE compositions have been integrated with data from Jannessary et al. (2012).

*Re-sulfurization*

The desulfurization process is the main event responsible of the PGE mobility in Abdasht-Soghan and Skyros, as suggested by the textural and chemical clues described above. However, there is also evidence of a later resulfurization event, not as pervasive as the desulfurization one and possibly related to circulation of more oxidizing fluids within the Abdasht-Soghan complex. The major clue supporting this hypothesis is the partial replacement of heazlewoodite and maucherite by millerite in some sulfide grains (Fig. 4.39). The event only affected BMM and possibly chromite, while PGM do not seem to have registered this late event. The late oxidizing event can be correlated to the partial and unevenly distributed chloritization and ferrian chromitization of chromitites. No clues of a later resulfurization have been detected within Skyros chromitites.

### 4.3.4 Conclusion

Chromitites from Skyros and Abdasht-Soghan show chromite mineral chemistry typical of ophiolite mantle chromitites. Only Agio Iohannis and Agio Alexandria spinels present some supra-Moho characteristics (relatively high $Al_2O_3$ and $TiO_2$ contents) and could have been generated within the Transition Zone, close to the contact between upper mantle peridotites and lower crust gabbros and cumulates.

Both Skyros and Abdasht-Soghan chromitites show PGM and BMM assemblages dominated by secondary sulfides and alloys and rare primary sulfides, mostly included within unaltered chromites. This testifies the occurrence in both complexes of a widespread alteration event, related to the circulation of low $fS_2$ and low $fO_2$ serpentinizing fluids. This alteration event caused the remobilization of PGE at different scales. Instability of laurite at low $fS_2$ resulted in subsolidus diffusion of PGE. Os was the most mobile and the first one to exit laurite lattice to form Os-rich alloys. Mass balance on partially altered laurite, on the other hand, shows that the PGM assemblage lost mainly Ru. A second, larger-scale remobilization can hence be inferred, where Ru acted as the most soluble PGE in the desulfurizing fluids, that differentially remobilized PGE. The mobility of PGE into the fluids follows the order: Ru>>Os>Ir. Less reliable data, due to the lower contents of PPGE, suggest that Rh is more mobile than Ru and that Pt and possibly Pd can be added to some extent to the system by fluids. This larger range mobility affects PGE whole rock content, giving rise to double peak and flat PGE patterns both within Skyros and Abdasht-Soghan. Results show that differential

mobility of PGE during the percolation of low $fS_2$ metamorphic fluids, can strongly affect PGE distribution and mineralogy within ophiolite chromitites and can play an important role in the economic assessment of this kind of PGE ore.

# CHAPTER 5: Chromite foundry sands

For the present study, chromite sands from different localities have been tested in order to assess their suitability for the chromite foundry market. Moreover, different silicate sands, representing the most common silicates within ophiolite chromitites, have been tested in order to assess their reactivity with binding resins. The aim of the work is to provide new insights into the production of foundry chromite sands from ophiolite-type deposits. Data and discussion have been already published:

- Bussolesi, M., Grieco, G., Eslami, A., & Cavallo, A. (2020). Ophiolite Chromite Deposits as a New Source for the Production of Refractory Chromite Sands. Sustainability, 12(17), 7096.

## 5.1. Introduction

Chromite foundry sands, bonded with resins, are employed in the industry to form molds for casting metal and steel when high performance of sand is required (Fig. 5.1A, B) (Carey, 2002). They have special properties, such as high melting point (2090 °C), low thermal expansion and neutral chemical behavior that make chromite sands the best solution for high demanding casting (Surekha et al., 2013) and are also the main reason why chromium has been included in the Critical Raw Material list (European Commission, 2014).

Chromite foundry sands are generally mixed with binding resins and hardeners to produce molds. They substitute silica sands to cast metals with high density and high melting point and are much cheaper when compared to zircon sand (Bengulur et al., 2013). They have to meet strict quality parameters in order to ensure a good final product (Laviosa Chimica Mineraria s.p.a., 2008). The most important ones are $Cr_2O_3$ content (higher than 44%), Fineness Index (between 40 and 75), $SiO_2$ content (below 2.5%), and Acid Demand (below 10, 8, and 6 at pH = 3, 4, and 5, respectively). The Fineness Index (FI) is a measure of the grain size distribution of the sand and it must be neither too high (preventing degassing during casting processes) nor too low (resulting in an uneven surface of the final product). Low silica content is required in order to avoid chemical reactions between silicate impurities within the sand and the binding resins, which could result in a decrease of the sand performance. As the reactivity of sand with resins is the most crucial parameter during casting, in addition to $SiO_2$ content, a specific test (Acid Demand Test, ADT) has been developed as a proxy of this process.

Foundry chromite production, a niche product in the chromite market but with a high added value, is almost completely dominated by South African companies, which provide the largest share of supply and the best foundry grade quality (Kogel et al., 2006; Koleli and Demir, 2016). These chromites derive from layered intrusion-type deposits. Some chrome ore companies, however, started producing

foundry sands from metallurgical-grade materials, coming from ophiolite-type deposits, widespread all over the world. While metallurgical-grade chromite is cheap and abundant, foundry sand grade is more expensive, as its high-quality parameters are much harder to attain. Thus, it is profitable for such companies to further enrich metallurgical-grade ore to reach foundry grade quality (Richard, 2015). As of April 2020, foundry chromite prices were between 380 and 540 $/ton. Expanding the chromite foundry sand market to other producers can widely contribute to lowering the criticality of this commodity, and triggering local production.

The present work aims to provide new insights into the production of foundry chromite grade from metallurgical-grade chromite coming from ophiolite-type deposits. For this purpose, two chromite concentrates from ophiolite deposits in Iran and Greece have been tested and compared with South African chromite sands. The first one is a sand used in the Iranian foundry market, the second one is a metallurgical-grade chromite concentrate. These sands were selected as potential candidates to replace South Africa chromite sands in the European foundry market. As the most critical difference between layered intrusions and ophiolite-type deposits for the production of foundry sands is the different mineralogy of silicate impurities within the sand concentrate, we then focused on the different effects that these impurities have on ADT values. This would provide an important tool in the production of chromite foundry sands from metallurgical-grade ophiolite-type chromite deposits.

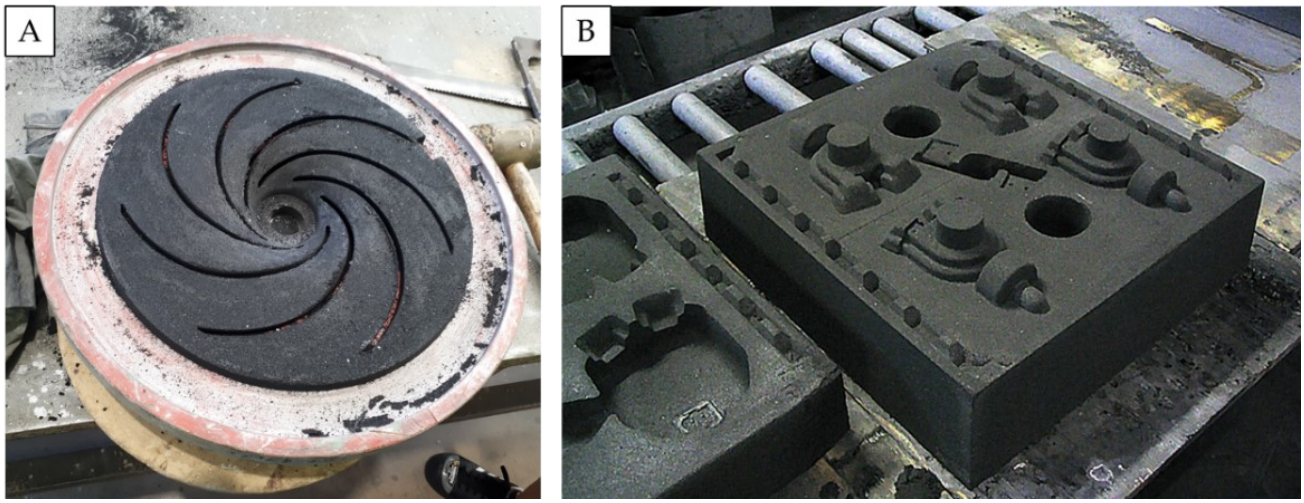


Fig. 5.1 A) and B) chromite sand molds for refractory use (Flowserve Foundry, Desio, Italy). From Bussolesi et al. (2020a).

## 5.2. Material and methods

Analyzed samples include one commercial South African chromite sand provided by Laviosa Chimica Mineraria S.p.A, two chromite concentrates from chromite enrichment plants and four rock samples (orthopyroxenite, dunite, serpentinized dunite, and chloritized dunite) representative of different

silicate impurities that can be found in chromite sands: orthopyroxene, olivine, serpentine, and chlorite. Moreover, two partially serpentinized dunites from the Aetoraches and Rizo mines have been selected and analyzed. These last two samples represent mixed serpentine-olivine assemblages that can be found within some ophiolite chromitites (Tab. 5.1). Concentrates where sampled directly from the separation plant at the mines in Aetoraches, Northern Greece, and Neyriz, Southern Iran. These mines exploit massive and disseminated chromitite bodies hosted in partially serpentinized peridotites of ophiolites (Ghorbani, 2013; Rajabzadeh et al., 2013; Rassios, 2014; Tzamos et al., 2017). Olivine and serpentine (i.e. lizardite) are the most common impurities in ophiolite chromite deposits and they often occur together in different proportions (Arai and Yurimoto, 1994; Grieco et al., 2018; Grieco and Merlini, 2012).

Tab. 5.1 List of samples and their location.

| Sample | Locality | Sample | Major silicates |
|---|---|---|---|
| SA | South Africa | Quality Proxy sand | Orthopyroxene |
| AE | Aetoraches (GR) | Chromite sand | Olivine + Serpentine |
| NE | Neyriz (IRN) | Chromite sand | Serpentine |
| CHL | Abdasht (IRN) | Chloritized sample | Chlorite |
| SRP | Neyriz (IRN) | Serpentinized sample | Serpentine |
| OLV | Finero (IT) | Dunite sample | Olivine |
| OPX | Ivrea Verbano (IT) | Orthopyroxenite sample | Orthopyroxene |
| RI-2 | Rizo (GR) | Serpentinized dunite sample | Olivine + Serpentine |
| AE-2 | Aetoraches (GR) | Serpentinized dunite sample | Olivine + Serpentine |

### 5.2.1. Grain size distribution

An important quality parameter of chromite sands is the Fineness Index, which is derived from grain size distribution analysis. Fineness Index values accepted for chromite foundry sands are comprised between 40 and 75 (Ente Nazionale di Unificazione, 1976). Grain size distribution is estimated using a sieve column, and Fineness Index is calculated through the following equation:

$$FI = \frac{p_1 a_1 + p_2 a_2 + p_3 a_3 + \cdots}{p_1 + p_2 + p_3 + \cdots}$$

Where:

FI = Fineness Index;

p = percentage of material collected by a specific sieve

a = sieve parameter (Tab. 5.2)

Grain size distribution was performed on samples SA and NE. For crushed samples (CHL, SRP, OLV, OPX) and for Aetoraches chromite sand (AE), a fixed FI (between 40 and 50) was assembled in order to have a comparison with samples SA and NE.

Tab. 5.2 Sieve parameters used to calculate FI (Ente Nazionale di Unificazione, 1976).

| Standard Column (μm)[1] | Sieve Parameter (a) |
|---|---|
| 3150 | 3 |
| 1600 | 5 |
| 800 | 11 |
| 630 | 18 |
| 400 | 31 |
| 315 | 38 |
| 200 | 52 |
| 160 | 66 |
| 100 | 102 |
| 80 | 130 |
| 50 | 210 |
| bottom | 300 |

[1] Standard column DIM4188

### 5.2.2. XRD powder diffraction

XRD analyses were performed on all samples using a High-resolution X-ray powder diffractometer Panalytical X'pert Pro at the department of Earth Sciences of the University of Milan. This powder diffractometer is equipped with an incident beam monochromator, that separates the Ka1 and the Ka2 and can work with the Bragg Brentano geometry (divergent beam) as well as with a parallel beam geometry. Ka1 and Ka2 are produced by a conventional X-ray tube equipped with a Cu anode, $\lambda \sim 1.54$ Å. The detector X'Celerator completes the instrument, allowing very fast data collection.

### 5.2.3. X-ray fluorescence

Chromite foundry sands were analyzed at the University of Milan Bicocca using energy-dispersive X-ray fluorescence (EDXRF, Panalytical Epsilon 3). Data were collected using the Omnian methodology, a standardless method which utilizes internal machine standards for the construction of a calibration curve. Calibration curves have been then corrected using five external standards, SARM8, SARM9, CHR-BHG, CHR-Pt, GR-55, and VV-4.

### 5.2.4. Acid Demand Test

The Acid Demand Test (ADT) is a standardized titration method used as a proxy for sand-resin reaction potential. The Acid Demand value keeps into account the amount of acid consumed at three different pH levels. The procedure, implemented by Laviosa Chimica Mineraria S.p.A (Laviosa Chimica Mineraria s.p.a., 2008) is here reported:

**Materials**

- 50g of foundry sand
- 50ml HCl (0.1M)
- 50ml NaOH (0.1M)
- $H_2O$

**Procedure**

- Mix 50g of chromite sand with 50ml of HCl, stir for 5 minutes and let the solution rest for 1h.
- Filter the solution adding distilled $H_2O$ until the solution reaches 150ml.
- Measure the pH value of the solution.
- Add NaOH until the solution reaches pH 3, 4 and 5, taking note of the volume of NaOH consumed after each step.

**Acid Demand Value**

ADT values for the three pH levels can be calculated through the following equation:

$$ADT_{pHn} = 50 - An * f$$

Where:

n = 3, 4, 5;

An = volumes of NaOH consumed to reach pH 3, 4, 5;

f = correction factor for HCl and NaOH, determined through blank tests

The accepted limits for the ADT parameter are 10 at pH = 3, 8 at pH = 4, and 6 at pH =5. In order to limit the grain size effect on the acid demand results, for the evaluation of the silicate gangue, a narrow range of Fineness Index (between 40 and 50) was chosen. Moreover, for the evaluation of silicate mineralogy effect on the ADT, pure silicate sands were used, and tests were performed at fixed SiO2 values of 2.5 wt % in 50 g of sand, that is 1.25 g of SiO2. The amount of starting material was recalculated based on the SiO2 content of each silicate mineral. The choice of the silicate samples was based on the most common silicate minerals of chromite deposits, which are pyroxene, olivine, serpentine, chlorite, or a mix of those.

# 5.3. Results

## 5.3.1. Fineness Index

Grain size distribution analysis was performed on standard South African sand (SA) and on chromite sands produced in the Neyriz enrichment plant (NE) (Fig. 5.2). The resulting FI are 50 and 41 respectively. For Aetoraches, as the metallurgical-grade final concentrate has a FI that does not meet foundry sand limits, a chromite sand with a FI of ~44 was assembled.

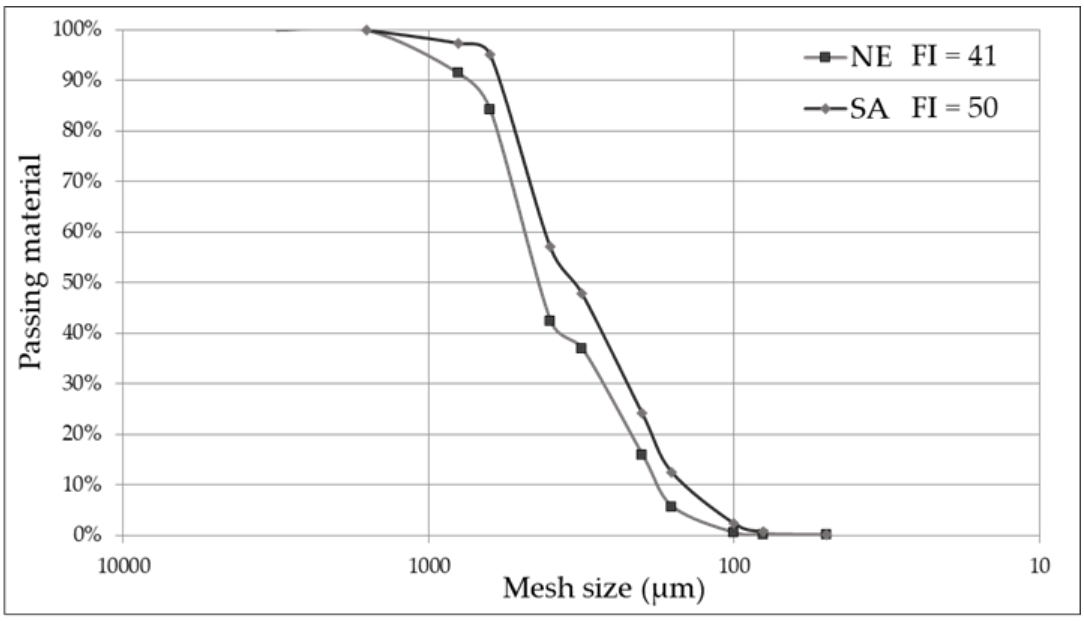


Fig. 5.2 Grain size distribution of chromite sands from South Africa and from Neyriz.

## 5.3.2. Mineralogy of silicates

Silicate content in chromite concentrates was too low to be detected through x-ray diffraction and, for these samples, silicate minerals were recognized optically and through EDS spectroscopy. South Africa foundry sand mineralogy is dominated by orthopyroxene with minor amounts of plagioclase and olivine, which is the typical silicate assemblage interstitial to chromite grains in layered intrusion chromite deposits (McLaren and De Villiers, 1982; Mondal and Mathez, 2007) (Fig. 5.3A). Ophiolite chromitites, on the other hand, typically have a silicate matrix consisting of olivine (Leblanc and Nicolas, 1992; Mondal and Griffin, 2018). Occasionally, diopside and pargasite can also be present in minor amounts (Augé, 1987; Leblanc and Nicolas, 1992; Mondal and Griffin, 2018). These deposits are often subject to hydrothermal alteration, which causes primary silicates to be replaced by secondary ones, mainly serpentine and chlorite (Leblanc and Nicolas, 1992). Carbonates within

ophiolite chromitites are rare, and they are usually indicative of late hydrothermal processes (Baccolo et al., 2019; Garuti et al., 2007).

Massive chromitites from the Vourinos complex, in which the Aetoraches deposit is included, are all partially serpentinized (Rassios et al., 2020). Within Aetoraches and the nearby Rizo deposit, the degree of serpentinization varies between 10 and 70%, and the silicate matrix is composed of serpentine and olivine in different proportions (Cazzaniga, 2009).

Massive chromitites from Neyriz deposit are composed of coarse-grained chromite with interstitial olivine, serpentine, and minor chlorite (Rajabzadeh et al., 2013). Disseminated ores show a silicate assemblage constituted by olivine and serpentine. Neyriz deposits show high degrees of serpentinization, up to 90% (Rajabzadeh et al., 2013).

Both the Neyriz and Aetoraches samples show the typical silicate assemblage of ophiolite chromite deposits, dominated by olivine that can be totally (NE) or partially (AE) replaced by serpentine (Fig. 5.3B and C) during retrograde metamorphism (Evans, 2004).

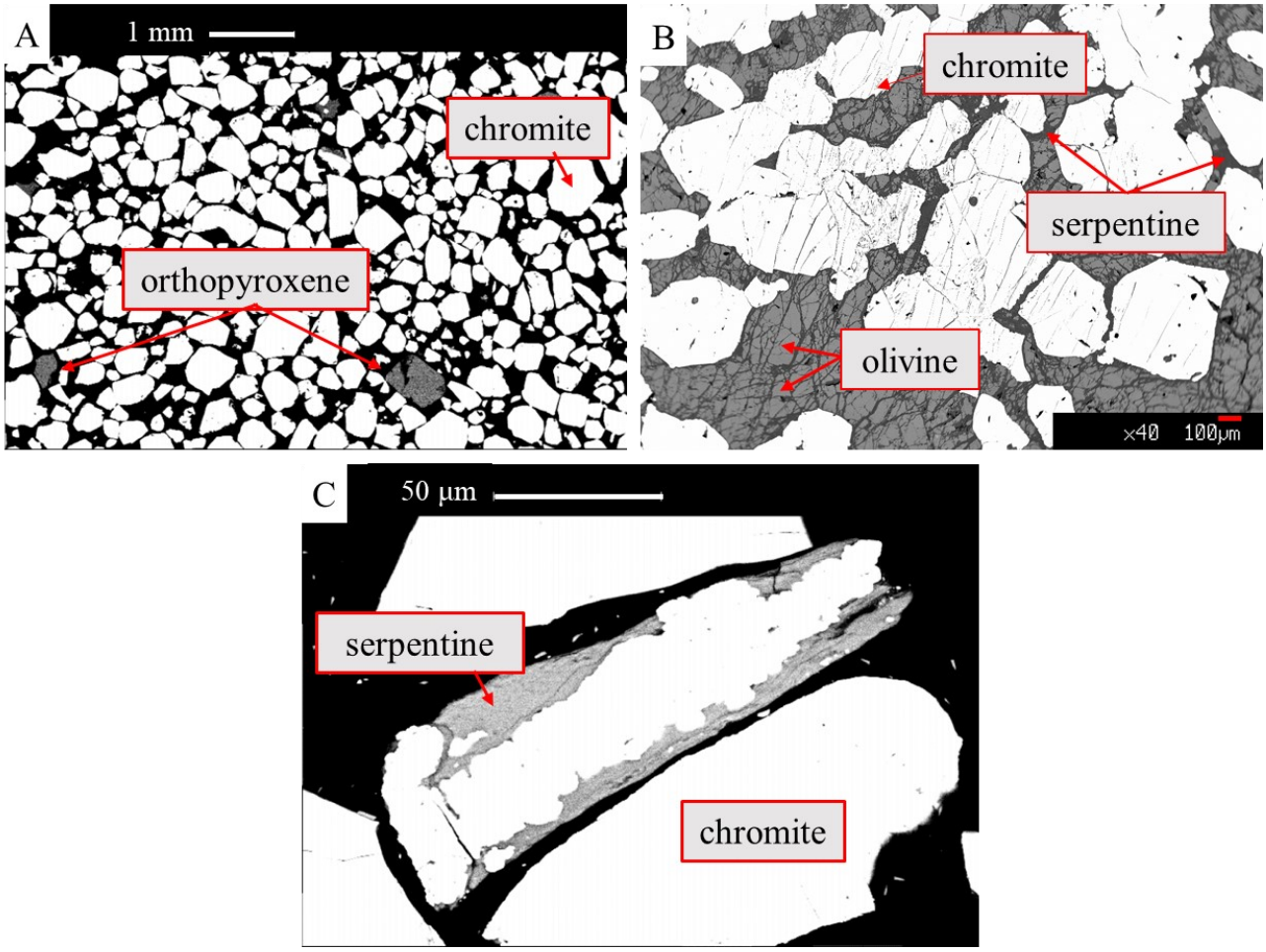


Fig. 5.3 BSE images of A) South Africa chromite sand; B) massive chromitite sample from Aetoraches, (C) mixed serpentine-chromite grains in the Neyriz chromite sand.

XRD analyses were performed on all the silicate samples, and qualitative results are reported in Fig. 5.4. Samples show mineralogical assemblages dominated by serpentine varieties, chlorite, orthopyroxene, and olivine, respectively. Minor impurities are brucite, chromite, and pargasite in such low amounts that cannot affect the results of ADT. Aetoraches and Rizo serpentinized dunites (AE-2 and RI-2) also show an assemblage dominated by olivine and serpentine with minor chromite and clinochlore.

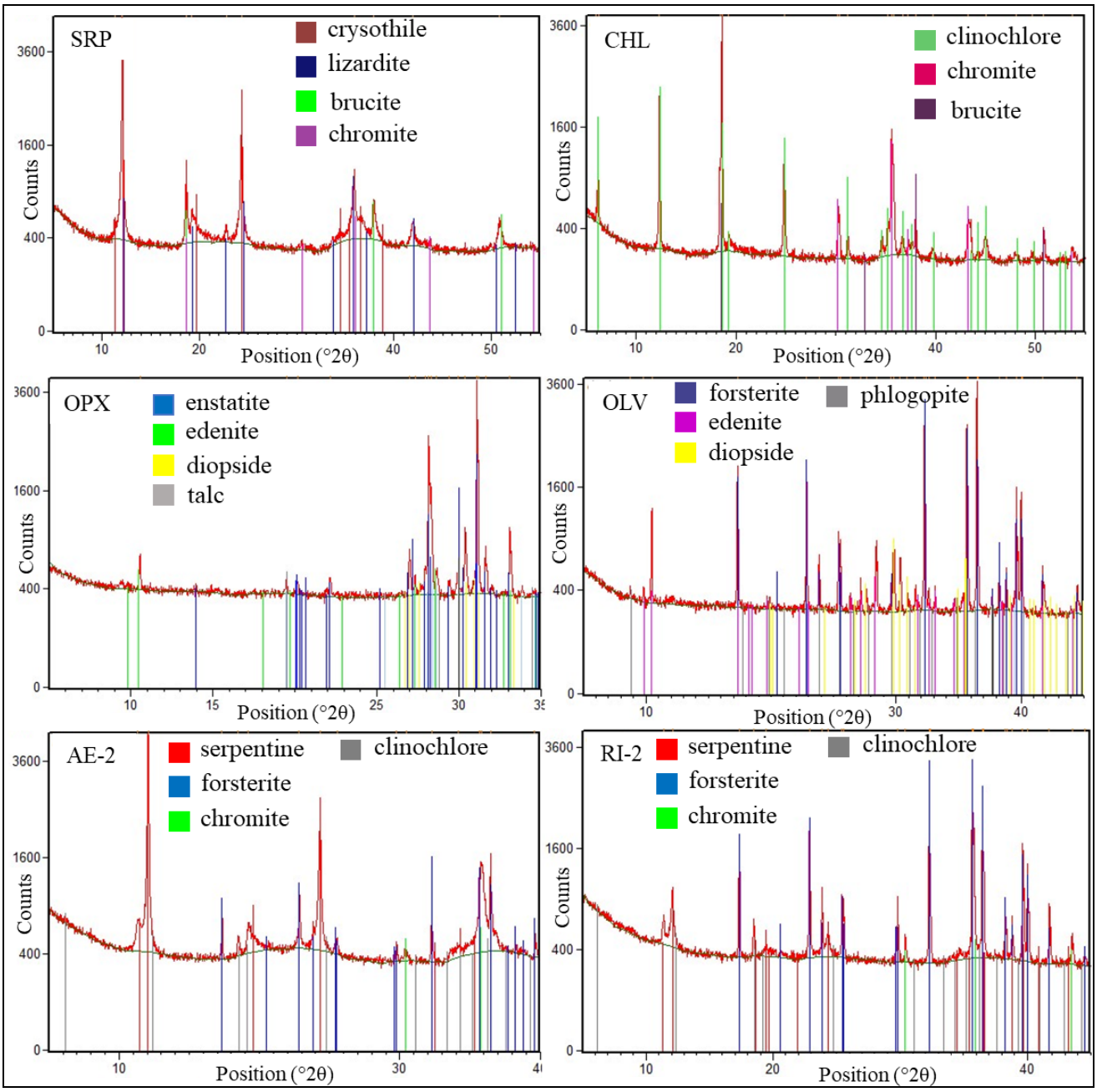


Fig. 5.4 XRD patterns of silicate samples (sample labels as in Tab. 5.1).

### 5.3.3. XRF

XRF analyses have been performed on the chromite concentrates. The results (Tab. 5.3) show that all three samples respect the $Cr_2O_3$ content threshold, with NE showing the highest $Cr_2O_3$ content of 56.27 wt%. Sample SA has the lowest $SiO_2$ content (0.70 wt%), followed by sample NE with a $SiO_2$ content of 2.01 wt%, both below the 2.5 wt% threshold. The only sample that exceeds the threshold is AE, with a $SiO_2$ content of 7.72 wt%, making this sand not suitable for foundry use.

Tab. 5.3. X-ray fluorescence results of chromite sands (wt%).

| Sample | $Cr_2O_3$ | $SiO_2$ | $Al_2O_3$ | CaO | $Fe_2O_3$ | MgO | MnO | $TiO_2$ |
|---|---|---|---|---|---|---|---|---|
| SA | 44.66 | 0.70 | 14.52 | 0.14 | 29.07 | 9.88 | 0.19 | 0.68 |
| NE | 56.27 | 2.01 | 12.08 | 0.18 | 15.68 | 13.08 | 0.20 | 0.09 |
| AE | 48.90 | 7.72 | 7.17 | 0.33 | 19.46 | 14.74 | 0.24 | 0.12 |

### 5.3.4. Acid Demand

During beneficiation, silica impurities are mostly separated from chromite, and reported to the tailing material. To have a foundry quality, chromite sands need to have Acid Demand values at pH =3, 4 and 5 not higher than 10, 8 and 6 respectively.

Acid Demand tests have been performed on chromite sands SA and NE, and on assembled chromite sand AE. In order to assess the behavior of different silicate impurities during Acid Demand, samples CHL, SRP, OLV, OPX, AE-2, and RI-2 have also been analyzed. Considering a $SiO_2$ limit of 2.5% in chromite foundry sands, the test was performed on the amount that would correspond to 2.5% $SiO_2$ within 50 g of a chromite sand, based on the silicate mineral chemistry (Tab. 5.4):

$$100[\%] : Y[\%] = x[g] : 1.25[g]$$

Where:

100(%) = total of the sand

Y(%) = % $SiO_2$ within the silicate mineral

X(g) = grams of sand to use for acid demand test

1.25(g) = grams of $SiO_2$ allowed within 50g of foundry sand (2.5%)

For mixed olivine-serpentine sands (RI-2 and AE-2), we considered a mean between the %$SiO_2$ of serpentine and olivine.

Tab. 5.4 Acid demand test results of chromite sands and silicate samples.

| Sample | Sand (g) | $SiO_2$% | Initial pH | ADT pH3 | ADT pH4 | ADT pH5 |
|---|---|---|---|---|---|---|
| SA | 50 | 0.70 | 1.52 | 8.9 | 6.6 | 6.0 |
| NE | 50 | 2.01 | 1.42 | 21.7 | 20.2 | 19.6 |
| AE | 50 | 7.7 | 2.62 | 40.7 | 33.3 | 32.3 |
| CHL | 4.12 | 2.5 | 1.93 | 23.5 | 20.8 | 20.2 |

| | | | | | | |
|---|---|---|---|---|---|---|
| OPX | 2.09 | 2.5 | 1.78 | 3.6 | 1.1 | 0.4 |
| OLV | 3.19 | 2.5 | 1.70 | 10.6 | 8.6 | 7.9 |
| SRP | 2.88 | 2.5 | 2.20 | 39.2 | 36.4 | 36.03 |
| AE-2 | 2.90 | 2.5 | 1.83 | 19.0 | 15.6 | 15.0 |
| RI-2 | 2.91 | 2.5 | 1.87 | 16.7 | 13.4 | 12.8 |

## 5.4. Discussion

Chromite sands for foundry use have to meet all four quality parameters (FI, $Cr_2O_3$, $SiO_2$ and ADT). South Africa (SA) sand, as expected, being the reference material for foundry market, meets all the required parameters. Neyriz (NE) chromite sand has a very high $Cr_2O_3$ content, a suitable grain size distribution and silica content lower than 2.5%. However, the acid demand values exceed the limits for all three pH (Fig. 5.5). Aetoraches (AE) sand meets only the $Cr_2O_3$ and FI parameters. Silica content is much higher than the threshold and the ADT is around four times the threshold for all pH.

The results on Aetoraches sand show that a typical metallurgical-grade chromite sand, with a $Cr_2O_3$ content around 48 wt % derived from ophiolite chromite deposits, is very far from meeting quality parameters for foundry use. The Neyriz sand, a substitute of unavailable South African sand in Iran, underwent a much deeper separation process in order to decrease $SiO_2$ content till meeting foundry sand quality. Our results show that the most demanding parameter is Acid Demand that is not met by NE sample in spite of its low $SiO_2$ content. This makes such sand unsuitable for the very demanding world foundry market.

If the high acid demand for Aetoraches sand is to be expected due to its high silica content, Neyriz acid demand values are more puzzling. The low difference in silica content between NE and SA cannot explain the high difference in Acid Demand values between the sands.

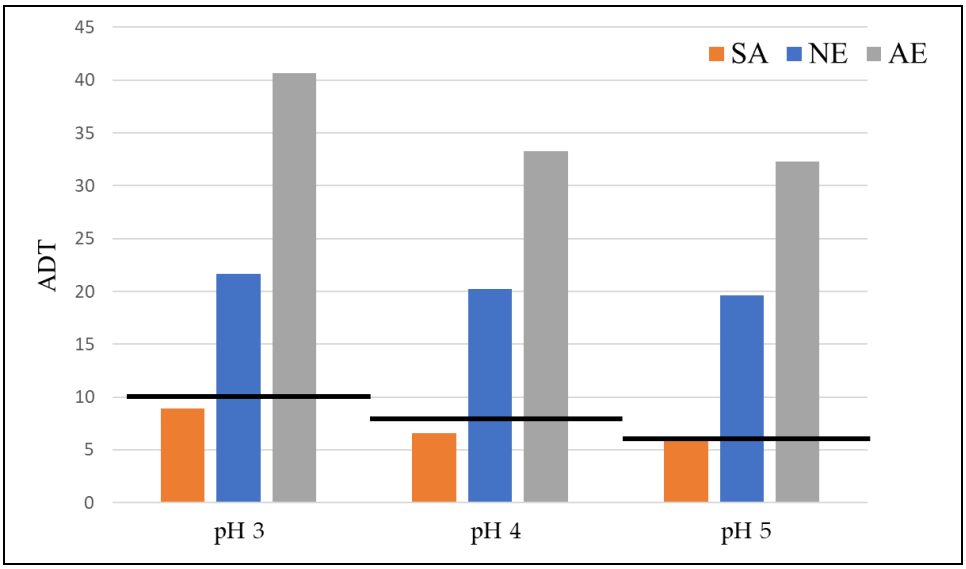


Fig. 5.5 ADT values at pH = 3, 4 and 5 of chromite sand concentrates from South Africa, Neyriz and Aetoraches; black lines represent ADT limits at each pH (labels as in Tab. 5.1)

The lack of linear correlation between $SiO_2$ content and acid demand values can be explained by the different reactivity of silicate minerals in the acid environment of the test. All the three chromite sands have been enriched through gravity methods, and their silica content ranges from 0.70 wt% (SA) to 7.7 wt% (AE). Acid Demand tests on pure silicate samples of chlorite, serpentine, olivine, pyroxene (Tab. 5.4) at a fixed silica content of 2.5% show a very different reactivity of the minerals (Fig. 5.6). For all pH values, the orthopyroxene gangue respects ADT limits, classifying as the least reactive mineral and, therefore, the best one (Fig. 5.6). This explains why South African sand is the most performing one, as its gangue is mostly composed of pyroxenes. Olivine performs worse than orthopyroxene, but exceeds the ADT limits at pH 3, 4 and 5 by a tiny amount. The worst performing silicate sands are chlorite (CHL) and serpentine (SRP), which are highly above the ADT limits.

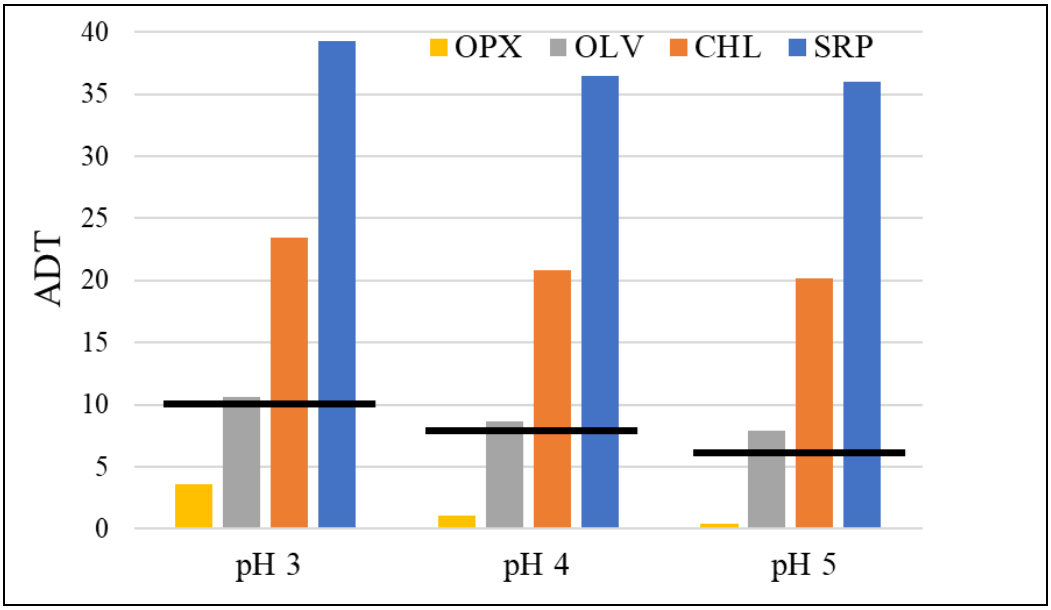


Fig. 5.6 ADT values at pH = 3, 4 and 5 for pure silicate gangues (orthopyroxene, olivine, chlorite and serpentine).

Acid demand tests performed on two mixed serpentine-olivine samples at 2.5% $SiO_2$ content (Tab. 5.4, Fig. 5.7), show ADT values comprised between those of pure olivine and pure serpentine. Sample RI-2 performs slightly better than sample AE-2, due to a lower degree of serpentinization. Both samples exceed the ADT limits for all three pH, however, they show values more similar to pure olivine than to pure serpentine. This means that the degree of serpentinization in the two samples is very low, and that a better constrain of the behavior of serpentine and olivine sands during Acid Demand tests could be pivotal for the production of chromite foundry sands from ophiolite chromitites.

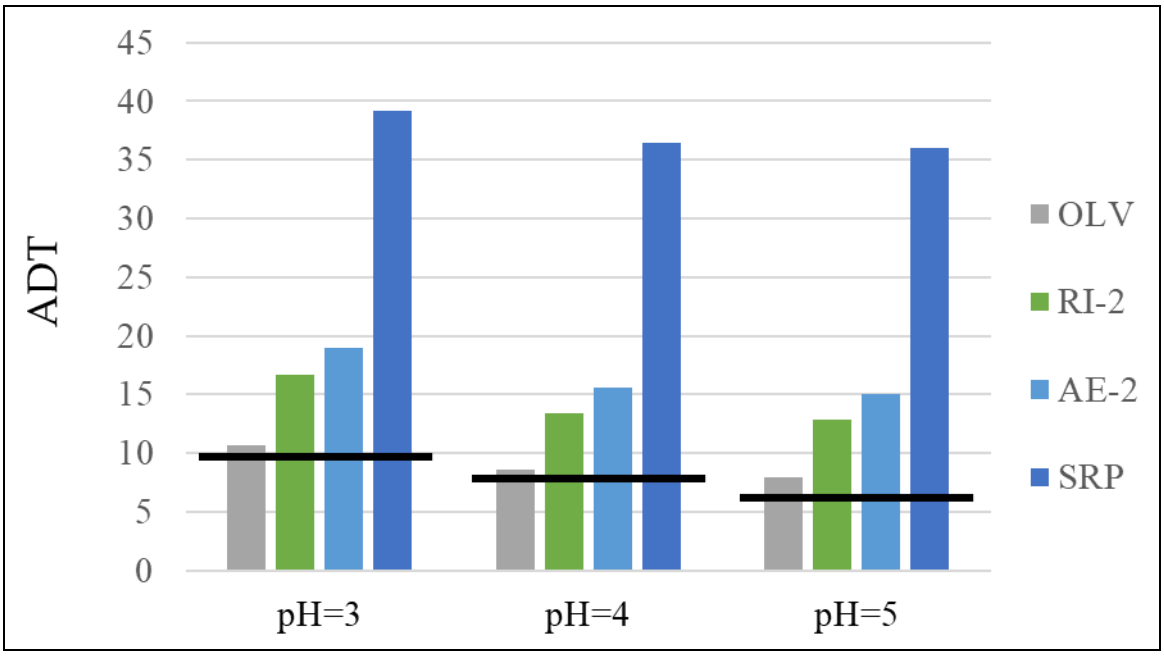


Fig. 5.7. ADT values at pH = 3, 4, and 5 for mixed olivine-serpentine silicate gangues in Aetoraches and Rizo.

The study of silicate mineralogy has a direct impact on the beneficiation processes of chromite sands. To produce chromite sand of foundry quality, enrichment plants must set machinery based on the mineralogy of the silicate assemblage. Orthopyroxene, a common silicate within layered intrusion chromite deposits, always respects the ADT limit for silica contents lower than 2.5%, so that when the sand meeting the $SiO_2$ quality parameter is produced, it will always meet also the ADT limits.

The results show that ophiolite chromites dominated by a chlorite or serpentine silicate assemblage cannot be enriched till meeting the foundry sand quality parameters. Hence, the possibility to produce foundry sand from these chromite deposits is limited to those with an olivine or mixed olivine-serpentine silicate assemblage that is quite common. In the following section, we focus on the impact of olivine and serpentine contents on the ADT value, in order to assess the maximum serpentine content of olivine-serpentine chromite sands that can be successfully enriched till foundry sand quality. For this purpose, two additional tests were performed (Tab. 5.5):

i. Olivine and serpentine sand mixes at different proportions (25%, 50% and 75% of serpentine) maintaining a fixed 2.5% of $SiO_2$, in order to simulate the behavior of partially serpentinized sands.
ii. Pure olivine and pure serpentine sands at $SiO_2$ contents lower than 2.5% (1.875%, 1.25% and 0.625%).

Mixed olivine-serpentine samples show ADT values (Fig. 5.8) comprised between the two pure end-members.

Tab. 5.5 Acid demand test results of mixed olivine-serpentine sands at fixed silica content and of pure olivine and pure serpentine sands at different silica contents.

| Sample | SERP (g) | OLV (g) | $SiO_2$% | Initial pH | ADT pH3 | ADT pH4 | ADT pH5 |
|---|---|---|---|---|---|---|---|
| 25-75 SRP-OLV | 0.76 | 2.28 | 2.50 | 2.03 | 30.5 | 27.2 | 26.6 |
| 50-50 SRP-OLV | 1.52 | 1.52 | 2.50 | 2.11 | 33.5 | 30.7 | 30.2 |
| 75-25 SRP-OLV | 2.22 | 0.74 | 2.50 | 2.15 | 36.2 | 33.3 | 32.6 |
| 25-SRP | 0.72 | 0 | 0.63 | 1.65 | 24.4 | 22.2 | 21.6 |
| 50-SRP | 1.44 | 0 | 1.25 | 1.83 | 32.1 | 29.7 | 29.0 |
| 75-SRP | 2.16 | 0 | 1.88 | 1.88 | 36.9 | 34.7 | 34.3 |
| 25-OLV | 0 | 0.80 | 0.63 | 1.45 | 5.9 | 4.3 | 4.0 |
| 50-OLV | 0 | 1.60 | 1.25 | 1.48 | 7.8 | 6.1 | 5.8 |
| 75-OLV | 0 | 2.40 | 1.88 | 1.46 | 8.7 | 6.9 | 6.4 |

* For mixed olivine-serpentine, an average between antigorite and forsterite $SiO_2$ contents has been calculated

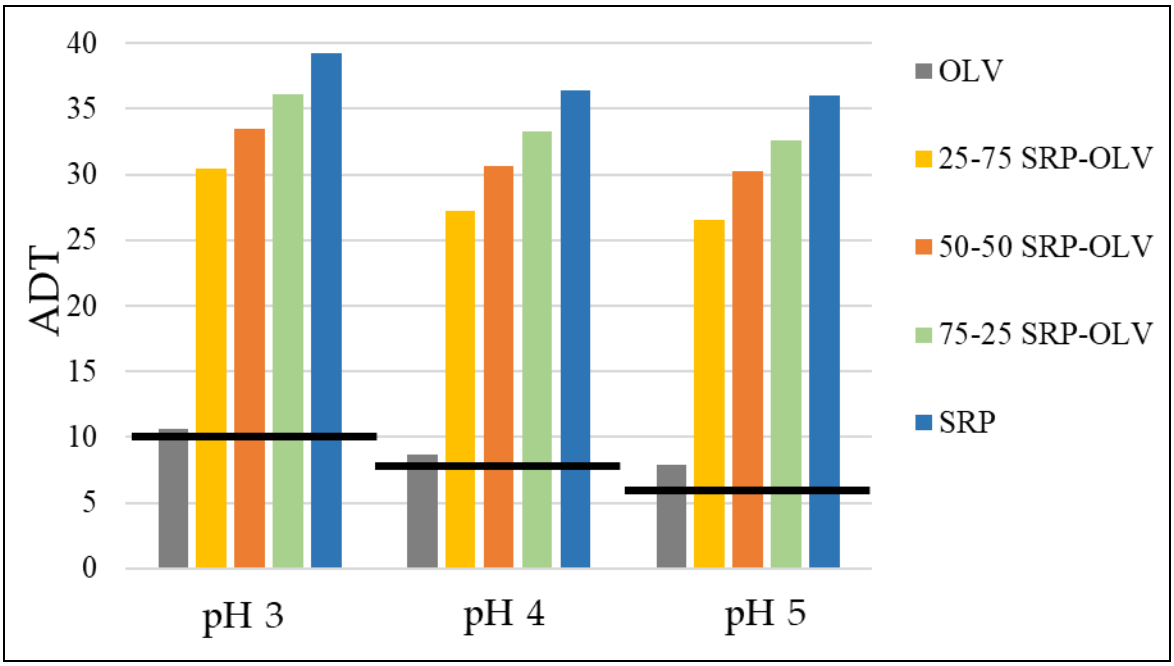


Fig. 5.8. ADT values at pH = 3, 4 and 5 for mixed serpentine and olivine silicate assemblage (labels as in Tab. 1 and 5).

ADT and serpentine modal contents (Fig. 5.9A) are not in a linear correlation, and even a small amount of serpentine leads to high ADT values, so that the mix serpentine-olivine at 25% serpentine fraction has ADT values more similar to the ones of pure serpentine than of pure olivine. The highest SiO2 contents that can result in a sand meeting the Acid Demand quality parameter can be calculated separately for olivine and serpentine from results shown in Fig. 5.9B.

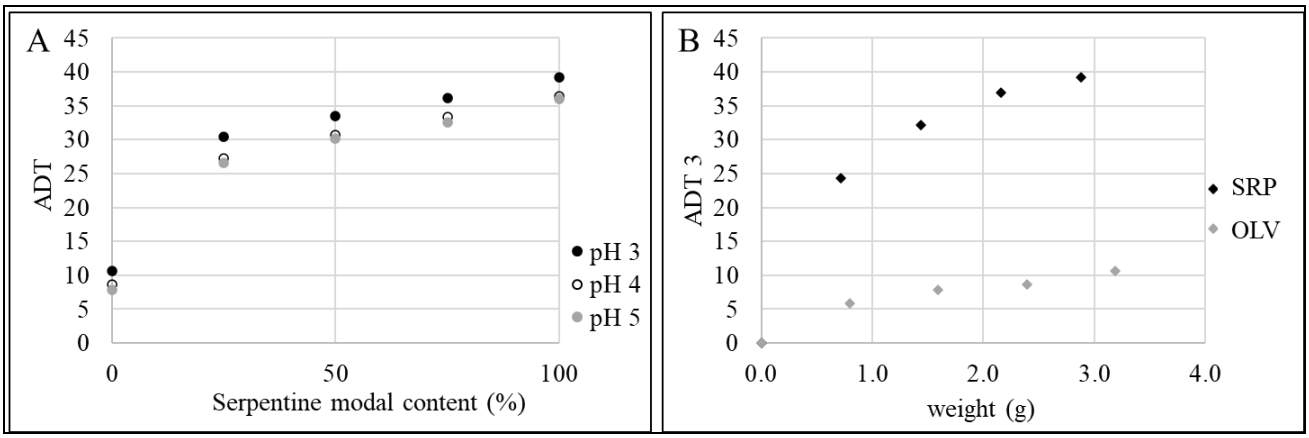


Fig. 5.9 A) ADT vs serpentine modal content in a mix of serpentine and olivine sands at $SiO_2$ 2.5%, at pH = 3, 4 and 5; B) ADT at pH = 3 vs weight of material (g) for pure olivine and serpentine sands.

The ADT parameter depends on the initial pH of the sand. As serpentine and olivine behave as bases, the initial pH is calculated from the equation of base dissociation constant:

$$pH_i = 14 + \frac{1}{2}(\log_{10} Kb + \log_{10} Cb)$$

Where:

pHi = initial pH of the sand

Kb = base dissociation constant

Cb = concentration of the base in the solution

As a consequence, ADT must be correlated by a base10 logarithmic function to the amount of silicate added during acid demand test. Due to the fact that in absence of silicates the ADT value is necessarily 0, the logarithmic curve was transposed by factor 1 on the x axis as a mathematical artifact necessary to get finite values. ADT and the base10 logarithm of w + 1, where w is the amount of silicate added (serpentine or olivine) have been then plotted (Fig. 5.10) and show a linear correlation with high $r^2$ values. The ADT and the amount of silicate are correlated through the following relation:

$$ADT = k * \log_{10}(w + 1)$$

Where:

k = coefficient of proportionality derived from the correlation;

w = amount of added silicate.

In order to estimate the amount of silicate that corresponds to the ADT3 threshold, we can resolve the relation for ADT = 10. The results are 0.36 g of serpentine and 2.70 g of olivine. Finally, from the mass of silicate we can calculate through the $SiO_2$ content of the mineral, the corresponding $SiO_2$ content of the chromite sand, that is 0.31% for serpentine and 2.11% for olivine.

These results mean that an ophiolite chromite with an only serpentine silicate assemblage should be purified to a final $SiO_2$ content as low as 0.31% to reach the ADT quality threshold, while an ophiolite chromite with an only olivine silicate assemblage should be purified to a much more easily affordable final $SiO_2$ content of 2.11% to reach the ADT quality threshold. For chromite sands with mixed olivine-serpentine assemblage, the serpentine works as a limiting factor as it is much more reactive than olivine, so it should anyway never exceed 0.36 g within the 50 g of chromite sand used in the test. That is less than 0.72% of serpentine in the sand, independently of the olivine content.

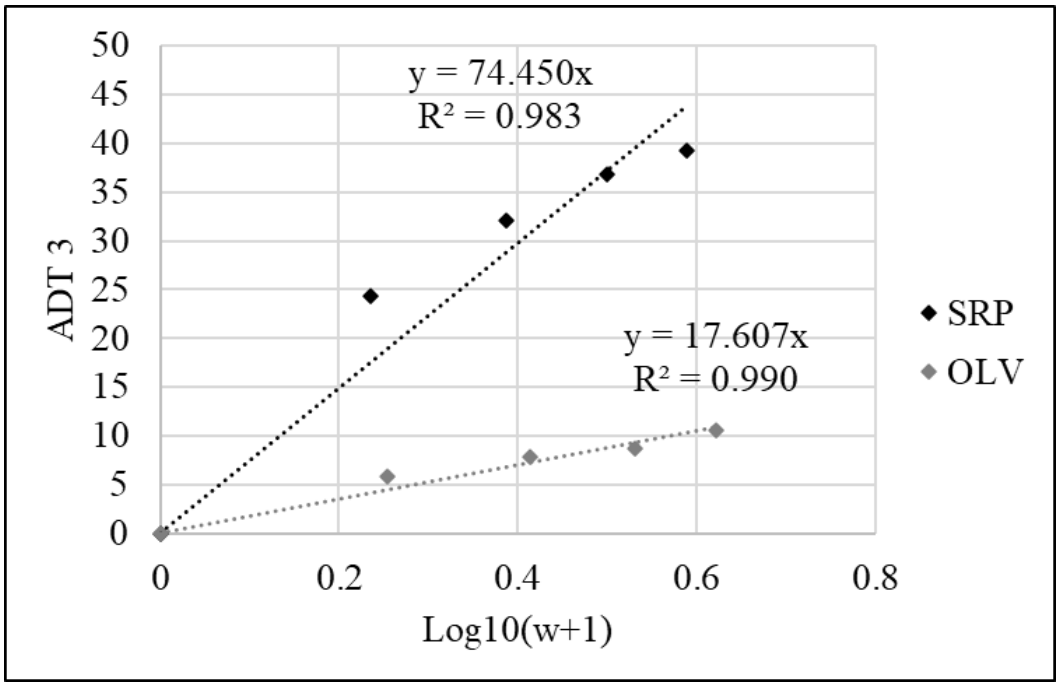


Fig. 5.10. Linear correlation between ADT values at pH = 3 and log10 of the weight (g) of material used for the tests.

## 5.5. Conclusion

Chromite foundry sand is a crucial commodity, irreplaceable in high demanding casting of steel and metals. The identification of new possible sources for the production of such commodity can dramatically decrease the criticality of chromite raw material. Ophiolite chromite concentrates do not meet the required quality parameters, and also refractory sand produced in Iran from ophiolite chromites does not respect the most critical parameter, that is Acid Demand value. This is due to the different mineralogy of the silicate assemblage of these sands when compared to South African ones. The presence of serpentine, even in small amounts, due to its high reactivity with acid, precludes the possibility to get acid demand values respecting the quality threshold. On the other hand, olivine, the other most common silicate in ophiolite chromites shows a performance close to that of

orthopyroxene, the best performing silicate, abundant in layered intrusion chromites, like those of South Africa.

The present work shows that the production of chromite foundry sands starting from ophiolite chromites is possible, but only for those where the silicate impurities assemblage is dominated by olivine, with very low or negligible amounts of serpentine. Two examples of ophiolite chromitites with a low degree of serpentinization are reported in the work. Both Aetoraches and Rizo exceed the Acid Demand thresholds by a low amount, and an affordable degree of purification could lower the ADT values and make them suitable for the foundry market.

# CHAPTER 6: Final Remarks

Chromitite layers, pods and lenses within ophiolite ultramafic rocks are major industrial chromium sources and contain sub-economic PGE enrichments. The study of altered chromitites can give us important insights on their evolution, as well as on the behavior of precious metals in contact with altering fluids.

In the present work, the three main post-magmatic processes affecting podiform chromitites have been addressed: high-T subsolidus re-equilibration of olivine and spinel, low-T circulation of high $fS_2$ and $fO_2$ chloritizing fluids and low-T circulation of low $fS_2$ and $fO_2$ serpentinizing fluids. The results are the following:

- Olivine and chromite diffusivity patterns, developed during subsolidus re-equilibration, are useful tools for the reconstruction of chromitites thermal history down to 650 °C. A new approach using an exponential function to model XMg variations with the distance from the grain boundary has been developed, and produced reliable primary and re-equilibrated XMg values. These values can be used to infer re-equilibrated and primary temperatures, as well as to estimate the cooling rates of the olivine- chromite-bearing rocks. The approach, developed starting from the case study of Finero subcontinental mantle has been used with good results also for two partially serpentinized ophiolite chromitites, Iballe and Nea Roda.
- Low-T circulating fluids at high $fS_2$ and $fO_2$ conditions can alter primary mineralogical assemblages and induce crystallization of secondary minerals, as observed within the ophiolite chromitite of Gomati and Nea Roda. The high sulfur and oxygen fugacities favor the replacement of primary silicates by Cr-chlorite, and the formation of ferrian chromitized rims. Primary BMM are altered and replaced by secondary ones, but no alloys are generated, as they are not stable under these conditions. PGM are not affected by the circulating fluids, and retain their magmatic imprint, as also confirmed by primary mantle-normalized PGE patterns, which present a peak for Ru.
- Low-T circulating fluids at low $fS_2$ and $fO_2$ conditions are the most common within ophiolite chromitites, and are responsible for the major altering process in this kind of deposit: serpentinization. The low sulfur and oxygen fugacities favor the replacement of primary silicates by serpentine, and the formation of magnetite. A distinctive feature of serpentinization is the replacement of primary BMM with base metal alloys, as well as with secondary sulfides. PGM are also highly affected by the serpentinizing conditions, and tend to lose sulfur and be transformed into alloys. This generates a remobilization of PGE into the circulating fluids. The remobilization, estimated within the Abdasht-Soghan complex through a mass balance calculation on a partially desulfurized laurite grain, occurred at two different scales. Os was the first element to exit laurite

lattice to form Os-rich alloys. However, the mass balance calculation showed that the PGM mostly lost Ru. This implied a second, larger scale remobilization where Ru acted as the most soluble PGE in the desulfurizing fluids. The mobility of PGE into the fluids hence follows the order: Ru>>Os>>Ir. This is confirmed by PGE patterns, which present a double peak, for Ru and Os.

Post-magmatic processes have a strong impact on the economic assessment of chromite ore deposits. In this study we focused on the quality parameters of a chromite sand for the foundry industry. Foundry chromite sands are the most valuable chromite commodity, and are currently not produced within the EU. The major producer of top-quality chromite foundry sands is South Africa. In order to find alternative sources of this critical commodity, we tested the behavior of two industrial ophiolite chromite sands from Iran and Greece, enriched through shaking tables and spirals:

- Ophiolite chromite sands do not meet the most critical quality parameter, the Acid Demand, due to the mineralogy of the silicate impurities. The presence of serpentine, a highly reactive mineral widespread in ophiolite chromitites, lowers the performance of chromite sands. On the contrary, olivine, the second most common silicate mineral in podiform chromitites, shows good performance. The present work shows that the production of chromite foundry sands starting from ophiolite chromites is possible, but only for those where the silicate impurities is dominated by olivine, with negligible or very low amounts of serpentine. Two examples of ophiolite chromitites with a low degree of serpentinization within the EU are Aetoraches and Rizo deposits, in Greece. Their chromite sands exceed the Acid Demand thresholds by a low amount, and an affordable degree of purification could lower the ADT values and make them suitable for the foundry market.

The remobilization of PGE and other precious metals during the circulation of fluids is a topic that requires further studies. The mechanisms that trap PGE both during the magmatic and post-magmatic stages are still largely unknown, but could be pivotal for future exploration. The present study highlighted interesting PGE concentrations within base metal minerals, and further studies are required in order to have a complete view of the phases that can host PGE and hence play a role in their remobilization and reconcentration. In particular, the enrichment in Pt and Pd of some secondary BMM suggests once again the importance of investigating possible PGE-bearing circulating fluids.

The results obtained in the evaluation of ophiolite chromitite for the foundry industry are also a first step for future studies. Chromium is a commodity which stands between the line of critical and non-critical material for the EU, and chromite sands of foundry quality are currently not produced in Europe. However, our results demonstrate that ophiolite chromitites can meet the quality parameters under certain circumstances, and therefore a more detailed assessment of partially serpentinized deposits could lead to the production of this valuable commodity in Europe.

# Acknowledgements

First of all, I would like to thank my PhD supervisor Prof. Giovanni Grieco, for his constant support during my research and for his presence and precious advices. I could not have hoped for a better mentor during these three years.

Many thanks also to Dr. Evangelos Tzamos, Dr. Federica Zaccarini, Dr. Annie Rassios, and Alireza Eslami, who helped me during all the stages of my research. I hope we can keep on working together for future projects.

Special thanks go to my past and present PhD fellows and colleagues as well as to all the people of the "kitchen", for giving me advices and make lunch, coffee times and drinks memorable.

I would like to thank the many people that made my Erasmus period in Leoben an amazing experience: the "Geology Dream Team Leoben", for all the Schnitzel we ate while discussing science, and all the Erasmus friends. I will never forget those three months.

I want to thank all my friends from home, university and also abroad, with whom I spent beautiful moments.

Last, but not least, I would like to thank my family and my boyfriend Stefano, for their continuous support during all these years. I couldn't have done this without you.

# References


Agiorgitis, G., Wolf, R., 1978. Aspects of osmium, ruthenium and iridium contents in some Greek chromites. Chem. Geol. 23, 267–272. https://doi.org/10.1016/0009-2541(78)90082-7

Ahmadipour, H., Sabzehei, M., Emami, M., Whitechurch, H., Rastad, E., 2003. Soghan complex as an evidence for paleospreading center and mantle diapirism in Sanandaj-Sirjan zone (south-east Iran). J. Sci. Islam. Repub. Iran 14, 157–172.

Ahmed, A., Arai, S., 2002. Unexpectedly high-PGE chromitite from the deeper mantle section of the northern Oman ophiolite and its tectonic implications. Contrib. to Mineral. Petrol. 143, 263–278. https://doi.org/10.1007/s00410-002-0347-8

Ahmed, A.H., 2007. Diversity of platinum-group minerals in podiform chromitites of the late Proterozoic ophiolite, Eastern Desert, Egypt: Genetic implications. Ore Geol. Rev. 32, 1–19. https://doi.org/10.1016/j.oregeorev.2006.05.008

Alard, O., Griffin, W.L., Lorand, J.P., Jackson, S.E., O'Reilly, S.Y., 2000. Non-chondritic distribution of the highly siderophile elements in mantle sulphides. Nature 407, 891–894. https://doi.org/10.1038/35038049

Alavi, M., 1994. Tectonics of the zagros orogenic belt of iran: new data and interpretations. Tectonophysics 229, 211–238. https://doi.org/10.1016/0040-1951(94)90030-2

Anders, B., Reischmann, T., Kostopoulos, D., 2007. Zircon geochronology of basement rocks from the Pelagonian Zone, Greece: constraints on the pre-Alpine evolution of the westernmost Internal Hellenides. Int. J. Earth Sci. 96, 639–661. https://doi.org/10.1007/s00531-006-0121-7

Anders, B., Reischmann, T., Kostopoulos, D., Poller, U., 2006. The oldest rocks of Greece: first evidence for a Precambrian terrane within the Pelagonian Zone. Geol. Mag. 143, 41–58. https://doi.org/10.1017/S0016756805001111

Andrews, D.R.A., Brenan, J.M., 2002. Phase-equilibrium constraints on the magmatic origin of laurite + Ru-Os-Ir alloy. Can. Mineral. 40, 1705–1716. https://doi.org/10.2113/gscanmin.40.6.1705

Arai, S., 1997. Control of wall-rock composition on the formation of podiform chromitites as a result of magma/peridotite interaction. Shigen-Chishitsu 47, 177–187.

Arai, S., Prichard, H.M., Matsumoto, I., Fisher, P.C., 1999. Platinum-Group Minerals in Podiform Chromitite from the Kamuikotan Zone, Hokkaido, Northern Japan. Resour. Geol. 49, 39–47. https://doi.org/10.1111/j.1751-3928.1999.tb00030.x

Arai, S., Uesugi, J., Ahmed, A.H., 2004. Upper crustal podiform chromitite from the northern Oman ophiolite as the stratigraphically shallowest chromitite in ophiolite and its implication for Cr concentration. Contrib. to Mineral. Petrol. 147, 145–154. https://doi.org/10.1007/s00410-004-0552-8

Arai, S., Yurimoto, H., 1994. Podiform chromitites of the Tari-Misaka ultramafic complex, southwestern Japan, as mantle-melt interaction products. Econ. Geol. 89, 1279–1288. https://doi.org/10.2113/gsecongeo.89.6.1279

Arvin, M., Pan, Y., Dargahi, S., Malekizadeh, A., Babaei, A., 2007. Petrochemistry of the Siah-Kuh granitoid stock southwest of Kerman, Iran: Implications for initiation of Neotethys subduction. J. Asian Earth Sci. 30, 474–489. https://doi.org/10.1016/j.jseaes.2007.01.001

Asvesta, A., Dimitriadis, S., 2010. Facies architecture of a Triassic rift-related Silicic Volcano-Sedimentary succession in the Tethyan realm, Peonias subzone, Vardar (Axios) Zone, northern Greece; Regional implications. J. Volcanol. Geotherm. Res. 193, 245–269. https://doi.org/10.1016/j.jvolgeores.2010.04.005

Augé, T., 1987. Chromite deposits in the northern Oman ophiolite: Mineralogical constraints. Miner. Depos. 22. https://doi.org/10.1007/BF00204235

Augé, T., 1985. Platinum-group mineral inclusions in ophiolitic chromitite from the Vourinos Complex, Greece. Can. Mineral. 23, 163–171.

Auge, T., Cabri, L.J., Legendre, O., McMahon, G., Cocherie, A., 1999. PGE distribution in base-metal alloys and sulfides of the New Caledonia Ophiolite. Can. Mineral. 37, 1147–1161.

Augé, T., Johan, Z., 1988. Comparative Study of Chromite Deposits from Troodos, Vourinos, North Oman and New Caledonia Ophiolites, in: Mineral Deposits within the European Community. Springer Berlin Heidelberg, Berlin, Heidelberg, pp. 267–288. https://doi.org/10.1007/978-3-642-51858-4_15

Auge, T., Legendre, O., 1994. Platinum-group element oxides from the Pirogues ophiolitic mineralization, New Caledonia; origin and significance. Econ. Geol. 89, 1454–1468. https://doi.org/10.2113/gsecongeo.89.7.1454

Baccolo, L.P., Grieco, G., Bussolesi, M., Eslami, A., 2019. Mineralogical study of rodingitized microgabbros and associated chromitite seams from the Nain ophiolite, Central Iran, in: EGU General Assembly.

Bach, W., Garrido, C.J., Paulick, H., Harvey, J., Rosner, M., 2004. Seawater-peridotite interactions: First insights from ODP Leg 209, MAR 15°N. Geochemistry, Geophys. Geosystems 5, n/a-n/a. https://doi.org/10.1029/2004GC000744

Bach, W., Paulick, H., Garrido, C.J., Ildefonse, B., Meurer, W.P., Humphris, S.E., 2006. Unraveling the sequence of serpentinization reactions: petrography, mineral chemistry, and petrophysics of serpentinites from MAR 15°N (ODP Leg 209, Site 1274). Geophys. Res. Lett. 33, L13306. https://doi.org/10.1029/2006GL025681

Badanina, I.Y., Malitch, K.N., Belousova, A., 2013. U-Pb and Hf isotope characteristics of zircon from chromites at Finero, in: Goldschmidt Abstracts 2013. Mineralogical Magazine. p. 639. https://doi.org/10.1180/minmag.2013.077.5.8

Ballhaus, C., 1998. Origin of podiform chromite deposits by magma mingling. Earth Planet. Sci. Lett. 156, 185–193. https://doi.org/http://dx.doi.org/10.1016/S0012-821X(98)00005-3

Ballhaus, C., Berry, R.F., Green, D.H., 1991. High pressure experimental calibration of the olivine-orthopyroxene-spinel oxygen geobarometer: implications for the oxidation state of the upper mantle. Contrib. to Mineral. Petrol. 107, 27–40.

Ballhaus, C., Bockrath, C., Wohlgemuth-Ueberwasser, C., Laurenz, V., Berndt, J., 2006. Fractionation of the noble metals by physical processes. Contrib. to Mineral. Petrol. 152, 667–684. https://doi.org/10.1007/s00410-006-0126-z

Barin, I., 1995. Thermochemical Data of Pure Substances, VCH Publishers, New York, NY.

Barkov, A.Y., Bindi, L., Tamura, N., Shvedov, G.I., Winkler, B., Stan, C. V., Morgenroth, W., Martin, R.F., Zaccarini, F., Stanley, C.J., 2019. Ognitite, NiBiTe, a new mineral species, and Co-rich maucherite from the Ognit ultramafic complex, Eastern Sayans, Russia. Mineral. Mag. 83, 695–703. https://doi.org/10.1180/mgm.2019.31

Barnes, S.-J., Cox, R.A., Zientek, M.L., 2006. Platinum-group element, Gold, Silver and Base Metal distribution in compositionally zoned sulfide droplets from the Medvezky Creek Mine, Noril'sk, Russia. Contrib. to Mineral. Petrol. 152, 187–200. https://doi.org/10.1007/s00410-006-0100-9

Barnes, S.J., Roeder, P.L., 2001. The Range of Spinel Compositions in Terrestrial Mafic and Ultramafic Rocks. J. Petrol. 42, 2279–2302. https://doi.org/10.1093/petrology/42.12.2279

Bazylev, B.A., Ledneva, G. V., Ishiwatari, A., 2013. High-pressure ultramafics in the lower crustal rocks of the Pekul'ney complex, central Chukchi Peninsula. 2. Internal structure of blocks and ultramafic bodies, geologic and geodynamic setting of rock formation. Petrology 21, 336–350. https://doi.org/10.1134/S0869591113040024

Beaufort, D., Rigault, C., Billon, S., Billault, V., Inoue, A., Inoue, S., Patrier, P., 2015. Chlorite and chloritization processes through mixed-layer mineral series in low-temperature geological systems – a review. Clay Miner. 50, 497–523. https://doi.org/10.1180/claymin.2015.050.4.06

Bébien, J., Dimo-Lahitte, A., Vergély, P., Insergueix-Filippi, D., Dupeyrat, L., 2000. Albanian ophiolites. I - magmatic and metamorphic processes associated with the initiation of a subduction. Ofioliti 25, 39–45.

Beccaluva, L., Coltorti, M., Premti, I., Saccani, E., Siena, F., Zeda, O., 1994. Mid-ocean ridge and suprasubduction affinities in the ophilitic belts from Albania. Ofioliti 19, 77–96.

Beccaluva, L., Coltorti, M., Saccani, E., Siena, F., 2005. Magma generation and crustal accretion as evidenced by supra-subduction ophiolites of the Albanide-Hellenide Subpelagonian zone. Isl. Arc 14, 551–563. https://doi.org/10.1111/j.1440-1738.2005.00483.x

Bédard, J.H., Hébert, R., 1998. Formation of chromitites by assimilation of crustal pyroxenites and gabbros into peridotitic intrusions: North Arm Mountain massif, Bay of Islands ophiolite, Newfoundland, Canada. J. Geophys. Res. Solid Earth 103, 5165–5184. https://doi.org/10.1029/97JB03291

Bengulur, S., Darwada, H.R., Gurram, K.R., Vundavilli, P.R., 2013. Experimental Studies on Properties of Chromite-based Resin Bonded Sand System. Recent Adv. Robot. Aeronaut. Mech. Eng. 230–238.

Berberian, M., King, G.C.P., 1981. Towards a paleogeography and tectonic evolution of Iran. Can. J. Earth Sci. 18, 210–265. https://doi.org/10.1139/e81-019

Berger, A., Herwegh, M., Schwarz, J.-O., Putlitz, B., 2011. Quantitative analysis of crystal/grain sizes and their distributions in 2D and 3D. J. Struct. Geol. 33, 1751–1763. https://doi.org/10.1016/j.jsg.2011.07.002

Bio Intelligence Service, 2015. Study on Data for a Raw Material System Analysis: Roadmap and Test of the Fully Operational MSA for Raw Materials – Final Report. Eur. Commision.

Bockrath, C., Ballhaus, C., Holzheid, A., 2004. Stabilities of laurite RuS2 and monosulfide liquid solution at magmatic temperature. Chem. Geol. 208, 265–271. https://doi.org/10.1016/j.chemgeo.2004.04.016

Bonazzi, P., Bindi, L., 2019. Dienerite, Ni3As: a mineralogical species to revalidate, in: Congresso SIMP-SGI-SOGEI Parma. p. 65.

Bonev, N., Dilek, Y., 2010. Geochemistry and tectonic significance of proto-ophiolitic metamafic units from the Serbo-Macedonian and western Rhodope massifs (Bulgaria-Greece). Int. Geol. Rev. 52, 298–335. https://doi.org/10.1080/00206810902757214

Bonev, N., Dilek, Y., Hanchar, J.M., Bogdanov, K., Klain, L., 2012. Nd – Sr – Pb isotopic composition and mantle sources of Triassic rift units in the Serbo-Macedonian and the western Rhodope massifs ( Bulgaria – Greece ). Geol. Mag. 149, 146–152. https://doi.org/10.1017/S0016756811000938

Bonev, N., Moritz, R., Borisova, M., Filipov, P., 2018. Therma–volvi–gomati complex of the serbo-macedonian massif, northern Greece: A middle triassic continental margin ophiolite of neotethyan origin. J. Geol. Soc. London. 176, 931–944. https://doi.org/10.1144/jgs2017-130

Bonev, N., Ovtcharova-Schaltegger, M., Moritz, R., Marchev, P., Ulianov, A., 2013. Peri-Gondwanan Ordovician crustal fragments in the high-grade basement of the Eastern Rhodope Massif, Bulgaria: evidence from U-Pb LA-ICP-MS zircon geochronology and geochemistry. Geodin. Acta 26, 207–229. https://doi.org/10.1080/09853111.2013.858942

Borsi, S., Ferrara, G., Mercier, J., 1965. Détermination de l'âge des séries métamorphiques du Massif Serbo-Macédonien au Nord-Est de Thessalonique (Grèce) par les méthodes Rb/Sr et K/Ar. Ann. la Société géologique du Nord 84, 223–225.

Bortolotti, V., Kodra, A., Marroni, M., Mustafa, F., Pandolfi, L., Principi, G., Saccani, E., 1996. Geology and petrology of the ophiolitic sequences in the Mirdita region (Northern Albania). Ofioliti 21.

Bortolotti, V., Marroni, M., Pandolfi, L., Principi, G., 2005. Mesozoic to Tertiary tectonic history of the Mirdita ophiolites, northern Albania. Isl. Arc 14, 471–493. https://doi.org/10.1111/j.1440-1738.2005.00479.x

Boudier, F., Nicolas, A., 1995. Nature of the Moho Transition Zone in the Oman Ophiolite. J. Petrol. 36, 777–796. https://doi.org/10.1093/petrology/36.3.777

Braun, M.G., Kelemen, P.B., 2002. Dunite distribution in the Oman Ophiolite: Implications for melt flux through porous dunite conduits. Geochemistry, Geophys. Geosystems 3, 1–21. https://doi.org/10.1029/2001GC000289

Brenan, J.M., 2008. The Platinum-Group Elements: "Admirably Adapted" for Science and Industry. Elements 4, 227–232. https://doi.org/10.2113/GSELEMENTS.4.4.227

Brenan, J.M., Andrews, D., 2001. High-temperature stability of laurite and Ru-Os-Ir alloy and their role in PGE fractionation in mafic magmas. Can. Mineral. 39, 341–360. https://doi.org/10.2113/gscanmin.39.2.341

British Geological Survey, 2016. World Production of Ferro Alloys (Ferro Chrome) 2010-2014.

British Geological Survey, 2009. Platinum: definition, mineralogy and deposits.

British Geological Survey, Brown, T.J., Idoine, N.E., Raycraft, E.R., Shaw, R.A., Hobbs, S.F., Everett, P., Deady, E.A., Bide, T., 2018. World mineral production 2012-2016.

Bussolesi, M., Grieco, G., Eslami, A., Cavallo, A., 2020a. Ophiolite Chromite Deposits as a New Source for the Production of Refractory Chromite Sands. Sustainability 12, 7096. https://doi.org/10.3390/su12177096

Bussolesi, M., Grieco, G., Tzamos, E., 2019. Olivine–Spinel Diffusivity Patterns in Chromitites and Dunites from the Finero Phlogopite-Peridotite (Ivrea-Verbano Zone, Southern Alps): Implications for the Thermal History of the Massif. Minerals 9, 75. https://doi.org/10.3390/min9020075

Bussolesi, M., Zaccarini, F., Grieco, G., Tzamos, E., 2020b. Rare and new compounds in the Ni-Cu-Sb-As system: first occurrence in the Gomati ophiolite, Greece. Period. di Mineral. 89, 63–76. https://doi.org/https://doi.org/10.2451/2020PM855

Cabri, L.J., 2002. The geology, geochemistry, mineralogy and mineral beneficiation of platinum-group elements. Canadian Institute of Mining Metallurgy and Petroleum.

Cabri, L.J., Laflamme, J.H.G., 1981. Analyses of minerals containing platinum-group elements. Platinum-gr. Elem. Mineral. Geol. Recover. 23, 151–173.

Cabri, L.J., Laflamme, J.H.G., 1976. The mineralogy of the platinum-group elements from some copper-nickel deposits of the Sudbury area, Ontario. Econ. Geol. 71, 1159–1195. https://doi.org/10.2113/gsecongeo.71.7.1159

Campbell, I.H., Naldrett, A.J., 1979. The influence of silicate:sulfide ratios on the geochemistry of magmatic sulfides. Econ. Geol. 74, 1503–1506. https://doi.org/10.2113/gsecongeo.74.6.1503

Carey, P., 2002. Sand/binders/sand preparation and coremaking. Foundry Manag. Technol 130, 39–52.

Cazzaniga, M., 2009. Parametri tessiturali di qualità delle cromiti di Aetoraches e Rizo (complesso di Vourinos, Grecia). University of Milan.

Centrella, S., Putnis, A., Lanari, P., Austrheim, H., 2018. Textural and chemical evolution of pyroxene during hydration and deformation: A consequence of retrograde metamorphism. Lithos 296–299, 245–264. https://doi.org/10.1016/j.lithos.2017.11.002

Chakraborty, K.L., 1968. Mineralogical note on the chrome-chlorite (kämmererite) and chrome-garnet (uvarovite) from the chromite deposits of Kalrangi, Orissa, India. Mineral. Mag. J. Mineral. Soc. 36, 962–965.

https://doi.org/10.1180/minmag.1968.283.036.07

Chamberlain, J.A., 1966. Heazlewoodite and awaruite in serpentinites of the Eastern Townships, Quebec. Can. Mineral. 8, 519–522.

Chou, C.L., 1978. Fractionation of siderophile elements in the Earth's upper mantle. Lunar Planet. Sci. Conf. Proc. 9.

Christodoulou, C., 1980. The Geochemistry of podiform chromite deposits from two ophiolite complexes, Chalkidiki peninsula, Northern Greece. Diss. Durham Univ.

Christy, A.G., 1989. The stability of sapphirine + clinopyroxene: implications for phase relations in the CaO-MgO-Al2O3-SiO2 system under deep-crustal and upper mantle conditions. Contrib. to Mineral. Petrol. 102, 422–428. https://doi.org/10.1007/BF00371085

Cocomazzi, G., Grieco, G., Tartarotti, P., Bussolesi, M., Zaccarini, F., Crispini, L., 2020. The formation of dunite channels within harzburgite in the wadi tayin massif, oman ophiolite: Insights from compositional variability of cr-spinel and olivine in holes ba1b and ba3a, oman drilling project. Minerals 10, 1–17. https://doi.org/10.3390/min10020167

Colás, V., González-Jiménez, J.M., Camprubí, A., Proenza, J.A., Griffin, W.L., Fanlo, I., O'Reilly, S.Y., Gervilla, F., González-Partida, E., 2019. A reappraisal of the metamorphic history of the Tehuitzingo chromitite, Puebla state, Mexico. Int. Geol. Rev. 61, 1706–1727. https://doi.org/10.1080/00206814.2018.1542633

Colás, V., Padrón-Navarta, J.A., González-Jiménez, J.M., Fanlo, I., López Sánchez-Vizcaíno, V., Gervilla, F., Castroviejo, R., 2017. The role of silica in the hydrous metamorphism of chromite. Ore Geol. Rev. 90, 274–286. https://doi.org/10.1016/j.oregeorev.2017.02.025

Coltorti, M., Siena, F., 1984. Mantle tectonite and fractionate peridotite at Finero (Italian Western Alps). NEUES Jahrb. FUR Mineral. 149, 225–244.

Cornelius, N.K., 2008. UHP metamorphic rocks of the Eastern Rhodope Massif, NE Greece: new constraints from petrology, geochemistry and zircon ages, in: PhD Thesis, University of Mainz, Germany.

Dai, J.-G., Wang, C.-S., Hébert, R., Santosh, M., Li, Y.-L., Xu, J.-Y., 2011. Petrology and geochemistry of peridotites in the Zhongba ophiolite, Yarlung Zangbo Suture Zone: Implications for the Early Cretaceous intra-oceanic subduction zone within the Neo-Tethys. Chem. Geol. 288, 133–148. https://doi.org/10.1016/j.chemgeo.2011.07.011

De Bono, A., Martini, R., Zaninetti, L., Hirsch, F., Stampfli, G.M., Vavassis, I., 2001. Permo-Triassic stratigraphy of the pelagonian zone in central Evia island (Greece). Eclogae Geol. Helv. 94, 289–311.

Deloitte Sustainability, British Geological Survey, Bureau de Recherches Géologiques et Minières, Netherlands Organisation for Applied Scientific Research, 2017a. Study on the review of the list of Critical Raw Materials: Criticality Assessment, Publications Office of the European Union. https://doi.org/https://doi.org/10.2873/876644

Deloitte Sustainability, Survey, B.G., Minières, B. de R.G. et, Research, N.O. for A.S., 2017b. Study on the review of the list of Critical Raw Materials - Critical Raw Materials Factsheets, European Commission. https://doi.org/10.2873/876644

Dilek, Y., Furnes, H., Shallo, M., 2008. Geochemistry of the Jurassic Mirdita Ophiolite (Albania) and the MORB to SSZ evolution of a marginal basin oceanic crust. Lithos 100, 174–209. https://doi.org/10.1016/j.lithos.2007.06.026

Dilek, Y., Furnes, H., Shallo, M., 2007. Suprasubduction zone ophiolite formation along the periphery of Mesozoic Gondwana. Gondwana Res. 11, 453–475. https://doi.org/10.1016/j.gr.2007.01.005

Dilek, Y., Shallo, M., Furnes, H., 2005. Rift-Drift, Seafloor Spreading, and Subduction Tectonics of Albanian Ophiolites. Int. Geol. Rev. 47, 147–176. https://doi.org/10.2747/0020-6814.47.2.147

Dimitriadis, S., Asvesta, A., 1993. Sedimentation and magmatism related to the Triassic rifting and later events in the

Vardar–Axios zone. Bull. Geol. Soc. Greece 28, 149–168.

Dixon, J.E., Dimitriadis, S., 1984. Metamorphosed ophiolitic rocks from the Serbo-Macedonian Massif, near Lake Volvi, north-east Greece. Geol. Soc. London, Spec. Publ. 17, 603–618.

Dohmen, R., Chakraborty, S., 2007. Fe-Mg diffusion in olivine II: Point defect chemistry, change of diffusion mechanisms and a model for calculation of diffusion coefficients in natural olivine. Phys. Chem. Miner. 34, 409–430. https://doi.org/10.1007/s00269-007-0158-6

Eckstrand, O.R., 1975. The Dumont serpentinite; a model for control of nickeliferous opaque mineral assemblages by alteration reactions in ultramafic rocks. Econ. Geol. 70, 183–201. https://doi.org/10.2113/gsecongeo.70.1.183

Economou-Eliopoulos, M., 2007. On the origin of the PGE-enrichment in chromitites associated with ophiolite complexes: The case of Skyros island, Greece. 9th SGA Meet. Andrew, CJ, Borg, G., Eds 1611–1614.

Economou-Eliopoulos, M., 1996. Platinum-group element distribution in chromite ores from ophiolite complexes : implications for their exploration. Ore Geol. Rev. 11, 363–381. https://doi.org/10.1016/S0169-1368(96)00008-X

Economou, M., 1984. On the chemical composition of the chromite ores from the Chalkidiki peninsula, Greece. Ofioliti 123–134.

Economou, M., Dimou, E., Economou, G., Migiros, G., Vacondios, I., 1986. Chromite deposits of Greece. Chromites UNESCÓS IGCP-197 Proj. Metallog. ophiolites 129–159.

Engi, M., 1983. Equilibria involving Al-Cr spinel: Mg-Fe exchange with olivine. Experiments, thermodynamic analysis, and consequences for geothermometry. Am. J. Sci.

Ente Nazionale di Unificazione, 1976. UNI462800.

Eslami, A., Grieco, G., Montanini, A., Cavallo, A., Arai, L.E., Szabo, C., Marchesi, C., 2018. Mineralogy of Cu-rich Hydrothermally Altered Pyroxenites in the Cheshmeh-Bid Chromitite Deposit, Khajeh-Jamali Ophiolitic Massifs, Iran: a First Report. 3rd Eur. Mantle Work. Pavia 42.

European Commission, 2017. Study on the review of the list of Critical Raw Materials: Non-critical Raw Materials Factsheets. https://doi.org/10.2873/876644

European Commission, 2014. Report on Critical Raw Materials for the Eu Critical Raw Materials Profiles. Eur. Commision 1–205. https://doi.org/Ref. Ares(2015)1819595 - 29/04/2015

Eurostat, 2016. International Trade Easy Comext Database [WWW Document]. URL http://epp.eurostat.ec.europa.eu/newxtweb/

Evans, B.W., 2004. The Serpentinite Multisystem Revisited: Chrysotile Is Metastable. Int. Geol. Rev. 46, 479–506. https://doi.org/10.2747/0020-6814.46.6.479

Exley, R.A., Sills, J.D., Smith, J. V., 1982. Geochemistry of micas from the Finero spinel-lherzolite, Italian Alps. Contrib. to Mineral. Petrol. 81, 59–63.

Fabriès, J., 1979. Spinel-olivine geothermometry in peridotites from ultramafic complexes. Contrib. to Mineral. Petrol. 69, 329–336.

Faupl, P., Wagreich, M., 2000. Late Jurassic to Eocene palaeogeography and geodynamic evolution of the Eastern Alps. Mitteilungen der Österreichischen Geol. Gesellschaft 92, 79–94.

Ferriere, J., Baumgartner, P.O., Chanier, F., 2016. The Maliac Ocean: the origin of the Tethyan Hellenic ophiolites. Int. J. Earth Sci. 105, 1941–1963. https://doi.org/10.1007/s00531-016-1303-6

Ferrière, J., Stais, A., 1995. Nouvelle intreprètation de la suture tèthysienne vardarienne d'après l'analyse de sèrie de Pèonias (Vardar oriental, Hellènides internes). Bull. Soc. Geol. Fr. 166, 327–339.

Finnigan, C.S., Brenan, J.M., Mungall, J.E., McDonough, W.F., 2008. Experiments and Models Bearing on the Role of Chromite as a Collector of Platinum Group Minerals by Local Reduction. J. Petrol. 49, 1647–1665. https://doi.org/10.1093/petrology/egn041

Fonseca, R.O.C., Laurenz, V., Mallmann, G., Luguet, A., Hoehne, N., Jochum, K.P., 2012. New constraints on the genesis and long-term stability of Os-rich alloys in the Earth's mantle. Geochim. Cosmochim. Acta 87, 227–242. https://doi.org/10.1016/j.gca.2012.04.002

Freer, R., 1981. Diffusion in silicate minerals and glasses: a data digest and guide to the literature. Contrib. to Mineral. Petrol. 76, 440–454.

Freer, R., O'reilly, W., 1980. The Diffusion of Fe2+ Ions in Spinels with Relevance to the Process of Maghemitization. Mineral. Mag. 43, 889–899. https://doi.org/10.1180/minmag.1980.043.331.12

Frost, B.R., 1985. On the Stability of Sulfides, Oxides, and Native Metals in Serpentinite. J. Petrol. 26, 31–63. https://doi.org/10.1093/petrology/26.1.31

Frost, R.B., Beard, J.S., 2007. On silica activity and serpentinization. J. Petrol. 48, 1351–1368. https://doi.org/10.1093/petrology/egm021

Gartzos, E., Migiros, G., Parcharidis, I., 1990. Chromites from ultramafic rocks of northern Evia (Greece) and their geotectonic significance. Schweizerische Mineral. und Petrogr. Mitteilungen 70, 301–307.

Garuti, G., Bea, F., Zaccarini, F., Montero, P., 2001. Age, Geochemistry and Petrogenesis of the Ultramafic Pipes in the Ivrea Zone, NW Italy. J. Petrol. 42, 433–457. https://doi.org/10.1093/petrology/42.2.433

Garuti, G., Gazzotti, M., Torres-Ruiz, J., 1995. Iridium, rhodium, and platinum sulfides in chromitites from the ultramafic massifs of Finero, Italy, and Ojen, Spain. Can. Mineral. 33, 509–520.

Garuti, G., Naldrett, A.J., Ferrario, A., 1990. Platinum-group elements in magmatic sulfides from the Ivrea Zone; their control by sulfide assimilation and silicate fractionation. Econ. Geol. 85, 328–336. https://doi.org/10.2113/gsecongeo.85.2.328

Garuti, G., Proenza, J.A., Zaccarini, F., 2007. Distribution and mineralogy of platinum-group elements in altered chromitites of the Campo Formoso layered intrusion (Bahia State, Brazil): control by magmatic and hydrothermal processes. Mineral. Petrol. 89, 159–188. https://doi.org/10.1007/s00710-006-0141-9

Garuti, G., Zaccarini, F., 1997. In situ alteration of platinum-group minerals at low temperature: evidence from serpentinised and weathered chromitite of the Vourinos complex, Greece. Can. Mineral. 35, 611–626.

Gentile, A., 2015. Chromite and PGM ores of Soghan and Abdasht mining districts, Kerman province, Iran. University of Milan.

Gervilla, F., Padrón-Navarta, J.A., Kerestedjian, T., Sergeeva, I., González-Jiménez, J.M., Fanlo, I., 2012. Formation of ferrian chromite in podiform chromitites from the Golyamo Kamenyane serpentinite, Eastern Rhodopes, SE Bulgaria: a two-stage process. Contrib. to Mineral. Petrol. 164, 643–657. https://doi.org/10.1007/s00410-012-0763-3

Gervilla, F., Proenza, J.A., Frei, R., González-Jiménez, J.M., Garrido, C.J., Melgarejo, J.C., Meibom, A., Díaz-Martínez, R., Lavaut, W., 2005. Distribution of platinum-group elements and Os isotopes in chromite ores from Mayarí-Baracoa Ophiolitic Belt (eastern Cuba). Contrib. to Mineral. Petrol. 150, 589–607. https://doi.org/10.1007/s00410-005-0039-2

Ghazi, J.M., Moazzen, M., 2015. Geodynamic evolution of the Sanandaj-Sirjan zone, Zagros orogen, Iran. Turkish J. Earth Sci. 24, 513–528.

Ghorbani, M., 2013. Economic geology of Iran (Vol. 581). Mineral deposits and natural resources: Springer.

Ghosh, B., Bhatta, K., 2014. Podiform chromitites in lherzolitic mantle rocks (Andaman ophiolite, India): the role of magma/rock interaction and parental melt composition. Bull. la Société Géologique Fr. 185, 123–130. https://doi.org/10.2113/gssgfbull.185.2.123

Ghosh, B., Morishita, T., 2011. Andradite-uvarovite solid solution from hydrothemally altered podiform chromitite, Rutland Ophiolite, Andaman, India. Can. Mineral. 49, 573–580. https://doi.org/10.3749/canmin.49.2.573

Giovanardi, T., Morishita, T., Zanetti, A., Mazzucchelli, M., Vannucci, R., 2013. Igneous sapphirine as a product of melt-peridotite interactions in the Finero Phlogopite-Peridotite Massif, Western Italian Alps. Eur. J. Mineral. 25, 17–31. https://doi.org/10.1016/j.bbrc.2017.05.005

González-Jiménez, J., Mondal, S., Ghosh, B., Griffin, W., O'Reilly, S., 2020. Re-Os Isotope Systematics of Sulfides in Chromitites and Host Lherzolites of the Andaman Ophiolite, India. Minerals 10, 686. https://doi.org/10.3390/min10080686

Gonzalez-Jimenez, J.M., Auge, T., Gervilla, F., Bailly, L., Proenza, J.A., Griffin, W.L., 2011a. Mineralogy and Geochemistry of Platinum-Rich Chromitites from the Mantle-Crust Transition Zone at Ouen Island, New Caledonia Ophiolite. Can. Mineral. 49, 1549–1569. https://doi.org/10.3749/canmin.49.6.1549

Gonzalez-Jimenez, J.M., Auge, T., Gervilla, F., Bailly, L., Proenza, J.A., Griffin, W.L., 2011b. Mineralogy and geochemistry of platinum-rich chromitites from the mantle-crust transition zone at Ouen Island, New Caledonia ophiolite. Can. Mineral. 49, 1549–1569. https://doi.org/10.3749/canmin.49.6.1549

González-Jiménez, J.M., Gervilla, F., Griffin, W.L., Proenza, J.A., Augé, T., O'Reilly, S.Y., Pearson, N.J., 2012. Os-isotope variability within sulfides from podiform chromitites. Chem. Geol. 291, 224–235. https://doi.org/10.1016/j.chemgeo.2011.10.016

González-Jiménez, J.M., Gervilla, F., Kerestedjian, T., Proenza, J.A., 2010. Alteration of Platinum-Group and Base-Metal Mineral Assemblages in Ophiolite Chromitites from the Dobromirtsi Massif, Rhodope Mountains (Bulgaria). Resour. Geol. 60, 315–334. https://doi.org/10.1111/j.1751-3928.2010.00138.x

González-Jiménez, J.M., Gervilla, F., Proenza, J.A., Kerestedjian, T., Augé, T., Bailly, L., 2009a. Zoning of laurite (RuS2)erlichmanite (OsS2): implications for the origin of PGM in ophiolite chromitites. Eur. J. Mineral. 21, 419–432. https://doi.org/10.1127/0935-1221/2009/0021-1921

González-Jiménez, J.M., Griffin, W.L., Gervilla, F., Proenza, J.A., O'Reilly, S.Y., Pearson, N.J., 2014a. Chromitites in ophiolites: How, where, when, why? Part I. A review and new ideas on the origin and significance of platinum-group minerals. Lithos 189, 127–139. https://doi.org/10.1016/j.lithos.2013.06.016

González-Jiménez, J.M., Griffin, W.L., Proenza, J.A., Gervilla, F., O'Reilly, S.Y., Akbulut, M., Pearson, N.J., Arai, S., 2014b. Chromitites in ophiolites: How, where, when, why? Part II. The crystallization of chromitites. Lithos 189, 140–158. https://doi.org/10.1016/j.lithos.2013.09.008

González-Jiménez, J.M., Kerestedjian, T., Proenza, J.A., Gervilla, F., 2009b. Metamorphism on chromite ores from the Dobromirtsi Ultramafic Massif, Rhodope Mountains (SE Bulgaria). Geol. Acta 7, 413–429. https://doi.org/10.1344/104.000001447

González-Jiménez, J.M., Proenza, J.A., Gervilla, F., Melgarejo, J.C., Blanco-Moreno, J.A., Ruiz-Sánchez, R., Griffin, W.L., 2011. High-Cr and high-Al chromitites from the Sagua de Tánamo district, Mayarí-Cristal ophiolitic massif (eastern Cuba): Constraints on their origin from mineralogy and geochemistry of chromian spinel and platinum-group elements. Lithos 125, 101–121. https://doi.org/10.1016/j.lithos.2011.01.016

Good, D.J., Crocket, J.H., Barnett, R.L., 1997. A secondary clinopyroxene-chlorite-spinel assemblage in clinopyroxenite of

the Mann complex, Abitibi Belt, Ontario: An unusual hydrothermal alteration suite. Mineral. Petrol. 59, 69–90. https://doi.org/10.1007/BF01163062

Greenfield, A.M.R., Ghent, E.D., Russell, J.K., 2013. Geothermobarometry of spinel peridotites from southern British Columbia: implications for the thermal conditions in the upper mantle. Can. J. Earth Sci. 50, 1019–1032. https://doi.org/10.1139/cjes-2013-0037

Grieco, G., Bussolesi, M., Eslami, A., Gentile, A., Cavallo, A., Lian, D., Yang, J., Ghaseminejad, F., 2020. Differential platinum group elements (PGE) re-mobilization at low fS2 in Abdasht and Soghan mafic-ultramafic complexes (Southern Iran). Lithos 366–367, 105523. https://doi.org/10.1016/j.lithos.2020.105523

Grieco, G., Bussolesi, M., Tzamos, E., Rassios, A.E., Kapsiotis, A., 2018. Processes of primary and re-equilibration mineralization affecting chromitite ore geochemistry within the Vourinos ultramafic sequence, Vourinos ophiolite (West Macedonia, Greece). Ore Geol. Rev. 95, 537–551. https://doi.org/10.1016/j.oregeorev.2018.03.009

Grieco, G., Diella, V., Chaplygina, N.L., Savelieva, G.N., 2007. Platinum group elements zoning and mineralogy of chromitites from the cumulate sequence of the Nurali massif (Southern Urals, Russia). Ore Geol. Rev. 30, 257–276. https://doi.org/10.1016/j.oregeorev.2006.03.002

Grieco, G., Ferrario, A., Mathez, E.A., 2004. The effect of metasomatism on the Cr-PGE mineralization in the Finero Complex, Ivrea Zone, Southern Alps. Ore Geol. Rev. 24, 299–314. https://doi.org/10.1016/j.oregeorev.2003.05.004

Grieco, G., Ferrario, A., Von Quadt, A., Koeppel, V., Mathez, E.A., 2001. The Zircon-Bearing Chromitites of the Phlogopite Peridotite of Finero (Ivrea Zone, Southern Alps): Evidence and Geochronology of a Metasomatized Mantle Slab. J. Petrol. 42, 89–101. https://doi.org/10.1093/petrology/42.1.89

Grieco, G., Merlini, A., 2012. Chromite alteration processes within Vourinos ophiolite. Int. J. Earth Sci. 101, 1523–1533. https://doi.org/10.1007/s00531-011-0693-8

Harder, H., Jacobshagen, V., Skala, W., Arafeh, M., Berndsen, J., 1983. Geologische Entwicklung und Struktur der Insel Skyros, Nord-Sporaden, Griechenland.

Hartmann, G., Wedepohl, K.H., 1993. The composition of peridotite tectonites from the Ivrea Complex, northern Italy: residues from melt extraction. Geochim. Cosmochim. Acta 57, 1761–1782.

Helgadóttir, H.M., Franzson, H., Óskarsson, N., Grönvold, K., Steinþórsson, S., 2015. Hydrothermal Alteration of Pyroxene in the Hellisheiði Geothermal Field, SW-Iceland, in: Proceedings World Geothermal Congress.

Henderson, P., 1976. Reaction trends shown by chrome-spinels of the Rhum layered intrusion, in: Chromium: Its Physicochemical Behavior and Petrologic Significance. Elsevier, pp. 1035–1044. https://doi.org/10.1016/B978-0-08-019954-2.50024-X

Henderson, P., Wood, R.J., 1982. Reaction relationships of chrome-spinels in igneous rocks ? further evidence from the layered intrusions of Rhum and Mull, Inner Hebrides, Scotland. Contrib. to Mineral. Petrol. 78, 225–229. https://doi.org/10.1007/BF00398917

Henk, A., Franz, L., Teufel, S., Oncken, O., 1997. Magmatic Underplating, Extension, and Crustal Reequilibration: Insights From A Cross-Section Through the Ivrea Zone and Strona-Ceneri Zone, Northern Italy. J. Geol. 105, 367–378. https://doi.org/10.1086/515932

Heraeus Precious Metals, 2018. Heraeus precious forecast.

Hewitt, D.F., 1948. A partial study of the NiAs-NiSb system. Econ. Geol. 43, 408–417.

Himmerikus, F., Reischmann, T., Kostopoulos, D., 2009. Triassic rift-related meta-granites in the Internal Hellenides, Greece. Geol. Mag. 146, 252–265. https://doi.org/10.1017/S001675680800592X

Holwell, D.A., McDonald, I., 2007. Distribution of platinum-group elements in the Platreef at Overysel, northern Bushveld Complex: a combined PGM and LA-ICP-MS study. Contrib. to Mineral. Petrol. 154, 171–190. https://doi.org/10.1007/s00410-007-0185-9

Hynes, A.J., Nisbet, E.G., Smith, A.G., Welland, M.J.P., Rex, D.C., 1972. Spreading and emplacement ages of some ophiolites in the Othris region (eastern central Greece). Zeitschrift der Dtsch. Geol. Gesellschaft 455–468.

Ibrahim, M., 2015. An Overview of the Albanian Ophiolite and Related Ore Minerals. Acta Geol. Sin. 2.

IGME, 1978. Geological map of Greece, Ierissos sheet, scale 1:50,000.

Irvine, T.N., 1977. Origin of chromitite layers in the Muskox intrusion and other stratiform intrusions: A new interpretation. Geology 5, 273–277. https://doi.org/10.1130/0091-7613(1977)5<273:OOCLIT>2.0.CO;2

Irvine, T.N., 1967. Chromian spinel as a petrogenetic indicator: Part 2. Petrologic applications. Can. J. Earth Sci. 4, 71–103.

Irvine, T.N., 1965. Chromian spinel as a petrogenetic indicator: Part 1. Theory. Can. J. Earth Sci. 2, 648–672.

Jackson, S.E., Fryer, B.J., Gosse, W., Healey, D.C., Longerich, H.P., Strong, D.F., 1990. Determination of the precious metals in geological materials by inductively coupled plasma-mass spectrometry (ICP-MS) with nickel sulphide fire-assay collection and tellurium coprecipitation. Chem. Geol. 83, 119–132. https://doi.org/10.1016/0009-2541(90)90144-V

Jacobshagen, V., Matarangas, D., 1972. Skyros Island, Geological Map of Greece 1:50.000. IGME, Athens.

Jamali, H., Dilek, Y., Daliran, F., Yaghubpur, A., Mehrabi, B., 2010. Metallogeny and tectonic evolution of the Cenozoic Ahar–Arasbaran volcanic belt, northern Iran. Int. Geol. Rev. 52, 608–630. https://doi.org/10.1080/00206810903416323

Jannessary, M.R., Melcher, F., Lodziak, J., Meisel, T.C., 2012. Review of platinum-group element distribution and mineralogy in chromitite ores from southern Iran. Ore Geol. Rev. 48, 278–305. https://doi.org/10.1016/j.oregeorev.2012.05.001

Jerram, D.A., Mock, A., Davis, G.R., Field, M., Brown, R.J., 2009. 3D crystal size distributions: A case study on quantifying olivine populations in kimberlites. Lithos 112, 223–235. https://doi.org/10.1016/j.lithos.2009.05.042

Jiménez–Franco, A., González–Jiménez, J.M., Roqué, J., Proenza, J.A., Gervilla, F., Nieto, F., 2020. Nanoscale constraints on the in situ transformation of Ru–Os–Ir sulfides to alloys at low temperature. Ore Geol. Rev. 124, 103640. https://doi.org/10.1016/j.oregeorev.2020.103640

Johnson Matthey, 2020. Pgm Market Report February 2020.

Jugo, P.J., 2004. An Experimental Study of the Sulfur Content in Basaltic Melts Saturated with Immiscible Sulfide or Sulfate Liquids at 1300 C and 1{middle dot}0 GPa. J. Petrol. 46, 783–798. https://doi.org/10.1093/petrology/egh097

Kamenetsky, V.S., Crawford, A.J., Meffre, S., 2001. Factors Controlling Chemistry of Magmatic Spinel: an Empirical Study of Associated Olivine, Cr-spinel and Melt Inclusions from Primitive Rocks. J. Petrol. 42, 655–671. https://doi.org/10.1093/petrology/42.4.655

Kanehira, K., S., B., Yui, S., 1975. Awaruite, heazlewoodite, and native copper in serpentinized peridotite from the Mineoka District, Southern Boso Peninsula. J. Japanese Assoc. Mineral. Petrol. Econ. Geol. 70, 388–394.

Kapsiotis, A., 2014. Composition and alteration of Cr-spinels from Milia and Pefki serpentinized mantle peridotites (Pindos Ophiolite Complex, Greece). Geol. Carpathica 65, 83–95. https://doi.org/10.2478/geoca-2013-0006

Kapsiotis, A., Grammatikopoulos, T.A. Tsikouras, B., Hatzipanagiotou, K., Zaccarini, F., Garuti, G., 2011. Mineralogy, composition and PGM of chromitites from Pefki, Pindos ophiolite complex (NW Greece): evidence for progressively

elevated fAs conditions in the upper mantle sequence. Mineral. Petrol. 101, 129–150.

Kapsiotis, A., Rassios, A.E., Uysal, I., Grieco, G., Akmaz, R.M., Saka, S., Bussolesi, M., 2018. Compositional fingerprints of chromian spinel from the refractory chrome ores of Metalleion, Othris (Greece): Implications for metallogeny and deformation of chromitites within a "hot" oceanic fault zone. J. Geochemical Explor. 185, 14–32. https://doi.org/10.1016/j.gexplo.2017.11.003

Kapsiotis, A.N., 2015. Alteration of chromitites from the Voidolakkos and Xerolivado mines, Vourinos ophiolite complex, Greece: implications for deformation-induced metamorphism. Geol. J. 50, 739–763. https://doi.org/10.1002/gj.2590

Karkalis, C., Magganas, A., Koutsovitis, P., 2017. Petrological, mineralogical and geochemical data from the Eohellenic Ophiolitic Nappe in the island of Skyros, Greece. Bull. Geol. Soc. Greece 50, 1867. https://doi.org/10.12681/bgsg.11926

Karup-Møller, S., Makovicky, E., 1995. The phase system Fe-Ni-S and 725 degree C. Neues Jahrb. fuer Mineral. Monatshefte 1, 1–10.

Katsikatsos, G., 1992. Geology of Greece. Univ. Patras 451.

Keays, R.R., 1995. The role of komatiitic and picritic magmatism and S-saturation in the formation of ore deposits. Lithos 34, 1–18. https://doi.org/10.1016/0024-4937(95)90003-9

Kelemen, P.B., 1990. Reaction Between Ultramafic Rock and Fractionating Basaltic Magma I. Phase Relations, the Origin of Calc-alkaline Magma Series, and the Formation of Discordant Dunite. J. Petrol. 31, 51–98. https://doi.org/10.1093/petrology/31.1.51

Kelemen, P.B., Braun, M., Hirth, G., 2000. Spatial distribution of melt conduits in the mantle beneath oceanic spreading ridges: Observations from the Ingalls and Oman ophiolites. Geochemistry, Geophys. Geosystems 1, n/a-n/a. https://doi.org/10.1029/1999GC000012

Kelemen, P.B., Dick, H.J.B., 1995. Focused melt flow and localized deformation in the upper mantle: Juxtaposition of replacive dunite and ductile shear zones in the Josephine peridotite, SW Oregon. J. Geophys. Res. Solid Earth 100, 423–438. https://doi.org/10.1029/94JB02063

Kelemen, P.B., Hirth, G., Shimizu, N., Spiegelman, M., Dick, H.J.B., 1999. A review of melt migration processes in the adiabatically upwelling mantle beneath oceanic spreading ridges, in: Mid-Ocean Ridges. Cambridge University Press, pp. 67–102. https://doi.org/10.1017/CBO9780511600050.005

Kelemen, P.B., Koga, K., Shimizu, N., 1997. Geochemistry of gabbro sills in the crust-mantle transition zone of the Oman ophiolite: implications for the origin of the oceanic lower crust. Earth Planet. Sci. Lett. 146, 475–488. https://doi.org/10.1016/S0012-821X(96)00235-X

Kelemen, P.B., Shimizu, N., Salters, V.J.M., 1995. Extraction of mid-ocean-ridge basalt from the upwelling mantle by focused flow of melt in dunite channels. Nature 375, 747–753. https://doi.org/10.1038/375747a0

Kerestedjian, T., Gervilla, F., Gonzalez-Jimenez, J.M., Proenza, J., 2007. Godlevskite Ni9S8 from Dobromirtsi, Central Rhodopes, Bulgaria: First report for the country and genetic implications. Geochemistry, Geophys. Geosystems 45, 19–28.

Kieser, N.B.J., 1994. In-situ modification of platinum-group minerals in Tosnia ultramafic complex, south-central Alaska: Implications for surficial dispersion and geochemical exploration. Trans. Inst. Min. Metall. (Section B Appl. Earth Sci. 103.

Kilias, A.A., Frisch, W., Avgerinas, A., Dunkl, I., Falalakis, G., Gawlick, H., 2010. Alpine architecture and kinematics of deformation of the northern Pelagonian nappe pile in the Hellenides. Austrian J. Earth Sci. 103, 4–28.

Kimball, K.L., 1990. Effects of hydrothermal alteration on the compositions of chromian spinels. Contrib. to Mineral. Petrol. 105, 337–346. https://doi.org/10.1007/BF00306543

Klein, F., Bach, W., 2009. Fe-Ni-Co-O-S Phase Relations in Peridotite-Seawater Interactions. J. Petrol. 50, 37–59. https://doi.org/10.1093/petrology/egn071

Klein, F., Bach, W., Jöns, N., McCollom, T., Moskowitz, B., Berquó, T., 2009. Iron partitioning and hydrogen generation during serpentinization of abyssal peridotites from 15°N on the Mid-Atlantic Ridge. Geochim. Cosmochim. Acta 73, 6868–6893. https://doi.org/10.1016/j.gca.2009.08.021

Klemme, S., Van Miltenburg, J.C., Javorsky, P., Wastin, F., 2005. Thermodynamic properties of uvarovite garnet (Ca3Cr2Si3O12). Am. Mineral. 90, 663–666. https://doi.org/10.2138/am.2005.1812

Kockel, F., 1977. Erläuterungen zur Geologischen Karte der Chalkidhiki und angrenzender Gebiete 1: 100 000 (Nord-Griechenland). Bundesanstalt für Geowissenschaften und Rohstoffe.

Kockel, F., Mollat, H., Walther, H.W., 1971. Geologie des Serbo-macedonischen massivs und seines mesozoichen rahmens (Nordgriecheland). Geol. Jahrb. 89, 529–551.

Kogel, J.E., Trivedi, N.C., Barker, J.M., Krukowski, S.T., 2006. Industrial minerals & rocks: commodities, markets, and uses. SME.

Koleli, N., Demir, A., 2016. Chromite. Environ. Mater. Waste 245–263.

Koukouvelas, I.K., Aydin, A., 2002. Fault structure and related basins of the North Aegean Sea and its surroundings. Tectonics 21, 10-1-10–17. https://doi.org/10.1029/2001TC901037

Koutsovitis, P., 2012. Gabbroic rocks in ophiolitic occurrences from East Othris, Greece: petrogenetic processes and geotectonic environment implications. Mineral. Petrol. 104, 249–265. https://doi.org/10.1007/s00710-011-0191-5

Kullerud, G., 1969. Phase relations in the Cu-Fe-S, Cu-Ni-S and Fe-Ni-S system. Magmat. ore Depos. 323–343.

Kullerud, G., 1963. Thermal stability of pentlandite. Can. Mineral. 7, 353–366.

Kullerud, G., Yund, R.A., 1962. The Ni-S System and Related Minerals. J. Petrol. 3, 126–175. https://doi.org/10.1093/petrology/3.1.126

Lago, B.L., Rabinowicz, M., Nicolas, A., 1982. Podiform Chromite Ore Bodies: a Genetic Model. J. Petrol. 23, 103–125. https://doi.org/10.1093/petrology/23.1.103

Laviosa Chimica Mineraria s.p.a., 2008. Acid Demand.

Lawley, C.J.M., Petts, D.C., Jackson, S.E., Zagorevski, A., Pearson, D.G., Kjarsgaard, B.A., Savard, D., Tschirhart, V., 2020. Precious metal mobility during serpentinization and breakdown of base metal sulphide. Lithos 354–355, 105278. https://doi.org/10.1016/j.lithos.2019.105278

Leblanc, M., Ceuleneer, G., 1991. Chromite crystallization in a multicellular magma flow: Evidence from a chromitite dike in the Oman ophiolite. Lithos 27, 231–257. https://doi.org/10.1016/0024-4937(91)90002-3

Leblanc, M., Nicolas, A., 1992. Ophiolitic Chromitites. Int. Geol. Rev. 34, 653–686. https://doi.org/10.1080/00206819209465629

Legendre, O., Augé, T., 1986. Mineralogy of platinum-group mineral inclusions in chromtites from different ophiolitic complexes, in: Conference Metallogeny of Basic and Ultrabasic Rocks. pp. 361–372.

Lehmann, J., 1983. Diffusion between olivine and spinel: application to geothermometry. Earth Planet. Sci. Lett. 64, 123–138. https://doi.org/10.1016/0012-821X(83)90057-2

Locmelis, M., Pearson, N.J., Barnes, S.J., Fiorentini, M.L., 2011. Ruthenium in komatiitic chromite. Geochim. Cosmochim. Acta 75, 3645–3661. https://doi.org/10.1016/j.gca.2011.03.041

Lorand, J.-P., Alard, O., 2001. Platinum-group element abundances in the upper mantle: new constraints from in situ and whole-rock analyses of Massif Central xenoliths (France). Geochim. Cosmochim. Acta 65, 2789–2806. https://doi.org/10.1016/S0016-7037(01)00627-5

Lorand, J.-P., Luguet, A., Alard, O., 2008. Platinum-Group Elements: A New Set of Key Tracers for the Earth's Interior. Elements 4, 247–252. https://doi.org/10.2113/GSELEMENTS.4.4.247

Lorand, J.P., 1987. Cu-Fe-Ni-S mineral assemblages in upper-mantle peridotites from the Table Mountain and Blow-Me-Down Mountain ophiolite massifs (Bay of Islands area, Newfoundland): Their relationships with fluids and silicate melts. Lithos 20, 59–76. https://doi.org/10.1016/0024-4937(87)90024-7

Luguet, A., Shirey, S.B., Lorand, J.-P., Horan, M.F., Carlson, R.W., 2007. Residual platinum-group minerals from highly depleted harzburgites of the Lherz massif (France) and their role in HSE fractionation of the mantle. Geochim. Cosmochim. Acta 71, 3082–3097. https://doi.org/10.1016/j.gca.2007.04.011

Malitch, K.N., Junk, S.A., Thalhammer, O.A.R., Melcher, F., Knauf, V.V., Pernicka, E., Stumpfl, E.F., 2003a. Laurite and ruarsite from podiform chromitites at Kraubath and Hochgrossen, Austria: new insights from Osmium isotopes. Can. Mineral. 41, 331–352. https://doi.org/10.2113/gscanmin.41.2.331

Malitch, K.N., Thalhammer, O.A., Knauf, V.V., Melcher, F., 2003b. Diversity of platinum-group mineral assemblages in banded and podiform chromitite from the Kraubath ultramafic massif, Austria: evidence for an ophiolitic transition zone? Miner. Depos. 38, 282–297. https://doi.org/10.1007/s00126-002-0308-1

Matveev, S., Ballhaus, C., 2002. Role of water in the origin of podiform chromitite deposits. Earth Planet. Sci. Lett. 203, 235–243. https://doi.org/10.1016/S0012-821X(02)00860-9

Maurel, C., Maurel, P., 1982. Étude expérimentale de la distribution de l'aluminium entre bain silicaté basique et spinelle chromifère. Implications pétrogénétiques: teneur en chrome des spinelles. Bull. Mineral. 105, 197–202.

Mavrogenes, J.A., O'Neill, H.S.., 1999. The relative effects of pressure, temperature and oxygen fugacity on the solubility of sulfide in mafic magmas. Geochim. Cosmochim. Acta 63, 1173–1180. https://doi.org/10.1016/S0016-7037(98)00289-0

McDonough, W.F., Sun, S.S., 1995. The composition of the Earth. Chem. Geol. 120, 223–253. https://doi.org/10.1016/0009-2541(94)00140-4

McElduff, B., Stumpfl, E.F., 1990. Platinum-group minerals from the Troodos ophiolite, Cyprus. Mineral. Petrol. 42, 211–232. https://doi.org/10.1007/BF01162692

McLaren, C.H., De Villiers, J.P.R., 1982. The platinum-group chemistry and mineralogy of the UG-2 chromitite layer of the Bushveld Complex. Econ. Geol. 77, 1348–1366. https://doi.org/10.2113/gsecongeo.77.6.1348

Medaris, L.G., 1975. Coexisting spinel and silicates in alpine peridotites of the granulite facies. Geochim. Cosmochim. Acta 39, 947–958.

Méducin, F., Redfern, S.A., Le Godec, Y., Stone, H.J., Tucker, M.G., Dove, M.T., Marshall, W.G., 2004. Study of cation order-disorder in MgAl2O4 spinel by in situ neutron diffraction up to 1600 K and 3.2 GPa. Am. Mineral. 89, 981–986.

Mehnert, K.R., 1975. The Ivrea Zone, a model of the deep crust. N. Jb. Miner. Abh 125, 156–199.

Melcher, F., Grum, W., Simon, G., Thalhammer, T. V., Stumpfl, E.F., 1997. Petrogenesis of the Ophiolitic Giant Chromite Deposits of Kempirsai, Kazakhstan: a Study of Solid and Fluid Inclusions in Chromite. J. Petrol. 38, 1419–1458. https://doi.org/10.1093/petroj/38.10.1419

Mellini, M., Rumori, C., Viti, C., 2005. Hydrothermally reset magmatic spinels in retrograde serpentinites: formation of

"ferritchromit" rims and chlorite aureoles. Contrib. to Mineral. Petrol. 149, 266–275. https://doi.org/10.1007/s00410-005-0654-y

Mercier, J., 1966. Paleogeographie, orogenese, metamorphisme et magmatisme des zones internes des Hellenides en Macedoine (Grece); vue d'ensemble. Bull. la Société Géologique Fr. S7-VIII, 1020–1049. https://doi.org/https://doi.org/10.2113/gssgfbull.S7-VIII.7.1020

Mercier, J., Vergély, P., Bébien, J., 1975. Les ophiolites helléniques "obductées" au Jurassique supérieur sont'elles les vestiges d'un Océan téthysien ou d'une mer marginale péri-européene? Société Géologique Fr. 17, 108–112.

Merlini, A., Grieco, G., Diella, V., 2009. Ferritchromite and chromian-chlorite formation in mélange-hosted Kalkan chromitite (Southern Urals, Russia). Am. Mineral. 94, 1459–1467. https://doi.org/10.2138/am.2009.3082

Michailidis, K.M., Soldatos, T.C., Christodoulou, C., 1995. Ultramafic rocks and associated chromite mineralisation from Nea Roda (Eastern Chalkidiki peninsula, Northern Greece). Ofioliti 20, 81–96.

Minerals4EU, 2014. European Minerals Yearbook [online].

Mittwede, S.K., Schandl, E.S., 1992. Rodingites from the southern Appalachian Piedmont, South Carolina, USA. Eur. J. Mineral. 4, 7–16.

Miura, M., Arai, S., Ahmed, A.H., Mizukami, T., Okuno, M., Yamamoto, S., 2012. Podiform chromitite classification revisited: A comparison of discordant and concordant chromitite pods from Wadi Hilti, northern Oman ophiolite. J. Asian Earth Sci. 59, 52–61. https://doi.org/10.1016/j.jseaes.2012.05.008

Mohajjel, M., Fergusson, C.L., 2000. Dextral transpression in Late Cretaceous continental collision, Sanandaj–Sirjan Zone, western Iran. J. Struct. Geol. 22, 1125–1139. https://doi.org/10.1016/S0191-8141(00)00023-7

Mondal, S.K., Griffin, W.L., 2018. Processes and Ore Deposits of Ultramafic-Mafic Magmas through Space and Time. Elsevier. https://doi.org/10.1016/C2016-0-00577-6

Mondal, S.K., Mathez, E.A., 2007. Origin of the UG2 chromitite layer, Bushveld Complex. J. Petrol. 48, 495–510. https://doi.org/10.1093/petrology/egl069

Moreno, T., Gibbons, W., Prichard, H.M., Lunar, R., 2001. Platiniferous chromitite and the tectonic setting of ultramafic rocks in Cabo Ortegal, NW Spain. J. Geol. Soc. London. 158, 601–614. https://doi.org/10.1144/jgs.158.4.601

Mountrakis, D., 1986. The Pelagonian Zone in Greece: A Polyphase-Deformed Fragment of the Cimmerian Continent and Its Role in the Geotectonic Evolution of the Eastern Mediterranean. J. Geol. 94, 335–347. https://doi.org/10.1086/629033

Mudd, G.M., 2012. Key trends in the resource sustainability of platinum group elements. Ore Geol. Rev. 46, 106–117. https://doi.org/10.1016/j.oregeorev.2012.02.005

Mukherjee, R., Mondal, S.K., Rosing, M.T., Frei, R., 2010. Compositional variations in the Mesoarchean chromites of the Nuggihalli schist belt, Western Dharwar Craton (India): potential parental melts and implications for tectonic setting. Contrib. to Mineral. Petrol. 160, 865–885. https://doi.org/10.1007/s00410-010-0511-5

Mungall, J.E., 2002. Kinetic Controls on the Partitioning of Trace Elements Between Silicate and Sulfide Liquids. J. Petrol. 43, 749–768. https://doi.org/10.1093/petrology/43.5.749

Mungall, J.E., Naldrett, A.J., 2008. Ore Deposits of the Platinum-Group Elements. Elements 4, 253–258. https://doi.org/10.2113/GSELEMENTS.4.4.253

Najafzadeh, A.R., Ahmadipour, H., 2016. Geochemistry of platinum-group elements and mineral composition in chromitites and associated rocks from the Abdasht ultramafic complex, Kerman, Southeastern Iran. Ore Geol. Rev. 75, 220–238. https://doi.org/10.1016/j.oregeorev.2015.12.018

Najafzadeh, A.R., Ahmadipour, H., 2014. Using platinum-group elements and Au geochemistry to constrain the genesis of podiform chromitites and associated peridotites from the Soghan mafic–ultramafic complex, Kerman, Southeastern Iran. Ore Geol. Rev. 60, 60–75. https://doi.org/10.1016/j.oregeorev.2013.12.014

Naldrett, A.J., 1973. Nickel sulfide deposits-their classification and genesis, with special emphasis on deposits of volcanic association. Cim Bull. 66, 45–63.

Naldrett, A.J., Cabri, L.J., 1976. Ultramafic and related mafic rocks; their classification and genesis with special reference to the concentration of nickel sulfides and platinum-group elements. Econ. Geol. 71, 1131–1158. https://doi.org/10.2113/gsecongeo.71.7.1131

Naldrett, A.J., Wilson, A.H., 1990. Horizontal and vertical variations in noble-metal distribution in the Great Dyke of Zimbabwe: A model for the origin of the PGE mineralization by fractional segregation of sulfide. Chem. Geol. 88, 279–300. https://doi.org/10.1016/0009-2541(90)90094-N

Naldrett, T., Kinnaird, J., Wilson, A., Chunnett, G., 2008. Concentration of PGE in the Earth's Crust with Special Reference to the Bushveld Complex. Earth Sci. Front. 15, 264–297. https://doi.org/10.1016/S1872-5791(09)60006-3

Nilsson, L.P., 1990. Platinum-group mineral inclusions in chromitite from the Osthammeren ultramafic tectonite body, South Central Norway. Mineral. Petrol. 42, 249–263. https://doi.org/10.1007/BF01162694

Nirta, G., Moratti, G., Piccardi, L., Montanari, D., Catanzariti, R., Carras, N., Papini, M., 2015. The Boeotian flysch revisited: new constraints on ophiolite obduction in central Greece. Ofioliti 40, 107–123. https://doi.org/10.4454/ofioliti.v40i2.438

Nixon, G.T., Cabri, L.J., Laflamme, J.H.G., 1990. Platinum-group-element mineralization in lode and placer deposits associated with the Tulameen Alaskan-type complex, British Columbia. Can. Mineral. 28, 503–535.

Norilsk Nickel, 2015. Mineral Reserves and Resources Statement [WWW Document]. URL http://www.nornik.ru/en/about-norilsk-nickel/operations/mineral-reserves-and-resources-statement

O'Hara, M.J., Fry, N., Prichard, H.M., 2001. Minor Phases as Carriers of Trace Elements in Non-Modal Crystal–Liquid Separation Processes II: Illustrations and Bearing on Behaviour of REE, U, Th and the PGE in Igneous Processes. J. Petrol. 42, 1887–1910. https://doi.org/10.1093/petrology/42.10.1887

O'Neill, H.S.C., Wall, V.J., 1987. The Olivine--Orthopyroxene--Spinel Oxygen Geobarometer, the Nickel Precipitation Curve, and the Oxygen Fugacity of the Earth's Upper Mantle. J. Petrol. 28, 1169–1191. https://doi.org/10.1093/petrology/28.6.1169

Oen, I.S., Kieft, C., Burke, E.A.J., Westerhof, A.B., 1980. Orcelite and associated minerals in the Ni — Fe — As — S system in chromitites and orthopyroxenites of Nebral, Málaga, Spain. Bull. Minéralogie 103, 198–208. https://doi.org/10.3406/bulmi.1980.7397

Okamoto, H., 2009. Ni-Sb (Nickel-Antimony). J. Phase Equilibria Diffus. 30, 301–302.

Omrani, J., Agard, P., Whitechurch, H., Benoit, M., Prouteau, G., Jolivet, L., 2008. Arc-magmatism and subduction history beneath the Zagros Mountains, Iran: A new report of adakites and geodynamic consequences. Lithos 106, 380–398. https://doi.org/10.1016/j.lithos.2008.09.008

Ozawa, K., 1984. Olivine-spinel geospeedometry: Analysis of diffusion-controlled Mg-Fe2+ exchange. Geochim. Cosmochim. Acta 48, 2597–2611.

Ozawa, K., 1983. Evaluation of Olivine-Spinel Geothermometry as an Indicator of Thermal History for Peridotites. Contrib. to Mineral. Petrol. 82, 52–65.

Pagé, P., Barnes, S.-J., 2009. Using Trace Elements in Chromites to Constrain the Origin of Podiform Chromitites in the

Thetford Mines Ophiolite , Québec , Canada. Econ. Geol. 104, 997–1018.

Pagé, P., Barnes, S.-J., Bédard, J.H., Zientek, M.L., 2012. In situ determination of Os, Ir, and Ru in chromites formed from komatiite, tholeiite and boninite magmas: Implications for chromite control of Os, Ir and Ru during partial melting and crystal fractionation. Chem. Geol. 302–303, 3–15. https://doi.org/10.1016/j.chemgeo.2011.06.006

Pal, T., Das, D., 2010. Uvarovite from chromite-bearing ultramafic intrusives, Orissa, India, a crystal-chemical characterization using 57Fe Mossbauer spectroscopy. Am. Mineral. 95, 839–843. https://doi.org/10.2138/am.2010.3328

Papanikolaou, D., 2013. Tectonostratigraphic models of the Alpine terranes and subduction history of the Hellenides. Tectonophysics 595–596, 1–24. https://doi.org/10.1016/j.tecto.2012.08.008

Papanikolaou, D., 1997. The tectonostratigraphic terranes of the Hellenides. Ann. Geol. des Pays Hell. 37.

Papantoniou, G., 2015. The Structure and History of the Strike—Slip Fault Zone of Skyros Island, Central—North Aegean. National and Kapodistrian University of Athens.

Papp, J.F., Lipin, B.R., 2001. Chromium, USGS Open-File Report. USGS.

Pe-Piper, G., Piper, D.J., Lentz, D.R., 2004. The igneous rocks of Greece: The anatomy of an orogen.

Pedrotti, M., 2012. Chromite: from the mineral to the commodity. University of Milan.

Pertsev, A.N., Spadea, P., Savelieva, G.N., Gaggero, L., 1997. Nature of the transition zone in the Nurali ophiolite, southern Urals. Tectonophysics 276, 163–180. https://doi.org/10.1016/S0040-1951(97)00056-5

Piña, R., Gervilla, F., Barnes, S.-J., Ortega, L., Lunar, R., 2015. Liquid immiscibility between arsenide and sulfide melts: evidence from a LA-ICP-MS study in magmatic deposits at Serranía de Ronda (Spain). Miner. Depos. 50, 265–279. https://doi.org/10.1007/s00126-014-0534-3

Price pressures on metals, 2019. . Nat. Catal. 2, 735–735. https://doi.org/10.1038/s41929-019-0359-7

Prichard, H.M., Economou-Eliopoulos, M., Fisher, P.C., 2008a. Platinum-group minerals in podiform chromitite in the Pindos ophiolite complex, Greece. Can. Mineral. 46, 329–341.

Prichard, H.M., Hutchinson, D., Fisher, P.C., 2004. Petrology and Crystallization History of Multiphase Sulfide Droplets in a Mafic Dike from Uruguay: Implications for the Origin of Cu-Ni-PGE Sulfide Deposits. Econ. Geol. 99, 365–376. https://doi.org/10.2113/gsecongeo.99.2.365

Prichard, H.M., Ixer, R.A., Lord, R.A., Maynard, N., Williams, N., 1994. Assemblages of platinum-group minerals and sulfides in silicate lithologies and chromite-rich rocks within the Shetland ophiolite. Can. Mineral. 32, 271–294.

Prichard, H.M., Lord, R.A., 1988. The Shetland Ophiolite: Evidence for a Supra-Subduction Zone Origin and Implications for Platinum-Group Element Mineralization, in: Mineral Deposits within the European Community. Springer Berlin Heidelberg, Berlin, Heidelberg, pp. 289–302. https://doi.org/10.1007/978-3-642-51858-4_16

Prichard, H.M., Lord, R.A., Neary, C.R., 1996. A model to explain the occurrence of platinum- and palladium-rich ophiolite complexes. J. Geol. Soc. London. 153, 323–328. https://doi.org/10.1144/gsjgs.153.2.0323

Prichard, H.M., Neary, C.R., Fisher, P.C., O'Hara, M.J., 2008b. PGE-rich Podiform Chromitites in the Al 'Ays Ophiolite Complex, Saudi Arabia: An Example of Critical Mantle Melting to Extract and Concentrate PGE. Econ. Geol. 103, 1507–1529. https://doi.org/10.2113/gsecongeo.103.7.1507

Prichard, H.M., Tarkian, M., 1988. Platinum and Palladium minerals from two PGE-rich localities in the Shetland ophiolite complex. Can. Mineral. 26, 979–990.

Proenza, J., Gervilla, F., Melgarejo, J., Vera, O., Alfonso, P., Fallick, A., 2001. Genesis of sulfide-rich chromite ores by the interaction between chromitite and pegmatitic olivine–norite dikes in the Potosí Mine (Moa-Baracoa ophiolitic

massif, eastern Cuba). Miner. Depos. 36, 658–669. https://doi.org/10.1007/s001260100193

Proenza, J., Solé, J., Melgarejo, J.C., 1999. Uvarovite in podiform chromitite; the Moa-Baracoa ophiolitic massif, Cuba. Can. Mineral. 37, 679–690.

Proenza, J.A., Ortega-Gutiérrez, F., Camprubí, A., Tritlla, J., Elías-Herrera, M., Reyes-Salas, M., 2004. Paleozoic serpentinite-enclosed chromitites from Tehuitzingo (Acatlán Complex, southern Mexico): a petrological and mineralogical study. J. South Am. Earth Sci. 16, 649–666. https://doi.org/10.1016/j.jsames.2003.12.003

Proenza, J.A., Zaccarini, F., Escayola, M., Cábana, C., Schalamuk, A., Garuti, G., 2008. Composition and textures of chromite and platinum-group minerals in chromitites of the western ophiolitic belt from Pampean Ranges of Córdoba, Argentina. Ore Geol. Rev. 33, 32–48. https://doi.org/10.1016/j.oregeorev.2006.05.009

Proenza, J.A., Zaccarini, F., Lewis, J.F., Longo, F., Garuti, G., 2007. Chromian spinel composition and the Platinum-group minerals of the PGE-rich Loma Peguera chromitites, Loma Caribe peridotite, Dominican Republic. Can. Mineral. 45, 631–648. https://doi.org/10.2113/gscanmin.45.3.631

Qiu, T., Yang, J., Milushi, I., Wu, W., Mekshiqi, N., Xiong, F., Zhang, C., Shen, T., 2018. Petrology and PGE Abundances of High-Cr and High-Al Podiform Chromitites and Peridotites from the Bulqiza Ultramafic Massif, Eastern Mirdita Ophiolite, Albania. Acta Geol. Sin. - English Ed. 92, 1063–1081. https://doi.org/10.1111/1755-6724.13592

Quick, J.E., Sinigoi, S., Mayer, A., 1994. Emplacement dynamics of a large mafic intrusion in the lower crust, Ivrea-Verbano Zone, northern Italy. J. Geophys. Res. Solid Earth 99, 21559–21573.

Raghavan, V., 2004. Fe-Ni-Sb (Iron-Nickel-Antimony). J. Phase Equilibria Diffus. 25, 553.

Rajabzadeh, M.A., Nazari Dehkordi, T., Caran, Ş., 2013. Mineralogy, geochemistry and geotectonic significance of mantle peridotites with high-Cr chromitites in the Neyriz ophiolite from the outer Zagros ophiolite belts, Iran. J. African Earth Sci. 78, 1–15. https://doi.org/10.1016/j.jafrearsci.2012.09.013

Rassios, A., 2014. Cooperative development for Greek chromite reserves: Initial Review. Inst. Geol. Miner. Explor. 27.

Rassios, A., Tzamos, E., Dilek, Y., Bussolesi, M., Grieco, G., Batsi, A., Gamaletsos, P.N., 2020. A structural approach to the genesis of chrome ores within the Vourinos ophiolite (Greece): Significance of ductile and brittle deformation processes in the formation of economic ore bodies in oceanic upper mantle peridotites. Ore Geol. Rev. 125, 103684. https://doi.org/10.1016/j.oregeorev.2020.103684

Rassios, A.E., Dilek, Y., 2009. Rotational deformation in the Jurassic Mesohellenic ophiolites, Greece, and its tectonic significance. Lithos 108, 207–223. https://doi.org/10.1016/j.lithos.2008.09.005

Richard, P., 2015. ICDA: overview of the global chrome market, in: 1st Indinox Stainless Steel Conference, Ahmedabad, India.

Ricou, L., Burg, J., Godfriaux, I., Ivanov, Z., Burg, J., Godfriaux, I., Rhodope, Z.I., 1998. Rhodope and Vardar : the metamorphic and the olistostromic paired belts related to the Cretaceous subduction under Europe Rhodope and Vardar : the metamorphic and the olistostromic paired belts related to the Cretaceous subduction under Europe. Geodin. Acta 11, 285–309.

Ricou, L.E., 1977. Le croissant ophiolitique peri-arabe, Une ceinture de nappes mises en place au Cretace superieur. Rev. géologie Dyn. géographie Phys. 327–350.

Ricou, L.E., 1971. Le metamorphisme au contact des peridotites de Neyriz (Zagros interne, Iran); developpement de skarns a pyroxene. Bull. la Société Géologique Fr. 7, 146–155.

Ripley, E.M., Li, C., 2013. Sulfide Saturation in Mafic Magmas: Is External Sulfur Required for Magmatic Ni-Cu-(PGE) Ore Genesis? Econ. Geol. 108, 45–58. https://doi.org/10.2113/econgeo.108.1.45

Robertson, A.H.F., 2012. Late Palaeozoic–Cenozoic tectonic development of Greece and Albania in the context of alternative reconstructions of Tethys in the Eastern Mediterranean region. Int. Geol. Rev. 54, 373–454. https://doi.org/10.1080/00206814.2010.543791

Robertson, A.H.F., Dixon, J.E., 1984. Introduction: aspects of the geological evolution of the Eastern Mediterranean. Geol. Soc. London, Spec. Publ. 17, 1–74. https://doi.org/10.1144/GSL.SP.1984.017.01.02

Robertson, A.H.F., Dixon, J.E., Brown, S., Collins, A., Morris, A., Pickett, E., Sharp, I., Ustaömer, T., 1996. Alternative tectonic models for the Late Palaeozoic-Early Tertiary development of Tethys in the Eastern Mediterranean region. Geol. Soc. London, Spec. Publ. 105, 239–263. https://doi.org/10.1144/GSL.SP.1996.105.01.22

Roeder, P.L., Campbell, I.H., 1985. The Effect of Postcumulus Reactions on Composition of Chrome-spinels from the Jimberlana Intrusion. J. Petrol. 26, 763–786. https://doi.org/10.1093/petrology/26.3.763

Roeder, P.L., Campbell, I.H., Jamieson, H.E., 1979. A re-evaluation of the olivine-spinel geothermometer. Contrib. to Mineral. Petrol. 68, 325–334. https://doi.org/10.1007/BF00371554

Rollinson, H., 2008. The geochemistry of mantle chromitites from the northern part of the Oman ophiolite: Inferred parental melt compositions. Contrib. to Mineral. Petrol. 156, 273–288. https://doi.org/10.1007/s00410-008-0284-2

Rudnick, R.L., Gao, S., 2003. Composition of the Continental Crust, in: Treatise on Geochemistry. Elsevier, pp. 1–64. https://doi.org/10.1016/B0-08-043751-6/03016-4

Saccani, E., Beccaluva, L., Photiades, A., Zeda, O., 2011. Petrogenesis and tectono-magmatic significance of basalts and mantle peridotites from the Albanian–Greek ophiolites and sub-ophiolitic mélanges. New constraints for the Triassic–Jurassic evolution of the Neo-Tethys in the Dinaride sector. Lithos 124, 227–242. https://doi.org/10.1016/j.lithos.2010.10.009

Saccani, E., Bortolotti, V., Marroni, M., Pandolfi, L., Photiades, A., Principi, G., 2008. The Jurassic association of backarc basin ophiolites and calc-alkaline volcanics in the Guevgueli Complex (Northern Greece): implication for the evolution of the Vardar Zone. Ofioliti 33, 209–227.

Saccani, E., Tassinari, R., 2015. The role of morb and SSZ magma-types in the formation of Jurassic ultramafic cumulates in the Mirdita Ophiolites (Albania) as deduced from chromian spinel and olivine chemistry. Ofioliti 40, 37–56. https://doi.org/10.4454/ofioliti.v40i1.434

Sack, R.O., Ghiorso, M.S., 1991. Chromian spinels as petrogenetic indicators: Thermodynamics and petrological applications. Am. Mineral. 76, 827–847. https://doi.org/10.1007/s00103-007-0219-5

Scarpelis, N., Economou, M., 1978. Genesis and metasomatism of chromite ore from the Gomati area, Chalkidiki, Greece. Ann. Geol. Pays Hell 29, 716–728.

Schenker, F.L., Burg, J.-P., Kostopoulos, D., Moulas, E., Larionov, A., von Quadt, A., 2014. From Mesoproterozoic magmatism to collisional Cretaceous anatexis: Tectonomagmatic history of the Pelagonian Zone, Greece. Tectonics 33, 1552–1576. https://doi.org/10.1002/2014TC003563

Schmid, S.M., Bernoulli, D., Fügenschuh, B., Matenco, L., Schefer, S., Schuster, R., Tischler, M., Ustaszewski, K., 2008. The Alpine-Carpathian-Dinaridic orogenic system: correlation and evolution of tectonic units. Swiss J. Geosci. 101, 139–183. https://doi.org/10.1007/s00015-008-1247-3

Schumaker, L.L., 1990. Reconstructing 3D objects from cross-sections. In Computation of Curves and Surfaces. Springer, Dordr. 275–309.

Şengör, A.M.C., 1990. A new model for the late Palaeozoic—Mesozoic tectonic evolution of Iran and implications for Oman. Geol. Soc. London, Spec. Publ. 49, 797–831. https://doi.org/10.1144/GSL.SP.1992.049.01.49

Şengör, A.M.C., Yılmaz, Y., Sungurlu, O., 1984. Tectonics of the Mediterranean Cimmerides: nature and evolution of the western termination of Palaeo-Tethys. Geol. Soc. London, Spec. Publ. 17, 77–112. https://doi.org/10.1144/GSL.SP.1984.017.01.04

Shallo, M., 1994. Outline of the Albanian ophiolites. Ofioliti 19, 57–75.

Shallo, M., Beqiraj, A., Beqiraj-Goga, E., 2010. Ultramafic intrusions in the Albanian ophiolites: petrological implications.

Shallo, M., Kote, D., Vranai, A., 1987. Geochemistry of the volcanics from ophiolitic belts of Albanides. Ofioliti 12, 125–136.

Sharp, I.R., Robertson, A.H.F., 1994. Late Jurassic-lower cretaceous ocenic crust and sediments of the eastern Almopias zone, NW Macedonia (Greece), Implications for the evolution of the eastern''Internal" Hellenides. Bull. Geol. Soc. Greece 30, 47–61.

Shvedov, G., Barkov, A., 2017. Primary and alteration assemblages of platinum-group minerals from the Ognit complex, Irkutskaya oblast, Eastern Sayans, Russia. Neues Jahrb. für Mineral. - Abhandlungen J. Mineral. Geochemistry 194, 35–48. https://doi.org/10.1127/njma/2016/0038

Siena, F., Coltorti, M., 1989. The petrogenesis of a hydrated mafic ultramafic complex and the role of amphibole fractionation at Finero (Italian Western Alps). NEUES Jahrb. FUR Mineral. 6, 255–274.

Sills, J.D., Ackermand, D., Herd, R.K., Windley, B.F., 1983. Bulk composition and mineral parageneses of sapphirine-bearing rocks along a gabbro-lherzolite contact at Finero, Ivrea Zone, N Italy. J. Metamorph. Geol. 1, 337–351.

Sinigoi, S., Quick, J.E., Clemens-Knott, D., Mayer, A., Demarchi, G., Mazzucchelli, M., Negrini, L., Rivalenti, G., 1994. Chemical evolution of a large mafic intrusion in the lower crust, Ivrea-Verbano Zone, northern Italy. J. Geophys. Res. 99, 21559–21573. https://doi.org/10.1029/94JB00113

Siron, C.R., Rhys, D., Thompson, J.F.H., Baker, T., Veligrakis, T., Camacho, A., Dalampiras, L., 2018. Structural Controls on Porphyry Au-Cu and Au-Rich Polymetallic Carbonate-Hosted Replacement Deposits of the Kassandra Mining District, Northern Greece. Econ. Geol. 113, 309–345. https://doi.org/10.5382/econgeo.2018.4552

Smye, A.J., Stockli, D.F., 2014. Rutile U-Pb age depth profiling: A continuous record of lithospheric thermal evolution. Earth Planet. Sci. Lett. 408, 171–182. https://doi.org/10.1016/j.epsl.2014.10.013

Spiegelman, M., Kelemen, P.B., 2003. Extreme chemical variability as a consequence of channelized melt transport. Geochemistry, Geophys. Geosystems 4. https://doi.org/10.1029/2002GC000336

Stöcklin, J., 1968. Structural History and Tectonics of Iran: A Review. Am. Assoc. Pet. Geol. Bull. 52. https://doi.org/10.1306/5D25C4A5-16C1-11D7-8645000102C1865D

Stockman, H.W., Hlava, P.F., 1984. Platinum-group minerals in alpine chromitites from southwestern Oregon. Econ. Geol. 79, 491–508. https://doi.org/10.2113/gsecongeo.79.3.491

Storni, N., 2020. The metallic mineral assemblage of Gomati and Nea Roda ophiolites, Serbo-Macedonian Massif, Chalkidiki, Greece. University of Milan.

Surekha, B., Hanumantha Rao, D., Krishna Mohana Rao, G., Pandu R, V., Parappagoudar, M.B., 2013. Application of response surface methodology for modeling the properties of chromite-based resin bonded sand cores. Int. J. Mech. 7, 443–458.

Tarkian, M., Economou-Eliopoulos, M., Eliopoulos, D.G., 1992. Platinum-group minerals and tetraauricupride in ophiolitic rocks of Skyros island, Greece. Mineral. Petrol. 47, 55–66. https://doi.org/10.1007/BF01165297

Tarkian, M., Encomou-Eliopoulos, M., Sambanis, G., 1996. Platinum-group minerals in chromitites from the Pindos

ophiolite complex, Greece. Neues Jahrb. fuer Mineral. Monatshefte 145–160.

Tarkian, M., Naidenova, E., Zhelyaskova-Panayotova, M., 1991. Platinum-group minerals in chromitites from the Eastern Rhodope ultramafic complex, Bulgaria. Mineral. Petrol. 44, 73–87. https://doi.org/10.1007/BF01167101

Thayer, T.., 1961. Application of geology in chromite exploration and mining, in: Symposium on Chrome Ore, Ankara, Turkey. pp. 197–223.

Torres-Ruiz, J., Garuti, G., Gazzotti, M., Gervilla, F., Hach-Ali, P.F., 1996. Platinum-group minerals in chromitites from the ojen lherzolite massif (Serrania de Ronda, Betic Cordillera, Southern Spain). Mineral. Petrol. 56, 25–50. https://doi.org/10.1007/BF01162656

Tranos, M.D., Kilias, A.A., Mountrakis, D.M., 1999. Geometry and kinematics of the Tertiary post-metamorphic Circum Rhodope Belt Thrust System (CRBTS), Northern Greece. Δελτίον της Ελληνικής Γεωλογικής Εταιρίας, 33, 5-16. Bull. Geol. Soc. Greece 33, 5–16.

Tredoux, M., Lindsay, N.M., Davies, G., McDonald, L., 1995. The fractionation of platinum-group elements in magmatic systems, with the suggestion of a novel causal mechanism. South African J. Geol. 98, 157–167.

Tredoux, M., Zaccarini, F., Garuti, G., Miller, D.E., 2016. Phases in the Ni–Sb–As system which occur in the Bon Accord oxide body, Barberton greenstone belt, South Africa. Mineral. Mag. 80, 187–198. https://doi.org/10.1180/minmag.2015.079.7.07

Tsoupas, G., Economou-Eliopoulos, M., 2008. High PGE contents and extremely abundant PGE-minerals hosted in chromitites from the Veria ophiolite complex, northern Greece. Ore Geol. Rev. 33, 3–19. https://doi.org/10.1016/j.oregeorev.2006.10.008

Tzamos, E., Filippidis, A., Michailidis, K., Koroneos, A., Rassios, A., Grieco, G., Pedrotti, M., Stamoulis, K., 2016. Mineral chemistry and formation of awaruite and heazlewoodite in the Xerolivado chrome mine, Vourinos, Greece. Bull. Geol. Soc. Greece 50, 2047–2056.

Tzamos, E., Kapsiotis, A., Filippidis, A., Koroneos, A., Grieco, G., Ewing Rassios, A., Kantiranis, N., Papadopoulos, A., Gamaletsos, P.N., Godelitsas, A., 2017. Metallogeny of the Chrome Ores of the Xerolivado-Skoumtsa Mine, Vourinos Ophiolite, Greece: Implications on the genesis of IPGE-bearing high-Cr chromitites within a heterogeneously depleted mantle section. Ore Geol. Rev. 90, 226–242. https://doi.org/10.1016/j.oregeorev.2017.03.013

Tzamos, E., Papadopoulos, A., Grieco, G., Stoulos, S., Bussolesi, M., Daftsis, E., Vagli, E., Dimitriadis, D., Godelitsas, A., 2019. Investigation of Trace and Critical Elements (Including Actinides) in Flotation Sulphide Concentrates of Kassandra Mines (Chalkidiki, Greece). Geosciences 9, 164. https://doi.org/10.3390/geosciences9040164

USGS, 2020a. Mineral Commodity Summaries: Cr. USGS.gov.

USGS, 2020b. Mineral commodity summaries.

Uysal, I., Zaccarini, F., Garuti, G., Meisel, T., Tarkian, M., Bernhardt, J.H., Sadiklar, M.B., 2007. Ophiolitic chromitites from the Kahramanmaras area, Southeastern Turkey: their platinum-group elements (PGE) geochemistry, mineralogy and Os-isotope signature. Ofioliti 32, 151–161.

Uysal, I., Zaccarini, F., Sadiklar, M.B., Bernhardt, H.-J., Bigi, S., Garuti, G., 2009. Occurrence of rare Ru-Fe-Os-Ir-oxide and associated Platinum-group minerals (PGM) in the chromitite of Muğla ophiolite, SW-Turkey. Neues Jahrb. für Mineral. - Abhandlungen 185, 323–333. https://doi.org/10.1127/0077-7757/2009/0131

Vavassis, I., De Bono, A., Stampli, G.M., Giorgis, D., Valloton, A., Amelin, Y., 2000. U-Pb and Ar-Ar geochronological data from the Pelagonian basement in Evia (Greece): geodynamic implications for the evolution of Paleotethys.

Schweizerische Mineral. und Petrogr. Mitteilungen 80, 21–43. https://doi.org/10.5169/seals-60948

Vogt, K., Dohmen, R., Chakraborty, S., 2015. Fe-Mg diffusion in spinel: New experimental data and a point defect model. Am. Mineral. 100, 2112–2122. https://doi.org/10.2138/am-2015-5109

Walshe, J.L., 1986. A six-component chlorite solid solution model and the conditions of chlorite formation in hydrothermal and geothermal systems. Econ. Geol. 81, 681–703. https://doi.org/10.2113/gsecongeo.81.3.681

Weber-Diefenbach, K., Davoudzadeh, M., Alavi-Tehrani, N., Lensch, G., 1986. Paleozoic ophiolites in Iran. Geology, geochemistry and geodynamic implication. Ofioliti 11, 305–338.

Wedepohl, H.K., 1995. The composition of the continental crust. Geochim. Cosmochim. Acta 59, 1217–1232. https://doi.org/10.1016/0016-7037(95)00038-2

Willis, P., Chapman, A., Fryer, A., 2012. Study of by-products of copper, Lead, Zinc and Nickel.

Wogelius, R.A., Bishop, F.C., 1989. Subsolidus emplacement history of the Lanzo massif, northern Italy. Geology 17, 995–999. https://doi.org/10.1130/0091-7613(1989)017<0995:SEHOTL>2.3.CO;2

Wolff, R., Dunkl, I., Kiesselbach, G., Wemmer, K., Siegesmund, S., 2012. Thermochronological constraints on the multiphase exhumation history of the Ivrea-Verbano Zone of the Southern Alps. Tectonophysics 579, 104–117. https://doi.org/10.1016/j.tecto.2012.03.019

Yang, K., Seccombe, P.K., 1993. Chemical variation of chromite in the ultramafic cumulates of the Great Serpentinite Belt, Upper Bingara to Doonba, New South Wales, Australia. Can. Mineral. 31, 75–87.

Yarwood, G.A., Aftalion, M., 1976. Field relations and U-Pb geochronology of a granite from the Pelagonian Zone of the Hellenides (High Pieira, Greece). Bull. la Société Géologique Fr. 7, 259–264.

Yund, R.A., 1961. Phase relations in the system Ni-As. Econ. Geol. 56, 1273–1296. https://doi.org/10.2113/gsecongeo.56.7.1273

Zaccarini, F., Garuti, G., Martin, R.F., 2006. Exotic accessory minerals in layered chromitites of the Campo Formoso complex Brazil). Geol. Acta 4, 461–469.

Zaccarini, F., Garuti, G., Proenza, J.A., Campos, L., Thalhammer, O.A., Aiglsperger, T., Lewis, J.F., 2011. Chromite and platinum group elements mineralization in the Santa Elena Ultramafic Nappe (Costa Rica): geodynamic implications. Geol. Acta an Int. earth Sci. J. 9, 407–423. https://doi.org/https://doi.org/10.1344/105.000001696

Zaccarini, F., Proenza, J.A., Ortega-Gutiérrez, F., Garuti, G., 2005. Platinum group minerals in ophiolitic chromitites from Tehuitzingo (Acatlán complex, southern Mexico): implications for post-magmatic modification. Mineral. Petrol. 84, 147–168. https://doi.org/10.1007/s00710-005-0075-7

Zaccarini, F., Proenza, J.A., Rudashevsky, N.S., Cabri, L.J., Garuti, G., Rudashevsky, V.N., Melgarejo, J.C., Lewis, J.F., Longo, F., Bakker, R.J., Stanley, C.J., 2009. The Loma Peguera ophiolitic chromitite (Central Dominican Republic): a source of new platinum group minerals (PGM) species. Neues Jahrb. für Mineral. - Abhandlungen 185, 335–349. https://doi.org/10.1127/0077-7757/2009/0127

Zaccarini, F., Pushkarev, E., Garuti, G., 2008. Platinum-group element mineralogy and geochemistry of chromitite of the Kluchevskoy ophiolite complex, central Urals (Russia). Ore Geol. Rev. 33, 20–30. https://doi.org/10.1016/j.oregeorev.2006.05.007

Zaccarini, F., Pushkarev, E. V., Fershtater, G.B., Garuti, G., 2004a. Composition and Mineralogy of PGE-rich Chromitites in the Nurali Lherzolite Gabbro Complex, Southern Urals, Russia. Can. Mineral. 42, 545–562. https://doi.org/10.2113/gscanmin.42.2.545

Zaccarini, F., Singh, A.K., Garuti, G., 2016. Platinum Group Minerals and Silicate Inclusions In Chromitite From the

Naga-Manipur Ophiolite Complex, Indo-Myanmar Orogenic Belt, Northeast India. Can. Mineral. 54, 409–427. https://doi.org/10.3749/canmin.1500034

Zaccarini, F., Stumpfl, E.F., Garuti, G., 2004b. Zirconolite and Zr-Th-U minerals in chromitites of the Finero Complex, Western Alps, Italy: Evidence for carbonatite-type metasomatism in a subcontinental mantle plume. Can. Mineral. 42, 1825–1845. https://doi.org/10.2113/gscanmin.42.6.1825

Zachariadis, P.T. (2007)., 2007. Ophiolites of the eastern Vardar zone, N. Greece, in: PhD Thesis, University of Mainz, Germany.

Zanetti, A., Giovanardi, T., Langone, A., Tiepolo, M., Wu, F.Y., Dallai, L., Mazzucchelli, M., 2016. Origin and age of zircon-bearing chromitite layers from the Finero phlogopite peridotite (Ivrea–Verbano Zone, Western Alps) and geodynamic consequences. Lithos 262, 58–74. https://doi.org/10.1016/j.lithos.2016.06.015

Zanetti, A., Mazzucchelli, M., Rivalenti, G., Vannucci, R., 1999. The Finero phlogopite-peridotite massif: An example of subduction-related metasomatism. Contrib. to Mineral. Petrol. 134, 107–122. https://doi.org/10.1007/s004100050472

Zhmodik, S.M., Agafonov, L.V., 2000. Shandite and other nickel minerals from chromitites of ophiolite association in the southeast of East Sayan. Geol. i Geofiz. 41, 712–721.

Zhou, M.-F., Robinson, P.T., 1997. Origin and tectonic environment of podiform chromite deposits. Econ. Geol. 92, 259–262. https://doi.org/10.2113/gsecongeo.92.2.259

Zhou, M.-F., Robinson, P.T., Malpas, J., Aitchison, J., Sun, M., Bai, W.-J., Hu, X.-F., Yang, J.-S., 2001. Melt/mantle interaction and melt evolution in the Sartohay high-Al chromite deposits of the Dalabute ophiolite (NW China). J. Asian Earth Sci. 19, 517–534. https://doi.org/10.1016/S1367-9120(00)00048-1

Zhou, M.-F., Robinson, P.T., Su, B.-X., Gao, J.-F., Li, J.-W., Yang, J.-S., Malpas, J., 2014. Compositions of chromite, associated minerals, and parental magmas of podiform chromite deposits: The role of slab contamination of asthenospheric melts in suprasubduction zone environments. Gondwana Res. 26, 262–283. https://doi.org/10.1016/j.gr.2013.12.011

Zhou, M.-F., Sun, M., Keays, R.R., Kerrich, R.W., 1998. Controls on Platinum-Group Elemental Distributions of Podiform Chromitites: A Case Study of High-Cr and High-Al Chromitites from Chinese Orogenic Belts. Geochim. Cosmochim. Acta 62, 677–688. https://doi.org/10.1016/S0016-7037(97)00382-7

Zhou, M.F., Robinson, P.T., Bai, W.J., 1994. Formation of podiform chromitites by melt/rock interaction in the upper mantle. Miner. Depos. 29, 98–101. https://doi.org/10.1007/BF03326400

Zhou, M.F., Robinson, P.T., Malpas, J., Li, Z., 1996. Podiform Chromitites in the Luobusa Ophiolite (Southern Tibet): Implications for Melt-Rock Interaction and Chromite Segregation in the Upper Mantle. J. Petrol. 37, 3–21. https://doi.org/10.1093/petrology/37.1.3

Zhu, Y., Tan, J., Qiu, T., 2016. Platinum group mineral (PGM) and Fe–Ni–As–S minerals in the Sartohay chromitite, Xinjiang (NW China): Implications for the mobility of Os, Ir, Sb, and As during hydrothermal processes. Ore Geol. Rev. 72, 299–312. https://doi.org/10.1016/j.oregeorev.2015.08.001

Zientek, M.L., Loferski, P.J., 2014. Platinum-Group Elements—So Many Excellent Properties. U.S. Geol. Surv. Fact Sheet 3064. https://doi.org/10.3133/fs20143064

# Appendix

## Chapter 3

Tab. A3.1 DUN-FIN microprobe analyses of olivine and chromite crystals; d(mm) distance from the intergranular limit.

| Analysis | 1-OL | 2-OL | 3-OL | 4-OL | 5-OL | 6-OL | 7-OL | 8-OL | 9-OL | 10-OL | 11-OL | d rim | 12-CHR | 13-CHR | 14-CHR |
|---|---|---|---|---|---|---|---|---|---|---|---|---|---|---|---|
| X | 62.0880 | 62.0855 | 62.0855 | 62.0850 | 62.0850 | 62.0830 | 62.0830 | 62.0830 | 62.0830 | 62.0830 | 62.0770 | 62.0880 | 62.0770 | 62.0770 | 62.0770 |
| Y | 67.7385 | 67.7685 | 67.8010 | 67.8305 | 67.8610 | 67.8925 | 67.9030 | 67.9145 | 67.9220 | 67.9295 | 67.9385 | 67.9385 | 67.9445 | 67.9475 | 67.9525 |
| **d (mm)** | **0.2000** | **0.1700** | **0.1375** | **0.1080** | **0.0776** | **0.0463** | **0.0359** | **0.0245** | **0.0172** | **0.0103** | **0.0110** | | **0.0125** | **0.0142** | **0.0178** |
| $SiO_2$ | 40.86 | 40.81 | 40.64 | 40.95 | 40.94 | 41.23 | 41.08 | 41.07 | 40.89 | 40.63 | 40.90 | | 0.18 | 0.02 | 0.03 |
| $TiO_2$ | 0.00 | 0.03 | 0.03 | 0.04 | 0.02 | 0.05 | 0.01 | 0.02 | 0.00 | 0.00 | 0.03 | | 0.02 | 0.06 | 0.06 |
| $Al_2O_3$ | 0.00 | 0.01 | 0.00 | 0.00 | 0.00 | 0.02 | 0.00 | 0.00 | 0.00 | 0.00 | 0.03 | | 5.12 | 5.92 | 6.15 |
| $Cr_2O_3$ | 0.03 | 0.00 | 0.03 | 0.01 | 0.02 | 0.03 | 0.08 | 0.14 | 0.24 | 0.32 | 0.51 | | 53.61 | 54.74 | 55.57 |
| $V_2O_3$ | 0.02 | 0.02 | 0.04 | 0.00 | 0.01 | 0.00 | 0.00 | 0.00 | 0.00 | 0.06 | 0.00 | | 0.10 | 0.06 | 0.10 |
| $Fe_2O_3$ | 0.00 | 0.00 | 0.00 | 0.00 | 0.00 | 0.00 | 0.00 | 0.00 | 0.00 | 0.00 | 0.00 | | 8.82 | 8.69 | 8.06 |
| FeO | 8.31 | 8.47 | 8.62 | 8.63 | 8.26 | 8.50 | 8.51 | 8.30 | 8.29 | 8.34 | 7.30 | | 26.49 | 25.23 | 25.29 |
| MnO | 0.08 | 0.20 | 0.18 | 0.17 | 0.14 | 0.12 | 0.18 | 0.12 | 0.19 | 0.16 | 0.12 | | 0.45 | 0.38 | 0.46 |
| MgO | 49.48 | 48.75 | 49.25 | 48.48 | 48.93 | 48.82 | 49.00 | 48.57 | 49.33 | 48.68 | 49.62 | | 3.13 | 4.50 | 4.52 |
| NiO | 0.39 | 0.32 | 0.41 | 0.40 | 0.35 | 0.40 | 0.40 | 0.37 | 0.42 | 0.28 | 0.35 | | 0.08 | 0.01 | 0.08 |
| ZnO | 0.00 | 0.00 | 0.00 | 0.00 | 0.11 | 0.02 | 0.06 | 0.00 | 0.08 | 0.05 | 0.00 | | 0.94 | 0.52 | 0.62 |
| TOT | 99.18 | 98.63 | 99.20 | 98.68 | 98.79 | 99.19 | 99.34 | 98.61 | 99.46 | 98.53 | 98.87 | | 98.94 | 100.14 | 100.95 |
| Si | 1.00 | 1.01 | 1.00 | 1.02 | 1.01 | 1.02 | 1.01 | 1.02 | 1.00 | 1.01 | 1.01 | | 0.01 | 0.00 | 0.00 |
| Ti | 0.00 | 0.00 | 0.00 | 0.00 | 0.00 | 0.00 | 0.00 | 0.00 | 0.00 | 0.00 | 0.00 | | 0.00 | 0.00 | 0.00 |
| Al | 0.00 | 0.00 | 0.00 | 0.00 | 0.00 | 0.00 | 0.00 | 0.00 | 0.00 | 0.00 | 0.00 | | 0.22 | 0.24 | 0.25 |
| Cr | 0.00 | 0.00 | 0.00 | 0.00 | 0.00 | 0.00 | 0.00 | 0.00 | 0.00 | 0.01 | 0.01 | | 1.53 | 1.52 | 1.53 |
| V | 0.00 | 0.00 | 0.00 | 0.00 | 0.00 | 0.00 | 0.00 | 0.00 | 0.00 | 0.00 | 0.00 | | 0.00 | 0.00 | 0.00 |
| $Fe^{3+}$ | 0.00 | 0.00 | 0.00 | 0.00 | 0.00 | 0.00 | 0.00 | 0.00 | 0.00 | 0.00 | 0.00 | | 0.24 | 0.23 | 0.21 |
| $Fe^{2+}$ | 0.17 | 0.18 | 0.18 | 0.18 | 0.17 | 0.18 | 0.18 | 0.17 | 0.17 | 0.17 | 0.15 | | 0.80 | 0.74 | 0.74 |
| Mn | 0.00 | 0.00 | 0.00 | 0.00 | 0.00 | 0.00 | 0.00 | 0.00 | 0.00 | 0.00 | 0.00 | | 0.01 | 0.01 | 0.01 |
| Mg | 1.81 | 1.80 | 1.81 | 1.79 | 1.80 | 1.79 | 1.80 | 1.80 | 1.81 | 1.80 | 1.82 | | 0.17 | 0.24 | 0.23 |
| Ni | 0.01 | 0.01 | 0.01 | 0.01 | 0.01 | 0.01 | 0.01 | 0.01 | 0.01 | 0.01 | 0.01 | | 0.00 | 0.00 | 0.00 |
| Zn | 0.00 | 0.00 | 0.00 | 0.00 | 0.00 | 0.00 | 0.00 | 0.00 | 0.00 | 0.00 | 0.00 | | 0.02 | 0.01 | 0.02 |

| Analysis | 15-CHR | 16-CHR | d rim | 17-CHR | 18-CHR | 19-CHR | 20-CHR | 21-CHR | 22-CHR | 23-CHR | 24-CHR | d rim | 25-OL | 26-OL | 27-OL | 28-OL |
|---|---|---|---|---|---|---|---|---|---|---|---|---|---|---|---|---|
| X | 62.0770 | 62.0770 | 62.0405 | 62.0770 | 62.0865 | 62.0785 | 62.0710 | 62.0600 | 62.0525 | 62.0470 | 62.0420 | 62.0400 | 62.0365 | 62.0340 | 62.0300 | 62.0245 |
| Y | 67.9580 | 67.9655 | 67.9750 | 67.9745 | 67.9825 | 67.9880 | 67.9930 | 68.0020 | 68.0090 | 68.0125 | 68.0150 | 68.0170 | 68.0180 | 68.0190 | 68.0210 | 68.0240 |
| **d (mm)** | **0.0224** | **0.0292** | | **0.0365** | **0.0440** | **0.0482** | **0.0392** | **0.0250** | **0.0148** | **0.0083** | **0.0028** | | **0.0036** | **0.0063** | **0.0108** | **0.0170** |
| $SiO_2$ | 0.01 | 0.00 | | 0.00 | 0.03 | 0.00 | 0.03 | 0.00 | 0.03 | 0.04 | 0.03 | | 40.08 | 40.84 | 40.62 | 40.35 |
| $TiO_2$ | 0.11 | 0.12 | | 0.08 | 0.06 | 0.15 | 0.08 | 0.05 | 0.05 | 0.10 | 0.06 | | 0.00 | 0.00 | 0.02 | 0.01 |
| $Al_2O_3$ | 5.98 | 5.95 | | 5.82 | 5.89 | 5.87 | 5.78 | 5.93 | 5.88 | 6.04 | 5.79 | | 0.00 | 0.00 | 0.01 | 0.01 |
| $Cr_2O_3$ | 56.03 | 56.74 | | 56.62 | 56.03 | 56.28 | 56.83 | 56.63 | 56.78 | 55.60 | 55.66 | | 0.82 | 0.38 | 0.30 | 0.19 |
| $V_2O_3$ | 0.04 | 0.01 | | 0.05 | 0.11 | 0.05 | 0.11 | 0.09 | 0.14 | 0.08 | 0.03 | | 0.00 | 0.00 | 0.00 | 0.00 |
| $Fe_2O_3$ | 7.36 | 7.01 | | 7.22 | 7.57 | 7.36 | 7.02 | 6.64 | 7.26 | 7.57 | 7.60 | | 0.00 | 0.00 | 0.00 | 0.00 |
| FeO | 24.97 | 25.16 | | 25.31 | 25.02 | 25.06 | 25.36 | 25.39 | 25.42 | 25.42 | 25.14 | | 7.41 | 7.59 | 8.14 | 8.33 |
| MnO | 0.41 | 0.40 | | 0.39 | 0.42 | 0.39 | 0.48 | 0.36 | 0.39 | 0.49 | 0.40 | | 0.08 | 0.19 | 0.08 | 0.16 |
| MgO | 4.62 | 4.57 | | 4.55 | 4.63 | 4.68 | 4.51 | 4.41 | 4.61 | 4.40 | 4.45 | | 48.01 | 49.69 | 49.22 | 49.69 |
| NiO | 0.07 | 0.01 | | 0.06 | 0.07 | 0.06 | 0.03 | 0.04 | 0.05 | 0.07 | 0.00 | | 0.33 | 0.31 | 0.46 | 0.36 |
| ZnO | 0.61 | 0.73 | | 0.42 | 0.58 | 0.55 | 0.48 | 0.44 | 0.42 | 0.49 | 0.57 | | 0.03 | 0.01 | 0.00 | 0.03 |
| TOT | 100.23 | 100.71 | | 100.55 | 100.41 | 100.45 | 100.74 | 100.02 | 101.04 | 100.30 | 99.74 | | 96.78 | 99.02 | 98.85 | 99.12 |
| Si | 0.00 | 0.00 | | 0.00 | 0.00 | 0.00 | 0.00 | 0.00 | 0.00 | 0.00 | 0.00 | | 1.01 | 1.00 | 1.00 | 0.99 |
| Ti | 0.00 | 0.00 | | 0.00 | 0.00 | 0.00 | 0.00 | 0.00 | 0.00 | 0.00 | 0.00 | | 0.00 | 0.00 | 0.00 | 0.00 |
| Al | 0.25 | 0.24 | | 0.24 | 0.24 | 0.24 | 0.24 | 0.25 | 0.24 | 0.25 | 0.24 | | 0.00 | 0.00 | 0.00 | 0.00 |
| Cr | 1.55 | 1.56 | | 1.56 | 1.55 | 1.56 | 1.57 | 1.57 | 1.56 | 1.54 | 1.55 | | 0.02 | 0.01 | 0.01 | 0.00 |
| V | 0.00 | 0.00 | | 0.00 | 0.00 | 0.00 | 0.00 | 0.00 | 0.00 | 0.00 | 0.00 | | 0.00 | 0.00 | 0.00 | 0.00 |

| | | | | | | | | | | | | | | |
|---|---|---|---|---|---|---|---|---|---|---|---|---|---|---|
| $Fe^{3+}$ | 0.19 | 0.18 | 0.19 | 0.20 | 0.19 | 0.18 | 0.18 | 0.19 | 0.20 | 0.20 | 0.00 | 0.00 | 0.00 | 0.00 |
| $Fe^{2+}$ | 0.73 | 0.73 | 0.74 | 0.73 | 0.73 | 0.74 | 0.75 | 0.74 | 0.74 | 0.74 | 0.16 | 0.16 | 0.17 | 0.17 |
| Mn | 0.01 | 0.01 | 0.01 | 0.01 | 0.01 | 0.01 | 0.01 | 0.01 | 0.01 | 0.01 | 0.00 | 0.00 | 0.00 | 0.00 |
| Mg | 0.24 | 0.24 | 0.24 | 0.24 | 0.24 | 0.23 | 0.23 | 0.24 | 0.23 | 0.23 | 1.81 | 1.82 | 1.81 | 1.82 |
| Ni | 0.00 | 0.00 | 0.00 | 0.00 | 0.00 | 0.00 | 0.00 | 0.00 | 0.00 | 0.00 | 0.01 | 0.01 | 0.01 | 0.01 |
| Zn | 0.02 | 0.02 | 0.01 | 0.01 | 0.01 | 0.01 | 0.01 | 0.01 | 0.01 | 0.01 | 0.00 | 0.00 | 0.00 | 0.00 |

| Analysis | 29-OL | 30-OL | 31-OL | 32-OL | 33-OL | 34-OL | 35-OL | 36-OL | 37-OL | 38-OL | d rim | 39-CHR | 40-CHR |
|---|---|---|---|---|---|---|---|---|---|---|---|---|---|
| X | 62.0175 | 62.0090 | 61.9910 | 61.9760 | 61.9595 | 61.9370 | 61.9165 | 61.8950 | 62.1520 | 62.1445 | 62.1425 | 62.1400 | 62.1340 |
| Y | 68.0285 | 68.0340 | 68.0500 | 68.0675 | 68.0815 | 68.0990 | 68.1200 | 68.1345 | 68.0055 | 68.0055 | 68.0055 | 68.0055 | 68.0055 |
| **d (mm)** | **0.0253** | **0.0354** | **0.0591** | **0.0815** | **0.1032** | **0.1317** | **0.1608** | **0.1866** | **0.0095** | **0.0020** | | **0.0025** | **0.0085** |
| $SiO_2$ | 40.58 | 40.54 | 40.71 | 40.67 | 40.55 | 40.83 | 40.74 | 40.72 | 40.35 | 40.81 | | 0.25 | 0.04 |
| $TiO_2$ | 0.01 | 0.00 | 0.01 | 0.00 | 0.03 | 0.01 | 0.03 | 0.00 | 0.00 | 0.04 | | 0.06 | 0.14 |
| $Al_2O_3$ | 0.00 | 0.02 | 0.00 | 0.01 | 0.00 | 0.01 | 0.00 | 0.01 | 0.00 | 0.00 | | 5.51 | 5.94 |
| $Cr_2O_3$ | 0.12 | 0.11 | 0.03 | 0.00 | 0.03 | 0.02 | 0.00 | 0.01 | 0.22 | 0.52 | | 52.61 | 54.77 |
| $V_2O_3$ | 0.00 | 0.00 | 0.02 | 0.01 | 0.03 | 0.00 | 0.00 | 0.03 | 0.00 | 0.03 | | 0.06 | 0.05 |
| $Fe_2O_3$ | 0.00 | 0.00 | 0.00 | 0.00 | 0.00 | 0.00 | 0.00 | 0.00 | 0.00 | 0.00 | | 10.01 | 8.44 |
| FeO | 8.55 | 8.31 | 8.62 | 8.27 | 8.35 | 8.61 | 8.37 | 8.78 | 8.64 | 8.12 | | 27.28 | 26.07 |
| MnO | 0.13 | 0.14 | 0.17 | 0.20 | 0.16 | 0.16 | 0.14 | 0.18 | 0.19 | 0.14 | | 0.49 | 0.43 |
| MgO | 49.01 | 49.31 | 48.93 | 49.67 | 48.76 | 48.99 | 48.85 | 48.69 | 49.26 | 49.17 | | 2.95 | 3.89 |
| NiO | 0.35 | 0.42 | 0.25 | 0.33 | 0.41 | 0.36 | 0.43 | 0.37 | 0.44 | 0.31 | | 0.00 | 0.11 |
| ZnO | 0.00 | 0.06 | 0.05 | 0.09 | 0.07 | 0.10 | 0.00 | 0.00 | 0.04 | 0.01 | | 1.05 | 0.73 |
| TOT | 98.77 | 98.91 | 98.80 | 99.25 | 98.39 | 99.10 | 98.56 | 98.80 | 99.14 | 99.17 | | 100.28 | 100.63 |
| Si | 1.00 | 1.00 | 1.01 | 1.00 | 1.01 | 1.01 | 1.01 | 1.01 | 0.99 | 1.01 | | 0.01 | 0.00 |
| Ti | 0.00 | 0.00 | 0.00 | 0.00 | 0.00 | 0.00 | 0.00 | 0.00 | 0.00 | 0.00 | | 0.00 | 0.00 |
| Al | 0.00 | 0.00 | 0.00 | 0.00 | 0.00 | 0.00 | 0.00 | 0.00 | 0.00 | 0.00 | | 0.23 | 0.25 |
| Cr | 0.00 | 0.00 | 0.00 | 0.00 | 0.00 | 0.00 | 0.00 | 0.00 | 0.00 | 0.01 | | 1.48 | 1.52 |
| V | 0.00 | 0.00 | 0.00 | 0.00 | 0.00 | 0.00 | 0.00 | 0.00 | 0.00 | 0.00 | | 0.00 | 0.00 |
| $Fe^{3+}$ | 0.00 | 0.00 | 0.00 | 0.00 | 0.00 | 0.00 | 0.00 | 0.00 | 0.00 | 0.00 | | 0.27 | 0.22 |
| $Fe^{2+}$ | 0.18 | 0.17 | 0.18 | 0.17 | 0.17 | 0.18 | 0.17 | 0.18 | 0.18 | 0.17 | | 0.81 | 0.77 |
| Mn | 0.00 | 0.00 | 0.00 | 0.00 | 0.00 | 0.00 | 0.00 | 0.00 | 0.00 | 0.00 | | 0.01 | 0.01 |
| Mg | 1.81 | 1.81 | 1.80 | 1.82 | 1.81 | 1.80 | 1.80 | 1.80 | 1.81 | 1.81 | | 0.16 | 0.20 |
| Ni | 0.01 | 0.01 | 0.00 | 0.01 | 0.01 | 0.01 | 0.01 | 0.01 | 0.01 | 0.01 | | 0.00 | 0.00 |
| Zn | 0.00 | 0.00 | 0.00 | 0.00 | 0.00 | 0.00 | 0.00 | 0.00 | 0.00 | 0.00 | | 0.03 | 0.02 |

Tab. A3.2 FIN01A microprobe analyses of olivine and chromite crystals; d(mm) distance from the intergranular limit.

| Analysis | FIN01A-1 | FIN01A-2 | FIN01A-3 | FIN01A-4 | FIN01A-5 | FIN01A-6 | FIN01A-7 | FIN01A-8 | FIN01A-9 | FIN01A-10 | d chr | FIN01A-11 | FIN01A-12 | FIN01A-13 | FIN01A-14 | FIN01A-15 | FIN01A-16 | FIN01A-17 | FIN01A-18 |
|---|---|---|---|---|---|---|---|---|---|---|---|---|---|---|---|---|---|---|---|
| | 92-OL | 93-OL | 94-CHR | 95-CHR | 96-OL | 97-CHR | 98-CHR | 99-CHR | 100-CHR | 101-CHR | | 102-OL | 103-OL | 104-OL | 105-OL | 106-OL | 107-OL | 108-OL | 109-OL |
| X | 53.23 | 53.22 | 53.17 | 53.29 | 53.29 | 52.13 | 52.07 | 52.01 | 51.97 | 51.94 | 51.93 | 51.92 | 51.90 | 51.89 | 51.82 | 51.73 | 51.66 | 51.62 | 51.54 |
| Y | 92.35 | 92.35 | 92.33 | 92.34 | 92.35 | 92.47 | 92.44 | 92.40 | 92.40 | 92.41 | 92.41 | 92.40 | 92.39 | 92.35 | 92.29 | 92.16 | 92.10 | 92.06 | 91.98 |
| **d (mm)** | | | | | | **0.21** | **0.14** | **0.08** | **0.04** | **0.01** | | **0.01** | **0.04** | **0.07** | **0.16** | **0.32** | **0.35** | **0.30** | **0.19** |
| $SiO_2$ | 40.27 | 41.16 | 0.09 | 0.11 | 40.90 | 0.01 | 0.03 | 0.02 | 0.00 | 0.04 | | 41.29 | 41.07 | 41.22 | 40.85 | 40.99 | 40.57 | 41.01 | 41.09 |
| $TiO_2$ | 0.05 | 0.01 | 0.44 | 0.46 | 0.02 | 0.58 | 0.60 | 0.55 | 0.54 | 0.43 | | 0.02 | 0.02 | 0.02 | 0.01 | 0.00 | 0.01 | 0.00 | 0.00 |
| $Al_2O_3$ | 0.16 | 0.01 | 14.02 | 14.58 | 0.02 | 13.86 | 13.75 | 13.72 | 13.67 | 12.69 | | 0.01 | 0.00 | 0.00 | 0.03 | 0.00 | 0.01 | 0.00 | 0.00 |
| $Cr_2O_3$ | 0.61 | 0.36 | 48.75 | 47.09 | 0.25 | 51.50 | 51.24 | 51.80 | 51.67 | 52.75 | | 0.38 | 0.07 | 0.04 | 0.00 | 0.06 | 0.00 | 0.01 | 0.00 |
| $V_2O_3$ | 0.01 | 0.00 | 0.09 | 0.02 | 0.01 | 0.10 | 0.07 | 0.02 | 0.05 | 0.00 | | 0.02 | 0.00 | 0.00 | 0.06 | 0.03 | 0.00 | 0.02 | 0.02 |
| $Fe_2O_3$ | 0.00 | 0.00 | 8.32 | 7.77 | 0.00 | 5.72 | 5.86 | 5.87 | 5.85 | 5.25 | | 0.00 | 0.00 | 0.00 | 0.00 | 0.00 | 0.00 | 0.00 | 0.00 |
| FeO | 3.80 | 3.73 | 17.81 | 20.12 | 4.08 | 18.51 | 18.55 | 18.28 | 18.17 | 18.77 | | 4.39 | 5.31 | 5.46 | 5.70 | 5.87 | 5.66 | 5.82 | 5.89 |
| MnO | 0.05 | 0.12 | 0.16 | 0.20 | 0.00 | 0.17 | 0.16 | 0.11 | 0.10 | 0.17 | | 0.07 | 0.09 | 0.07 | 0.10 | 0.09 | 0.02 | 0.15 | 0.05 |
| MgO | 53.02 | 52.88 | 10.99 | 9.34 | 51.71 | 10.60 | 10.56 | 10.78 | 10.81 | 10.11 | | 52.51 | 51.50 | 51.66 | 51.75 | 50.80 | 51.23 | 51.23 | 51.69 |
| NiO | 0.29 | 0.37 | 0.10 | 0.14 | 0.36 | 0.10 | 0.08 | 0.07 | 0.06 | 0.00 | | 0.39 | 0.32 | 0.38 | 0.31 | 0.35 | 0.30 | 0.33 | 0.34 |
| ZnO | 0.00 | 0.01 | 0.03 | 0.00 | 0.00 | 0.10 | 0.14 | 0.17 | 0.09 | 0.16 | | 0.07 | 0.00 | 0.08 | 0.00 | 0.05 | 0.02 | 0.11 | 0.08 |
| TOT | 98.26 | 98.66 | 100.84 | 99.86 | 97.36 | 101.28 | 101.05 | 101.41 | 101.01 | 100.37 | | 99.15 | 98.40 | 98.95 | 98.81 | 98.24 | 97.82 | 98.71 | 99.18 |
| Si | 0.98 | 1.00 | 0.00 | 0.00 | 1.01 | 0.00 | 0.00 | 0.00 | 0.00 | 0.00 | | 1.00 | 1.00 | 1.00 | 0.99 | 1.01 | 1.00 | 1.00 | 1.00 |
| Ti | 0.00 | 0.00 | 0.01 | 0.01 | 0.00 | 0.01 | 0.01 | 0.01 | 0.01 | 0.01 | | 0.00 | 0.00 | 0.00 | 0.00 | 0.00 | 0.00 | 0.00 | 0.00 |

| | | | | | | | | | | | | | | | | | | |
|---|---|---|---|---|---|---|---|---|---|---|---|---|---|---|---|---|---|---|
| Al | 0.00 | 0.00 | 0.53 | 0.56 | 0.00 | 0.52 | 0.52 | 0.52 | 0.52 | 0.49 | 0.00 | 0.00 | 0.00 | 0.00 | 0.00 | 0.00 | 0.00 | 0.00 |
| Cr | 0.01 | 0.01 | 1.24 | 1.22 | 0.00 | 1.31 | 1.30 | 1.31 | 1.31 | 1.36 | 0.01 | 0.00 | 0.00 | 0.00 | 0.00 | 0.00 | 0.00 | 0.00 |
| V | 0.00 | 0.00 | 0.00 | 0.00 | 0.00 | 0.00 | 0.00 | 0.00 | 0.00 | 0.00 | 0.00 | 0.00 | 0.00 | 0.00 | 0.00 | 0.00 | 0.00 | 0.00 |
| $Fe^{3+}$ | 0.00 | 0.00 | 0.20 | 0.19 | 0.00 | 0.14 | 0.14 | 0.14 | 0.14 | 0.13 | 0.00 | 0.00 | 0.00 | 0.00 | 0.00 | 0.00 | 0.00 | 0.00 |
| $Fe^{2+}$ | 0.08 | 0.08 | 0.48 | 0.55 | 0.08 | 0.50 | 0.50 | 0.49 | 0.49 | 0.51 | 0.09 | 0.11 | 0.11 | 0.12 | 0.12 | 0.12 | 0.12 | 0.12 |
| Mn | 0.00 | 0.00 | 0.00 | 0.01 | 0.00 | 0.00 | 0.00 | 0.00 | 0.00 | 0.00 | 0.00 | 0.00 | 0.00 | 0.00 | 0.00 | 0.00 | 0.00 | 0.00 |
| Mg | 1.92 | 1.91 | 0.53 | 0.46 | 1.90 | 0.51 | 0.51 | 0.51 | 0.52 | 0.49 | 1.89 | 1.88 | 1.87 | 1.88 | 1.86 | 1.88 | 1.87 | 1.87 |
| Ni | 0.01 | 0.01 | 0.00 | 0.00 | 0.01 | 0.00 | 0.00 | 0.00 | 0.00 | 0.00 | 0.01 | 0.01 | 0.01 | 0.01 | 0.01 | 0.01 | 0.01 | 0.01 |
| Zn | 0.00 | 0.00 | 0.00 | 0.00 | 0.00 | 0.00 | 0.00 | 0.00 | 0.00 | 0.00 | 0.00 | 0.00 | 0.00 | 0.00 | 0.00 | 0.00 | 0.00 | 0.00 |

| Analysis | FIN01A-19 | FIN01A-20 | FIN01A-21 | FIN01A-22 | FIN01A-23 | FIN01A-24 | d chr | FIN01A-25 | FIN01A-26 | FIN01A-27 | FIN01A-28 | FIN01A-29 | FIN01A-30 | FIN01A-31 | FIN01A-32 | FIN01A-33 | FIN01A-34 | FIN01A-35 | FIN01A-36 | FIN01A-37 |
|---|---|---|---|---|---|---|---|---|---|---|---|---|---|---|---|---|---|---|---|---|
| | 110-OL | 111-OL | 112-OL | 113-OL | 114-OL | 115-OL | | 116-CHR | 117-CHR | 118-CHR | 119-CHR | 120-CHR | 121-CHR | 122-CHR | 123-CHR | 124-CHR | 125-CHR | 126-CHR | 127-CHR | 128-CHR |
| X | 51.51 | 51.47 | 51.45 | 51.42 | 51.40 | 51.39 | 51.38 | 51.37 | 51.36 | 51.34 | 51.32 | 51.29 | 51.25 | 51.20 | 51.16 | 38.39 | 38.39 | 38.42 | 38.45 | 38.45 |
| Y | 91.94 | 91.92 | 91.90 | 91.89 | 91.88 | 91.90 | 91.89 | 91.89 | 91.88 | 91.87 | 91.86 | 91.84 | 91.81 | 91.78 | 91.71 | 89.76 | 89.95 | 90.11 | 90.23 | 90.37 |
| **d (mm)** | **0.14** | **0.10** | **0.07** | **0.05** | **0.03** | **0.01** | | **0.00** | **0.02** | **0.04** | **0.07** | **0.10** | **0.15** | **0.20** | **0.28** | **1.02** | **0.83** | **0.69** | **0.58** | **0.45** |
| $SiO_2$ | 41.07 | 40.70 | 41.03 | 40.89 | 41.03 | 41.14 | | 1.91 | 0.04 | 0.02 | 0.02 | 0.25 | 0.01 | 0.00 | 0.04 | 0.00 | 0.00 | 0.03 | 0.00 | 0.02 |
| $TiO_2$ | 0.01 | 0.00 | 0.00 | 0.02 | 0.02 | 0.01 | | 0.64 | 0.70 | 0.70 | 0.61 | 0.70 | 0.64 | 0.50 | 0.53 | 0.63 | 0.63 | 0.65 | 0.64 | 0.66 |
| $Al_2O_3$ | 0.00 | 0.00 | 0.00 | 0.02 | 0.00 | 0.00 | | 21.51 | 14.01 | 14.22 | 14.72 | 16.35 | 15.22 | 13.59 | 13.49 | 14.67 | 14.26 | 14.51 | 13.69 | 13.96 |
| $Cr_2O_3$ | 0.00 | 0.06 | 0.00 | 0.07 | 0.15 | 0.24 | | 42.58 | 50.49 | 51.03 | 51.26 | 49.55 | 50.06 | 51.39 | 52.14 | 50.47 | 51.47 | 50.96 | 51.97 | 51.17 |
| $V_2O_3$ | 0.00 | 0.00 | 0.00 | 0.00 | 0.00 | 0.02 | | 0.04 | 0.09 | 0.01 | 0.06 | 0.08 | 0.06 | 0.06 | 0.02 | 0.03 | 0.02 | 0.06 | 0.00 | 0.04 |
| $Fe_2O_3$ | 0.00 | 0.00 | 0.00 | 0.00 | 0.00 | 0.00 | | 8.62 | 6.95 | 6.56 | 6.09 | 6.81 | 6.16 | 6.19 | 6.28 | 6.40 | 5.72 | 5.87 | 5.83 | 6.21 |
| FeO | 5.64 | 5.26 | 5.04 | 4.84 | 4.56 | 4.32 | | 13.66 | 18.06 | 17.87 | 17.83 | 16.82 | 17.41 | 17.34 | 17.59 | 17.22 | 17.72 | 18.15 | 17.91 | 17.64 |
| MnO | 0.07 | 0.12 | 0.06 | 0.09 | 0.08 | 0.06 | | 0.00 | 0.14 | 0.17 | 0.15 | 0.11 | 0.19 | 0.14 | 0.21 | 0.14 | 0.14 | 0.16 | 0.09 | 0.19 |
| MgO | 51.30 | 51.96 | 51.93 | 51.76 | 52.17 | 52.38 | | 17.31 | 11.15 | 11.36 | 11.40 | 12.79 | 11.54 | 11.22 | 11.18 | 11.52 | 11.28 | 11.07 | 11.12 | 11.20 |
| NiO | 0.42 | 0.28 | 0.35 | 0.30 | 0.43 | 0.38 | | 0.22 | 0.07 | 0.08 | 0.09 | 0.03 | 0.10 | 0.11 | 0.04 | 0.20 | 0.11 | 0.11 | 0.06 | 0.10 |
| ZnO | 0.00 | 0.08 | 0.07 | 0.00 | 0.00 | 0.10 | | 0.16 | 0.15 | 0.03 | 0.10 | 0.11 | 0.10 | 0.00 | 0.26 | 0.15 | 0.00 | 0.06 | 0.12 | 0.18 |
| TOT | 98.51 | 98.49 | 98.49 | 98.00 | 98.44 | 98.66 | | 106.67 | 101.86 | 102.05 | 102.34 | 103.63 | 101.51 | 100.53 | 101.80 | 101.44 | 101.37 | 101.64 | 101.43 | 101.39 |
| Si | 1.00 | 0.99 | 1.00 | 1.00 | 1.00 | 1.00 | | 0.05 | 0.00 | 0.00 | 0.00 | 0.01 | 0.00 | 0.00 | 0.00 | 0.00 | 0.00 | 0.00 | 0.00 | 0.00 |
| Ti | 0.00 | 0.00 | 0.00 | 0.00 | 0.00 | 0.00 | | 0.01 | 0.02 | 0.02 | 0.01 | 0.02 | 0.02 | 0.01 | 0.01 | 0.02 | 0.02 | 0.02 | 0.02 | 0.02 |
| Al | 0.00 | 0.00 | 0.00 | 0.00 | 0.00 | 0.00 | | 0.72 | 0.53 | 0.53 | 0.55 | 0.59 | 0.57 | 0.52 | 0.51 | 0.55 | 0.54 | 0.54 | 0.52 | 0.53 |
| Cr | 0.00 | 0.00 | 0.00 | 0.00 | 0.00 | 0.00 | | 0.96 | 1.27 | 1.28 | 1.28 | 1.20 | 1.25 | 1.31 | 1.31 | 1.27 | 1.30 | 1.28 | 1.31 | 1.29 |
| V | 0.00 | 0.00 | 0.00 | 0.00 | 0.00 | 0.00 | | 0.00 | 0.00 | 0.00 | 0.00 | 0.00 | 0.00 | 0.00 | 0.00 | 0.00 | 0.00 | 0.00 | 0.00 | 0.00 |
| $Fe^{3+}$ | 0.00 | 0.00 | 0.00 | 0.00 | 0.00 | 0.00 | | 0.18 | 0.17 | 0.16 | 0.14 | 0.16 | 0.15 | 0.15 | 0.15 | 0.15 | 0.14 | 0.14 | 0.14 | 0.15 |
| $Fe^{2+}$ | 0.12 | 0.11 | 0.10 | 0.10 | 0.09 | 0.09 | | 0.32 | 0.48 | 0.47 | 0.47 | 0.43 | 0.46 | 0.47 | 0.47 | 0.46 | 0.47 | 0.48 | 0.48 | 0.47 |
| Mn | 0.00 | 0.00 | 0.00 | 0.00 | 0.00 | 0.00 | | 0.00 | 0.00 | 0.00 | 0.00 | 0.00 | 0.00 | 0.00 | 0.01 | 0.00 | 0.00 | 0.00 | 0.00 | 0.01 |
| Mg | 1.87 | 1.89 | 1.89 | 1.89 | 1.89 | 1.90 | | 0.73 | 0.53 | 0.54 | 0.54 | 0.59 | 0.54 | 0.54 | 0.53 | 0.55 | 0.54 | 0.52 | 0.53 | 0.53 |
| Ni | 0.01 | 0.01 | 0.01 | 0.01 | 0.01 | 0.01 | | 0.01 | 0.00 | 0.00 | 0.00 | 0.00 | 0.00 | 0.00 | 0.00 | 0.01 | 0.00 | 0.00 | 0.00 | 0.00 |
| Zn | 0.00 | 0.00 | 0.00 | 0.00 | 0.00 | 0.00 | | 0.00 | 0.00 | 0.00 | 0.00 | 0.00 | 0.00 | 0.00 | 0.01 | 0.00 | 0.00 | 0.00 | 0.00 | 0.00 |

| Analysis | FIN01A-38 | FIN01A-39 | FIN01A-40 | FIN01A-41 | FIN01A-42 | d chr | FIN01A-43 | FIN01A-44 | FIN01A-45 | FIN01A-46 | FIN01A-47 | FIN01A-48 | FIN01A-49 | FIN01A-50 | FIN01A-51 | FIN01A-52 | FIN01A-53 | d chr | FIN01A-54 | FIN01A-55 | FIN01A-56 |
|---|---|---|---|---|---|---|---|---|---|---|---|---|---|---|---|---|---|---|---|---|---|
| | 129-CHR | 130-CHR | 131-CHR | 132-CHR | 133-CHR | | 134-OL | 135-OL | 136-OL | 137-OL | 138-OL | 139-OL | 140-OL | 141-OL | 142-OL | 143-OL | 144-OL | | 145-CHR | 146-CHR | 147-CHR |
| X | 38.45 | 38.45 | 38.46 | 38.46 | 38.22 | 38.22 | 38.22 | 38.22 | 38.21 | 38.22 | 38.19 | 38.17 | 38.19 | 38.17 | 38.17 | 38.18 | 38.18 | 38.18 | 38.17 | 38.16 | 38.16 |
| Y | 90.54 | 90.60 | 90.64 | 90.68 | 90.76 | 90.77 | 90.78 | 90.85 | 90.99 | 91.16 | 91.33 | 91.44 | 91.56 | 91.65 | 91.69 | 91.74 | 91.75 | 91.76 | 91.76 | 91.78 | 91.81 |
| **d (mm)** | **0.32** | **0.28** | **0.27** | **0.25** | **0.01** | | **0.01** | **0.08** | **0.22** | **0.39** | **0.43** | **0.32** | **0.20** | **0.11** | **0.06** | **0.02** | **0.01** | | **0.01** | **0.03** | **0.05** |
| $SiO_2$ | 0.02 | 0.01 | 0.03 | 0.01 | 0.01 | | 41.52 | 40.84 | 41.26 | 40.99 | 40.73 | 40.34 | 40.84 | 40.77 | 40.56 | 41.34 | 40.82 | | 0.01 | 0.04 | 0.04 |
| $TiO_2$ | 0.64 | 0.63 | 0.59 | 0.59 | 0.43 | | 0.00 | 0.01 | 0.00 | 0.05 | 0.04 | 0.00 | 0.00 | 0.01 | 0.00 | 0.00 | 0.00 | | 0.31 | 0.39 | 0.43 |
| $Al_2O_3$ | 14.09 | 13.73 | 13.60 | 13.31 | 12.30 | | 0.01 | 0.01 | 0.00 | 0.00 | 0.00 | 0.00 | 0.03 | 0.00 | 0.00 | 0.00 | 0.00 | | 12.40 | 13.51 | 13.77 |
| $Cr_2O_3$ | 51.60 | 51.69 | 52.05 | 52.81 | 54.28 | | 0.40 | 0.00 | 0.00 | 0.01 | 0.00 | 0.00 | 0.05 | 0.00 | 0.05 | 0.10 | 0.11 | | 51.90 | 51.56 | 51.75 |
| $V_2O_3$ | 0.03 | 0.05 | 0.07 | 0.00 | 0.06 | | 0.02 | 0.02 | 0.00 | 0.00 | 0.01 | 0.02 | 0.00 | 0.00 | 0.03 | 0.00 | 0.00 | | 0.09 | 0.09 | 0.04 |
| $Fe_2O_3$ | 5.74 | 5.73 | 5.45 | 5.71 | 5.11 | | 0.00 | 0.00 | 0.00 | 0.00 | 0.00 | 0.00 | 0.00 | 0.00 | 0.00 | 0.00 | 0.00 | | 6.55 | 6.47 | 6.31 |
| FeO | 18.35 | 18.04 | 17.98 | 17.72 | 17.66 | | 4.06 | 5.42 | 6.08 | 6.06 | 6.21 | 6.03 | 5.69 | 5.17 | 5.26 | 4.76 | 4.60 | | 18.47 | 17.93 | 17.38 |
| MnO | 0.18 | 0.07 | 0.14 | 0.21 | 0.17 | | 0.04 | 0.08 | 0.06 | 0.09 | 0.05 | 0.10 | 0.10 | 0.06 | 0.09 | 0.03 | 0.07 | | 0.19 | 0.12 | 0.11 |

| | | | | | | | | | | | | | | | | | | | |
|---|---|---|---|---|---|---|---|---|---|---|---|---|---|---|---|---|---|---|---|
| MgO | 10.85 | 11.02 | 10.95 | 11.11 | 10.98 | 52.49 | 51.94 | 51.15 | 51.01 | 50.59 | 50.70 | 51.75 | 51.28 | 51.40 | 52.03 | 52.15 | 10.06 | 10.87 | 11.35 |
| NiO | 0.11 | 0.10 | 0.08 | 0.07 | 0.03 | 0.32 | 0.37 | 0.43 | 0.38 | 0.26 | 0.33 | 0.33 | 0.38 | 0.36 | 0.38 | 0.39 | 0.04 | 0.09 | 0.12 |
| ZnO | 0.17 | 0.00 | 0.08 | 0.21 | 0.03 | 0.00 | 0.05 | 0.08 | 0.07 | 0.05 | 0.00 | 0.07 | 0.00 | 0.00 | 0.01 | 0.00 | 0.20 | 0.14 | 0.04 |
| TOT | 101.78 | 101.07 | 101.03 | 101.74 | 101.06 | 98.88 | 98.77 | 99.06 | 98.66 | 97.95 | 97.52 | 98.87 | 97.69 | 97.75 | 98.65 | 98.14 | 100.24 | 101.21 | 101.35 |
| Si | 0.00 | 0.00 | 0.00 | 0.00 | 0.00 | 1.01 | 0.99 | 1.01 | 1.00 | 1.00 | 1.00 | 0.99 | 1.00 | 1.00 | 1.01 | 1.00 | 0.00 | 0.00 | 0.00 |
| Ti | 0.02 | 0.02 | 0.01 | 0.01 | 0.01 | 0.00 | 0.00 | 0.00 | 0.00 | 0.00 | 0.00 | 0.00 | 0.00 | 0.00 | 0.00 | 0.00 | 0.01 | 0.01 | 0.01 |
| Al | 0.53 | 0.52 | 0.51 | 0.50 | 0.47 | 0.00 | 0.00 | 0.00 | 0.00 | 0.00 | 0.00 | 0.00 | 0.00 | 0.00 | 0.00 | 0.00 | 0.48 | 0.51 | 0.52 |
| Cr | 1.30 | 1.31 | 1.32 | 1.33 | 1.38 | 0.01 | 0.00 | 0.00 | 0.00 | 0.00 | 0.00 | 0.00 | 0.00 | 0.00 | 0.00 | 0.00 | 1.34 | 1.31 | 1.31 |
| V | 0.00 | 0.00 | 0.00 | 0.00 | 0.00 | 0.00 | 0.00 | 0.00 | 0.00 | 0.00 | 0.00 | 0.00 | 0.00 | 0.00 | 0.00 | 0.00 | 0.00 | 0.00 | 0.00 |
| $Fe^{3+}$ | 0.14 | 0.14 | 0.13 | 0.14 | 0.12 | 0.00 | 0.00 | 0.00 | 0.00 | 0.00 | 0.00 | 0.00 | 0.00 | 0.00 | 0.00 | 0.00 | 0.16 | 0.16 | 0.15 |
| $Fe^{2+}$ | 0.49 | 0.48 | 0.48 | 0.47 | 0.48 | 0.08 | 0.11 | 0.12 | 0.12 | 0.13 | 0.12 | 0.12 | 0.11 | 0.11 | 0.10 | 0.09 | 0.51 | 0.48 | 0.46 |
| Mn | 0.00 | 0.00 | 0.00 | 0.01 | 0.00 | 0.00 | 0.00 | 0.00 | 0.00 | 0.00 | 0.00 | 0.00 | 0.00 | 0.00 | 0.00 | 0.00 | 0.01 | 0.00 | 0.00 |
| Mg | 0.52 | 0.53 | 0.52 | 0.53 | 0.53 | 1.90 | 1.88 | 1.86 | 1.86 | 1.86 | 1.87 | 1.88 | 1.88 | 1.88 | 1.89 | 1.90 | 0.49 | 0.52 | 0.54 |
| Ni | 0.00 | 0.00 | 0.00 | 0.00 | 0.00 | 0.01 | 0.01 | 0.01 | 0.01 | 0.01 | 0.01 | 0.01 | 0.01 | 0.01 | 0.01 | 0.01 | 0.00 | 0.00 | 0.00 |
| Zn | 0.00 | 0.00 | 0.00 | 0.00 | 0.00 | 0.00 | 0.00 | 0.00 | 0.00 | 0.00 | 0.00 | 0.00 | 0.00 | 0.00 | 0.00 | 0.00 | 0.00 | 0.00 | 0.00 |

Tab. A3.3 FIN01B-1 microprobe analyses of olivine and chromite crystals; d(mm) distance from the intergranular limit

| Analysis | GRID 1-1 | GRID 1-2 | GRID 1-3 | GRID 1-4 | GRID 1-5 | GRID 1-6 | GRID 1-7 | GRID 2-1 | GRID 2-2 | GRID 2-3 | GRID 2-4 | GRID 2-5 | GRID 2-6 | GRID 2-7 | GRID 3-1 | GRID 3-2 | GRID 3-3 | GRID 3-4 | GRID 3-5 | GRID 3-6 |
|---|---|---|---|---|---|---|---|---|---|---|---|---|---|---|---|---|---|---|---|---|
| | 60-OL | 61-OL | 62-OL | 63-OL | 64-OL | 65-OL | 66-OL | 67-OL | 68-OL | 69-OL | 70-OL | 71-OL | 72-OL | 73-OL | 74-OL | 75-OL | 76-OL | 77-OL | 78-OL | 79-OL |
| X | 75.52 | 75.52 | 75.52 | 75.52 | 75.52 | 75.52 | 75.52 | 75.62 | 75.62 | 75.62 | 75.62 | 75.62 | 75.62 | 75.62 | 75.72 | 75.72 | 75.72 | 75.72 | 75.72 | 75.72 |
| Y | 69.97 | 70.07 | 70.17 | 70.27 | 70.37 | 70.47 | 70.57 | 69.97 | 70.07 | 70.17 | 70.27 | 70.37 | 70.47 | 70.57 | 69.97 | 70.07 | 70.17 | 70.27 | 70.37 | 70.47 |
| **d (mm)** | **0.40** | **0.35** | **0.32** | **0.32** | **0.34** | **0.39** | **0.45** | **0.33** | **0.26** | **0.22** | **0.21** | **0.24** | **0.30** | **0.38** | **0.26** | **0.18** | **0.13** | **0.11** | **0.16** | **0.24** |
| $SiO_2$ | 41.02 | 41.34 | 41.08 | 41.22 | 41.18 | 41.19 | 41.86 | 41.46 | 41.32 | 41.31 | 40.96 | 41.29 | 41.24 | 41.07 | 41.37 | 41.02 | 41.36 | 41.17 | 40.98 | 41.26 |
| $TiO_2$ | 0.03 | 0.02 | 0.03 | 0.00 | 0.00 | 0.03 | 0.04 | 0.00 | 0.00 | 0.00 | 0.00 | 0.07 | 0.00 | 0.02 | 0.00 | 0.00 | 0.01 | 0.02 | 0.02 | 0.00 |
| $Al_2O_3$ | 0.01 | 0.01 | 0.00 | 0.00 | 0.00 | 0.01 | 0.00 | 0.00 | 0.00 | 0.00 | 0.01 | 0.04 | 0.00 | 0.02 | 0.00 | 0.03 | 0.00 | 0.00 | 0.00 | 0.00 |
| $Cr_2O_3$ | 0.00 | 0.03 | 0.02 | 0.00 | 0.04 | 0.00 | 0.05 | 0.00 | 0.01 | 0.00 | 0.00 | 0.02 | 0.01 | 0.00 | 0.00 | 0.00 | 0.03 | 0.00 | 0.00 | 0.00 |
| $V_2O_3$ | 0.02 | 0.01 | 0.02 | 0.00 | 0.01 | 0.00 | 0.01 | 0.05 | 0.00 | 0.00 | 0.00 | 0.00 | 0.00 | 0.00 | 0.00 | 0.07 | 0.00 | 0.00 | 0.04 | 0.00 |
| $Fe_2O_3$ | 0.00 | 0.00 | 0.00 | 0.00 | 0.00 | 0.00 | 0.00 | 0.00 | 0.00 | 0.00 | 0.00 | 0.00 | 0.00 | 0.00 | 0.00 | 0.00 | 0.00 | 0.00 | 0.00 | 0.00 |
| FeO | 8.49 | 7.99 | 8.43 | 8.25 | 8.24 | 8.24 | 8.23 | 8.28 | 8.16 | 8.02 | 8.36 | 7.94 | 8.42 | 8.53 | 8.17 | 8.31 | 8.40 | 8.30 | 8.29 | 8.29 |
| MnO | 0.10 | 0.09 | 0.12 | 0.15 | 0.16 | 0.16 | 0.13 | 0.12 | 0.09 | 0.17 | 0.13 | 0.13 | 0.16 | 0.12 | 0.14 | 0.10 | 0.12 | 0.13 | 0.06 | 0.07 |
| MgO | 49.88 | 50.45 | 50.11 | 50.24 | 50.42 | 50.01 | 50.24 | 50.14 | 50.37 | 49.91 | 50.31 | 50.42 | 50.43 | 50.60 | 50.80 | 50.62 | 50.26 | 50.41 | 50.40 | 50.42 |
| NiO | 0.34 | 0.31 | 0.27 | 0.35 | 0.40 | 0.33 | 0.29 | 0.34 | 0.28 | 0.31 | 0.35 | 0.23 | 0.34 | 0.37 | 0.27 | 0.39 | 0.32 | 0.33 | 0.29 | 0.36 |
| ZnO | 0.00 | 0.00 | 0.01 | 0.05 | 0.07 | 0.08 | 0.00 | 0.10 | 0.02 | 0.11 | 0.00 | 0.16 | 0.00 | 0.00 | 0.04 | 0.00 | 0.00 | 0.00 | 0.01 | 0.00 |
| TOT | 99.92 | 100.26 | 100.11 | 100.29 | 100.54 | 100.06 | 100.87 | 100.54 | 100.28 | 99.86 | 100.14 | 100.32 | 100.61 | 100.76 | 100.80 | 100.54 | 100.52 | 100.38 | 100.09 | 100.42 |
| Si | 1.00 | 1.00 | 1.00 | 1.00 | 1.00 | 1.00 | 1.01 | 1.01 | 1.00 | 1.01 | 1.00 | 1.00 | 1.00 | 0.99 | 1.00 | 0.99 | 1.00 | 1.00 | 1.00 | 1.00 |
| Ti | 0.00 | 0.00 | 0.00 | 0.00 | 0.00 | 0.00 | 0.00 | 0.00 | 0.00 | 0.00 | 0.00 | 0.00 | 0.00 | 0.00 | 0.00 | 0.00 | 0.00 | 0.00 | 0.00 | 0.00 |
| Al | 0.00 | 0.00 | 0.00 | 0.00 | 0.00 | 0.00 | 0.00 | 0.00 | 0.00 | 0.00 | 0.00 | 0.00 | 0.00 | 0.00 | 0.00 | 0.00 | 0.00 | 0.00 | 0.00 | 0.00 |
| Cr | 0.00 | 0.00 | 0.00 | 0.00 | 0.00 | 0.00 | 0.00 | 0.00 | 0.00 | 0.00 | 0.00 | 0.00 | 0.00 | 0.00 | 0.00 | 0.00 | 0.00 | 0.00 | 0.00 | 0.00 |
| V | 0.00 | 0.00 | 0.00 | 0.00 | 0.00 | 0.00 | 0.00 | 0.00 | 0.00 | 0.00 | 0.00 | 0.00 | 0.00 | 0.00 | 0.00 | 0.00 | 0.00 | 0.00 | 0.00 | 0.00 |
| $Fe^{3+}$ | 0.00 | 0.00 | 0.00 | 0.00 | 0.00 | 0.00 | 0.00 | 0.00 | 0.00 | 0.00 | 0.00 | 0.00 | 0.00 | 0.00 | 0.00 | 0.00 | 0.00 | 0.00 | 0.00 | 0.00 |
| $Fe^{2+}$ | 0.17 | 0.16 | 0.17 | 0.17 | 0.17 | 0.17 | 0.17 | 0.17 | 0.17 | 0.16 | 0.17 | 0.16 | 0.17 | 0.17 | 0.16 | 0.17 | 0.17 | 0.17 | 0.17 | 0.17 |
| Mn | 0.00 | 0.00 | 0.00 | 0.00 | 0.00 | 0.00 | 0.00 | 0.00 | 0.00 | 0.00 | 0.00 | 0.00 | 0.00 | 0.00 | 0.00 | 0.00 | 0.00 | 0.00 | 0.00 | 0.00 |
| Mg | 1.81 | 1.83 | 1.82 | 1.82 | 1.82 | 1.82 | 1.81 | 1.81 | 1.82 | 1.82 | 1.82 | 1.82 | 1.82 | 1.82 | 1.83 | 1.83 | 1.82 | 1.82 | 1.83 | 1.82 |
| Ni | 0.01 | 0.01 | 0.01 | 0.01 | 0.01 | 0.01 | 0.01 | 0.01 | 0.01 | 0.01 | 0.01 | 0.00 | 0.01 | 0.01 | 0.01 | 0.01 | 0.01 | 0.01 | 0.01 | 0.01 |
| Zn | 0.00 | 0.00 | 0.00 | 0.00 | 0.00 | 0.00 | 0.00 | 0.00 | 0.00 | 0.00 | 0.00 | 0.00 | 0.00 | 0.00 | 0.00 | 0.00 | 0.00 | 0.00 | 0.00 | 0.00 |

| Analysis | GRID 3-7 | GRID 4-1 | GRID 4-2 | GRID 4-3 | GRID 4-4 | GRID 4-5 | GRID 4-6 | GRID 4-7 | GRID 5-1 | GRID 5-2 | GRID 5-3 | GRID 5-4 | GRID 5-5 | GRID 5-6 | GRID 5-7 | GRID 6-1 | GRID 6-2 | GRID 6-3 | GRID 6-4 | GRID 6-5 |
|---|---|---|---|---|---|---|---|---|---|---|---|---|---|---|---|---|---|---|---|---|
| | 80-OL | 81-OL | 82-OL | 83-OL | 84-OL | 85-OL | 86-OL | 87-OL | 88-OL | 89-OL | 90-OL | 91-OL | 92-OL | 93-OL | 94-OL | 95-OL | 96-OL | 97-OL | 98-OL | 99-OL |
| X | 75.72 | 75.82 | 75.82 | 75.82 | 75.82 | 75.82 | 75.82 | 75.82 | 75.92 | 75.92 | 75.92 | 75.92 | 75.92 | 75.92 | 75.92 | 76.02 | 76.02 | 76.02 | 76.02 | 76.02 |
| Y | 70.57 | 69.97 | 70.07 | 70.17 | 70.27 | 70.37 | 70.47 | 70.57 | 69.97 | 70.07 | 70.17 | 70.27 | 70.37 | 70.47 | 70.57 | 69.97 | 70.07 | 70.17 | 70.27 | 70.37 |
| **d (mm)** | **0.33** | **0.23** | **0.13** | **0.04** | **0.01** | **0.11** | **0.21** | **0.31** | **0.23** | **0.13** | **0.04** | **0.02** | **0.12** | **0.22** | **0.32** | **0.27** | **0.18** | **0.13** | **0.12** | **0.17** |
| $SiO_2$ | 41.11 | 41.12 | 41.02 | 41.34 | 40.96 | 40.97 | 41.24 | 41.27 | 40.97 | 41.30 | 40.83 | 41.26 | 41.24 | 41.50 | 41.03 | 41.11 | 41.14 | 40.97 | 40.95 | 40.94 |

| | | | | | | | | | | | | | | | | | | | | |
|---|---|---|---|---|---|---|---|---|---|---|---|---|---|---|---|---|---|---|---|---|
| $TiO_2$ | 0.01 | 0.00 | 0.03 | 0.00 | 0.00 | 0.02 | 0.03 | 0.00 | 0.00 | 0.04 | 0.02 | 0.02 | 0.03 | 0.00 | 0.04 | 0.04 | 0.00 | 0.00 | 0.00 | 0.02 |
| $Al_2O_3$ | 0.01 | 0.00 | 0.01 | 0.00 | 0.01 | 0.01 | 0.01 | 0.00 | 0.00 | 0.00 | 0.01 | 0.00 | 0.00 | 0.00 | 0.00 | 0.02 | 0.00 | 0.00 | 0.00 | 0.00 |
| $Cr_2O_3$ | 0.05 | 0.02 | 0.00 | 0.09 | 0.42 | 0.00 | 0.00 | 0.00 | 0.03 | 0.00 | 0.03 | 0.07 | 0.00 | 0.00 | 0.00 | 0.00 | 0.00 | 0.00 | 0.00 | 0.00 |
| $V_2O_3$ | 0.00 | 0.00 | 0.00 | 0.04 | 0.01 | 0.01 | 0.00 | 0.00 | 0.03 | 0.00 | 0.00 | 0.00 | 0.00 | 0.02 | 0.00 | 0.00 | 0.00 | 0.00 | 0.00 | 0.04 |
| $Fe_2O_3$ | 0.00 | 0.00 | 0.00 | 0.00 | 0.00 | 0.00 | 0.00 | 0.00 | 0.00 | 0.00 | 0.00 | 0.00 | 0.00 | 0.00 | 0.00 | 0.00 | 0.00 | 0.00 | 0.00 | 0.00 |
| FeO | 8.42 | 8.32 | 8.40 | 8.24 | 6.80 | 8.18 | 8.17 | 8.42 | 8.05 | 8.07 | 8.23 | 8.06 | 8.15 | 7.99 | 8.08 | 8.28 | 8.35 | 8.40 | 8.65 | 8.15 |
| MnO | 0.14 | 0.11 | 0.17 | 0.14 | 0.11 | 0.19 | 0.12 | 0.09 | 0.12 | 0.15 | 0.09 | 0.13 | 0.10 | 0.21 | 0.13 | 0.12 | 0.17 | 0.16 | 0.10 | 0.14 |
| MgO | 50.45 | 50.42 | 50.60 | 50.34 | 51.43 | 50.80 | 50.29 | 50.53 | 50.58 | 50.62 | 50.67 | 50.66 | 50.39 | 50.59 | 50.42 | 50.03 | 49.71 | 50.16 | 50.25 | 50.42 |
| NiO | 0.38 | 0.31 | 0.42 | 0.33 | 0.25 | 0.39 | 0.38 | 0.27 | 0.35 | 0.33 | 0.28 | 0.29 | 0.34 | 0.25 | 0.32 | 0.32 | 0.29 | 0.31 | 0.31 | 0.31 |
| ZnO | 0.06 | 0.06 | 0.10 | 0.00 | 0.05 | 0.00 | 0.06 | 0.25 | 0.00 | 0.06 | 0.06 | 0.07 | 0.00 | 0.16 | 0.00 | 0.00 | 0.01 | 0.00 | 0.00 | 0.00 |
| TOT | 100.63 | 100.38 | 100.78 | 100.54 | 100.05 | 100.58 | 100.32 | 100.85 | 100.13 | 100.59 | 100.24 | 100.58 | 100.25 | 100.74 | 100.03 | 99.92 | 99.70 | 100.01 | 100.27 | 100.04 |
| Si | 1.00 | 1.00 | 0.99 | 1.00 | 0.99 | 0.99 | 1.00 | 1.00 | 1.00 | 1.00 | 0.99 | 1.00 | 1.00 | 1.00 | 1.00 | 1.00 | 1.01 | 1.00 | 1.00 | 1.00 |
| Ti | 0.00 | 0.00 | 0.00 | 0.00 | 0.00 | 0.00 | 0.00 | 0.00 | 0.00 | 0.00 | 0.00 | 0.00 | 0.00 | 0.00 | 0.00 | 0.00 | 0.00 | 0.00 | 0.00 | 0.00 |
| Al | 0.00 | 0.00 | 0.00 | 0.00 | 0.00 | 0.00 | 0.00 | 0.00 | 0.00 | 0.00 | 0.00 | 0.00 | 0.00 | 0.00 | 0.00 | 0.00 | 0.00 | 0.00 | 0.00 | 0.00 |
| Cr | 0.00 | 0.00 | 0.00 | 0.00 | 0.01 | 0.00 | 0.00 | 0.00 | 0.00 | 0.00 | 0.00 | 0.00 | 0.00 | 0.00 | 0.00 | 0.00 | 0.00 | 0.00 | 0.00 | 0.00 |
| V | 0.00 | 0.00 | 0.00 | 0.00 | 0.00 | 0.00 | 0.00 | 0.00 | 0.00 | 0.00 | 0.00 | 0.00 | 0.00 | 0.00 | 0.00 | 0.00 | 0.00 | 0.00 | 0.00 | 0.00 |
| $Fe^{3+}$ | 0.00 | 0.00 | 0.00 | 0.00 | 0.00 | 0.00 | 0.00 | 0.00 | 0.00 | 0.00 | 0.00 | 0.00 | 0.00 | 0.00 | 0.00 | 0.00 | 0.00 | 0.00 | 0.00 | 0.00 |
| $Fe^{2+}$ | 0.17 | 0.17 | 0.17 | 0.17 | 0.14 | 0.16 | 0.17 | 0.17 | 0.16 | 0.16 | 0.17 | 0.16 | 0.17 | 0.16 | 0.16 | 0.17 | 0.17 | 0.17 | 0.18 | 0.17 |
| Mn | 0.00 | 0.00 | 0.00 | 0.00 | 0.00 | 0.00 | 0.00 | 0.00 | 0.00 | 0.00 | 0.00 | 0.00 | 0.00 | 0.00 | 0.00 | 0.00 | 0.00 | 0.00 | 0.00 | 0.00 |
| Mg | 1.82 | 1.82 | 1.82 | 1.82 | 1.86 | 1.83 | 1.82 | 1.82 | 1.83 | 1.83 | 1.83 | 1.83 | 1.82 | 1.82 | 1.83 | 1.82 | 1.81 | 1.82 | 1.82 | 1.83 |
| Ni | 0.01 | 0.01 | 0.01 | 0.01 | 0.00 | 0.01 | 0.01 | 0.01 | 0.01 | 0.01 | 0.01 | 0.01 | 0.01 | 0.00 | 0.01 | 0.01 | 0.01 | 0.01 | 0.01 | 0.01 |
| Zn | 0.00 | 0.00 | 0.00 | 0.00 | 0.00 | 0.00 | 0.00 | 0.00 | 0.00 | 0.00 | 0.00 | 0.00 | 0.00 | 0.00 | 0.00 | 0.00 | 0.00 | 0.00 | 0.00 | 0.00 |

| Analysis | GRID 6-6 | GRID 6-7 | GRID 7-1 | GRID 7-2 | GRID 7-3 | GRID 7-4 | GRID 7-5 | GRID 7-6 | GRID 7-7 | FIN02B-1 | FIN02B-2 | FIN02B-3 | FIN02B-4 | FIN02B-5 | GRID 1-1 | GRID 1-2 | GRID 1-3 | GRID 1-4 | GRID 1-5 | GRID 1-6 |
|---|---|---|---|---|---|---|---|---|---|---|---|---|---|---|---|---|---|---|---|---|
| | 100-OL | 101-OL | 102-OL | 103-OL | 104-OL | 105-OL | 106-OL | 107-OL | 108-OL | OL-rim | CHR-rim | CHR-core | CHR-rim | OL-rim | 114-OL | 115-OL | 116-OL | 117-OL | 118-OL | 119-OL |
| X | 76.02 | 76.02 | 76.12 | 76.12 | 76.12 | 76.12 | 76.12 | 76.12 | 76.12 | 75.86 | 75.86 | 75.86 | 75.86 | 75.86 | 75.73 | 75.73 | 75.73 | 75.73 | 75.73 | 75.73 |
| Y | 70.47 | 70.57 | 69.97 | 70.07 | 70.17 | 70.27 | 70.37 | 70.47 | 70.57 | 70.17 | 70.20 | 70.23 | 70.26 | 70.28 | 70.10 | 70.14 | 70.18 | 70.22 | 70.26 | 70.30 |
| **d (mm)** | **0.25** | **0.34** | **0.33** | **0.27** | **0.23** | **0.22** | **0.25** | **0.32** | **0.39** | **0.01** | **0.01** | **0.03** | **0.01** | **0.01** | **0.15** | **0.12** | **0.11** | **0.10** | **0.10** | **0.11** |
| $SiO_2$ | 41.21 | 41.48 | 40.91 | 41.19 | 41.30 | 41.53 | 41.41 | 41.39 | 41.46 | 41.15 | 0.12 | 0.09 | 0.23 | 41.43 | 41.37 | 41.65 | 41.22 | 41.21 | 41.56 | 41.30 |
| $TiO_2$ | 0.02 | 0.02 | 0.07 | 0.00 | 0.00 | 0.01 | 0.03 | 0.00 | 0.01 | 0.01 | 0.62 | 0.66 | 0.66 | 0.00 | 0.03 | 0.01 | 0.00 | 0.04 | 0.00 | 0.00 |
| $Al_2O_3$ | 0.01 | 0.00 | 0.02 | 0.03 | 0.00 | 0.00 | 0.01 | 0.00 | 0.01 | 0.03 | 12.78 | 13.03 | 12.88 | 0.01 | 0.00 | 0.00 | 0.00 | 0.00 | 0.00 | 0.00 |
| $Cr_2O_3$ | 0.00 | 0.03 | 0.00 | 0.03 | 0.04 | 0.00 | 0.01 | 0.00 | 0.00 | 0.30 | 48.66 | 49.17 | 48.55 | 0.29 | 0.00 | 0.00 | 0.04 | 0.00 | 0.00 | 0.00 |
| $V_2O_3$ | 0.00 | 0.00 | 0.00 | 0.00 | 0.01 | 0.00 | 0.00 | 0.01 | 0.02 | 0.07 | 0.19 | 0.15 | 0.13 | 0.00 | 0.00 | 0.00 | 0.00 | 0.00 | 0.01 | 0.03 |
| $Fe_2O_3$ | 0.00 | 0.00 | 0.00 | 0.00 | 0.00 | 0.00 | 0.00 | 0.00 | 0.00 | 0.00 | 7.54 | 7.23 | 7.25 | 0.00 | 0.37 | 0.00 | 0.00 | 0.00 | 0.00 | 0.00 |
| FeO | 8.69 | 8.49 | 8.20 | 8.27 | 8.01 | 8.08 | 8.11 | 8.21 | 8.52 | 7.94 | 23.24 | 23.52 | 23.25 | 7.43 | 8.04 | 8.22 | 8.17 | 8.16 | 8.01 | 8.14 |
| MnO | 0.13 | 0.11 | 0.13 | 0.13 | 0.16 | 0.12 | 0.11 | 0.17 | 0.13 | 0.15 | 0.40 | 0.36 | 0.27 | 0.16 | 0.10 | 0.09 | 0.12 | 0.13 | 0.18 | 0.14 |
| MgO | 50.02 | 50.89 | 50.25 | 50.27 | 49.59 | 50.30 | 50.81 | 50.02 | 50.47 | 50.38 | 7.27 | 7.16 | 7.35 | 51.08 | 50.77 | 50.28 | 50.50 | 50.58 | 50.55 | 50.52 |
| NiO | 0.33 | 0.31 | 0.35 | 0.32 | 0.32 | 0.29 | 0.36 | 0.30 | 0.34 | 0.32 | 0.10 | 0.11 | 0.16 | 0.28 | 0.32 | 0.30 | 0.27 | 0.33 | 0.30 | 0.33 |
| ZnO | 0.00 | 0.00 | 0.00 | 0.00 | 0.00 | 0.00 | 0.04 | 0.00 | 0.00 | 0.00 | 0.20 | 0.42 | 0.36 | 0.00 | 0.17 | 0.00 | 0.00 | 0.13 | 0.10 | 0.10 |
| TOT | 100.43 | 101.34 | 99.94 | 100.26 | 99.45 | 100.35 | 100.90 | 100.12 | 100.97 | 100.35 | 101.13 | 101.91 | 101.09 | 100.68 | 101.21 | 100.56 | 100.34 | 100.60 | 100.72 | 100.59 |
| Si | 1.00 | 1.00 | 1.00 | 1.00 | 1.01 | 1.01 | 1.00 | 1.01 | 1.00 | 1.00 | 0.00 | 0.00 | 0.01 | 1.00 | 1.00 | 1.01 | 1.00 | 1.00 | 1.00 | 1.00 |
| Ti | 0.00 | 0.00 | 0.00 | 0.00 | 0.00 | 0.00 | 0.00 | 0.00 | 0.00 | 0.00 | 0.02 | 0.02 | 0.02 | 0.00 | 0.00 | 0.00 | 0.00 | 0.00 | 0.00 | 0.00 |
| Al | 0.00 | 0.00 | 0.00 | 0.00 | 0.00 | 0.00 | 0.00 | 0.00 | 0.00 | 0.00 | 0.50 | 0.50 | 0.50 | 0.00 | 0.00 | 0.00 | 0.00 | 0.00 | 0.00 | 0.00 |
| Cr | 0.00 | 0.00 | 0.00 | 0.00 | 0.00 | 0.00 | 0.00 | 0.00 | 0.00 | 0.01 | 1.27 | 1.28 | 1.27 | 0.01 | 0.00 | 0.00 | 0.00 | 0.00 | 0.00 | 0.00 |
| V | 0.00 | 0.00 | 0.00 | 0.00 | 0.00 | 0.00 | 0.00 | 0.00 | 0.00 | 0.00 | 0.01 | 0.00 | 0.00 | 0.00 | 0.00 | 0.00 | 0.00 | 0.00 | 0.00 | 0.00 |
| $Fe^{3+}$ | 0.00 | 0.00 | 0.00 | 0.00 | 0.00 | 0.00 | 0.00 | 0.00 | 0.00 | 0.00 | 0.19 | 0.18 | 0.18 | 0.00 | 0.01 | 0.00 | 0.00 | 0.00 | 0.00 | 0.00 |
| $Fe^{2+}$ | 0.18 | 0.17 | 0.17 | 0.17 | 0.16 | 0.16 | 0.16 | 0.17 | 0.17 | 0.16 | 0.64 | 0.65 | 0.64 | 0.15 | 0.16 | 0.17 | 0.17 | 0.17 | 0.16 | 0.16 |
| Mn | 0.00 | 0.00 | 0.00 | 0.00 | 0.00 | 0.00 | 0.00 | 0.00 | 0.00 | 0.00 | 0.01 | 0.01 | 0.01 | 0.00 | 0.00 | 0.00 | 0.00 | 0.00 | 0.00 | 0.00 |
| Mg | 1.81 | 1.82 | 1.83 | 1.82 | 1.81 | 1.82 | 1.83 | 1.82 | 1.82 | 1.82 | 0.36 | 0.35 | 0.36 | 1.84 | 1.82 | 1.82 | 1.83 | 1.82 | 1.82 | 1.82 |
| Ni | 0.01 | 0.01 | 0.01 | 0.01 | 0.01 | 0.01 | 0.01 | 0.01 | 0.01 | 0.01 | 0.00 | 0.00 | 0.00 | 0.01 | 0.01 | 0.01 | 0.01 | 0.01 | 0.01 | 0.01 |
| Zn | 0.00 | 0.00 | 0.00 | 0.00 | 0.00 | 0.00 | 0.00 | 0.00 | 0.00 | 0.00 | 0.00 | 0.01 | 0.01 | 0.00 | 0.00 | 0.00 | 0.00 | 0.00 | 0.00 | 0.00 |

# Appendix: Chapter 3

| Analysis | GRID 1-7 | GRID 2-1 | GRID 2-2 | GRID 2-3 | GRID 2-4 | GRID 2-5 | GRID 2-6 | GRID 2-7 | GRID 3-1 | GRID 3-2 | GRID 3-3 | GRID 3-4 | GRID 3-5 | GRID 3-6 | GRID 3-7 | GRID 4-1 | GRID 4-2 | GRID 4-3 | GRID 4-4 | GRID 4-5 |
|---|---|---|---|---|---|---|---|---|---|---|---|---|---|---|---|---|---|---|---|---|
| | 120-OL | 121-OL | 122-OL | 123-OL | 124-OL | 125-OL | 126-OL | 127-OL | 128-OL | 129-OL | 130-OL | 131-OL | 132-OL | 133-OL | 134-OL | 135-OL | 136-OL | 137-OL | 138-CHR | 139-CHR |
| X | 75.73 | 75.77 | 75.77 | 75.77 | 75.77 | 75.77 | 75.77 | 75.77 | 75.81 | 75.81 | 75.81 | 75.81 | 75.81 | 75.81 | 75.81 | 75.85 | 75.85 | 75.85 | 75.85 | 75.85 |
| Y | 70.34 | 70.10 | 70.14 | 70.18 | 70.22 | 70.26 | 70.30 | 70.34 | 70.10 | 70.14 | 70.18 | 70.22 | 70.26 | 70.30 | 70.34 | 70.10 | 70.14 | 70.18 | 70.22 | 70.26 |
| **d (mm)** | **0.13** | **0.12** | **0.09** | **0.07** | **0.06** | **0.06** | **0.07** | **0.10** | **0.10** | **0.06** | **0.03** | **0.02** | **0.01** | **0.05** | **0.08** | **0.09** | **0.05** | **0.01** | **0.03** | **0.01** |
| $SiO_2$ | 41.38 | 41.32 | 41.46 | 41.45 | 41.27 | 41.52 | 41.48 | 41.21 | 41.17 | 41.24 | 41.56 | 41.62 | 41.84 | 41.32 | 41.36 | 41.31 | 41.08 | 40.96 | 0.05 | 0.20 |
| $TiO_2$ | 0.00 | 0.00 | 0.01 | 0.03 | 0.00 | 0.04 | 0.01 | 0.04 | 0.00 | 0.03 | 0.01 | 0.00 | 0.00 | 0.02 | 0.00 | 0.00 | 0.00 | 0.09 | 0.65 | 0.60 |
| $Al_2O_3$ | 0.01 | 0.00 | 0.01 | 0.01 | 0.01 | 0.01 | 0.03 | 0.00 | 0.00 | 0.00 | 0.03 | 0.04 | 0.03 | 0.01 | 0.00 | 0.01 | 0.01 | 0.03 | 13.11 | 12.90 |
| $Cr_2O_3$ | 0.02 | 0.00 | 0.13 | 0.07 | 0.06 | 0.00 | 0.00 | 0.02 | 0.05 | 0.04 | 0.18 | 0.54 | 0.29 | 0.06 | 0.04 | 0.02 | 0.02 | 0.27 | 48.61 | 48.51 |
| $V_2O_3$ | 0.00 | 0.00 | 0.01 | 0.00 | 0.00 | 0.04 | 0.06 | 0.00 | 0.00 | 0.00 | 0.00 | 0.02 | 0.00 | 0.00 | 0.00 | 0.04 | 0.00 | 0.04 | 0.14 | 0.18 |
| $Fe_2O_3$ | 0.00 | 0.00 | 0.00 | 0.00 | 0.00 | 0.00 | 0.00 | 0.00 | 0.00 | 0.00 | 0.00 | 0.00 | 0.00 | 0.00 | 0.00 | 0.00 | 0.00 | 0.00 | 7.56 | 7.19 |
| FeO | 8.16 | 8.07 | 8.26 | 8.02 | 8.19 | 8.18 | 7.85 | 7.79 | 8.24 | 8.36 | 8.10 | 7.33 | 6.48 | 7.98 | 8.00 | 8.19 | 8.23 | 7.52 | 23.39 | 23.04 |
| MnO | 0.13 | 0.15 | 0.10 | 0.12 | 0.18 | 0.12 | 0.15 | 0.14 | 0.15 | 0.15 | 0.11 | 0.09 | 0.05 | 0.15 | 0.10 | 0.15 | 0.18 | 0.11 | 0.31 | 0.27 |
| MgO | 50.57 | 50.75 | 50.31 | 50.82 | 50.46 | 50.66 | 50.59 | 50.99 | 50.35 | 50.37 | 50.65 | 50.95 | 51.29 | 50.54 | 50.49 | 50.46 | 50.31 | 50.58 | 7.24 | 7.43 |
| NiO | 0.34 | 0.41 | 0.36 | 0.32 | 0.33 | 0.28 | 0.30 | 0.32 | 0.32 | 0.29 | 0.32 | 0.29 | 0.35 | 0.32 | 0.22 | 0.39 | 0.28 | 0.35 | 0.02 | 0.04 |
| ZnO | 0.04 | 0.01 | 0.00 | 0.00 | 0.01 | 0.00 | 0.00 | 0.16 | 0.00 | 0.00 | 0.00 | 0.02 | 0.00 | 0.08 | 0.08 | 0.13 | 0.03 | 0.08 | 0.38 | 0.32 |
| TOT | 100.67 | 100.73 | 100.66 | 100.84 | 100.51 | 100.88 | 100.51 | 100.69 | 100.29 | 100.47 | 100.98 | 100.93 | 100.35 | 100.50 | 100.29 | 100.69 | 100.16 | 100.08 | 101.47 | 100.68 |
| Si | 1.00 | 1.00 | 1.00 | 1.00 | 1.00 | 1.00 | 1.00 | 0.99 | 1.00 | 1.00 | 1.00 | 1.00 | 1.01 | 1.00 | 1.00 | 1.00 | 1.00 | 1.00 | 0.00 | 0.01 |
| Ti | 0.00 | 0.00 | 0.00 | 0.00 | 0.00 | 0.00 | 0.00 | 0.00 | 0.00 | 0.00 | 0.00 | 0.00 | 0.00 | 0.00 | 0.00 | 0.00 | 0.00 | 0.00 | 0.02 | 0.01 |
| Al | 0.00 | 0.00 | 0.00 | 0.00 | 0.00 | 0.00 | 0.00 | 0.00 | 0.00 | 0.00 | 0.00 | 0.00 | 0.00 | 0.00 | 0.00 | 0.00 | 0.00 | 0.00 | 0.51 | 0.50 |
| Cr | 0.00 | 0.00 | 0.00 | 0.00 | 0.00 | 0.00 | 0.00 | 0.00 | 0.00 | 0.00 | 0.00 | 0.01 | 0.01 | 0.00 | 0.00 | 0.00 | 0.00 | 0.01 | 1.26 | 1.27 |
| V | 0.00 | 0.00 | 0.00 | 0.00 | 0.00 | 0.00 | 0.00 | 0.00 | 0.00 | 0.00 | 0.00 | 0.00 | 0.00 | 0.00 | 0.00 | 0.00 | 0.00 | 0.00 | 0.00 | 0.00 |
| $Fe^{3+}$ | 0.00 | 0.00 | 0.00 | 0.00 | 0.00 | 0.00 | 0.00 | 0.00 | 0.00 | 0.00 | 0.00 | 0.00 | 0.00 | 0.00 | 0.00 | 0.00 | 0.00 | 0.00 | 0.19 | 0.18 |
| $Fe^{2+}$ | 0.17 | 0.16 | 0.17 | 0.16 | 0.17 | 0.17 | 0.16 | 0.16 | 0.17 | 0.17 | 0.16 | 0.15 | 0.13 | 0.16 | 0.16 | 0.17 | 0.17 | 0.15 | 0.64 | 0.64 |
| Mn | 0.00 | 0.00 | 0.00 | 0.00 | 0.00 | 0.00 | 0.00 | 0.00 | 0.00 | 0.00 | 0.00 | 0.00 | 0.00 | 0.00 | 0.00 | 0.00 | 0.00 | 0.00 | 0.01 | 0.01 |
| Mg | 1.82 | 1.83 | 1.82 | 1.83 | 1.82 | 1.82 | 1.83 | 1.83 | 1.82 | 1.82 | 1.82 | 1.83 | 1.84 | 1.82 | 1.83 | 1.82 | 1.82 | 1.83 | 0.36 | 0.37 |
| Ni | 0.01 | 0.01 | 0.01 | 0.01 | 0.01 | 0.01 | 0.01 | 0.01 | 0.01 | 0.01 | 0.01 | 0.01 | 0.01 | 0.01 | 0.00 | 0.01 | 0.01 | 0.01 | 0.00 | 0.00 |
| Zn | 0.00 | 0.00 | 0.00 | 0.00 | 0.00 | 0.00 | 0.00 | 0.00 | 0.00 | 0.00 | 0.00 | 0.00 | 0.00 | 0.00 | 0.00 | 0.00 | 0.00 | 0.00 | 0.01 | 0.01 |

| Analysis | GRID 4-6 | GRID 4-7 | GRID 5-1 | GRID 5-2 | GRID 5-3 | GRID 5-4 | GRID 5-5 | GRID 5-6 | GRID 5-7 | GRID 6-1 | GRID 6-2 | GRID 6-3 | GRID 6-4 | GRID 6-5 | GRID 6-6 | GRID 6-7 | GRID 7-1 | GRID 7-2 | GRID 7-3 | GRID 7-4 |
|---|---|---|---|---|---|---|---|---|---|---|---|---|---|---|---|---|---|---|---|---|
| | 140-OL | 141-OL | 142-OL | 143-OL | 144-OL | 145-CHR | 146-OL | 147-OL | 148-OL | 149-OL | 150-OL | 151-OL | 152-OL | 153-OL | 154-OL | 155-OL | 156-OL | 157-OL | 158-OL | 159-OL |
| X | 75.85 | 75.85 | 75.89 | 75.89 | 75.89 | 75.89 | 75.89 | 75.89 | 75.89 | 75.93 | 75.93 | 75.93 | 75.93 | 75.93 | 75.93 | 75.93 | 75.97 | 75.97 | 75.97 | 75.97 |
| Y | 70.30 | 70.34 | 70.10 | 70.14 | 70.18 | 70.22 | 70.26 | 70.30 | 70.34 | 70.10 | 70.14 | 70.18 | 70.22 | 70.26 | 70.30 | 70.34 | 70.10 | 70.14 | 70.18 | 70.22 |
| **d (mm)** | **0.04** | **0.07** | **0.09** | **0.05** | **0.01** | **0.01** | **0.00** | **0.04** | **0.08** | **0.10** | **0.07** | **0.04** | **0.03** | **0.03** | **0.06** | **0.09** | **0.12** | **0.09** | **0.08** | **0.07** |
| $SiO_2$ | 41.28 | 41.31 | 41.29 | 41.11 | 41.05 | 0.74 | 41.33 | 41.16 | 41.23 | 41.17 | 41.11 | 41.17 | 41.16 | 41.19 | 41.22 | 41.36 | 41.10 | 41.21 | 41.49 | 41.27 |
| $TiO_2$ | 0.02 | 0.03 | 0.00 | 0.01 | 0.00 | 0.51 | 0.00 | 0.02 | 0.02 | 0.01 | 0.00 | 0.00 | 0.00 | 0.00 | 0.03 | 0.00 | 0.00 | 0.00 | 0.00 | 0.00 |
| $Al_2O_3$ | 0.02 | 0.00 | 0.00 | 0.00 | 0.04 | 14.50 | 0.00 | 0.01 | 0.00 | 0.00 | 0.01 | 0.01 | 0.01 | 0.00 | 0.02 | 0.01 | 0.01 | 0.00 | 0.00 | 0.00 |
| $Cr_2O_3$ | 0.05 | 0.02 | 0.06 | 0.01 | 0.20 | 44.67 | 0.44 | 0.07 | 0.00 | 0.00 | 0.02 | 0.06 | 0.07 | 0.02 | 0.03 | 0.00 | 0.00 | 0.03 | 0.00 | 0.02 |
| $V_2O_3$ | 0.00 | 0.00 | 0.02 | 0.00 | 0.01 | 0.19 | 0.00 | 0.03 | 0.00 | 0.01 | 0.00 | 0.00 | 0.00 | 0.02 | 0.02 | 0.01 | 0.00 | 0.00 | 0.00 | 0.03 |
| $Fe_2O_3$ | 0.00 | 0.00 | 0.00 | 0.00 | 0.00 | 9.97 | 0.00 | 0.00 | 0.00 | 0.00 | 0.00 | 0.00 | 0.00 | 0.00 | 0.00 | 0.00 | 0.00 | 0.00 | 0.00 | 0.00 |
| FeO | 8.42 | 8.04 | 8.33 | 7.88 | 7.79 | 21.77 | 7.32 | 8.32 | 8.26 | 8.09 | 8.24 | 8.19 | 7.85 | 8.33 | 8.64 | 8.41 | 7.99 | 8.29 | 8.21 | 8.51 |
| MnO | 0.10 | 0.03 | 0.18 | 0.13 | 0.16 | 0.30 | 0.11 | 0.16 | 0.14 | 0.07 | 0.14 | 0.10 | 0.17 | 0.11 | 0.11 | 0.13 | 0.08 | 0.12 | 0.13 | 0.13 |
| MgO | 50.53 | 50.63 | 50.35 | 50.82 | 51.66 | 9.17 | 50.84 | 50.58 | 50.77 | 50.50 | 50.58 | 50.24 | 50.56 | 50.23 | 50.27 | 49.88 | 50.53 | 50.43 | 50.45 | 50.08 |
| NiO | 0.37 | 0.38 | 0.34 | 0.36 | 0.34 | 0.07 | 0.31 | 0.29 | 0.38 | 0.39 | 0.38 | 0.33 | 0.24 | 0.37 | 0.31 | 0.39 | 0.34 | 0.28 | 0.35 | 0.30 |
| ZnO | 0.00 | 0.02 | 0.07 | 0.07 | 0.11 | 0.14 | 0.00 | 0.07 | 0.06 | 0.00 | 0.07 | 0.00 | 0.00 | 0.03 | 0.00 | 0.04 | 0.15 | 0.02 | 0.06 | 0.04 |
| TOT | 100.81 | 100.46 | 100.65 | 100.43 | 101.35 | 102.03 | 100.36 | 100.71 | 100.91 | 100.26 | 100.59 | 100.11 | 100.07 | 100.31 | 100.67 | 100.25 | 100.22 | 100.41 | 100.69 | 100.40 |
| Si | 1.00 | 1.00 | 1.00 | 0.99 | 0.98 | 0.02 | 1.00 | 1.00 | 0.99 | 1.00 | 1.00 | 1.00 | 1.00 | 1.00 | 1.00 | 1.01 | 1.00 | 1.00 | 1.00 | 1.00 |
| Ti | 0.00 | 0.00 | 0.00 | 0.00 | 0.00 | 0.01 | 0.00 | 0.00 | 0.00 | 0.00 | 0.00 | 0.00 | 0.00 | 0.00 | 0.00 | 0.00 | 0.00 | 0.00 | 0.00 | 0.00 |
| Al | 0.00 | 0.00 | 0.00 | 0.00 | 0.00 | 0.55 | 0.00 | 0.00 | 0.00 | 0.00 | 0.00 | 0.00 | 0.00 | 0.00 | 0.00 | 0.00 | 0.00 | 0.00 | 0.00 | 0.00 |
| Cr | 0.00 | 0.00 | 0.00 | 0.00 | 0.00 | 1.13 | 0.01 | 0.00 | 0.00 | 0.00 | 0.00 | 0.00 | 0.00 | 0.00 | 0.00 | 0.00 | 0.00 | 0.00 | 0.00 | 0.00 |
| V | 0.00 | 0.00 | 0.00 | 0.00 | 0.00 | 0.00 | 0.00 | 0.00 | 0.00 | 0.00 | 0.00 | 0.00 | 0.00 | 0.00 | 0.00 | 0.00 | 0.00 | 0.00 | 0.00 | 0.00 |
| $Fe^{3+}$ | 0.00 | 0.00 | 0.00 | 0.00 | 0.00 | 0.24 | 0.00 | 0.00 | 0.00 | 0.00 | 0.00 | 0.00 | 0.00 | 0.00 | 0.00 | 0.00 | 0.00 | 0.00 | 0.00 | 0.00 |
| $Fe^{2+}$ | 0.17 | 0.16 | 0.17 | 0.16 | 0.16 | 0.58 | 0.15 | 0.17 | 0.17 | 0.16 | 0.17 | 0.17 | 0.16 | 0.17 | 0.18 | 0.17 | 0.16 | 0.17 | 0.17 | 0.17 |

| | | | | | | | | | | | | | | | | | | | | |
|---|---|---|---|---|---|---|---|---|---|---|---|---|---|---|---|---|---|---|---|---|
| Mn | 0.00 | 0.00 | 0.00 | 0.00 | 0.00 | 0.01 | 0.00 | 0.00 | 0.00 | 0.00 | 0.00 | 0.00 | 0.00 | 0.00 | 0.00 | 0.00 | 0.00 | 0.00 | 0.00 | 0.00 |
| Mg | 1.82 | 1.83 | 1.82 | 1.83 | 1.84 | 0.44 | 1.83 | 1.82 | 1.83 | 1.83 | 1.83 | 1.82 | 1.83 | 1.82 | 1.82 | 1.81 | 1.83 | 1.82 | 1.82 | 1.81 |
| Ni | 0.01 | 0.01 | 0.01 | 0.01 | 0.01 | 0.00 | 0.01 | 0.01 | 0.01 | 0.01 | 0.01 | 0.01 | 0.00 | 0.01 | 0.01 | 0.01 | 0.01 | 0.01 | 0.01 | 0.01 |
| Zn | 0.00 | 0.00 | 0.00 | 0.00 | 0.00 | 0.00 | 0.00 | 0.00 | 0.00 | 0.00 | 0.00 | 0.00 | 0.00 | 0.00 | 0.00 | 0.00 | 0.00 | 0.00 | 0.00 | 0.00 |

| Analysis | GRID 7-5 160-OL | GRID 7-6 161-OL | GRID 7-7 162-OL | FIN02B-1 18-OL | FIN02B-2 19-CHR | FIN02B-3 20-CHR | FIN02B-4 21-CHR | FIN02B-5 22-CHR | FIN02B-6 23-CHR | FIN02B-7 24-CHR | d-CHR | FIN02B-8 25-CHR | FIN02B-9 26-CHR | FIN02B-10 27-CHR | FIN02B-11 28-CHR | FIN02B-12 29-CHR | FIN02B-13 30-OL | d-CHR |
|---|---|---|---|---|---|---|---|---|---|---|---|---|---|---|---|---|---|---|
| X | 75.97 | 75.97 | 75.97 | 47.36 | 47.35 | 47.35 | 47.34 | 47.34 | 47.33 | 47.32 | 47.35 | 47.30 | 47.29 | 47.29 | 47.28 | 47.28 | 47.27 | 47.28 |
| Y | 70.26 | 70.30 | 70.34 | 71.00 | 71.00 | 71.00 | 71.00 | 71.00 | 71.00 | 71.01 | 71.00 | 71.01 | 71.01 | 71.01 | 71.01 | 71.01 | 71.01 | 71.01 |
| **d (mm)** | **0.07** | **0.09** | **0.11** | **28.46** | **28.47** | **28.47** | **28.48** | **28.48** | **28.49** | **28.51** | | **28.62** | **28.63** | **28.63** | **28.64** | **28.64** | **28.65** | |
| $SiO_2$ | 41.06 | 41.21 | 41.24 | 41.47 | 0.01 | 0.04 | 0.01 | 0.06 | 0.03 | 0.02 | | 0.03 | 0.02 | 0.06 | 0.02 | 0.05 | 41.88 | |
| $TiO_2$ | 0.00 | 0.00 | 0.01 | 0.00 | 0.66 | 0.72 | 0.75 | 0.70 | 0.67 | 0.71 | | 0.68 | 0.60 | 0.69 | 0.54 | 0.59 | 0.00 | |
| $Al_2O_3$ | 0.00 | 0.01 | 0.00 | 0.01 | 14.23 | 13.74 | 13.38 | 13.39 | 13.17 | 13.35 | | 13.11 | 13.20 | 13.10 | 13.56 | 13.86 | 0.00 | |
| $Cr_2O_3$ | 0.02 | 0.00 | 0.12 | 0.55 | 47.54 | 48.25 | 49.07 | 49.17 | 49.35 | 49.52 | | 49.30 | 49.03 | 49.03 | 48.01 | 47.40 | 0.37 | |
| $V_2O_3$ | 0.00 | 0.05 | 0.02 | 0.02 | 0.16 | 0.15 | 0.14 | 0.15 | 0.11 | 0.16 | | 0.15 | 0.20 | 0.17 | 0.20 | 0.18 | 0.00 | |
| $Fe_2O_3$ | 0.00 | 0.00 | 0.00 | 0.00 | 8.18 | 7.49 | 7.33 | 7.26 | 7.10 | 7.39 | | 7.60 | 7.12 | 7.73 | 8.03 | 8.35 | 0.00 | |
| FeO | 8.22 | 8.46 | 8.29 | 6.95 | 23.77 | 24.26 | 24.24 | 24.19 | 24.05 | 24.21 | | 24.11 | 24.12 | 24.34 | 23.87 | 23.90 | 7.42 | |
| MnO | 0.14 | 0.10 | 0.11 | 0.16 | 0.29 | 0.32 | 0.22 | 0.31 | 0.34 | 0.31 | | 0.33 | 0.20 | 0.36 | 0.34 | 0.24 | 0.11 | |
| MgO | 50.04 | 50.54 | 50.25 | 51.96 | 7.23 | 6.97 | 7.06 | 7.06 | 7.04 | 7.11 | | 7.02 | 6.89 | 6.97 | 6.94 | 7.08 | 51.66 | |
| NiO | 0.28 | 0.43 | 0.31 | 0.36 | 0.13 | 0.04 | 0.06 | 0.12 | 0.00 | 0.04 | | 0.11 | 0.06 | 0.08 | 0.08 | 0.13 | 0.34 | |
| ZnO | 0.02 | 0.00 | 0.06 | 0.00 | 0.45 | 0.30 | 0.27 | 0.25 | 0.21 | 0.35 | | 0.28 | 0.28 | 0.17 | 0.34 | 0.33 | 0.15 | |
| TOT | 99.78 | 100.81 | 100.42 | 101.48 | 102.64 | 102.31 | 102.56 | 102.65 | 102.07 | 103.17 | | 102.73 | 101.72 | 102.69 | 101.95 | 102.11 | 101.93 | |
| Si | 1.00 | 1.00 | 1.00 | 0.99 | 0.00 | 0.00 | 0.00 | 0.00 | 0.00 | 0.00 | | 0.00 | 0.00 | 0.00 | 0.00 | 0.00 | 1.00 | |
| Ti | 0.00 | 0.00 | 0.00 | 0.00 | 0.02 | 0.02 | 0.02 | 0.02 | 0.02 | 0.02 | | 0.02 | 0.01 | 0.02 | 0.01 | 0.01 | 0.00 | |
| Al | 0.00 | 0.00 | 0.00 | 0.00 | 0.54 | 0.53 | 0.51 | 0.51 | 0.51 | 0.51 | | 0.50 | 0.51 | 0.50 | 0.52 | 0.53 | 0.00 | |
| Cr | 0.00 | 0.00 | 0.00 | 0.01 | 1.22 | 1.25 | 1.26 | 1.27 | 1.28 | 1.27 | | 1.27 | 1.28 | 1.26 | 1.24 | 1.22 | 0.01 | |
| V | 0.00 | 0.00 | 0.00 | 0.00 | 0.00 | 0.00 | 0.00 | 0.00 | 0.00 | 0.00 | | 0.00 | 0.01 | 0.00 | 0.01 | 0.00 | 0.00 | |
| $Fe^{3+}$ | 0.00 | 0.00 | 0.00 | 0.00 | 0.20 | 0.18 | 0.18 | 0.18 | 0.18 | 0.18 | | 0.19 | 0.18 | 0.19 | 0.20 | 0.21 | 0.00 | |
| $Fe^{2+}$ | 0.17 | 0.17 | 0.17 | 0.14 | 0.64 | 0.66 | 0.66 | 0.66 | 0.66 | 0.66 | | 0.66 | 0.66 | 0.66 | 0.65 | 0.65 | 0.15 | |
| Mn | 0.00 | 0.00 | 0.00 | 0.00 | 0.01 | 0.01 | 0.01 | 0.01 | 0.01 | 0.01 | | 0.01 | 0.01 | 0.01 | 0.01 | 0.01 | 0.00 | |
| Mg | 1.82 | 1.82 | 1.82 | 1.85 | 0.35 | 0.34 | 0.34 | 0.34 | 0.34 | 0.34 | | 0.34 | 0.34 | 0.34 | 0.34 | 0.34 | 1.83 | |
| Ni | 0.01 | 0.01 | 0.01 | 0.01 | 0.00 | 0.00 | 0.00 | 0.00 | 0.00 | 0.00 | | 0.00 | 0.00 | 0.00 | 0.00 | 0.00 | 0.01 | |
| Zn | 0.00 | 0.00 | 0.00 | 0.00 | 0.01 | 0.01 | 0.01 | 0.01 | 0.01 | 0.01 | | 0.01 | 0.01 | 0.00 | 0.01 | 0.01 | 0.00 | |

Tab. A3.4 FIN01B-2 microprobe analyses of olivine and chromite crystals; d(mm) distance from the intergranular limit

| Analysis | FIN02B-14 31-OL | FIN02B-15 32-OL | FIN02B-16 33-OL | FIN02B-17 34-OL | d-CHR | FIN02B-18 35-CHR | FIN02B-19 36-CHR | FIN02B-20 37-CHR | FIN02B-21 38-CHR | FIN02B-22 39-CHR | FIN02B-23 40-CHR | FIN02B-24 41-CHR | FIN02B-25 42-CHR | FIN02B-26 43-CHR | FIN02B-27 44-CHR | FIN02B-28 45-CHR | FIN02B-29 46-CHR | FIN02B-30 47-CHR | FIN02B-31 48-CHR |
|---|---|---|---|---|---|---|---|---|---|---|---|---|---|---|---|---|---|---|---|
| X | 44.472 | 44.420 | 44.395 | 44.377 | 44.369 | 44.366 | 44.362 | 44.357 | 44.347 | 44.326 | 44.276 | 44.247 | 44.206 | 44.157 | 44.116 | 44.096 | 44.080 | 44.072 | 44.065 |
| Y | 66.700 | 66.702 | 66.703 | 66.698 | 66.697 | 66.695 | 66.693 | 66.691 | 66.691 | 66.687 | 66.687 | 66.687 | 66.688 | 66.689 | 66.690 | 66.690 | 66.690 | 66.690 | 66.690 |
| **d (mm)** | **0.103** | **0.051** | **0.026** | **0.008** | | **0.004** | **0.009** | **0.013** | **0.023** | **0.044** | **0.094** | **0.122** | **0.149** | **0.100** | **0.059** | **0.039** | **0.023** | **0.015** | **0.008** |
| $SiO_2$ | 41.40 | 41.51 | 41.92 | 41.91 | | 0.02 | 0.04 | 0.03 | 0.01 | 0.04 | 0.02 | 0.04 | 0.03 | 0.04 | 0.00 | 0.05 | 0.01 | 0.01 | 0.03 |
| $TiO_2$ | 0.03 | 0.00 | 0.01 | 0.00 | | 0.66 | 0.64 | 0.67 | 0.72 | 0.69 | 0.50 | 0.45 | 0.69 | 0.75 | 0.52 | 0.70 | 0.74 | 0.67 | 1.63 |
| $Al_2O_3$ | 0.00 | 0.00 | 0.00 | 0.00 | | 13.34 | 13.41 | 13.42 | 13.71 | 14.06 | 13.91 | 13.66 | 13.42 | 13.12 | 13.22 | 13.12 | 13.18 | 13.17 | 13.14 |
| $Cr_2O_3$ | 0.02 | 0.12 | 0.15 | 0.47 | | 49.95 | 50.19 | 50.07 | 49.31 | 49.27 | 49.66 | 50.03 | 49.73 | 49.89 | 49.66 | 49.59 | 49.84 | 50.10 | 48.27 |
| $V_2O_3$ | 0.03 | 0.00 | 0.00 | 0.02 | | 0.14 | 0.11 | 0.11 | 0.13 | 0.14 | 0.16 | 0.14 | 0.15 | 0.23 | 0.19 | 0.14 | 0.17 | 0.14 | 0.16 |
| $Fe_2O_3$ | 0.00 | 0.00 | 0.00 | 0.00 | | 7.00 | 7.13 | 6.94 | 7.19 | 6.95 | 7.08 | 7.21 | 7.36 | 7.41 | 8.04 | 7.59 | 7.64 | 7.55 | 7.55 |
| FeO | 8.18 | 7.84 | 7.28 | 6.23 | | 22.41 | 22.42 | 22.61 | 22.21 | 22.35 | 22.46 | 22.06 | 22.33 | 22.10 | 21.87 | 22.39 | 22.54 | 22.32 | 23.39 |
| MnO | 0.14 | 0.13 | 0.13 | 0.09 | | 0.25 | 0.20 | 0.23 | 0.20 | 0.30 | 0.19 | 0.18 | 0.26 | 0.24 | 0.30 | 0.25 | 0.22 | 0.27 | 0.31 |
| MgO | 50.67 | 51.27 | 51.54 | 52.69 | | 8.15 | 8.34 | 8.13 | 8.39 | 8.34 | 8.18 | 8.42 | 8.27 | 8.45 | 8.39 | 8.23 | 8.31 | 8.35 | 8.24 |
| NiO | 0.32 | 0.28 | 0.40 | 0.40 | | 0.11 | 0.14 | 0.12 | 0.12 | 0.11 | 0.05 | 0.06 | 0.17 | 0.11 | 0.10 | 0.10 | 0.02 | 0.08 | 0.08 |
| ZnO | 0.00 | 0.02 | 0.00 | 0.00 | | 0.18 | 0.04 | 0.12 | 0.11 | 0.10 | 0.24 | 0.19 | 0.19 | 0.21 | 0.20 | 0.15 | 0.14 | 0.14 | 0.10 |
| TOT | 100.82 | 101.20 | 101.44 | 101.82 | | 102.21 | 102.65 | 102.45 | 102.10 | 102.35 | 102.44 | 102.45 | 102.61 | 102.56 | 102.53 | 102.31 | 102.82 | 102.80 | 102.88 |
| Si | 1.00 | 1.00 | 1.00 | 0.99 | | 0.00 | 0.00 | 0.00 | 0.00 | 0.00 | 0.00 | 0.00 | 0.00 | 0.00 | 0.00 | 0.00 | 0.00 | 0.00 | 0.00 |
| Ti | 0.00 | 0.00 | 0.00 | 0.00 | | 0.02 | 0.02 | 0.02 | 0.02 | 0.02 | 0.01 | 0.01 | 0.02 | 0.02 | 0.01 | 0.02 | 0.02 | 0.02 | 0.04 |

| | | | | | | | | | | | | | | | | | | | |
|---|---|---|---|---|---|---|---|---|---|---|---|---|---|---|---|---|---|---|---|
| Al | 0.00 | 0.00 | 0.00 | 0.00 | | 0.51 | 0.51 | 0.51 | 0.52 | 0.53 | 0.53 | 0.52 | 0.51 | 0.50 | 0.50 | 0.50 | 0.50 | 0.50 | 0.50 |
| Cr | 0.00 | 0.00 | 0.00 | 0.01 | | 1.28 | 1.28 | 1.28 | 1.26 | 1.26 | 1.27 | 1.28 | 1.27 | 1.28 | 1.27 | 1.27 | 1.27 | 1.28 | 1.23 |
| V | 0.00 | 0.00 | 0.00 | 0.00 | | 0.00 | 0.00 | 0.00 | 0.00 | 0.00 | 0.00 | 0.00 | 0.00 | 0.01 | 0.00 | 0.00 | 0.00 | 0.00 | 0.00 |
| $Fe^{3+}$ | 0.00 | 0.00 | 0.00 | 0.00 | | 0.17 | 0.17 | 0.17 | 0.18 | 0.17 | 0.17 | 0.18 | 0.18 | 0.18 | 0.20 | 0.19 | 0.19 | 0.18 | 0.18 |
| $Fe^{2+}$ | 0.17 | 0.16 | 0.15 | 0.12 | | 0.61 | 0.61 | 0.61 | 0.60 | 0.60 | 0.61 | 0.60 | 0.60 | 0.60 | 0.59 | 0.61 | 0.61 | 0.60 | 0.63 |
| Mn | 0.00 | 0.00 | 0.00 | 0.00 | | 0.01 | 0.01 | 0.01 | 0.01 | 0.01 | 0.01 | 0.00 | 0.01 | 0.01 | 0.01 | 0.01 | 0.01 | 0.01 | 0.01 |
| Mg | 1.82 | 1.83 | 1.84 | 1.86 | | 0.39 | 0.40 | 0.39 | 0.41 | 0.40 | 0.39 | 0.41 | 0.40 | 0.41 | 0.40 | 0.40 | 0.40 | 0.40 | 0.40 |
| Ni | 0.01 | 0.01 | 0.01 | 0.01 | | 0.00 | 0.00 | 0.00 | 0.00 | 0.00 | 0.00 | 0.00 | 0.00 | 0.00 | 0.00 | 0.00 | 0.00 | 0.00 | 0.00 |
| Zn | 0.00 | 0.00 | 0.00 | 0.00 | | 0.00 | 0.00 | 0.00 | 0.00 | 0.00 | 0.01 | 0.00 | 0.00 | 0.01 | 0.00 | 0.00 | 0.00 | 0.00 | 0.00 |

| Analysis | d-CHR | FIN02B-32 | FIN02B-33 | FIN02B-34 | FIN02B-35 | FIN02B-36 | FIN02B-37 | FIN02B-38 | FIN02B-39 | FIN02B-40 | d-CHR | FIN02B-41 | FIN02B-42 | FIN02B-43 | FIN02B-44 | FIN02B-45 | FIN02B-46 | FIN02B-47 | FIN02B-48 |
|---|---|---|---|---|---|---|---|---|---|---|---|---|---|---|---|---|---|---|---|
| | | 49-OL | 50-OL | 51-OL | 52-OL | 53-OL | 54-OL | 55-OL | 56-OL | 57-OL | | 58-CHR | 59-CHR | 60-CHR | 61-OL | 62-OL | 63-OL | 64-OL | 65-OL |
| X | 44.057 | 44.049 | 44.038 | 44.024 | 43.983 | 44.281 | 44.269 | 44.258 | 44.255 | 44.253 | 44.250 | 44.246 | 44.241 | 44.231 | 43.981 | 44.075 | 44.099 | 44.106 | 44.126 |
| Y | 66.690 | 66.690 | 66.690 | 66.690 | 66.691 | 66.468 | 66.508 | 66.538 | 66.553 | 66.563 | 66.570 | 66.575 | 66.590 | 66.617 | 66.953 | 66.887 | 66.871 | 66.872 | 66.861 |
| **d (mm)** | | **0.008** | **0.019** | **0.034** | **0.075** | **0.106** | **0.064** | **0.033** | **0.018** | **0.008** | | **0.006** | **0.022** | **0.051** | **0.188** | **0.073** | **0.044** | **0.039** | **0.017** |
| $SiO_2$ | | 40.81 | 41.11 | 40.54 | 41.25 | 41.06 | 41.14 | 41.04 | 41.24 | 41.27 | | 0.03 | 0.04 | 0.00 | 41.20 | 41.49 | 41.62 | 41.06 | 41.01 |
| $TiO_2$ | | 0.02 | 0.03 | 0.00 | 0.04 | 0.01 | 0.00 | 0.01 | 0.00 | 0.00 | | 0.56 | 0.66 | 0.64 | 0.00 | 0.00 | 0.00 | 0.05 | 0.02 |
| $Al_2O_3$ | | 0.00 | 0.00 | 0.04 | 0.00 | 0.01 | 0.00 | 0.00 | 0.01 | 0.03 | | 12.29 | 13.21 | 13.60 | 0.01 | 0.02 | 0.00 | 0.00 | 0.00 |
| $Cr_2O_3$ | | 0.28 | 0.12 | 0.06 | 0.00 | 0.00 | 0.01 | 0.12 | 0.31 | 0.52 | | 51.66 | 50.21 | 49.85 | 0.03 | 0.01 | 0.02 | 0.07 | 0.31 |
| $V_2O_3$ | | 0.00 | 0.00 | 0.00 | 0.00 | 0.04 | 0.00 | 0.00 | 0.00 | 0.02 | | 0.14 | 0.16 | 0.12 | 0.02 | 0.00 | 0.00 | 0.01 | 0.00 |
| $Fe_2O_3$ | | 0.00 | 0.00 | 0.00 | 0.00 | 0.00 | 0.00 | 0.00 | 0.00 | 0.00 | | 6.46 | 6.77 | 6.46 | 0.00 | 0.00 | 0.00 | 0.00 | 0.00 |
| FeO | | 6.55 | 7.05 | 7.51 | 7.81 | 8.25 | 7.74 | 7.48 | 6.80 | 6.37 | | 22.21 | 22.05 | 22.61 | 8.63 | 8.02 | 7.51 | 7.42 | 6.89 |
| MnO | | 0.13 | 0.18 | 0.14 | 0.14 | 0.09 | 0.14 | 0.06 | 0.04 | 0.07 | | 0.27 | 0.22 | 0.22 | 0.17 | 0.13 | 0.11 | 0.09 | 0.10 |
| MgO | | 51.65 | 51.56 | 51.04 | 50.60 | 50.37 | 50.88 | 50.89 | 51.22 | 51.88 | | 8.01 | 8.38 | 7.92 | 49.90 | 50.82 | 50.72 | 50.80 | 51.46 |
| NiO | | 0.31 | 0.40 | 0.32 | 0.29 | 0.26 | 0.29 | 0.30 | 0.37 | 0.35 | | 0.11 | 0.02 | 0.10 | 0.32 | 0.23 | 0.32 | 0.28 | 0.32 |
| ZnO | | 0.00 | 0.13 | 0.07 | 0.00 | 0.00 | 0.05 | 0.00 | 0.01 | 0.02 | | 0.31 | 0.24 | 0.25 | 0.00 | 0.05 | 0.05 | 0.08 | 0.00 |
| TOT | | 99.76 | 100.59 | 99.73 | 100.16 | 100.09 | 100.25 | 99.93 | 100.03 | 100.54 | | 102.04 | 101.96 | 101.77 | 100.29 | 100.78 | 100.38 | 99.88 | 100.13 |
| Si | | 0.99 | 0.99 | 0.99 | 1.00 | 1.00 | 1.00 | 1.00 | 1.00 | 0.99 | | 0.00 | 0.00 | 0.00 | 1.00 | 1.00 | 1.01 | 1.00 | 0.99 |
| Ti | | 0.00 | 0.00 | 0.00 | 0.00 | 0.00 | 0.00 | 0.00 | 0.00 | 0.00 | | 0.01 | 0.02 | 0.02 | 0.00 | 0.00 | 0.00 | 0.00 | 0.00 |
| Al | | 0.00 | 0.00 | 0.00 | 0.00 | 0.00 | 0.00 | 0.00 | 0.00 | 0.00 | | 0.47 | 0.51 | 0.52 | 0.00 | 0.00 | 0.00 | 0.00 | 0.00 |
| Cr | | 0.01 | 0.00 | 0.00 | 0.00 | 0.00 | 0.00 | 0.00 | 0.01 | 0.01 | | 1.33 | 1.29 | 1.28 | 0.00 | 0.00 | 0.00 | 0.00 | 0.01 |
| V | | 0.00 | 0.00 | 0.00 | 0.00 | 0.00 | 0.00 | 0.00 | 0.00 | 0.00 | | 0.00 | 0.00 | 0.00 | 0.00 | 0.00 | 0.00 | 0.00 | 0.00 |
| $Fe^{3+}$ | | 0.00 | 0.00 | 0.00 | 0.00 | 0.00 | 0.00 | 0.00 | 0.00 | 0.00 | | 0.16 | 0.17 | 0.16 | 0.00 | 0.00 | 0.00 | 0.00 | 0.00 |
| $Fe^{2+}$ | | 0.13 | 0.14 | 0.15 | 0.16 | 0.17 | 0.16 | 0.15 | 0.14 | 0.13 | | 0.61 | 0.60 | 0.62 | 0.18 | 0.16 | 0.15 | 0.15 | 0.14 |
| Mn | | 0.00 | 0.00 | 0.00 | 0.00 | 0.00 | 0.00 | 0.00 | 0.00 | 0.00 | | 0.01 | 0.01 | 0.01 | 0.00 | 0.00 | 0.00 | 0.00 | 0.00 |
| Mg | | 1.86 | 1.85 | 1.85 | 1.83 | 1.83 | 1.84 | 1.84 | 1.85 | 1.86 | | 0.39 | 0.41 | 0.38 | 1.81 | 1.83 | 1.83 | 1.84 | 1.85 |
| Ni | | 0.01 | 0.01 | 0.01 | 0.01 | 0.01 | 0.01 | 0.01 | 0.01 | 0.01 | | 0.00 | 0.00 | 0.00 | 0.01 | 0.00 | 0.01 | 0.01 | 0.01 |
| Zn | | 0.00 | 0.00 | 0.00 | 0.00 | 0.00 | 0.00 | 0.00 | 0.00 | 0.00 | | 0.01 | 0.01 | 0.01 | 0.00 | 0.00 | 0.00 | 0.00 | 0.00 |

| Analysis | FIN02B-49 | d-CHR | FIN02B-50 | FIN02B-51 | FIN02B-52 | FIN02B-53 | FIN02B-54 | FIN02B-55 | FIN02B-56 | FIN02B-57 | FIN02B-58 | FIN02B-59 | FIN02B-60 | d-CHR | FIN02B-61 | FIN02B-62 | FIN02B-63 | FIN02B-64 | FIN02B-65 |
|---|---|---|---|---|---|---|---|---|---|---|---|---|---|---|---|---|---|---|---|
| | 66-OL | | 67-CHR | 68-CHR | 69-CHR | 70-CHR | 71-OL | 72-OL | 73-OL | 74-OL | 75-OL | 76-OL | 77-OL | | 78-CHR | 79-CHR | 80-CHR | 81-CHR | 82-CHR |
| X | 44.132 | 44.137 | 44.142 | 44.148 | 44.158 | 44.173 | 43.907 | 43.944 | 43.985 | 44.022 | 44.040 | 44.054 | 44.066 | 44.070 | 44.074 | 44.079 | 44.086 | 44.097 | 44.118 |
| Y | 66.852 | 66.848 | 66.845 | 66.839 | 66.830 | 66.817 | 66.494 | 66.516 | 66.548 | 66.578 | 66.588 | 66.600 | 66.601 | 66.604 | 66.606 | 66.609 | 66.613 | 66.621 | 66.633 |
| **d (mm)** | **0.006** | | **0.006** | **0.015** | **0.028** | **0.047** | **0.197** | **0.154** | **0.101** | **0.054** | **0.034** | **0.016** | **0.005** | | **0.005** | **0.011** | **0.019** | **0.032** | **0.057** |
| $SiO_2$ | 41.10 | | 0.03 | 0.05 | 0.02 | 0.02 | 41.10 | 40.92 | 40.32 | 40.31 | 40.55 | 40.52 | 40.65 | | 0.15 | 0.04 | 0.00 | 0.05 | 0.01 |
| $TiO_2$ | 0.00 | | 0.69 | 0.66 | 0.72 | 0.71 | 0.04 | 0.00 | 0.00 | 0.07 | 0.02 | 0.03 | 0.01 | | 0.82 | 0.76 | 0.84 | 0.70 | 0.83 |
| $Al_2O_3$ | 0.00 | | 13.52 | 13.45 | 13.42 | 13.22 | 0.01 | 0.00 | 0.00 | 0.02 | 0.00 | 0.00 | 0.04 | | 15.15 | 14.43 | 13.32 | 13.12 | 13.20 |
| $Cr_2O_3$ | 0.58 | | 49.66 | 50.26 | 50.55 | 49.69 | 0.01 | 0.02 | 0.00 | 0.03 | 0.06 | 0.13 | 0.40 | | 44.98 | 47.40 | 48.65 | 49.60 | 49.92 |
| $V_2O_3$ | 0.00 | | 0.17 | 0.18 | 0.22 | 0.14 | 0.03 | 0.02 | 0.05 | 0.00 | 0.00 | 0.00 | 0.03 | | 0.07 | 0.20 | 0.10 | 0.14 | 0.12 |
| $Fe_2O_3$ | 0.00 | | 6.97 | 6.72 | 5.97 | 7.13 | 0.00 | 0.00 | 0.00 | 0.00 | 0.00 | 0.00 | 0.00 | | 9.00 | 8.43 | 8.22 | 7.60 | 6.99 |

| | | | | | | | | | | | | | | | | | | |
|---|---|---|---|---|---|---|---|---|---|---|---|---|---|---|---|---|---|---|
| FeO | 5.48 | | 22.22 | 22.37 | 22.83 | 22.31 | 8.37 | 8.17 | 8.43 | 7.93 | 7.79 | 7.19 | 6.57 | | 22.55 | 22.42 | 22.86 | 22.61 | 22.77 |
| MnO | 0.08 | | 0.15 | 0.20 | 0.17 | 0.20 | 0.12 | 0.09 | 0.13 | 0.15 | 0.14 | 0.10 | 0.14 | | 0.24 | 0.26 | 0.22 | 0.21 | 0.24 |
| MgO | 53.02 | | 8.39 | 8.32 | 8.02 | 8.26 | 50.14 | 50.04 | 50.74 | 50.30 | 50.75 | 50.94 | 51.95 | | 8.26 | 8.37 | 8.04 | 8.17 | 8.02 |
| NiO | 0.33 | | 0.10 | 0.03 | 0.08 | 0.02 | 0.39 | 0.36 | 0.36 | 0.34 | 0.29 | 0.26 | 0.35 | | 0.13 | 0.10 | 0.03 | 0.11 | 0.08 |
| ZnO | 0.00 | | 0.12 | 0.23 | 0.13 | 0.15 | 0.06 | 0.00 | 0.12 | 0.01 | 0.00 | 0.00 | 0.13 | | 0.22 | 0.26 | 0.20 | 0.09 | 0.25 |
| TOT | 100.59 | | 102.02 | 102.47 | 102.13 | 101.86 | 100.29 | 99.63 | 100.16 | 99.17 | 99.63 | 99.18 | 100.31 | | 101.60 | 102.66 | 102.51 | 102.41 | 102.44 |
| Si | 0.98 | | 0.00 | 0.00 | 0.00 | 0.00 | 1.00 | 1.00 | 0.98 | 0.99 | 0.99 | 0.99 | 0.98 | | 0.00 | 0.00 | 0.00 | 0.00 | 0.00 |
| Ti | 0.00 | | 0.02 | 0.02 | 0.02 | 0.02 | 0.00 | 0.00 | 0.00 | 0.00 | 0.00 | 0.00 | 0.00 | | 0.02 | 0.02 | 0.02 | 0.02 | 0.02 |
| Al | 0.00 | | 0.52 | 0.51 | 0.51 | 0.51 | 0.00 | 0.00 | 0.00 | 0.00 | 0.00 | 0.00 | 0.00 | | 0.58 | 0.55 | 0.51 | 0.50 | 0.50 |
| Cr | 0.01 | | 1.27 | 1.28 | 1.30 | 1.28 | 0.00 | 0.00 | 0.00 | 0.00 | 0.00 | 0.00 | 0.01 | | 1.15 | 1.20 | 1.25 | 1.27 | 1.28 |
| V | 0.00 | | 0.00 | 0.00 | 0.01 | 0.00 | 0.00 | 0.00 | 0.00 | 0.00 | 0.00 | 0.00 | 0.00 | | 0.00 | 0.01 | 0.00 | 0.00 | 0.00 |
| $Fe^{3+}$ | 0.00 | | 0.17 | 0.16 | 0.15 | 0.17 | 0.00 | 0.00 | 0.00 | 0.00 | 0.00 | 0.00 | 0.00 | | 0.22 | 0.20 | 0.20 | 0.19 | 0.17 |
| $Fe^{2+}$ | 0.11 | | 0.60 | 0.60 | 0.62 | 0.61 | 0.17 | 0.17 | 0.17 | 0.16 | 0.16 | 0.15 | 0.13 | | 0.61 | 0.60 | 0.62 | 0.61 | 0.62 |
| Mn | 0.00 | | 0.00 | 0.01 | 0.00 | 0.01 | 0.00 | 0.00 | 0.00 | 0.00 | 0.00 | 0.00 | 0.00 | | 0.01 | 0.01 | 0.01 | 0.01 | 0.01 |
| Mg | 1.89 | | 0.41 | 0.40 | 0.39 | 0.40 | 1.82 | 1.82 | 1.84 | 1.84 | 1.84 | 1.85 | 1.87 | | 0.40 | 0.40 | 0.39 | 0.39 | 0.39 |
| Ni | 0.01 | | 0.00 | 0.00 | 0.00 | 0.00 | 0.01 | 0.01 | 0.01 | 0.01 | 0.01 | 0.01 | 0.01 | | 0.00 | 0.00 | 0.00 | 0.00 | 0.00 |
| Zn | 0.00 | | 0.00 | 0.01 | 0.00 | 0.00 | 0.00 | 0.00 | 0.00 | 0.00 | 0.00 | 0.00 | 0.00 | | 0.01 | 0.01 | 0.00 | 0.00 | 0.01 |

| Analysis | FIN02B-66 | FIN02B-67 | FIN02B-68 | FIN02B-69 | FIN02B-70 | FIN02B-71 | FIN02B-72 | FIN02B-73 | FIN02B-74 | FIN02B-75 | d-CHR | FIN02B-76 | FIN02B-77 | FIN02B-78 | FIN02B-79 | FIN02B-80 | FIN02B-81 |
|---|---|---|---|---|---|---|---|---|---|---|---|---|---|---|---|---|---|
| | 83-CHR | 84-CHR | 85-CHR | 86-OL | 87-OL | 88-OL | 89-OL | 90-OL | 91-OL | 92-OL | | 93-CHR | 94-CHR | 95-CHR | 96-CHR | 97-CHR | 98-CHR |
| X | 44.152 | 44.162 | 44.298 | 44.328 | 44.312 | 44.298 | 44.290 | 44.282 | 44.272 | 44.267 | 44.265 | 44.262 | 44.258 | 44.252 | 44.244 | 44.232 | 44.218 |
| Y | 66.653 | 66.722 | 66.721 | 66.993 | 66.941 | 66.901 | 66.878 | 66.860 | 66.853 | 66.847 | 66.841 | 66.838 | 66.833 | 66.826 | 66.814 | 66.797 | 66.775 |
| **d (mm)** | **0.096** | **0.109** | **0.100** | **0.164** | **0.110** | **0.069** | **0.044** | **0.025** | **0.013** | **0.006** | | **0.004** | **0.011** | **0.020** | **0.034** | **0.055** | **0.081** |
| $SiO_2$ | 0.03 | 0.05 | 0.00 | 39.62 | 39.52 | 39.95 | 39.56 | 40.17 | 40.07 | 40.03 | | 0.01 | 0.01 | 0.06 | 0.03 | 0.05 | 0.00 |
| $TiO_2$ | 0.69 | 0.79 | 0.70 | 0.00 | 0.04 | 0.01 | 0.01 | 0.02 | 0.00 | 0.05 | | 0.74 | 0.78 | 0.72 | 0.72 | 0.65 | 0.44 |
| $Al_2O_3$ | 13.00 | 13.21 | 13.70 | 0.00 | 0.00 | 0.01 | 0.00 | 0.00 | 0.00 | 0.00 | | 13.77 | 13.38 | 13.38 | 13.52 | 13.49 | 13.64 |
| $Cr_2O_3$ | 49.57 | 50.65 | 49.01 | 0.04 | 0.06 | 0.08 | 0.10 | 0.19 | 0.34 | 0.62 | | 49.44 | 49.31 | 49.28 | 49.45 | 50.45 | 50.39 |
| $V_2O_3$ | 0.20 | 0.12 | 0.17 | 0.00 | 0.00 | 0.00 | 0.02 | 0.00 | 0.02 | 0.00 | | 0.18 | 0.19 | 0.15 | 0.17 | 0.17 | 0.15 |
| $Fe_2O_3$ | 7.63 | 6.75 | 7.09 | 0.00 | 0.00 | 0.00 | 0.00 | 0.00 | 0.00 | 0.00 | | 6.60 | 6.43 | 6.67 | 7.06 | 6.38 | 6.47 |
| FeO | 22.03 | 23.19 | 22.44 | 8.19 | 7.92 | 8.03 | 7.56 | 6.74 | 6.61 | 5.70 | | 23.10 | 23.08 | 22.71 | 22.78 | 23.13 | 22.48 |
| MnO | 0.31 | 0.30 | 0.22 | 0.06 | 0.16 | 0.16 | 0.11 | 0.12 | 0.12 | 0.02 | | 0.14 | 0.29 | 0.37 | 0.25 | 0.20 | 0.25 |
| MgO | 8.28 | 7.96 | 8.06 | 50.85 | 51.00 | 50.92 | 51.25 | 51.23 | 51.97 | 52.03 | | 7.84 | 7.70 | 7.71 | 8.00 | 7.89 | 7.99 |
| NiO | 0.08 | 0.12 | 0.05 | 0.36 | 0.24 | 0.30 | 0.37 | 0.40 | 0.34 | 0.34 | | 0.12 | 0.04 | 0.09 | 0.02 | 0.14 | 0.10 |
| ZnO | 0.29 | 0.09 | 0.31 | 0.07 | 0.00 | 0.00 | 0.03 | 0.00 | 0.00 | 0.02 | | 0.14 | 0.00 | 0.34 | 0.21 | 0.07 | 0.15 |
| TOT | 102.11 | 103.22 | 101.75 | 99.23 | 98.96 | 99.46 | 99.02 | 98.89 | 99.47 | 98.82 | | 102.09 | 101.21 | 101.49 | 102.21 | 102.62 | 102.05 |
| Si | 0.00 | 0.00 | 0.00 | 0.97 | 0.97 | 0.97 | 0.97 | 0.98 | 0.97 | 0.97 | | 0.00 | 0.00 | 0.00 | 0.00 | 0.00 | 0.00 |
| Ti | 0.02 | 0.02 | 0.02 | 0.00 | 0.00 | 0.00 | 0.00 | 0.00 | 0.00 | 0.00 | | 0.02 | 0.02 | 0.02 | 0.02 | 0.02 | 0.01 |
| Al | 0.50 | 0.50 | 0.53 | 0.00 | 0.00 | 0.00 | 0.00 | 0.00 | 0.00 | 0.00 | | 0.53 | 0.52 | 0.52 | 0.52 | 0.51 | 0.52 |
| Cr | 1.27 | 1.29 | 1.26 | 0.00 | 0.00 | 0.00 | 0.00 | 0.00 | 0.01 | 0.01 | | 1.27 | 1.28 | 1.28 | 1.27 | 1.29 | 1.29 |
| V | 0.01 | 0.00 | 0.00 | 0.00 | 0.00 | 0.00 | 0.00 | 0.00 | 0.00 | 0.00 | | 0.00 | 0.00 | 0.00 | 0.00 | 0.00 | 0.00 |
| $Fe^{3+}$ | 0.19 | 0.16 | 0.17 | 0.00 | 0.00 | 0.00 | 0.00 | 0.00 | 0.00 | 0.00 | | 0.16 | 0.16 | 0.16 | 0.17 | 0.16 | 0.16 |
| $Fe^{2+}$ | 0.60 | 0.62 | 0.61 | 0.17 | 0.16 | 0.16 | 0.15 | 0.14 | 0.13 | 0.12 | | 0.63 | 0.63 | 0.62 | 0.62 | 0.63 | 0.61 |
| Mn | 0.01 | 0.01 | 0.01 | 0.00 | 0.00 | 0.00 | 0.00 | 0.00 | 0.00 | 0.00 | | 0.00 | 0.01 | 0.01 | 0.01 | 0.01 | 0.01 |
| Mg | 0.40 | 0.38 | 0.39 | 1.85 | 1.86 | 1.85 | 1.87 | 1.87 | 1.88 | 1.89 | | 0.38 | 0.38 | 0.38 | 0.39 | 0.38 | 0.39 |
| Ni | 0.00 | 0.00 | 0.00 | 0.01 | 0.00 | 0.01 | 0.01 | 0.01 | 0.01 | 0.01 | | 0.00 | 0.00 | 0.00 | 0.00 | 0.00 | 0.00 |
| Zn | 0.01 | 0.00 | 0.01 | 0.00 | 0.00 | 0.00 | 0.00 | 0.00 | 0.00 | 0.00 | | 0.00 | 0.00 | 0.01 | 0.00 | 0.00 | 0.00 |

Tab. A3.5 PO4A-GRID1 microprobe analyses of olivine and chromite crystals; d(mm) distance from the intergranular limit

| Analysis | GRID 1-1 | GRID 1-2 | GRID 1-3 | GRID 1-4 | GRID 1-5 | GRID 1-6 | GRID 1-7 | GRID 1-8 | GRID 1-9 | GRID 2-1 | GRID 2-2 | GRID 2-3 | GRID 2-4 | GRID 2-5 | GRID 2-7 | GRID 2-8 | GRID 2-9 | GRID 3-1 |
|---|---|---|---|---|---|---|---|---|---|---|---|---|---|---|---|---|---|---|

# Appendix: Chapter 3

| | 163-CHR | 164-CHR | 165-OL | 166-OL | 167-OL | 168-OL | 169-OL | 170-OL | 171-CHR | 172-OL | 173-OL | 174-OL | 175-CHR | 176-OL | 178-OL | 179-OL | 180-OL | 181-OL |
|---|---|---|---|---|---|---|---|---|---|---|---|---|---|---|---|---|---|---|
| X | 37.87 | 37.87 | 37.87 | 37.87 | 37.87 | 37.87 | 37.87 | 37.87 | 37.87 | 38.07 | 38.07 | 38.07 | 38.07 | 38.07 | 38.07 | 38.07 | 38.07 | 38.27 |
| Y | 82.06 | 82.26 | 82.46 | 82.66 | 82.86 | 83.06 | 83.26 | 83.46 | 83.66 | 82.06 | 82.26 | 82.46 | 82.66 | 82.86 | 83.26 | 83.46 | 83.66 | 82.06 |
| **d (mm)** | **0.141** | **0.029** | **0.118** | **0.059** | **0.024** | | **0.247** | **0.176** | **0.006** | **0.029** | **0.141** | **0.071** | **0.035** | **0.035** | **0.329** | | **0.194** | **0.153** |
| $SiO_2$ | 0.00 | 0.02 | 41.50 | 41.78 | 41.46 | 45.40 | 41.54 | 41.86 | 0.10 | 41.67 | 41.52 | 41.62 | 0.02 | 41.56 | 41.48 | 42.97 | 41.59 | 41.09 |
| $TiO_2$ | 0.56 | 0.57 | 0.00 | 0.00 | 0.05 | 0.00 | 0.02 | 0.00 | 0.51 | 0.01 | 0.05 | 0.00 | 0.62 | 0.01 | 0.00 | 0.00 | 0.00 | 0.05 |
| $Al_2O_3$ | 15.08 | 15.58 | 0.00 | 0.00 | 0.00 | 0.02 | 0.00 | 0.00 | 14.00 | 0.00 | 0.00 | 0.03 | 16.34 | 0.00 | 0.00 | 0.28 | 0.00 | 0.03 |
| $Cr_2O_3$ | 51.70 | 51.86 | 0.00 | 0.03 | 0.19 | 0.12 | 0.00 | 0.00 | 52.13 | 0.10 | 0.01 | 0.00 | 50.26 | 0.08 | 0.01 | 0.27 | 0.00 | 0.00 |
| $V_2O_3$ | 0.13 | 0.07 | 0.00 | 0.00 | 0.00 | 0.00 | 0.01 | 0.00 | 0.10 | 0.00 | 0.00 | 0.02 | 0.09 | 0.00 | 0.00 | 0.02 | 0.00 | 0.00 |
| $Fe_2O_3$ | 4.99 | 4.18 | 0.00 | 0.00 | 0.00 | 0.00 | 0.00 | 0.00 | 4.94 | 0.00 | 0.00 | 0.00 | 4.42 | 0.00 | 0.00 | 0.00 | 0.00 | 0.00 |
| FeO | 17.34 | 17.34 | 5.72 | 4.71 | 4.84 | 5.73 | 5.65 | 5.80 | 17.83 | 5.32 | 5.79 | 5.51 | 17.93 | 6.44 | 6.19 | 6.31 | 6.31 | 5.65 |
| MnO | 0.20 | 0.09 | 0.05 | 0.05 | 0.08 | 0.09 | 0.11 | 0.05 | 0.15 | 0.12 | 0.08 | 0.04 | 0.20 | 0.09 | 0.05 | 0.10 | 0.10 | 0.09 |
| MgO | 11.55 | 11.60 | 52.31 | 52.74 | 52.60 | 44.34 | 51.79 | 51.90 | 11.08 | 52.12 | 51.85 | 51.97 | 11.31 | 51.63 | 51.92 | 44.05 | 51.48 | 52.24 |
| NiO | 0.11 | 0.13 | 0.58 | 0.50 | 0.54 | 0.46 | 0.52 | 0.39 | 0.05 | 0.47 | 0.52 | 0.41 | 0.08 | 0.47 | 0.47 | 0.44 | 0.46 | 0.49 |
| ZnO | 0.12 | 0.25 | 0.00 | 0.08 | 0.09 | 0.14 | 0.00 | 0.00 | 0.16 | 0.07 | 0.00 | 0.00 | 0.10 | 0.00 | 0.00 | 0.02 | 0.00 | 0.03 |
| TOT | 101.80 | 101.70 | 100.16 | 99.89 | 99.87 | 96.37 | 99.65 | 100.02 | 101.05 | 99.89 | 99.83 | 99.61 | 101.37 | 100.29 | 100.13 | 94.68 | 99.96 | 99.68 |
| Si | 0.00 | 0.00 | 1.00 | 1.00 | 1.00 | 1.16 | 1.00 | 1.01 | 0.00 | 1.00 | 1.00 | 1.01 | 0.00 | 1.00 | 1.00 | 1.12 | 1.01 | 0.99 |
| Ti | 0.01 | 0.01 | 0.00 | 0.00 | 0.00 | 0.00 | 0.00 | 0.00 | 0.01 | 0.00 | 0.00 | 0.00 | 0.01 | 0.00 | 0.00 | 0.00 | 0.00 | 0.00 |
| Al | 0.56 | 0.58 | 0.00 | 0.00 | 0.00 | 0.00 | 0.00 | 0.00 | 0.53 | 0.00 | 0.00 | 0.00 | 0.61 | 0.00 | 0.00 | 0.01 | 0.00 | 0.00 |
| Cr | 1.29 | 1.29 | 0.00 | 0.00 | 0.00 | 0.00 | 0.00 | 0.00 | 1.32 | 0.00 | 0.00 | 0.00 | 1.25 | 0.00 | 0.00 | 0.01 | 0.00 | 0.00 |
| V | 0.00 | 0.00 | 0.00 | 0.00 | 0.00 | 0.00 | 0.00 | 0.00 | 0.00 | 0.00 | 0.00 | 0.00 | 0.00 | 0.00 | 0.00 | 0.00 | 0.00 | 0.00 |
| $Fe^{3+}$ | 0.12 | 0.10 | 0.00 | 0.00 | 0.00 | 0.00 | 0.00 | 0.00 | 0.12 | 0.00 | 0.00 | 0.00 | 0.10 | 0.00 | 0.00 | 0.00 | 0.00 | 0.00 |
| $Fe^{2+}$ | 0.46 | 0.46 | 0.11 | 0.09 | 0.10 | 0.12 | 0.11 | 0.12 | 0.48 | 0.11 | 0.12 | 0.11 | 0.47 | 0.13 | 0.13 | 0.14 | 0.13 | 0.11 |
| Mn | 0.01 | 0.00 | 0.00 | 0.00 | 0.00 | 0.00 | 0.00 | 0.00 | 0.00 | 0.00 | 0.00 | 0.00 | 0.01 | 0.00 | 0.00 | 0.00 | 0.00 | 0.00 |
| Mg | 0.54 | 0.55 | 1.88 | 1.89 | 1.89 | 1.69 | 1.87 | 1.86 | 0.53 | 1.87 | 1.87 | 1.87 | 0.53 | 1.86 | 1.87 | 1.71 | 1.86 | 1.88 |
| Ni | 0.00 | 0.00 | 0.01 | 0.01 | 0.01 | 0.01 | 0.01 | 0.01 | 0.00 | 0.01 | 0.01 | 0.01 | 0.00 | 0.01 | 0.01 | 0.01 | 0.01 | 0.01 |
| Zn | 0.00 | 0.01 | 0.00 | 0.00 | 0.00 | 0.00 | 0.00 | 0.00 | 0.00 | 0.00 | 0.00 | 0.00 | 0.00 | 0.00 | 0.00 | 0.00 | 0.00 | 0.00 |

| Analysis | GRID 3-2 | GRID 3-3 | GRID 3-4 | GRID 3-6 | GRID 3-7 | GRID 3-8 | GRID 3-9 | GRID 4-1 | GRID 4-3 | GRID 4-4 | GRID 4-5 | GRID 4-6 | GRID 4-7 | GRID 4-8 | GRID 4-9 | GRID 5-1 | GRID 5-2 | GRID 5-3 |
|---|---|---|---|---|---|---|---|---|---|---|---|---|---|---|---|---|---|---|
| | 182-OL | 183-CHR | 184-OL | 186-OL | 187-OL | 188-OL | 189-OL | 190-CHR | 192-OL | 193-OL | 194-CHR | 195-OL | 196-OL | 197-CHR | 198-OL | 199-CHR | 200-CHR | 201-OL |
| X | 38.27 | 38.27 | 38.27 | 38.27 | 38.27 | 38.27 | 38.27 | 38.47 | 38.47 | 38.47 | 38.47 | 38.47 | 38.47 | 38.47 | 38.47 | 38.67 | 38.67 | 38.67 |
| Y | 82.26 | 82.46 | 82.66 | 83.06 | 83.26 | 83.46 | 83.66 | 82.06 | 82.46 | 82.66 | 82.86 | 83.06 | 83.26 | 83.46 | 83.66 | 82.06 | 82.26 | 82.46 |
| **d (mm)** | **0.018** | **0.091** | **0.059** | **0.235** | **0.212** | **0.047** | **0.118** | **0.018** | **0.082** | **0.129** | **0.016** | **0.082** | **0.035** | **0.059** | **0.094** | **0.141** | **0.047** | **0.106** |
| $SiO_2$ | 41.68 | 0.04 | 41.27 | 41.61 | 42.21 | 41.66 | 41.71 | 0.01 | 41.65 | 41.53 | 0.06 | 41.54 | 41.15 | 0.02 | 41.72 | 0.02 | 0.01 | 41.43 |
| $TiO_2$ | 0.04 | 0.69 | 0.03 | 0.00 | 0.00 | 0.00 | 0.00 | 0.50 | 0.02 | 0.00 | 0.53 | 0.01 | 0.06 | 0.60 | 0.00 | 0.55 | 0.53 | 0.00 |
| $Al_2O_3$ | 0.05 | 14.63 | 0.02 | 0.00 | 0.04 | 0.01 | 0.00 | 14.43 | 0.00 | 0.00 | 14.52 | 0.01 | 0.02 | 15.21 | 0.00 | 14.25 | 15.22 | 0.00 |
| $Cr_2O_3$ | 0.54 | 52.33 | 0.00 | 0.02 | 0.03 | 0.07 | 0.00 | 52.34 | 0.00 | 0.00 | 51.71 | 0.01 | 0.21 | 51.10 | 0.01 | 52.23 | 50.97 | 0.00 |
| $V_2O_3$ | 0.00 | 0.08 | 0.00 | 0.00 | 0.02 | 0.00 | 0.00 | 0.13 | 0.02 | 0.03 | 0.11 | 0.00 | 0.04 | 0.12 | 0.00 | 0.12 | 0.14 | 0.05 |
| $Fe_2O_3$ | 0.00 | 4.09 | 0.00 | 0.00 | 0.00 | 0.00 | 0.00 | 5.03 | 0.00 | 0.00 | 4.80 | 0.00 | 0.00 | 4.96 | 0.00 | 4.40 | 5.18 | 0.00 |
| FeO | 4.82 | 18.20 | 5.77 | 5.36 | 5.86 | 5.55 | 6.17 | 17.61 | 5.54 | 5.98 | 18.23 | 5.58 | 5.31 | 17.67 | 5.99 | 17.58 | 16.95 | 5.75 |
| MnO | 0.06 | 0.10 | 0.11 | 0.06 | 0.09 | 0.10 | 0.10 | 0.18 | 0.06 | 0.05 | 0.26 | 0.08 | 0.08 | 0.16 | 0.13 | 0.20 | 0.22 | 0.11 |
| MgO | 52.77 | 11.01 | 51.13 | 52.05 | 51.78 | 51.92 | 51.73 | 11.26 | 51.89 | 52.33 | 10.80 | 52.21 | 52.63 | 11.29 | 52.26 | 11.14 | 11.66 | 51.91 |
| NiO | 0.51 | 0.05 | 0.57 | 0.46 | 0.47 | 0.45 | 0.47 | 0.16 | 0.46 | 0.45 | 0.03 | 0.39 | 0.56 | 0.16 | 0.47 | 0.09 | 0.13 | 0.38 |
| ZnO | 0.00 | 0.31 | 0.14 | 0.00 | 0.03 | 0.03 | 0.00 | 0.13 | 0.20 | 0.09 | 0.22 | 0.09 | 0.14 | 0.16 | 0.00 | 0.07 | 0.11 | 0.00 |
| TOT | 100.50 | 101.52 | 99.05 | 99.56 | 100.53 | 99.80 | 100.19 | 101.79 | 99.87 | 100.47 | 101.30 | 99.91 | 100.20 | 101.48 | 100.59 | 100.67 | 101.13 | 99.65 |
| Si | 1.00 | 0.00 | 1.01 | 1.01 | 1.01 | 1.01 | 1.01 | 0.00 | 1.01 | 1.00 | 0.00 | 1.00 | 0.99 | 0.00 | 1.00 | 0.00 | 0.00 | 1.00 |
| Ti | 0.00 | 0.02 | 0.00 | 0.00 | 0.00 | 0.00 | 0.00 | 0.01 | 0.00 | 0.00 | 0.01 | 0.00 | 0.00 | 0.01 | 0.00 | 0.01 | 0.01 | 0.00 |
| Al | 0.00 | 0.55 | 0.00 | 0.00 | 0.00 | 0.00 | 0.00 | 0.54 | 0.00 | 0.00 | 0.55 | 0.00 | 0.00 | 0.57 | 0.00 | 0.54 | 0.57 | 0.00 |
| Cr | 0.01 | 1.32 | 0.00 | 0.00 | 0.00 | 0.00 | 0.00 | 1.31 | 0.00 | 0.00 | 1.31 | 0.00 | 0.00 | 1.28 | 0.00 | 1.32 | 1.28 | 0.00 |
| V | 0.00 | 0.00 | 0.00 | 0.00 | 0.00 | 0.00 | 0.00 | 0.00 | 0.00 | 0.00 | 0.00 | 0.00 | 0.00 | 0.00 | 0.00 | 0.00 | 0.00 | 0.00 |

| | | | | | | | | | | | | | | | | | | |
|---|---|---|---|---|---|---|---|---|---|---|---|---|---|---|---|---|---|---|
| $Fe^{3+}$ | 0.00 | 0.10 | 0.00 | 0.00 | 0.00 | 0.00 | 0.00 | 0.12 | 0.00 | 0.00 | 0.12 | 0.00 | 0.00 | 0.12 | 0.00 | 0.11 | 0.12 | 0.00 |
| $Fe^{2+}$ | 0.10 | 0.48 | 0.12 | 0.11 | 0.12 | 0.11 | 0.12 | 0.47 | 0.11 | 0.12 | 0.49 | 0.11 | 0.11 | 0.47 | 0.12 | 0.47 | 0.45 | 0.12 |
| Mn | 0.00 | 0.00 | 0.00 | 0.00 | 0.00 | 0.00 | 0.00 | 0.00 | 0.00 | 0.00 | 0.01 | 0.00 | 0.00 | 0.00 | 0.00 | 0.01 | 0.01 | 0.00 |
| Mg | 1.88 | 0.52 | 1.86 | 1.88 | 1.85 | 1.87 | 1.86 | 0.53 | 1.87 | 1.87 | 0.51 | 1.88 | 1.88 | 0.53 | 1.87 | 0.53 | 0.55 | 1.87 |
| Ni | 0.01 | 0.00 | 0.01 | 0.01 | 0.01 | 0.01 | 0.01 | 0.00 | 0.01 | 0.01 | 0.00 | 0.01 | 0.01 | 0.00 | 0.01 | 0.00 | 0.00 | 0.01 |
| Zn | 0.00 | 0.01 | 0.00 | 0.00 | 0.00 | 0.00 | 0.00 | 0.00 | 0.00 | 0.00 | 0.01 | 0.00 | 0.00 | 0.00 | 0.00 | 0.00 | 0.00 | 0.00 |

| Analysis | GRID 5-4 | GRID 5-5 | GRID 5-6 | GRID 5-7 | GRID 5-8 | GRID 5-9 | GRID 6-1 | GRID 6-2 | GRID 6-3 | GRID 6-4 | GRID 6-5 | GRID 6-6 | GRID 6-7 | GRID 6-8 | GRID 6-9 | GRID 7-1 | GRID 7-2 | GRID 7-4 |
|---|---|---|---|---|---|---|---|---|---|---|---|---|---|---|---|---|---|---|
| | 202-OL | 203-CHR | 204-OL | 205-CHR | 206-CHR | 207-OL | 208-CHR | 209-CHR | 210-CHR | 211-OL | 212-CHR | 213-OL | 214-CHR | 215-CHR | 216-OL | 217-CHR | 218-CHR | 220-OL |
| X | 38.67 | 38.67 | 38.67 | 38.67 | 38.67 | 38.67 | 38.87 | 38.87 | 38.87 | 38.87 | 38.87 | 38.87 | 38.87 | 38.87 | 38.87 | 39.07 | 39.07 | 39.07 |
| Y | 82.66 | 82.86 | 83.06 | 83.26 | 83.46 | 83.66 | 82.06 | 82.26 | 82.46 | 82.66 | 82.86 | 83.06 | 83.26 | 83.46 | 83.66 | 82.06 | 82.26 | 82.66 |
| **d (mm)** | **0.076** | **0.118** | **0.012** | **0.129** | **0.024** | **0.212** | **0.294** | **0.176** | **0.047** | **0.082** | **0.029** | **0.006** | **0.047** | **0.024** | **0.082** | **0.318** | **0.153** | **0.094** |
| $SiO_2$ | 41.74 | 0.03 | 41.66 | 0.05 | 0.17 | 41.67 | 0.01 | 0.01 | 0.00 | 41.17 | 0.07 | 41.44 | 0.00 | 0.16 | 41.88 | 0.03 | 0.00 | 41.69 |
| $TiO_2$ | 0.00 | 0.57 | 0.10 | 0.56 | 0.40 | 0.00 | 0.67 | 0.54 | 0.55 | 0.05 | 0.55 | 0.02 | 0.64 | 0.51 | 0.00 | 0.54 | 0.61 | 0.06 |
| $Al_2O_3$ | 0.00 | 15.01 | 0.07 | 14.57 | 12.47 | 0.00 | 15.29 | 15.22 | 15.36 | 0.00 | 14.67 | 0.03 | 15.36 | 13.21 | 0.00 | 15.01 | 15.04 | 0.00 |
| $Cr_2O_3$ | 0.02 | 51.97 | 0.69 | 51.80 | 54.00 | 0.03 | 51.38 | 51.92 | 51.95 | 0.04 | 51.55 | 0.31 | 51.52 | 52.68 | 0.04 | 52.41 | 51.66 | 0.01 |
| $V_2O_3$ | 0.00 | 0.11 | 0.00 | 0.10 | 0.12 | 0.00 | 0.10 | 0.12 | 0.07 | 0.00 | 0.05 | 0.02 | 0.11 | 0.03 | 0.01 | 0.19 | 0.12 | 0.01 |
| $Fe_2O_3$ | 0.00 | 4.68 | 0.00 | 5.16 | 4.86 | 0.00 | 4.18 | 4.46 | 4.56 | 0.00 | 4.43 | 0.00 | 4.64 | 4.95 | 0.00 | 4.23 | 4.51 | 0.00 |
| FeO | 5.68 | 18.22 | 4.28 | 17.77 | 18.22 | 5.64 | 17.65 | 17.46 | 17.52 | 5.85 | 18.08 | 5.15 | 18.15 | 18.34 | 5.68 | 17.88 | 17.44 | 5.92 |
| MnO | 0.11 | 0.19 | 0.07 | 0.16 | 0.24 | 0.04 | 0.09 | 0.17 | 0.08 | 0.09 | 0.17 | 0.13 | 0.17 | 0.16 | 0.08 | 0.10 | 0.15 | 0.12 |
| MgO | 52.12 | 11.06 | 53.36 | 11.20 | 10.69 | 52.07 | 11.41 | 11.38 | 11.49 | 52.70 | 10.86 | 53.06 | 11.16 | 10.69 | 52.30 | 11.39 | 11.44 | 51.91 |
| NiO | 0.52 | 0.09 | 0.54 | 0.09 | 0.02 | 0.40 | 0.13 | 0.10 | 0.25 | 0.53 | 0.09 | 0.46 | 0.06 | 0.10 | 0.48 | 0.09 | 0.05 | 0.42 |
| ZnO | 0.18 | 0.22 | 0.12 | 0.31 | 0.16 | 0.00 | 0.00 | 0.34 | 0.13 | 0.01 | 0.16 | 0.13 | 0.21 | 0.05 | 0.00 | 0.00 | 0.19 | 0.02 |
| TOT | 100.40 | 102.15 | 100.94 | 101.77 | 101.36 | 99.91 | 100.93 | 101.72 | 101.98 | 100.46 | 100.70 | 100.75 | 102.02 | 100.91 | 100.49 | 101.87 | 101.20 | 100.16 |
| Si | 1.00 | 0.00 | 0.99 | 0.00 | 0.01 | 1.00 | 0.00 | 0.00 | 0.00 | 0.99 | 0.00 | 0.99 | 0.00 | 0.01 | 1.00 | 0.00 | 0.00 | 1.00 |
| Ti | 0.00 | 0.01 | 0.00 | 0.01 | 0.01 | 0.00 | 0.02 | 0.01 | 0.01 | 0.00 | 0.01 | 0.00 | 0.02 | 0.01 | 0.00 | 0.01 | 0.01 | 0.00 |
| Al | 0.00 | 0.56 | 0.00 | 0.54 | 0.47 | 0.00 | 0.57 | 0.57 | 0.57 | 0.00 | 0.55 | 0.00 | 0.57 | 0.50 | 0.00 | 0.56 | 0.56 | 0.00 |
| Cr | 0.00 | 1.30 | 0.01 | 1.30 | 1.38 | 0.00 | 1.29 | 1.30 | 1.29 | 0.00 | 1.31 | 0.01 | 1.29 | 1.34 | 0.00 | 1.31 | 1.30 | 0.00 |
| V | 0.00 | 0.00 | 0.00 | 0.00 | 0.00 | 0.00 | 0.00 | 0.00 | 0.00 | 0.00 | 0.00 | 0.00 | 0.00 | 0.00 | 0.00 | 0.00 | 0.00 | 0.00 |
| $Fe^{3+}$ | 0.00 | 0.11 | 0.00 | 0.12 | 0.12 | 0.00 | 0.10 | 0.11 | 0.11 | 0.00 | 0.11 | 0.00 | 0.11 | 0.12 | 0.00 | 0.10 | 0.11 | 0.00 |
| $Fe^{2+}$ | 0.11 | 0.48 | 0.09 | 0.47 | 0.49 | 0.11 | 0.47 | 0.46 | 0.46 | 0.12 | 0.48 | 0.10 | 0.48 | 0.49 | 0.11 | 0.47 | 0.46 | 0.12 |
| Mn | 0.00 | 0.01 | 0.00 | 0.00 | 0.01 | 0.00 | 0.00 | 0.00 | 0.00 | 0.00 | 0.00 | 0.00 | 0.00 | 0.00 | 0.00 | 0.00 | 0.00 | 0.00 |
| Mg | 1.87 | 0.52 | 1.89 | 0.53 | 0.51 | 1.87 | 0.54 | 0.54 | 0.54 | 1.88 | 0.52 | 1.89 | 0.53 | 0.51 | 1.87 | 0.54 | 0.54 | 1.86 |
| Ni | 0.01 | 0.00 | 0.01 | 0.00 | 0.00 | 0.01 | 0.00 | 0.00 | 0.01 | 0.01 | 0.00 | 0.01 | 0.00 | 0.00 | 0.01 | 0.00 | 0.00 | 0.01 |
| Zn | 0.00 | 0.01 | 0.00 | 0.01 | 0.00 | 0.00 | 0.00 | 0.01 | 0.00 | 0.00 | 0.00 | 0.00 | 0.00 | 0.00 | 0.00 | 0.00 | 0.00 | 0.00 |

| Analysis | GRID 7-5 | GRID 7-6 | GRID 7-7 | GRID 7-9 | GRID 8-1 | GRID 8-2 | GRID 8-3 | GRID 8-4 | GRID 8-5 | GRID 8-6 | GRID 8-8 | GRID 8-9 | GRID 9-2 | GRID 9-3 | GRID 9-5 | GRID 9-6 | GRID 9-7 | GRID 9-9 |
|---|---|---|---|---|---|---|---|---|---|---|---|---|---|---|---|---|---|---|
| | 221-CHR | 222-OL | 223-OL | 225-CHR | 226-CHR | 227-CHR | 228-OL | 229-OL | 230-CHR | 231-OL | 233-OL | 234-CHR | 236-CHR | 237-CHR | 239-CHR | 240-CHR | 241-OL | 243-OL |
| X | 39.07 | 39.07 | 39.07 | 39.07 | 39.27 | 39.27 | 39.27 | 39.27 | 39.27 | 39.27 | 39.27 | 39.27 | 39.47 | 39.47 | 39.47 | 39.47 | 39.47 | 39.47 |
| Y | 82.86 | 83.06 | 83.26 | 83.66 | 82.06 | 82.26 | 82.46 | 82.66 | 82.86 | 83.06 | 83.46 | 83.66 | 82.26 | 82.46 | 82.86 | 83.06 | 83.26 | 83.66 |
| **d (mm)** | **0.047** | **0.059** | **0.035** | **0.001** | **0.106** | **0.041** | **0.065** | **0.029** | **0.129** | **0.047** | **0.082** | **0.106** | **0.001** | **0.129** | **0.071** | **0.001** | **0.188** | **0.012** |
| $SiO_2$ | 0.01 | 41.57 | 41.53 | 0.12 | 0.00 | 0.07 | 41.79 | 41.28 | 0.01 | 41.55 | 41.60 | 0.04 | 0.08 | 0.01 | 0.00 | 0.20 | 41.32 | 41.17 |
| $TiO_2$ | 0.51 | 0.00 | 0.00 | 0.54 | 0.59 | 0.55 | 0.02 | 0.03 | 0.58 | 0.01 | 0.00 | 0.55 | 0.54 | 0.56 | 0.55 | 0.43 | 0.00 | 0.05 |
| $Al_2O_3$ | 14.65 | 0.00 | 0.02 | 14.07 | 15.32 | 13.58 | 0.02 | 0.55 | 14.91 | 0.00 | 0.01 | 14.99 | 14.94 | 15.98 | 14.92 | 12.29 | 0.03 | 0.01 |
| $Cr_2O_3$ | 52.19 | 0.00 | 0.11 | 52.17 | 51.55 | 53.20 | 0.04 | 0.20 | 51.92 | 0.00 | 0.07 | 52.05 | 53.03 | 51.47 | 51.42 | 52.97 | 0.00 | 0.27 |
| $V_2O_3$ | 0.09 | 0.00 | 0.06 | 0.14 | 0.06 | 0.13 | 0.00 | 0.00 | 0.12 | 0.06 | 0.00 | 0.05 | 0.16 | 0.15 | 0.07 | 0.11 | 0.00 | 0.00 |
| $Fe_2O_3$ | 4.29 | 0.00 | 0.00 | 4.82 | 4.78 | 4.41 | 0.00 | 0.00 | 4.85 | 0.00 | 0.00 | 4.25 | 3.47 | 4.25 | 4.54 | 5.37 | 0.00 | 0.21 |
| FeO | 18.51 | 5.00 | 5.24 | 18.30 | 16.99 | 18.32 | 5.19 | 5.77 | 17.88 | 5.50 | 5.61 | 18.16 | 18.74 | 17.12 | 18.10 | 18.47 | 6.09 | 5.14 |
| MnO | 0.18 | 0.13 | 0.03 | 0.20 | 0.19 | 0.14 | 0.05 | 0.12 | 0.09 | 0.08 | 0.08 | 0.12 | 0.22 | 0.09 | 0.10 | 0.22 | 0.11 | 0.03 |
| MgO | 10.71 | 52.44 | 52.44 | 10.86 | 11.69 | 10.87 | 52.45 | 52.11 | 11.19 | 52.10 | 52.26 | 11.00 | 10.82 | 11.74 | 10.97 | 10.31 | 52.22 | 52.24 |

| | | | | | | | | | | | | | | | | | | |
|---|---|---|---|---|---|---|---|---|---|---|---|---|---|---|---|---|---|---|
| NiO | 0.01 | 0.50 | 0.49 | 0.18 | 0.05 | 0.06 | 0.57 | 0.57 | 0.08 | 0.46 | 0.43 | 0.20 | 0.07 | 0.15 | 0.14 | 0.14 | 0.52 | 0.47 |
| ZnO | 0.13 | 0.00 | 0.00 | 0.01 | 0.39 | 0.02 | 0.00 | 0.01 | 0.40 | 0.04 | 0.00 | 0.10 | 0.08 | 0.36 | 0.00 | 0.23 | 0.00 | 0.00 |
| TOT | 101.29 | 99.66 | 99.92 | 101.43 | 101.62 | 101.36 | 100.13 | 100.65 | 102.03 | 99.82 | 100.06 | 101.51 | 102.16 | 101.89 | 100.81 | 100.73 | 100.31 | 99.60 |
| Si | 0.00 | 1.00 | 1.00 | 0.00 | 0.00 | 0.00 | 1.00 | 0.99 | 0.00 | 1.00 | 1.00 | 0.00 | 0.00 | 0.00 | 0.00 | 0.01 | 0.99 | 0.99 |
| Ti | 0.01 | 0.00 | 0.00 | 0.01 | 0.01 | 0.01 | 0.00 | 0.00 | 0.01 | 0.00 | 0.00 | 0.01 | 0.01 | 0.01 | 0.01 | 0.01 | 0.00 | 0.00 |
| Al | 0.55 | 0.00 | 0.00 | 0.53 | 0.57 | 0.51 | 0.00 | 0.02 | 0.56 | 0.00 | 0.00 | 0.56 | 0.56 | 0.59 | 0.56 | 0.47 | 0.00 | 0.00 |
| Cr | 1.32 | 0.00 | 0.00 | 1.32 | 1.29 | 1.35 | 0.00 | 0.00 | 1.30 | 0.00 | 0.00 | 1.31 | 1.33 | 1.28 | 1.30 | 1.36 | 0.00 | 0.01 |
| V | 0.00 | 0.00 | 0.00 | 0.00 | 0.00 | 0.00 | 0.00 | 0.00 | 0.00 | 0.00 | 0.00 | 0.00 | 0.00 | 0.00 | 0.00 | 0.00 | 0.00 | 0.00 |
| $Fe^{3+}$ | 0.10 | 0.00 | 0.00 | 0.12 | 0.11 | 0.11 | 0.00 | 0.00 | 0.12 | 0.00 | 0.00 | 0.10 | 0.08 | 0.10 | 0.11 | 0.13 | 0.00 | 0.00 |
| $Fe^{2+}$ | 0.49 | 0.10 | 0.11 | 0.49 | 0.45 | 0.49 | 0.10 | 0.12 | 0.47 | 0.11 | 0.11 | 0.48 | 0.50 | 0.45 | 0.48 | 0.50 | 0.12 | 0.10 |
| Mn | 0.00 | 0.00 | 0.00 | 0.01 | 0.01 | 0.00 | 0.00 | 0.00 | 0.00 | 0.00 | 0.00 | 0.00 | 0.01 | 0.00 | 0.00 | 0.01 | 0.00 | 0.00 |
| Mg | 0.51 | 1.88 | 1.88 | 0.52 | 0.55 | 0.52 | 1.88 | 1.86 | 0.53 | 1.87 | 1.87 | 0.52 | 0.51 | 0.55 | 0.52 | 0.50 | 1.87 | 1.88 |
| Ni | 0.00 | 0.01 | 0.01 | 0.00 | 0.00 | 0.00 | 0.01 | 0.01 | 0.00 | 0.01 | 0.01 | 0.01 | 0.00 | 0.00 | 0.00 | 0.00 | 0.01 | 0.01 |
| Zn | 0.00 | 0.00 | 0.00 | 0.00 | 0.01 | 0.00 | 0.00 | 0.00 | 0.01 | 0.00 | 0.00 | 0.00 | 0.00 | 0.01 | 0.00 | 0.01 | 0.00 | 0.00 |

| Analysis | PO4A-1 | PO4A-2 | PO4A-3 | PO4A-4 | PO4A-5 | PO4A-3 | PO4A-4 | PO4A-5 | PO4A-6 | PO4A-7 | PO4A-8 | PO4A-9 |
|---|---|---|---|---|---|---|---|---|---|---|---|---|
| | OL-rim | CHR-rim | CHR-core | CHR-rim | OL-rim | 43-CHR | 44-CHR | 45-OL | 46-CHR | 47-OL | 48-OL | 49-OL |
| X | 38.80 | 38.78 | 38.64 | 38.49 | 38.46 | 38.29 | 38.24 | 38.23 | 38.09 | 38.08 | 37.98 | 37.86 |
| Y | 82.71 | 82.74 | 82.88 | 82.95 | 82.96 | 84.16 | 84.13 | 84.12 | 84.36 | 84.36 | 84.33 | 84.27 |
| **d (mm)** | **0.006** | **0.012** | **0.129** | **0.001** | **0.012** | **0.061** | **0.004** | **0.008** | **0.008** | **0.012** | **0.113** | **0.242** |
| $SiO_2$ | 41.45 | 0.08 | 0.00 | 0.17 | 41.68 | 0.04 | 0.00 | 41.44 | 0.06 | 41.52 | 41.10 | 41.31 |
| $TiO_2$ | 0.00 | 0.66 | 0.58 | 0.48 | 0.00 | 0.60 | 0.32 | 0.00 | 0.43 | 0.01 | 0.00 | 0.01 |
| $Al_2O_3$ | 0.07 | 14.68 | 14.80 | 14.42 | 0.05 | 14.88 | 12.87 | 0.00 | 14.53 | 0.01 | 0.00 | 0.00 |
| $Cr_2O_3$ | 0.25 | 50.83 | 51.71 | 51.73 | 0.32 | 52.51 | 53.91 | 0.28 | 52.20 | 0.28 | 0.06 | 0.02 |
| $V_2O_3$ | 0.00 | 0.12 | 0.06 | 0.14 | 0.00 | 0.00 | 0.02 | 0.00 | 0.03 | 0.00 | 0.00 | 0.02 |
| $Fe_2O_3$ | 0.00 | 5.12 | 4.67 | 4.61 | 0.00 | 3.83 | 4.58 | 0.00 | 4.30 | 0.00 | 0.00 | 0.00 |
| FeO | 5.26 | 18.48 | 17.97 | 18.47 | 5.05 | 18.61 | 17.55 | 4.15 | 18.24 | 4.64 | 5.75 | 6.05 |
| MnO | 0.05 | 0.08 | 0.14 | 0.12 | 0.03 | 0.16 | 0.10 | 0.05 | 0.12 | 0.07 | 0.04 | 0.08 |
| MgO | 52.51 | 10.87 | 11.02 | 10.77 | 52.58 | 10.86 | 10.82 | 52.39 | 10.75 | 53.05 | 51.51 | 51.23 |
| NiO | 0.38 | 0.13 | 0.07 | 0.00 | 0.51 | 0.01 | 0.13 | 0.47 | 0.03 | 0.52 | 0.50 | 0.59 |
| ZnO | 0.00 | 0.02 | 0.25 | 0.23 | 0.05 | 0.05 | 0.16 | 0.00 | 0.22 | 0.00 | 0.00 | 0.00 |
| TOT | 99.97 | 101.08 | 101.27 | 101.17 | 100.28 | 101.57 | 100.47 | 98.80 | 100.94 | 100.12 | 98.98 | 99.36 |
| Si | 1.00 | 0.00 | 0.00 | 0.01 | 1.00 | 0.01 | 0.01 | 0.00 | 0.01 | 0.00 | 0.00 | 0.00 |
| Ti | 0.00 | 0.02 | 0.01 | 0.01 | 0.00 | 0.56 | 0.49 | 0.00 | 0.55 | 0.00 | 0.00 | 0.00 |
| Al | 0.00 | 0.55 | 0.56 | 0.54 | 0.00 | 1.32 | 1.38 | 0.01 | 1.32 | 0.01 | 0.00 | 0.00 |
| Cr | 0.00 | 1.28 | 1.30 | 1.31 | 0.01 | 0.00 | 0.00 | 0.00 | 0.00 | 0.00 | 0.00 | 0.00 |
| V | 0.00 | 0.00 | 0.00 | 0.00 | 0.00 | 0.09 | 0.11 | 0.00 | 0.10 | 0.00 | 0.00 | 0.00 |
| $Fe^{3+}$ | 0.00 | 0.12 | 0.11 | 0.11 | 0.00 | 0.49 | 0.48 | 0.08 | 0.49 | 0.09 | 0.12 | 0.12 |
| $Fe^{2+}$ | 0.11 | 0.49 | 0.48 | 0.49 | 0.10 | 0.00 | 0.00 | 0.00 | 0.00 | 0.00 | 0.00 | 0.00 |
| Mn | 0.00 | 0.00 | 0.00 | 0.00 | 0.00 | 0.51 | 0.52 | 1.89 | 0.51 | 1.89 | 1.87 | 1.86 |
| Mg | 1.88 | 0.52 | 0.52 | 0.51 | 1.88 | 0.00 | 0.00 | 0.01 | 0.00 | 0.01 | 0.01 | 0.01 |
| Ni | 0.01 | 0.00 | 0.00 | 0.00 | 0.01 | 0.00 | 0.00 | 0.00 | 0.00 | 0.00 | 0.00 | 0.00 |
| Zn | 0.00 | 0.00 | 0.01 | 0.01 | 0.00 | 0.00 | 0.00 | 0.00 | 0.00 | 0.00 | 0.00 | 0.00 |

Tab. A3.6 PO4A-GRID2 microprobe analyses of olivine and chromite crystals; d(mm) distance from the intergranular limit

| Analysis | GRID 1-1 | GRID 1-2 | GRID 1-3 | GRID 1-4 | GRID 1-5 | GRID 1-6 | GRID 1-7 | GRID 1-8 | GRID 1-9 | GRID 2-1 | GRID 2-2 | GRID 2-3 | GRID 2-4 | GRID 2-6 | GRID 2-7 | GRID 2-8 | GRID 2-9 | GRID 3-1 |
|---|---|---|---|---|---|---|---|---|---|---|---|---|---|---|---|---|---|---|
| | 249-OL | 250-OL | 251-CHR | 252-CHR | 253-OL | 254-OL | 255-OL | 256-OL | 257-CHR | 258-OL | 259-OL | 260-CHR | 261-CHR | 263-CHR | 264-CHR | 265-OL | 266-CHR | 267-CHR |
| X | 37.38 | 37.38 | 37.38 | 37.38 | 37.38 | 37.38 | 37.38 | 37.38 | 37.38 | 37.58 | 37.58 | 37.58 | 37.58 | 37.58 | 37.58 | 37.58 | 37.58 | 37.78 |
| Y | 79.97 | 80.17 | 80.37 | 80.57 | 80.77 | 80.97 | 81.17 | 81.37 | 81.57 | 79.97 | 80.17 | 80.37 | 80.57 | 80.97 | 81.17 | 81.37 | 81.57 | 79.97 |

| d (mm) | 0.206 | 0.023 | 0.120 | 0.063 | 0.103 | 0.031 | 0.029 | 0.103 | 0.069 | 0.074 | 0.017 | 0.137 | 0.109 | 0.006 | 0.109 | 0.069 | 0.002 | 0.103 |
|---|---|---|---|---|---|---|---|---|---|---|---|---|---|---|---|---|---|---|
| $SiO_2$ | 41.58 | 41.65 | 0.03 | 0.03 | 41.89 | 41.93 | 41.31 | 42.05 | 0.01 | 41.33 | 41.64 | 0.04 | 0.00 | 0.03 | 0.01 | 41.78 | 0.01 | 0.02 |
| $TiO_2$ | 0.02 | 0.00 | 0.48 | 0.52 | 0.00 | 0.03 | 0.00 | 0.01 | 0.57 | 0.00 | 0.02 | 0.57 | 0.59 | 0.61 | 0.66 | 0.00 | 0.64 | 0.60 |
| $Al_2O_3$ | 0.02 | 0.03 | 14.76 | 15.13 | 0.02 | 0.00 | 0.00 | 0.00 | 15.28 | 0.00 | 0.06 | 14.70 | 14.89 | 15.35 | 15.03 | 0.00 | 15.11 | 15.18 |
| $Cr_2O_3$ | 0.00 | 0.12 | 52.32 | 51.72 | 0.03 | 0.02 | 0.23 | 0.01 | 51.37 | 0.00 | 0.28 | 51.89 | 52.14 | 51.25 | 51.46 | 0.00 | 51.42 | 51.63 |
| $V_2O_3$ | 0.02 | 0.03 | 0.07 | 0.13 | 0.01 | 0.00 | 0.00 | 0.00 | 0.10 | 0.02 | 0.00 | 0.06 | 0.11 | 0.09 | 0.10 | 0.00 | 0.16 | 0.10 |
| $Fe_2O_3$ | 0.00 | 0.00 | 4.07 | 4.81 | 0.00 | 0.00 | 0.00 | 0.00 | 4.90 | 0.00 | 0.00 | 4.75 | 4.54 | 5.02 | 4.51 | 0.00 | 4.81 | 4.52 |
| FeO | 6.47 | 5.23 | 18.12 | 17.65 | 5.28 | 5.47 | 5.28 | 5.26 | 17.39 | 5.84 | 4.94 | 17.68 | 17.72 | 17.73 | 18.23 | 5.29 | 17.49 | 17.92 |
| MnO | 0.08 | 0.12 | 0.13 | 0.11 | 0.01 | 0.05 | 0.10 | 0.15 | 0.16 | 0.09 | 0.09 | 0.24 | 0.21 | 0.20 | 0.10 | 0.06 | 0.21 | 0.14 |
| MgO | 51.26 | 52.52 | 10.97 | 11.49 | 52.68 | 52.50 | 53.12 | 52.44 | 11.57 | 51.96 | 53.09 | 11.28 | 11.32 | 11.30 | 11.01 | 52.28 | 11.30 | 11.23 |
| NiO | 0.42 | 0.49 | 0.06 | 0.12 | 0.49 | 0.48 | 0.43 | 0.48 | 0.11 | 0.46 | 0.48 | 0.13 | 0.11 | 0.10 | 0.05 | 0.44 | 0.20 | 0.11 |
| ZnO | 0.06 | 0.00 | 0.07 | 0.00 | 0.07 | 0.02 | 0.15 | 0.00 | 0.06 | 0.12 | 0.00 | 0.00 | 0.08 | 0.34 | 0.19 | 0.00 | 0.39 | 0.13 |
| TOT | 99.93 | 100.21 | 101.09 | 101.72 | 100.50 | 100.53 | 100.64 | 100.42 | 101.55 | 99.83 | 100.62 | 101.33 | 101.72 | 102.05 | 101.36 | 99.86 | 101.74 | 101.58 |
| Si | 1.01 | 1.00 | 0.00 | 0.00 | 1.00 | 1.00 | 0.99 | 1.01 | 0.00 | 1.00 | 0.99 | 0.00 | 0.00 | 0.00 | 0.00 | 1.01 | 0.00 | 0.00 |
| Ti | 0.00 | 0.00 | 0.01 | 0.01 | 0.00 | 0.00 | 0.00 | 0.00 | 0.01 | 0.00 | 0.00 | 0.01 | 0.01 | 0.01 | 0.02 | 0.00 | 0.02 | 0.01 |
| Al | 0.00 | 0.00 | 0.56 | 0.56 | 0.00 | 0.00 | 0.00 | 0.00 | 0.57 | 0.00 | 0.00 | 0.55 | 0.56 | 0.57 | 0.56 | 0.00 | 0.56 | 0.57 |
| Cr | 0.00 | 0.00 | 1.32 | 1.29 | 0.00 | 0.00 | 0.00 | 0.00 | 1.28 | 0.00 | 0.01 | 1.30 | 1.31 | 1.28 | 1.29 | 0.00 | 1.29 | 1.29 |
| V | 0.00 | 0.00 | 0.00 | 0.00 | 0.00 | 0.00 | 0.00 | 0.00 | 0.00 | 0.00 | 0.00 | 0.00 | 0.00 | 0.00 | 0.00 | 0.00 | 0.00 | 0.00 |
| $Fe^{3+}$ | 0.00 | 0.00 | 0.10 | 0.11 | 0.00 | 0.00 | 0.02 | 0.00 | 0.12 | 0.00 | 0.00 | 0.11 | 0.11 | 0.12 | 0.11 | 0.00 | 0.11 | 0.11 |
| $Fe^{2+}$ | 0.13 | 0.10 | 0.48 | 0.47 | 0.11 | 0.11 | 0.08 | 0.11 | 0.46 | 0.12 | 0.10 | 0.47 | 0.47 | 0.47 | 0.49 | 0.11 | 0.46 | 0.47 |
| Mn | 0.00 | 0.00 | 0.00 | 0.00 | 0.00 | 0.00 | 0.00 | 0.00 | 0.00 | 0.00 | 0.00 | 0.01 | 0.01 | 0.01 | 0.00 | 0.00 | 0.01 | 0.00 |
| Mg | 1.85 | 1.88 | 0.52 | 0.54 | 1.88 | 1.87 | 1.89 | 1.87 | 0.55 | 1.87 | 1.89 | 0.53 | 0.53 | 0.53 | 0.52 | 1.88 | 0.53 | 0.53 |
| Ni | 0.01 | 0.01 | 0.00 | 0.00 | 0.01 | 0.01 | 0.01 | 0.01 | 0.00 | 0.01 | 0.01 | 0.00 | 0.00 | 0.00 | 0.00 | 0.01 | 0.01 | 0.00 |
| Zn | 0.00 | 0.00 | 0.00 | 0.00 | 0.00 | 0.00 | 0.00 | 0.00 | 0.00 | 0.00 | 0.00 | 0.00 | 0.00 | 0.01 | 0.00 | 0.00 | 0.01 | 0.00 |

| Analysis | GRID 3-2 268-OL | GRID 3-3 269-CHR | GRID 3-4 270-CHR | GRID 3-5 271-CHR | GRID 3-6 272-CHR | GRID 3-7 273-OL | GRID 3-8 274-OL | GRID 4-1 276-CHR | GRID 4-3 278-CHR | GRID 4-4 279-CHR | GRID 4-5 280-CHR | GRID 4-6 281-CHR | GRID 4-7 282-CHR | GRID 4-9 284-OL | GRID 5-1 285-OL | GRID 5-2 286-CHR | GRID 5-3 287-OL | GRID 5-4 288-OL |
|---|---|---|---|---|---|---|---|---|---|---|---|---|---|---|---|---|---|---|
| X | 37.78 | 37.78 | 37.78 | 37.78 | 37.78 | 37.78 | 37.78 | 37.98 | 37.98 | 37.98 | 37.98 | 37.98 | 37.98 | 37.98 | 38.18 | 38.18 | 38.18 | 38.18 |
| Y | 80.17 | 80.37 | 80.57 | 80.77 | 80.97 | 81.17 | 81.37 | 79.97 | 80.37 | 80.57 | 80.77 | 80.97 | 81.17 | 81.57 | 79.97 | 80.17 | 80.37 | 80.57 |
| d (mm) | 0.006 | 0.023 | | 0.126 | 0.046 | 0.011 | 0.057 | | 0.034 | 0.091 | 0.149 | 0.011 | 0.131 | 0.086 | 0.011 | 0.040 | 0.046 | 0.006 |
| $SiO_2$ | 42.91 | 0.04 | 1.92 | 0.00 | 0.06 | 41.37 | 41.52 | 0.19 | 0.04 | 0.01 | 0.01 | 0.14 | 0.05 | 42.34 | 42.35 | 0.03 | 42.03 | 41.57 |
| $TiO_2$ | 0.00 | 0.56 | 0.57 | 0.53 | 0.58 | 0.00 | 0.00 | 0.54 | 0.60 | 0.58 | 0.60 | 0.59 | 0.60 | 0.00 | 0.00 | 0.59 | 0.01 | 0.01 |
| $Al_2O_3$ | 0.03 | 14.72 | 14.02 | 15.24 | 15.08 | 0.03 | 0.03 | 16.99 | 15.24 | 15.03 | 14.85 | 13.42 | 14.89 | 0.01 | 0.03 | 15.94 | 0.01 | 0.22 |
| $Cr_2O_3$ | 0.49 | 51.95 | 48.54 | 51.37 | 51.52 | 0.30 | 0.03 | 49.46 | 51.21 | 51.50 | 52.16 | 52.12 | 51.39 | 0.00 | 0.61 | 50.86 | 0.09 | 1.35 |
| $V_2O_3$ | 0.03 | 0.13 | 0.11 | 0.13 | 0.11 | 0.06 | 0.03 | 0.14 | 0.07 | 0.09 | 0.10 | 0.12 | 0.12 | 0.00 | 0.00 | 0.10 | 0.01 | 0.01 |
| $Fe_2O_3$ | 0.00 | 4.80 | 3.15 | 4.73 | 4.78 | 0.00 | 0.00 | 4.54 | 4.78 | 4.87 | 4.01 | 5.25 | 4.81 | 0.00 | 0.00 | 4.12 | 0.00 | 0.00 |
| FeO | 4.78 | 17.86 | 17.45 | 17.49 | 17.77 | 5.13 | 5.58 | 17.14 | 17.68 | 17.20 | 17.72 | 18.13 | 17.66 | 5.56 | 4.80 | 17.27 | 4.88 | 3.89 |
| MnO | 0.10 | 0.21 | 0.18 | 0.08 | 0.14 | 0.09 | 0.06 | 0.15 | 0.16 | 0.21 | 0.16 | 0.15 | 0.13 | 0.08 | 0.09 | 0.15 | 0.10 | 0.02 |
| MgO | 51.85 | 11.16 | 12.40 | 11.43 | 11.30 | 52.58 | 52.45 | 11.88 | 11.42 | 11.49 | 11.29 | 10.86 | 11.39 | 52.34 | 52.24 | 11.59 | 52.72 | 53.35 |
| NiO | 0.45 | 0.11 | 0.12 | 0.14 | 0.13 | 0.46 | 0.48 | 0.24 | 0.09 | 0.14 | 0.05 | 0.16 | 0.11 | 0.45 | 0.52 | 0.08 | 0.46 | 0.46 |
| ZnO | 0.08 | 0.17 | 0.08 | 0.10 | 0.20 | 0.00 | 0.03 | 0.05 | 0.03 | 0.23 | 0.02 | 0.09 | 0.00 | 0.00 | 0.00 | 0.15 | 0.00 | 0.00 |
| TOT | 100.74 | 101.74 | 98.55 | 101.24 | 101.66 | 100.02 | 100.22 | 101.41 | 101.33 | 101.34 | 100.98 | 101.05 | 101.16 | 100.78 | 100.64 | 100.88 | 100.33 | 100.88 |
| Si | 1.03 | 0.00 | 0.06 | 0.00 | 0.00 | 0.99 | 1.00 | 0.01 | 0.00 | 0.00 | 0.00 | 0.00 | 0.00 | 1.01 | 1.01 | 0.00 | 1.01 | 0.99 |
| Ti | 0.00 | 0.01 | 0.01 | 0.01 | 0.01 | 0.00 | 0.00 | 0.01 | 0.01 | 0.01 | 0.01 | 0.01 | 0.01 | 0.00 | 0.00 | 0.01 | 0.00 | 0.00 |
| Al | 0.00 | 0.55 | 0.53 | 0.57 | 0.56 | 0.00 | 0.00 | 0.63 | 0.57 | 0.56 | 0.56 | 0.51 | 0.56 | 0.00 | 0.00 | 0.60 | 0.00 | 0.01 |
| Cr | 0.01 | 1.30 | 1.24 | 1.29 | 1.29 | 0.01 | 0.00 | 1.23 | 1.28 | 1.29 | 1.31 | 1.32 | 1.29 | 0.00 | 0.01 | 1.27 | 0.00 | 0.03 |
| V | 0.00 | 0.00 | 0.00 | 0.00 | 0.00 | 0.00 | 0.00 | 0.00 | 0.00 | 0.00 | 0.00 | 0.00 | 0.00 | 0.00 | 0.00 | 0.00 | 0.00 | 0.00 |
| $Fe^{3+}$ | 0.00 | 0.11 | 0.08 | 0.11 | 0.11 | 0.00 | 0.00 | 0.11 | 0.11 | 0.12 | 0.10 | 0.13 | 0.12 | 0.00 | 0.00 | 0.10 | 0.00 | 0.00 |
| $Fe^{2+}$ | 0.10 | 0.47 | 0.47 | 0.46 | 0.47 | 0.10 | 0.11 | 0.45 | 0.47 | 0.46 | 0.47 | 0.49 | 0.47 | 0.11 | 0.10 | 0.46 | 0.10 | 0.08 |
| Mn | 0.00 | 0.01 | 0.00 | 0.00 | 0.00 | 0.00 | 0.00 | 0.00 | 0.00 | 0.01 | 0.00 | 0.00 | 0.00 | 0.00 | 0.00 | 0.00 | 0.00 | 0.00 |

| | | | | | | | | | | | | | | | | | | |
|---|---|---|---|---|---|---|---|---|---|---|---|---|---|---|---|---|---|---|
| Mg | 1.85 | 0.53 | 0.60 | 0.54 | 0.53 | 1.88 | 1.88 | 0.55 | 0.54 | 0.54 | 0.54 | 0.52 | 0.54 | 1.87 | 1.87 | 0.55 | 1.88 | 1.89 |
| Ni | 0.01 | 0.00 | 0.00 | 0.00 | 0.00 | 0.01 | 0.01 | 0.01 | 0.00 | 0.00 | 0.00 | 0.00 | 0.00 | 0.01 | 0.01 | 0.00 | 0.01 | 0.01 |
| Zn | 0.00 | 0.00 | 0.00 | 0.00 | 0.00 | 0.00 | 0.00 | 0.00 | 0.00 | 0.01 | 0.00 | 0.00 | 0.00 | 0.00 | 0.00 | 0.00 | 0.00 | 0.00 |

| Analysis | GRID 5-5 289-CHR | GRID 5-6 290-CHR | GRID 5-7 291-CHR | GRID 5-8 292-OL | GRID 5-9 293-CHR | GRID 6-1 294-CHR | GRID 6-2 295-CHR | GRID 6-3 296-CHR | GRID 6-4 297-CHR | GRID 6-5 298-OL | GRID 6-6 299-CHR | GRID 6-7 300-CHR | GRID 6-8 301-OL | GRID 6-9 302-CHR | GRID 7-1 303-CHR | GRID 7-2 304-CHR | GRID 7-3 305-CHR | GRID 7-4 306-CHR |
|---|---|---|---|---|---|---|---|---|---|---|---|---|---|---|---|---|---|---|
| X | 38.18 | 38.18 | 38.18 | 38.18 | 38.18 | 38.38 | 38.38 | 38.38 | 38.38 | 38.38 | 38.38 | 38.38 | 38.38 | 38.38 | 38.58 | 38.58 | 38.58 | 38.58 |
| Y | 80.77 | 80.97 | 81.17 | 81.37 | 81.57 | 79.97 | 80.17 | 80.37 | 80.57 | 80.77 | 80.97 | 81.17 | 81.37 | 81.57 | 79.97 | 80.17 | 80.37 | 80.57 |
| d (mm) | 0.034 | 0.063 | 0.069 | 0.069 | 0.046 | 0.137 | 0.171 | 0.109 | 0.137 | 0.046 | 0.109 | 0.131 | 0.046 | 0.031 | 0.114 | 0.017 | 0.189 | 0.200 |
| $SiO_2$ | 0.04 | 0.02 | 0.02 | 41.74 | 0.04 | 0.00 | 0.02 | 0.00 | 0.00 | 41.63 | 0.02 | 0.02 | 41.74 | 0.02 | 0.02 | 0.00 | 0.02 | 0.01 |
| $TiO_2$ | 0.60 | 0.65 | 0.59 | 0.06 | 0.54 | 0.57 | 0.55 | 0.60 | 0.57 | 0.00 | 0.54 | 0.52 | 0.00 | 0.53 | 0.61 | 0.53 | 0.57 | 0.60 |
| $Al_2O_3$ | 15.47 | 14.79 | 14.60 | 0.01 | 15.20 | 14.57 | 15.24 | 15.17 | 15.24 | 0.00 | 15.08 | 15.12 | 0.00 | 14.43 | 14.97 | 15.08 | 15.02 | 15.32 |
| $Cr_2O_3$ | 51.58 | 51.85 | 52.24 | 0.02 | 51.42 | 52.26 | 51.64 | 51.64 | 51.99 | 0.09 | 52.26 | 52.19 | 0.00 | 52.19 | 51.72 | 51.41 | 51.97 | 51.42 |
| $V_2O_3$ | 0.15 | 0.16 | 0.14 | 0.02 | 0.14 | 0.13 | 0.12 | 0.09 | 0.11 | 0.01 | 0.13 | 0.11 | 0.00 | 0.18 | 0.15 | 0.11 | 0.14 | 0.15 |
| $Fe_2O_3$ | 4.76 | 4.47 | 4.68 | 0.00 | 4.57 | 4.61 | 4.81 | 4.61 | 4.43 | 0.00 | 4.60 | 4.14 | 0.00 | 4.80 | 4.70 | 5.10 | 4.04 | 4.20 |
| FeO | 17.61 | 17.73 | 18.12 | 5.29 | 17.81 | 17.85 | 17.28 | 17.65 | 17.34 | 5.04 | 17.90 | 17.48 | 5.18 | 17.82 | 17.65 | 17.50 | 17.83 | 17.61 |
| MnO | 0.23 | 0.05 | 0.12 | 0.07 | 0.14 | 0.22 | 0.23 | 0.19 | 0.14 | 0.06 | 0.16 | 0.15 | 0.06 | 0.16 | 0.15 | 0.17 | 0.19 | 0.11 |
| MgO | 11.48 | 11.39 | 11.05 | 52.40 | 11.19 | 11.18 | 11.56 | 11.28 | 11.51 | 52.35 | 11.33 | 11.41 | 52.57 | 11.21 | 11.34 | 11.30 | 11.17 | 11.41 |
| NiO | 0.19 | 0.05 | 0.13 | 0.41 | 0.20 | 0.10 | 0.03 | 0.07 | 0.16 | 0.48 | 0.11 | 0.05 | 0.49 | 0.10 | 0.14 | 0.10 | 0.07 | 0.03 |
| ZnO | 0.19 | 0.08 | 0.21 | 0.00 | 0.12 | 0.05 | 0.29 | 0.32 | 0.24 | 0.00 | 0.09 | 0.23 | 0.13 | 0.01 | 0.18 | 0.35 | 0.08 | 0.08 |
| TOT | 102.31 | 101.27 | 101.92 | 100.05 | 101.37 | 101.55 | 101.77 | 101.63 | 101.76 | 99.68 | 102.23 | 101.43 | 100.19 | 101.45 | 101.64 | 101.66 | 101.12 | 100.94 |
| Si | 0.00 | 0.00 | 0.00 | 1.00 | 0.00 | 0.00 | 0.00 | 0.00 | 0.00 | 1.00 | 0.00 | 0.00 | 1.00 | 0.00 | 0.00 | 0.00 | 0.00 | 0.00 |
| Ti | 0.01 | 0.02 | 0.01 | 0.00 | 0.01 | 0.01 | 0.01 | 0.01 | 0.01 | 0.00 | 0.01 | 0.01 | 0.00 | 0.01 | 0.01 | 0.01 | 0.01 | 0.01 |
| Al | 0.57 | 0.55 | 0.55 | 0.00 | 0.57 | 0.55 | 0.57 | 0.57 | 0.57 | 0.00 | 0.56 | 0.56 | 0.00 | 0.54 | 0.56 | 0.56 | 0.56 | 0.57 |
| Cr | 1.28 | 1.30 | 1.31 | 0.00 | 1.29 | 1.31 | 1.29 | 1.29 | 1.30 | 0.00 | 1.30 | 1.31 | 0.00 | 1.31 | 1.30 | 1.29 | 1.31 | 1.29 |
| V | 0.00 | 0.00 | 0.00 | 0.00 | 0.00 | 0.00 | 0.00 | 0.00 | 0.00 | 0.00 | 0.00 | 0.00 | 0.00 | 0.00 | 0.00 | 0.00 | 0.00 | 0.00 |
| $Fe^{3+}$ | 0.11 | 0.11 | 0.11 | 0.00 | 0.11 | 0.11 | 0.11 | 0.11 | 0.11 | 0.00 | 0.11 | 0.10 | 0.00 | 0.11 | 0.11 | 0.12 | 0.10 | 0.10 |
| $Fe^{2+}$ | 0.46 | 0.47 | 0.48 | 0.11 | 0.47 | 0.47 | 0.46 | 0.47 | 0.46 | 0.10 | 0.47 | 0.46 | 0.10 | 0.47 | 0.47 | 0.46 | 0.47 | 0.47 |
| Mn | 0.01 | 0.00 | 0.00 | 0.00 | 0.00 | 0.01 | 0.01 | 0.01 | 0.00 | 0.00 | 0.00 | 0.00 | 0.00 | 0.00 | 0.00 | 0.00 | 0.01 | 0.00 |
| Mg | 0.54 | 0.54 | 0.52 | 1.88 | 0.53 | 0.53 | 0.54 | 0.53 | 0.54 | 1.88 | 0.53 | 0.54 | 1.88 | 0.53 | 0.54 | 0.53 | 0.53 | 0.54 |
| Ni | 0.00 | 0.00 | 0.00 | 0.01 | 0.01 | 0.00 | 0.00 | 0.00 | 0.00 | 0.01 | 0.00 | 0.00 | 0.01 | 0.00 | 0.00 | 0.00 | 0.00 | 0.00 |
| Zn | 0.00 | 0.00 | 0.00 | 0.00 | 0.00 | 0.00 | 0.01 | 0.01 | 0.01 | 0.00 | 0.00 | 0.01 | 0.00 | 0.00 | 0.00 | 0.01 | 0.00 | 0.00 |

| Analysis | GRID 7-5 307-CHR | GRID 7-6 308-CHR | GRID 7-7 309-CHR | GRID 7-8 310-OL | GRID 7-9 311-CHR | GRID 8-2 313-OL | GRID 8-3 314-CHR | GRID 8-4 315-CHR | GRID 8-5 316-CHR | GRID 8-6 317-CHR | GRID 8-7 318-CHR | GRID 8-8 319-CHR | GRID 8-9 320-CHR | GRID 9-1 321-OL | GRID 9-2 322-OL | GRID 9-3 323-OL | GRID 9-4 324-CHR | GRID 9-5 325-CHR |
|---|---|---|---|---|---|---|---|---|---|---|---|---|---|---|---|---|---|---|
| X | 38.58 | 38.58 | 38.58 | 38.58 | 38.58 | 38.78 | 38.78 | 38.78 | 38.78 | 38.78 | 38.78 | 38.78 | 38.78 | 38.98 | 38.98 | 38.98 | 38.98 | 38.98 |
| Y | 80.77 | 80.97 | 81.17 | 81.37 | 81.57 | 80.17 | 80.37 | 80.57 | 80.77 | 80.97 | 81.17 | 81.37 | 81.57 | 79.97 | 80.17 | 80.37 | 80.57 | 80.77 |
| d (mm) | 0.047 | 0.005 | 0.126 | 0.034 | 0.051 | 0.074 | 0.008 | 0.103 | 0.137 | 0.126 | 0.034 | 0.089 | 0.002 | 0.120 | 0.149 | 0.011 | 0.046 | 0.006 |
| $SiO_2$ | 0.00 | 0.03 | 0.00 | 41.84 | 0.00 | 40.70 | 0.12 | 0.03 | 0.02 | 0.04 | 0.06 | 0.01 | 0.04 | 41.07 | 41.73 | 41.15 | 0.00 | 0.09 |
| $TiO_2$ | 0.57 | 0.56 | 0.52 | 0.00 | 0.49 | 0.01 | 0.48 | 0.64 | 0.49 | 0.62 | 0.54 | 0.66 | 0.50 | 0.02 | 0.00 | 0.03 | 0.55 | 0.61 |
| $Al_2O_3$ | 14.69 | 14.29 | 15.21 | 0.00 | 15.19 | 0.00 | 14.51 | 15.06 | 13.91 | 14.82 | 14.48 | 14.94 | 14.12 | 0.00 | 0.03 | 0.04 | 14.85 | 13.78 |
| $Cr_2O_3$ | 52.23 | 52.56 | 51.94 | 0.04 | 51.60 | 0.03 | 51.66 | 51.92 | 53.92 | 51.87 | 52.38 | 52.17 | 52.78 | 0.02 | 0.00 | 0.48 | 51.74 | 53.13 |
| $V_2O_3$ | 0.09 | 0.09 | 0.12 | 0.03 | 0.15 | 0.00 | 0.14 | 0.07 | 0.16 | 0.10 | 0.06 | 0.12 | 0.08 | 0.00 | 0.00 | 0.00 | 0.09 | 0.12 |
| $Fe_2O_3$ | 4.76 | 4.34 | 4.29 | 0.00 | 4.84 | 0.00 | 4.84 | 4.60 | 4.25 | 4.42 | 4.93 | 4.31 | 4.71 | 0.00 | 0.00 | 0.00 | 4.77 | 4.24 |
| FeO | 17.80 | 17.79 | 17.56 | 5.08 | 17.42 | 5.60 | 17.63 | 17.77 | 18.03 | 17.91 | 18.09 | 17.72 | 18.07 | 5.75 | 5.69 | 4.20 | 17.46 | 18.27 |
| MnO | 0.09 | 0.05 | 0.18 | 0.08 | 0.20 | 0.04 | 0.15 | 0.12 | 0.04 | 0.16 | 0.15 | 0.10 | 0.14 | 0.10 | 0.08 | 0.04 | 0.20 | 0.13 |
| MgO | 11.27 | 11.07 | 11.34 | 52.78 | 11.37 | 54.78 | 11.19 | 11.40 | 11.13 | 11.26 | 11.17 | 11.44 | 10.96 | 52.37 | 52.24 | 52.79 | 11.29 | 11.00 |
| NiO | 0.11 | 0.17 | 0.09 | 0.56 | 0.14 | 0.44 | 0.21 | 0.09 | 0.05 | 0.04 | 0.00 | 0.09 | 0.07 | 0.42 | 0.48 | 0.50 | 0.13 | 0.08 |
| ZnO | 0.14 | 0.28 | 0.17 | 0.06 | 0.23 | 0.00 | 0.09 | 0.20 | 0.25 | 0.02 | 0.19 | 0.09 | 0.26 | 0.00 | 0.16 | 0.05 | 0.20 | 0.00 |
| TOT | 101.79 | 101.24 | 101.42 | 100.47 | 101.63 | 101.61 | 101.03 | 101.91 | 102.27 | 101.26 | 102.04 | 101.66 | 101.72 | 99.76 | 100.43 | 99.31 | 101.29 | 101.45 |

| | | | | | | | | | | | | | | | | | | |
|---|---|---|---|---|---|---|---|---|---|---|---|---|---|---|---|---|---|---|
| Si | 0.00 | 0.00 | 0.00 | 1.00 | 0.00 | 0.96 | 0.00 | 0.00 | 0.00 | 0.00 | 0.00 | 0.00 | 0.00 | 0.99 | 1.00 | 0.99 | 0.00 | 0.00 |
| Ti | 0.01 | 0.01 | 0.01 | 0.00 | 0.01 | 0.00 | 0.01 | 0.02 | 0.01 | 0.01 | 0.01 | 0.02 | 0.01 | 0.00 | 0.00 | 0.00 | 0.01 | 0.01 |
| Al | 0.55 | 0.54 | 0.57 | 0.00 | 0.57 | 0.00 | 0.55 | 0.56 | 0.52 | 0.56 | 0.54 | 0.56 | 0.53 | 0.00 | 0.00 | 0.00 | 0.56 | 0.52 |
| Cr | 1.31 | 1.33 | 1.30 | 0.00 | 1.29 | 0.00 | 1.30 | 1.30 | 1.35 | 1.30 | 1.31 | 1.31 | 1.33 | 0.00 | 0.00 | 0.01 | 1.30 | 1.34 |
| V | 0.00 | 0.00 | 0.00 | 0.00 | 0.00 | 0.00 | 0.00 | 0.00 | 0.00 | 0.00 | 0.00 | 0.00 | 0.00 | 0.00 | 0.00 | 0.00 | 0.00 | 0.00 |
| $Fe^{3+}$ | 0.11 | 0.10 | 0.10 | 0.00 | 0.12 | 0.00 | 0.12 | 0.11 | 0.10 | 0.11 | 0.12 | 0.10 | 0.11 | 0.00 | 0.00 | 0.00 | 0.11 | 0.10 |
| $Fe^{2+}$ | 0.47 | 0.48 | 0.47 | 0.10 | 0.46 | 0.11 | 0.47 | 0.47 | 0.48 | 0.48 | 0.48 | 0.47 | 0.48 | 0.12 | 0.11 | 0.09 | 0.46 | 0.49 |
| Mn | 0.00 | 0.00 | 0.00 | 0.00 | 0.01 | 0.00 | 0.00 | 0.00 | 0.00 | 0.00 | 0.00 | 0.00 | 0.00 | 0.00 | 0.00 | 0.00 | 0.01 | 0.00 |
| Mg | 0.53 | 0.53 | 0.54 | 1.88 | 0.54 | 1.92 | 0.53 | 0.54 | 0.53 | 0.53 | 0.53 | 0.54 | 0.52 | 1.88 | 1.87 | 1.90 | 0.54 | 0.52 |
| Ni | 0.00 | 0.00 | 0.00 | 0.01 | 0.00 | 0.01 | 0.01 | 0.00 | 0.00 | 0.00 | 0.00 | 0.00 | 0.00 | 0.01 | 0.01 | 0.01 | 0.00 | 0.00 |
| Zn | 0.00 | 0.01 | 0.00 | 0.00 | 0.01 | 0.00 | 0.00 | 0.00 | 0.01 | 0.00 | 0.00 | 0.00 | 0.01 | 0.00 | 0.00 | 0.00 | 0.00 | 0.00 |

| Analysis | GRID 9-6 | GRID 9-7 | GRID 9-8 | GRID 9-9 | PO4A-6 | PO4A-7 | PO4A-12 | d-CHR | PO4A-13 | PO4A-14 | PO4A-15 |
|---|---|---|---|---|---|---|---|---|---|---|---|
| | 326-CHR | 327-OL | 328-CHR | 329-CHR | CHR-rim | OL-rim | 52-CHR | | 53-OL | 54-OL | 55-OL |
| X | 38.98 | 38.98 | 38.98 | 38.98 | 38.24 | 38.26 | 38.41 | 38.42 | 38.43 | 38.49 | 38.63 |
| Y | 80.97 | 81.17 | 81.37 | 81.57 | 80.76 | 80.80 | 81.27 | 81.26 | 81.26 | 81.18 | 81.10 |
| d (mm) | 0.040 | 0.017 | 0.091 | 0.080 | 0.011 | 0.006 | 0.011 | | 0.012 | 0.107 | 0.261 |
| $SiO_2$ | 0.09 | 41.68 | 0.02 | 0.04 | 0.13 | 41.46 | 0.02 | | 41.23 | 41.02 | 40.76 |
| $TiO_2$ | 0.53 | 0.00 | 0.55 | 0.54 | 0.57 | 0.01 | 0.61 | | 0.00 | 0.03 | 0.06 |
| $Al_2O_3$ | 14.47 | 0.05 | 15.12 | 15.01 | 15.74 | 0.01 | 14.80 | | 0.01 | 0.03 | 0.00 |
| $Cr_2O_3$ | 52.91 | 0.44 | 51.69 | 51.98 | 50.86 | 0.45 | 52.08 | | 0.27 | 0.02 | 0.01 |
| $V_2O_3$ | 0.14 | 0.00 | 0.08 | 0.13 | 0.16 | 0.00 | 0.08 | | 0.01 | 0.01 | 0.00 |
| $Fe_2O_3$ | 4.26 | 0.00 | 4.53 | 4.43 | 4.47 | 0.00 | 4.37 | | 0.00 | 0.00 | 0.00 |
| FeO | 18.09 | 4.49 | 17.57 | 17.51 | 17.80 | 4.85 | 18.42 | | 4.76 | 5.71 | 5.94 |
| MnO | 0.13 | 0.11 | 0.19 | 0.18 | 0.19 | 0.08 | 0.17 | | 0.02 | 0.03 | 0.03 |
| MgO | 11.19 | 53.33 | 11.33 | 11.50 | 11.35 | 52.69 | 10.83 | | 51.96 | 51.18 | 51.29 |
| NiO | 0.10 | 0.46 | 0.07 | 0.07 | 0.08 | 0.51 | 0.10 | | 0.52 | 0.48 | 0.53 |
| ZnO | 0.10 | 0.08 | 0.17 | 0.02 | 0.24 | 0.00 | 0.17 | | 0.00 | 0.00 | 0.03 |
| TOT | 102.02 | 100.65 | 101.33 | 101.43 | 101.61 | 100.07 | 101.68 | | 98.79 | 98.54 | 98.66 |
| Si | 0.00 | 0.99 | 0.00 | 0.00 | 0.00 | 1.00 | 0.01 | | 0.00 | 0.00 | 0.00 |
| Ti | 0.01 | 0.00 | 0.01 | 0.01 | 0.01 | 0.00 | 0.55 | | 0.00 | 0.00 | 0.00 |
| Al | 0.54 | 0.00 | 0.57 | 0.56 | 0.59 | 0.00 | 1.31 | | 0.01 | 0.00 | 0.00 |
| Cr | 1.32 | 0.01 | 1.30 | 1.30 | 1.27 | 0.01 | 0.00 | | 0.00 | 0.00 | 0.00 |
| V | 0.00 | 0.00 | 0.00 | 0.00 | 0.00 | 0.00 | 0.10 | | 0.00 | 0.00 | 0.00 |
| $Fe^{3+}$ | 0.10 | 0.00 | 0.11 | 0.11 | 0.11 | 0.00 | 0.49 | | 0.10 | 0.12 | 0.12 |
| $Fe^{2+}$ | 0.48 | 0.09 | 0.47 | 0.46 | 0.47 | 0.10 | 0.00 | | 0.00 | 0.00 | 0.00 |
| Mn | 0.00 | 0.00 | 0.00 | 0.00 | 0.01 | 0.00 | 0.51 | | 1.88 | 1.87 | 1.87 |
| Mg | 0.53 | 1.89 | 0.54 | 0.54 | 0.53 | 1.89 | 0.00 | | 0.01 | 0.01 | 0.01 |
| Ni | 0.00 | 0.01 | 0.00 | 0.00 | 0.00 | 0.01 | 0.00 | | 0.00 | 0.00 | 0.00 |
| Zn | 0.00 | 0.00 | 0.00 | 0.00 | 0.01 | 0.00 | 0.00 | | 0.00 | 0.00 | 0.00 |

Tab. A3.7 PO4A-GRID3 microprobe analyses of olivine and chromite crystals; d(mm) distance from the intergranular limit

| Analysis | GRID 1-1 | GRID 1-2 | GRID 1-3 | GRID 1-4 | GRID 1-5 | GRID 1-7 | GRID 2-1 | GRID 2-2 | GRID 2-4 | GRID 2-5 | GRID 2-6 | GRID 2-7 | GRID 3-1 | GRID 3-2 | GRID 3-3 | GRID 3-5 | GRID 3-6 | GRID 3-7 |
|---|---|---|---|---|---|---|---|---|---|---|---|---|---|---|---|---|---|---|
| | 332-OL | 333-OL | 334-OL | 335-OL | 336-OL | 338-OL | 339-OL | 340-OL | 342-OL | 343-OL | 344-OL | 345-OL | 346-OL | 347-OL | 348-OL | 350-OL | 351-OL | 352-OL |
| X | 34.12 | 34.12 | 34.12 | 34.12 | 34.12 | 34.12 | 34.22 | 34.22 | 34.22 | 34.22 | 34.22 | 34.22 | 34.32 | 34.32 | 34.32 | 34.32 | 34.32 | 34.32 |
| Y | 65.74 | 65.84 | 65.94 | 66.04 | 66.14 | 66.34 | 65.74 | 65.84 | 66.04 | 66.14 | 66.24 | 66.34 | 65.74 | 65.84 | 65.94 | 66.14 | 66.24 | 66.34 |
| **d (mm)** | **0.154** | **0.077** | **0.087** | **0.128** | **0.241** | **0.333** | **0.128** | **0.026** | **0.092** | **0.123** | **0.162** | **0.279** | **0.149** | **0.067** | **0.041** | **0.049** | **0.138** | **0.236** |
| $SiO_2$ | 41.22 | 41.34 | 41.55 | 41.14 | 41.34 | 41.53 | 41.26 | 41.07 | 40.99 | 40.89 | 41.09 | 41.22 | 41.49 | 41.25 | 41.45 | 41.35 | 41.57 | 41.36 |
| $TiO_2$ | 0.00 | 0.02 | 0.02 | 0.02 | 0.02 | 0.08 | 0.02 | 0.02 | 0.00 | 0.02 | 0.00 | 0.03 | 0.06 | 0.00 | 0.02 | 0.00 | 0.01 | 0.00 |

| | | | | | | | | | | | | | | | | | | |
|---|---|---|---|---|---|---|---|---|---|---|---|---|---|---|---|---|---|---|
| $Al_2O_3$ | 0.03 | 0.00 | 0.00 | 0.00 | 0.00 | 0.00 | 0.00 | 0.00 | 0.00 | 0.00 | 0.01 | 0.02 | 0.00 | 0.00 | 0.01 | 0.01 | 0.02 | 0.01 |
| $Cr_2O_3$ | 0.06 | 0.01 | 0.05 | 0.00 | 0.03 | 0.00 | 0.00 | 0.06 | 0.00 | 0.00 | 0.00 | 0.05 | 0.05 | 0.06 | 0.03 | 0.02 | 0.00 | 0.00 |
| $V_2O_3$ | 0.02 | 0.00 | 0.03 | 0.00 | 0.00 | 0.00 | 0.03 | 0.00 | 0.00 | 0.04 | 0.03 | 0.02 | 0.01 | 0.02 | 0.00 | 0.04 | 0.01 | 0.00 |
| $Fe_2O_3$ | 0.00 | 0.00 | 0.00 | 0.00 | 0.00 | 0.00 | 0.00 | 0.00 | 0.00 | 0.00 | 0.00 | 0.00 | 0.00 | 0.00 | 0.00 | 0.00 | 0.00 | 0.00 |
| FeO | 7.39 | 7.21 | 7.35 | 7.24 | 7.14 | 7.36 | 7.60 | 7.02 | 7.12 | 7.30 | 7.30 | 7.26 | 7.32 | 7.33 | 7.24 | 7.21 | 7.22 | 7.41 |
| MnO | 0.14 | 0.05 | 0.13 | 0.09 | 0.16 | 0.11 | 0.14 | 0.21 | 0.10 | 0.07 | 0.12 | 0.09 | 0.16 | 0.11 | 0.14 | 0.16 | 0.13 | 0.17 |
| MgO | 50.99 | 51.13 | 50.46 | 50.55 | 51.04 | 50.65 | 50.63 | 51.60 | 50.88 | 50.95 | 51.06 | 50.73 | 51.02 | 51.33 | 51.77 | 51.47 | 50.61 | 51.07 |
| NiO | 0.54 | 0.44 | 0.52 | 0.50 | 0.45 | 0.41 | 0.47 | 0.49 | 0.44 | 0.49 | 0.39 | 0.40 | 0.42 | 0.43 | 0.41 | 0.52 | 0.48 | 0.45 |
| ZnO | 0.00 | 0.09 | 0.04 | 0.00 | 0.01 | 0.00 | 0.00 | 0.07 | 0.23 | 0.04 | 0.00 | 0.00 | 0.10 | 0.00 | 0.16 | 0.01 | 0.00 | 0.04 |
| TOT | 100.40 | 100.31 | 100.16 | 99.55 | 100.19 | 100.15 | 100.17 | 100.54 | 99.77 | 99.83 | 100.03 | 99.83 | 100.64 | 100.56 | 101.22 | 100.79 | 100.06 | 100.51 |
| Si | 1.00 | 1.00 | 1.01 | 1.00 | 1.00 | 1.01 | 1.00 | 0.99 | 1.00 | 0.99 | 1.00 | 1.00 | 1.00 | 0.99 | 0.99 | 0.99 | 1.01 | 1.00 |
| Ti | 0.00 | 0.00 | 0.00 | 0.00 | 0.00 | 0.00 | 0.00 | 0.00 | 0.00 | 0.00 | 0.00 | 0.00 | 0.00 | 0.00 | 0.00 | 0.00 | 0.00 | 0.00 |
| Al | 0.00 | 0.00 | 0.00 | 0.00 | 0.00 | 0.00 | 0.00 | 0.00 | 0.00 | 0.00 | 0.00 | 0.00 | 0.00 | 0.00 | 0.00 | 0.00 | 0.00 | 0.00 |
| Cr | 0.00 | 0.00 | 0.00 | 0.00 | 0.00 | 0.00 | 0.00 | 0.00 | 0.00 | 0.00 | 0.00 | 0.00 | 0.00 | 0.00 | 0.00 | 0.00 | 0.00 | 0.00 |
| V | 0.00 | 0.00 | 0.00 | 0.00 | 0.00 | 0.00 | 0.00 | 0.00 | 0.00 | 0.00 | 0.00 | 0.00 | 0.00 | 0.00 | 0.00 | 0.00 | 0.00 | 0.00 |
| $Fe^{3+}$ | 0.00 | 0.00 | 0.00 | 0.00 | 0.00 | 0.00 | 0.00 | 0.00 | 0.00 | 0.00 | 0.00 | 0.00 | 0.00 | 0.00 | 0.00 | 0.00 | 0.00 | 0.00 |
| $Fe^{2+}$ | 0.15 | 0.15 | 0.15 | 0.15 | 0.14 | 0.15 | 0.15 | 0.14 | 0.15 | 0.15 | 0.15 | 0.15 | 0.15 | 0.15 | 0.15 | 0.15 | 0.15 | 0.15 |
| Mn | 0.00 | 0.00 | 0.00 | 0.00 | 0.00 | 0.00 | 0.00 | 0.00 | 0.00 | 0.00 | 0.00 | 0.00 | 0.00 | 0.00 | 0.00 | 0.00 | 0.00 | 0.00 |
| Mg | 1.84 | 1.84 | 1.83 | 1.84 | 1.84 | 1.83 | 1.83 | 1.85 | 1.84 | 1.84 | 1.84 | 1.84 | 1.84 | 1.84 | 1.85 | 1.85 | 1.83 | 1.84 |
| Ni | 0.01 | 0.01 | 0.01 | 0.01 | 0.01 | 0.01 | 0.01 | 0.01 | 0.01 | 0.01 | 0.01 | 0.01 | 0.01 | 0.01 | 0.01 | 0.01 | 0.01 | 0.01 |
| Zn | 0.00 | 0.00 | 0.00 | 0.00 | 0.00 | 0.00 | 0.00 | 0.00 | 0.00 | 0.00 | 0.00 | 0.00 | 0.00 | 0.00 | 0.00 | 0.00 | 0.00 | 0.00 |

| Analysis | GRID 4-1 | GRID 4-2 | GRID 4-4 | GRID 4-5 | GRID 4-6 | GRID 4-7 | GRID 5-1 | GRID 5-2 | GRID 5-3 | GRID 5-4 | GRID 5-5 | GRID 5-6 | GRID 5-7 | GRID 6-1 | GRID 6-2 | GRID 6-3 | GRID 6-4 | GRID 6-5 |
|---|---|---|---|---|---|---|---|---|---|---|---|---|---|---|---|---|---|---|
| | 353-OL | 354-OL | 356-CHR | 357-OL | 358-OL | 359-OL | 360-OL | 361-OL | 362-OL | 363-OL | 364-OL | 365-OL | 366-OL | 367-OL | 368-OL | 369-CHR | 370-OL | 371-OL |
| X | 34.42 | 34.42 | 34.42 | 34.42 | 34.42 | 34.42 | 34.52 | 34.52 | 34.52 | 34.52 | 34.52 | 34.52 | 34.52 | 34.62 | 34.62 | 34.62 | 34.62 | 34.62 |
| Y | 65.74 | 65.84 | 66.04 | 66.14 | 66.24 | 66.34 | 65.74 | 65.84 | 65.94 | 66.04 | 66.14 | 66.24 | 66.34 | 65.74 | 65.84 | 65.94 | 66.04 | 66.14 |
| **d (mm)** | **0.190** | **0.087** | **0.056** | **0.021** | **0.128** | **0.231** | **0.190** | **0.121** | **0.046** | **0.008** | **0.056** | **0.138** | **0.231** | **0.123** | **0.046** | **0.003** | **0.031** | **0.113** |
| $SiO_2$ | 41.34 | 41.40 | 0.03 | 41.21 | 41.18 | 41.16 | 41.27 | 41.26 | 41.28 | 41.32 | 41.39 | 41.31 | 41.40 | 41.53 | 41.41 | 0.19 | 41.36 | 41.55 |
| $TiO_2$ | 0.00 | 0.00 | 0.54 | 0.05 | 0.00 | 0.01 | 0.06 | 0.00 | 0.00 | 0.07 | 0.02 | 0.04 | 0.00 | 0.00 | 0.02 | 0.54 | 0.00 | 0.10 |
| $Al_2O_3$ | 0.00 | 0.00 | 14.73 | 0.01 | 0.00 | 0.01 | 0.02 | 0.00 | 0.00 | 0.02 | 0.00 | 0.01 | 0.00 | 0.00 | 0.01 | 14.18 | 0.04 | 0.00 |
| $Cr_2O_3$ | 0.00 | 0.05 | 51.22 | 0.34 | 0.03 | 0.00 | 0.00 | 0.00 | 0.03 | 0.36 | 0.15 | 0.02 | 0.04 | 0.00 | 0.08 | 50.65 | 0.21 | 0.00 |
| $V_2O_3$ | 0.00 | 0.00 | 0.06 | 0.00 | 0.01 | 0.00 | 0.01 | 0.04 | 0.04 | 0.03 | 0.02 | 0.01 | 0.00 | 0.00 | 0.00 | 0.07 | 0.00 | 0.01 |
| $Fe_2O_3$ | 0.00 | 0.00 | 4.50 | 0.00 | 0.00 | 0.00 | 0.00 | 0.00 | 0.00 | 0.00 | 0.00 | 0.00 | 0.00 | 0.00 | 0.00 | 5.28 | 0.00 | 0.00 |
| FeO | 7.13 | 7.20 | 20.97 | 6.04 | 7.30 | 8.04 | 7.07 | 7.35 | 6.80 | 6.07 | 6.69 | 7.15 | 7.27 | 6.93 | 6.88 | 20.99 | 6.61 | 7.22 |
| MnO | 0.11 | 0.08 | 0.23 | 0.12 | 0.11 | 0.17 | 0.16 | 0.15 | 0.10 | 0.07 | 0.14 | 0.07 | 0.13 | 0.09 | 0.08 | 0.18 | 0.10 | 0.09 |
| MgO | 51.19 | 50.91 | 9.13 | 52.30 | 50.23 | 49.88 | 51.50 | 50.82 | 50.78 | 52.12 | 51.84 | 51.17 | 50.74 | 50.73 | 51.14 | 9.14 | 51.28 | 50.71 |
| NiO | 0.48 | 0.41 | 0.13 | 0.55 | 0.49 | 0.38 | 0.49 | 0.39 | 0.48 | 0.44 | 0.46 | 0.42 | 0.45 | 0.47 | 0.49 | 0.04 | 0.41 | 0.48 |
| ZnO | 0.00 | 0.17 | 0.10 | 0.18 | 0.06 | 0.00 | 0.02 | 0.00 | 0.00 | 0.00 | 0.02 | 0.12 | 0.00 | 0.00 | 0.03 | 0.26 | 0.05 | 0.00 |
| TOT | 100.27 | 100.23 | 101.65 | 100.81 | 99.44 | 99.67 | 100.63 | 100.00 | 99.51 | 100.54 | 100.74 | 100.32 | 100.04 | 99.78 | 100.17 | 101.54 | 100.06 | 100.16 |
| Si | 1.00 | 1.00 | 0.00 | 0.99 | 1.01 | 1.01 | 0.99 | 1.00 | 1.01 | 0.99 | 0.99 | 1.00 | 1.00 | 1.01 | 1.00 | 0.01 | 1.00 | 1.01 |
| Ti | 0.00 | 0.00 | 0.01 | 0.00 | 0.00 | 0.00 | 0.00 | 0.00 | 0.00 | 0.00 | 0.00 | 0.00 | 0.00 | 0.00 | 0.00 | 0.01 | 0.00 | 0.00 |
| Al | 0.00 | 0.00 | 0.56 | 0.00 | 0.00 | 0.00 | 0.00 | 0.00 | 0.00 | 0.00 | 0.00 | 0.00 | 0.00 | 0.00 | 0.00 | 0.54 | 0.00 | 0.00 |
| Cr | 0.00 | 0.00 | 1.30 | 0.01 | 0.00 | 0.00 | 0.00 | 0.00 | 0.00 | 0.01 | 0.00 | 0.00 | 0.00 | 0.00 | 0.00 | 1.29 | 0.00 | 0.00 |
| V | 0.00 | 0.00 | 0.00 | 0.00 | 0.00 | 0.00 | 0.00 | 0.00 | 0.00 | 0.00 | 0.00 | 0.00 | 0.00 | 0.00 | 0.00 | 0.00 | 0.00 | 0.00 |
| $Fe^{3+}$ | 0.00 | 0.00 | 0.11 | 0.00 | 0.00 | 0.00 | 0.00 | 0.00 | 0.00 | 0.00 | 0.00 | 0.00 | 0.00 | 0.00 | 0.00 | 0.13 | 0.00 | 0.00 |
| $Fe^{2+}$ | 0.14 | 0.15 | 0.56 | 0.12 | 0.15 | 0.16 | 0.14 | 0.15 | 0.14 | 0.12 | 0.13 | 0.15 | 0.15 | 0.14 | 0.14 | 0.57 | 0.13 | 0.15 |
| Mn | 0.00 | 0.00 | 0.01 | 0.00 | 0.00 | 0.00 | 0.00 | 0.00 | 0.00 | 0.00 | 0.00 | 0.00 | 0.00 | 0.00 | 0.00 | 0.01 | 0.00 | 0.00 |
| Mg | 1.84 | 1.84 | 0.44 | 1.87 | 1.83 | 1.82 | 1.85 | 1.84 | 1.84 | 1.87 | 1.86 | 1.84 | 1.84 | 1.84 | 1.84 | 0.44 | 1.85 | 1.83 |
| Ni | 0.01 | 0.01 | 0.00 | 0.01 | 0.01 | 0.01 | 0.01 | 0.01 | 0.01 | 0.01 | 0.01 | 0.01 | 0.01 | 0.01 | 0.01 | 0.00 | 0.01 | 0.01 |
| Zn | 0.00 | 0.00 | 0.00 | 0.00 | 0.00 | 0.00 | 0.00 | 0.00 | 0.00 | 0.00 | 0.00 | 0.00 | 0.00 | 0.00 | 0.00 | 0.01 | 0.00 | 0.00 |

| Analysis | GRID 6-6 | GRID 6-7 | GRID 7-1 | GRID 7-2 | GRID 7-3 | GRID 7-4 | GRID 7-5 | GRID 7-6 | GRID 7-7 | PO4A-8 | PO4A-9 | PO4A-10 | PO4A-11 | PO4A-12 | PO4A-16 | PO4A-17 | PO4A-18 | PO4A-19 |
|---|---|---|---|---|---|---|---|---|---|---|---|---|---|---|---|---|---|---|
| | 372-OL | 373-OL | 374-OL | 375-CHR | 376-CHR | 377-CHR | 378-OL | 379-OL | 380-OL | OL-rim | CHR-rim | CHR-core | CHR-rim | OL-rim | 56-CHR | 57-CHR | 58-CHR | 59-CHR |
| X | 34.62 | 34.62 | 34.72 | 34.72 | 34.72 | 34.72 | 34.72 | 34.72 | 34.72 | 34.46 | 34.45 | 34.41 | 34.35 | 34.32 | 34.45 | 34.44 | 34.42 | 34.40 |
| Y | 66.24 | 66.34 | 65.74 | 65.84 | 65.94 | 66.04 | 66.14 | 66.24 | 66.34 | 65.94 | 65.97 | 66.04 | 66.09 | 66.12 | 66.89 | 66.87 | 66.86 | 66.84 |
| **d (mm)** | **0.210** | **0.308** | **0.077** | **0.010** | **0.092** | **0.005** | **0.097** | **0.200** | **0.303** | **0.005** | **0.082** | **0.018** | **0.005** | **0.026** | **0.096** | **0.070** | **0.048** | **0.023** |
| $SiO_2$ | 41.11 | 41.17 | 41.03 | 0.14 | 0.02 | 0.13 | 39.64 | 39.97 | 41.12 | 41.43 | 0.07 | 0.02 | 0.14 | 41.61 | 0.01 | 0.00 | 0.03 | 0.02 |
| $TiO_2$ | 0.01 | 0.02 | 0.01 | 0.46 | 0.55 | 0.61 | 0.00 | 0.00 | 0.05 | 0.04 | 0.56 | 0.59 | 0.42 | 0.00 | 0.59 | 0.59 | 0.57 | 0.51 |
| $Al_2O_3$ | 0.00 | 0.00 | 0.00 | 17.51 | 15.11 | 14.28 | 0.16 | 0.04 | 0.01 | 0.05 | 16.42 | 14.75 | 13.63 | 0.00 | 15.22 | 15.67 | 16.23 | 16.73 |
| $Cr_2O_3$ | 0.00 | 0.00 | 0.05 | 47.56 | 50.73 | 51.12 | 0.12 | 0.09 | 0.03 | 0.34 | 48.60 | 51.40 | 52.03 | 0.18 | 51.32 | 50.57 | 50.19 | 49.70 |
| $V_2O_3$ | 0.00 | 0.00 | 0.00 | 0.12 | 0.12 | 0.19 | 0.00 | 0.00 | 0.02 | 0.02 | 0.05 | 0.18 | 0.07 | 0.02 | 0.02 | 0.09 | 0.00 | 0.10 |
| $Fe_2O_3$ | 0.00 | 0.00 | 0.00 | 5.39 | 4.78 | 4.94 | 0.00 | 0.00 | 0.00 | 0.00 | 4.86 | 4.21 | 4.64 | 0.00 | 4.42 | 4.13 | 4.36 | 4.52 |
| FeO | 7.27 | 7.29 | 7.28 | 19.24 | 20.34 | 20.96 | 6.80 | 3.14 | 7.30 | 6.53 | 20.55 | 21.23 | 20.61 | 6.46 | 21.11 | 20.98 | 20.73 | 20.41 |
| MnO | 0.06 | 0.12 | 0.06 | 0.17 | 0.20 | 0.25 | 0.11 | 0.07 | 0.14 | 0.05 | 0.15 | 0.09 | 0.19 | 0.12 | 0.15 | 0.08 | 0.19 | 0.25 |
| MgO | 50.80 | 50.83 | 51.45 | 10.45 | 9.55 | 9.18 | 53.64 | 53.90 | 51.00 | 51.70 | 9.56 | 9.02 | 9.16 | 51.69 | 9.22 | 9.23 | 9.53 | 9.77 |
| NiO | 0.44 | 0.41 | 0.46 | 0.12 | 0.11 | 0.14 | 0.41 | 0.49 | 0.43 | 0.46 | 0.13 | 0.14 | 0.15 | 0.44 | 0.15 | 0.16 | 0.07 | 0.14 |
| ZnO | 0.00 | 0.00 | 0.00 | 0.30 | 0.21 | 0.27 | 0.01 | 0.00 | 0.00 | 0.03 | 0.05 | 0.26 | 0.17 | 0.07 | 0.26 | 0.23 | 0.27 | 0.10 |
| TOT | 99.73 | 99.85 | 100.38 | 101.49 | 101.71 | 102.06 | 100.99 | 97.75 | 100.12 | 100.65 | 101.01 | 101.91 | 101.20 | 100.59 | 102.46 | 101.75 | 102.17 | 102.26 |
| Si | 1.00 | 1.00 | 0.99 | 0.00 | 0.00 | 0.00 | 0.94 | 0.97 | 1.00 | 1.00 | 0.00 | 0.00 | 0.00 | 1.00 | 0.00 | 0.00 | 0.00 | 0.00 |
| Ti | 0.00 | 0.00 | 0.00 | 0.01 | 0.01 | 0.01 | 0.00 | 0.00 | 0.00 | 0.00 | 0.01 | 0.01 | 0.01 | 0.00 | 0.01 | 0.01 | 0.01 | 0.01 |
| Al | 0.00 | 0.00 | 0.00 | 0.65 | 0.57 | 0.54 | 0.00 | 0.00 | 0.00 | 0.00 | 0.62 | 0.56 | 0.52 | 0.00 | 0.57 | 0.59 | 0.61 | 0.62 |
| Cr | 0.00 | 0.00 | 0.00 | 1.19 | 1.28 | 1.30 | 0.00 | 0.00 | 0.00 | 0.01 | 1.23 | 1.31 | 1.33 | 0.00 | 1.29 | 1.28 | 1.26 | 1.24 |
| V | 0.00 | 0.00 | 0.00 | 0.00 | 0.00 | 0.00 | 0.00 | 0.00 | 0.00 | 0.00 | 0.00 | 0.00 | 0.00 | 0.00 | 0.00 | 0.00 | 0.00 | 0.00 |
| $Fe^{3+}$ | 0.00 | 0.00 | 0.00 | 0.13 | 0.12 | 0.12 | 0.00 | 0.00 | 0.00 | 0.00 | 0.12 | 0.10 | 0.11 | 0.00 | 0.11 | 0.10 | 0.10 | 0.11 |
| $Fe^{2+}$ | 0.15 | 0.15 | 0.15 | 0.51 | 0.54 | 0.56 | 0.14 | 0.06 | 0.15 | 0.13 | 0.55 | 0.57 | 0.56 | 0.13 | 0.56 | 0.56 | 0.55 | 0.54 |
| Mn | 0.00 | 0.00 | 0.00 | 0.00 | 0.01 | 0.01 | 0.00 | 0.00 | 0.00 | 0.00 | 0.00 | 0.00 | 0.01 | 0.00 | 0.00 | 0.00 | 0.01 | 0.01 |
| Mg | 1.84 | 1.84 | 1.85 | 0.49 | 0.46 | 0.44 | 1.90 | 1.95 | 1.84 | 1.85 | 0.46 | 0.43 | 0.44 | 1.85 | 0.44 | 0.44 | 0.45 | 0.46 |
| Ni | 0.01 | 0.01 | 0.01 | 0.00 | 0.00 | 0.00 | 0.01 | 0.01 | 0.01 | 0.01 | 0.00 | 0.00 | 0.00 | 0.01 | 0.00 | 0.00 | 0.00 | 0.00 |
| Zn | 0.00 | 0.00 | 0.00 | 0.01 | 0.00 | 0.01 | 0.00 | 0.00 | 0.00 | 0.00 | 0.00 | 0.01 | 0.00 | 0.00 | 0.01 | 0.01 | 0.01 | 0.00 |

| Analysis | PO4A-20 | d (mm) | PO4A-21 | PO4A-22 | PO4A-23 | PO4A-24 | PO4A-25 | d (mm) | PO4A-26 |
|---|---|---|---|---|---|---|---|---|---|
| | 60-CHR | | 61-OL | 62-OL | 63-OL | 64-CHR | 65-CHR | | 66-OL |
| X | 34.39 | 34.39 | 34.39 | 34.37 | 34.35 | 34.12 | 34.11 | 34.11 | 34.11 |
| Y | 66.83 | 66.82 | 66.82 | 66.80 | 66.77 | 67.03 | 67.08 | 67.08 | 67.09 |
| **d (mm)** | **0.007** | | **0.005** | **0.032** | **0.067** | **0.054** | **0.007** | | **0.006** |
| $SiO_2$ | 0.06 | | 40.94 | 41.06 | 40.93 | 0.00 | 0.00 | | 41.25 |
| $TiO_2$ | 0.47 | | 0.12 | 0.03 | 0.00 | 0.55 | 0.44 | | 0.00 |
| $Al_2O_3$ | 16.34 | | 0.03 | 0.00 | 0.00 | 14.82 | 13.81 | | 0.00 |
| $Cr_2O_3$ | 49.47 | | 0.28 | 0.04 | 0.00 | 51.12 | 52.51 | | 0.33 |
| $V_2O_3$ | 0.01 | | 0.00 | 0.04 | 0.00 | 0.02 | 0.04 | | 0.04 |
| $Fe_2O_3$ | 4.40 | | 0.00 | 0.00 | 0.00 | 3.99 | 4.21 | | 0.00 |
| FeO | 21.71 | | 5.71 | 6.70 | 7.07 | 21.51 | 21.59 | | 5.73 |
| MnO | 0.11 | | 0.10 | 0.10 | 0.16 | 0.16 | 0.27 | | 0.06 |
| MgO | 8.96 | | 51.59 | 50.88 | 50.18 | 8.71 | 8.47 | | 51.66 |
| NiO | 0.06 | | 0.49 | 0.42 | 0.49 | 0.08 | 0.18 | | 0.40 |
| ZnO | 0.00 | | 0.13 | 0.04 | 0.00 | 0.16 | 0.11 | | 0.05 |
| TOT | 101.61 | | 99.41 | 99.32 | 98.85 | 101.12 | 101.65 | | 99.54 |
| Si | 0.00 | | 0.99 | 1.00 | 1.00 | 0.00 | 0.00 | | 1.00 |
| Ti | 0.01 | | 0.00 | 0.00 | 0.00 | 0.01 | 0.01 | | 0.00 |
| Al | 0.62 | | 0.00 | 0.00 | 0.00 | 0.57 | 0.53 | | 0.00 |
| Cr | 1.25 | | 0.01 | 0.00 | 0.00 | 1.31 | 1.35 | | 0.01 |

| | | | | | | | | |
|---|---|---|---|---|---|---|---|---|
| V | 0.00 | | 0.00 | 0.00 | 0.00 | 0.00 | 0.00 | 0.00 |
| $Fe^{3+}$ | 0.11 | | 0.00 | 0.00 | 0.00 | 0.10 | 0.10 | 0.00 |
| $Fe^{2+}$ | 0.58 | | 0.12 | 0.14 | 0.15 | 0.58 | 0.59 | 0.12 |
| Mn | 0.00 | | 0.00 | 0.00 | 0.00 | 0.00 | 0.01 | 0.00 |
| Mg | 0.43 | | 1.87 | 1.85 | 1.84 | 0.42 | 0.41 | 1.87 |
| Ni | 0.00 | | 0.01 | 0.01 | 0.01 | 0.00 | 0.00 | 0.01 |
| Zn | 0.00 | | 0.00 | 0.00 | 0.00 | 0.00 | 0.00 | 0.00 |

Tab. A3.8 GR63B-GRID1 (Nea Roda) microprobe analyses of olivine and chromite crystals; d(mm) distance from the intergranular limit

| Analysis | GRID1-1 | GRID1-3 | GRID1-4 | GRID1-7 | GRID2-3 | GRID2-5 | GRID2-6 | GRID3-6 | GRID4-2 | GRID4-4 | GRID5-1 | GRID5-2 | GRID5-6 | GRID6-1 | GRID6-2 | GRID6-3 | GRID6-4 | GRID6-5 | GRID6-6 |
|---|---|---|---|---|---|---|---|---|---|---|---|---|---|---|---|---|---|---|---|
| | 142-OL | 144-OL | 145-OL | 148-OL | 151-OL | 153-OL | 154-OL | 161-OL | 164-OL | 166-CHR | 170-OL | 171-OL | 175-OL | 177-OL | 178-OL | 179-OL | 180-OL | 181-OL | 182-OL |
| X | 42.67 | 42.67 | 42.67 | 42.67 | 42.77 | 42.77 | 42.77 | 42.87 | 42.97 | 42.97 | 43.07 | 43.07 | 43.07 | 43.17 | 43.17 | 43.17 | 43.17 | 43.17 | 43.17 |
| Y | 71.65 | 71.85 | 71.95 | 72.25 | 71.85 | 72.05 | 72.15 | 72.15 | 71.75 | 71.95 | 71.65 | 71.75 | 72.15 | 71.65 | 71.75 | 71.85 | 71.95 | 72.05 | 72.15 |
| d (mm) | | | | | | | | | | | | | | | | | | | |
| $SiO_2$ | 41.70 | 41.39 | 41.88 | 41.52 | 42.12 | 41.56 | 41.22 | 41.33 | 41.62 | 0.06 | 41.48 | 41.46 | 42.04 | 41.66 | 41.03 | 41.97 | 41.50 | 41.04 | 42.03 |
| $TiO_2$ | 0.00 | 0.00 | 0.04 | 0.00 | 0.00 | 0.00 | 0.00 | 0.02 | 0.03 | 0.20 | 0.01 | 0.02 | 0.02 | 0.00 | 0.00 | 0.08 | 0.02 | 0.00 | 0.02 |
| $Al_2O_3$ | 0.04 | 0.00 | 0.01 | 0.00 | 0.01 | 0.00 | 0.02 | 0.01 | 0.00 | 12.30 | 0.00 | 0.00 | 0.02 | 0.00 | 0.00 | 0.01 | 0.04 | 0.02 | 0.01 |
| $Cr_2O_3$ | 0.00 | 0.05 | 0.00 | 0.03 | 0.06 | 0.00 | 0.04 | 0.05 | 0.02 | 53.71 | 0.02 | 0.02 | 0.00 | 0.00 | 0.06 | 0.02 | 0.00 | 0.00 | 0.03 |
| $V_2O_3$ | 0.00 | 0.00 | 0.00 | 0.00 | 0.00 | 0.00 | 0.00 | 0.00 | 0.00 | 0.08 | 0.00 | 0.00 | 0.00 | 0.00 | 0.00 | 0.00 | 0.00 | 0.00 | 0.00 |
| $Fe_2O_3$ | 0.00 | 0.00 | 0.00 | 0.00 | 0.00 | 0.00 | 0.00 | 0.00 | 0.00 | 4.57 | 0.00 | 0.00 | 0.00 | 0.00 | 0.00 | 0.00 | 0.00 | 0.00 | 0.00 |
| FeO | 6.51 | 6.77 | 6.35 | 6.48 | 6.51 | 6.58 | 6.70 | 7.33 | 6.84 | 21.13 | 6.55 | 6.81 | 6.48 | 6.68 | 6.86 | 6.60 | 6.83 | 6.92 | 6.55 |
| MnO | 0.03 | 0.11 | 0.12 | 0.09 | 0.02 | 0.11 | 0.05 | 0.09 | 0.08 | 0.34 | 0.05 | 0.13 | 0.07 | 0.09 | 0.16 | 0.11 | 0.09 | 0.11 | 0.08 |
| MgO | 51.54 | 52.50 | 51.58 | 51.51 | 51.46 | 51.72 | 52.59 | 49.47 | 51.62 | 8.33 | 52.06 | 51.99 | 51.40 | 51.32 | 52.96 | 51.36 | 52.01 | 52.31 | 51.69 |
| NiO | 0.44 | 0.38 | 0.44 | 0.41 | 0.45 | 0.42 | 0.36 | 0.42 | 0.39 | 0.00 | 0.43 | 0.40 | 0.46 | 0.39 | 0.49 | 0.45 | 0.45 | 0.40 | 0.42 |
| ZnO | 0.11 | 0.21 | 0.00 | 0.00 | 0.11 | 0.00 | 0.16 | 0.02 | 0.00 | 0.36 | 0.06 | 0.05 | 0.09 | 0.00 | 0.03 | 0.04 | 0.00 | 0.00 | 0.06 |
| TOT | 100.38 | 101.44 | 100.45 | 100.08 | 100.77 | 100.40 | 101.16 | 98.76 | 100.64 | 101.08 | 100.68 | 100.89 | 100.58 | 100.14 | 101.63 | 100.65 | 100.96 | 100.80 | 100.91 |
| Si | 1.00 | 0.99 | 1.01 | 1.00 | 1.01 | 1.00 | 0.98 | 1.02 | 1.00 | 0.00 | 1.00 | 0.99 | 1.01 | 1.01 | 0.97 | 1.01 | 0.99 | 0.98 | 1.01 |
| Ti | 0.00 | 0.00 | 0.00 | 0.00 | 0.00 | 0.00 | 0.00 | 0.00 | 0.00 | 0.01 | 0.00 | 0.00 | 0.00 | 0.00 | 0.00 | 0.00 | 0.00 | 0.00 | 0.00 |
| Al | 0.00 | 0.00 | 0.00 | 0.00 | 0.00 | 0.00 | 0.00 | 0.00 | 0.00 | 0.48 | 0.00 | 0.00 | 0.00 | 0.00 | 0.00 | 0.00 | 0.00 | 0.00 | 0.00 |
| Cr | 0.00 | 0.00 | 0.00 | 0.00 | 0.00 | 0.00 | 0.00 | 0.00 | 0.00 | 1.40 | 0.00 | 0.00 | 0.00 | 0.00 | 0.00 | 0.00 | 0.00 | 0.00 | 0.00 |
| V | 0.00 | 0.00 | 0.00 | 0.00 | 0.00 | 0.00 | 0.00 | 0.00 | 0.00 | 0.00 | 0.00 | 0.00 | 0.00 | 0.00 | 0.00 | 0.00 | 0.00 | 0.00 | 0.00 |
| $Fe^{3+}$ | 0.00 | 0.00 | 0.00 | 0.00 | 0.00 | 0.00 | 0.00 | 0.00 | 0.00 | 0.11 | 0.00 | 0.00 | 0.00 | 0.00 | 0.00 | 0.00 | 0.00 | 0.00 | 0.00 |
| $Fe^{2+}$ | 0.13 | 0.13 | 0.13 | 0.13 | 0.13 | 0.13 | 0.13 | 0.15 | 0.14 | 0.58 | 0.13 | 0.14 | 0.13 | 0.14 | 0.14 | 0.13 | 0.14 | 0.14 | 0.13 |
| Mn | 0.00 | 0.00 | 0.00 | 0.00 | 0.00 | 0.00 | 0.00 | 0.00 | 0.00 | 0.01 | 0.00 | 0.00 | 0.00 | 0.00 | 0.00 | 0.00 | 0.00 | 0.00 | 0.00 |
| Mg | 1.85 | 1.86 | 1.85 | 1.85 | 1.84 | 1.86 | 1.87 | 1.82 | 1.85 | 0.41 | 1.86 | 1.86 | 1.84 | 1.85 | 1.87 | 1.84 | 1.86 | 1.87 | 1.85 |
| Ni | 0.01 | 0.01 | 0.01 | 0.01 | 0.01 | 0.01 | 0.01 | 0.01 | 0.01 | 0.00 | 0.01 | 0.01 | 0.01 | 0.01 | 0.01 | 0.01 | 0.01 | 0.01 | 0.01 |
| Zn | 0.00 | 0.00 | 0.00 | 0.00 | 0.00 | 0.00 | 0.00 | 0.00 | 0.00 | 0.01 | 0.00 | 0.00 | 0.00 | 0.00 | 0.00 | 0.00 | 0.00 | 0.00 | 0.00 |

| Analysis | GRID6-7 | GRID7-1 | GRID7-2 | GR63B-1 | GR63B-2 | GR63B-3 | GR63B-1 | GR63B-2 | GR63B-3 | d-CHR | GR63B-4 | GR63B-5 | GR63B-6 | GR63B-7 | GR63B-8 | GR63B-9 | GR63B-10 | GR63B-11 | GR63B-12 |
|---|---|---|---|---|---|---|---|---|---|---|---|---|---|---|---|---|---|---|---|
| | 183-OL | 184-OL | 185-OL | 191-FeCHR | CHRcore | CHRrim | 99-OL | 100-OL | 101-OL | | 102-FeCHR | 103-FeCHR | 104-CHR | 105-CHR | 106-CHR | 107-CHR | 108-CHR | 109-OL | 110-OL |
| X | 43.17 | 43.27 | 43.27 | 42.97 | 42.98 | 43.05 | 15.12 | 15.10 | 15.08 | 15.06 | 15.06 | 15.05 | 15.05 | 15.04 | 15.03 | 15.02 | 15.00 | 15.16 | 15.15 |
| Y | 72.25 | 71.65 | 71.75 | 72.02 | 71.94 | 71.95 | 73.87 | 73.87 | 73.87 | 73.87 | 73.87 | 73.87 | 73.87 | 73.87 | 73.88 | 73.88 | 73.88 | 73.95 | 73.95 |
| d (mm) | | | | | | | 0.06 | 0.04 | 0.02 | | 0.00 | 0.01 | 0.01 | 0.02 | 0.03 | 0.04 | 0.06 | 0.12 | 0.11 |
| $SiO_2$ | 41.39 | 41.65 | 35.69 | 0.17 | 0.04 | 0.15 | 39.66 | 39.47 | 39.55 | | 6.06 | 0.04 | 0.02 | 0.01 | 0.04 | 0.01 | 0.00 | 38.49 | 38.43 |
| $TiO_2$ | 0.02 | 0.02 | 0.00 | 0.30 | 0.16 | 0.28 | 0.00 | 0.00 | 0.00 | | 0.24 | 0.29 | 0.22 | 0.25 | 0.30 | 0.23 | 0.17 | 0.00 | 0.00 |
| $Al_2O_3$ | 0.00 | 0.00 | 2.98 | 4.79 | 12.42 | 9.43 | 0.01 | 0.00 | 0.01 | | 2.92 | 7.81 | 11.63 | 11.87 | 12.41 | 12.59 | 12.40 | 0.00 | 0.01 |
| $Cr_2O_3$ | 0.03 | 0.00 | 0.04 | 61.05 | 53.99 | 54.02 | 0.04 | 0.10 | 0.19 | | 42.09 | 55.43 | 53.29 | 54.27 | 53.60 | 53.75 | 54.21 | 0.08 | 0.01 |
| $V_2O_3$ | 0.00 | 0.00 | 0.00 | 0.09 | 0.07 | 0.11 | 0.00 | 0.00 | 0.00 | | 0.17 | 0.13 | 0.06 | 0.07 | 0.05 | 0.10 | 0.10 | 0.00 | 0.00 |

| | | | | | | | | | | | | | | | | | | | |
|---|---|---|---|---|---|---|---|---|---|---|---|---|---|---|---|---|---|---|---|
| $Fe_2O_3$ | 0.00 | 0.00 | 0.00 | 3.34 | 4.36 | 5.58 | 0.00 | 0.00 | 0.00 | | 20.30 | 5.95 | 5.54 | 4.07 | 4.40 | 4.38 | 4.26 | 0.00 | 0.00 |
| FeO | 6.52 | 6.46 | 7.28 | 23.89 | 21.31 | 23.34 | 6.65 | 6.78 | 6.73 | | 5.46 | 24.89 | 23.56 | 23.58 | 22.68 | 22.25 | 22.15 | 6.84 | 6.82 |
| MnO | 0.10 | 0.11 | 0.17 | 0.40 | 0.29 | 0.42 | 0.08 | 0.10 | 0.09 | | 0.34 | 0.33 | 0.21 | 0.22 | 0.29 | 0.25 | 0.28 | 0.14 | 0.09 |
| MgO | 51.81 | 51.59 | 51.52 | 5.71 | 8.38 | 6.58 | 50.82 | 50.98 | 50.55 | | 22.40 | 5.29 | 6.94 | 6.90 | 7.62 | 7.79 | 7.83 | 51.13 | 50.95 |
| NiO | 0.44 | 0.42 | 0.42 | 0.00 | 0.00 | 0.04 | 0.39 | 0.43 | 0.45 | | 0.20 | 0.07 | 0.05 | 0.02 | 0.00 | 0.04 | 0.00 | 0.47 | 0.41 |
| ZnO | 0.13 | 0.00 | 0.07 | 0.24 | 0.11 | 0.07 | 0.13 | 0.01 | 0.00 | | 0.15 | 0.40 | 0.15 | 0.27 | 0.19 | 0.33 | 0.27 | 0.07 | 0.06 |
| TOT | 100.44 | 100.25 | 98.44 | 99.98 | 101.14 | 100.02 | 97.79 | 97.90 | 97.60 | | 100.34 | 100.63 | 101.67 | 101.54 | 101.59 | 101.74 | 101.67 | 97.22 | 96.79 |
| Si | 1.00 | 1.00 | 0.87 | 0.01 | 0.00 | 0.01 | 0.98 | 0.97 | 0.98 | | 0.19 | 0.00 | 0.00 | 0.00 | 0.00 | 0.00 | 0.00 | 0.95 | 0.96 |
| Ti | 0.00 | 0.00 | 0.00 | 0.01 | 0.00 | 0.01 | 0.00 | 0.00 | 0.00 | | 0.01 | 0.01 | 0.01 | 0.01 | 0.01 | 0.01 | 0.00 | 0.00 | 0.00 |
| Al | 0.00 | 0.00 | 0.09 | 0.20 | 0.48 | 0.38 | 0.00 | 0.00 | 0.00 | | 0.11 | 0.32 | 0.45 | 30.46 | 0.48 | 0.49 | 0.48 | 0.00 | 0.00 |
| Cr | 0.00 | 0.00 | 0.00 | 1.69 | 1.40 | 1.45 | 0.00 | 0.00 | 0.00 | | 1.03 | 1.51 | 1.39 | 1.42 | 1.39 | 1.39 | 1.40 | 0.00 | 0.00 |
| V | 0.00 | 0.00 | 0.00 | 0.00 | 0.00 | 0.00 | 0.00 | 0.00 | 0.00 | | 0.00 | 0.00 | 0.00 | 0.00 | 0.00 | 0.00 | 0.00 | 0.00 | 0.00 |
| $Fe^{3+}$ | 0.00 | 0.00 | 0.00 | 0.09 | 0.11 | 0.14 | 0.00 | 0.00 | 0.00 | | 0.47 | 0.15 | 0.14 | 0.10 | 0.11 | 0.11 | 0.11 | 0.00 | 0.00 |
| $Fe^{2+}$ | 0.13 | 0.13 | 0.15 | 0.70 | 0.58 | 0.66 | 0.14 | 0.14 | 0.14 | | 0.14 | 0.72 | 0.65 | 0.65 | 0.62 | 0.61 | 0.61 | 0.14 | 0.14 |
| Mn | 0.00 | 0.00 | 0.00 | 0.01 | 0.01 | 0.01 | 0.00 | 0.00 | 0.00 | | 0.01 | 0.01 | 0.01 | 0.01 | 0.01 | 0.01 | 0.01 | 0.00 | 0.00 |
| Mg | 1.86 | 1.85 | 1.87 | 0.30 | 0.41 | 0.33 | 1.87 | 1.87 | 1.87 | | 1.03 | 0.27 | 0.34 | 0.34 | 0.37 | 0.38 | 0.38 | 1.89 | 1.89 |
| Ni | 0.01 | 0.01 | 0.01 | 0.00 | 0.00 | 0.00 | 0.01 | 0.01 | 0.01 | | 0.00 | 0.00 | 0.00 | 0.00 | 0.00 | 0.00 | 0.00 | 0.01 | 0.01 |
| Zn | 0.00 | 0.00 | 0.00 | 0.01 | 0.00 | 0.00 | 0.00 | 0.00 | 0.00 | | 0.00 | 0.01 | 0.00 | 0.01 | 0.00 | 0.01 | 0.01 | 0.00 | 0.00 |

| Analysis | GR63B-13 | GR63B-14 | GR63B-15 | GR63B-16 | d-CHR | GR63B-17 | GR63B-18 | GR63B-19 | GR63B-20 | GR63B-21 | GR63B-22 | GR63B-23 | GR63B-24 | GR63B-25 | d-CHR | GR63B-26 | GR63B-27 | GR63B-28 | GR63B-29 | d-CHR |
|---|---|---|---|---|---|---|---|---|---|---|---|---|---|---|---|---|---|---|---|---|
| | 111-OL | 112-OL | 113-OL | 114-OL | | 115-CHR | 116-CHR | 117-CHR | 118-CHR | 119-CHR | 120-CHR | 121-CHR | 122-CHR | 123-CHR | | 124-OL | 125-OL | 126-OL | 127-OL | |
| X | 15.14 | 15.12 | 15.10 | 15.08 | 15.06 | 15.06 | 15.05 | 15.04 | 15.03 | 15.02 | 15.02 | 15.01 | 15.01 | 15.00 | 15.02 | 14.85 | 14.86 | 14.87 | 14.87 | 14.90 |
| Y | 73.94 | 73.94 | 73.93 | 73.92 | 73.90 | 73.90 | 73.90 | 73.89 | 73.88 | 73.93 | 73.93 | 73.93 | 73.93 | 73.92 | 73.93 | 73.93 | 73.93 | 73.92 | 73.92 | 73.91 |
| d (mm) | 0.09 | 0.08 | 0.06 | 0.04 | | 0.00 | 0.01 | 0.02 | 0.03 | 0.00 | 0.00 | 0.01 | 0.01 | 0.03 | | 0.05 | 0.04 | 0.03 | 0.03 | |
| $SiO_2$ | 38.59 | 38.34 | 38.55 | 39.17 | | 0.05 | 0.02 | 0.00 | 0.04 | 0.04 | 0.02 | 0.01 | 0.00 | 0.04 | | 40.42 | 40.45 | 40.34 | 39.23 | |
| $TiO_2$ | 0.00 | 0.01 | 0.00 | 0.01 | | 0.27 | 0.22 | 0.25 | 0.34 | 0.30 | 0.31 | 0.30 | 0.23 | 0.24 | | 0.00 | 0.00 | 0.03 | 0.00 | |
| $Al_2O_3$ | 0.00 | 0.00 | 0.00 | 0.02 | | 6.56 | 11.54 | 10.37 | 12.32 | 9.95 | 12.91 | 13.05 | 12.75 | 12.48 | | 0.00 | 0.00 | 0.00 | 0.00 | |
| $Cr_2O_3$ | 0.04 | 0.02 | 0.04 | 0.14 | | 56.75 | 53.37 | 57.85 | 53.59 | 54.55 | 52.33 | 53.03 | 53.69 | 54.02 | | 0.08 | 0.14 | 0.15 | 0.11 | |
| $V_2O_3$ | 0.00 | 0.00 | 0.00 | 0.00 | | 0.12 | 0.16 | 0.11 | 0.14 | 0.13 | 0.11 | 0.12 | 0.10 | 0.08 | | 0.00 | 0.00 | 0.00 | 0.00 | |
| $Fe_2O_3$ | 0.00 | 0.00 | 0.00 | 0.00 | | 5.96 | 5.25 | 2.42 | 4.43 | 5.37 | 4.40 | 4.22 | 4.08 | 4.32 | | 0.00 | 0.00 | 0.00 | 0.00 | |
| FeO | 6.65 | 6.69 | 6.74 | 6.75 | | 25.01 | 23.52 | 23.23 | 22.19 | 24.33 | 22.94 | 22.77 | 22.49 | 21.81 | | 6.59 | 6.60 | 6.91 | 7.06 | |
| MnO | 0.14 | 0.07 | 0.12 | 0.14 | | 0.37 | 0.25 | 0.19 | 0.34 | 0.26 | 0.26 | 0.32 | 0.33 | 0.20 | | 0.13 | 0.06 | 0.15 | 0.10 | |
| MgO | 50.63 | 50.72 | 51.25 | 50.63 | | 5.15 | 6.78 | 7.06 | 7.85 | 6.16 | 7.29 | 7.59 | 7.59 | 8.07 | | 51.22 | 51.23 | 51.21 | 52.82 | |
| NiO | 0.42 | 0.44 | 0.48 | 0.39 | | 0.02 | 0.09 | 0.01 | 0.11 | 0.07 | 0.09 | 0.12 | 0.14 | 0.10 | | 0.36 | 0.48 | 0.44 | 0.42 | |
| ZnO | 0.00 | 0.09 | 0.00 | 0.00 | | 0.23 | 0.34 | 0.23 | 0.15 | 0.27 | 0.19 | 0.05 | 0.21 | 0.40 | | 0.00 | 0.00 | 0.00 | 0.00 | |
| TOT | 96.48 | 96.40 | 97.18 | 97.27 | | 100.49 | 101.55 | 101.74 | 101.49 | 101.46 | 100.84 | 101.56 | 101.61 | 101.76 | | 98.83 | 98.99 | 99.28 | 99.75 | |
| Si | 0.96 | 0.96 | 0.96 | 0.97 | | 0.00 | 0.00 | 0.00 | 0.00 | 0.00 | 0.00 | 0.00 | 0.00 | 0.00 | | 0.99 | 0.99 | 0.98 | 0.95 | |
| Ti | 0.00 | 0.00 | 0.00 | 0.00 | | 0.01 | 0.01 | 0.01 | 0.01 | 0.01 | 0.01 | 0.01 | 0.01 | 0.01 | | 0.00 | 0.00 | 0.00 | 0.00 | |
| Al | 0.00 | 0.00 | 0.00 | 0.00 | | 0.27 | 0.45 | 0.41 | 0.48 | 0.39 | 0.50 | 0.50 | 0.49 | 0.48 | | 0.00 | 0.00 | 0.00 | 0.00 | |
| Cr | 0.00 | 0.00 | 0.00 | 0.00 | | 1.56 | 1.40 | 1.52 | 1.39 | 1.45 | 1.37 | 1.37 | 1.39 | 1.40 | | 0.00 | 0.00 | 0.00 | 0.00 | |
| V | 0.00 | 0.00 | 0.00 | 0.00 | | 0.00 | 0.00 | 0.00 | 0.00 | 0.00 | 0.00 | 0.00 | 0.00 | 0.00 | | 0.00 | 0.00 | 0.00 | 0.00 | |
| $Fe^{3+}$ | 0.00 | 0.00 | 0.00 | 0.00 | | 0.16 | 0.13 | 0.06 | 0.11 | 0.14 | 0.11 | 0.10 | 0.10 | 0.11 | | 0.00 | 0.00 | 0.00 | 0.00 | |
| $Fe^{2+}$ | 0.14 | 0.14 | 0.14 | 0.14 | | 0.73 | 0.65 | 0.65 | 0.61 | 0.68 | 0.63 | 0.62 | 0.62 | 0.60 | | 0.13 | 0.13 | 0.14 | 0.14 | |
| Mn | 0.00 | 0.00 | 0.00 | 0.00 | | 0.01 | 0.01 | 0.01 | 0.01 | 0.01 | 0.01 | 0.01 | 0.01 | 0.01 | | 0.00 | 0.00 | 0.00 | 0.00 | |
| Mg | 1.88 | 1.89 | 1.89 | 1.87 | | 0.27 | 0.34 | 0.35 | 0.38 | 0.31 | 0.36 | 0.37 | 0.37 | 0.39 | | 1.87 | 1.86 | 1.86 | 1.90 | |
| Ni | 0.01 | 0.01 | 0.01 | 0.01 | | 0.00 | 0.00 | 0.00 | 0.00 | 0.00 | 0.00 | 0.00 | 0.00 | 0.00 | | 0.01 | 0.01 | 0.01 | 0.01 | |
| Zn | 0.00 | 0.00 | 0.00 | 0.00 | | 0.01 | 0.01 | 0.01 | 0.00 | 0.01 | 0.00 | 0.00 | 0.01 | 0.01 | | 0.00 | 0.00 | 0.00 | 0.00 | |

| Analysis | GR63B-30 | GR63B-31 | GR63B-32 | GR63B-33 | GR63B-34 | GR63B-35 | GR63B-36 | GR63B-37 | GR63B-38 | d-CHR | GR63B-39 | GR63B-40 | GR63B-41 | GR63B-42 | GR63B-43 | GR63B-44 | GR63B-45 | d-CHR | GR63B-46 | GR63B-47 | GR63B-48 | GR63B-49 |
|---|---|---|---|---|---|---|---|---|---|---|---|---|---|---|---|---|---|---|---|---|---|---|
| | 128-CHR | 129-CHR | 130-CHR | 131-CHR | 132-CHR | 133-CHR | 134-OL | 135-OL | 136-OL | | 137-FeCHR | 138-FeCHR | 139-CHR | 140-CHR | 141-CHR | 142-OL | 143-OL | | 144-CHR | 145-CHR | 146-CHR | 147-CHR |

| | | | | | | | | | | | | | | | | | | | | | | |
|---|---|---|---|---|---|---|---|---|---|---|---|---|---|---|---|---|---|---|---|---|---|---|
| X | 14.90 | 14.90 | 14.91 | 14.91 | 14.92 | 14.95 | 14.83 | 14.84 | 14.85 | 14.90 | 14.87 | 14.88 | 14.89 | 14.90 | 14.92 | 14.93 | 14.93 | 14.93 | 14.93 | 14.93 | 14.93 | 14.93 |
| Y | 73.91 | 73.91 | 73.91 | 73.91 | 73.90 | 73.89 | 73.80 | 73.81 | 73.82 | 73.91 | 73.84 | 73.84 | 73.85 | 73.86 | 73.87 | 73.80 | 73.80 | 73.82 | 73.83 | 73.83 | 73.84 | 73.85 |
| d (mm) | 0.00 | 0.00 | 0.01 | 0.01 | 0.02 | 0.05 | 0.14 | 0.12 | 0.11 | | 0.08 | 0.07 | 0.06 | 0.05 | 0.05 | 0.03 | 0.02 | | 0.00 | 0.01 | 0.02 | 0.03 |
| $SiO_2$ | 0.00 | 0.03 | 0.01 | 0.02 | 0.01 | 0.06 | 39.19 | 39.37 | 36.27 | | 0.10 | 0.04 | 0.02 | 0.02 | 0.01 | 35.47 | 39.35 | | 15.40 | 0.01 | 0.03 | 0.03 |
| $TiO_2$ | 0.26 | 0.22 | 0.28 | 0.24 | 0.25 | 0.19 | 0.00 | 0.03 | 0.00 | | 0.37 | 0.30 | 0.27 | 0.17 | 0.28 | 0.00 | 0.09 | | 0.13 | 0.30 | 0.30 | 0.31 |
| $Al_2O_3$ | 12.21 | 12.92 | 12.98 | 12.93 | 12.56 | 12.58 | 0.00 | 0.00 | 0.00 | | 3.08 | 3.39 | 3.57 | 11.87 | 11.77 | 0.04 | 0.00 | | 0.39 | 10.00 | 13.05 | 11.97 |
| $Cr_2O_3$ | 52.76 | 52.69 | 52.77 | 52.91 | 54.62 | 54.08 | 0.01 | 0.02 | 0.12 | | 58.42 | 59.70 | 60.32 | 53.32 | 54.86 | 0.18 | 0.35 | | 34.33 | 53.67 | 51.90 | 53.73 |
| $V_2O_3$ | 0.13 | 0.14 | 0.09 | 0.14 | 0.11 | 0.09 | 0.00 | 0.00 | 0.00 | | 0.13 | 0.12 | 0.11 | 0.09 | 0.08 | 0.00 | 0.00 | | 0.05 | 0.11 | 0.11 | 0.13 |
| $Fe_2O_3$ | 5.16 | 4.39 | 5.07 | 4.68 | 4.26 | 3.91 | 0.00 | 0.00 | 0.00 | | 5.56 | 5.71 | 5.82 | 5.01 | 3.96 | 0.00 | 0.00 | | 8.84 | 5.91 | 5.14 | 4.52 |
| FeO | 23.74 | 23.29 | 22.89 | 22.60 | 22.77 | 22.47 | 6.81 | 6.70 | 6.77 | | 27.63 | 26.73 | 25.81 | 23.53 | 22.86 | 7.31 | 7.21 | | 20.24 | 24.33 | 23.03 | 23.43 |
| MnO | 0.27 | 0.33 | 0.32 | 0.25 | 0.26 | 0.18 | 0.11 | 0.12 | 0.11 | | 0.41 | 0.33 | 0.43 | 0.30 | 0.24 | 0.07 | 0.10 | | 0.54 | 0.35 | 0.27 | 0.29 |
| MgO | 6.76 | 7.14 | 7.49 | 7.68 | 7.84 | 7.78 | 51.13 | 51.02 | 54.98 | | 2.78 | 3.63 | 4.28 | 6.82 | 7.40 | 43.70 | 51.05 | | 20.29 | 6.00 | 7.35 | 7.09 |
| NiO | 0.04 | 0.11 | 0.17 | 0.02 | 0.06 | 0.08 | 0.38 | 0.46 | 0.42 | | 0.13 | 0.00 | 0.07 | 0.15 | 0.05 | 0.45 | 0.46 | | 0.47 | 0.12 | 0.11 | 0.13 |
| ZnO | 0.32 | 0.06 | 0.21 | 0.23 | 0.06 | 0.09 | 0.05 | 0.01 | 0.00 | | 0.15 | 0.35 | 0.31 | 0.07 | 0.27 | 0.00 | 0.00 | | 0.06 | 0.20 | 0.19 | 0.09 |
| TOT | 101.67 | 101.33 | 102.30 | 101.70 | 102.79 | 101.54 | 97.71 | 97.73 | 98.67 | | 98.77 | 100.31 | 101.01 | 101.37 | 101.79 | 87.41 | 98.62 | | 100.84 | 101.01 | 101.50 | 101.71 |
| Si | 0.00 | 0.00 | 0.00 | 0.00 | 0.00 | 0.00 | 0.97 | 0.97 | 0.87 | | 0.00 | 0.00 | 0.00 | 0.00 | 0.00 | 0.99 | 0.97 | | 0.47 | 0.00 | 0.00 | 0.00 |
| Ti | 0.01 | 0.01 | 0.01 | 0.01 | 0.01 | 0.00 | 0.00 | 0.00 | 0.00 | | 0.01 | 0.01 | 0.01 | 0.00 | 0.01 | 0.00 | 0.00 | | 0.00 | 0.01 | 0.01 | 0.01 |
| Al | 0.48 | 0.50 | 0.50 | 0.50 | 0.48 | 0.49 | 0.00 | 0.00 | 0.00 | | 0.13 | 0.14 | 0.15 | 0.46 | 0.46 | 0.00 | 0.00 | | 0.01 | 0.40 | 0.51 | 0.47 |
| Cr | 1.38 | 1.37 | 1.36 | 1.37 | 1.40 | 1.40 | 0.00 | 0.00 | 0.00 | | 1.68 | 1.68 | 1.68 | 1.40 | 1.43 | 0.00 | 0.01 | | 0.83 | 1.43 | 1.35 | 1.40 |
| V | 0.00 | 0.00 | 0.00 | 0.00 | 0.00 | 0.00 | 0.00 | 0.00 | 0.00 | | 0.00 | 0.00 | 0.00 | 0.00 | 0.00 | 0.00 | 0.00 | | 0.00 | 0.00 | 0.00 | 0.00 |
| $Fe^{3+}$ | 0.13 | 0.11 | 0.12 | 0.12 | 0.10 | 0.10 | 0.00 | 0.00 | 0.00 | | 0.15 | 0.15 | 0.15 | 0.13 | 0.10 | 0.00 | 0.00 | | 0.20 | 0.15 | 0.13 | 0.11 |
| $Fe^{2+}$ | 0.66 | 0.64 | 0.62 | 0.62 | 0.62 | 0.62 | 0.14 | 0.14 | 0.14 | | 0.84 | 0.80 | 0.76 | 0.65 | 0.63 | 0.17 | 0.15 | | 0.52 | 0.69 | 0.63 | 0.65 |
| Mn | 0.01 | 0.01 | 0.01 | 0.01 | 0.01 | 0.00 | 0.00 | 0.00 | 0.00 | | 0.01 | 0.01 | 0.01 | 0.01 | 0.01 | 0.00 | 0.00 | | 0.01 | 0.01 | 0.01 | 0.01 |
| Mg | 0.33 | 0.35 | 0.36 | 0.37 | 0.38 | 0.38 | 1.88 | 1.88 | 1.98 | | 0.15 | 0.19 | 0.22 | 0.34 | 0.36 | 1.82 | 1.87 | | 0.93 | 0.30 | 0.36 | 0.35 |
| Ni | 0.00 | 0.00 | 0.00 | 0.00 | 0.00 | 0.00 | 0.01 | 0.01 | 0.01 | | 0.00 | 0.00 | 0.00 | 0.00 | 0.00 | 0.01 | 0.01 | | 0.01 | 0.00 | 0.00 | 0.00 |
| Zn | 0.01 | 0.00 | 0.01 | 0.01 | 0.00 | 0.00 | 0.00 | 0.00 | 0.00 | | 0.00 | 0.01 | 0.01 | 0.00 | 0.01 | 0.00 | 0.00 | | 0.00 | 0.01 | 0.00 | 0.00 |

Tab. A3.9 GR63B GRID 2 (Nea Roda)microprobe analyses of olivine and chromite crystals; d(mm) distance from the intergranular limit

| Analysis | GRID1-6 | GRID2-2 | GRID2-3 | GRID2-7 | GRID2-8 | GRID2-9 | GRID3-3 | GRID3-5 | GRID3-6 | GRID3-7 | GRID3-8 | GRID4-6 | GRID4-7 | GRID4-8 | GRID4-9 | GRID5-1 | GRID5-2 | GRID5-3 | GRID5-5 | GRID5-7 |
|---|---|---|---|---|---|---|---|---|---|---|---|---|---|---|---|---|---|---|---|---|
| | 200-OL | 205-OL | 206-OL | 210-CHR | 211-CHR | 212-CHR | 215-OL | 217-FeCHR | 218-CHR | 219-CHR | 220-CHR | 227-CHR | 228-CHR | 229-CHR | 230-CHR | 231-OL | 232-CHR | 233-CHR | 235-OL | 237-CHR |
| X | 40.93 | 41.03 | 41.03 | 41.03 | 41.03 | 41.03 | 41.13 | 41.13 | 41.13 | 41.13 | 41.13 | 41.23 | 41.23 | 41.23 | 41.23 | 41.33 | 41.33 | 41.33 | 41.33 | 41.33 |
| Y | 94.02 | 93.62 | 93.72 | 94.12 | 94.22 | 94.32 | 93.72 | 93.92 | 94.02 | 94.12 | 94.22 | 94.02 | 94.12 | 94.22 | 94.32 | 93.52 | 93.62 | 93.72 | 93.92 | 94.12 |
| d (mm) | 0.11 | 0.26 | 0.17 | 0.01 | 0.05 | 0.02 | 0.09 | 0.06 | 0.10 | 0.15 | 0.08 | 0.04 | 0.09 | 0.17 | 0.06 | 0.07 | 0.01 | 0.02 | 0.08 | 0.03 |
| $SiO_2$ | 41.28 | 41.66 | 42.11 | 0.06 | 0.03 | 0.03 | 41.51 | 0.04 | 0.01 | 0.00 | 0.03 | 0.03 | 0.00 | 0.01 | 0.00 | 41.61 | 0.07 | 0.08 | 41.68 | 0.03 |
| $TiO_2$ | 0.01 | 0.00 | 0.02 | 0.25 | 0.17 | 0.18 | 0.00 | 0.20 | 0.15 | 0.16 | 0.23 | 0.14 | 0.16 | 0.16 | 0.13 | 0.03 | 0.20 | 0.19 | 0.00 | 0.21 |
| $Al_2O_3$ | 0.00 | 0.01 | 0.00 | 13.42 | 12.99 | 12.95 | 0.03 | 3.92 | 13.41 | 13.05 | 13.00 | 13.30 | 13.05 | 12.94 | 12.85 | 0.00 | 13.32 | 13.15 | 0.00 | 13.24 |
| $Cr_2O_3$ | 0.06 | 0.00 | 0.00 | 52.82 | 53.21 | 53.77 | 0.04 | 61.02 | 53.43 | 54.58 | 54.35 | 53.93 | 54.23 | 54.13 | 54.61 | 0.06 | 52.63 | 53.35 | 0.05 | 53.66 |
| $V_2O_3$ | 0.00 | 0.00 | 0.00 | 0.06 | 0.09 | 0.10 | 0.00 | 0.11 | 0.11 | 0.08 | 0.11 | 0.09 | 0.10 | 0.09 | 0.04 | 0.00 | 0.11 | 0.15 | 0.00 | 0.08 |
| $Fe_2O_3$ | 0.00 | 0.00 | 0.00 | 4.33 | 4.17 | 4.02 | 0.00 | 5.04 | 3.88 | 3.81 | 3.51 | 3.91 | 3.84 | 4.30 | 3.63 | 0.00 | 4.73 | 3.81 | 0.00 | 4.28 |
| FeO | 6.60 | 6.72 | 6.70 | 20.98 | 20.60 | 21.01 | 6.22 | 23.96 | 20.70 | 20.72 | 20.75 | 21.03 | 20.50 | 20.02 | 20.75 | 6.57 | 21.28 | 20.69 | 6.43 | 21.06 |
| MnO | 0.08 | 0.06 | 0.12 | 0.28 | 0.32 | 0.26 | 0.10 | 0.35 | 0.24 | 0.26 | 0.26 | 0.30 | 0.25 | 0.23 | 0.25 | 0.10 | 0.28 | 0.16 | 0.08 | 0.17 |
| MgO | 51.66 | 52.07 | 51.53 | 8.66 | 8.74 | 8.53 | 51.82 | 5.51 | 8.80 | 8.92 | 8.89 | 8.62 | 9.01 | 9.26 | 8.81 | 51.51 | 8.44 | 8.84 | 51.92 | 8.71 |
| NiO | 0.38 | 0.46 | 0.35 | 0.06 | 0.11 | 0.07 | 0.47 | 0.04 | 0.05 | 0.05 | 0.00 | 0.09 | 0.07 | 0.04 | 0.03 | 0.39 | 0.09 | 0.03 | 0.33 | 0.08 |
| ZnO | 0.00 | 0.02 | 0.00 | 0.26 | 0.01 | 0.27 | 0.00 | 0.19 | 0.13 | 0.12 | 0.11 | 0.23 | 0.00 | 0.21 | 0.00 | 0.00 | 0.32 | 0.16 | 0.19 | 0.32 |
| TOT | 100.07 | 101.01 | 100.84 | 101.20 | 100.43 | 101.19 | 100.19 | 100.38 | 100.92 | 101.77 | 101.25 | 101.66 | 101.20 | 101.41 | 101.11 | 100.29 | 101.47 | 100.63 | 100.71 | 101.85 |
| Si | 1.00 | 1.00 | 1.01 | 0.00 | 0.00 | 0.00 | 1.00 | 0.00 | 0.00 | 0.00 | 0.00 | 0.00 | 0.00 | 0.00 | 0.00 | 1.00 | 0.00 | 0.00 | 1.00 | 0.00 |
| Ti | 0.00 | 0.00 | 0.00 | 0.01 | 0.00 | 0.00 | 0.00 | 0.01 | 0.00 | 0.00 | 0.01 | 0.00 | 0.00 | 0.00 | 0.00 | 0.00 | 0.00 | 0.00 | 0.00 | 0.01 |
| Al | 0.00 | 0.00 | 0.00 | 0.52 | 0.50 | 0.50 | 0.00 | 0.16 | 0.52 | 0.50 | 0.50 | 0.51 | 0.50 | 0.49 | 0.49 | 0.00 | 0.51 | 0.51 | 0.00 | 0.51 |
| Cr | 0.00 | 0.00 | 0.00 | 1.36 | 1.38 | 1.39 | 0.00 | 1.69 | 1.38 | 1.40 | 1.40 | 1.38 | 1.40 | 1.39 | 1.41 | 0.00 | 1.36 | 1.38 | 0.00 | 1.38 |
| V | 0.00 | 0.00 | 0.00 | 0.00 | 0.00 | 0.00 | 0.00 | 0.00 | 0.00 | 0.00 | 0.00 | 0.00 | 0.00 | 0.00 | 0.00 | 0.00 | 0.00 | 0.00 | 0.00 | 0.00 |

| | | | | | | | | | | | | | | | | | | | | |
|---|---|---|---|---|---|---|---|---|---|---|---|---|---|---|---|---|---|---|---|---|
| $Fe^{3+}$ | 0.00 | 0.00 | 0.00 | 0.11 | 0.10 | 0.10 | 0.00 | 0.13 | 0.10 | 0.09 | 0.09 | 0.10 | 0.09 | 0.10 | 0.09 | 0.00 | 0.12 | 0.09 | 0.00 | 0.10 |
| $Fe^{2+}$ | 0.13 | 0.13 | 0.13 | 0.57 | 0.57 | 0.57 | 0.13 | 0.70 | 0.56 | 0.56 | 0.56 | 0.57 | 0.56 | 0.54 | 0.57 | 0.13 | 0.58 | 0.57 | 0.13 | 0.57 |
| Mn | 0.00 | 0.00 | 0.00 | 0.01 | 0.01 | 0.01 | 0.00 | 0.01 | 0.01 | 0.01 | 0.01 | 0.01 | 0.01 | 0.01 | 0.01 | 0.00 | 0.01 | 0.00 | 0.00 | 0.00 |
| Mg | 1.86 | 1.86 | 1.84 | 0.42 | 0.43 | 0.42 | 1.86 | 0.29 | 0.43 | 0.43 | 0.43 | 0.42 | 0.44 | 0.45 | 0.43 | 1.85 | 0.41 | 0.43 | 1.86 | 0.42 |
| Ni | 0.01 | 0.01 | 0.01 | 0.00 | 0.00 | 0.00 | 0.01 | 0.00 | 0.00 | 0.00 | 0.00 | 0.00 | 0.00 | 0.00 | 0.00 | 0.01 | 0.00 | 0.00 | 0.01 | 0.00 |
| Zn | 0.00 | 0.00 | 0.00 | 0.01 | 0.00 | 0.01 | 0.00 | 0.00 | 0.00 | 0.00 | 0.00 | 0.01 | 0.00 | 0.00 | 0.00 | 0.00 | 0.01 | 0.00 | 0.00 | 0.01 |

| Analysis | GRID5-8 | GRID5-9 | GRID6-1 | GRID6-2 | GRID6-3 | GRID6-4 | GRID6-5 | GRID6-8 | GRID6-9 | GRID7-1 | GRID7-3 | GRID7-4 | GRID7-8 | GRID7-9 | GRID8-6 | GRID8-7 | GRID8-8 | GRID9-1 | GRID9-2 | GRID9-3 |
|---|---|---|---|---|---|---|---|---|---|---|---|---|---|---|---|---|---|---|---|---|
| | 238-CHR | 239-CHR | 240-OL | 241-CHR | 242-CHR | 243-CHR | 244-OL | 247-CHR | 248-CHR | 249-OL | 251-CHR | 252-CHR | 256-CHR | 257-CHR | 263-OL | 264-OL | 265-OL | 267-CHR | 268-OL | 269-OL |
| X | 41.33 | 41.33 | 41.43 | 41.43 | 41.43 | 41.43 | 41.43 | 41.43 | 41.43 | 41.53 | 41.53 | 41.53 | 41.53 | 41.53 | 41.63 | 41.63 | 41.63 | 41.73 | 41.73 | 41.73 |
| Y | 94.22 | 94.32 | 93.52 | 93.62 | 93.72 | 93.82 | 93.92 | 94.22 | 94.32 | 93.52 | 93.72 | 93.82 | 94.22 | 94.32 | 94.02 | 94.12 | 94.22 | 93.52 | 93.62 | 93.72 |
| d (mm) | 0.13 | 0.12 | 0.04 | 0.08 | 0.10 | 0.01 | 0.09 | 0.09 | 0.07 | 0.08 | 0.02 | 0.00 | 0.02 | 0.02 | 0.19 | 0.12 | 0.07 | 0.04 | 0.19 | 0.16 |
| $SiO_2$ | 0.00 | 0.11 | 41.60 | 0.00 | 0.04 | 0.15 | 41.59 | 0.04 | 0.05 | 41.57 | 0.02 | 0.13 | 0.07 | 0.01 | 41.93 | 41.78 | 41.70 | 0.00 | 41.55 | 41.54 |
| $TiO_2$ | 0.22 | 0.20 | 0.00 | 0.17 | 0.14 | 0.22 | 0.00 | 0.15 | 0.23 | 0.04 | 0.14 | 0.24 | 0.20 | 0.22 | 0.00 | 0.02 | 0.00 | 0.18 | 0.00 | 0.00 |
| $Al_2O_3$ | 13.09 | 12.82 | 0.02 | 13.28 | 13.17 | 12.65 | 0.00 | 13.12 | 13.29 | 0.00 | 13.26 | 10.93 | 13.14 | 13.25 | 0.00 | 0.00 | 0.01 | 13.29 | 0.06 | 0.00 |
| $Cr_2O_3$ | 54.83 | 54.51 | 0.08 | 54.14 | 53.98 | 53.49 | 0.02 | 54.51 | 54.00 | 0.06 | 53.95 | 52.83 | 53.64 | 54.34 | 0.00 | 0.03 | 0.09 | 53.28 | 0.03 | 0.01 |
| $V_2O_3$ | 0.08 | 0.11 | 0.00 | 0.10 | 0.07 | 0.11 | 0.00 | 0.11 | 0.11 | 0.00 | 0.12 | 0.13 | 0.11 | 0.10 | 0.00 | 0.00 | 0.00 | 0.10 | 0.00 | 0.00 |
| $Fe_2O_3$ | 3.51 | 3.37 | 0.00 | 3.62 | 4.06 | 4.44 | 0.00 | 3.79 | 3.86 | 0.00 | 3.85 | 6.23 | 4.29 | 4.07 | 0.00 | 0.00 | 0.00 | 3.90 | 0.00 | 0.00 |
| FeO | 20.62 | 20.93 | 6.32 | 21.15 | 20.94 | 21.28 | 6.62 | 20.97 | 20.82 | 6.65 | 21.18 | 22.08 | 21.44 | 21.42 | 6.75 | 6.56 | 6.47 | 21.00 | 6.48 | 6.44 |
| MnO | 0.18 | 0.17 | 0.13 | 0.24 | 0.20 | 0.27 | 0.14 | 0.21 | 0.25 | 0.13 | 0.35 | 0.31 | 0.32 | 0.24 | 0.09 | 0.15 | 0.07 | 0.30 | 0.11 | 0.09 |
| MgO | 9.09 | 8.90 | 51.71 | 8.58 | 8.77 | 8.43 | 51.61 | 8.93 | 8.89 | 52.00 | 8.64 | 7.65 | 8.48 | 8.67 | 52.04 | 52.28 | 51.60 | 8.49 | 51.60 | 51.65 |
| NiO | 0.06 | 0.01 | 0.39 | 0.04 | 0.02 | 0.08 | 0.42 | 0.03 | 0.11 | 0.40 | 0.00 | 0.05 | 0.06 | 0.06 | 0.44 | 0.43 | 0.45 | 0.05 | 0.44 | 0.36 |
| ZnO | 0.08 | 0.01 | 0.11 | 0.24 | 0.25 | 0.39 | 0.04 | 0.00 | 0.19 | 0.00 | 0.00 | 0.22 | 0.14 | 0.12 | 0.00 | 0.00 | 0.00 | 0.22 | 0.03 | 0.09 |
| TOT | 101.77 | 101.16 | 100.36 | 101.57 | 101.64 | 101.52 | 100.46 | 101.88 | 101.84 | 100.86 | 101.52 | 100.80 | 101.91 | 102.51 | 101.25 | 101.25 | 100.42 | 100.81 | 100.32 | 100.19 |
| Si | 0.00 | 0.00 | 1.00 | 0.00 | 0.00 | 0.00 | 1.00 | 0.00 | 0.00 | 1.00 | 0.00 | 0.00 | 0.00 | 0.00 | 1.00 | 1.00 | 1.00 | 0.00 | 1.00 | 1.00 |
| Ti | 0.01 | 0.00 | 0.00 | 0.00 | 0.00 | 0.01 | 0.00 | 0.00 | 0.01 | 0.00 | 0.00 | 0.01 | 0.00 | 0.01 | 0.00 | 0.00 | 0.00 | 0.00 | 0.00 | 0.00 |
| Al | 0.50 | 0.49 | 0.00 | 0.51 | 0.50 | 0.49 | 0.00 | 0.50 | 0.51 | 0.00 | 0.51 | 0.43 | 0.50 | 0.50 | 0.00 | 0.00 | 0.00 | 0.51 | 0.00 | 0.00 |
| Cr | 1.40 | 1.40 | 0.00 | 1.39 | 1.39 | 1.38 | 0.00 | 1.39 | 1.38 | 0.00 | 1.39 | 1.39 | 1.38 | 1.38 | 0.00 | 0.00 | 0.00 | 1.38 | 0.00 | 0.00 |
| V | 0.00 | 0.00 | 0.00 | 0.00 | 0.00 | 0.00 | 0.00 | 0.00 | 0.00 | 0.00 | 0.00 | 0.00 | 0.00 | 0.00 | 0.00 | 0.00 | 0.00 | 0.00 | 0.00 | 0.00 |
| $Fe^{3+}$ | 0.09 | 0.08 | 0.00 | 0.09 | 0.10 | 0.11 | 0.00 | 0.09 | 0.09 | 0.00 | 0.09 | 0.16 | 0.10 | 0.10 | 0.00 | 0.00 | 0.00 | 0.10 | 0.00 | 0.00 |
| $Fe^{2+}$ | 0.56 | 0.57 | 0.13 | 0.58 | 0.57 | 0.58 | 0.13 | 0.57 | 0.56 | 0.13 | 0.58 | 0.62 | 0.58 | 0.58 | 0.13 | 0.13 | 0.13 | 0.57 | 0.13 | 0.13 |
| Mn | 0.00 | 0.00 | 0.00 | 0.01 | 0.01 | 0.01 | 0.00 | 0.01 | 0.01 | 0.00 | 0.01 | 0.01 | 0.01 | 0.01 | 0.00 | 0.00 | 0.00 | 0.01 | 0.00 | 0.00 |
| Mg | 0.44 | 0.43 | 1.86 | 0.42 | 0.42 | 0.41 | 1.85 | 0.43 | 0.43 | 1.86 | 0.42 | 0.38 | 0.41 | 0.42 | 1.85 | 1.86 | 1.85 | 0.41 | 1.85 | 1.86 |
| Ni | 0.00 | 0.00 | 0.01 | 0.00 | 0.00 | 0.00 | 0.01 | 0.00 | 0.00 | 0.01 | 0.00 | 0.00 | 0.00 | 0.00 | 0.01 | 0.01 | 0.01 | 0.00 | 0.01 | 0.01 |
| Zn | 0.00 | 0.00 | 0.00 | 0.01 | 0.01 | 0.01 | 0.00 | 0.00 | 0.00 | 0.00 | 0.00 | 0.01 | 0.00 | 0.00 | 0.00 | 0.00 | 0.00 | 0.01 | 0.00 | 0.00 |

| Analysis | GRID9-6 | GRID9-7 | GRID9-8 | GR63B-50 | GR63B-51 | GR63B-52 | d-CHR | GR63B-53 | GR63B-54 | GR63B-55 | GR63B-56 | GR63B-57 | GR63B-58 | GR63B-59 | GR63B-60 | GR63B-61 | d-CHR | GR63B-63 | GR63B-64 | GR63B-65 |
|---|---|---|---|---|---|---|---|---|---|---|---|---|---|---|---|---|---|---|---|---|
| | 272-OL | 273-OL | 274-OL | 148-OL | 149-OL | 150-OL | | oliv-bad | 152-CHR | 153-CHR | 154-CHR | 155-CHR | 156-CHR | 157-OL | 158-OL | 159-OL | | 161-CHR | 162-CHR | 163-CHR |
| X | 41.73 | 41.73 | 41.73 | 13.35 | 13.33 | 13.33 | 13.32 | 13.32 | 13.32 | 13.32 | 13.31 | 13.30 | 13.28 | 13.33 | 13.32 | 13.30 | 13.28 | 13.28 | 13.28 | 13.27 |
| Y | 94.02 | 94.12 | 94.22 | 95.99 | 96.00 | 96.02 | 96.02 | 96.03 | 96.03 | 96.03 | 96.04 | 96.04 | 96.07 | 95.96 | 95.96 | 95.98 | 95.98 | 95.99 | 95.99 | 95.99 |
| d (mm) | 0.25 | 0.20 | 0.16 | 0.04 | 0.02 | 0.01 | | | 0.01 | 0.01 | 0.02 | 0.03 | 0.06 | 0.05 | 0.04 | 0.02 | | 0.01 | 0.01 | 0.02 |
| $SiO_2$ | 41.63 | 41.76 | 41.93 | 0.04 | 0.02 | 0.01 | | 0.00 | 0.01 | 0.01 | 0.02 | 0.03 | 0.06 | 0.05 | 0.04 | 0.02 | | 0.01 | 0.01 | 0.02 |
| $TiO_2$ | 0.01 | 0.00 | 0.00 | 29.45 | 40.44 | 39.47 | | 40.10 | 0.12 | 0.01 | 0.03 | 0.02 | 0.00 | 40.38 | 40.65 | 40.51 | | 0.10 | 0.02 | 0.03 |
| $Al_2O_3$ | 0.00 | 0.00 | 0.00 | 0.03 | 0.01 | 0.00 | | 0.00 | 0.26 | 0.31 | 0.22 | 0.17 | 0.18 | 0.00 | 0.04 | 0.00 | | 0.22 | 0.28 | 0.19 |
| $Cr_2O_3$ | 0.05 | 0.02 | 0.02 | 1.08 | 0.02 | 0.00 | | 0.04 | 6.57 | 11.14 | 13.17 | 13.58 | 13.44 | 0.01 | 0.00 | 0.00 | | 6.96 | 10.84 | 13.42 |
| $V_2O_3$ | 0.00 | 0.00 | 0.00 | 0.14 | 0.23 | 0.35 | | 0.86 | 57.15 | 53.83 | 53.77 | 54.38 | 54.53 | 0.18 | 0.21 | 0.49 | | 58.29 | 55.05 | 54.38 |
| $Fe_2O_3$ | 0.00 | 0.00 | 0.00 | 0.00 | 0.00 | 0.00 | | 0.04 | 0.13 | 0.07 | 0.13 | 0.15 | 0.04 | 0.00 | 0.00 | 0.00 | | 0.13 | 0.09 | 0.08 |
| FeO | 6.68 | 6.47 | 6.59 | 0.00 | 0.00 | 0.00 | | 0.00 | 6.61 | 5.43 | 3.89 | 3.33 | 3.17 | 0.00 | 0.00 | 0.00 | | 5.60 | 5.13 | 3.67 |
| MnO | 0.10 | 0.03 | 0.10 | 6.32 | 6.71 | 6.42 | | 3.80 | 23.51 | 22.68 | 22.11 | 21.71 | 21.13 | 6.39 | 6.75 | 6.28 | | 22.87 | 22.56 | 21.70 |
| MgO | 51.65 | 51.78 | 52.10 | 0.09 | 0.11 | 0.07 | | 0.05 | 0.38 | 0.22 | 0.22 | 0.29 | 0.28 | 0.11 | 0.10 | 0.13 | | 0.32 | 0.34 | 0.29 |

# Appendix: Chapter 3

| | | | | | | | | | | | | | | | | | | | |
|---|---|---|---|---|---|---|---|---|---|---|---|---|---|---|---|---|---|---|---|
| NiO | 0.42 | 0.46 | 0.39 | 50.19 | 51.37 | 51.11 | | 38.81 | 6.39 | 7.47 | 8.16 | 8.51 | 8.54 | 51.55 | 51.56 | 51.20 | | 6.84 | 7.59 | 8.38 |
| ZnO | 0.02 | 0.00 | 0.00 | 0.04 | 0.02 | 0.00 | | 0.02 | 0.01 | 0.01 | 0.00 | 0.00 | 0.03 | 0.01 | 0.01 | 0.00 | | 0.00 | 0.01 | 0.01 |
| TOT | 100.56 | 100.52 | 101.16 | 87.69 | 99.38 | 97.89 | | 83.89 | 101.32 | 101.29 | 101.80 | 102.18 | 101.74 | 99.22 | 99.76 | 99.06 | | 101.63 | 102.05 | 102.51 |
| Si | 1.00 | 1.00 | 1.00 | 0.79 | 0.98 | 0.97 | | 1.18 | 0.00 | 0.00 | 0.00 | 0.00 | 0.00 | 0.98 | 0.98 | 0.99 | | 0.00 | 0.00 | 0.00 |
| Ti | 0.00 | 0.00 | 0.00 | 0.00 | 0.00 | 0.00 | | 0.00 | 0.01 | 0.01 | 0.01 | 0.00 | 0.00 | 0.00 | 0.00 | 0.00 | | 0.01 | 0.01 | 0.00 |
| Al | 0.00 | 0.00 | 0.00 | 0.03 | 0.00 | 0.00 | | 0.00 | 0.26 | 0.44 | 0.51 | 0.52 | 0.51 | 0.00 | 0.00 | 0.00 | | 0.28 | 0.42 | 0.51 |
| Cr | 0.00 | 0.00 | 0.00 | 0.00 | 0.00 | 0.01 | | 0.02 | 1.54 | 1.41 | 1.38 | 1.39 | 1.40 | 0.00 | 0.00 | 0.01 | | 1.56 | 1.43 | 1.39 |
| V | 0.00 | 0.00 | 0.00 | 0.00 | 0.00 | 0.00 | | 0.00 | 0.00 | 0.00 | 0.00 | 0.00 | 0.00 | 0.00 | 0.00 | 0.00 | | 0.00 | 0.00 | 0.00 |
| $Fe^{3+}$ | 0.00 | 0.00 | 0.00 | 0.00 | 0.00 | 0.00 | | 0.00 | 0.17 | 0.14 | 0.10 | 0.08 | 0.08 | 0.00 | 0.00 | 0.00 | | 0.14 | 0.13 | 0.09 |
| $Fe^{2+}$ | 0.13 | 0.13 | 0.13 | 0.14 | 0.14 | 0.13 | | 0.09 | 0.67 | 0.63 | 0.60 | 0.59 | 0.57 | 0.13 | 0.14 | 0.13 | | 0.65 | 0.62 | 0.59 |
| Mn | 0.00 | 0.00 | 0.00 | 0.00 | 0.00 | 0.00 | | 0.00 | 0.01 | 0.01 | 0.01 | 0.01 | 0.01 | 0.00 | 0.00 | 0.00 | | 0.01 | 0.01 | 0.01 |
| Mg | 1.85 | 1.86 | 1.86 | 2.02 | 1.86 | 1.88 | | 1.70 | 0.32 | 0.37 | 0.40 | 0.41 | 0.41 | 1.87 | 1.86 | 1.86 | | 0.34 | 0.37 | 0.40 |
| Ni | 0.01 | 0.01 | 0.01 | 0.01 | 0.01 | 0.01 | | 0.00 | 0.00 | 0.00 | 0.00 | 0.00 | 0.00 | 0.01 | 0.01 | 0.01 | | 0.00 | 0.00 | 0.00 |
| Zn | 0.00 | 0.00 | 0.00 | 0.00 | 0.00 | 0.00 | | 0.00 | 0.00 | 0.00 | 0.00 | 0.00 | 0.01 | 0.00 | 0.00 | 0.00 | | 0.01 | 0.00 | 0.01 |

| Analysis | GR63B-66 | GR63B-67 | GR63B-68 | GR63B-69 | GR63B-70 | d-CHR | GR63B-71 | GR63B-72 | GR63B-73 | GR63B-74 | GR63B-75 | GR63B-76 | d-CHR | GR63B-77 | GR63B-78 | GR63B-79 | GR63B-80 | GR63B-81 | d-CHR | GR63B-82 |
|---|---|---|---|---|---|---|---|---|---|---|---|---|---|---|---|---|---|---|---|---|
| | 164-CHR | 165-CHR | 166-OL | 167-OL | 168-OL | | 169-CHR | 170-CHR | 171-CHR | 172-CHR | 173-CHR | 174-CHR | | 175-OL | 176-OL | 177-OL | 178-OL | 179-OL | | 180-CHR |
| X | 13.26 | 13.23 | 13.64 | 13.62 | 13.60 | 13.58 | 13.57 | 13.57 | 13.55 | 13.51 | 13.25 | 13.26 | 13.27 | 13.29 | 13.30 | 13.33 | 13.36 | 13.39 | 13.42 | 13.42 |
| Y | 96.00 | 96.02 | 96.18 | 96.18 | 96.18 | 96.18 | 96.19 | 96.19 | 96.19 | 96.19 | 95.93 | 95.93 | 95.92 | 95.92 | 95.90 | 95.88 | 95.85 | 95.81 | 95.77 | 95.77 |
| d (mm) | 0.03 | 0.07 | 0.06 | 0.04 | 0.03 | | | 0.01 | 0.03 | 0.07 | 0.02 | | | 0.02 | 0.04 | 0.08 | 0.10 | | | 0.01 |
| $SiO_2$ | 0.03 | 0.07 | 0.06 | 0.04 | 0.03 | | 0.00 | 0.01 | 0.03 | 0.07 | 0.02 | 0.00 | | 0.02 | 0.04 | 0.08 | 0.10 | 0.05 | | 0.01 |
| $TiO_2$ | 0.00 | 0.04 | 39.82 | 39.84 | 41.01 | | 33.59 | 0.06 | 0.04 | 0.04 | 0.04 | 4.29 | | 36.81 | 40.29 | 40.29 | 40.28 | 15.12 | | 0.03 |
| $Al_2O_3$ | 0.28 | 0.14 | 0.01 | 0.04 | 0.00 | | 0.00 | 0.34 | 0.21 | 0.18 | 0.18 | 0.05 | | 0.00 | 0.01 | 0.00 | 0.03 | 0.01 | | 0.21 |
| $Cr_2O_3$ | 13.63 | 13.46 | 0.00 | 0.01 | 0.00 | | 0.01 | 7.56 | 13.42 | 13.37 | 13.07 | 0.88 | | 0.03 | 0.02 | 0.00 | 0.00 | 0.01 | | 12.86 |
| $V_2O_3$ | 54.63 | 54.88 | 0.06 | 0.08 | 0.23 | | 0.86 | 57.47 | 54.10 | 54.91 | 53.78 | 20.49 | | 0.34 | 0.26 | 0.01 | 0.09 | 0.09 | | 53.57 |
| $Fe_2O_3$ | 0.10 | 0.09 | 0.00 | 0.00 | 0.00 | | 0.00 | 0.14 | 0.15 | 0.06 | 0.11 | 0.03 | | 0.00 | 0.00 | 0.00 | 0.00 | 0.00 | | 0.07 |
| FeO | 2.94 | 3.03 | 0.00 | 0.00 | 0.00 | | 0.00 | 5.21 | 3.22 | 2.80 | 4.05 | 42.31 | | 0.00 | 0.00 | 0.00 | 0.00 | 0.00 | | 4.26 |
| MnO | 21.92 | 21.21 | 6.52 | 6.69 | 6.47 | | 3.96 | 24.29 | 22.05 | 22.11 | 22.07 | -16.78 | | 5.59 | 6.69 | 6.72 | 6.61 | 6.13 | | 22.46 |
| MgO | 0.22 | 0.21 | 0.11 | 0.13 | 0.05 | | 0.02 | 0.27 | 0.14 | 0.14 | 0.18 | 0.20 | | 0.10 | 0.12 | 0.11 | 0.05 | 0.13 | | 0.25 |
| NiO | 8.42 | 8.65 | 50.74 | 51.33 | 50.07 | | 39.88 | 6.15 | 8.17 | 8.27 | 8.17 | 31.34 | | 49.25 | 50.92 | 51.16 | 51.02 | 36.92 | | 7.74 |
| ZnO | 0.00 | 0.02 | 0.00 | 0.00 | 0.01 | | 0.02 | 0.00 | 0.00 | 0.00 | 0.00 | 0.07 | | 0.03 | 0.01 | 0.01 | 0.00 | 0.20 | | 0.02 |
| TOT | 102.29 | 102.09 | 97.69 | 98.51 | 98.44 | | 78.39 | 101.65 | 101.77 | 101.97 | 101.76 | 83.23 | | 92.57 | 98.73 | 98.78 | 98.57 | 59.18 | | 101.76 |
| Si | 0.00 | 0.00 | 0.98 | 0.98 | 1.01 | | 1.04 | 0.00 | 0.00 | 0.00 | 0.00 | 0.15 | | 0.95 | 0.99 | 0.99 | 0.99 | 0.60 | | 0.00 |
| Ti | 0.01 | 0.00 | 0.00 | 0.00 | 0.00 | | 0.00 | 0.01 | 0.01 | 0.00 | 0.00 | 0.00 | | 0.00 | 0.00 | 0.00 | 0.00 | 0.00 | | 0.01 |
| Al | 0.52 | 0.51 | 0.00 | 0.00 | 0.00 | | 0.00 | 0.30 | 0.51 | 0.51 | 0.50 | 0.04 | | 0.00 | 0.00 | 0.00 | 0.00 | 0.00 | | 0.50 |
| Cr | 1.39 | 1.40 | 0.00 | 0.00 | 0.00 | | 0.02 | 1.54 | 1.39 | 1.41 | 1.38 | 0.56 | | 0.01 | 0.01 | 0.00 | 0.00 | 0.00 | | 1.39 |
| V | 0.00 | 0.00 | 0.00 | 0.00 | 0.00 | | 0.00 | 0.00 | 0.00 | 0.00 | 0.00 | 0.00 | | 0.00 | 0.00 | 0.00 | 0.00 | 0.00 | | 0.00 |
| $Fe^{3+}$ | 0.07 | 0.07 | 0.00 | 0.00 | 0.00 | | 0.00 | 0.13 | 0.08 | 0.07 | 0.10 | 1.10 | | 0.00 | 0.00 | 0.00 | 0.00 | 0.00 | | 0.10 |
| $Fe^{2+}$ | 0.59 | 0.57 | 0.13 | 0.14 | 0.13 | | 0.10 | 0.69 | 0.60 | 0.60 | 0.60 | -0.49 | | 0.12 | 0.14 | 0.14 | 0.14 | 0.20 | | 0.61 |
| Mn | 0.01 | 0.01 | 0.00 | 0.00 | 0.00 | | 0.00 | 0.01 | 0.00 | 0.00 | 0.00 | 0.01 | | 0.00 | 0.00 | 0.00 | 0.00 | 0.00 | | 0.01 |
| Mg | 0.41 | 0.42 | 1.87 | 1.87 | 1.84 | | 1.84 | 0.31 | 0.40 | 0.40 | 0.40 | 1.62 | | 1.90 | 1.86 | 1.87 | 1.86 | 2.17 | | 0.38 |
| Ni | 0.00 | 0.00 | 0.01 | 0.01 | 0.01 | | 0.00 | 0.00 | 0.00 | 0.00 | 0.00 | 0.01 | | 0.01 | 0.01 | 0.01 | 0.01 | 0.01 | | 0.00 |
| Zn | 0.00 | 0.01 | 0.00 | 0.00 | 0.00 | | 0.00 | 0.00 | 0.01 | 0.00 | 0.00 | 0.00 | | 0.00 | 0.00 | 0.00 | 0.00 | 0.00 | | 0.01 |

| Analysis | GR63B-83 | GR63B-84 | GR63B-85 | GR63B-86 | GR63B-87 | d-CHR | GR63B-88 | GR63B-89 | GR63B-90 | GR63B-91 | GR63B-92 | GR63B-93 | GR63B-94 | GR63B-95 | GR63B-96 | d-CHR | GR63B-97 | GR63B-98 | GR63B-99 | GR63B-100 | GR63B-101 |
|---|---|---|---|---|---|---|---|---|---|---|---|---|---|---|---|---|---|---|---|---|---|
| | 181-CHR | 182-CHR | 183-OL | 184-OL | 185-OL | | 186-CHR | 187-CHR | 188-CHR | 189-CHR | 190-CHR | 191-OL | 192-OL | 193-OL | 194-OL | | 195-CHR | 196-CHR | 197-CHR | 198-CHR | 199-CHR |
| X | 13.43 | 13.45 | 13.61 | 13.60 | 13.58 | 13.57 | 13.57 | 13.57 | 13.56 | 13.55 | 13.53 | 13.53 | 13.52 | 13.51 | 13.50 | 13.49 | 13.48 | 13.48 | 13.48 | 13.47 | 13.46 |
| Y | 95.76 | 95.74 | 95.78 | 95.76 | 95.75 | 95.74 | 95.74 | 95.74 | 95.73 | 95.72 | 95.71 | 95.44 | 95.46 | 95.48 | 95.50 | 95.52 | 95.52 | 95.53 | 95.53 | 95.54 | 95.55 |
| d (mm) | 0.02 | 0.05 | 0.06 | 0.03 | 0.01 | | 0.00 | 0.01 | 0.01 | 0.03 | 0.06 | 0.09 | 0.07 | 0.05 | 0.03 | | | 0.01 | 0.01 | 0.03 | 0.04 |
| $SiO_2$ | 0.02 | 0.05 | 0.06 | 0.03 | 0.01 | | 0.00 | 0.01 | 0.01 | 0.03 | 0.06 | 0.09 | 0.07 | 0.05 | 0.03 | | 0.00 | 0.01 | 0.01 | 0.03 | 0.04 |

| | | | | | | | | | | | | | | | | | | | |
|---|---|---|---|---|---|---|---|---|---|---|---|---|---|---|---|---|---|---|---|
| $TiO_2$ | 0.03 | 0.00 | 39.96 | 40.27 | 41.50 | 0.00 | 0.00 | 0.00 | 0.01 | 0.00 | 36.16 | 39.32 | 39.55 | 40.14 | 16.00 | 0.03 | 0.04 | 0.01 | 0.00 |
| $Al_2O_3$ | 0.15 | 0.19 | 0.03 | 0.03 | 0.00 | 0.28 | 0.16 | 0.24 | 0.20 | 0.19 | 0.00 | 0.02 | 0.01 | 0.00 | 0.00 | 0.24 | 0.19 | 0.19 | 0.14 |
| $Cr_2O_3$ | 13.10 | 13.10 | 0.00 | 0.02 | 0.01 | 9.96 | 12.90 | 13.70 | 13.54 | 13.61 | 0.00 | 0.00 | 0.00 | 0.00 | 0.12 | 7.03 | 12.39 | 13.12 | 13.28 |
| $V_2O_3$ | 54.22 | 54.78 | 0.02 | 0.15 | 0.43 | 54.43 | 53.22 | 53.11 | 54.16 | 54.22 | 0.00 | 0.04 | 0.08 | 0.24 | 12.16 | 56.28 | 54.11 | 53.86 | 54.23 |
| $Fe_2O_3$ | 0.16 | 0.10 | 0.00 | 0.00 | 0.00 | 0.12 | 0.06 | 0.05 | 0.10 | 0.11 | 0.00 | 0.00 | 0.00 | 0.00 | 0.00 | 0.18 | 0.10 | 0.14 | 0.11 |
| FeO | 3.37 | 2.97 | 0.00 | 0.00 | 0.00 | 5.76 | 4.83 | 4.15 | 3.56 | 3.38 | 0.00 | 0.00 | 0.00 | 0.00 | 30.75 | 6.06 | 4.72 | 3.96 | 3.66 |
| MnO | 21.56 | 21.84 | 6.49 | 6.46 | 6.68 | 23.22 | 22.22 | 21.56 | 21.95 | 21.56 | 6.33 | 6.70 | 6.66 | 6.91 | -7.17 | 23.76 | 22.28 | 21.45 | 21.79 |
| MgO | 0.22 | 0.27 | 0.06 | 0.04 | 0.09 | 0.31 | 0.27 | 0.24 | 0.31 | 0.28 | 0.04 | 0.12 | 0.09 | 0.05 | 0.07 | 0.35 | 0.24 | 0.27 | 0.19 |
| NiO | 8.30 | 8.19 | 51.25 | 51.33 | 42.72 | 6.79 | 7.85 | 8.46 | 8.27 | 8.41 | 49.69 | 51.30 | 51.06 | 51.20 | 35.39 | 5.82 | 7.90 | 8.38 | 8.37 |
| ZnO | 0.00 | 0.01 | 0.00 | 0.00 | 0.10 | 0.00 | 0.02 | 0.03 | 0.00 | 0.02 | 0.06 | 0.00 | 0.00 | 0.02 | 0.09 | 0.00 | 0.02 | 0.02 | 0.03 |
| TOT | 101.37 | 101.58 | 98.25 | 98.74 | 92.08 | 101.19 | 101.78 | 101.74 | 102.29 | 102.08 | 92.74 | 97.89 | 97.83 | 99.02 | 89.30 | 100.16 | 102.29 | 101.66 | 101.80 |
| Si | 0.00 | 0.00 | 0.98 | 0.98 | 1.11 | 0.00 | 0.00 | 0.00 | 0.00 | 0.00 | 0.94 | 0.97 | 0.98 | 0.98 | 0.49 | 0.00 | 0.00 | 0.00 | 0.00 |
| Ti | 0.00 | 0.00 | 0.00 | 0.00 | 0.00 | 0.01 | 0.00 | 0.01 | 0.00 | 0.00 | 0.00 | 0.00 | 0.00 | 0.00 | 0.00 | 0.01 | 0.00 | 0.00 | 0.00 |
| Al | 0.50 | 0.50 | 0.00 | 0.00 | 0.00 | 0.39 | 0.50 | 0.52 | 0.52 | 0.52 | 0.00 | 0.00 | 0.00 | 0.00 | 0.00 | 0.29 | 0.48 | 0.50 | 0.51 |
| Cr | 1.40 | 1.41 | 0.00 | 0.00 | 0.01 | 1.44 | 1.37 | 1.36 | 1.38 | 1.39 | 0.00 | 0.00 | 0.00 | 0.00 | 0.30 | 1.54 | 1.39 | 1.39 | 1.39 |
| V | 0.00 | 0.00 | 0.00 | 0.00 | 0.00 | 0.00 | 0.00 | 0.00 | 0.00 | 0.00 | 0.00 | 0.00 | 0.00 | 0.00 | 0.00 | 0.01 | 0.00 | 0.00 | 0.00 |
| $Fe^{3+}$ | 0.08 | 0.07 | 0.00 | 0.00 | 0.00 | 0.15 | 0.12 | 0.10 | 0.09 | 0.08 | 0.00 | 0.00 | 0.00 | 0.00 | 0.71 | 0.16 | 0.12 | 0.10 | 0.09 |
| $Fe^{2+}$ | 0.59 | 0.60 | 0.13 | 0.13 | 0.15 | 0.65 | 0.61 | 0.58 | 0.59 | 0.58 | 0.14 | 0.14 | 0.14 | 0.14 | -0.18 | 0.69 | 0.61 | 0.58 | 0.59 |
| Mn | 0.01 | 0.01 | 0.00 | 0.00 | 0.00 | 0.01 | 0.01 | 0.01 | 0.01 | 0.01 | 0.00 | 0.00 | 0.00 | 0.00 | 0.00 | 0.01 | 0.01 | 0.01 | 0.01 |
| Mg | 0.40 | 0.40 | 1.88 | 1.87 | 1.71 | 0.34 | 0.38 | 0.41 | 0.40 | 0.41 | 1.92 | 1.88 | 1.88 | 1.86 | 1.63 | 0.30 | 0.38 | 0.41 | 0.41 |
| Ni | 0.00 | 0.00 | 0.01 | 0.01 | 0.01 | 0.00 | 0.00 | 0.00 | 0.00 | 0.00 | 0.01 | 0.01 | 0.01 | 0.01 | 0.05 | 0.01 | 0.00 | 0.00 | 0.00 |
| Zn | 0.01 | 0.00 | 0.00 | 0.00 | 0.00 | 0.01 | 0.00 | 0.00 | 0.00 | 0.00 | 0.00 | 0.00 | 0.00 | 0.00 | 0.00 | 0.01 | 0.00 | 0.00 | 0.00 |

Tab. A3.10 GR62 (Nea Roda) microprobe analyses of olivine and chromite crystals; d(mm) distance from the intergranular limit

| Analysis | GR62-1 | GR62-2 | GR62-3 | GR62-4 | GR62-5 | GR62-6 | GR62-7 | GR62-8 | GR62-9 | GR62-10 | GR62-11 | GR62-12 | GR62-13 | bordo chr | GR62-15 | GR62-16 | GR62-17 | GR62-18 | GR62-19 | GR62-20 | GR62-21 |
|---|---|---|---|---|---|---|---|---|---|---|---|---|---|---|---|---|---|---|---|---|---|
| | CHR-254 | CHR-255 | CHR-256 | CHR-257 | CHR-258 | CHR-259 | CHR-260 | CHR-261 | CHR-262 | CHR-263 | CHR-264 | CHR-265 | CHR-266 | | OL-268 | OL-269 | OL-270 | OL-271 | OL-272 | OL-273 | OL-274 |
| X | 12.25 | 12.26 | 12.27 | 12.29 | 12.31 | 12.33 | 12.34 | 12.36 | 12.37 | 12.38 | 12.39 | 12.39 | 12.40 | 12.40 | 12.41 | 12.41 | 12.41 | 12.41 | 12.42 | 12.42 | 12.43 |
| Y | 67.02 | 67.03 | 67.04 | 67.07 | 67.09 | 67.13 | 67.14 | 67.16 | 67.18 | 67.20 | 67.21 | 67.21 | 67.22 | 67.22 | 67.23 | 67.23 | 67.23 | 67.23 | 67.24 | 67.25 | 67.25 |
| d (mm) | 0.25 | 0.24 | 0.22 | 0.19 | 0.16 | 0.11 | 0.10 | 0.07 | 0.05 | 0.03 | 0.02 | 0.01 | 0.00 | | 0.01 | 0.01 | 0.02 | 0.02 | 0.03 | 0.04 | 0.04 |
| $SiO_2$ | 0.00 | 0.00 | 0.02 | 0.00 | 0.04 | 0.06 | 0.00 | 0.03 | 0.02 | 0.00 | 0.04 | 0.51 | 0.11 | | 42.85 | 41.64 | 41.80 | 42.31 | 42.27 | 42.43 | 41.90 |
| $TiO_2$ | 0.20 | 0.13 | 0.18 | 0.12 | 0.16 | 0.19 | 0.15 | 0.13 | 0.18 | 0.13 | 0.16 | 0.19 | 0.24 | | 0.00 | 0.00 | 0.01 | 0.00 | 0.00 | 0.01 | 0.00 |
| $Al_2O_3$ | 13.65 | 13.60 | 13.60 | 13.76 | 13.72 | 13.71 | 13.60 | 13.83 | 13.82 | 13.78 | 11.65 | 10.05 | 6.65 | | 0.18 | 0.01 | 0.00 | 0.00 | 0.03 | 0.02 | 0.00 |
| $Cr_2O_3$ | 55.34 | 55.87 | 55.68 | 55.75 | 55.05 | 55.31 | 55.41 | 55.51 | 55.23 | 54.57 | 56.25 | 55.94 | 57.76 | | 0.66 | 0.47 | 0.31 | 0.29 | 0.20 | 0.15 | 0.12 |
| $V_2O_3$ | 0.00 | 0.00 | 0.00 | 0.00 | 0.00 | 0.00 | 0.00 | 0.00 | 0.00 | 0.00 | 0.00 | 0.00 | 0.00 | | 0.00 | 0.00 | 0.00 | 0.00 | 0.00 | 0.00 | 0.00 |
| $Fe_2O_3$ | 0.54 | 0.39 | 0.44 | 0.61 | 0.52 | 0.20 | 0.69 | 0.21 | 0.87 | 1.17 | 2.16 | 2.14 | 4.49 | | 0.00 | 0.00 | 0.00 | 0.00 | 0.00 | 0.00 | 0.00 |
| FeO | 23.60 | 23.60 | 23.69 | 23.59 | 23.75 | 23.94 | 24.00 | 24.40 | 24.38 | 24.90 | 25.27 | 25.49 | 25.68 | | 9.12 | 7.28 | 7.09 | 7.01 | 7.02 | 6.90 | 6.92 |
| MnO | 0.35 | 0.20 | 0.21 | 0.19 | 0.26 | 0.12 | 0.29 | 0.20 | 0.35 | 0.25 | 0.34 | 0.12 | 0.34 | | 0.07 | 0.15 | 0.14 | 0.10 | 0.16 | 0.07 | 0.13 |
| MgO | 6.94 | 6.98 | 7.02 | 7.11 | 6.87 | 6.86 | 6.76 | 6.58 | 6.60 | 6.18 | 5.83 | 5.75 | 4.77 | | 42.38 | 51.10 | 51.72 | 51.03 | 50.70 | 51.27 | 51.24 |
| NiO | 0.01 | 0.06 | 0.03 | 0.06 | 0.05 | 0.01 | 0.00 | 0.01 | 0.00 | 0.02 | 0.02 | 0.06 | 0.00 | | 0.45 | 0.32 | 0.41 | 0.36 | 0.38 | 0.33 | 0.35 |
| ZnO | 0.06 | 0.05 | 0.02 | 0.03 | 0.00 | 0.09 | 0.00 | 0.05 | 0.09 | 0.02 | 0.12 | 0.14 | 0.12 | | 0.00 | 0.04 | 0.04 | 0.02 | 0.00 | 0.00 | 0.00 |
| TOT | 100.68 | 100.90 | 100.88 | 101.21 | 100.41 | 100.50 | 100.92 | 100.96 | 101.55 | 101.06 | 101.85 | 100.41 | 100.19 | | 95.85 | 101.02 | 101.51 | 101.13 | 100.77 | 101.17 | 100.66 |
| Si | 0.00 | 0.00 | 0.00 | 0.00 | 0.00 | 0.00 | 0.00 | 0.00 | 0.00 | 0.00 | 0.00 | 0.02 | 0.00 | | 1.12 | 1.00 | 1.00 | 1.02 | 1.02 | 1.02 | 1.01 |
| Ti | 0.01 | 0.00 | 0.00 | 0.00 | 0.00 | 0.00 | 0.00 | 0.00 | 0.00 | 0.00 | 0.00 | 0.00 | 0.01 | | 0.00 | 0.00 | 0.00 | 0.00 | 0.00 | 0.00 | 0.00 |
| Al | 0.53 | 0.53 | 0.53 | 0.53 | 0.54 | 0.53 | 0.53 | 0.54 | 0.53 | 0.54 | 0.46 | 0.40 | 0.27 | | 0.01 | 0.00 | 0.00 | 0.00 | 0.00 | 0.00 | 0.00 |
| Cr | 1.45 | 1.46 | 1.45 | 1.45 | 1.44 | 1.45 | 1.45 | 1.45 | 1.43 | 1.43 | 1.48 | 1.50 | 1.59 | | 0.01 | 0.01 | 0.01 | 0.01 | 0.00 | 0.00 | 0.00 |
| V | 0.00 | 0.00 | 0.00 | 0.00 | 0.00 | 0.00 | 0.00 | 0.00 | 0.00 | 0.00 | 0.00 | 0.00 | 0.00 | | 0.00 | 0.00 | 0.00 | 0.00 | 0.00 | 0.00 | 0.00 |
| $Fe^{3+}$ | 0.01 | 0.01 | 0.01 | 0.02 | 0.01 | 0.01 | 0.02 | 0.01 | 0.02 | 0.03 | 0.05 | 0.05 | 0.12 | | 0.00 | 0.00 | 0.00 | 0.00 | 0.00 | 0.00 | 0.00 |
| $Fe^{2+}$ | 0.65 | 0.65 | 0.65 | 0.65 | 0.66 | 0.66 | 0.66 | 0.67 | 0.67 | 0.69 | 0.70 | 0.72 | 0.75 | | 0.20 | 0.15 | 0.14 | 0.14 | 0.14 | 0.14 | 0.14 |
| Mn | 0.01 | 0.01 | 0.01 | 0.01 | 0.01 | 0.00 | 0.01 | 0.01 | 0.01 | 0.01 | 0.01 | 0.00 | 0.01 | | 0.00 | 0.00 | 0.00 | 0.00 | 0.00 | 0.00 | 0.00 |
| Mg | 0.34 | 0.34 | 0.34 | 0.35 | 0.34 | 0.34 | 0.33 | 0.32 | 0.32 | 0.30 | 0.29 | 0.29 | 0.25 | | 1.65 | 1.83 | 1.84 | 1.83 | 1.82 | 1.83 | 1.84 |

| | | | | | | | | | | | | | | | | | | | | | |
|---|---|---|---|---|---|---|---|---|---|---|---|---|---|---|---|---|---|---|---|---|---|
| Ni | 0.00 | 0.00 | 0.00 | 0.00 | 0.00 | 0.00 | 0.00 | 0.00 | 0.00 | 0.00 | 0.00 | 0.00 | 0.00 | | 0.01 | 0.01 | 0.01 | 0.01 | 0.01 | 0.01 | 0.01 |
| Zn | 0.00 | 0.00 | 0.00 | 0.00 | 0.00 | 0.00 | 0.00 | 0.00 | 0.00 | 0.00 | 0.00 | 0.00 | 0.00 | | 0.00 | 0.00 | 0.00 | 0.00 | 0.00 | 0.00 | 0.00 |

| Analysis | GR62-22 | bordo chr | GR62-23 | GR62-24 | GR62-25 | GR62-26 | GR62-27 | GR62-28 | GR62-29 | GR62-30 | GR62-31 | GR62-32 | GR62-33 | GR62-34 | GR62-35 | GR62-36 | GR62-37 | GR62-38 | bordo chr | GR62-41 | GR62-42 |
|---|---|---|---|---|---|---|---|---|---|---|---|---|---|---|---|---|---|---|---|---|---|
| | OL-275 | | OL-276 | OL-277 | OL-278 | OL-279 | OL-280 | OL-281 | OL-282 | OL-283 | OL-284 | OL-285 | OL-286 | OL-287 | OL-288 | OL-289 | OL-290 | OL-291 | | CHR-294 | CHR-295 |
| X | 12.44 | 12.34 | 12.42 | 12.43 | 12.46 | 12.71 | 12.73 | 12.77 | 12.76 | 12.78 | 12.79 | 12.80 | 12.79 | 12.80 | 12.81 | 12.82 | 12.82 | 12.83 | 12.84 | 12.85 | 12.85 |
| Y | 67.26 | 67.25 | 67.34 | 67.36 | 67.39 | 67.37 | 67.39 | 67.41 | 67.47 | 67.48 | 67.49 | 67.50 | 67.54 | 67.55 | 67.56 | 67.56 | 67.56 | 67.57 | 67.58 | 67.58 | 67.58 |
| d (mm) | 0.057 | | 0.121 | 0.142 | 0.182 | 0.241 | 0.215 | 0.180 | 0.130 | 0.116 | 0.102 | 0.087 | 0.060 | 0.044 | 0.032 | 0.025 | 0.020 | 0.017 | | 0.010 | 0.014 |
| $SiO_2$ | 42.04 | | 42.52 | 41.70 | 42.36 | 42.58 | 42.68 | 43.16 | 41.51 | 41.73 | 42.82 | 42.27 | 42.81 | 42.46 | 42.49 | 42.13 | 42.22 | 42.07 | | 0.01 | 0.03 |
| $TiO_2$ | 0.00 | | 0.00 | 0.00 | 0.00 | 0.00 | 0.03 | 0.00 | 0.02 | 0.00 | 0.00 | 0.01 | 0.00 | 0.03 | 0.01 | 0.00 | 0.00 | 0.01 | | 0.20 | 0.16 |
| $Al_2O_3$ | 0.00 | | 0.00 | 0.00 | 0.00 | 0.00 | 0.01 | 0.00 | 0.00 | 0.02 | 0.01 | 0.02 | 0.00 | 0.00 | 0.00 | 0.00 | 0.00 | 0.00 | | 8.60 | 10.49 |
| $Cr_2O_3$ | 0.07 | | 0.08 | 0.07 | 0.05 | 0.00 | 0.01 | 0.01 | 0.02 | 0.02 | 0.02 | 0.06 | 0.05 | 0.10 | 0.19 | 0.21 | 0.26 | 0.27 | | 57.69 | 56.21 |
| $V_2O_3$ | 0.00 | | 0.00 | 0.00 | 0.00 | 0.00 | 0.00 | 0.00 | 0.00 | 0.00 | 0.00 | 0.00 | 0.00 | 0.00 | 0.00 | 0.00 | 0.00 | 0.00 | | 0.00 | 0.00 |
| $Fe_2O_3$ | 0.00 | | 0.00 | 0.00 | 0.00 | 0.00 | 0.00 | 0.00 | 0.00 | 0.00 | 0.00 | 0.00 | 0.00 | 0.00 | 0.00 | 0.00 | 0.00 | 0.00 | | 3.40 | 2.75 |
| FeO | 6.83 | | 7.26 | 7.05 | 7.05 | 7.14 | 7.16 | 7.32 | 6.77 | 7.21 | 7.31 | 7.35 | 7.27 | 7.26 | 7.16 | 7.19 | 7.09 | 7.32 | | 25.87 | 25.74 |
| MnO | 0.17 | | 0.08 | 0.05 | 0.17 | 0.12 | 0.19 | 0.02 | 0.13 | 0.13 | 0.12 | 0.20 | 0.02 | 0.08 | 0.04 | 0.06 | 0.14 | 0.10 | | 0.17 | 0.15 |
| MgO | 50.66 | | 50.82 | 51.17 | 51.09 | 51.13 | 50.78 | 51.53 | 52.63 | 52.32 | 51.74 | 51.29 | 51.49 | 51.02 | 51.68 | 52.01 | 51.18 | 50.70 | | 5.10 | 5.35 |
| NiO | 0.38 | | 0.33 | 0.42 | 0.36 | 0.33 | 0.38 | 0.34 | 0.38 | 0.36 | 0.36 | 0.40 | 0.39 | 0.38 | 0.39 | 0.43 | 0.35 | 0.45 | | 0.01 | 0.08 |
| ZnO | 0.05 | | 0.06 | 0.01 | 0.00 | 0.00 | 0.00 | 0.00 | 0.00 | 0.05 | 0.00 | 0.00 | 0.00 | 0.01 | 0.02 | 0.02 | 0.02 | 0.01 | | 0.09 | 0.06 |
| TOT | 100.20 | | 101.15 | 100.46 | 101.07 | 101.30 | 101.25 | 102.40 | 101.47 | 101.83 | 102.38 | 101.62 | 102.04 | 101.37 | 101.97 | 102.04 | 101.26 | 100.94 | | 101.16 | 101.01 |
| Si | 1.02 | | 1.02 | 1.01 | 1.02 | 1.02 | 1.03 | 1.02 | 0.99 | 0.99 | 1.02 | 1.01 | 1.02 | 1.02 | 1.01 | 1.00 | 1.01 | 1.01 | | 0.00 | 0.00 |
| Ti | 0.00 | | 0.00 | 0.00 | 0.00 | 0.00 | 0.00 | 0.00 | 0.00 | 0.00 | 0.00 | 0.00 | 0.00 | 0.00 | 0.00 | 0.00 | 0.00 | 0.00 | | 0.01 | 0.00 |
| Al | 0.00 | | 0.00 | 0.00 | 0.00 | 0.00 | 0.00 | 0.00 | 0.00 | 0.00 | 0.00 | 0.00 | 0.00 | 0.00 | 0.00 | 0.00 | 0.00 | 0.00 | | 0.35 | 0.42 |
| Cr | 0.00 | | 0.00 | 0.00 | 0.00 | 0.00 | 0.00 | 0.00 | 0.00 | 0.00 | 0.00 | 0.00 | 0.00 | 0.00 | 0.00 | 0.00 | 0.00 | 0.01 | | 1.56 | 1.50 |
| V | 0.00 | | 0.00 | 0.00 | 0.00 | 0.00 | 0.00 | 0.00 | 0.00 | 0.00 | 0.00 | 0.00 | 0.00 | 0.00 | 0.00 | 0.00 | 0.00 | 0.00 | | 0.00 | 0.00 |
| $Fe^{3+}$ | 0.00 | | 0.00 | 0.00 | 0.00 | 0.00 | 0.00 | 0.00 | 0.00 | 0.00 | 0.00 | 0.00 | 0.00 | 0.00 | 0.00 | 0.00 | 0.00 | 0.00 | | 0.09 | 0.07 |
| $Fe^{2+}$ | 0.14 | | 0.15 | 0.14 | 0.14 | 0.14 | 0.14 | 0.15 | 0.13 | 0.14 | 0.15 | 0.15 | 0.14 | 0.15 | 0.14 | 0.14 | 0.14 | 0.15 | | 0.74 | 0.73 |
| Mn | 0.00 | | 0.00 | 0.00 | 0.00 | 0.00 | 0.00 | 0.00 | 0.00 | 0.00 | 0.00 | 0.00 | 0.00 | 0.00 | 0.00 | 0.00 | 0.00 | 0.00 | | 0.01 | 0.00 |
| Mg | 1.83 | | 1.82 | 1.84 | 1.83 | 1.83 | 1.82 | 1.82 | 1.87 | 1.85 | 1.83 | 1.83 | 1.83 | 1.82 | 1.83 | 1.84 | 1.83 | 1.82 | | 0.26 | 0.27 |
| Ni | 0.01 | | 0.01 | 0.01 | 0.01 | 0.01 | 0.01 | 0.01 | 0.01 | 0.01 | 0.01 | 0.01 | 0.01 | 0.01 | 0.01 | 0.01 | 0.01 | 0.01 | | 0.00 | 0.00 |
| Zn | 0.00 | | 0.00 | 0.00 | 0.00 | 0.00 | 0.00 | 0.00 | 0.00 | 0.00 | 0.00 | 0.00 | 0.00 | 0.00 | 0.00 | 0.00 | 0.00 | 0.00 | | 0.00 | 0.00 |

| Analysis | GR62-43 | GR62-44 | GR62-45 | GR62-46 | GR62-47 | GR62-48 | GR62-49 | GR62-50 | GR62-51 | GR62-52 | GR62-53 | GR62-54 | GR62-55 | GR62-56 | GR62-57 | GR62-58 | GR62-59 | GR62-60 | GR62-61 | bordo chr | GR62-64 |
|---|---|---|---|---|---|---|---|---|---|---|---|---|---|---|---|---|---|---|---|---|---|
| | CHR-296 | CHR-297 | CHR-298 | CHR-299 | CHR-300 | CHR-301 | CHR-302 | CHR-303 | CHR-304 | CHR-305 | CHR-306 | CHR-307 | CHR-308 | CHR-309 | CHR-310 | CHR-311 | CHR-312 | CHR-313 | CHR-314 | | OL-317 |
| X | 12.85 | 12.86 | 12.86 | 12.87 | 12.89 | 12.92 | 12.66 | 12.65 | 12.60 | 12.56 | 12.53 | 12.50 | 12.44 | 12.43 | 12.42 | 12.40 | 12.39 | 12.38 | 12.38 | 12.38 | 12.35 |
| Y | 67.59 | 67.59 | 67.59 | 67.60 | 67.60 | 67.61 | 78.37 | 78.32 | 78.25 | 78.18 | 78.11 | 78.09 | 78.04 | 77.99 | 77.97 | 77.95 | 77.93 | 77.91 | 77.90 | 77.89 | 77.84 |
| d (mm) | 0.016 | 0.018 | 0.027 | 0.035 | 0.055 | 0.089 | 0.556 | 0.505 | 0.421 | 0.337 | 0.260 | 0.229 | 0.166 | 0.110 | 0.092 | 0.063 | 0.043 | 0.019 | 0.008 | | 0.063 |
| $SiO_2$ | 0.00 | 0.01 | 0.01 | 0.02 | 0.01 | 0.02 | 0.04 | 0.03 | 0.00 | 0.00 | 0.05 | 0.00 | 0.03 | 0.00 | 0.20 | 0.00 | 0.02 | 0.03 | 0.26 | | 40.94 |
| $TiO_2$ | 0.17 | 0.18 | 0.18 | 0.24 | 0.21 | 0.18 | 0.16 | 0.20 | 0.14 | 0.17 | 0.18 | 0.18 | 0.13 | 0.12 | 0.17 | 0.17 | 0.19 | 0.14 | 0.19 | | 0.00 |
| $Al_2O_3$ | 11.25 | 11.92 | 13.53 | 13.34 | 13.48 | 13.57 | 13.82 | 13.72 | 13.69 | 13.64 | 13.35 | 13.55 | 13.53 | 13.51 | 13.56 | 13.55 | 13.60 | 12.77 | 9.13 | | 1.66 |
| $Cr_2O_3$ | 55.86 | 54.82 | 53.44 | 53.80 | 54.04 | 53.87 | 56.07 | 55.87 | 55.79 | 55.74 | 55.86 | 56.62 | 56.11 | 55.50 | 55.55 | 55.51 | 54.83 | 54.72 | 56.85 | | 0.55 |
| $V_2O_3$ | 0.00 | 0.00 | 0.00 | 0.00 | 0.00 | 0.00 | 0.00 | 0.00 | 0.00 | 0.00 | 0.00 | 0.00 | 0.00 | 0.00 | 0.00 | 0.00 | 0.00 | 0.00 | 0.00 | | 0.00 |
| $Fe_2O_3$ | 2.63 | 2.30 | 1.69 | 1.68 | 1.28 | 1.34 | 0.00 | 0.02 | 0.65 | 0.60 | 0.54 | 0.20 | 0.20 | 0.68 | 0.19 | 0.77 | 1.26 | 2.30 | 3.35 | | 0.00 |
| FeO | 25.26 | 24.98 | 24.72 | 24.68 | 24.58 | 24.20 | 22.25 | 22.15 | 22.11 | 22.08 | 22.55 | 22.90 | 23.26 | 23.39 | 23.75 | 23.98 | 24.54 | 25.69 | 26.49 | | 9.44 |
| MnO | 0.28 | 0.27 | 0.32 | 0.23 | 0.28 | 0.19 | 0.18 | 0.26 | 0.19 | 0.23 | 0.21 | 0.33 | 0.12 | 0.23 | 0.22 | 0.15 | 0.27 | 0.28 | 0.33 | | 0.09 |
| MgO | 5.67 | 5.78 | 6.05 | 6.22 | 6.22 | 6.47 | 7.81 | 7.84 | 7.97 | 7.91 | 7.69 | 7.54 | 7.27 | 7.04 | 7.10 | 6.80 | 6.49 | 5.69 | 4.92 | | 41.09 |
| NiO | 0.09 | 0.04 | 0.05 | 0.00 | 0.03 | 0.04 | 0.00 | 0.07 | 0.00 | 0.03 | 0.00 | 0.01 | 0.04 | 0.09 | 0.00 | 0.07 | 0.04 | 0.04 | 0.01 | | 0.31 |
| ZnO | 0.09 | 0.12 | 0.01 | 0.08 | 0.04 | 0.03 | 0.00 | 0.03 | 0.04 | 0.08 | 0.04 | 0.04 | 0.05 | 0.01 | 0.03 | 0.14 | 0.00 | 0.07 | 0.13 | | 0.05 |
| TOT | 101.29 | 100.42 | 100.00 | 100.28 | 100.17 | 99.93 | 100.34 | 100.22 | 100.56 | 100.48 | 100.45 | 101.37 | 100.74 | 100.55 | 100.82 | 101.14 | 101.25 | 101.73 | 101.69 | | 95.09 |
| Si | 0.00 | 0.00 | 0.00 | 0.00 | 0.00 | 0.00 | 0.00 | 0.00 | 0.00 | 0.00 | 0.00 | 0.00 | 0.00 | 0.00 | 0.01 | 0.00 | 0.00 | 0.00 | 0.01 | | 1.08 |

| | | | | | | | | | | | | | | | | | | | | | |
|---|---|---|---|---|---|---|---|---|---|---|---|---|---|---|---|---|---|---|---|---|---|
| Ti | 0.00 | 0.00 | 0.00 | 0.01 | 0.01 | 0.00 | 0.00 | 0.00 | 0.00 | 0.00 | 0.00 | 0.00 | 0.00 | 0.00 | 0.00 | 0.00 | 0.00 | 0.00 | 0.00 | | 0.00 |
| Al | 0.44 | 0.47 | 0.53 | 0.52 | 0.53 | 0.53 | 0.54 | 0.53 | 0.53 | 0.53 | 0.52 | 0.52 | 0.53 | 0.53 | 0.53 | 0.53 | 0.53 | 0.50 | 0.36 | | 0.05 |
| Cr | 1.48 | 1.46 | 1.41 | 1.42 | 1.43 | 1.42 | 1.46 | 1.46 | 1.45 | 1.45 | 1.46 | 1.46 | 1.46 | 1.45 | 1.45 | 1.45 | 1.43 | 1.43 | 1.52 | | 0.01 |
| V | 0.00 | 0.00 | 0.00 | 0.00 | 0.00 | 0.00 | 0.00 | 0.00 | 0.00 | 0.00 | 0.00 | 0.00 | 0.00 | 0.00 | 0.00 | 0.00 | 0.00 | 0.00 | 0.00 | | 0.00 |
| $Fe^{3+}$ | 0.07 | 0.06 | 0.04 | 0.04 | 0.03 | 0.03 | 0.00 | 0.00 | 0.02 | 0.01 | 0.01 | 0.00 | 0.00 | 0.02 | 0.00 | 0.02 | 0.03 | 0.06 | 0.09 | | 0.00 |
| $Fe^{2+}$ | 0.71 | 0.70 | 0.69 | 0.69 | 0.69 | 0.68 | 0.61 | 0.61 | 0.61 | 0.61 | 0.62 | 0.63 | 0.64 | 0.65 | 0.65 | 0.66 | 0.68 | 0.71 | 0.75 | | 0.21 |
| Mn | 0.01 | 0.01 | 0.01 | 0.01 | 0.01 | 0.01 | 0.01 | 0.01 | 0.01 | 0.01 | 0.01 | 0.01 | 0.00 | 0.01 | 0.01 | 0.00 | 0.01 | 0.01 | 0.01 | | 0.00 |
| Mg | 0.28 | 0.29 | 0.30 | 0.31 | 0.31 | 0.32 | 0.38 | 0.39 | 0.39 | 0.39 | 0.38 | 0.37 | 0.36 | 0.35 | 0.35 | 0.33 | 0.32 | 0.28 | 0.25 | | 1.61 |
| Ni | 0.00 | 0.00 | 0.00 | 0.00 | 0.00 | 0.00 | 0.00 | 0.00 | 0.00 | 0.00 | 0.00 | 0.00 | 0.00 | 0.00 | 0.00 | 0.00 | 0.00 | 0.00 | 0.00 | | 0.01 |
| Zn | 0.00 | 0.00 | 0.00 | 0.00 | 0.00 | 0.00 | 0.00 | 0.00 | 0.00 | 0.00 | 0.00 | 0.00 | 0.00 | 0.00 | 0.00 | 0.00 | 0.00 | 0.00 | 0.00 | | 0.00 |

| Analysis | GR62-65 | GR62-66 | GR62-67 | GR62-68 | GR62-69 | GR62-70 | GR62-71 | GR62-72 | GR62-73 | GR62-74 | GR62-75 | GR62-76 | GR62-77 | GR62-78 | bordo chr | GR62-79 | GR62-80 | GR62-81 | GR62-82 | GR62-83 | GR62-84 |
|---|---|---|---|---|---|---|---|---|---|---|---|---|---|---|---|---|---|---|---|---|---|
| | OL-318 | OL-319 | OL-320 | OL-321 | OL-322 | OL-323 | OL-324 | CHR-325 | CHR-326 | CHR-327 | CHR-328 | CHR-329 | CHR-330 | CHR-331 | | OL-332 | OL-333 | OL-334 | OL-335 | OL-336 | OL-337 |
| X | 12.35 | 12.33 | 12.32 | 12.30 | 12.28 | 12.22 | 12.18 | 10.63 | 10.65 | 10.68 | 10.70 | 10.72 | 10.72 | 10.73 | 10.73 | 10.74 | 10.74 | 10.74 | 10.75 | 10.81 | 10.79 |
| Y | 77.84 | 77.82 | 77.82 | 77.80 | 77.76 | 77.70 | 77.66 | 77.16 | 77.15 | 77.14 | 77.14 | 77.13 | 77.13 | 77.13 | 77.13 | 77.13 | 77.13 | 77.14 | 77.14 | 77.14 | 77.10 |
| d (mm) | 0.064 | 0.088 | 0.095 | 0.119 | 0.163 | 0.251 | 0.307 | 0.104 | 0.080 | 0.052 | 0.031 | 0.013 | 0.004 | 0.003 | | 0.008 | 0.010 | 0.017 | 0.024 | 0.080 | 0.050 |
| $SiO_2$ | 41.18 | 42.17 | 41.94 | 41.79 | 42.10 | 42.20 | 42.84 | 0.01 | 0.00 | 0.00 | 0.05 | 0.07 | 0.16 | 0.00 | | 38.27 | 41.84 | 43.04 | 42.61 | 41.95 | 42.62 |
| $TiO_2$ | 0.00 | 0.01 | 0.00 | 0.02 | 0.00 | 0.00 | 0.00 | 0.16 | 0.19 | 0.20 | 0.18 | 0.21 | 0.13 | 0.14 | | 0.01 | 0.00 | 0.00 | 0.02 | 0.02 | 0.00 |
| $Al_2O_3$ | 1.27 | 0.00 | 0.01 | 0.00 | 0.02 | 0.00 | 0.02 | 13.43 | 13.19 | 12.41 | 12.54 | 10.63 | 8.23 | 7.55 | | 0.46 | 0.00 | 0.00 | 0.00 | 0.00 | 0.03 |
| $Cr_2O_3$ | 0.51 | 0.00 | 0.04 | 0.05 | 0.02 | 0.03 | 0.05 | 54.91 | 55.77 | 56.08 | 55.25 | 56.71 | 57.51 | 57.34 | | 0.65 | 0.35 | 0.22 | 0.15 | 0.09 | 0.04 |
| $V_2O_3$ | 0.00 | 0.00 | 0.00 | 0.00 | 0.00 | 0.00 | 0.00 | 0.00 | 0.00 | 0.00 | 0.00 | 0.00 | 0.00 | 0.00 | | 0.00 | 0.00 | 0.00 | 0.00 | 0.00 | 0.00 |
| $Fe_2O_3$ | 0.00 | 0.00 | 0.00 | 0.00 | 0.00 | 0.00 | 0.00 | 1.91 | 1.40 | 1.32 | 1.99 | 2.80 | 3.98 | 4.76 | | 0.00 | 0.00 | 0.00 | 0.00 | 0.00 | 0.00 |
| FeO | 8.92 | 7.44 | 7.69 | 7.91 | 7.98 | 7.07 | 7.18 | 24.41 | 24.55 | 24.57 | 25.14 | 26.48 | 26.87 | 26.62 | | 8.01 | 7.83 | 7.50 | 7.81 | 8.31 | 7.71 |
| MnO | 0.01 | 0.07 | 0.17 | 0.00 | 0.07 | 0.10 | 0.12 | 0.33 | 0.44 | 0.25 | 0.28 | 0.22 | 0.28 | 0.27 | | 0.14 | 0.12 | 0.20 | 0.02 | 0.09 | 0.08 |
| MgO | 44.26 | 52.04 | 51.77 | 51.41 | 51.50 | 52.21 | 52.28 | 6.58 | 6.48 | 6.30 | 6.09 | 5.23 | 4.57 | 4.35 | | 49.70 | 52.64 | 51.84 | 51.39 | 50.67 | 50.93 |
| NiO | 0.31 | 0.37 | 0.38 | 0.37 | 0.38 | 0.40 | 0.47 | 0.06 | 0.04 | 0.09 | 0.01 | 0.00 | 0.00 | 0.03 | | 0.30 | 0.35 | 0.41 | 0.39 | 0.37 | 0.32 |
| ZnO | 0.03 | 0.02 | 0.00 | 0.00 | 0.00 | 0.03 | 0.00 | 0.04 | 0.05 | 0.06 | 0.03 | 0.10 | 0.12 | 0.14 | | 0.00 | 0.02 | 0.00 | 0.02 | 0.00 | 0.00 |
| TOT | 97.22 | 102.14 | 102.02 | 101.56 | 102.07 | 102.03 | 102.98 | 101.85 | 102.10 | 101.28 | 101.56 | 102.45 | 101.85 | 101.21 | | 97.70 | 103.16 | 103.20 | 102.42 | 101.52 | 101.74 |
| Si | 1.05 | 1.00 | 1.00 | 1.00 | 1.00 | 1.00 | 1.01 | 0.00 | 0.00 | 0.00 | 0.00 | 0.00 | 0.01 | 0.00 | | 0.95 | 0.98 | 1.01 | 1.01 | 1.01 | 1.02 |
| Ti | 0.00 | 0.00 | 0.00 | 0.00 | 0.00 | 0.00 | 0.00 | 0.00 | 0.00 | 0.00 | 0.00 | 0.01 | 0.00 | 0.00 | | 0.00 | 0.00 | 0.00 | 0.00 | 0.00 | 0.00 |
| Al | 0.04 | 0.00 | 0.00 | 0.00 | 0.00 | 0.00 | 0.00 | 0.52 | 0.51 | 0.49 | 0.49 | 0.42 | 0.33 | 0.31 | | 0.01 | 0.00 | 0.00 | 0.00 | 0.00 | 0.00 |
| Cr | 0.01 | 0.00 | 0.00 | 0.00 | 0.00 | 0.00 | 0.00 | 1.42 | 1.45 | 1.47 | 1.45 | 1.50 | 1.55 | 1.56 | | 0.01 | 0.01 | 0.00 | 0.00 | 0.00 | 0.00 |
| V | 0.00 | 0.00 | 0.00 | 0.00 | 0.00 | 0.00 | 0.00 | 0.00 | 0.00 | 0.00 | 0.00 | 0.00 | 0.00 | 0.00 | | 0.00 | 0.00 | 0.00 | 0.00 | 0.00 | 0.00 |
| $Fe^{3+}$ | 0.00 | 0.00 | 0.00 | 0.00 | 0.00 | 0.00 | 0.00 | 0.05 | 0.03 | 0.03 | 0.05 | 0.07 | 0.10 | 0.12 | | 0.00 | 0.00 | 0.00 | 0.00 | 0.00 | 0.00 |
| $Fe^{2+}$ | 0.19 | 0.15 | 0.15 | 0.16 | 0.16 | 0.14 | 0.14 | 0.67 | 0.67 | 0.68 | 0.70 | 0.74 | 0.77 | 0.77 | | 0.17 | 0.15 | 0.15 | 0.16 | 0.17 | 0.15 |
| Mn | 0.00 | 0.00 | 0.00 | 0.00 | 0.00 | 0.00 | 0.00 | 0.01 | 0.01 | 0.01 | 0.01 | 0.01 | 0.01 | 0.01 | | 0.00 | 0.00 | 0.00 | 0.00 | 0.00 | 0.00 |
| Mg | 1.68 | 1.84 | 1.84 | 1.83 | 1.83 | 1.85 | 1.84 | 0.32 | 0.32 | 0.31 | 0.30 | 0.26 | 0.23 | 0.22 | | 1.84 | 1.85 | 1.82 | 1.82 | 1.81 | 1.82 |
| Ni | 0.01 | 0.01 | 0.01 | 0.01 | 0.01 | 0.01 | 0.01 | 0.00 | 0.00 | 0.00 | 0.00 | 0.00 | 0.00 | 0.00 | | 0.01 | 0.01 | 0.01 | 0.01 | 0.01 | 0.01 |
| Zn | 0.00 | 0.00 | 0.00 | 0.00 | 0.00 | 0.00 | 0.00 | 0.00 | 0.00 | 0.00 | 0.00 | 0.00 | 0.00 | 0.00 | | 0.00 | 0.00 | 0.00 | 0.00 | 0.00 | 0.00 |

| Analysis | bordo chr | GR62-85 | GR62-86 | GR62-87 | bordo chr | GR62-88 | GR62-89 | GR62-90 | GR62-91 |
|---|---|---|---|---|---|---|---|---|---|
| | | OL-338 | OL-339 | OL-340 | | CHR-341 | CHR-342 | CHR-343 | CHR-344 |
| X | 10.74 | 10.76 | 10.75 | 10.75 | 10.71 | 10.71 | 10.69 | 10.68 | 10.66 |
| Y | 77.10 | 77.04 | 77.04 | 77.05 | 77.07 | 77.07 | 77.07 | 77.08 | 77.10 |
| d (mm) | | 0.060 | 0.052 | 0.045 | | 0.002 | 0.018 | 0.031 | 0.058 |
| $SiO_2$ | | 42.26 | 42.76 | 41.63 | | 0.02 | 0.04 | 0.02 | 0.03 |
| $TiO_2$ | | 0.00 | 0.03 | 0.00 | | 0.16 | 0.18 | 0.22 | 0.19 |
| $Al_2O_3$ | | 0.01 | 0.01 | 0.00 | | 7.52 | 12.18 | 13.14 | 13.16 |
| $Cr_2O_3$ | | 0.03 | 0.01 | 0.10 | | 57.99 | 54.82 | 54.09 | 54.29 |
| $V_2O_3$ | | 0.00 | 0.00 | 0.00 | | 0.00 | 0.00 | 0.00 | 0.00 |
| $Fe_2O_3$ | | 0.00 | 0.00 | 0.00 | | 3.52 | 2.44 | 2.34 | 1.41 |
| FeO | | 7.26 | 7.40 | 7.32 | | 26.85 | 25.70 | 25.51 | 24.66 |

| | | | | | | | |
|---|---|---|---|---|---|---|---|
| MnO | 0.00 | 0.11 | 0.15 | 0.31 | 0.22 | 0.24 | 0.17 |
| MgO | 51.38 | 51.42 | 51.69 | 4.11 | 5.58 | 5.89 | 6.22 |
| NiO | 0.39 | 0.36 | 0.38 | 0.02 | 0.02 | 0.01 | 0.00 |
| ZnO | 0.00 | 0.03 | 0.01 | 0.15 | 0.12 | 0.03 | 0.09 |
| TOT | 101.33 | 102.12 | 101.29 | 100.65 | 101.30 | 101.50 | 100.22 |
| Si | 1.01 | 1.02 | 1.00 | 0.00 | 0.00 | 0.00 | 0.00 |
| Ti | 0.00 | 0.00 | 0.00 | 0.00 | 0.00 | 0.01 | 0.00 |
| Al | 0.00 | 0.00 | 0.00 | 0.31 | 0.48 | 0.51 | 0.52 |
| Cr | 0.00 | 0.00 | 0.00 | 1.59 | 1.45 | 1.42 | 1.43 |
| V | 0.00 | 0.00 | 0.00 | 0.00 | 0.00 | 0.00 | 0.00 |
| $Fe^{3+}$ | 0.00 | 0.00 | 0.00 | 0.09 | 0.06 | 0.06 | 0.04 |
| $Fe^{2+}$ | 0.15 | 0.15 | 0.15 | 0.78 | 0.72 | 0.71 | 0.69 |
| Mn | 0.00 | 0.00 | 0.00 | 0.01 | 0.01 | 0.01 | 0.00 |
| Mg | 1.83 | 1.82 | 1.84 | 0.21 | 0.28 | 0.29 | 0.31 |
| Ni | 0.01 | 0.01 | 0.01 | 0.00 | 0.00 | 0.00 | 0.00 |
| Zn | 0.00 | 0.00 | 0.00 | 0.00 | 0.00 | 0.00 | 0.00 |

Tab. A3.11 GR58C (Nea Roda) microprobe analyses of olivine and chromite crystals; d(mm) distance from the intergranular limit

| Analysis | GR58-1 | GR58-2 | GR58-3 | GR58-5 | GR58-6 | GR58-7 | GR58-8 | GR58-9 | d chr | GR58-10 | GR58-11 | GR58-12 | d chr | GR58-13 | d chr | GR58-14 | GR58-15 | GR58-16 | d chr | GR58-17 | GR58-18 | GR58-19 | GR58-20 | GR58-21 |
|---|---|---|---|---|---|---|---|---|---|---|---|---|---|---|---|---|---|---|---|---|---|---|---|---|
| | 152-OL | 153-OL | 154-OL | 156-OL | 157-OL | 158-OL | 159-OL | 160-OL | | 161-CHR | 162-CHR | 163-CHR | | 164-CHR | | 165-CHL | 166-OL | 167-OL | | 168-CHR | 169-CHR | 170-CHR | 171-CHR | 172-CHR |
| X | 18.90 | 18.90 | 18.90 | 18.90 | 18.87 | 18.85 | 18.83 | 18.82 | 18.81 | 18.81 | 18.81 | 18.82 | 18.84 | 18.83 | 18.81 | 18.77 | 18.64 | 18.67 | 18.71 | 18.71 | 18.72 | 18.73 | 18.74 | 18.76 |
| Y | 92.42 | 92.47 | 92.53 | 92.60 | 92.67 | 92.71 | 92.73 | 92.76 | 92.78 | 92.79 | 92.80 | 92.82 | 92.79 | 92.84 | 92.85 | 92.85 | 92.83 | 92.85 | 92.88 | 92.89 | 92.90 | 92.92 | 92.95 | 93.02 |
| d (mm) | 0.371 | 0.322 | 0.264 | 0.199 | 0.124 | 0.080 | 0.051 | 0.025 | | 0.008 | 0.018 | 0.029 | | 0.030 | | 0.035 | 0.087 | 0.055 | | 0.010 | 0.022 | 0.049 | 0.082 | 0.117 |
| $SiO_2$ | 41.23 | 40.92 | 40.86 | 40.90 | 41.10 | 41.47 | 41.39 | 41.16 | | 0.05 | 0.05 | 0.00 | | 0.00 | | | 41.16 | 41.66 | | 0.04 | 0.00 | 0.02 | 0.03 | 0.01 |
| $TiO_2$ | 0.01 | 0.07 | 0.02 | 0.06 | 0.01 | 0.00 | 0.01 | 0.08 | | 0.16 | 0.11 | 0.11 | | 0.09 | | | 0.00 | 0.02 | | 0.15 | 0.10 | 0.08 | 0.10 | 0.08 |
| $Al_2O_3$ | 0.00 | 0.00 | 0.00 | 0.00 | 0.00 | 0.03 | 0.00 | 0.00 | | 8.14 | 9.42 | 9.56 | | 9.57 | | | 0.00 | 0.00 | | 7.20 | 8.84 | 9.95 | 9.74 | 9.80 |
| $Cr_2O_3$ | 0.00 | 0.00 | 0.00 | 0.08 | 0.00 | 0.02 | 0.10 | 0.09 | | 59.89 | 60.07 | 60.04 | | 60.19 | | | 0.06 | 0.12 | | 60.84 | 60.48 | 59.98 | 60.18 | 60.36 |
| $V_2O_3$ | 0.00 | 0.04 | 0.00 | 0.00 | 0.02 | 0.01 | 0.00 | 0.00 | | 0.11 | 0.09 | 0.05 | | 0.08 | | | 0.00 | 0.00 | | 0.07 | 0.03 | 0.06 | 0.08 | 0.08 |
| $Fe_2O_3$ | | | | | | | | | | 2.76 | 2.22 | 1.74 | | 1.85 | | | | | | 2.86 | 1.91 | 1.52 | 2.20 | 1.86 |
| FeO | 5.05 | 4.91 | 4.83 | 4.92 | 4.68 | 4.69 | 4.56 | 5.01 | | 20.64 | 19.61 | 20.56 | | 20.29 | | | 4.64 | 5.03 | | 20.23 | 20.44 | 19.76 | 18.68 | 18.05 |
| MnO | 0.09 | 0.05 | 0.06 | 0.05 | 0.10 | 0.11 | 0.06 | 0.05 | | 0.28 | 0.24 | 0.22 | | 0.26 | | | 0.10 | 0.07 | | 0.24 | 0.22 | 0.16 | 0.16 | 0.10 |
| MgO | 51.86 | 51.87 | 51.95 | 51.90 | 51.75 | 51.96 | 52.22 | 52.00 | | 8.19 | 9.21 | 8.58 | | 8.71 | | | 51.54 | 51.71 | | 8.34 | 8.49 | 9.08 | 9.80 | 10.22 |
| NiO | 0.38 | 0.37 | 0.45 | 0.50 | 0.37 | 0.49 | 0.43 | 0.38 | | 0.01 | 0.00 | 0.02 | | 0.00 | | | 0.46 | 0.39 | | 0.13 | 0.01 | 0.01 | 0.10 | 0.06 |
| ZnO | 0.00 | 0.04 | 0.00 | 0.04 | 0.03 | 0.06 | 0.09 | 0.09 | | 0.25 | 0.11 | 0.00 | | 0.16 | | | 0.00 | 0.01 | | 0.00 | 0.06 | 0.15 | 0.19 | 0.03 |
| TOT | 98.62 | 98.27 | 98.17 | 98.47 | 98.10 | 98.84 | 98.88 | 98.86 | | 100.48 | 101.16 | 100.91 | | 101.22 | | | 97.98 | 99.03 | | 100.14 | 100.61 | 100.79 | 101.27 | 100.66 |
| Si | 1.00 | 1.00 | 1.00 | 1.00 | 1.01 | 1.01 | 1.00 | 1.00 | | 0.00 | 0.00 | 0.00 | | 0.00 | | | 1.01 | 1.01 | | 0.00 | 0.00 | 0.00 | 0.00 | 0.00 |
| Ti | 0.00 | 0.00 | 0.00 | 0.00 | 0.00 | 0.00 | 0.00 | 0.00 | | 0.00 | 0.00 | 0.00 | | 0.00 | | | 0.00 | 0.00 | | 0.00 | 0.00 | 0.00 | 0.00 | 0.00 |
| Al | 0.00 | 0.00 | 0.00 | 0.00 | 0.00 | 0.00 | 0.00 | 0.00 | | 0.32 | 0.37 | 0.37 | | 0.37 | | | 0.00 | 0.00 | | 0.29 | 0.35 | 0.39 | 0.38 | 0.38 |
| Cr | 0.00 | 0.00 | 0.00 | 0.00 | 0.00 | 0.00 | 0.00 | 0.00 | | 1.59 | 1.57 | 1.58 | | 1.57 | | | 0.00 | 0.00 | | 1.63 | 1.60 | 1.57 | 1.56 | 1.57 |
| V | 0.00 | 0.00 | 0.00 | 0.00 | 0.00 | 0.00 | 0.00 | 0.00 | | 0.00 | 0.00 | 0.00 | | 0.00 | | | 0.00 | 0.00 | | 0.00 | 0.00 | 0.00 | 0.00 | 0.00 |
| $Fe^{3+}$ | | | | | | | | | | 0.07 | 0.06 | 0.04 | | 0.05 | | | | | | 0.07 | 0.05 | 0.04 | 0.05 | 0.05 |
| $Fe^{2+}$ | 0.10 | 0.10 | 0.10 | 0.10 | 0.10 | 0.10 | 0.09 | 0.10 | | 0.58 | 0.54 | 0.57 | | 0.56 | | | 0.10 | 0.10 | | 0.57 | 0.57 | 0.55 | 0.51 | 0.50 |
| Mn | 0.00 | 0.00 | 0.00 | 0.00 | 0.00 | 0.00 | 0.00 | 0.00 | | 0.01 | 0.01 | 0.01 | | 0.01 | | | 0.00 | 0.00 | | 0.01 | 0.01 | 0.00 | 0.00 | 0.00 |
| Mg | 1.88 | 1.89 | 1.89 | 1.89 | 1.89 | 1.88 | 1.89 | 1.88 | | 0.41 | 0.45 | 0.42 | | 0.43 | | | 1.88 | 1.87 | | 0.42 | 0.42 | 0.45 | 0.48 | 0.50 |
| Ni | 0.01 | 0.01 | 0.01 | 0.01 | 0.01 | 0.01 | 0.01 | 0.01 | | 0.00 | 0.00 | 0.00 | | 0.00 | | | 0.01 | 0.01 | | 0.00 | 0.00 | 0.00 | 0.00 | 0.00 |
| Zn | 0.00 | 0.00 | 0.00 | 0.00 | 0.00 | 0.00 | 0.00 | 0.00 | | 0.01 | 0.00 | 0.00 | | 0.00 | | | 0.00 | 0.00 | | 0.00 | 0.00 | 0.00 | 0.00 | 0.00 |

Tab. A3.12 PUKA-3 (Iballe) microprobe analyses of olivine and chromite crystals; d(mm) distance from the intergranular limit

| Analysis | GRID 1-2 | GRID 1-3 | GRID 1-4 | GRID 1-5 | GRID 1-6 | GRID 1-7 | GRID 2-1 | GRID 2-2 | GRID 2-3 | GRID 2-4 | GRID 2-5 | GRID 2-6 | GRID 2-7 | GRID 3-1 | GRID 3-2 | GRID 3-3 | GRID 3-4 | GRID 3-5 | GRID 3-6 | GRID 3-7 |
|---|---|---|---|---|---|---|---|---|---|---|---|---|---|---|---|---|---|---|---|---|
| | 2-CHR | 3-CHR | 4-CHR | 5-CHR | 6-CHR | 7-CHR | 8-CHR | 9-CHR | 10-CHR | 11-CHR | 12-CHR | 13-CHR | 14-CHR | 15-CHR | 16-CHR | 17-CHR | 18-OL | 19-CHR | 20-CHR | 21-CHR |
| X | 78.052 | 78.052 | 78.052 | 78.052 | 78.052 | 78.052 | 78.152 | 78.152 | 78.152 | 78.152 | 78.152 | 78.152 | 78.152 | 78.252 | 78.252 | 78.252 | 78.252 | 78.252 | 78.252 | 78.252 |
| Y | 89.051 | 89.151 | 89.251 | 89.351 | 89.451 | 89.551 | 88.951 | 89.051 | 89.151 | 89.251 | 89.351 | 89.451 | 89.551 | 88.951 | 89.051 | 89.151 | 89.251 | 89.351 | 89.451 | 89.551 |
| $SiO_2$ | 0.03 | 0.00 | 0.00 | 0.00 | 0.01 | 0.00 | 0.01 | 0.02 | 0.02 | 0.05 | 0.00 | 0.00 | 0.03 | 0.00 | 0.02 | 0.05 | 41.69 | 0.03 | 0.06 | 0.01 |
| $TiO_2$ | 0.07 | 0.05 | 0.04 | 0.10 | 0.04 | 0.01 | 0.09 | 0.09 | 0.10 | 0.06 | 0.08 | 0.08 | 0.11 | 0.06 | 0.06 | 0.06 | 0.02 | 0.08 | 0.09 | 0.11 |
| $Al_2O_3$ | 24.23 | 24.23 | 24.24 | 23.72 | 23.70 | 23.07 | 24.19 | 23.35 | 22.71 | 24.47 | 23.64 | 23.20 | 22.64 | 24.30 | 23.91 | 24.22 | 0.02 | 24.02 | 23.37 | 23.28 |
| $Cr_2O_3$ | 46.41 | 45.77 | 45.57 | 46.18 | 45.96 | 45.78 | 45.55 | 46.76 | 47.40 | 45.72 | 45.82 | 46.14 | 46.76 | 45.74 | 45.57 | 45.81 | 0.22 | 46.14 | 46.64 | 46.60 |
| $V_2O_3$ | 0.23 | 0.24 | 0.20 | 0.21 | 0.19 | 0.13 | 0.29 | 0.26 | 0.21 | 0.24 | 0.17 | 0.20 | 0.19 | 0.21 | 0.21 | 0.16 | 0.00 | 0.23 | 0.24 | 0.18 |
| $Fe_2O_3$ | 2.49 | 2.72 | 2.91 | 3.33 | 3.08 | 3.80 | 2.99 | 2.56 | 3.13 | 2.64 | 3.38 | 3.33 | 3.05 | 2.73 | 3.08 | 2.22 | 0.00 | 3.11 | 3.06 | 3.22 |
| FeO | 11.92 | 11.91 | 11.82 | 11.55 | 11.74 | 11.25 | 11.58 | 11.83 | 11.45 | 11.87 | 11.43 | 11.36 | 11.97 | 11.71 | 11.47 | 11.61 | 4.21 | 11.66 | 11.81 | 11.78 |
| MnO | 0.00 | 0.04 | 0.04 | 0.04 | 0.07 | 0.08 | 0.04 | 0.09 | 0.05 | 0.13 | 0.01 | 0.04 | 0.05 | 0.03 | 0.05 | 0.02 | 0.04 | 0.00 | 0.09 | 0.04 |
| MgO | 15.82 | 15.73 | 15.66 | 15.99 | 15.67 | 15.73 | 15.89 | 15.61 | 15.92 | 15.74 | 15.85 | 15.85 | 15.52 | 15.88 | 15.84 | 15.82 | 53.17 | 15.93 | 15.73 | 15.75 |
| NiO | 0.24 | 0.14 | 0.23 | 0.21 | 0.17 | 0.25 | 0.19 | 0.15 | 0.24 | 0.21 | 0.09 | 0.21 | 0.09 | 0.15 | 0.19 | 0.12 | 0.90 | 0.27 | 0.18 | 0.23 |
| ZnO | 0.11 | 0.00 | 0.11 | 0.03 | 0.12 | 0.07 | 0.15 | 0.16 | 0.03 | 0.13 | 0.30 | 0.01 | 0.00 | 0.00 | 0.09 | 0.08 | 0.00 | 0.13 | 0.21 | 0.07 |
| TOT | 101.55 | 100.82 | 100.82 | 101.36 | 100.75 | 100.17 | 100.98 | 100.89 | 101.24 | 101.26 | 100.78 | 100.43 | 100.40 | 100.81 | 100.48 | 100.18 | 100.27 | 101.60 | 101.47 | 101.28 |
| Si | 0.00 | 0.00 | 0.00 | 0.00 | 0.00 | 0.00 | 0.00 | 0.00 | 0.00 | 0.00 | 0.00 | 0.00 | 0.00 | 0.00 | 0.00 | 0.00 | 1.00 | 0.00 | 0.00 | 0.00 |
| Ti | 0.00 | 0.00 | 0.00 | 0.00 | 0.00 | 0.00 | 0.00 | 0.00 | 0.00 | 0.00 | 0.00 | 0.00 | 0.00 | 0.00 | 0.00 | 0.00 | 0.00 | 0.00 | 0.00 | 0.00 |
| Al | 0.85 | 0.85 | 0.85 | 0.83 | 0.84 | 0.82 | 0.85 | 0.82 | 0.80 | 0.86 | 0.83 | 0.82 | 0.80 | 0.85 | 0.84 | 0.86 | 0.00 | 0.84 | 0.82 | 0.82 |
| Cr | 1.09 | 1.08 | 1.08 | 1.09 | 1.09 | 1.09 | 1.07 | 1.11 | 1.12 | 1.07 | 1.08 | 1.10 | 1.12 | 1.08 | 1.08 | 1.09 | 0.00 | 1.08 | 1.10 | 1.10 |
| V | 0.01 | 0.01 | 0.00 | 0.00 | 0.00 | 0.00 | 0.01 | 0.01 | 0.00 | 0.01 | 0.00 | 0.00 | 0.00 | 0.01 | 0.00 | 0.00 | 0.00 | 0.01 | 0.01 | 0.00 |
| $Fe^{3+}$ | 0.06 | 0.06 | 0.07 | 0.07 | 0.07 | 0.09 | 0.07 | 0.06 | 0.07 | 0.06 | 0.08 | 0.08 | 0.07 | 0.06 | 0.07 | 0.05 | 0.00 | 0.07 | 0.07 | 0.07 |
| $Fe^{2+}$ | 0.30 | 0.30 | 0.30 | 0.29 | 0.29 | 0.28 | 0.29 | 0.30 | 0.29 | 0.29 | 0.29 | 0.29 | 0.30 | 0.29 | 0.29 | 0.29 | 0.08 | 0.29 | 0.29 | 0.29 |
| Mn | 0.00 | 0.00 | 0.00 | 0.00 | 0.00 | 0.00 | 0.00 | 0.00 | 0.00 | 0.00 | 0.00 | 0.00 | 0.00 | 0.00 | 0.00 | 0.00 | 0.00 | 0.00 | 0.00 | 0.00 |
| Mg | 0.70 | 0.70 | 0.70 | 0.71 | 0.70 | 0.71 | 0.71 | 0.70 | 0.71 | 0.70 | 0.71 | 0.71 | 0.70 | 0.71 | 0.71 | 0.71 | 1.90 | 0.70 | 0.70 | 0.70 |
| Ni | 0.01 | 0.00 | 0.01 | 0.01 | 0.00 | 0.01 | 0.00 | 0.00 | 0.01 | 0.01 | 0.00 | 0.01 | 0.00 | 0.00 | 0.00 | 0.00 | 0.02 | 0.01 | 0.00 | 0.01 |
| Zn | 0.00 | 0.00 | 0.00 | 0.00 | 0.00 | 0.00 | 0.00 | 0.00 | 0.00 | 0.00 | 0.01 | 0.00 | 0.00 | 0.00 | 0.00 | 0.00 | 0.00 | 0.00 | 0.00 | 0.00 |

| Analysis | GRID 4-1 | GRID 4-2 | GRID 4-3 | GRID 4-4 | GRID 4-5 | GRID 4-6 | GRID 4-7 | GRID 5-2 | GRID 5-3 | GRID 5-6 | GRID 5-7 | GRID 6-1 | GRID 6-2 | GRID 6-3 | GRID 6-4 | GRID 6-6 | GRID 6-7 | GRID 7-1 | GRID 7-2 | GRID 7-3 |
|---|---|---|---|---|---|---|---|---|---|---|---|---|---|---|---|---|---|---|---|---|
| | 22-CHR | 23-CHR | 24-CHR | 25-OL | 26-CHR | 27-CHR | 28-CHR | 30-CHR | 31-CHR | 34-CHR | 35-CHR | 36-CHR | 37-CHR | 38-CHR | 39-CHR | 41-OL | 42-CHR | 43-CHR | 44-CHR | 45-CHR |
| X | 78.352 | 78.352 | 78.352 | 78.352 | 78.352 | 78.352 | 78.352 | 78.452 | 78.452 | 78.452 | 78.452 | 78.552 | 78.552 | 78.552 | 78.552 | 78.552 | 78.552 | 78.652 | 78.652 | 78.652 |
| Y | 88.951 | 89.051 | 89.151 | 89.251 | 89.351 | 89.451 | 89.551 | 89.051 | 89.151 | 89.451 | 89.551 | 88.951 | 89.051 | 89.151 | 89.251 | 89.451 | 89.551 | 88.951 | 89.051 | 89.151 |
| $SiO_2$ | 0.00 | 0.01 | 0.00 | 41.54 | 0.04 | 0.00 | 0.01 | 0.02 | 0.03 | 0.00 | 0.00 | 0.04 | 0.01 | 0.02 | 0.01 | 41.61 | 0.08 | 0.00 | 0.01 | 0.02 |
| $TiO_2$ | 0.06 | 0.05 | 0.04 | 0.01 | 0.08 | 0.05 | 0.09 | 0.04 | 0.05 | 0.05 | 0.06 | 0.00 | 0.06 | 0.05 | 0.06 | 0.00 | 0.07 | 0.05 | 0.05 | 0.08 |
| $Al_2O_3$ | 25.05 | 24.69 | 24.43 | 0.00 | 24.43 | 23.99 | 24.56 | 24.82 | 24.28 | 20.80 | 24.72 | 22.33 | 24.74 | 24.47 | 24.67 | 0.02 | 23.98 | 24.93 | 24.20 | 24.35 |
| $Cr_2O_3$ | 45.86 | 45.75 | 45.68 | 0.09 | 45.78 | 45.96 | 46.70 | 45.43 | 46.26 | 51.43 | 46.64 | 49.18 | 45.99 | 45.34 | 45.40 | 0.08 | 44.74 | 45.77 | 46.22 | 45.98 |
| $V_2O_3$ | 0.20 | 0.21 | 0.23 | 0.00 | 0.21 | 0.24 | 0.17 | 0.19 | 0.21 | 0.17 | 0.21 | 0.28 | 0.23 | 0.21 | 0.23 | 0.00 | 0.20 | 0.21 | 0.18 | 0.25 |
| $Fe_2O_3$ | 2.31 | 2.89 | 2.68 | 0.00 | 2.85 | 3.22 | 1.96 | 2.89 | 2.61 | 1.70 | 1.70 | 1.98 | 2.81 | 3.21 | 2.81 | 0.00 | 3.90 | 2.43 | 2.91 | 3.29 |
| FeO | 11.78 | 11.75 | 11.65 | 4.22 | 11.89 | 11.51 | 11.81 | 11.56 | 11.99 | 12.03 | 12.06 | 11.68 | 11.69 | 11.54 | 11.65 | 4.08 | 11.56 | 11.74 | 11.79 | 11.63 |
| MnO | 0.02 | 0.01 | 0.07 | 0.08 | 0.02 | 0.03 | 0.06 | 0.08 | 0.07 | 0.11 | 0.10 | 0.00 | 0.07 | 0.06 | 0.01 | 0.07 | 0.06 | 0.02 | 0.05 | 0.06 |
| MgO | 15.99 | 15.94 | 15.78 | 53.45 | 15.91 | 16.00 | 15.96 | 15.94 | 15.73 | 15.55 | 15.75 | 15.75 | 16.10 | 15.94 | 15.88 | 53.06 | 15.92 | 16.01 | 15.90 | 16.09 |
| NiO | 0.12 | 0.21 | 0.23 | 0.69 | 0.20 | 0.15 | 0.18 | 0.16 | 0.18 | 0.06 | 0.21 | 0.16 | 0.23 | 0.20 | 0.25 | 0.68 | 0.13 | 0.20 | 0.19 | 0.24 |
| ZnO | 0.14 | 0.18 | 0.13 | 0.00 | 0.02 | 0.06 | 0.05 | 0.28 | 0.15 | 0.00 | 0.00 | 0.17 | 0.00 | 0.16 | 0.17 | 0.00 | 0.10 | 0.00 | 0.05 | 0.08 |
| TOT | 101.53 | 101.69 | 100.92 | 100.08 | 101.42 | 101.22 | 101.54 | 101.41 | 101.57 | 101.90 | 101.46 | 101.57 | 101.92 | 101.20 | 101.16 | 99.60 | 100.72 | 101.35 | 101.57 | 102.06 |
| Si | 0.00 | 0.00 | 0.00 | 0.99 | 0.00 | 0.00 | 0.00 | 0.00 | 0.00 | 0.00 | 0.00 | 0.00 | 0.00 | 0.00 | 0.00 | 1.00 | 0.00 | 0.00 | 0.00 | 0.00 |
| Ti | 0.00 | 0.00 | 0.00 | 0.00 | 0.00 | 0.00 | 0.00 | 0.00 | 0.00 | 0.00 | 0.00 | 0.00 | 0.00 | 0.00 | 0.00 | 0.00 | 0.00 | 0.00 | 0.00 | 0.00 |
| Al | 0.87 | 0.86 | 0.86 | 0.00 | 0.85 | 0.84 | 0.86 | 0.87 | 0.85 | 0.74 | 0.86 | 0.79 | 0.86 | 0.86 | 0.86 | 0.00 | 0.84 | 0.87 | 0.85 | 0.85 |
| Cr | 1.07 | 1.07 | 1.08 | 0.00 | 1.07 | 1.08 | 1.09 | 1.06 | 1.08 | 1.22 | 1.09 | 1.16 | 1.07 | 1.06 | 1.07 | 0.00 | 1.06 | 1.07 | 1.08 | 1.07 |
| V | 0.00 | 0.00 | 0.01 | 0.00 | 0.00 | 0.01 | 0.00 | 0.00 | 0.01 | 0.00 | 0.00 | 0.01 | 0.01 | 0.01 | 0.01 | 0.00 | 0.00 | 0.00 | 0.00 | 0.01 |

| | | | | | | | | | | | | | | | | | | | | |
|---|---|---|---|---|---|---|---|---|---|---|---|---|---|---|---|---|---|---|---|---|
| $Fe^{3+}$ | 0.05 | 0.06 | 0.06 | 0.00 | 0.06 | 0.07 | 0.04 | 0.06 | 0.06 | 0.04 | 0.04 | 0.04 | 0.06 | 0.07 | 0.06 | 0.00 | 0.09 | 0.05 | 0.06 | 0.07 |
| $Fe^{2+}$ | 0.29 | 0.29 | 0.29 | 0.08 | 0.29 | 0.29 | 0.29 | 0.29 | 0.30 | 0.30 | 0.30 | 0.29 | 0.29 | 0.29 | 0.29 | 0.08 | 0.29 | 0.29 | 0.29 | 0.29 |
| Mn | 0.00 | 0.00 | 0.00 | 0.00 | 0.00 | 0.00 | 0.00 | 0.00 | 0.00 | 0.00 | 0.00 | 0.00 | 0.00 | 0.00 | 0.00 | 0.00 | 0.00 | 0.00 | 0.00 | 0.00 |
| Mg | 0.70 | 0.70 | 0.70 | 1.90 | 0.70 | 0.71 | 0.70 | 0.70 | 0.70 | 0.70 | 0.70 | 0.70 | 0.71 | 0.71 | 0.70 | 1.90 | 0.71 | 0.71 | 0.70 | 0.71 |
| Ni | 0.00 | 0.01 | 0.01 | 0.01 | 0.00 | 0.00 | 0.00 | 0.00 | 0.00 | 0.00 | 0.01 | 0.00 | 0.01 | 0.00 | 0.01 | 0.01 | 0.00 | 0.00 | 0.00 | 0.01 |
| Zn | 0.00 | 0.00 | 0.00 | 0.00 | 0.00 | 0.00 | 0.00 | 0.01 | 0.00 | 0.00 | 0.00 | 0.00 | 0.00 | 0.00 | 0.00 | 0.00 | 0.00 | 0.00 | 0.00 | 0.00 |

| Analysis | GRID 7-4 | GRID 7-5 | GRID 7-6 | GRID 7-7 | PUKA3-50 | PUKA3-51 | PUKA3-53 | PUKA3-54 | PUKA3-55 | PUKA3-56 | 67-CHR | 68-CHR | 69-CHR | 70-CHR | 71-CHR | 73-OL | 74-OL | 75-OL | 76-OL | 77-OL |
|---|---|---|---|---|---|---|---|---|---|---|---|---|---|---|---|---|---|---|---|---|
| | 46-CHR | 47-CHR | 48-OL | 49-OL | 50-OL | 51-OL | 53-Fe-CHR | 54-CHR | 55-CHR | 56-CHR | | | | | | | | | | |
| X | 78.652 | 78.652 | 78.652 | 78.652 | 78.343 | 78.210 | 78.145 | 78.098 | 78.875 | 78.967 | 79.05 | 78.99 | 78.95 | 78.92 | 78.91 | 78.89 | 78.88 | 78.86 | 78.84 | 78.83 |
| Y | 89.251 | 89.351 | 89.451 | 89.551 | 89.256 | 89.208 | 89.199 | 89.195 | 89.257 | 89.292 | 88.746 | 88.819 | 88.883 | 88.986 | 89.005 | 89.026 | 89.034 | 89.047 | 89.061 | 89.075 |
| d (mm) | | | | | | | | | | | 0.304 | 0.212 | 0.137 | 0.029 | 0.008 | 0.022 | 0.034 | 0.059 | 0.052 | 0.034 |
| $SiO_2$ | 0.00 | 0.13 | 41.62 | 41.56 | 41.80 | 42.04 | 0.04 | 0.00 | 0.04 | 0.04 | 0.01 | 0.04 | 0.00 | 0.02 | 0.03 | 41.13 | 41.30 | 40.95 | 41.23 | 41.40 |
| $TiO_2$ | 0.05 | 0.06 | 0.02 | 0.00 | 0.00 | 0.00 | 0.08 | 0.08 | 0.04 | 0.09 | 0.10 | 0.01 | 0.01 | 0.06 | 0.07 | 0.00 | 0.00 | 0.01 | 0.00 | 0.00 |
| $Al_2O_3$ | 24.34 | 25.46 | 0.00 | 0.08 | 0.00 | 0.07 | 12.13 | 24.69 | 21.59 | 15.55 | 25.11 | 24.45 | 23.61 | 24.33 | 24.27 | 0.00 | 0.00 | 0.04 | 0.01 | 0.00 |
| $Cr_2O_3$ | 45.67 | 45.83 | 0.00 | 0.26 | 0.08 | 0.43 | 56.80 | 45.86 | 50.26 | 49.25 | 46.10 | 46.08 | 46.55 | 46.59 | 46.81 | 0.24 | 0.18 | 0.12 | 0.06 | 0.14 |
| $V_2O_3$ | 0.22 | 0.14 | 0.00 | 0.00 | 0.00 | 0.00 | 0.18 | 0.23 | 0.19 | 0.20 | 0.13 | 0.12 | 0.12 | 0.11 | 0.09 | 0.01 | 0.00 | 0.00 | 0.00 | 0.01 |
| $Fe_2O_3$ | 3.37 | 1.86 | 0.00 | 0.00 | 0.00 | 0.00 | 5.97 | 2.89 | 1.35 | 9.10 | 1.67 | 2.24 | 3.01 | 2.27 | 1.87 | | | | | |
| FeO | 11.34 | 11.46 | 4.30 | 3.74 | 4.17 | 4.13 | 11.97 | 11.75 | 12.43 | 12.63 | 12.24 | 12.13 | 11.85 | 12.62 | 12.29 | 3.88 | 4.39 | 4.54 | 4.22 | 4.05 |
| MnO | 0.08 | 0.06 | 0.10 | 0.06 | 0.05 | 0.08 | 0.10 | 0.01 | 0.06 | 0.19 | 0.00 | 0.04 | 0.01 | 0.06 | 0.05 | 0.08 | 0.08 | 0.05 | 0.06 | 0.08 |
| MgO | 16.14 | 16.46 | 52.71 | 53.71 | 53.25 | 52.66 | 14.62 | 16.05 | 15.27 | 14.38 | 15.70 | 15.59 | 15.67 | 15.44 | 15.55 | 51.93 | 51.83 | 51.56 | 51.73 | 51.57 |
| NiO | 0.24 | 0.07 | 0.82 | 0.78 | 0.72 | 0.96 | 0.06 | 0.19 | 0.11 | 0.22 | 0.22 | 0.14 | 0.25 | 0.18 | 0.14 | 0.93 | 0.90 | 0.91 | 0.92 | 0.76 |
| ZnO | 0.00 | 0.00 | 0.11 | 0.00 | 0.00 | 0.03 | 0.23 | 0.09 | 0.02 | 0.00 | 0.07 | 0.13 | 0.00 | 0.00 | 0.09 | 0.01 | 0.06 | 0.00 | 0.00 | 0.00 |
| TOT | 101.46 | 101.53 | 99.68 | 100.19 | 100.07 | 100.40 | 102.17 | 101.84 | 101.36 | 101.65 | 101.37 | 100.96 | 101.10 | 101.70 | 101.27 | 98.25 | 98.77 | 98.18 | 98.23 | 98.01 |
| Si | 0.00 | 0.00 | 1.00 | 0.99 | 1.00 | 1.01 | 0.00 | 0.00 | 0.00 | 0.00 | 0.00 | 0.00 | 0.00 | 0.00 | 0.00 | 1.00 | 1.01 | 1.00 | 1.01 | 1.01 |
| Ti | 0.00 | 0.00 | 0.00 | 0.00 | 0.00 | 0.00 | 0.00 | 0.00 | 0.00 | 0.00 | 0.00 | 0.00 | 0.00 | 0.00 | 0.00 | 0.00 | 0.00 | 0.00 | 0.00 | 0.00 |
| Al | 0.85 | 0.88 | 0.00 | 0.00 | 0.00 | 0.00 | 0.45 | 0.86 | 0.77 | 0.57 | 0.88 | 0.86 | 0.83 | 0.85 | 0.85 | 0.00 | 0.00 | 0.00 | 0.00 | 0.00 |
| Cr | 1.07 | 1.06 | 0.00 | 0.00 | 0.00 | 0.01 | 1.40 | 1.07 | 1.20 | 1.21 | 1.08 | 1.09 | 1.10 | 1.09 | 1.10 | 0.00 | 0.00 | 0.00 | 0.00 | 0.00 |
| V | 0.01 | 0.00 | 0.00 | 0.00 | 0.00 | 0.00 | 0.00 | 0.01 | 0.00 | 0.00 | 0.00 | 0.00 | 0.00 | 0.00 | 0.00 | 0.00 | 0.00 | 0.00 | 0.00 | 0.00 |
| $Fe^{3+}$ | 0.08 | 0.04 | 0.00 | 0.00 | 0.00 | 0.00 | 0.14 | 0.06 | 0.03 | 0.21 | 0.04 | 0.05 | 0.07 | 0.05 | 0.04 | | | | | |
| $Fe^{2+}$ | 0.28 | 0.28 | 0.09 | 0.07 | 0.08 | 0.08 | 0.31 | 0.29 | 0.31 | 0.33 | 0.30 | 0.30 | 0.30 | 0.31 | 0.31 | 0.08 | 0.09 | 0.09 | 0.09 | 0.08 |
| Mn | 0.00 | 0.00 | 0.00 | 0.00 | 0.00 | 0.00 | 0.00 | 0.00 | 0.00 | 0.00 | 0.00 | 0.00 | 0.00 | 0.00 | 0.00 | 0.00 | 0.00 | 0.00 | 0.00 | 0.00 |
| Mg | 0.71 | 0.72 | 1.89 | 1.91 | 1.90 | 1.88 | 0.68 | 0.71 | 0.68 | 0.66 | 0.69 | 0.69 | 0.70 | 0.68 | 0.69 | 1.89 | 1.88 | 1.88 | 1.89 | 1.88 |
| Ni | 0.01 | 0.00 | 0.02 | 0.01 | 0.01 | 0.02 | 0.00 | 0.00 | 0.00 | 0.01 | 0.01 | 0.00 | 0.01 | 0.00 | 0.00 | 0.02 | 0.02 | 0.02 | 0.02 | 0.01 |
| Zn | 0.00 | 0.00 | 0.00 | 0.00 | 0.00 | 0.00 | 0.01 | 0.00 | 0.00 | 0.00 | 0.00 | 0.00 | 0.00 | 0.00 | 0.00 | 0.00 | 0.00 | 0.00 | 0.00 | 0.00 |

| Analysis | 78-OL | 79-OL | 81-CHR | 82-CHR | 83-CHR |
|---|---|---|---|---|---|
| X | 78.82 | 78.81 | 78.79 | 78.78 | 78.76 |
| Y | 89.083 | 89.090 | 89.113 | 89.124 | 89.148 |
| d (mm) | 0.022 | 0.011 | 0.016 | 0.032 | 0.065 |
| $SiO_2$ | 41.00 | 41.23 | 0.04 | 0.01 | 0.00 |
| $TiO_2$ | 0.03 | 0.00 | 0.07 | 0.12 | 0.02 |
| $Al_2O_3$ | 0.00 | 0.00 | 24.33 | 24.36 | 24.16 |
| $Cr_2O_3$ | 0.21 | 0.24 | 46.59 | 46.56 | 46.64 |
| $V_2O_3$ | 0.00 | 0.00 | 0.12 | 0.13 | 0.11 |
| $Fe_2O_3$ | | | 2.28 | 2.50 | 2.32 |
| FeO | 4.23 | 4.27 | 12.42 | 12.12 | 12.27 |
| MnO | 0.05 | 0.04 | 0.01 | 0.00 | 0.00 |
| MgO | 51.83 | 51.57 | 15.63 | 15.83 | 15.52 |
| NiO | 0.85 | 0.88 | 0.16 | 0.18 | 0.24 |
| ZnO | 0.06 | 0.05 | 0.04 | 0.10 | 0.00 |

| TOT | 98.28 | 98.29 | 101.70 | 101.91 | 101.30 |
|---|---|---|---|---|---|
| Si | 1.00 | 1.01 | 0.00 | 0.00 | 0.00 |
| Ti | 0.00 | 0.00 | 0.00 | 0.00 | 0.00 |
| Al | 0.00 | 0.00 | 0.85 | 0.85 | 0.85 |
| Cr | 0.00 | 0.00 | 1.09 | 1.09 | 1.10 |
| V | 0.00 | 0.00 | 0.00 | 0.00 | 0.00 |
| $Fe^{3+}$ | | | 0.05 | 0.06 | 0.05 |
| $Fe^{2+}$ | 0.09 | 0.09 | 0.31 | 0.30 | 0.31 |
| Mn | 0.00 | 0.00 | 0.00 | 0.00 | 0.00 |
| Mg | 1.89 | 1.88 | 0.69 | 0.70 | 0.69 |
| Ni | 0.02 | 0.02 | 0.00 | 0.00 | 0.01 |
| Zn | 0.00 | 0.00 | 0.00 | 0.00 | 0.00 |

Tab. A3.13 PUKA-2 (Iballe) microprobe analyses of olivine and chromite crystals; d(mm) distance from the intergranular limit

| Analysis | PUKA2-1 CHR-110 | PUKA2-2 CHR-111 | PUKA2-3 CHR-112 | PUKA2-4 CHR-113 | PUKA2-5 CHR-114 | PUKA2-6 CHR-115 | PUKA2-7 CHR-116 | PUKA2-8 CHR-117 | PUKA2-9 CHR-118 | PUKA2-10 CHR-119 | PUKA2-11 CHR-120 | PUKA2-12 CHR-121 | PUKA2-13 CHR-122 | PUKA2-14 CHR-123 | PUKA2-15 CHR-124 | PUKA2-16 CHR-125 | PUKA2-17 CHR-126 | PUKA2-18 CHR-127 | PUKA2-19 CHR-128 |
|---|---|---|---|---|---|---|---|---|---|---|---|---|---|---|---|---|---|---|---|
| X | 47.174 | 47.167 | 47.162 | 47.162 | 47.168 | 47.163 | 47.161 | 47.163 | 47.100 | 47.089 | 47.083 | 47.076 | 47.078 | 47.078 | 47.076 | 47.074 | 47.072 | 47.072 | 47.070 |
| Y | 71.810 | 71.838 | 71.869 | 71.931 | 71.980 | 72.022 | 72.063 | 72.128 | 72.154 | 72.180 | 72.206 | 72.223 | 72.242 | 72.254 | 72.272 | 72.284 | 72.300 | 72.308 | 72.318 |
| d(mm) | 0.551 | 0.522 | 0.491 | 0.431 | 0.384 | 0.343 | 0.303 | 0.242 | 0.199 | 0.172 | 0.145 | 0.128 | 0.109 | 0.097 | 0.079 | 0.067 | 0.051 | 0.043 | 0.033 |
| $SiO_2$ | 0.00 | 0.00 | 0.00 | 0.02 | 0.00 | 0.00 | 0.00 | 0.00 | 0.00 | 0.00 | 0.00 | 0.02 | 0.00 | 0.04 | 0.00 | 0.03 | 0.00 | 0.00 | 0.01 |
| $TiO_2$ | 0.09 | 0.11 | 0.12 | 0.12 | 0.17 | 0.11 | 0.10 | 0.14 | 0.12 | 0.11 | 0.11 | 0.09 | 0.10 | 0.11 | 0.14 | 0.14 | 0.11 | 0.13 | 0.14 |
| $Al_2O_3$ | 26.14 | 26.10 | 26.35 | 26.09 | 26.25 | 26.38 | 26.53 | 26.48 | 26.61 | 26.44 | 26.40 | 26.37 | 26.43 | 26.36 | 26.70 | 26.46 | 26.65 | 26.77 | 26.87 |
| $Cr_2O_3$ | 43.22 | 43.27 | 42.89 | 43.10 | 42.98 | 43.57 | 43.58 | 43.32 | 43.22 | 43.20 | 44.43 | 43.37 | 43.24 | 43.61 | 43.25 | 43.37 | 43.43 | 43.05 | 42.99 |
| $V_2O_3$ | 0.00 | 0.00 | 0.00 | 0.00 | 0.00 | 0.00 | 0.00 | 0.00 | 0.00 | 0.00 | 0.00 | 0.00 | 0.00 | 0.00 | 0.00 | 0.00 | 0.00 | 0.00 | 0.00 |
| $Fe_2O_3$ | 3.13 | 3.10 | 3.48 | 3.48 | 3.60 | 2.87 | 3.33 | 3.51 | 3.90 | 3.68 | 3.26 | 3.19 | 3.46 | 3.46 | 3.42 | 3.86 | 3.33 | 3.50 | 3.48 |
| FeO | 12.39 | 12.20 | 12.19 | 11.84 | 11.78 | 12.46 | 11.93 | 12.13 | 11.66 | 11.64 | 12.08 | 12.20 | 11.74 | 11.87 | 11.93 | 11.70 | 11.98 | 12.26 | 11.99 |
| MnO | 0.10 | 0.00 | 0.03 | 0.15 | 0.09 | 0.00 | 0.12 | 0.03 | 0.10 | 0.03 | 0.06 | 0.13 | 0.06 | 0.04 | 0.01 | 0.04 | 0.08 | 0.00 | 0.05 |
| MgO | 15.58 | 15.75 | 15.85 | 15.94 | 16.08 | 15.72 | 16.12 | 16.06 | 16.38 | 16.29 | 16.24 | 15.85 | 16.16 | 16.24 | 16.23 | 16.38 | 16.10 | 16.03 | 16.23 |
| NiO | 0.16 | 0.14 | 0.16 | 0.16 | 0.17 | 0.20 | 0.19 | 0.18 | 0.18 | 0.17 | 0.17 | 0.09 | 0.17 | 0.19 | 0.18 | 0.21 | 0.16 | 0.18 | 0.11 |
| ZnO | 0.00 | 0.02 | 0.00 | 0.01 | 0.01 | 0.00 | 0.00 | 0.00 | 0.00 | 0.05 | 0.00 | 0.00 | 0.00 | 0.01 | 0.00 | 0.03 | 0.11 | 0.00 | 0.00 |
| TOT | 100.81 | 100.70 | 101.06 | 100.90 | 101.15 | 101.32 | 101.91 | 101.85 | 102.16 | 101.60 | 102.75 | 101.36 | 101.37 | 101.93 | 101.86 | 102.23 | 101.93 | 101.92 | 101.88 |
| Si | 0.00 | 0.00 | 0.00 | 0.00 | 0.00 | 0.00 | 0.00 | 0.00 | 0.00 | 0.00 | 0.00 | 0.00 | 0.00 | 0.00 | 0.00 | 0.00 | 0.00 | 0.00 | 0.00 |
| Ti | 0.00 | 0.00 | 0.00 | 0.00 | 0.00 | 0.00 | 0.00 | 0.00 | 0.00 | 0.00 | 0.00 | 0.00 | 0.00 | 0.00 | 0.00 | 0.00 | 0.00 | 0.00 | 0.00 |
| Al | 0.91 | 0.91 | 0.92 | 0.91 | 0.91 | 0.92 | 0.91 | 0.91 | 0.91 | 0.91 | 0.90 | 0.91 | 0.91 | 0.91 | 0.92 | 0.91 | 0.92 | 0.92 | 0.92 |
| Cr | 1.01 | 1.01 | 1.00 | 1.01 | 1.00 | 1.02 | 1.01 | 1.00 | 1.00 | 1.00 | 1.02 | 1.01 | 1.00 | 1.01 | 1.00 | 1.00 | 1.00 | 1.00 | 0.99 |
| V | 0.00 | 0.00 | 0.00 | 0.00 | 0.00 | 0.00 | 0.00 | 0.00 | 0.00 | 0.00 | 0.00 | 0.00 | 0.00 | 0.00 | 0.00 | 0.00 | 0.00 | 0.00 | 0.00 |
| $Fe^{3+}$ | 0.07 | 0.07 | 0.08 | 0.08 | 0.08 | 0.06 | 0.07 | 0.08 | 0.09 | 0.08 | 0.07 | 0.07 | 0.08 | 0.08 | 0.08 | 0.08 | 0.07 | 0.08 | 0.08 |
| $Fe^{2+}$ | 0.31 | 0.30 | 0.30 | 0.29 | 0.29 | 0.31 | 0.29 | 0.30 | 0.28 | 0.29 | 0.29 | 0.30 | 0.29 | 0.29 | 0.29 | 0.29 | 0.29 | 0.30 | 0.29 |
| Mn | 0.00 | 0.00 | 0.00 | 0.00 | 0.00 | 0.00 | 0.00 | 0.00 | 0.00 | 0.00 | 0.00 | 0.00 | 0.00 | 0.00 | 0.00 | 0.00 | 0.00 | 0.00 | 0.00 |
| Mg | 0.69 | 0.70 | 0.70 | 0.70 | 0.71 | 0.69 | 0.70 | 0.70 | 0.71 | 0.71 | 0.70 | 0.70 | 0.71 | 0.71 | 0.71 | 0.71 | 0.70 | 0.70 | 0.71 |
| Ni | 0.00 | 0.00 | 0.00 | 0.00 | 0.00 | 0.00 | 0.00 | 0.00 | 0.00 | 0.00 | 0.00 | 0.00 | 0.00 | 0.00 | 0.00 | 0.00 | 0.00 | 0.00 | 0.00 |
| Zn | 0.00 | 0.00 | 0.00 | 0.00 | 0.00 | 0.00 | 0.00 | 0.00 | 0.00 | 0.00 | 0.00 | 0.00 | 0.00 | 0.00 | 0.00 | 0.00 | 0.00 | 0.00 | 0.00 |

| Analysis | PUKA2-20 CHR-129 | PUKA2-21 CHR-130 | PUKA2-22 CHR-131 | PUKA2-23 CHR-132 | PUKA2-24 CHR-133 | PUKA2-25 CHR-134 | bordo chr | PUKA2-26 OL-135 | PUKA2-27 OL-136 | PUKA2-28 OL-137 | PUKA2-29 OL-138 | PUKA2-30 OL-139 | PUKA2-31 OL-140 | PUKA2-32 OL-141 | PUKA2-33 OL-142 | PUKA2-34 OL-143 | PUKA2-35 OL-144 | PUKA2-36 OL-145 | PUKA2-37 OL-146 |
|---|---|---|---|---|---|---|---|---|---|---|---|---|---|---|---|---|---|---|---|
| X | 47.069 | 47.069 | 47.068 | 47.068 | 47.067 | 47.069 | 47.068 | 47.066 | 47.066 | 47.065 | 47.065 | 47.064 | 47.062 | 47.062 | 47.061 | 47.060 | 47.059 | 47.058 | 47.056 |
| Y | 72.324 | 72.329 | 72.333 | 72.337 | 72.340 | 72.347 | 72.351 | 72.362 | 72.363 | 72.364 | 72.365 | 72.366 | 72.367 | 72.368 | 72.371 | 72.376 | 72.380 | 72.384 | 72.390 |
| d(mm) | 0.027 | 0.022 | 0.018 | 0.014 | 0.011 | 0.004 | | 0.011 | 0.013 | 0.014 | 0.014 | 0.016 | 0.017 | 0.018 | 0.022 | 0.026 | 0.031 | 0.035 | 0.041 |
| $SiO_2$ | 0.00 | 0.01 | 0.34 | 0.13 | 0.23 | 0.38 | | 41.23 | 41.76 | 41.85 | 41.44 | 40.99 | 41.49 | 41.99 | 41.39 | 41.12 | 41.91 | 41.67 | 41.73 |
| $TiO_2$ | 0.13 | 0.14 | 0.13 | 0.13 | 0.15 | 0.06 | | 0.00 | 0.00 | 0.02 | 0.00 | 0.00 | 0.01 | 0.01 | 0.00 | 0.00 | 0.00 | 0.00 | 0.01 |

# Appendix: Chapter 3

| | | | | | | | | | | | | | | | | | | |
|---|---|---|---|---|---|---|---|---|---|---|---|---|---|---|---|---|---|---|
| $Al_2O_3$ | 26.94 | 24.17 | 26.18 | 27.16 | 26.99 | 22.75 | | 0.47 | 0.05 | 0.00 | 0.01 | 0.00 | 0.00 | 0.00 | 0.01 | 0.00 | 0.00 | 0.01 | 0.00 |
| $Cr_2O_3$ | 43.16 | 43.43 | 41.68 | 41.88 | 42.03 | 41.00 | | 0.48 | 0.35 | 0.26 | 0.23 | 0.27 | 0.24 | 0.18 | 0.17 | 0.18 | 0.12 | 0.11 | 0.11 |
| $V_2O_3$ | 0.00 | 0.00 | 0.00 | 0.00 | 0.00 | 0.00 | | 0.00 | 0.00 | 0.00 | 0.00 | 0.00 | 0.00 | 0.00 | 0.00 | 0.00 | 0.00 | 0.00 | 0.00 |
| $Fe_2O_3$ | 3.65 | 5.79 | 4.24 | 2.80 | 3.51 | 10.38 | | 0.00 | 0.00 | 0.00 | 0.00 | 0.00 | 0.00 | 0.00 | 0.00 | 0.00 | 0.00 | 0.00 | 0.00 |
| FeO | 12.21 | 11.13 | 10.61 | 12.11 | 11.00 | 6.27 | | 4.30 | 4.57 | 4.56 | 4.41 | 4.58 | 4.34 | 4.41 | 4.04 | 4.82 | 4.37 | 4.66 | 4.69 |
| MnO | 0.03 | 0.00 | 0.00 | 0.06 | 0.09 | 0.16 | | 0.07 | 0.08 | 0.16 | 0.04 | 0.12 | 0.11 | 0.12 | 0.03 | 0.14 | 0.06 | 0.08 | 0.05 |
| MgO | 16.21 | 16.35 | 17.01 | 15.90 | 16.80 | 19.32 | | 50.34 | 52.66 | 52.52 | 52.35 | 52.92 | 52.50 | 53.09 | 53.16 | 52.82 | 53.02 | 52.39 | 52.62 |
| NiO | 0.09 | 0.13 | 0.14 | 0.17 | 0.15 | 0.20 | | 0.59 | 0.62 | 0.67 | 0.54 | 0.65 | 0.57 | 0.62 | 0.60 | 0.55 | 0.63 | 0.58 | 0.60 |
| ZnO | 0.03 | 0.02 | 0.00 | 0.06 | 0.06 | 0.03 | | 0.00 | 0.01 | 0.01 | 0.00 | 0.01 | 0.00 | 0.00 | 0.00 | 0.00 | 0.00 | 0.03 | 0.00 |
| TOT | 102.46 | 101.16 | 100.38 | 100.41 | 101.04 | 100.56 | | 97.55 | 100.13 | 100.06 | 99.03 | 99.54 | 99.27 | 100.43 | 99.41 | 99.64 | 100.13 | 99.57 | 99.80 |
| Si | 0.00 | 0.00 | 0.01 | 0.00 | 0.01 | 0.01 | | 1.02 | 1.00 | 1.01 | 1.00 | 0.99 | 1.00 | 1.00 | 1.00 | 0.99 | 1.00 | 1.01 | 1.00 |
| Ti | 0.00 | 0.00 | 0.00 | 0.00 | 0.00 | 0.00 | | 0.00 | 0.00 | 0.00 | 0.00 | 0.00 | 0.00 | 0.00 | 0.00 | 0.00 | 0.00 | 0.00 | 0.00 |
| Al | 0.92 | 0.85 | 0.91 | 0.95 | 0.93 | 0.79 | | 0.01 | 0.00 | 0.00 | 0.00 | 0.00 | 0.00 | 0.00 | 0.00 | 0.00 | 0.00 | 0.00 | 0.00 |
| Cr | 0.99 | 1.02 | 0.97 | 0.98 | 0.97 | 0.96 | | 0.01 | 0.01 | 0.00 | 0.00 | 0.01 | 0.00 | 0.00 | 0.00 | 0.00 | 0.00 | 0.00 | 0.00 |
| V | 0.00 | 0.00 | 0.00 | 0.00 | 0.00 | 0.00 | | 0.00 | 0.00 | 0.00 | 0.00 | 0.00 | 0.00 | 0.00 | 0.00 | 0.00 | 0.00 | 0.00 | 0.00 |
| $Fe^{3+}$ | 0.08 | 0.13 | 0.09 | 0.06 | 0.08 | 0.23 | | 0.00 | 0.00 | 0.00 | 0.00 | 0.00 | 0.00 | 0.00 | 0.00 | 0.00 | 0.00 | 0.00 | 0.00 |
| $Fe^{2+}$ | 0.30 | 0.28 | 0.26 | 0.30 | 0.27 | 0.15 | | 0.09 | 0.09 | 0.09 | 0.09 | 0.09 | 0.09 | 0.09 | 0.08 | 0.10 | 0.09 | 0.09 | 0.09 |
| Mn | 0.00 | 0.00 | 0.00 | 0.00 | 0.00 | 0.00 | | 0.00 | 0.00 | 0.00 | 0.00 | 0.00 | 0.00 | 0.00 | 0.00 | 0.00 | 0.00 | 0.00 | 0.00 |
| Mg | 0.70 | 0.72 | 0.75 | 0.70 | 0.73 | 0.85 | | 1.85 | 1.88 | 1.88 | 1.89 | 1.90 | 1.89 | 1.89 | 1.91 | 1.90 | 1.89 | 1.88 | 1.89 |
| Ni | 0.00 | 0.00 | 0.00 | 0.00 | 0.00 | 0.00 | | 0.01 | 0.01 | 0.01 | 0.01 | 0.01 | 0.01 | 0.01 | 0.01 | 0.01 | 0.01 | 0.01 | 0.01 |
| Zn | 0.00 | 0.00 | 0.00 | 0.00 | 0.00 | 0.00 | | 0.00 | 0.00 | 0.00 | 0.00 | 0.00 | 0.00 | 0.00 | 0.00 | 0.00 | 0.00 | 0.00 | 0.00 |

| Analysis | PUKA2-38 | PUKA2-39 | PUKA2-40 | PUKA2-41 | PUKA2-42 | PUKA2-43 | PUKA2-44 | PUKA2-45 | PUKA2-46 | PUKA2-47 | PUKA2-48 | PUKA2-49 | PUKA2-50 | PUKA2-51 | PUKA2-52 | PUKA2-53 | PUKA2-54 | PUKA2-55 | PUKA2-56 |
|---|---|---|---|---|---|---|---|---|---|---|---|---|---|---|---|---|---|---|---|
| | OL-147 | OL-148 | OL-149 | OL-150 | OL-151 | OL-152 | OL-153 | OL-154 | OL-155 | OL-156 | OL-157 | OL-158 | OL-159 | OL-160 | OL-161 | OL-162 | OL-163 | OL-164 | OL-165 |
| X | 47.055 | 47.052 | 47.044 | 47.040 | 47.036 | 47.032 | 47.029 | 47.032 | 47.031 | 47.033 | 47.036 | 47.034 | 47.040 | 47.045 | 47.047 | 47.049 | 47.050 | 47.052 | 47.055 |
| Y | 72.419 | 72.433 | 72.457 | 72.477 | 72.496 | 72.525 | 72.546 | 72.574 | 72.637 | 72.668 | 72.690 | 72.714 | 72.742 | 72.771 | 72.787 | 72.796 | 72.818 | 72.828 | 72.843 |
| d(mm) | 0.069 | 0.084 | 0.109 | 0.129 | 0.149 | 0.178 | 0.199 | 0.226 | 0.277 | 0.245 | 0.223 | 0.200 | 0.171 | 0.142 | 0.126 | 0.116 | 0.095 | 0.084 | 0.070 |
| $SiO_2$ | 41.49 | 40.78 | 39.52 | 40.77 | 41.12 | 41.04 | 40.63 | 41.84 | 40.93 | 40.71 | 41.25 | 41.26 | 42.25 | 42.51 | 41.74 | 42.35 | 41.93 | 41.11 | 40.95 |
| $TiO_2$ | 0.00 | 0.02 | 0.01 | 0.00 | 0.03 | 0.02 | 0.02 | 0.01 | 0.00 | 0.00 | 0.03 | 0.03 | 0.00 | 0.00 | 0.00 | 0.00 | 0.00 | 0.03 | 0.02 |
| $Al_2O_3$ | 0.00 | 0.00 | 0.00 | 0.01 | 0.01 | 0.01 | 0.00 | 0.00 | 0.01 | 0.00 | 0.02 | 0.02 | 0.00 | 0.00 | 0.00 | 0.00 | 0.01 | 0.01 | 0.00 |
| $Cr_2O_3$ | 0.07 | 0.07 | 0.07 | 0.00 | 0.06 | 0.03 | 0.01 | 0.00 | 0.00 | 0.02 | 0.00 | 0.03 | 0.00 | 0.04 | 0.02 | 0.02 | 0.03 | 0.05 | 0.05 |
| $V_2O_3$ | 0.00 | 0.00 | 0.00 | 0.00 | 0.00 | 0.00 | 0.00 | 0.00 | 0.00 | 0.00 | 0.00 | 0.00 | 0.00 | 0.00 | 0.00 | 0.00 | 0.00 | 0.00 | 0.00 |
| $Fe_2O_3$ | 0.00 | 0.00 | 0.00 | 0.00 | 0.00 | 0.00 | 0.00 | 0.00 | 0.00 | 0.00 | 0.00 | 0.00 | 0.00 | 0.00 | 0.00 | 0.00 | 0.00 | 0.00 | 0.00 |
| FeO | 4.83 | 4.99 | 5.18 | 5.06 | 5.33 | 5.44 | 5.28 | 5.43 | 5.71 | 5.23 | 4.99 | 5.05 | 5.04 | 5.25 | 5.25 | 5.21 | 5.42 | 5.30 | 5.25 |
| MnO | 0.13 | 0.05 | 0.13 | 0.00 | 0.09 | 0.11 | 0.01 | 0.11 | 0.11 | 0.11 | 0.00 | 0.06 | 0.19 | 0.09 | 0.04 | 0.00 | 0.01 | 0.03 | 0.06 |
| MgO | 52.37 | 52.76 | 53.35 | 53.32 | 53.17 | 53.41 | 53.17 | 53.11 | 53.11 | 53.02 | 53.58 | 53.80 | 52.91 | 52.90 | 52.57 | 52.58 | 52.33 | 52.22 | 52.42 |
| NiO | 0.58 | 0.51 | 0.51 | 0.56 | 0.56 | 0.54 | 0.61 | 0.63 | 0.57 | 0.62 | 0.66 | 0.58 | 0.55 | 0.60 | 0.62 | 0.60 | 0.56 | 0.55 | 0.61 |
| ZnO | 0.00 | 0.00 | 0.00 | 0.00 | 0.02 | 0.00 | 0.00 | 0.02 | 0.03 | 0.01 | 0.07 | 0.00 | 0.00 | 0.01 | 0.01 | 0.00 | 0.00 | 0.00 | 0.00 |
| TOT | 99.51 | 99.18 | 98.77 | 99.74 | 100.40 | 100.60 | 99.78 | 101.17 | 100.48 | 99.76 | 100.60 | 100.82 | 100.94 | 101.41 | 100.28 | 100.76 | 100.30 | 99.34 | 99.36 |
| Si | 1.00 | 0.99 | 0.96 | 0.98 | 0.98 | 0.98 | 0.98 | 0.99 | 0.98 | 0.98 | 0.98 | 0.98 | 1.01 | 1.01 | 1.00 | 1.01 | 1.01 | 0.99 | 0.99 |
| Ti | 0.00 | 0.00 | 0.00 | 0.00 | 0.00 | 0.00 | 0.00 | 0.00 | 0.00 | 0.00 | 0.00 | 0.00 | 0.00 | 0.00 | 0.00 | 0.00 | 0.00 | 0.00 | 0.00 |
| Al | 0.00 | 0.00 | 0.00 | 0.00 | 0.00 | 0.00 | 0.00 | 0.00 | 0.00 | 0.00 | 0.00 | 0.00 | 0.00 | 0.00 | 0.00 | 0.00 | 0.00 | 0.00 | 0.00 |
| Cr | 0.00 | 0.00 | 0.00 | 0.00 | 0.00 | 0.00 | 0.00 | 0.00 | 0.00 | 0.00 | 0.00 | 0.00 | 0.00 | 0.00 | 0.00 | 0.00 | 0.00 | 0.00 | 0.00 |
| V | 0.00 | 0.00 | 0.00 | 0.00 | 0.00 | 0.00 | 0.00 | 0.00 | 0.00 | 0.00 | 0.00 | 0.00 | 0.00 | 0.00 | 0.00 | 0.00 | 0.00 | 0.00 | 0.00 |
| $Fe^{3+}$ | 0.00 | 0.00 | 0.00 | 0.00 | 0.00 | 0.00 | 0.00 | 0.00 | 0.00 | 0.00 | 0.00 | 0.00 | 0.00 | 0.00 | 0.00 | 0.00 | 0.00 | 0.00 | 0.00 |
| $Fe^{2+}$ | 0.10 | 0.10 | 0.10 | 0.10 | 0.11 | 0.11 | 0.11 | 0.11 | 0.11 | 0.11 | 0.10 | 0.10 | 0.10 | 0.10 | 0.11 | 0.10 | 0.11 | 0.11 | 0.11 |
| Mn | 0.00 | 0.00 | 0.00 | 0.00 | 0.00 | 0.00 | 0.00 | 0.00 | 0.00 | 0.00 | 0.00 | 0.00 | 0.00 | 0.00 | 0.00 | 0.00 | 0.00 | 0.00 | 0.00 |
| Mg | 1.88 | 1.90 | 1.92 | 1.91 | 1.90 | 1.90 | 1.90 | 1.88 | 1.89 | 1.90 | 1.90 | 1.91 | 1.88 | 1.87 | 1.88 | 1.87 | 1.87 | 1.88 | 1.89 |
| Ni | 0.01 | 0.01 | 0.01 | 0.01 | 0.01 | 0.01 | 0.01 | 0.01 | 0.01 | 0.01 | 0.01 | 0.01 | 0.01 | 0.01 | 0.01 | 0.01 | 0.01 | 0.01 | 0.01 |
| Zn | 0.00 | 0.00 | 0.00 | 0.00 | 0.00 | 0.00 | 0.00 | 0.00 | 0.00 | 0.00 | 0.00 | 0.00 | 0.00 | 0.00 | 0.00 | 0.00 | 0.00 | 0.00 | 0.00 |

| Analysis | PUKA2-57 | PUKA2-58 | PUKA2-59 | PUKA2-60 | PUKA2-61 | PUKA2-62 | bordo chr | PUKA2-63 | PUKA2-64 | PUKA2-65 | PUKA2-66 | PUKA2-67 | PUKA2-68 | PUKA2-69 | PUKA2-70 | PUKA2-71 | PUKA2-72 | PUKA2-73 | PUKA2-74 |
|---|---|---|---|---|---|---|---|---|---|---|---|---|---|---|---|---|---|---|---|

| | OL-166 | OL-167 | OL-168 | OL-169 | OL-170 | OL-171 | | CHR-172 | CHR-173 | CHR-174 | CHR-175 | CHR-176 | CHR-177 | CHR-178 | CHR-179 | CHR-180 | CHR-181 | CHR-182 | CHR-183 |
|---|---|---|---|---|---|---|---|---|---|---|---|---|---|---|---|---|---|---|---|
| X | 47.056 | 47.057 | 47.060 | 47.059 | 47.057 | 47.063 | 47.064 | 47.064 | 47.064 | 47.063 | 47.063 | 47.062 | 47.063 | 47.063 | 47.063 | 47.062 | 47.062 | 47.061 | 47.058 |
| Y | 72.857 | 72.870 | 72.883 | 72.891 | 72.898 | 72.900 | 72.912 | 72.915 | 72.916 | 72.918 | 72.918 | 72.921 | 72.923 | 72.923 | 72.927 | 72.933 | 72.941 | 72.953 | 72.970 |
| d(mm) | 0.056 | 0.043 | 0.029 | 0.021 | 0.015 | 0.012 | | 0.003 | 0.004 | 0.006 | 0.006 | 0.009 | 0.011 | 0.012 | 0.016 | 0.021 | 0.029 | 0.041 | 0.059 |
| $SiO_2$ | 41.17 | 41.58 | 41.49 | 40.77 | 41.67 | 42.04 | | 0.04 | 0.00 | 0.00 | 0.04 | 0.03 | 0.04 | 0.03 | 0.04 | 0.00 | 0.01 | 0.07 | 0.00 |
| $TiO_2$ | 0.02 | 0.01 | 0.00 | 0.00 | 0.00 | 0.00 | | 0.10 | 0.12 | 0.15 | 0.15 | 0.14 | 0.12 | 0.14 | 0.14 | 0.12 | 0.08 | 0.13 | 0.13 |
| $Al_2O_3$ | 0.01 | 0.02 | 0.00 | 0.00 | 0.00 | 0.03 | | 29.03 | 28.77 | 28.31 | 28.16 | 27.59 | 27.13 | 27.47 | 26.99 | 26.52 | 26.49 | 26.53 | 26.35 |
| $Cr_2O_3$ | 0.07 | 0.06 | 0.13 | 0.22 | 0.27 | 0.30 | | 41.11 | 41.01 | 41.54 | 41.09 | 41.79 | 42.40 | 42.16 | 42.49 | 42.62 | 42.58 | 43.12 | 43.18 |
| $V_2O_3$ | 0.00 | 0.00 | 0.00 | 0.00 | 0.00 | 0.00 | | 0.00 | 0.00 | 0.00 | 0.00 | 0.00 | 0.00 | 0.00 | 0.00 | 0.00 | 0.00 | 0.00 | 0.00 |
| $Fe_2O_3$ | 0.00 | 0.00 | 0.00 | 0.00 | 0.00 | 0.00 | | 2.36 | 2.46 | 3.00 | 2.83 | 3.05 | 2.98 | 3.04 | 3.87 | 3.89 | 3.85 | 3.71 | 3.67 |
| FeO | 5.12 | 5.13 | 5.04 | 4.81 | 4.78 | 4.83 | | 12.20 | 12.19 | 12.21 | 12.41 | 12.83 | 12.97 | 12.87 | 12.77 | 12.46 | 12.73 | 12.90 | 12.30 |
| MnO | 0.09 | 0.11 | 0.03 | 0.08 | 0.04 | 0.08 | | 0.04 | 0.00 | 0.00 | 0.06 | 0.01 | 0.00 | 0.00 | 0.00 | 0.13 | 0.01 | 0.00 | 0.06 |
| MgO | 52.13 | 52.35 | 52.46 | 52.56 | 53.37 | 52.80 | | 16.19 | 16.07 | 16.15 | 15.87 | 15.64 | 15.54 | 15.68 | 15.80 | 15.73 | 15.57 | 15.77 | 15.90 |
| NiO | 0.66 | 0.59 | 0.57 | 0.64 | 0.62 | 0.60 | | 0.13 | 0.15 | 0.17 | 0.14 | 0.14 | 0.11 | 0.13 | 0.20 | 0.16 | 0.21 | 0.15 | 0.09 |
| ZnO | 0.00 | 0.03 | 0.00 | 0.01 | 0.00 | 0.00 | | 0.01 | 0.00 | 0.01 | 0.00 | 0.02 | 0.00 | 0.00 | 0.03 | 0.00 | 0.00 | 0.00 | 0.07 |
| TOT | 99.29 | 99.88 | 99.74 | 99.13 | 100.76 | 100.72 | | 101.21 | 100.77 | 101.57 | 100.73 | 101.24 | 101.29 | 101.54 | 102.37 | 101.65 | 101.54 | 102.38 | 101.76 |
| Si | 1.00 | 1.00 | 1.00 | 0.99 | 0.99 | 1.00 | | 0.00 | 0.00 | 0.00 | 0.00 | 0.00 | 0.00 | 0.00 | 0.00 | 0.00 | 0.00 | 0.00 | 0.00 |
| Ti | 0.00 | 0.00 | 0.00 | 0.00 | 0.00 | 0.00 | | 0.00 | 0.00 | 0.00 | 0.00 | 0.00 | 0.00 | 0.00 | 0.00 | 0.00 | 0.00 | 0.00 | 0.00 |
| Al | 0.00 | 0.00 | 0.00 | 0.00 | 0.00 | 0.00 | | 1.00 | 0.99 | 0.97 | 0.97 | 0.95 | 0.94 | 0.95 | 0.93 | 0.92 | 0.92 | 0.91 | 0.91 |
| Cr | 0.00 | 0.00 | 0.00 | 0.00 | 0.01 | 0.01 | | 0.95 | 0.95 | 0.96 | 0.95 | 0.97 | 0.99 | 0.98 | 0.98 | 0.99 | 0.99 | 1.00 | 1.00 |
| V | 0.00 | 0.00 | 0.00 | 0.00 | 0.00 | 0.00 | | 0.00 | 0.00 | 0.00 | 0.00 | 0.00 | 0.00 | 0.00 | 0.00 | 0.00 | 0.00 | 0.00 | 0.00 |
| $Fe^{3+}$ | 0.00 | 0.00 | 0.00 | 0.00 | 0.00 | 0.00 | | 0.05 | 0.05 | 0.07 | 0.06 | 0.07 | 0.07 | 0.07 | 0.08 | 0.09 | 0.09 | 0.08 | 0.08 |
| $Fe^{2+}$ | 0.10 | 0.10 | 0.10 | 0.10 | 0.10 | 0.10 | | 0.30 | 0.30 | 0.30 | 0.30 | 0.32 | 0.32 | 0.32 | 0.31 | 0.31 | 0.31 | 0.32 | 0.30 |
| Mn | 0.00 | 0.00 | 0.00 | 0.00 | 0.00 | 0.00 | | 0.00 | 0.00 | 0.00 | 0.00 | 0.00 | 0.00 | 0.00 | 0.00 | 0.00 | 0.00 | 0.00 | 0.00 |
| Mg | 1.88 | 1.88 | 1.88 | 1.90 | 1.89 | 1.88 | | 0.70 | 0.70 | 0.70 | 0.69 | 0.68 | 0.68 | 0.68 | 0.69 | 0.69 | 0.68 | 0.69 | 0.70 |
| Ni | 0.01 | 0.01 | 0.01 | 0.01 | 0.01 | 0.01 | | 0.00 | 0.00 | 0.00 | 0.00 | 0.00 | 0.00 | 0.00 | 0.00 | 0.00 | 0.00 | 0.00 | 0.00 |
| Zn | 0.00 | 0.00 | 0.00 | 0.00 | 0.00 | 0.00 | | 0.00 | 0.00 | 0.00 | 0.00 | 0.00 | 0.00 | 0.00 | 0.00 | 0.00 | 0.00 | 0.00 | 0.00 |

| Analysis | PUKA2-75 | PUKA2-76 | PUKA2-77 | PUKA2-78 | PUKA2-79 | PUKA2-80 | PUKA2-81 | PUKA2-82 | PUKA2-83 | PUKA2-84 | PUKA2-85 | PUKA2-86 | PUKA2-87 | PUKA2-88 | PUKA2-89 | PUKA2-90 | PUKA2-91 | PUKA2-92 | PUKA2-93 |
|---|---|---|---|---|---|---|---|---|---|---|---|---|---|---|---|---|---|---|---|
| | CHR-184 | CHR-185 | CHR-186 | CHR-187 | CHR-188 | CHR-189 | CHR-190 | CHR-191 | CHR-192 | CHR-193 | CHR-194 | CHR-195 | CHR-196 | CHR-197 | CHR-198 | CHR-199 | CHR-200 | CHR-201 | CHR-202 |
| X | 47.057 | 47.056 | 47.059 | 47.064 | 47.065 | 42.715 | 42.669 | 42.608 | 42.549 | 42.469 | 42.396 | 42.359 | 42.309 | 42.292 | 42.256 | 42.219 | 42.201 | 42.174 | 42.143 |
| Y | 72.986 | 72.999 | 73.015 | 73.049 | 73.058 | 93.247 | 93.260 | 93.290 | 93.323 | 93.335 | 93.380 | 93.383 | 93.396 | 93.410 | 93.425 | 93.440 | 93.444 | 93.454 | 93.461 |
| d(mm) | 0.074 | 0.088 | 0.103 | 0.138 | 0.146 | 0.702 | 0.655 | 0.587 | 0.521 | 0.441 | 0.358 | 0.321 | 0.270 | 0.250 | 0.211 | 0.171 | 0.153 | 0.124 | 0.093 |
| $SiO_2$ | 0.01 | 0.00 | 0.03 | 0.03 | 0.00 | 0.02 | 0.00 | 0.03 | 0.01 | 0.01 | 0.00 | 0.00 | 0.04 | 0.00 | 0.01 | 0.05 | 0.02 | 0.00 | 0.00 |
| $TiO_2$ | 0.13 | 0.10 | 0.11 | 0.10 | 0.13 | 0.13 | 0.10 | 0.15 | 0.10 | 0.17 | 0.17 | 0.10 | 0.12 | 0.13 | 0.11 | 0.11 | 0.14 | 0.12 | 0.15 |
| $Al_2O_3$ | 26.22 | 26.10 | 26.28 | 26.28 | 26.18 | 26.63 | 26.40 | 26.63 | 26.34 | 26.36 | 26.56 | 26.39 | 26.32 | 26.31 | 26.61 | 26.57 | 26.18 | 26.31 | 25.69 |
| $Cr_2O_3$ | 43.05 | 43.32 | 43.59 | 43.39 | 43.60 | 43.29 | 43.41 | 43.20 | 42.94 | 43.79 | 43.61 | 43.09 | 43.75 | 42.87 | 43.07 | 43.49 | 43.32 | 43.56 | 43.71 |
| $V_2O_3$ | 0.00 | 0.00 | 0.00 | 0.00 | 0.00 | 0.00 | 0.00 | 0.00 | 0.00 | 0.00 | 0.00 | 0.00 | 0.00 | 0.00 | 0.00 | 0.00 | 0.00 | 0.00 | 0.00 |
| $Fe_2O_3$ | 4.00 | 3.83 | 3.78 | 3.53 | 3.63 | 2.84 | 3.17 | 2.87 | 3.01 | 2.80 | 3.41 | 3.65 | 3.28 | 3.16 | 3.32 | 3.28 | 3.54 | 3.52 | 3.98 |
| FeO | 12.55 | 12.32 | 12.35 | 12.45 | 12.26 | 12.28 | 12.17 | 12.37 | 12.01 | 12.66 | 12.18 | 12.31 | 12.62 | 12.55 | 12.42 | 12.51 | 12.30 | 12.33 | 12.07 |
| MnO | 0.01 | 0.00 | 0.00 | 0.10 | 0.03 | 0.05 | 0.11 | 0.12 | 0.03 | 0.00 | 0.04 | 0.15 | 0.15 | 0.03 | 0.03 | 0.12 | 0.09 | 0.06 | 0.09 |
| MgO | 15.79 | 15.89 | 16.03 | 15.81 | 15.92 | 15.89 | 15.89 | 15.77 | 15.80 | 15.72 | 16.10 | 15.82 | 15.74 | 15.57 | 15.84 | 15.84 | 15.85 | 15.90 | 15.95 |
| NiO | 0.16 | 0.13 | 0.12 | 0.14 | 0.13 | 0.13 | 0.11 | 0.20 | 0.17 | 0.16 | 0.21 | 0.13 | 0.18 | 0.11 | 0.12 | 0.19 | 0.14 | 0.16 | 0.18 |
| ZnO | 0.00 | 0.00 | 0.05 | 0.02 | 0.14 | 0.00 | 0.02 | 0.01 | 0.03 | 0.01 | 0.04 | 0.01 | 0.00 | 0.00 | 0.04 | 0.00 | 0.05 | 0.02 | 0.03 |
| TOT | 101.93 | 101.69 | 102.34 | 101.85 | 102.02 | 101.26 | 101.37 | 101.34 | 100.47 | 101.69 | 102.32 | 101.65 | 102.19 | 100.73 | 101.56 | 102.19 | 101.64 | 101.99 | 101.88 |
| Si | 0.00 | 0.00 | 0.00 | 0.00 | 0.00 | 0.00 | 0.00 | 0.00 | 0.00 | 0.00 | 0.00 | 0.00 | 0.00 | 0.00 | 0.00 | 0.00 | 0.00 | 0.00 | 0.00 |
| Ti | 0.00 | 0.00 | 0.00 | 0.00 | 0.00 | 0.00 | 0.00 | 0.00 | 0.00 | 0.00 | 0.00 | 0.00 | 0.00 | 0.00 | 0.00 | 0.00 | 0.00 | 0.00 | 0.00 |
| Al | 0.91 | 0.90 | 0.90 | 0.91 | 0.90 | 0.92 | 0.92 | 0.92 | 0.92 | 0.91 | 0.91 | 0.91 | 0.91 | 0.92 | 0.92 | 0.91 | 0.91 | 0.91 | 0.89 |
| Cr | 1.00 | 1.01 | 1.01 | 1.01 | 1.01 | 1.01 | 1.01 | 1.00 | 1.01 | 1.02 | 1.01 | 1.00 | 1.01 | 1.00 | 1.00 | 1.00 | 1.01 | 1.01 | 1.02 |
| V | 0.00 | 0.00 | 0.00 | 0.00 | 0.00 | 0.00 | 0.00 | 0.00 | 0.00 | 0.00 | 0.00 | 0.00 | 0.00 | 0.00 | 0.00 | 0.00 | 0.00 | 0.00 | 0.00 |
| $Fe^{3+}$ | 0.09 | 0.08 | 0.08 | 0.08 | 0.08 | 0.06 | 0.07 | 0.06 | 0.07 | 0.06 | 0.07 | 0.08 | 0.07 | 0.07 | 0.07 | 0.07 | 0.08 | 0.08 | 0.09 |
| $Fe^{2+}$ | 0.31 | 0.30 | 0.30 | 0.31 | 0.30 | 0.30 | 0.30 | 0.30 | 0.30 | 0.31 | 0.30 | 0.30 | 0.31 | 0.31 | 0.30 | 0.31 | 0.30 | 0.30 | 0.30 |
| Mn | 0.00 | 0.00 | 0.00 | 0.00 | 0.00 | 0.00 | 0.00 | 0.00 | 0.00 | 0.00 | 0.00 | 0.00 | 0.00 | 0.00 | 0.00 | 0.00 | 0.00 | 0.00 | 0.00 |
| Mg | 0.69 | 0.70 | 0.70 | 0.69 | 0.70 | 0.70 | 0.70 | 0.69 | 0.70 | 0.69 | 0.70 | 0.69 | 0.69 | 0.69 | 0.69 | 0.69 | 0.69 | 0.69 | 0.70 |
| Ni | 0.00 | 0.00 | 0.00 | 0.00 | 0.00 | 0.00 | 0.00 | 0.00 | 0.00 | 0.00 | 0.00 | 0.00 | 0.00 | 0.00 | 0.00 | 0.00 | 0.00 | 0.00 | 0.00 |

| Zn | 0.00 | 0.00 | 0.00 | 0.00 | 0.00 | 0.00 | 0.00 | 0.00 | 0.00 | 0.00 | 0.00 | 0.00 | 0.00 | 0.00 | 0.00 | 0.00 | 0.00 | 0.00 | 0.00 |
|---|---|---|---|---|---|---|---|---|---|---|---|---|---|---|---|---|---|---|---|

| Analysis | PUKA2-94 CHR-203 | PUKA2-95 CHR-204 | PUKA2-96 CHR-205 | PUKA2-97 CHR-206 | PUKA2-98 CHR-207 | PUKA2-99 CHR-208 | bordo chr | PUKA2-103 OL-212 | PUKA2-104 OL-213 | PUKA2-105 OL-214 | PUKA2-106 OL-215 | PUKA2-107 OL-216 | PUKA2-108 OL-217 | PUKA2-109 OL-218 | PUKA2-110 OL-219 | PUKA2-111 OL-220 | PUKA2-112 OL-221 | PUKA2-113 OL-222 | PUKA2-114 OL-223 |
|---|---|---|---|---|---|---|---|---|---|---|---|---|---|---|---|---|---|---|---|
| X | 42.116 | 42.098 | 42.081 | 42.074 | 42.068 | 42.061 | 42.052 | 42.029 | 42.028 | 42.025 | 42.020 | 41.993 | 41.969 | 41.937 | 41.895 | 41.837 | 41.745 | 41.717 | 41.559 |
| Y | 93.467 | 93.472 | 93.469 | 93.469 | 93.471 | 93.474 | 93.480 | 93.502 | 93.503 | 93.503 | 93.503 | 93.526 | 93.526 | 93.533 | 93.540 | 93.569 | 93.615 | 93.672 | 93.620 |
| d(mm) | 0.065 | 0.047 | 0.031 | 0.024 | 0.018 | 0.011 | | 0.032 | 0.034 | 0.036 | 0.040 | 0.075 | 0.095 | 0.127 | 0.168 | 0.233 | 0.335 | 0.386 | 0.459 |
| $SiO_2$ | 0.03 | 0.02 | 0.00 | 0.00 | 0.00 | 0.05 | | 42.37 | 42.07 | 42.35 | 42.30 | 40.64 | 42.10 | 41.80 | 41.35 | 42.56 | 42.18 | 41.82 | 41.70 |
| $TiO_2$ | 0.13 | 0.10 | 0.09 | 0.10 | 0.11 | 0.09 | | 0.00 | 0.02 | 0.00 | 0.00 | 0.00 | 0.00 | 0.00 | 0.00 | 0.00 | 0.00 | 0.00 | 0.00 |
| $Al_2O_3$ | 25.80 | 25.41 | 25.44 | 25.71 | 25.71 | 22.70 | | 0.01 | 0.02 | 0.01 | 0.01 | 0.03 | 0.00 | 0.30 | 0.05 | 0.00 | 0.03 | 0.01 | 0.00 |
| $Cr_2O_3$ | 44.62 | 44.80 | 43.73 | 44.41 | 45.25 | 48.42 | | 0.09 | 0.08 | 0.08 | 0.08 | 0.05 | 0.03 | 0.02 | 0.00 | 0.00 | 0.00 | 0.00 | 0.02 |
| $V_2O_3$ | 0.00 | 0.00 | 0.00 | 0.00 | 0.00 | 0.00 | | 0.00 | 0.00 | 0.00 | 0.00 | 0.00 | 0.00 | 0.00 | 0.00 | 0.00 | 0.00 | 0.00 | 0.00 |
| $Fe_2O_3$ | 3.34 | 3.68 | 3.67 | 2.88 | 1.97 | 1.09 | | 0.00 | 0.00 | 0.00 | 0.00 | 0.00 | 0.00 | 0.00 | 0.00 | 0.00 | 0.00 | 0.00 | 0.00 |
| FeO | 12.91 | 13.14 | 12.63 | 13.19 | 13.90 | 14.76 | | 4.80 | 4.77 | 4.83 | 4.52 | 4.88 | 5.15 | 4.13 | 4.99 | 5.24 | 5.87 | 6.07 | 6.08 |
| MnO | 0.07 | 0.13 | 0.00 | 0.02 | 0.04 | 0.00 | | 0.03 | 0.07 | 0.03 | 0.12 | 0.04 | 0.08 | 0.02 | 0.05 | 0.08 | 0.07 | 0.07 | 0.01 |
| MgO | 15.70 | 15.47 | 15.52 | 15.28 | 14.86 | 13.88 | | 53.28 | 53.56 | 53.75 | 56.43 | 56.37 | 53.07 | 53.00 | 53.07 | 53.54 | 53.02 | 52.68 | 52.85 |
| NiO | 0.11 | 0.11 | 0.13 | 0.11 | 0.15 | 0.17 | | 0.57 | 0.55 | 0.54 | 0.54 | 0.51 | 0.56 | 0.48 | 0.53 | 0.57 | 0.53 | 0.56 | 0.55 |
| ZnO | 0.00 | 0.00 | 0.00 | 0.00 | 0.00 | 0.00 | | 0.00 | 0.00 | 0.00 | 0.01 | 0.01 | 0.00 | 0.01 | 0.00 | 0.00 | 0.02 | 0.02 | 0.00 |
| TOT | 102.70 | 102.86 | 101.21 | 101.71 | 101.99 | 101.16 | | 101.14 | 101.14 | 101.61 | 104.02 | 102.56 | 100.99 | 99.77 | 100.05 | 102.00 | 101.74 | 101.24 | 101.22 |
| Si | 0.00 | 0.00 | 0.00 | 0.00 | 0.00 | 0.00 | | 1.01 | 1.00 | 1.00 | 0.97 | 0.94 | 1.00 | 1.00 | 0.99 | 1.00 | 1.00 | 1.00 | 0.99 |
| Ti | 0.00 | 0.00 | 0.00 | 0.00 | 0.00 | 0.00 | | 0.00 | 0.00 | 0.00 | 0.00 | 0.00 | 0.00 | 0.00 | 0.00 | 0.00 | 0.00 | 0.00 | 0.00 |
| Al | 0.89 | 0.88 | 0.89 | 0.89 | 0.89 | 0.81 | | 0.00 | 0.00 | 0.00 | 0.00 | 0.00 | 0.00 | 0.01 | 0.00 | 0.00 | 0.00 | 0.00 | 0.00 |
| Cr | 1.03 | 1.04 | 1.03 | 1.04 | 1.06 | 1.16 | | 0.00 | 0.00 | 0.00 | 0.00 | 0.00 | 0.00 | 0.00 | 0.00 | 0.00 | 0.00 | 0.00 | 0.00 |
| V | 0.00 | 0.00 | 0.00 | 0.00 | 0.00 | 0.00 | | 0.00 | 0.00 | 0.00 | 0.00 | 0.00 | 0.00 | 0.00 | 0.00 | 0.00 | 0.00 | 0.00 | 0.00 |
| $Fe^{3+}$ | 0.07 | 0.08 | 0.08 | 0.06 | 0.04 | 0.02 | | 0.00 | 0.00 | 0.00 | 0.00 | 0.00 | 0.00 | 0.00 | 0.00 | 0.00 | 0.00 | 0.00 | 0.00 |
| $Fe^{2+}$ | 0.32 | 0.32 | 0.31 | 0.33 | 0.34 | 0.37 | | 0.10 | 0.09 | 0.10 | 0.09 | 0.09 | 0.10 | 0.08 | 0.10 | 0.10 | 0.12 | 0.12 | 0.12 |
| Mn | 0.00 | 0.00 | 0.00 | 0.00 | 0.00 | 0.00 | | 0.00 | 0.00 | 0.00 | 0.00 | 0.00 | 0.00 | 0.00 | 0.00 | 0.00 | 0.00 | 0.00 | 0.00 |
| Mg | 0.68 | 0.68 | 0.69 | 0.67 | 0.65 | 0.63 | | 1.89 | 1.89 | 1.89 | 1.93 | 1.95 | 1.88 | 1.90 | 1.90 | 1.88 | 1.87 | 1.87 | 1.88 |
| Ni | 0.00 | 0.00 | 0.00 | 0.00 | 0.00 | 0.00 | | 0.01 | 0.01 | 0.01 | 0.01 | 0.01 | 0.01 | 0.01 | 0.01 | 0.01 | 0.01 | 0.01 | 0.01 |
| Zn | 0.00 | 0.00 | 0.00 | 0.00 | 0.00 | 0.00 | | 0.00 | 0.00 | 0.00 | 0.00 | 0.00 | 0.00 | 0.00 | 0.00 | 0.00 | 0.00 | 0.00 | 0.00 |

| Analysis | PUKA2-115 OL-224 | PUKA2-116 OL-225 | PUKA2-117 OL-226 | PUKA2-118 OL-227 | PUKA2-119 OL-228 | PUKA2-120 OL-229 | PUKA2-121 OL-230 | PUKA2-122 OL-231 | PUKA2-123 OL-232 | PUKA2-124 OL-233 | PUKA2-125 OL-234 | PUKA2-126 OL-235 | PUKA2-127 OL-236 | PUKA2-128 OL-237 | PUKA2-129 OL-238 | PUKA2-130 OL-239 | PUKA2-131 OL-240 | bordo chr | PUKA2-133 CHR-242 |
|---|---|---|---|---|---|---|---|---|---|---|---|---|---|---|---|---|---|---|---|
| X | 41.509 | 41.475 | 41.443 | 41.398 | 41.379 | 41.336 | 41.287 | 41.272 | 41.297 | 41.291 | 41.269 | 41.257 | 41.246 | 41.237 | 41.232 | 41.226 | 41.223 | 41.213 | 41.208 |
| Y | 93.636 | 93.667 | 93.687 | 93.720 | 93.732 | 93.779 | 93.767 | 93.771 | 93.882 | 93.892 | 93.900 | 93.905 | 93.909 | 93.913 | 93.914 | 93.916 | 93.917 | 93.922 | 93.923 |
| d(mm) | 0.412 | 0.366 | 0.329 | 0.274 | 0.252 | 0.189 | 0.172 | 0.162 | 0.093 | 0.083 | 0.060 | 0.047 | 0.036 | 0.026 | 0.020 | 0.015 | 0.011 | | 0.005 |
| $SiO_2$ | 41.83 | 42.13 | 42.65 | 42.57 | 42.43 | 42.63 | 42.05 | 42.51 | 42.71 | 42.78 | 42.75 | 42.70 | 42.66 | 42.32 | 43.27 | 42.49 | 36.03 | | 0.00 |
| $TiO_2$ | 0.02 | 0.05 | 0.02 | 0.02 | 0.00 | 0.01 | 0.00 | 0.00 | 0.00 | 0.00 | 0.00 | 0.00 | 0.01 | 0.00 | 0.03 | 0.01 | 0.01 | | 0.10 |
| $Al_2O_3$ | 0.01 | 0.00 | 0.04 | 0.02 | 0.00 | 0.01 | 0.00 | 0.00 | 0.00 | 0.00 | 0.00 | 0.00 | 0.00 | 0.03 | 0.00 | 0.00 | 0.61 | | 25.88 |
| $Cr_2O_3$ | 0.00 | 0.00 | 0.04 | 0.00 | 0.00 | 0.02 | 0.03 | 0.00 | 0.01 | 0.05 | 0.05 | 0.05 | 0.20 | 0.15 | 0.24 | 0.31 | 0.53 | | 44.58 |
| $V_2O_3$ | 0.00 | 0.00 | 0.00 | 0.00 | 0.00 | 0.00 | 0.00 | 0.00 | 0.00 | 0.00 | 0.00 | 0.00 | 0.00 | 0.00 | 0.00 | 0.00 | 0.00 | | 0.00 |
| $Fe_2O_3$ | 0.00 | 0.00 | 0.00 | 0.00 | 0.00 | 0.00 | 0.00 | 0.00 | 0.00 | 0.00 | 0.00 | 0.00 | 0.00 | 0.00 | 0.00 | 0.00 | 0.00 | | 1.58 |
| FeO | 5.79 | 5.92 | 5.84 | 5.62 | 5.80 | 5.45 | 5.65 | 5.33 | 4.97 | 4.46 | 4.28 | 4.76 | 4.62 | 4.56 | 4.52 | 4.18 | 3.20 | | 13.59 |
| MnO | 0.08 | 0.07 | 0.08 | 0.06 | 0.07 | 0.02 | 0.03 | 0.06 | 0.01 | 0.04 | 0.09 | 0.11 | 0.06 | 0.01 | 0.11 | 0.06 | 0.10 | | 0.06 |
| MgO | 52.79 | 51.28 | 51.58 | 51.92 | 51.31 | 51.78 | 51.56 | 51.47 | 52.05 | 52.28 | 52.46 | 52.85 | 52.56 | 52.75 | 53.64 | 53.52 | 52.24 | | 14.82 |
| NiO | 0.49 | 0.47 | 0.59 | 0.53 | 0.62 | 0.51 | 0.49 | 0.52 | 0.56 | 0.53 | 0.61 | 0.51 | 0.61 | 0.57 | 0.54 | 0.56 | 0.59 | | 0.12 |
| ZnO | 0.00 | 0.00 | 0.04 | 0.03 | 0.03 | 0.06 | 0.00 | 0.03 | 0.04 | 0.00 | 0.00 | 0.00 | 0.00 | 0.00 | 0.03 | 0.07 | 0.03 | | 0.00 |
| TOT | 101.01 | 99.94 | 100.90 | 100.76 | 100.30 | 100.50 | 99.83 | 99.93 | 100.35 | 100.15 | 100.24 | 100.99 | 100.72 | 100.41 | 102.41 | 101.19 | 93.38 | | 100.74 |
| Si | 1.00 | 1.02 | 1.02 | 1.02 | 1.02 | 1.02 | 1.02 | 1.03 | 1.03 | 1.03 | 1.02 | 1.02 | 1.02 | 1.01 | 1.02 | 1.01 | 0.91 | | 0.00 |
| Ti | 0.00 | 0.00 | 0.00 | 0.00 | 0.00 | 0.00 | 0.00 | 0.00 | 0.00 | 0.00 | 0.00 | 0.00 | 0.00 | 0.00 | 0.00 | 0.00 | 0.00 | | 0.00 |
| Al | 0.00 | 0.00 | 0.00 | 0.00 | 0.00 | 0.00 | 0.00 | 0.00 | 0.00 | 0.00 | 0.00 | 0.00 | 0.00 | 0.00 | 0.00 | 0.00 | 0.02 | | 0.91 |
| Cr | 0.00 | 0.00 | 0.00 | 0.00 | 0.00 | 0.00 | 0.00 | 0.00 | 0.00 | 0.00 | 0.00 | 0.00 | 0.00 | 0.00 | 0.00 | 0.01 | 0.01 | | 1.05 |

| | | | | | | | | | | | | | | | | | | |
|---|---|---|---|---|---|---|---|---|---|---|---|---|---|---|---|---|---|---|
| V | 0.00 | 0.00 | 0.00 | 0.00 | 0.00 | 0.00 | 0.00 | 0.00 | 0.00 | 0.00 | 0.00 | 0.00 | 0.00 | 0.00 | 0.00 | 0.00 | 0.00 | 0.00 |
| $Fe^{3+}$ | 0.00 | 0.00 | 0.00 | 0.00 | 0.00 | 0.00 | 0.00 | 0.00 | 0.00 | 0.00 | 0.00 | 0.00 | 0.00 | 0.00 | 0.00 | 0.00 | 0.00 | 0.04 |
| $Fe^{2+}$ | 0.12 | 0.12 | 0.12 | 0.11 | 0.12 | 0.11 | 0.11 | 0.11 | 0.10 | 0.09 | 0.09 | 0.09 | 0.09 | 0.09 | 0.09 | 0.08 | 0.07 | 0.34 |
| Mn | 0.00 | 0.00 | 0.00 | 0.00 | 0.00 | 0.00 | 0.00 | 0.00 | 0.00 | 0.00 | 0.00 | 0.00 | 0.00 | 0.00 | 0.00 | 0.00 | 0.00 | 0.00 |
| Mg | 1.88 | 1.85 | 1.84 | 1.85 | 1.84 | 1.85 | 1.86 | 1.85 | 1.86 | 1.87 | 1.87 | 1.88 | 1.87 | 1.88 | 1.88 | 1.89 | 1.97 | 0.66 |
| Ni | 0.01 | 0.01 | 0.01 | 0.01 | 0.01 | 0.01 | 0.01 | 0.01 | 0.01 | 0.01 | 0.01 | 0.01 | 0.01 | 0.01 | 0.01 | 0.01 | 0.01 | 0.00 |
| Zn | 0.00 | 0.00 | 0.00 | 0.00 | 0.00 | 0.00 | 0.00 | 0.00 | 0.00 | 0.00 | 0.00 | 0.00 | 0.00 | 0.00 | 0.00 | 0.00 | 0.00 | 0.00 |

| Analysis | PUKA2-134 | PUKA2-135 | PUKA2-136 | PUKA2-137 | PUKA2-138 | PUKA2-139 | PUKA2-140 | PUKA2-141 | PUKA2-142 | PUKA2-143 | PUKA2-144 |
|---|---|---|---|---|---|---|---|---|---|---|---|
| | CHR-243 | CHR-244 | CHR-245 | CHR-246 | CHR-247 | CHR-248 | CHR-249 | CHR-250 | CHR-251 | CHR-252 | CHR-253 |
| X | 41.205 | 41.197 | 41.193 | 41.184 | 41.179 | 41.171 | 41.146 | 41.130 | 41.087 | 41.025 | 40.953 |
| Y | 93.924 | 93.927 | 93.928 | 93.932 | 93.935 | 93.940 | 93.952 | 93.955 | 93.972 | 93.995 | 94.042 |
| d(mm) | 0.008 | 0.017 | 0.021 | 0.030 | 0.036 | 0.045 | 0.074 | 0.090 | 0.135 | 0.201 | 0.286 |
| $SiO_2$ | 0.01 | 0.02 | 0.03 | 0.00 | 0.01 | 0.04 | 0.03 | 0.04 | 0.00 | 0.00 | 0.02 |
| $TiO_2$ | 0.09 | 0.11 | 0.10 | 0.10 | 0.12 | 0.13 | 0.11 | 0.10 | 0.15 | 0.14 | 0.14 |
| $Al_2O_3$ | 26.64 | 26.61 | 26.51 | 26.33 | 26.28 | 26.78 | 26.64 | 26.39 | 26.69 | 26.28 | 26.55 |
| $Cr_2O_3$ | 43.56 | 43.60 | 43.88 | 43.26 | 43.66 | 43.83 | 43.70 | 43.54 | 43.60 | 43.12 | 43.24 |
| $V_2O_3$ | 0.00 | 0.00 | 0.00 | 0.00 | 0.00 | 0.00 | 0.00 | 0.00 | 0.00 | 0.00 | 0.00 |
| $Fe_2O_3$ | 2.48 | 2.78 | 2.94 | 3.11 | 3.54 | 2.77 | 3.42 | 3.54 | 3.59 | 3.52 | 3.58 |
| FeO | 12.68 | 12.54 | 12.14 | 12.25 | 11.84 | 12.76 | 12.57 | 11.99 | 12.20 | 12.09 | 12.22 |
| MnO | 0.14 | 0.01 | 0.04 | 0.09 | 0.05 | 0.03 | 0.02 | 0.11 | 0.07 | 0.08 | 0.04 |
| MgO | 15.52 | 15.83 | 16.10 | 15.75 | 16.18 | 15.88 | 15.99 | 16.16 | 16.21 | 15.91 | 16.05 |
| NiO | 0.18 | 0.06 | 0.10 | 0.14 | 0.14 | 0.06 | 0.15 | 0.11 | 0.14 | 0.17 | 0.21 |
| ZnO | 0.00 | 0.02 | 0.03 | 0.03 | 0.11 | 0.01 | 0.00 | 0.01 | 0.00 | 0.04 | 0.00 |
| TOT | 101.29 | 101.57 | 101.89 | 101.05 | 101.93 | 102.27 | 102.64 | 101.98 | 102.66 | 101.35 | 102.05 |
| Si | 0.00 | 0.00 | 0.00 | 0.00 | 0.00 | 0.00 | 0.00 | 0.00 | 0.00 | 0.00 | 0.00 |
| Ti | 0.00 | 0.00 | 0.00 | 0.00 | 0.00 | 0.00 | 0.00 | 0.00 | 0.00 | 0.00 | 0.00 |
| Al | 0.93 | 0.92 | 0.91 | 0.92 | 0.91 | 0.92 | 0.91 | 0.91 | 0.91 | 0.91 | 0.91 |
| Cr | 1.02 | 1.01 | 1.01 | 1.01 | 1.01 | 1.01 | 1.01 | 1.01 | 1.00 | 1.00 | 1.00 |
| V | 0.00 | 0.00 | 0.00 | 0.00 | 0.00 | 0.00 | 0.00 | 0.00 | 0.00 | 0.00 | 0.00 |
| $Fe^{3+}$ | 0.05 | 0.06 | 0.06 | 0.07 | 0.08 | 0.06 | 0.07 | 0.08 | 0.08 | 0.08 | 0.08 |
| $Fe^{2+}$ | 0.31 | 0.31 | 0.30 | 0.30 | 0.29 | 0.31 | 0.31 | 0.29 | 0.30 | 0.30 | 0.30 |
| Mn | 0.00 | 0.00 | 0.00 | 0.00 | 0.00 | 0.00 | 0.00 | 0.00 | 0.00 | 0.00 | 0.00 |
| Mg | 0.68 | 0.69 | 0.70 | 0.69 | 0.71 | 0.69 | 0.69 | 0.70 | 0.70 | 0.70 | 0.70 |
| Ni | 0.00 | 0.00 | 0.00 | 0.00 | 0.00 | 0.00 | 0.00 | 0.00 | 0.00 | 0.00 | 0.00 |
| Zn | 0.00 | 0.00 | 0.00 | 0.00 | 0.00 | 0.00 | 0.00 | 0.00 | 0.00 | 0.00 | 0.00 |

Tab. A3.14 OLPU1-GRID1 (Iballe) microprobe analyses of olivine and chromite crystals; d(mm) distance from the intergranular limit

| Analysis | GRID1-1 | GRID1-3 | GRID1-4 | GRID1-8 | GRID1-9 | GRID2-1 | GRID2-2 | GRID2-3 | GRID2-4 | GRID2-5 | GRID2-7 | GRID2-8 | GRID2-9 | GRID3-1 | GRID3-3 | GRID3-4 | GRID3-7 | GRID3-8 | GRID3-9 |
|---|---|---|---|---|---|---|---|---|---|---|---|---|---|---|---|---|---|---|---|
| | 57-OL | 59-OL | 60-OL | 64-OL | 65-OL | 66-OL | 67-OL | 68-OL | 69-OL | 70-OL | 72-OL | 73-OL | 74-OL | 75-OL | 77-OL | 78-OL | 81-OL | 82-OL | 83-OL |
| X | 74.68 | 74.68 | 74.68 | 74.68 | 74.68 | 74.78 | 74.78 | 74.78 | 74.78 | 74.78 | 74.78 | 74.78 | 74.78 | 74.88 | 74.88 | 74.88 | 74.88 | 74.88 | 74.88 |
| Y | 74.65 | 74.85 | 74.95 | 75.35 | 75.45 | 74.65 | 74.75 | 74.85 | 74.95 | 75.05 | 75.25 | 75.35 | 75.45 | 74.65 | 74.85 | 74.95 | 75.25 | 75.35 | 75.45 |
| $SiO_2$ | 40.44 | 40.83 | 41.00 | 41.46 | 41.12 | 42.91 | 41.00 | 40.91 | 41.32 | 42.50 | 41.32 | 41.24 | 41.61 | 40.00 | 40.38 | 40.46 | 41.70 | 40.91 | 41.03 |
| $TiO_2$ | 0.00 | 0.00 | 0.04 | 0.00 | 0.00 | 0.00 | 0.00 | 0.07 | 0.00 | 0.00 | 0.00 | 0.00 | 0.00 | 0.00 | 0.00 | 0.00 | 0.01 | 0.03 | 0.00 |
| $Al_2O_3$ | 0.05 | 0.01 | 0.01 | 0.02 | 0.01 | 0.00 | 0.02 | 0.02 | 0.00 | 0.00 | 0.01 | 0.01 | 0.00 | 0.02 | 0.00 | 0.01 | 0.00 | 0.01 | 0.00 |
| $Cr_2O_3$ | 0.01 | 0.01 | 0.00 | 0.00 | 0.00 | 0.00 | 0.00 | 0.04 | 0.04 | 0.00 | 0.02 | 0.00 | 0.00 | 0.00 | 0.00 | 0.03 | 0.00 | 0.00 | 0.00 |
| $V_2O_3$ | 0.00 | 0.00 | 0.00 | 0.00 | 0.00 | 0.00 | 0.00 | 0.00 | 0.00 | 0.00 | 0.00 | 0.00 | 0.00 | 0.00 | 0.00 | 0.00 | 0.00 | 0.00 | 0.00 |
| $Fe_2O_3$ | 0.00 | 0.00 | 0.00 | 0.00 | 0.00 | 0.00 | 0.00 | 0.00 | 0.00 | 0.00 | 0.00 | 0.00 | 0.00 | 0.00 | 0.00 | 0.00 | 0.00 | 0.00 | 0.00 |
| FeO | 5.85 | 5.65 | 5.84 | 5.93 | 5.76 | 5.84 | 5.92 | 6.12 | 5.99 | 5.98 | 6.13 | 5.79 | 5.81 | 5.71 | 5.83 | 5.46 | 5.82 | 5.88 | 6.03 |
| MnO | 0.07 | 0.08 | 0.05 | 0.11 | 0.07 | 0.12 | 0.05 | 0.05 | 0.10 | 0.05 | 0.11 | 0.11 | 0.10 | 0.10 | 0.06 | 0.06 | 0.08 | 0.04 | 0.07 |

# Appendix: Chapter 3

| | | | | | | | | | | | | | | | | | | | |
|---|---|---|---|---|---|---|---|---|---|---|---|---|---|---|---|---|---|---|---|
| MgO | 54.64 | 52.18 | 51.60 | 52.31 | 52.69 | 49.34 | 51.61 | 51.82 | 51.84 | 51.19 | 51.99 | 52.51 | 52.21 | 51.47 | 51.96 | 52.64 | 51.97 | 52.02 | 52.12 |
| NiO | 0.47 | 0.40 | 0.42 | 0.32 | 0.43 | 0.45 | 0.46 | 0.43 | 0.33 | 0.51 | 0.38 | 0.51 | 0.48 | 0.50 | 0.48 | 0.42 | 0.44 | 0.43 | 0.43 |
| ZnO | 0.07 | 0.01 | 0.05 | 0.07 | 0.00 | 0.00 | 0.00 | 0.07 | 0.00 | 0.00 | 0.15 | 0.04 | 0.00 | 0.00 | 0.00 | 0.14 | 0.00 | 0.00 | 0.01 |
| TOT | 101.61 | 99.20 | 99.02 | 100.25 | 100.13 | 98.68 | 99.06 | 99.54 | 99.63 | 100.23 | 100.15 | 100.23 | 100.23 | 97.81 | 98.74 | 99.24 | 100.04 | 99.34 | 99.73 |
| Si | 0.95 | 0.99 | 1.00 | 1.00 | 0.99 | 1.06 | 1.00 | 0.99 | 1.00 | 1.03 | 1.00 | 0.99 | 1.00 | 0.98 | 0.98 | 0.98 | 1.00 | 0.99 | 0.99 |
| Ti | 0.00 | 0.00 | 0.00 | 0.00 | 0.00 | 0.00 | 0.00 | 0.00 | 0.00 | 0.00 | 0.00 | 0.00 | 0.00 | 0.00 | 0.00 | 0.00 | 0.00 | 0.00 | 0.00 |
| Al | 0.00 | 0.00 | 0.00 | 0.00 | 0.00 | 0.00 | 0.00 | 0.00 | 0.00 | 0.00 | 0.00 | 0.00 | 0.00 | 0.00 | 0.00 | 0.00 | 0.00 | 0.00 | 0.00 |
| Cr | 0.00 | 0.00 | 0.00 | 0.00 | 0.00 | 0.00 | 0.00 | 0.00 | 0.00 | 0.00 | 0.00 | 0.00 | 0.00 | 0.00 | 0.00 | 0.00 | 0.00 | 0.00 | 0.00 |
| V | 0.00 | 0.00 | 0.00 | 0.00 | 0.00 | 0.00 | 0.00 | 0.00 | 0.00 | 0.00 | 0.00 | 0.00 | 0.00 | 0.00 | 0.00 | 0.00 | 0.00 | 0.00 | 0.00 |
| $Fe^{3+}$ | 0.00 | 0.00 | 0.00 | 0.00 | 0.00 | 0.00 | 0.00 | 0.00 | 0.00 | 0.00 | 0.00 | 0.00 | 0.00 | 0.00 | 0.00 | 0.00 | 0.00 | 0.00 | 0.00 |
| $Fe^{2+}$ | 0.12 | 0.11 | 0.12 | 0.12 | 0.12 | 0.12 | 0.12 | 0.12 | 0.12 | 0.12 | 0.12 | 0.12 | 0.12 | 0.12 | 0.12 | 0.11 | 0.12 | 0.12 | 0.12 |
| Mn | 0.00 | 0.00 | 0.00 | 0.00 | 0.00 | 0.00 | 0.00 | 0.00 | 0.00 | 0.00 | 0.00 | 0.00 | 0.00 | 0.00 | 0.00 | 0.00 | 0.00 | 0.00 | 0.00 |
| Mg | 1.92 | 1.89 | 1.87 | 1.87 | 1.89 | 1.81 | 1.87 | 1.87 | 1.87 | 1.84 | 1.87 | 1.88 | 1.87 | 1.89 | 1.89 | 1.90 | 1.87 | 1.88 | 1.88 |
| Ni | 0.01 | 0.01 | 0.01 | 0.01 | 0.01 | 0.01 | 0.01 | 0.01 | 0.01 | 0.01 | 0.01 | 0.01 | 0.01 | 0.01 | 0.01 | 0.01 | 0.01 | 0.01 | 0.01 |
| Zn | 0.00 | 0.00 | 0.00 | 0.00 | 0.00 | 0.00 | 0.00 | 0.00 | 0.00 | 0.00 | 0.00 | 0.00 | 0.00 | 0.00 | 0.00 | 0.00 | 0.00 | 0.00 | 0.00 |

| Analysis | GRID4-1 | GRID4-2 | GRID4-3 | GRID4-4 | GRID4-5 | GRID4-6 | GRID4-7 | GRID4-8 | GRID4-9 | GRID5-1 | GRID5-2 | GRID5-3 | GRID5-4 | GRID5-5 | GRID5-6 | GRID5-7 | GRID5-8 | GRID5-9 | GRID6-1 | GRID6-2 |
|---|---|---|---|---|---|---|---|---|---|---|---|---|---|---|---|---|---|---|---|---|
| | 84-OL | 85-OL | 86-OL | 87-CHR | 88-CHR | 89-CHR | 90-OL | 91-OL | 92-OL | 93-OL | 94-OL | 95-OL | 96-CHR | 97-CHR | 98-CHR | 99-OL | 100-OL | 101-OL | 102-OL | 103-OL |
| X | 74.98 | 74.98 | 74.98 | 74.98 | 74.98 | 74.98 | 74.98 | 74.98 | 74.98 | 75.08 | 75.08 | 75.08 | 75.08 | 75.08 | 75.08 | 75.08 | 75.08 | 75.08 | 75.18 | 75.18 |
| Y | 74.65 | 74.75 | 74.85 | 74.95 | 75.05 | 75.15 | 75.25 | 75.35 | 75.45 | 74.65 | 74.75 | 74.85 | 74.95 | 75.05 | 75.15 | 75.25 | 75.35 | 75.45 | 74.65 | 74.75 |
| $SiO_2$ | 40.38 | 40.37 | 43.16 | 0.09 | 0.04 | 0.06 | 41.48 | 41.16 | 41.28 | 40.58 | 40.72 | 41.15 | 0.05 | 0.04 | 0.03 | 41.92 | 41.39 | 41.42 | 40.72 | 40.59 |
| $TiO_2$ | 0.00 | 0.00 | 0.00 | 0.01 | 0.05 | 0.10 | 0.01 | 0.00 | 0.01 | 0.00 | 0.03 | 0.02 | 0.00 | 0.06 | 0.12 | 0.00 | 0.02 | 0.04 | 0.00 | 0.03 |
| $Al_2O_3$ | 0.01 | 0.00 | 0.07 | 8.44 | 8.70 | 8.56 | 0.03 | 0.01 | 0.00 | 0.02 | 0.00 | 0.00 | 8.73 | 8.78 | 8.76 | 0.00 | 0.01 | 0.01 | 0.01 | 0.01 |
| $Cr_2O_3$ | 0.00 | 0.01 | 0.05 | 61.33 | 61.95 | 61.76 | 0.03 | 0.02 | 0.03 | 0.00 | 0.00 | 0.05 | 61.99 | 62.48 | 62.67 | 0.08 | 0.04 | 0.00 | 0.00 | 0.03 |
| $V_2O_3$ | 0.00 | 0.00 | 0.00 | 0.18 | 0.17 | 0.22 | 0.00 | 0.00 | 0.00 | 0.00 | 0.00 | 0.00 | 0.19 | 0.16 | 0.10 | 0.00 | 0.00 | 0.00 | 0.00 | 0.00 |
| $Fe_2O_3$ | 0.00 | 0.00 | 0.00 | 1.83 | 2.22 | 2.16 | 0.00 | 0.00 | 0.00 | 0.00 | 0.00 | 0.00 | 1.81 | 2.14 | 1.90 | 0.00 | 0.00 | 0.00 | 0.00 | 0.00 |
| FeO | 5.75 | 5.76 | 5.67 | 18.70 | 16.78 | 17.10 | 5.76 | 6.02 | 5.83 | 6.08 | 5.91 | 5.81 | 17.30 | 16.18 | 16.59 | 5.52 | 5.78 | 5.96 | 6.20 | 5.95 |
| MnO | 0.09 | 0.08 | 0.03 | 0.15 | 0.18 | 0.07 | 0.10 | 0.05 | 0.15 | 0.11 | 0.05 | 0.13 | 0.11 | 0.17 | 0.14 | 0.07 | 0.08 | 0.09 | 0.15 | 0.09 |
| MgO | 51.72 | 52.62 | 50.55 | 9.51 | 10.88 | 10.77 | 52.22 | 52.21 | 52.32 | 51.72 | 52.01 | 51.88 | 10.66 | 11.42 | 11.17 | 52.17 | 52.44 | 52.05 | 52.18 | 51.57 |
| NiO | 0.42 | 0.45 | 0.53 | 0.02 | 0.08 | 0.03 | 0.34 | 0.41 | 0.35 | 0.38 | 0.44 | 0.47 | 0.09 | 0.00 | 0.10 | 0.48 | 0.37 | 0.51 | 0.37 | 0.37 |
| ZnO | 0.11 | 0.06 | 0.00 | 0.31 | 0.23 | 0.25 | 0.02 | 0.04 | 0.06 | 0.11 | 0.00 | 0.02 | 0.00 | 0.28 | 0.30 | 0.00 | 0.00 | 0.00 | 0.17 | 0.10 |
| TOT | 98.51 | 99.38 | 100.06 | 100.58 | 101.31 | 101.08 | 100.01 | 99.94 | 100.07 | 99.04 | 99.17 | 99.56 | 100.93 | 101.71 | 101.89 | 100.28 | 100.17 | 100.13 | 99.84 | 98.77 |
| Si | 0.99 | 0.98 | 1.05 | 0.00 | 0.00 | 0.00 | 1.00 | 0.99 | 0.99 | 0.99 | 0.99 | 1.00 | 0.00 | 0.00 | 0.00 | 1.01 | 0.99 | 1.00 | 0.98 | 0.99 |
| Ti | 0.00 | 0.00 | 0.00 | 0.00 | 0.00 | 0.00 | 0.00 | 0.00 | 0.00 | 0.00 | 0.00 | 0.00 | 0.00 | 0.00 | 0.00 | 0.00 | 0.00 | 0.00 | 0.00 | 0.00 |
| Al | 0.00 | 0.00 | 0.00 | 0.33 | 0.34 | 0.33 | 0.00 | 0.00 | 0.00 | 0.00 | 0.00 | 0.00 | 0.34 | 0.34 | 0.34 | 0.00 | 0.00 | 0.00 | 0.00 | 0.00 |
| Cr | 0.00 | 0.00 | 0.00 | 1.61 | 1.60 | 1.60 | 0.00 | 0.00 | 0.00 | 0.00 | 0.00 | 0.00 | 1.61 | 1.60 | 1.61 | 0.00 | 0.00 | 0.00 | 0.00 | 0.00 |
| V | 0.00 | 0.00 | 0.00 | 0.00 | 0.00 | 0.01 | 0.00 | 0.00 | 0.00 | 0.00 | 0.00 | 0.00 | 0.00 | 0.00 | 0.00 | 0.00 | 0.00 | 0.00 | 0.00 | 0.00 |
| $Fe^{3+}$ | 0.00 | 0.00 | 0.00 | 0.05 | 0.05 | 0.05 | 0.00 | 0.00 | 0.00 | 0.00 | 0.00 | 0.00 | 0.04 | 0.05 | 0.05 | 0.00 | 0.00 | 0.00 | 0.00 | 0.00 |
| $Fe^{2+}$ | 0.12 | 0.12 | 0.11 | 0.52 | 0.46 | 0.47 | 0.12 | 0.12 | 0.12 | 0.12 | 0.12 | 0.12 | 0.47 | 0.44 | 0.45 | 0.11 | 0.12 | 0.12 | 0.13 | 0.12 |
| Mn | 0.00 | 0.00 | 0.00 | 0.00 | 0.00 | 0.00 | 0.00 | 0.00 | 0.00 | 0.00 | 0.00 | 0.00 | 0.00 | 0.00 | 0.00 | 0.00 | 0.00 | 0.00 | 0.00 | 0.00 |
| Mg | 1.88 | 1.90 | 1.83 | 0.47 | 0.53 | 0.53 | 1.87 | 1.88 | 1.88 | 1.88 | 1.88 | 1.87 | 0.52 | 0.55 | 0.54 | 1.87 | 1.88 | 1.87 | 1.88 | 1.88 |
| Ni | 0.01 | 0.01 | 0.01 | 0.00 | 0.00 | 0.00 | 0.01 | 0.01 | 0.01 | 0.01 | 0.01 | 0.01 | 0.00 | 0.00 | 0.00 | 0.01 | 0.01 | 0.01 | 0.01 | 0.01 |
| Zn | 0.00 | 0.00 | 0.00 | 0.01 | 0.01 | 0.01 | 0.00 | 0.00 | 0.00 | 0.00 | 0.00 | 0.00 | 0.00 | 0.01 | 0.01 | 0.00 | 0.00 | 0.00 | 0.00 | 0.00 |

| Analysis | GRID6-4 | GRID6-5 | GRID6-6 | GRID6-7 | GRID7-1 | GRID7-2 | GRID7-3 | GRID7-4 | GRID7-6 | GRID7-7 | GRID7-8 | GRID7-9 | GRID8-3 | GRID8-7 | GRID8-8 | GRID8-9 | GRID9-1 | GRID9-2 | GRID9-6 | GRID9-7 |
|---|---|---|---|---|---|---|---|---|---|---|---|---|---|---|---|---|---|---|---|---|
| | 105-CHR | 106-CHR | 107-CHR | 108-OL | 111-OL | 112-OL | 113-OL | 114-OL | 116-OL | 117-OL | 118-OL | 119-OL | 122-OL | 126-OL | 127-OL | 128-OL | 129-OL | 130-OL | 134-OL | 135-OL |
| X | 75.18 | 75.18 | 75.18 | 75.18 | 75.28 | 75.28 | 75.28 | 75.28 | 75.28 | 75.28 | 75.28 | 75.28 | 75.38 | 75.38 | 75.38 | 75.38 | 75.48 | 75.48 | 75.48 | 75.48 |
| Y | 74.95 | 75.05 | 75.15 | 75.25 | 74.65 | 74.75 | 74.85 | 74.95 | 75.15 | 75.25 | 75.35 | 75.45 | 74.85 | 75.25 | 75.35 | 75.45 | 74.65 | 74.75 | 75.15 | 75.25 |
| d(mm) | | | | | | | | | | | | | | | | | | | | |
| $SiO_2$ | 0.07 | 0.01 | 0.05 | 42.16 | 40.69 | 42.35 | 41.20 | 41.74 | 41.89 | 41.61 | 41.65 | 41.46 | 41.16 | 41.49 | 41.46 | 41.83 | 41.11 | 41.20 | 41.28 | 41.07 |
| $TiO_2$ | 0.07 | 0.07 | 0.06 | 0.00 | 0.00 | 0.03 | 0.00 | 0.00 | 0.04 | 0.00 | 0.00 | 0.00 | 0.01 | 0.08 | 0.00 | 0.00 | 0.00 | 0.02 | 0.00 | 0.05 |

| | | | | | | | | | | | | | | | | | | | | |
|---|---|---|---|---|---|---|---|---|---|---|---|---|---|---|---|---|---|---|---|---|
| $Al_2O_3$ | 8.62 | 8.76 | 8.74 | 0.03 | 0.00 | 0.04 | 0.03 | 0.01 | 0.00 | 0.00 | 0.01 | 0.00 | 0.00 | 0.02 | 0.00 | 0.01 | 0.00 | 0.00 | 0.00 | 0.02 |
| $Cr_2O_3$ | 61.41 | 62.36 | 61.72 | 0.14 | 0.00 | 0.02 | 0.01 | 0.17 | 0.06 | 0.00 | 0.00 | 0.01 | 0.00 | 0.03 | 0.00 | 0.00 | 0.00 | 0.00 | 0.00 | 0.01 |
| $V_2O_3$ | 0.22 | 0.18 | 0.23 | 0.00 | 0.00 | 0.00 | 0.00 | 0.00 | 0.00 | 0.00 | 0.00 | 0.00 | 0.00 | 0.00 | 0.00 | 0.00 | 0.00 | 0.00 | 0.00 | 0.00 |
| $Fe_2O_3$ | 1.92 | 1.68 | 2.06 | 0.00 | 0.00 | 0.00 | 0.00 | 0.00 | 0.00 | 0.00 | 0.00 | 0.00 | 0.00 | 0.00 | 0.00 | 0.00 | 0.00 | 0.00 | 0.00 | 0.00 |
| FeO | 18.51 | 17.06 | 17.10 | 4.75 | 5.87 | 5.83 | 5.91 | 5.86 | 5.64 | 5.82 | 5.56 | 6.08 | 5.76 | 6.03 | 5.91 | 6.22 | 5.99 | 6.08 | 5.83 | 5.95 |
| MnO | 0.12 | 0.19 | 0.20 | 0.08 | 0.07 | 0.09 | 0.07 | 0.13 | 0.08 | 0.08 | 0.06 | 0.05 | 0.07 | 0.09 | 0.09 | 0.08 | 0.05 | 0.04 | 0.04 | 0.13 |
| MgO | 9.87 | 10.79 | 10.74 | 49.86 | 51.77 | 50.16 | 52.52 | 51.95 | 52.42 | 52.30 | 51.84 | 52.39 | 51.82 | 52.27 | 52.32 | 52.68 | 52.27 | 51.81 | 52.61 | 52.77 |
| NiO | 0.03 | 0.04 | 0.06 | 0.33 | 0.41 | 0.39 | 0.44 | 0.42 | 0.47 | 0.46 | 0.45 | 0.43 | 0.41 | 0.46 | 0.45 | 0.45 | 0.44 | 0.36 | 0.50 | 0.49 |
| ZnO | 0.11 | 0.13 | 0.11 | 0.02 | 0.01 | 0.02 | 0.02 | 0.13 | 0.00 | 0.00 | 0.03 | 0.00 | 0.04 | 0.00 | 0.00 | 0.00 | 0.08 | 0.00 | 0.00 | 0.12 |
| TOT | 100.95 | 101.26 | 101.08 | 97.37 | 98.84 | 98.96 | 100.20 | 100.41 | 100.62 | 100.31 | 99.64 | 100.46 | 99.29 | 100.49 | 100.29 | 101.32 | 99.96 | 99.56 | 100.30 | 100.66 |
| Si | 0.00 | 0.00 | 0.00 | 1.05 | 0.99 | 1.04 | 0.99 | 1.00 | 1.00 | 1.00 | 1.01 | 0.99 | 1.00 | 1.00 | 1.00 | 1.00 | 0.99 | 1.00 | 0.99 | 0.98 |
| Ti | 0.00 | 0.00 | 0.00 | 0.00 | 0.00 | 0.00 | 0.00 | 0.00 | 0.00 | 0.00 | 0.00 | 0.00 | 0.00 | 0.00 | 0.00 | 0.00 | 0.00 | 0.00 | 0.00 | 0.00 |
| Al | 0.34 | 0.34 | 0.34 | 0.00 | 0.00 | 0.00 | 0.00 | 0.00 | 0.00 | 0.00 | 0.00 | 0.00 | 0.00 | 0.00 | 0.00 | 0.00 | 0.00 | 0.00 | 0.00 | 0.00 |
| Cr | 1.60 | 1.61 | 1.60 | 0.00 | 0.00 | 0.00 | 0.00 | 0.00 | 0.00 | 0.00 | 0.00 | 0.00 | 0.00 | 0.00 | 0.00 | 0.00 | 0.00 | 0.00 | 0.00 | 0.00 |
| V | 0.01 | 0.00 | 0.01 | 0.00 | 0.00 | 0.00 | 0.00 | 0.00 | 0.00 | 0.00 | 0.00 | 0.00 | 0.00 | 0.00 | 0.00 | 0.00 | 0.00 | 0.00 | 0.00 | 0.00 |
| $Fe^{3+}$ | 0.05 | 0.04 | 0.05 | 0.00 | 0.00 | 0.00 | 0.00 | 0.00 | 0.00 | 0.00 | 0.00 | 0.00 | 0.00 | 0.00 | 0.00 | 0.00 | 0.00 | 0.00 | 0.00 | 0.00 |
| $Fe^{2+}$ | 0.51 | 0.47 | 0.47 | 0.10 | 0.12 | 0.12 | 0.12 | 0.12 | 0.11 | 0.12 | 0.11 | 0.12 | 0.12 | 0.12 | 0.12 | 0.12 | 0.12 | 0.12 | 0.12 | 0.12 |
| Mn | 0.00 | 0.01 | 0.01 | 0.00 | 0.00 | 0.00 | 0.00 | 0.00 | 0.00 | 0.00 | 0.00 | 0.00 | 0.00 | 0.00 | 0.00 | 0.00 | 0.00 | 0.00 | 0.00 | 0.00 |
| Mg | 0.49 | 0.53 | 0.52 | 1.84 | 1.88 | 1.83 | 1.88 | 1.86 | 1.87 | 1.87 | 1.87 | 1.87 | 1.87 | 1.87 | 1.87 | 1.87 | 1.88 | 1.87 | 1.88 | 1.88 |
| Ni | 0.00 | 0.00 | 0.00 | 0.01 | 0.01 | 0.01 | 0.01 | 0.01 | 0.01 | 0.01 | 0.01 | 0.01 | 0.01 | 0.01 | 0.01 | 0.01 | 0.01 | 0.01 | 0.01 | 0.01 |
| Zn | 0.00 | 0.00 | 0.00 | 0.00 | 0.00 | 0.00 | 0.00 | 0.00 | 0.00 | 0.00 | 0.00 | 0.00 | 0.00 | 0.00 | 0.00 | 0.00 | 0.00 | 0.00 | 0.00 | 0.00 |

| Analysis | GRID9-8 | GRID9-9 | OLPU1-4 | OLPU1-1 | OLPU1-2 | OLPU1-3 | d-CHR | OLPU1-4 | OLPU1-5 | d-CHR | OLPU1-6 | OLPU1-7 | d-CHR | GRID1-7-4 | OLPU1-8 | OLPU1-9 | d-CHR | OLPU1-10 | OLPU1-11 |
|---|---|---|---|---|---|---|---|---|---|---|---|---|---|---|---|---|---|---|---|
| | 136-OL | 137-OL | 141-CHR | 1-OL | 2-OL | 3-OL | | 4-OL | 5-OL | | 6-CHR | 7-CHR | | OL | 8-OL | 9-CHR | | 10-OL | 11-CHR |
| X | 75.48 | 75.48 | 74.35 | 74.93 | 74.93 | 74.93 | 74.94 | 74.93 | 75.15 | 75.14 | 75.14 | 75.17 | 75.17 | old an. | 75.03 | 75.03 | 75.03 | 74.90 | 74.92 |
| Y | 75.35 | 75.45 | 90.24 | 75.67 | 75.67 | 75.67 | 75.66 | 75.67 | 75.63 | 75.63 | 75.62 | 75.46 | 75.46 | | 75.36 | 75.38 | 75.37 | 75.39 | 75.41 |
| d(mm) | | | | 0.01 | 0.01 | 0.01 | | 0.01 | 0.01 | | 0.00 | 0.00 | | 0.04 | 0.01 | 0.00 | | 0.02 | 0.00 |
| $SiO_2$ | 41.75 | 41.78 | 0.03 | 41.31 | 41.34 | 41.26 | | 40.66 | 41.68 | | 0.04 | 0.02 | | 41.74 | 42.02 | 0.06 | | 41.47 | 0.05 |
| $TiO_2$ | 0.00 | 0.00 | 0.11 | 0.01 | 0.00 | 0.03 | | 0.00 | 0.00 | | 0.05 | 0.03 | | 0.00 | 0.00 | 0.09 | | 0.01 | 0.04 |
| $Al_2O_3$ | 0.00 | 0.00 | 9.36 | 0.00 | 0.00 | 0.00 | | 0.00 | 0.01 | | 8.87 | 8.81 | | 0.01 | 0.00 | 9.05 | | 0.00 | 8.72 |
| $Cr_2O_3$ | 0.00 | 0.04 | 61.61 | 0.31 | 0.30 | 0.29 | | 0.29 | 0.34 | | 60.68 | 61.85 | | 0.17 | 0.37 | 60.86 | | 0.27 | 60.80 |
| $V_2O_3$ | 0.00 | 0.00 | 0.15 | 0.00 | 0.00 | 0.00 | | 0.00 | 0.00 | | 0.21 | 0.13 | | 0.00 | 0.00 | 0.07 | | 0.00 | 0.25 |
| $Fe_2O_3$ | 0.00 | 0.00 | 2.64 | 0.00 | 0.00 | 0.00 | | 0.00 | 0.00 | | 2.86 | 1.47 | | 0.00 | 0.00 | 2.36 | | 0.00 | 2.37 |
| FeO | 6.04 | 5.97 | 14.56 | 5.35 | 5.26 | 5.34 | | 5.26 | 5.22 | | 19.02 | 19.65 | | 5.86 | 5.33 | 19.24 | | 5.84 | 19.44 |
| MnO | 0.10 | 0.11 | 0.15 | 0.08 | 0.05 | 0.07 | | 0.09 | 0.03 | | 0.22 | 0.17 | | 0.13 | 0.11 | 0.19 | | 0.09 | 0.31 |
| MgO | 52.16 | 52.49 | 12.43 | 53.18 | 52.94 | 53.06 | | 52.65 | 53.21 | | 9.52 | 9.13 | | 51.95 | 53.22 | 9.40 | | 52.72 | 9.11 |
| NiO | 0.45 | 0.44 | 0.00 | 0.45 | 0.48 | 0.42 | | 0.43 | 0.47 | | 0.10 | 0.00 | | 0.42 | 0.35 | 0.08 | | 0.28 | 0.12 |
| ZnO | 0.00 | 0.04 | 0.38 | 0.05 | 0.06 | 0.00 | | 0.00 | 0.09 | | 0.22 | 0.15 | | 0.13 | 0.08 | 0.29 | | 0.06 | 0.15 |
| TOT | 100.53 | 100.92 | 101.45 | 100.79 | 100.45 | 100.48 | | 99.42 | 101.08 | | 101.80 | 101.43 | | 100.41 | 101.53 | 101.72 | | 100.74 | 101.38 |
| Si | 1.00 | 1.00 | 0.00 | 0.99 | 0.99 | 0.99 | | 0.98 | 0.99 | | 0.00 | 0.00 | | 1.00 | 1.00 | 0.00 | | 0.99 | 0.00 |
| Ti | 0.00 | 0.00 | 0.00 | 0.00 | 0.00 | 0.00 | | 0.00 | 0.00 | | 0.00 | 0.00 | | 0.00 | 0.00 | 0.00 | | 0.00 | 0.00 |
| Al | 0.00 | 0.00 | 0.36 | 0.00 | 0.00 | 0.00 | | 0.00 | 0.00 | | 0.34 | 0.34 | | 0.00 | 0.00 | 0.35 | | 0.00 | 0.34 |
| Cr | 0.00 | 0.00 | 1.57 | 0.01 | 0.01 | 0.01 | | 0.01 | 0.01 | | 1.58 | 1.61 | | 0.00 | 0.01 | 1.58 | | 0.01 | 1.59 |
| V | 0.00 | 0.00 | 0.00 | 0.00 | 0.00 | 0.00 | | 0.00 | 0.00 | | 0.01 | 0.00 | | 0.00 | 0.00 | 0.00 | | 0.00 | 0.01 |
| $Fe^{3+}$ | 0.00 | 0.00 | 0.06 | 0.00 | 0.00 | 0.00 | | 0.00 | 0.00 | | 0.07 | 0.04 | | 0.00 | 0.00 | 0.06 | | 0.00 | 0.06 |
| $Fe^{2+}$ | 0.12 | 0.12 | 0.39 | 0.11 | 0.11 | 0.11 | | 0.11 | 0.10 | | 0.52 | 0.54 | | 0.12 | 0.11 | 0.53 | | 0.12 | 0.54 |
| Mn | 0.00 | 0.00 | 0.00 | 0.00 | 0.00 | 0.00 | | 0.00 | 0.00 | | 0.01 | 0.00 | | 0.00 | 0.00 | 0.01 | | 0.00 | 0.01 |
| Mg | 1.86 | 1.87 | 0.60 | 1.89 | 1.89 | 1.89 | | 1.89 | 1.89 | | 0.47 | 0.45 | | 1.86 | 1.88 | 0.46 | | 1.88 | 0.45 |
| Ni | 0.01 | 0.01 | 0.00 | 0.01 | 0.01 | 0.01 | | 0.01 | 0.01 | | 0.00 | 0.00 | | 0.01 | 0.01 | 0.00 | | 0.01 | 0.00 |
| Zn | 0.00 | 0.00 | 0.01 | 0.00 | 0.00 | 0.00 | | 0.00 | 0.00 | | 0.01 | 0.00 | | 0.00 | 0.00 | 0.01 | | 0.00 | 0.00 |

| Analysis | d-CHR | OLPU1-12 | OLPU1-13 | d-CHR | OLPU1-14 | OLPU1-15 | OLPU1-16 | OLPU1-17 | d-CHR |
|---|---|---|---|---|---|---|---|---|---|

| | | 12-OL | 13-CHR | | 14-OL | 15-OL | 16-CHR | 17-CHR | |
|---|---|---|---|---|---|---|---|---|---|
| X | 74.91 | 74.78 | 74.86 | 74.82 | 74.84 | 74.87 | 74.89 | 74.93 | 74.88 |
| Y | 75.40 | 75.56 | 75.59 | 75.58 | 75.44 | 75.45 | 75.46 | 75.48 | 75.46 |
| d(mm) | | 0.05 | 0.04 | | 0.05 | 0.01 | 0.01 | 0.05 | |
| $SiO_2$ | | 41.41 | 0.02 | | 41.51 | 41.62 | 0.02 | 0.01 | |
| $TiO_2$ | | 0.04 | 0.06 | | 0.00 | 0.00 | 0.09 | 0.10 | |
| $Al_2O_3$ | | 0.00 | 8.74 | | 0.00 | 0.00 | 8.53 | 8.91 | |
| $Cr_2O_3$ | | 0.08 | 62.25 | | 0.00 | 0.28 | 61.59 | 62.15 | |
| $V_2O_3$ | | 0.00 | 0.18 | | 0.00 | 0.00 | 0.16 | 0.17 | |
| $Fe_2O_3$ | | 0.00 | 1.98 | | 0.00 | 0.00 | 2.01 | 1.60 | |
| FeO | | 5.76 | 18.48 | | 5.73 | 5.42 | 19.26 | 17.56 | |
| MnO | | 0.09 | 0.14 | | 0.11 | 0.10 | 0.12 | 0.15 | |
| MgO | | 52.18 | 10.09 | | 52.44 | 52.57 | 9.45 | 10.48 | |
| NiO | | 0.44 | 0.02 | | 0.45 | 0.49 | 0.03 | 0.05 | |
| ZnO | | 0.04 | 0.09 | | 0.03 | 0.07 | 0.01 | 0.22 | |
| TOT | | 100.08 | 102.06 | | 100.32 | 100.56 | 101.29 | 101.42 | |
| Si | | 1.00 | 0.00 | | 1.00 | 1.00 | 0.00 | 0.00 | |
| Ti | | 0.00 | 0.00 | | 0.00 | 0.00 | 0.00 | 0.00 | |
| Al | | 0.00 | 0.34 | | 0.00 | 0.00 | 0.33 | 0.34 | |
| Cr | | 0.00 | 1.61 | | 0.00 | 0.01 | 1.61 | 1.61 | |
| V | | 0.00 | 0.00 | | 0.00 | 0.00 | 0.00 | 0.00 | |
| $Fe^{3+}$ | | 0.00 | 0.05 | | 0.00 | 0.00 | 0.05 | 0.04 | |
| $Fe^{2+}$ | | 0.12 | 0.50 | | 0.12 | 0.11 | 0.53 | 0.48 | |
| Mn | | 0.00 | 0.00 | | 0.00 | 0.00 | 0.00 | 0.00 | |
| Mg | | 1.87 | 0.49 | | 1.88 | 1.88 | 0.47 | 0.51 | |
| Ni | | 0.01 | 0.00 | | 0.01 | 0.01 | 0.00 | 0.00 | |
| Zn | | 0.00 | 0.00 | | 0.00 | 0.00 | 0.00 | 0.01 | |

Tab. A3.15 OLPU1-GRID2 (Iballe) microprobe analyses of olivine and chromite crystals; d(mm) distance from the intergranular limit

| Analysis | GRID1-1 | GRID1-2 | GRID1-3 | GRID1-4 | GRID1-6 | GRID1-8 | GRID1-9 | GRID2-2 | GRID2-3 | GRID2-4 | GRID2-5 | GRID2-6 | GRID2-8 | GRID2-9 | GRID3-1 |
|---|---|---|---|---|---|---|---|---|---|---|---|---|---|---|---|
| | 374-OL | 375-OL | 376-OL | 377-OL | 379-OL | 381-OL | 382-OL | 384-OL | 385-OL | 386-CHR | 387-CHR | 388-CHR | 390-OL | 391-OL | 392-OL |
| X | 64.348 | 64.348 | 64.348 | 64.348 | 64.348 | 64.348 | 64.348 | 64.448 | 64.448 | 64.448 | 64.448 | 64.448 | 64.448 | 64.448 | 64.548 |
| Y | 71.869 | 71.969 | 72.069 | 72.169 | 72.369 | 72.569 | 72.669 | 71.969 | 72.069 | 72.169 | 72.269 | 72.369 | 72.569 | 72.669 | 71.869 |
| $SiO_2$ | 43.30 | 41.43 | 41.73 | 41.65 | 41.92 | 41.84 | 41.85 | 42.09 | 42.04 | 0.07 | 0.05 | 0.04 | 41.52 | 41.69 | 41.56 |
| $TiO_2$ | 0.00 | 0.01 | 0.02 | 0.00 | 0.01 | 0.01 | 0.00 | 0.00 | 0.02 | 0.11 | 0.02 | 0.11 | 0.00 | 0.00 | 0.00 |
| $Al_2O_3$ | 0.00 | 0.00 | 0.03 | 0.00 | 0.00 | 0.00 | 0.00 | 0.01 | 0.00 | 9.03 | 9.24 | 9.02 | 0.02 | 0.00 | 0.00 |
| $Cr_2O_3$ | 0.03 | 0.00 | 0.00 | 0.02 | 0.06 | 0.01 | 0.00 | 0.02 | 0.10 | 61.92 | 61.49 | 61.41 | 0.03 | 0.00 | 0.04 |
| $V_2O_3$ | 0.00 | 0.00 | 0.00 | 0.05 | 0.00 | 0.00 | 0.00 | 0.00 | 0.00 | 0.18 | 0.15 | 0.15 | 0.00 | 0.00 | 0.00 |
| $Fe_2O_3$ | | | | | | | | | | 1.89 | 2.11 | 2.60 | | | |
| FeO | 5.83 | 5.84 | 5.82 | 5.95 | 5.81 | 5.79 | 5.94 | 5.87 | 5.05 | 17.73 | 16.73 | 16.84 | 5.96 | 5.70 | 5.79 |
| MnO | 0.12 | 0.10 | 0.11 | 0.08 | 0.01 | 0.09 | 0.06 | 0.04 | 0.08 | 0.23 | 0.15 | 0.18 | 0.08 | 0.04 | 0.08 |
| MgO | 51.57 | 52.50 | 51.99 | 52.67 | 52.87 | 53.39 | 52.46 | 52.31 | 53.17 | 10.44 | 10.97 | 11.01 | 54.47 | 52.16 | 52.66 |
| NiO | 0.42 | 0.37 | 0.53 | 0.43 | 0.40 | 0.43 | 0.49 | 0.47 | 0.44 | 0.06 | 0.11 | 0.08 | 0.40 | 0.46 | 0.51 |
| ZnO | 0.01 | 0.00 | 0.00 | 0.03 | 0.00 | 0.00 | 0.00 | 0.03 | 0.05 | 0.34 | 0.24 | 0.19 | 0.10 | 0.02 | 0.07 |
| TOT | 101.35 | 100.29 | 100.26 | 100.88 | 101.10 | 101.56 | 100.82 | 100.85 | 100.97 | 101.98 | 101.27 | 101.63 | 102.60 | 100.07 | 100.72 |
| Si | 1.03 | 0.99 | 1.00 | 0.99 | 1.00 | 0.99 | 1.00 | 1.01 | 1.00 | 0.00 | 0.00 | 0.00 | 0.97 | 1.00 | 0.99 |
| Ti | 0.00 | 0.00 | 0.00 | 0.00 | 0.00 | 0.00 | 0.00 | 0.00 | 0.00 | 0.00 | 0.00 | 0.00 | 0.00 | 0.00 | 0.00 |
| Al | 0.00 | 0.00 | 0.00 | 0.00 | 0.00 | 0.00 | 0.00 | 0.00 | 0.00 | 0.35 | 0.36 | 0.35 | 0.00 | 0.00 | 0.00 |
| Cr | 0.00 | 0.00 | 0.00 | 0.00 | 0.00 | 0.00 | 0.00 | 0.00 | 0.00 | 1.59 | 1.58 | 1.58 | 0.00 | 0.00 | 0.00 |
| V | 0.00 | 0.00 | 0.00 | 0.00 | 0.00 | 0.00 | 0.00 | 0.00 | 0.00 | 0.00 | 0.00 | 0.00 | 0.00 | 0.00 | 0.00 |

| | | | | | | | | | | | | | | | | |
|---|---|---|---|---|---|---|---|---|---|---|---|---|---|---|---|---|
| $Fe^{3+}$ | | | | | | | | | | 0.05 | 0.05 | 0.06 | | | | |
| $Fe^{2+}$ | 0.12 | 0.12 | 0.12 | 0.12 | 0.12 | 0.11 | 0.12 | 0.12 | 0.10 | 0.48 | 0.46 | 0.46 | 0.12 | 0.11 | 0.12 | |
| Mn | 0.00 | 0.00 | 0.00 | 0.00 | 0.00 | 0.00 | 0.00 | 0.00 | 0.00 | 0.01 | 0.00 | 0.00 | 0.00 | 0.00 | 0.00 | |
| Mg | 1.84 | 1.88 | 1.86 | 1.87 | 1.88 | 1.88 | 1.87 | 1.86 | 1.89 | 0.51 | 0.53 | 0.53 | 1.90 | 1.87 | 1.88 | |
| Ni | 0.01 | 0.01 | 0.01 | 0.01 | 0.01 | 0.01 | 0.01 | 0.01 | 0.01 | 0.00 | 0.00 | 0.00 | 0.01 | 0.01 | 0.01 | |
| Zn | 0.00 | 0.00 | 0.00 | 0.00 | 0.00 | 0.00 | 0.00 | 0.00 | 0.00 | 0.01 | 0.01 | 0.00 | 0.00 | 0.00 | 0.00 | |

| Analysis | GRID3-2 393-OL | GRID3-3 394-CHR | GRID3-4 395-CHR | GRID3-5 396-CHR | GRID3-6 397-CHR | GRID3-7 398-CHR | GRID3-8 399-OL | GRID3-9 400-OL | GRID4-1 401-OL | GRID4-8 408-OL | GRID8-5 | GRID-8-7 |
|---|---|---|---|---|---|---|---|---|---|---|---|---|
| X | 64.548 | 64.548 | 64.548 | 64.548 | 64.548 | 64.548 | 64.548 | 64.548 | | | | |
| Y | 71.969 | 72.069 | 72.169 | 72.269 | 72.369 | 72.469 | 72.569 | 72.669 | | | | |
| $SiO_2$ | 41.94 | 0.05 | 0.08 | 0.00 | 0.05 | 0.12 | 43.06 | 38.46 | 41.55 | 41.28 | 41.50 | 41.62 |
| $TiO_2$ | 0.00 | 0.05 | 0.08 | 0.10 | 0.05 | 0.07 | 0.00 | 0.00 | 0.00 | 0.03 | 0.00 | 0.00 |
| $Al_2O_3$ | 0.00 | 8.57 | 9.07 | 9.22 | 9.16 | 9.40 | 0.01 | 0.08 | 0.00 | 0.40 | 0.03 | 0.01 |
| $Cr_2O_3$ | 0.11 | 62.17 | 61.70 | 61.54 | 61.84 | 61.33 | 0.02 | 0.02 | 0.00 | 0.00 | 0.01 | 0.00 |
| $V_2O_3$ | 0.03 | 0.20 | 0.15 | 0.19 | 0.13 | 0.24 | 0.00 | 0.02 | 0.01 | 0.00 | 0.00 | 0.21 |
| $Fe_2O_3$ | | 2.07 | 1.75 | 1.91 | 2.46 | 1.88 | | | | | | |
| FeO | 5.62 | 17.28 | 16.82 | 16.19 | 16.09 | 17.81 | 5.69 | 5.81 | 5.99 | 5.42 | 5.23 | 5.57 |
| MnO | 0.08 | 0.18 | 0.12 | 0.12 | 0.18 | 0.18 | 0.07 | 0.14 | 0.08 | 0.09 | 0.05 | 0.03 |
| MgO | 52.48 | 10.64 | 10.92 | 11.39 | 11.54 | 10.45 | 51.78 | 53.14 | 52.24 | 52.73 | 53.10 | 52.52 |
| NiO | 0.39 | 0.09 | 0.00 | 0.00 | 0.08 | 0.04 | 0.46 | 0.45 | 0.44 | 0.40 | 0.44 | 0.43 |
| ZnO | 0.00 | 0.12 | 0.35 | 0.14 | 0.13 | 0.31 | 0.00 | 0.00 | 0.00 | 0.00 | 0.00 | 0.00 |
| TOT | 100.65 | 101.44 | 101.06 | 100.80 | 101.73 | 101.87 | 101.10 | 98.15 | 100.33 | 100.35 | 100.39 | 100.41 |
| Si | 1.00 | 0.00 | 0.00 | 0.00 | 0.00 | 0.00 | 1.03 | 0.94 | 1.00 | 0.99 | 0.99 | 1.00 |
| Ti | 0.00 | 0.00 | 0.00 | 0.00 | 0.00 | 0.00 | 0.00 | 0.00 | 0.00 | 0.00 | 0.00 | 0.00 |
| Al | 0.00 | 0.33 | 0.35 | 0.35 | 0.35 | 0.36 | 0.00 | 0.00 | 0.00 | 0.01 | 0.00 | 0.00 |
| Cr | 0.00 | 1.61 | 1.59 | 1.59 | 1.58 | 1.58 | 0.00 | 0.00 | 0.00 | 0.00 | 0.00 | 0.00 |
| V | 0.00 | 0.01 | 0.00 | 0.00 | 0.00 | 0.01 | 0.00 | 0.00 | 0.00 | 0.00 | 0.00 | 0.00 |
| $Fe^{3+}$ | | 0.05 | 0.04 | 0.05 | 0.06 | 0.05 | | | | 0.00 | | |
| $Fe^{2+}$ | 0.11 | 0.47 | 0.46 | 0.44 | 0.44 | 0.48 | 0.11 | 0.12 | 0.12 | 0.11 | 0.10 | 0.11 |
| Mn | 0.00 | 0.01 | 0.00 | 0.00 | 0.00 | 0.01 | 0.00 | 0.00 | 0.00 | 0.00 | 0.00 | 0.00 |
| Mg | 1.87 | 0.52 | 0.53 | 0.55 | 0.56 | 0.51 | 1.85 | 1.93 | 1.87 | 1.88 | 1.89 | 1.88 |
| Ni | 0.01 | 0.00 | 0.00 | 0.00 | 0.00 | 0.00 | 0.01 | 0.01 | 0.01 | 0.01 | 0.01 | 0.01 |
| Zn | 0.00 | 0.00 | 0.01 | 0.00 | 0.00 | 0.01 | 0.00 | 0.00 | 0.00 | 0.00 | 0.00 | 0.00 |

Tab. A3.16 OLPU1-GRID2 (Iballe) microprobe analyses of olivine and chromite crystals; d(mm) distance from the intergranular limit

| Analysis | OLPU3-1 OL-1 | OLPU3-2 OL-2 | OLPU3-3 OL-3 | OLPU3-4 OL-4 | OLPU3-5 OL-5 | OLPU3-6 OL-6 | OLPU3-7 OL-7 | OLPU3-8 OL-8 | OLPU3-9 OL-9 | OLPU3-10 OL-10 | OLPU3-11 OL-11 | OLPU3-12 OL-12 | OLPU3-13 OL-13 | OLPU3-14 OL-14 | OLPU3-15 OL-15 | OLPU3-16 OL-16 | OLPU3-17 OL-17 | OLPU3-18 OL-18 |
|---|---|---|---|---|---|---|---|---|---|---|---|---|---|---|---|---|---|---|
| X | 76.202 | 76.164 | 76.083 | 76.064 | 76.046 | 76.024 | 76.010 | 75.989 | 75.974 | 75.963 | 75.934 | 75.928 | 75.921 | 75.914 | 75.906 | 75.889 | 75.868 | 75.844 |
| Y | 93.510 | 93.472 | 93.407 | 93.382 | 93.363 | 93.349 | 93.333 | 93.320 | 93.304 | 93.291 | 93.280 | 93.276 | 93.271 | 93.267 | 93.261 | 93.247 | 93.249 | 93.239 |
| d(mm) | 0.474 | 0.421 | 0.317 | 0.288 | 0.263 | 0.237 | 0.216 | 0.191 | 0.170 | 0.155 | 0.123 | 0.116 | 0.108 | 0.100 | 0.090 | 0.069 | 0.051 | 0.026 |
| $SiO_2$ | 40.78 | 40.43 | 41.23 | 40.64 | 40.80 | 40.30 | 40.49 | 40.89 | 40.41 | 40.98 | 41.26 | 39.48 | 39.97 | 41.18 | 40.47 | 31.22 | 37.76 | 40.09 |
| $TiO_2$ | 0.02 | 0.00 | 0.00 | 0.02 | 0.00 | 0.05 | 0.03 | 0.00 | 0.00 | 0.00 | 0.03 | 0.00 | 0.00 | 0.01 | 0.00 | 0.02 | 0.01 | 0.03 |
| $Al_2O_3$ | 0.00 | 0.00 | 0.00 | 0.00 | 0.00 | 0.00 | 0.01 | 0.00 | 0.03 | 0.01 | 0.00 | 0.02 | 0.00 | 0.03 | 0.00 | 0.00 | 0.03 | 0.00 |
| $Cr_2O_3$ | 0.00 | 0.01 | 0.00 | 0.00 | 0.00 | 0.01 | 0.00 | 0.05 | 0.03 | 0.02 | 0.00 | 0.03 | 0.04 | 0.10 | 0.13 | 0.15 | 0.23 | 0.55 |
| $V_2O_3$ | 0.00 | 0.00 | 0.00 | 0.00 | 0.00 | 0.00 | 0.00 | 0.00 | 0.00 | 0.00 | 0.00 | 0.00 | 0.00 | 0.00 | 0.00 | 0.00 | 0.00 | 0.00 |
| $Fe_2O_3$ | 0.00 | 0.00 | 0.00 | 0.00 | 0.00 | 0.00 | 0.00 | 0.00 | 0.00 | 0.00 | 0.00 | 0.00 | 0.00 | 0.00 | 0.00 | 0.00 | 0.00 | 0.00 |
| FeO | 6.66 | 6.40 | 6.64 | 6.28 | 6.38 | 6.31 | 6.47 | 6.42 | 6.38 | 6.24 | 6.18 | 6.01 | 6.18 | 6.00 | 6.08 | 5.41 | 5.24 | 5.30 |
| MnO | 0.08 | 0.09 | 0.02 | 0.12 | 0.00 | 0.08 | 0.14 | 0.11 | 0.08 | 0.10 | 0.16 | 0.05 | 0.00 | 0.02 | 0.07 | 0.07 | 0.03 | 0.10 |
| MgO | 52.51 | 52.06 | 51.39 | 52.07 | 51.86 | 51.24 | 52.31 | 52.56 | 52.41 | 52.70 | 52.36 | 51.54 | 52.93 | 53.54 | 53.15 | 52.55 | 50.32 | 55.07 |

| | | | | | | | | | | | | | | | | | | |
|---|---|---|---|---|---|---|---|---|---|---|---|---|---|---|---|---|---|---|
| NiO | 0.38 | 0.38 | 0.39 | 0.38 | 0.40 | 0.38 | 0.38 | 0.41 | 0.36 | 0.37 | 0.37 | 0.40 | 0.37 | 0.40 | 0.43 | 0.36 | 0.40 | 0.36 |
| ZnO | 0.00 | 0.00 | 0.00 | 0.00 | 0.00 | 0.00 | 0.06 | 0.00 | 0.00 | 0.03 | 0.00 | 0.03 | 0.00 | 0.00 | 0.03 | 0.02 | 0.05 | 0.00 |
| TOT | 100.48 | 99.43 | 99.71 | 99.54 | 99.49 | 98.42 | 99.90 | 100.47 | 99.74 | 100.47 | 100.36 | 97.54 | 99.48 | 101.30 | 100.36 | 89.83 | 94.07 | 101.50 |
| Si | 0.98 | 0.98 | 1.00 | 0.98 | 0.99 | 0.99 | 0.98 | 0.98 | 0.98 | 0.98 | 0.99 | 0.97 | 0.96 | 0.98 | 0.97 | 0.82 | 0.96 | 0.94 |
| Ti | 0.00 | 0.00 | 0.00 | 0.00 | 0.00 | 0.00 | 0.00 | 0.00 | 0.00 | 0.00 | 0.00 | 0.00 | 0.00 | 0.00 | 0.00 | 0.00 | 0.00 | 0.00 |
| Al | 0.00 | 0.00 | 0.00 | 0.00 | 0.00 | 0.00 | 0.00 | 0.00 | 0.00 | 0.00 | 0.00 | 0.00 | 0.00 | 0.00 | 0.00 | 0.00 | 0.00 | 0.00 |
| Cr | 0.00 | 0.00 | 0.00 | 0.00 | 0.00 | 0.00 | 0.00 | 0.00 | 0.00 | 0.00 | 0.00 | 0.00 | 0.00 | 0.00 | 0.00 | 0.00 | 0.00 | 0.01 |
| V | 0.00 | 0.00 | 0.00 | 0.00 | 0.00 | 0.00 | 0.00 | 0.00 | 0.00 | 0.00 | 0.00 | 0.00 | 0.00 | 0.00 | 0.00 | 0.00 | 0.00 | 0.00 |
| $Fe^{3+}$ | 0.00 | 0.00 | 0.00 | 0.00 | 0.00 | 0.00 | 0.00 | 0.00 | 0.00 | 0.00 | 0.00 | 0.00 | 0.00 | 0.00 | 0.00 | 0.00 | 0.00 | 0.00 |
| $Fe^{2+}$ | 0.13 | 0.13 | 0.13 | 0.13 | 0.13 | 0.13 | 0.13 | 0.13 | 0.13 | 0.13 | 0.12 | 0.12 | 0.12 | 0.12 | 0.12 | 0.12 | 0.11 | 0.10 |
| Mn | 0.00 | 0.00 | 0.00 | 0.00 | 0.00 | 0.00 | 0.00 | 0.00 | 0.00 | 0.00 | 0.00 | 0.00 | 0.00 | 0.00 | 0.00 | 0.00 | 0.00 | 0.00 |
| Mg | 1.88 | 1.88 | 1.86 | 1.88 | 1.87 | 1.87 | 1.88 | 1.88 | 1.89 | 1.88 | 1.87 | 1.89 | 1.90 | 1.89 | 1.90 | 2.05 | 1.91 | 1.93 |
| Ni | 0.01 | 0.01 | 0.01 | 0.01 | 0.01 | 0.01 | 0.01 | 0.01 | 0.01 | 0.01 | 0.01 | 0.01 | 0.01 | 0.01 | 0.01 | 0.01 | 0.01 | 0.01 |
| Zn | 0.00 | 0.00 | 0.00 | 0.00 | 0.00 | 0.00 | 0.00 | 0.00 | 0.00 | 0.00 | 0.00 | 0.00 | 0.00 | 0.00 | 0.00 | 0.00 | 0.00 | 0.00 |

| Analysis | OLPU3-19 | bordo chr | OLPU3-20 | OLPU3-21 | OLPU3-22 | OLPU3-23 | OLPU3-24 | OLPU3-25 | OLPU3-26 | OLPU3-27 | OLPU3-28 | OLPU3-29 | OLPU3-30 | OLPU3-31 | OLPU3-32 | OLPU3-33 | OLPU3-34 | OLPU3-35 |
|---|---|---|---|---|---|---|---|---|---|---|---|---|---|---|---|---|---|---|
| | OL-19 | | CHR-20 | CHR-21 | CHR-22 | CHR-23 | CHR-24 | CHR-25 | CHR-26 | CHR-27 | CHR-28 | CHR-29 | CHR-30 | CHR-31 | CHR-32 | CHR-33 | CHR-34 | CHR-35 |
| X | 75.839 | 75.824 | 75.817 | 75.813 | 75.809 | 75.803 | 75.794 | 75.789 | 75.782 | 75.775 | 75.765 | 75.753 | 75.748 | 75.738 | 75.728 | 75.716 | 75.710 | 75.706 |
| Y | 93.233 | 93.224 | 93.227 | 93.222 | 93.216 | 93.210 | 93.200 | 93.193 | 93.186 | 93.178 | 93.168 | 93.157 | 93.151 | 93.140 | 93.130 | 93.118 | 93.109 | 93.103 |
| d(mm) | 0.018 | | 0.008 | 0.011 | 0.017 | 0.025 | 0.038 | 0.046 | 0.057 | 0.067 | 0.081 | 0.083 | 0.076 | 0.061 | 0.047 | 0.030 | 0.020 | 0.015 |
| $SiO_2$ | 29.84 | | 0.04 | 0.00 | 0.01 | 0.00 | 0.04 | 0.03 | 0.02 | 0.02 | 0.04 | 0.00 | 0.00 | 0.00 | 0.00 | 0.04 | 0.00 | 0.00 |
| $TiO_2$ | 0.00 | | 0.07 | 0.05 | 0.08 | 0.05 | 0.08 | 0.04 | 0.11 | 0.07 | 0.09 | 0.11 | 0.07 | 0.11 | 0.12 | 0.06 | 0.03 | 0.04 |
| $Al_2O_3$ | 0.42 | | 7.23 | 7.28 | 7.66 | 7.75 | 7.84 | 7.94 | 8.11 | 8.10 | 8.11 | 8.01 | 8.09 | 8.12 | 8.21 | 8.09 | 8.22 | 7.87 |
| $Cr_2O_3$ | 0.66 | | 63.72 | 64.12 | 63.97 | 63.78 | 63.19 | 63.48 | 63.85 | 63.20 | 63.51 | 63.21 | 62.66 | 63.30 | 62.75 | 63.05 | 63.46 | 62.64 |
| $V_2O_3$ | 0.00 | | 0.00 | 0.00 | 0.00 | 0.00 | 0.00 | 0.00 | 0.00 | 0.00 | 0.00 | 0.00 | 0.00 | 0.00 | 0.00 | 0.00 | 0.00 | 0.00 |
| $Fe_2O_3$ | 0.00 | | 0.27 | 0.27 | 0.00 | 0.00 | 0.13 | 0.00 | 0.00 | 0.00 | 0.00 | 0.00 | 0.21 | 0.00 | 0.00 | 0.11 | 0.20 | 0.64 |
| FeO | 5.29 | | 22.50 | 21.88 | 21.55 | 21.44 | 21.08 | 20.32 | 20.56 | 19.96 | 20.26 | 20.33 | 20.12 | 20.55 | 20.87 | 21.43 | 21.77 | 22.08 |
| MnO | 0.09 | | 0.18 | 0.07 | 0.24 | 0.00 | 0.16 | 0.14 | 0.04 | 0.14 | 0.18 | 0.11 | 0.24 | 0.09 | 0.08 | 0.11 | 0.24 | 0.13 |
| MgO | 40.87 | | 7.18 | 7.64 | 7.65 | 7.74 | 8.04 | 8.26 | 8.18 | 8.40 | 8.56 | 8.38 | 8.46 | 8.20 | 8.10 | 7.88 | 7.75 | 7.38 |
| NiO | 0.45 | | 0.01 | 0.03 | 0.06 | 0.01 | 0.10 | 0.06 | 0.00 | 0.03 | 0.07 | 0.10 | 0.03 | 0.04 | 0.01 | 0.08 | 0.06 | 0.00 |
| ZnO | 0.00 | | 0.06 | 0.08 | 0.01 | 0.10 | 0.02 | 0.11 | 0.13 | 0.03 | 0.07 | 0.01 | 0.04 | 0.00 | 0.09 | 0.03 | 0.06 | 0.14 |
| TOT | 77.65 | | 101.28 | 101.41 | 101.24 | 100.88 | 100.69 | 100.36 | 101.01 | 99.96 | 100.87 | 100.27 | 99.94 | 100.41 | 100.23 | 100.91 | 101.78 | 100.94 |
| Si | 0.93 | | 0.00 | 0.00 | 0.00 | 0.00 | 0.00 | 0.00 | 0.00 | 0.00 | 0.00 | 0.00 | 0.00 | 0.00 | 0.00 | 0.00 | 0.00 | 0.00 |
| Ti | 0.00 | | 0.00 | 0.00 | 0.00 | 0.00 | 0.00 | 0.00 | 0.00 | 0.00 | 0.00 | 0.00 | 0.00 | 0.00 | 0.00 | 0.00 | 0.00 | 0.00 |
| Al | 0.02 | | 0.29 | 0.29 | 0.30 | 0.31 | 0.31 | 0.31 | 0.32 | 0.32 | 0.32 | 0.32 | 0.32 | 0.32 | 0.33 | 0.32 | 0.32 | 0.31 |
| Cr | 0.02 | | 1.70 | 1.70 | 1.70 | 1.70 | 1.68 | 1.69 | 1.69 | 1.68 | 1.68 | 1.68 | 1.67 | 1.68 | 1.67 | 1.67 | 1.67 | 1.67 |
| V | 0.00 | | 0.00 | 0.00 | 0.00 | 0.00 | 0.00 | 0.00 | 0.00 | 0.00 | 0.00 | 0.00 | 0.00 | 0.00 | 0.00 | 0.00 | 0.00 | 0.00 |
| $Fe^{3+}$ | 0.00 | | 0.01 | 0.01 | 0.00 | 0.00 | 0.00 | 0.00 | 0.00 | 0.00 | 0.00 | 0.00 | 0.01 | 0.00 | 0.00 | 0.00 | 0.00 | 0.02 |
| $Fe^{2+}$ | 0.14 | | 0.63 | 0.61 | 0.60 | 0.60 | 0.59 | 0.57 | 0.58 | 0.56 | 0.57 | 0.57 | 0.57 | 0.58 | 0.59 | 0.60 | 0.61 | 0.62 |
| Mn | 0.00 | | 0.01 | 0.00 | 0.01 | 0.00 | 0.00 | 0.00 | 0.00 | 0.00 | 0.01 | 0.00 | 0.01 | 0.00 | 0.00 | 0.00 | 0.01 | 0.00 |
| Mg | 1.89 | | 0.36 | 0.38 | 0.38 | 0.39 | 0.40 | 0.41 | 0.41 | 0.42 | 0.43 | 0.42 | 0.43 | 0.41 | 0.41 | 0.39 | 0.38 | 0.37 |
| Ni | 0.01 | | 0.00 | 0.00 | 0.00 | 0.00 | 0.00 | 0.00 | 0.00 | 0.00 | 0.00 | 0.00 | 0.00 | 0.00 | 0.00 | 0.00 | 0.00 | 0.00 |
| Zn | 0.00 | | 0.00 | 0.00 | 0.00 | 0.00 | 0.00 | 0.00 | 0.00 | 0.00 | 0.00 | 0.00 | 0.00 | 0.00 | 0.00 | 0.00 | 0.00 | 0.00 |

| Analysis | OLPU3-36 | bordo chr | OLPU3-37 | OLPU3-38 | OLPU3-39 | OLPU3-40 | OLPU3-41 | OLPU3-42 | OLPU3-43 | OLPU3-44 | OLPU3-45 | OLPU3-46 | OLPU3-47 | OLPU3-48 | OLPU3-49 | OLPU3-50 | OLPU3-51 | bordo chr |
|---|---|---|---|---|---|---|---|---|---|---|---|---|---|---|---|---|---|---|
| | CHR-36 | | OL-37 | OL-38 | OL-39 | OL-40 | OL-41 | OL-42 | OL-43 | OL-44 | CHR-45 | CHR-46 | CHR-47 | CHR-48 | CHR-49 | CHR-50 | CHR-51 | |
| X | 75.695 | 75.692 | 75.677 | 75.674 | 75.670 | 75.664 | 75.662 | 75.658 | 75.655 | 75.647 | 75.775 | 75.771 | 75.769 | 75.763 | 75.759 | 75.755 | 75.753 | 75.751 |
| Y | 93.105 | 93.101 | 93.101 | 93.097 | 93.094 | 93.088 | 93.084 | 93.080 | 93.076 | 93.066 | 93.084 | 93.078 | 93.074 | 93.072 | 93.070 | 93.065 | 93.062 | 93.057 |
| d(mm) | 0.006 | | 0.014 | 0.018 | 0.023 | 0.031 | 0.034 | 0.040 | 0.044 | 0.057 | 0.036 | 0.029 | 0.024 | 0.019 | 0.015 | 0.008 | 0.006 | |
| $SiO_2$ | 0.22 | | 40.39 | 40.56 | 40.99 | 41.06 | 40.23 | 39.66 | 40.31 | 39.93 | 0.00 | 0.05 | 0.00 | 0.02 | 0.09 | 0.02 | 0.31 | |
| $TiO_2$ | 0.04 | | 0.01 | 0.01 | 0.00 | 0.01 | 0.02 | 0.00 | 0.00 | 0.01 | 0.06 | 0.10 | 0.06 | 0.05 | 0.04 | 0.04 | 0.04 | |
| $Al_2O_3$ | 6.51 | | 0.01 | 0.01 | 0.00 | 0.00 | 0.00 | 0.01 | 0.00 | 0.02 | 8.03 | 8.13 | 8.01 | 7.84 | 7.97 | 8.40 | 8.86 | |

| | | | | | | | | | | | | | | | | | | |
|---|---|---|---|---|---|---|---|---|---|---|---|---|---|---|---|---|---|---|
| $Cr_2O_3$ | 58.05 | | 0.53 | 0.40 | 0.31 | 0.28 | 0.24 | 0.16 | 0.12 | 0.09 | 62.87 | 63.10 | 63.95 | 62.86 | 63.14 | 62.83 | 59.44 | |
| $V_2O_3$ | 0.00 | | 0.00 | 0.00 | 0.00 | 0.00 | 0.00 | 0.00 | 0.00 | 0.00 | 0.00 | 0.00 | 0.00 | 0.00 | 0.00 | 0.00 | 0.00 | |
| $Fe_2O_3$ | 6.00 | | 0.00 | 0.00 | 0.00 | 0.00 | 0.00 | 0.00 | 0.00 | 0.00 | 0.41 | 0.00 | 0.00 | 0.38 | 0.00 | 0.56 | 2.86 | |
| FeO | 23.98 | | 5.60 | 5.75 | 5.78 | 5.94 | 5.97 | 5.78 | 6.26 | 6.27 | 20.71 | 20.94 | 21.47 | 21.66 | 21.91 | 22.28 | 23.25 | |
| MnO | 0.53 | | 0.09 | 0.00 | 0.05 | 0.06 | 0.05 | 0.03 | 0.09 | 0.20 | 0.19 | 0.11 | 0.08 | 0.25 | 0.18 | 0.26 | 0.18 | |
| MgO | 5.98 | | 53.01 | 52.56 | 53.47 | 53.30 | 53.41 | 52.92 | 53.42 | 55.45 | 8.23 | 8.08 | 7.88 | 7.62 | 7.44 | 7.50 | 7.21 | |
| NiO | 0.09 | | 0.42 | 0.36 | 0.38 | 0.35 | 0.43 | 0.43 | 0.37 | 0.43 | 0.03 | 0.05 | 0.02 | 0.00 | 0.08 | 0.01 | 0.02 | |
| ZnO | 0.06 | | 0.01 | 0.00 | 0.02 | 0.00 | 0.01 | 0.00 | 0.00 | 0.01 | 0.04 | 0.01 | 0.02 | 0.06 | 0.10 | 0.06 | 0.07 | |
| TOT | 101.48 | | 100.07 | 99.68 | 101.00 | 100.99 | 100.37 | 99.00 | 100.57 | 102.42 | 100.59 | 100.59 | 101.49 | 100.74 | 100.94 | 101.97 | 102.26 | |
| Si | 0.01 | | 0.97 | 0.98 | 0.97 | 0.98 | 0.96 | 0.96 | 0.96 | 0.93 | 0.00 | 0.00 | 0.00 | 0.00 | 0.00 | 0.00 | 0.01 | |
| Ti | 0.00 | | 0.00 | 0.00 | 0.00 | 0.00 | 0.00 | 0.00 | 0.00 | 0.00 | 0.00 | 0.00 | 0.00 | 0.00 | 0.00 | 0.00 | 0.00 | |
| Al | 0.26 | | 0.00 | 0.00 | 0.00 | 0.00 | 0.00 | 0.00 | 0.00 | 0.00 | 0.32 | 0.32 | 0.32 | 0.31 | 0.32 | 0.33 | 0.35 | |
| Cr | 1.57 | | 0.01 | 0.01 | 0.01 | 0.01 | 0.00 | 0.00 | 0.00 | 0.00 | 1.67 | 1.68 | 1.69 | 1.68 | 1.68 | 1.65 | 1.56 | |
| V | 0.00 | | 0.00 | 0.00 | 0.00 | 0.00 | 0.00 | 0.00 | 0.00 | 0.00 | 0.00 | 0.00 | 0.00 | 0.00 | 0.00 | 0.00 | 0.00 | |
| $Fe^{3+}$ | 0.15 | | 0.00 | 0.00 | 0.00 | 0.00 | 0.00 | 0.00 | 0.00 | 0.00 | 0.01 | 0.00 | 0.00 | 0.01 | 0.00 | 0.01 | 0.07 | |
| $Fe^{2+}$ | 0.68 | | 0.11 | 0.12 | 0.11 | 0.12 | 0.12 | 0.12 | 0.13 | 0.12 | 0.58 | 0.59 | 0.60 | 0.61 | 0.62 | 0.62 | 0.65 | |
| Mn | 0.02 | | 0.00 | 0.00 | 0.00 | 0.00 | 0.00 | 0.00 | 0.00 | 0.00 | 0.01 | 0.00 | 0.00 | 0.01 | 0.01 | 0.01 | 0.01 | |
| Mg | 0.30 | | 1.90 | 1.89 | 1.90 | 1.89 | 1.90 | 1.91 | 1.90 | 1.93 | 0.41 | 0.40 | 0.39 | 0.38 | 0.37 | 0.37 | 0.36 | |
| Ni | 0.00 | | 0.01 | 0.01 | 0.01 | 0.01 | 0.01 | 0.01 | 0.01 | 0.01 | 0.00 | 0.00 | 0.00 | 0.00 | 0.00 | 0.00 | 0.00 | |
| Zn | 0.00 | | 0.00 | 0.00 | 0.00 | 0.00 | 0.00 | 0.00 | 0.00 | 0.00 | 0.00 | 0.00 | 0.00 | 0.00 | 0.00 | 0.00 | 0.00 | |

| Analysis | OLPU3-52 | OLPU3-53 | OLPU3-54 | OLPU3-55 | OLPU3-56 | OLPU3-57 | OLPU3-58 | OLPU3-59 | OLPU3-60 | OLPU3-61 | OLPU3-62 | OLPU3-63 | OLPU3-64 | OLPU3-65 | OLPU3-66 | OLPU3-67 | OLPU3-68 | OLPU3-69 |
|---|---|---|---|---|---|---|---|---|---|---|---|---|---|---|---|---|---|---|
| | OL-52 | OL-53 | OL-54 | OL-55 | OL-56 | OL-57 | OL-58 | OL-59 | OL-60 | OL-61 | OL-62 | OL-63 | OL-64 | OL-65 | OL-66 | OL-67 | OL-68 | OL-69 |
| X | 75.750 | 75.748 | 75.745 | 75.746 | 65.219 | 65.251 | 65.287 | 65.307 | 65.340 | 65.365 | 65.400 | 65.435 | 65.471 | 65.495 | 65.509 | 65.514 | 65.519 | 65.526 |
| Y | 93.055 | 93.052 | 93.049 | 93.045 | 83.942 | 83.928 | 83.911 | 83.899 | 83.885 | 83.871 | 83.854 | 83.831 | 83.806 | 83.788 | 83.774 | 83.769 | 83.765 | 83.760 |
| d(mm) | 0.003 | 0.006 | 0.010 | 0.013 | 0.373 | 0.338 | 0.299 | 0.276 | 0.240 | 0.211 | 0.173 | 0.132 | 0.088 | 0.058 | 0.038 | 0.031 | 0.025 | 0.016 |
| $SiO_2$ | 39.81 | 40.53 | 39.18 | 40.26 | 40.11 | 39.31 | 40.06 | 41.55 | 40.98 | 40.16 | 40.21 | 41.16 | 41.30 | 40.32 | 40.15 | 40.74 | 41.27 | 40.35 |
| $TiO_2$ | 0.00 | 0.00 | 0.00 | 0.03 | 0.00 | 0.00 | 0.04 | 0.00 | 0.00 | 0.04 | 0.03 | 0.00 | 0.00 | 0.01 | 0.00 | 0.01 | 0.01 | 0.02 |
| $Al_2O_3$ | 0.00 | 0.01 | 0.00 | 0.02 | 0.00 | 0.01 | 0.00 | 0.00 | 0.02 | 0.00 | 0.00 | 0.00 | 0.00 | 0.00 | 0.00 | 0.00 | 0.01 | 0.00 |
| $Cr_2O_3$ | 0.70 | 0.65 | 0.53 | 0.48 | 0.00 | 0.00 | 0.00 | 0.00 | 0.00 | 0.00 | 0.01 | 0.02 | 0.01 | 0.03 | 0.10 | 0.14 | 0.10 | 0.13 |
| $V_2O_3$ | 0.00 | 0.00 | 0.00 | 0.00 | 0.00 | 0.00 | 0.00 | 0.00 | 0.00 | 0.00 | 0.00 | 0.00 | 0.00 | 0.00 | 0.00 | 0.00 | 0.00 | 0.00 |
| $Fe_2O_3$ | 0.00 | 0.00 | 0.00 | 0.00 | 0.00 | 0.00 | 0.00 | 0.00 | 0.00 | 0.00 | 0.00 | 0.00 | 0.00 | 0.00 | 0.00 | 0.00 | 0.00 | 0.00 |
| FeO | 5.58 | 5.52 | 5.29 | 5.24 | 6.64 | 6.87 | 6.87 | 6.91 | 6.70 | 6.69 | 6.62 | 6.86 | 6.47 | 6.36 | 6.35 | 6.29 | 5.77 | 5.46 |
| MnO | 0.01 | 0.05 | 0.09 | 0.06 | 0.08 | 0.13 | 0.04 | 0.12 | 0.01 | 0.17 | 0.07 | 0.13 | 0.01 | 0.10 | 0.11 | 0.04 | 0.07 | 0.08 |
| MgO | 54.57 | 54.77 | 55.65 | 56.47 | 52.70 | 52.56 | 52.15 | 51.74 | 52.00 | 51.68 | 52.10 | 51.97 | 52.35 | 52.21 | 52.34 | 52.44 | 52.30 | 52.24 |
| NiO | 0.42 | 0.36 | 0.42 | 0.34 | 0.34 | 0.40 | 0.42 | 0.43 | 0.41 | 0.29 | 0.35 | 0.46 | 0.41 | 0.36 | 0.32 | 0.38 | 0.37 | 0.48 |
| TOT | 101.10 | 101.94 | 101.17 | 102.90 | 99.93 | 99.32 | 99.62 | 100.82 | 100.16 | 99.08 | 99.45 | 100.60 | 100.57 | 99.42 | 99.40 | 100.08 | 99.89 | 98.76 |
| Si | 0.94 | 0.95 | 0.92 | 0.93 | 0.97 | 0.95 | 0.97 | 1.00 | 0.99 | 0.98 | 0.97 | 0.99 | 0.99 | 0.98 | 0.97 | 0.98 | 0.99 | 0.98 |
| Ti | 0.00 | 0.00 | 0.00 | 0.00 | 0.00 | 0.00 | 0.00 | 0.00 | 0.00 | 0.00 | 0.00 | 0.00 | 0.00 | 0.00 | 0.00 | 0.00 | 0.00 | 0.00 |
| Al | 0.00 | 0.00 | 0.00 | 0.00 | 0.00 | 0.00 | 0.00 | 0.00 | 0.00 | 0.00 | 0.00 | 0.00 | 0.00 | 0.00 | 0.00 | 0.00 | 0.00 | 0.00 |
| Cr | 0.01 | 0.01 | 0.01 | 0.01 | 0.00 | 0.00 | 0.00 | 0.00 | 0.00 | 0.00 | 0.00 | 0.00 | 0.00 | 0.00 | 0.00 | 0.00 | 0.00 | 0.00 |
| V | 0.00 | 0.00 | 0.00 | 0.00 | 0.00 | 0.00 | 0.00 | 0.00 | 0.00 | 0.00 | 0.00 | 0.00 | 0.00 | 0.00 | 0.00 | 0.00 | 0.00 | 0.00 |
| $Fe^{3+}$ | 0.00 | 0.00 | 0.00 | 0.00 | 0.00 | 0.00 | 0.00 | 0.00 | 0.00 | 0.00 | 0.00 | 0.00 | 0.00 | 0.00 | 0.00 | 0.00 | 0.00 | 0.00 |
| $Fe^{2+}$ | 0.11 | 0.11 | 0.10 | 0.10 | 0.13 | 0.14 | 0.14 | 0.14 | 0.13 | 0.14 | 0.13 | 0.14 | 0.13 | 0.13 | 0.13 | 0.13 | 0.12 | 0.11 |
| Mn | 0.00 | 0.00 | 0.00 | 0.00 | 0.00 | 0.00 | 0.00 | 0.00 | 0.00 | 0.00 | 0.00 | 0.00 | 0.00 | 0.00 | 0.00 | 0.00 | 0.00 | 0.00 |
| Mg | 1.93 | 1.92 | 1.95 | 1.95 | 1.89 | 1.90 | 1.88 | 1.85 | 1.87 | 1.88 | 1.88 | 1.86 | 1.87 | 1.88 | 1.89 | 1.88 | 1.88 | 1.89 |
| Ni | 0.01 | 0.01 | 0.01 | 0.01 | 0.01 | 0.01 | 0.01 | 0.01 | 0.01 | 0.01 | 0.01 | 0.01 | 0.01 | 0.01 | 0.01 | 0.01 | 0.01 | 0.01 |

| Analysis | OLPU3-70 | bordo chr | OLPU3-71 | OLPU3-72 | OLPU3-73 | OLPU3-74 | OLPU3-75 | OLPU3-76 | OLPU3-77 | OLPU3-78 | OLPU3-79 | OLPU3-80 | OLPU3-81 | OLPU3-82 | OLPU3-83 | OLPU3-84 | OLPU3-85 | OLPU3-86 |
|---|---|---|---|---|---|---|---|---|---|---|---|---|---|---|---|---|---|---|
| | OL-70 | | CHR-71 | CHR-72 | CHR-73 | CHR-74 | CHR-75 | CHR-76 | CHR-77 | CHR-78 | CHR-79 | CHR-80 | CHR-81 | CHR-82 | CHR-83 | CHR-84 | CHR-85 | CHR-86 |
| X | 65.529 | 65.539 | 65.543 | 65.545 | 65.550 | 65.553 | 65.558 | 65.569 | 65.581 | 65.600 | 65.613 | 65.622 | 65.691 | 65.700 | 65.718 | 65.730 | 65.741 | 65.750 |
| Y | 83.757 | 83.750 | 83.747 | 83.742 | 83.737 | 83.733 | 83.727 | 83.719 | 83.706 | 83.689 | 83.674 | 83.661 | 83.650 | 83.641 | 83.629 | 83.616 | 83.607 | 83.598 |

# Appendix: Chapter 3

| d(mm) | 0.012 | 0.005 | 0.010 | 0.017 | 0.023 | 0.030 | 0.043 | 0.061 | 0.086 | 0.107 | 0.122 | 0.095 | 0.082 | 0.060 | 0.043 | 0.029 | 0.016 |
|---|---|---|---|---|---|---|---|---|---|---|---|---|---|---|---|---|---|
| $SiO_2$ | 40.69 | 1.09 | 0.06 | 0.04 | 0.02 | 0.02 | 0.01 | 0.00 | 0.00 | 0.00 | 0.02 | 0.00 | 0.03 | 0.00 | 0.04 | 0.00 | 0.00 |
| $TiO_2$ | 0.01 | 0.03 | 0.05 | 0.08 | 0.07 | 0.07 | 0.07 | 0.04 | 0.07 | 0.05 | 0.10 | 0.07 | 0.09 | 0.08 | 0.06 | 0.08 | 0.07 |
| $Al_2O_3$ | 0.01 | 4.10 | 8.73 | 8.17 | 8.29 | 8.42 | 8.37 | 8.19 | 8.35 | 8.20 | 8.17 | 8.31 | 8.24 | 8.28 | 8.13 | 8.28 | 8.20 |
| $Cr_2O_3$ | 0.24 | 23.46 | 60.49 | 61.79 | 61.49 | 62.70 | 62.52 | 62.74 | 62.44 | 62.82 | 62.20 | 62.20 | 63.00 | 63.20 | 63.23 | 61.90 | 61.75 |
| $V_2O_3$ | 0.00 | 0.00 | 0.00 | 0.00 | 0.00 | 0.00 | 0.00 | 0.00 | 0.00 | 0.00 | 0.00 | 0.00 | 0.00 | 0.00 | 0.00 | 0.00 | 0.00 |
| $Fe_2O_3$ | 0.00 | 43.19 | 1.14 | 0.23 | 0.25 | 0.00 | 0.00 | 0.00 | 0.03 | 0.14 | 0.12 | 0.00 | 0.00 | 0.00 | 0.00 | 0.31 | 0.29 |
| FeO | 5.59 | 19.10 | 21.50 | 21.44 | 20.85 | 20.45 | 20.33 | 20.18 | 19.94 | 19.91 | 19.73 | 19.73 | 19.65 | 19.89 | 20.39 | 20.68 | 20.98 |
| MnO | 0.07 | 0.69 | 0.17 | 0.02 | 0.22 | 0.21 | 0.17 | 0.18 | 0.04 | 0.18 | 0.25 | 0.14 | 0.13 | 0.13 | 0.29 | 0.20 | 0.20 |
| MgO | 52.47 | 8.85 | 7.67 | 7.74 | 7.91 | 8.16 | 8.22 | 8.27 | 8.68 | 8.68 | 8.60 | 8.60 | 8.46 | 8.43 | 8.31 | 8.12 | 7.85 |
| NiO | 0.36 | 0.49 | 0.08 | 0.03 | 0.02 | 0.02 | 0.05 | 0.00 | 0.00 | 0.00 | 0.05 | 0.04 | 0.00 | 0.10 | 0.01 | 0.04 | 0.04 |
| TOT | 99.44 | 101.02 | 99.97 | 99.56 | 99.13 | 100.13 | 99.83 | 99.68 | 99.64 | 100.07 | 99.31 | 99.12 | 99.59 | 100.13 | 100.55 | 99.60 | 99.39 |
| Si | 0.98 | 0.04 | 0.00 | 0.00 | 0.00 | 0.00 | 0.00 | 0.00 | 0.00 | 0.00 | 0.00 | 0.00 | 0.00 | 0.00 | 0.00 | 0.00 | 0.00 |
| Ti | 0.00 | 0.00 | 0.00 | 0.00 | 0.00 | 0.00 | 0.00 | 0.00 | 0.00 | 0.00 | 0.00 | 0.00 | 0.00 | 0.00 | 0.00 | 0.00 | 0.00 |
| Al | 0.00 | 0.17 | 0.35 | 0.33 | 0.33 | 0.33 | 0.33 | 0.33 | 0.33 | 0.32 | 0.33 | 0.33 | 0.33 | 0.33 | 0.32 | 0.33 | 0.33 |
| Cr | 0.00 | 0.64 | 1.62 | 1.66 | 1.66 | 1.67 | 1.67 | 1.68 | 1.66 | 1.67 | 1.66 | 1.67 | 1.68 | 1.68 | 1.68 | 1.66 | 1.66 |
| V | 0.00 | 0.00 | 0.00 | 0.00 | 0.00 | 0.00 | 0.00 | 0.00 | 0.00 | 0.00 | 0.00 | 0.00 | 0.00 | 0.00 | 0.00 | 0.00 | 0.00 |
| $Fe^{3+}$ | 0.00 | 1.12 | 0.03 | 0.01 | 0.01 | 0.00 | 0.00 | 0.00 | 0.00 | 0.00 | 0.00 | 0.00 | 0.00 | 0.00 | 0.00 | 0.01 | 0.01 |
| $Fe^{2+}$ | 0.11 | 0.55 | 0.61 | 0.61 | 0.59 | 0.58 | 0.57 | 0.57 | 0.56 | 0.56 | 0.56 | 0.56 | 0.56 | 0.56 | 0.57 | 0.59 | 0.60 |
| Mn | 0.00 | 0.02 | 0.00 | 0.00 | 0.01 | 0.01 | 0.00 | 0.01 | 0.00 | 0.01 | 0.01 | 0.00 | 0.00 | 0.00 | 0.01 | 0.01 | 0.01 |
| Mg | 1.89 | 0.45 | 0.39 | 0.39 | 0.40 | 0.41 | 0.41 | 0.42 | 0.44 | 0.43 | 0.43 | 0.43 | 0.43 | 0.42 | 0.42 | 0.41 | 0.40 |
| Ni | 0.01 | 0.01 | 0.00 | 0.00 | 0.00 | 0.00 | 0.00 | 0.00 | 0.00 | 0.00 | 0.00 | 0.00 | 0.00 | 0.00 | 0.00 | 0.00 | 0.00 |

| Analysis | OLPU3-87 CHR-87 | OLPU3-88 CHR-88 | bordo chr | OLPU3-89 OL-89 | OLPU3-90 OL-90 | OLPU3-91 OL-91 | OLPU3-92 OL-92 | OLPU3-93 OL-93 | OLPU3-94 OL-94 | OLPU3-95 OL-95 | OLPU3-96 OL-96 | OLPU3-97 OL-97 | OLPU3-98 OL-98 | OLPU3-99 OL-99 | OLPU3-100 OL-100 | OLPU3-101 OL-101 | OLPU3-102 OL-102 |
|---|---|---|---|---|---|---|---|---|---|---|---|---|---|---|---|---|---|
| X | 65.754 | 65.757 | 65.761 | 65.767 | 65.768 | 65.772 | 65.776 | 65.782 | 65.788 | 65.794 | 65.797 | 65.802 | 65.809 | 65.816 | 65.819 | 65.826 | 65.836 |
| Y | 83.593 | 83.589 | 83.587 | 83.583 | 83.580 | 83.578 | 83.576 | 83.572 | 83.569 | 83.566 | 83.564 | 83.560 | 83.554 | 83.548 | 83.543 | 83.537 | 83.530 |
| d(mm) | 0.010 | 0.005 | | 0.007 | 0.010 | 0.014 | 0.018 | 0.025 | 0.032 | 0.039 | 0.043 | 0.049 | 0.058 | 0.067 | 0.073 | 0.082 | 0.094 |
| $SiO_2$ | 0.00 | 0.01 | | 33.89 | 40.29 | 40.34 | 40.34 | 40.05 | 41.09 | 40.69 | 40.68 | 40.28 | 40.85 | 40.47 | 41.18 | 40.61 | 40.85 |
| $TiO_2$ | 0.09 | 0.12 | | 0.00 | 0.00 | 0.02 | 0.02 | 0.00 | 0.01 | 0.00 | 0.01 | 0.02 | 0.00 | 0.00 | 0.01 | 0.00 | 0.00 |
| $Al_2O_3$ | 8.17 | 8.19 | | 0.07 | 0.01 | 0.00 | 0.00 | 0.00 | 0.00 | 0.00 | 0.02 | 0.01 | 0.00 | 0.00 | 0.00 | 0.00 | 0.00 |
| $Cr_2O_3$ | 61.93 | 61.57 | | 0.82 | 0.51 | 0.34 | 0.34 | 0.19 | 0.17 | 0.11 | 0.13 | 0.08 | 0.06 | 0.03 | 0.03 | 0.02 | 0.02 |
| $V_2O_3$ | 0.00 | 0.00 | | 0.00 | 0.00 | 0.00 | 0.00 | 0.00 | 0.00 | 0.00 | 0.00 | 0.00 | 0.00 | 0.00 | 0.00 | 0.00 | 0.00 |
| $Fe_2O_3$ | 0.24 | 0.64 | | 0.00 | 0.00 | 0.00 | 0.00 | 0.00 | 0.00 | 0.00 | 0.00 | 0.00 | 0.00 | 0.00 | 0.00 | 0.00 | 0.00 |
| FeO | 21.43 | 21.65 | | 5.10 | 5.18 | 5.57 | 5.57 | 5.84 | 6.11 | 6.17 | 6.12 | 5.94 | 6.71 | 6.34 | 6.52 | 6.19 | 6.39 |
| MnO | 0.15 | 0.17 | | 0.01 | 0.01 | 0.20 | 0.20 | 0.13 | 0.09 | 0.21 | 0.19 | 0.03 | 0.02 | 0.06 | 0.07 | 0.10 | 0.04 |
| MgO | 7.66 | 7.56 | | 55.36 | 55.45 | 53.31 | 53.31 | 52.22 | 52.09 | 51.93 | 52.32 | 52.39 | 52.58 | 52.83 | 53.44 | 52.16 | 52.15 |
| NiO | 0.03 | 0.03 | | 0.22 | 0.46 | 0.33 | 0.33 | 0.35 | 0.38 | 0.31 | 0.34 | 0.33 | 0.34 | 0.38 | 0.39 | 0.41 | 0.42 |
| ZnO | 0.03 | 0.06 | | 0.05 | 0.00 | 0.02 | 0.02 | 0.00 | 0.08 | 0.00 | 0.02 | 0.03 | 0.02 | 0.00 | 0.02 | 0.00 | 0.00 |
| TOT | 99.72 | 100.01 | | 95.52 | 101.92 | 100.13 | 100.13 | 98.78 | 100.02 | 99.42 | 99.85 | 99.12 | 100.60 | 100.13 | 101.69 | 99.51 | 99.91 |
| Si | 0.00 | 0.00 | | 0.84 | 0.94 | 0.97 | 0.97 | 0.97 | 0.99 | 0.99 | 0.98 | 0.98 | 0.98 | 0.97 | 0.97 | 0.98 | 0.99 |
| Ti | 0.00 | 0.00 | | 0.00 | 0.00 | 0.00 | 0.00 | 0.00 | 0.00 | 0.00 | 0.00 | 0.00 | 0.00 | 0.00 | 0.00 | 0.00 | 0.00 |
| Al | 0.33 | 0.33 | | 0.00 | 0.00 | 0.00 | 0.00 | 0.00 | 0.00 | 0.00 | 0.00 | 0.00 | 0.00 | 0.00 | 0.00 | 0.00 | 0.00 |
| Cr | 1.66 | 1.65 | | 0.02 | 0.01 | 0.01 | 0.01 | 0.00 | 0.00 | 0.00 | 0.00 | 0.00 | 0.00 | 0.00 | 0.00 | 0.00 | 0.00 |
| V | 0.00 | 0.00 | | 0.00 | 0.00 | 0.00 | 0.00 | 0.00 | 0.00 | 0.00 | 0.00 | 0.00 | 0.00 | 0.00 | 0.00 | 0.00 | 0.00 |
| $Fe^{3+}$ | 0.01 | 0.02 | | 0.00 | 0.00 | 0.00 | 0.00 | 0.00 | 0.00 | 0.00 | 0.00 | 0.00 | 0.00 | 0.00 | 0.00 | 0.00 | 0.00 |
| $Fe^{2+}$ | 0.61 | 0.61 | | 0.11 | 0.10 | 0.11 | 0.11 | 0.12 | 0.12 | 0.13 | 0.12 | 0.12 | 0.13 | 0.13 | 0.13 | 0.13 | 0.13 |
| Mn | 0.00 | 0.00 | | 0.00 | 0.00 | 0.00 | 0.00 | 0.00 | 0.00 | 0.00 | 0.00 | 0.00 | 0.00 | 0.00 | 0.00 | 0.00 | 0.00 |
| Mg | 0.39 | 0.38 | | 2.04 | 1.94 | 1.90 | 1.90 | 1.89 | 1.87 | 1.88 | 1.88 | 1.89 | 1.88 | 1.89 | 1.89 | 1.88 | 1.88 |
| Ni | 0.00 | 0.00 | | 0.00 | 0.01 | 0.01 | 0.01 | 0.01 | 0.01 | 0.01 | 0.01 | 0.01 | 0.01 | 0.01 | 0.01 | 0.01 | 0.01 |
| Zn | 0.00 | 0.00 | | 0.00 | 0.00 | 0.00 | 0.00 | 0.00 | 0.00 | 0.00 | 0.00 | 0.00 | 0.00 | 0.00 | 0.00 | 0.00 | 0.00 |

# Chapter 4

Tab. A4.1 Spinels microprobe analyses (core and rim) of Nea Roda massive chromitites.

| wt% | NRO9-4 | NRO9-5 | NRO9-10 | NRO9-12 | NRO9-14 | NRO9-3 | NRO9-6 | NRO9-9 | NRO9-11 | NRO913 |
|---|---|---|---|---|---|---|---|---|---|---|
| | core | core | core | core | core | rim | rim | rim | rim | rim |
| $TiO_2$ | 0.20 | 0.17 | 0.17 | 0.25 | 0.20 | 0.13 | 0.20 | 0.21 | 0.15 | 0.24 |
| MnO | 0.07 | 0.10 | 0.11 | 0.05 | 0.12 | 0.26 | 0.16 | 0.21 | 0.20 | 0.27 |
| MgO | 13.49 | 14.22 | 13.66 | 13.73 | 12.37 | 9.36 | 10.86 | 9.76 | 9.47 | 9.16 |
| $Cr_2O_3$ | 53.41 | 52.68 | 53.93 | 54.27 | 57.97 | 67.94 | 64.37 | 66.87 | 65.26 | 66.63 |
| Feo | 15.39 | 14.72 | 15.11 | 15.38 | 16.76 | 19.16 | 18.17 | 19.35 | 20.61 | 20.74 |
| $Fe_2O_3$ | 1.06 | 1.23 | 1.10 | 1.06 | 1.06 | 0.57 | 1.05 | 0.89 | 0.34 | 1.50 |
| $Al_2O_3$ | 16.85 | 17.68 | 16.40 | 16.52 | 12.80 | 3.80 | 6.78 | 4.22 | 3.24 | 3.22 |
| NiO | 0.08 | 0.07 | 0.11 | 0.08 | 0.01 | 0.04 | 0.04 | 0.00 | 0.07 | 0.09 |
| Total | 100.59 | 100.91 | 100.67 | 101.40 | 101.34 | 101.30 | 101.69 | 101.63 | 100.95 | 102.00 |
| Ti | 0.00 | 0.00 | 0.00 | 0.01 | 0.00 | 0.00 | 0.00 | 0.01 | 0.00 | 0.01 |
| Mn | 0.00 | 0.00 | 0.00 | 0.00 | 0.00 | 0.01 | 0.00 | 0.01 | 0.01 | 0.01 |
| Mg | 0.63 | 0.65 | 0.63 | 0.63 | 0.58 | 0.47 | 0.53 | 0.49 | 0.48 | 0.46 |
| Cr | 1.32 | 1.28 | 1.33 | 1.33 | 1.45 | 1.81 | 1.67 | 1.77 | 1.74 | 1.77 |
| $Fe^{2+}$ | 0.40 | 0.38 | 0.39 | 0.40 | 0.44 | 0.54 | 0.50 | 0.54 | 0.58 | 0.58 |
| $Fe^{3+}$ | 0.03 | 0.03 | 0.03 | 0.03 | 0.03 | 0.02 | 0.03 | 0.02 | 0.01 | 0.04 |
| Al | 0.62 | 0.64 | 0.60 | 0.60 | 0.48 | 0.15 | 0.26 | 0.17 | 0.13 | 0.13 |
| Ni | 0.00 | 0.00 | 0.00 | 0.00 | 0.00 | 0.00 | 0.00 | 0.00 | 0.00 | 0.00 |

Tab. A4.2 Spinel microprobe analyses (core and rim) of St. George (Gomati) massive chromitites.

| wt% | GOM2A-1 | GOM2A-2 | GOM2A-4 | GOM2A-6 | GOM2A-7 | GOM2A-8 | GOM2A-9 | GOM2A-11 | GOM2A-13 | GOM2A-14 | GOM2A-15 | GOM2A-16 | GOM2A-17 | GOM2A-18 | GOM2A-19 | GOM2A-20 | GOM2A-21 | GOM2A-22 |
|---|---|---|---|---|---|---|---|---|---|---|---|---|---|---|---|---|---|---|
| | core | core | core | core | core | core | core | core | core | core | core | core | core | core | core | core | core | core |
| $TiO_2$ | 0.21 | 0.35 | 0.24 | 0.37 | 0.24 | 0.28 | 0.21 | 0.33 | 0.32 | 0.30 | 0.30 | 0.41 | 0.39 | 0.25 | 0.23 | 0.26 | 0.10 | 0.21 |
| $Al_2O_3$ | 11.91 | 11.41 | 6.24 | 11.55 | 11.48 | 11.63 | 11.05 | 12.06 | 11.34 | 11.57 | 11.23 | 11.13 | 10.60 | 11.34 | 10.97 | 6.41 | 12.03 | 11.71 |
| $Cr_2O_3$ | 56.02 | 56.59 | 62.92 | 55.98 | 55.97 | 54.75 | 57.63 | 56.56 | 55.78 | 56.68 | 56.11 | 55.99 | 57.76 | 56.92 | 56.79 | 62.96 | 55.36 | 56.14 |
| $V_2O_3$ | 0.00 | 0.00 | 0.00 | 0.00 | 0.00 | 0.00 | 0.00 | 0.00 | 0.00 | 0.00 | 0.00 | 0.00 | 0.00 | 0.00 | 0.00 | 0.00 | 0.00 | 0.00 |
| $Fe_2O_3$ | 2.34 | 1.17 | 1.72 | 2.41 | 2.13 | 2.16 | 0.89 | 0.55 | 2.25 | 2.40 | 3.16 | 3.40 | 1.95 | 1.68 | 1.73 | 1.17 | 2.14 | 1.76 |
| FeO | 21.48 | 21.77 | 23.21 | 21.81 | 21.21 | 21.14 | 21.48 | 22.05 | 20.99 | 21.20 | 20.81 | 21.35 | 22.15 | 21.44 | 21.25 | 22.95 | 20.82 | 21.27 |
| MnO | 0.14 | 0.13 | 0.24 | 0.16 | 0.25 | 0.13 | 0.07 | 0.04 | 0.00 | 0.20 | 0.19 | 0.10 | 0.18 | 0.14 | 0.06 | 0.26 | 0.09 | 0.00 |
| MgO | 8.27 | 8.07 | 6.61 | 8.01 | 8.10 | 8.35 | 7.95 | 7.81 | 8.33 | 8.46 | 8.53 | 8.43 | 7.80 | 8.18 | 8.16 | 6.73 | 8.27 | 8.18 |
| NiO | 0.03 | 0.09 | 0.08 | 0.10 | 0.05 | 0.11 | 0.11 | 0.10 | 0.10 | 0.11 | 0.09 | 0.04 | 0.07 | 0.05 | 0.03 | 0.03 | 0.12 | 0.11 |
| ZnO | 0.03 | 0.03 | 0.08 | 0.04 | 0.00 | 0.00 | 0.00 | 0.00 | 0.02 | 0.03 | 0.11 | 0.06 | 0.06 | 0.04 | 0.05 | 0.04 | 0.02 | 0.00 |
| Total | 100.47 | 99.78 | 101.36 | 100.43 | 99.43 | 98.82 | 99.37 | 99.51 | 99.13 | 100.98 | 100.53 | 100.91 | 100.96 | 100.10 | 99.34 | 100.81 | 98.93 | 99.38 |
| Ti | 0.01 | 0.01 | 0.01 | 0.01 | 0.01 | 0.01 | 0.01 | 0.01 | 0.01 | 0.01 | 0.01 | 0.01 | 0.01 | 0.01 | 0.01 | 0.01 | 0.00 | 0.01 |
| Al | 0.46 | 0.45 | 0.25 | 0.45 | 0.45 | 0.46 | 0.44 | 0.47 | 0.45 | 0.45 | 0.44 | 0.43 | 0.41 | 0.44 | 0.43 | 0.26 | 0.48 | 0.46 |
| Cr | 1.46 | 1.49 | 1.69 | 1.47 | 1.48 | 1.45 | 1.53 | 1.49 | 1.48 | 1.48 | 1.47 | 1.46 | 1.52 | 1.50 | 1.51 | 1.70 | 1.47 | 1.48 |
| V | 0.00 | 0.00 | 0.00 | 0.00 | 0.00 | 0.00 | 0.00 | 0.00 | 0.00 | 0.00 | 0.00 | 0.00 | 0.00 | 0.00 | 0.00 | 0.00 | 0.00 | 0.00 |
| $Fe^{3+}$ | 0.06 | 0.03 | 0.04 | 0.06 | 0.05 | 0.05 | 0.02 | 0.01 | 0.06 | 0.06 | 0.08 | 0.08 | 0.05 | 0.04 | 0.04 | 0.03 | 0.05 | 0.04 |
| $Fe^{2+}$ | 0.59 | 0.61 | 0.66 | 0.61 | 0.59 | 0.59 | 0.60 | 0.62 | 0.59 | 0.58 | 0.58 | 0.59 | 0.62 | 0.60 | 0.60 | 0.66 | 0.58 | 0.59 |
| Mn | 0.00 | 0.00 | 0.01 | 0.00 | 0.01 | 0.00 | 0.00 | 0.00 | 0.00 | 0.01 | 0.01 | 0.00 | 0.01 | 0.00 | 0.00 | 0.01 | 0.00 | 0.00 |
| Mg | 0.41 | 0.40 | 0.34 | 0.40 | 0.40 | 0.42 | 0.40 | 0.39 | 0.42 | 0.42 | 0.42 | 0.42 | 0.39 | 0.41 | 0.41 | 0.34 | 0.41 | 0.41 |
| Ni | 0.00 | 0.00 | 0.00 | 0.00 | 0.00 | 0.00 | 0.00 | 0.00 | 0.00 | 0.00 | 0.00 | 0.00 | 0.00 | 0.00 | 0.00 | 0.00 | 0.00 | 0.00 |

| | | | | | | | | | | | | | | | | | | |
|---|---|---|---|---|---|---|---|---|---|---|---|---|---|---|---|---|---|---|
| Zn | 0.00 | 0.00 | 0.00 | 0.00 | 0.00 | 0.00 | 0.00 | 0.00 | 0.00 | 0.00 | 0.00 | 0.00 | 0.00 | 0.00 | 0.00 | 0.00 | 0.00 | 0.00 |

| wt% | GOM2A-24 core | GOM2A-25 core | GOM2A-26 core | GOM2A-27 core | GOM2A-28 core | GOM2A-29 core | GOM2A-30 core | GOM2A-5 rim | GOM2A-3 rim | GOM2A-10 rim | GOM2B-1 core | GOM2B-4 core | GOM2B-5 core | GOM2B-6 core | GOM2B-7 core | GOM2B-13 core | GOM2B-14 core | GOM2B-15 core |
|---|---|---|---|---|---|---|---|---|---|---|---|---|---|---|---|---|---|---|
| $TiO_2$ | 0.31 | 0.36 | 0.29 | 0.17 | 0.26 | 0.27 | 0.28 | 0.17 | 0.06 | 0.24 | 0.36 | 0.44 | 0.39 | 0.43 | 0.46 | 0.40 | 0.33 | 0.49 |
| $Al_2O_3$ | 10.34 | 11.58 | 11.74 | 7.70 | 11.41 | 11.86 | 11.96 | 4.96 | 3.78 | 5.51 | 11.22 | 12.23 | 12.20 | 10.31 | 6.26 | 6.38 | 12.25 | 10.14 |
| $Cr_2O_3$ | 56.25 | 55.24 | 55.80 | 60.79 | 56.80 | 55.99 | 55.79 | 65.44 | 67.13 | 66.29 | 52.10 | 51.43 | 51.13 | 53.15 | 56.01 | 55.46 | 51.99 | 52.78 |
| $V_2O_3$ | 0.00 | 0.00 | 0.00 | 0.00 | 0.00 | 0.00 | 0.00 | 0.00 | 0.00 | 0.00 | 0.17 | 0.18 | 0.18 | 0.21 | 0.23 | 0.21 | 0.17 | 0.17 |
| $Fe_2O_3$ | 2.64 | 2.46 | 2.20 | 1.95 | 2.23 | 1.84 | 2.04 | 1.27 | 0.00 | 0.00 | 5.10 | 4.06 | 4.16 | 4.98 | 6.56 | 6.47 | 3.76 | 4.69 |
| FeO | 21.49 | 21.37 | 21.30 | 22.56 | 21.60 | 20.99 | 21.11 | 23.61 | 23.22 | 22.79 | 25.55 | 25.04 | 25.03 | 25.99 | 26.80 | 26.49 | 25.03 | 25.67 |
| MnO | 0.17 | 0.18 | 0.24 | 0.24 | 0.19 | 0.06 | 0.08 | 0.19 | 0.16 | 0.14 | 0.41 | 0.32 | 0.24 | 0.36 | 0.27 | 0.43 | 0.29 | 0.38 |
| MgO | 7.78 | 8.09 | 8.17 | 6.99 | 8.09 | 8.37 | 8.42 | 6.41 | 6.10 | 6.76 | 5.33 | 5.78 | 5.77 | 5.05 | 4.28 | 4.18 | 5.69 | 5.14 |
| NiO | 0.07 | 0.08 | 0.10 | 0.03 | 0.09 | 0.09 | 0.05 | 0.03 | 0.09 | 0.07 | 0.08 | 0.07 | 0.04 | 0.06 | 0.06 | 0.04 | 0.04 | 0.10 |
| ZnO | 0.04 | 0.00 | 0.00 | 0.06 | 0.06 | 0.14 | 0.00 | 0.06 | 0.01 | 0.10 | 0.01 | 0.00 | 0.00 | 0.10 | 0.00 | 0.02 | 0.11 | 0.00 |
| Total | 99.08 | 99.36 | 99.86 | 100.48 | 100.75 | 99.62 | 99.74 | 102.14 | 100.57 | 101.91 | 100.34 | 99.58 | 99.21 | 100.61 | 100.93 | 100.08 | 99.67 | 99.63 |
| Ti | 0.01 | 0.01 | 0.01 | 0.00 | 0.01 | 0.01 | 0.01 | 0.00 | 0.00 | 0.01 | 0.01 | 0.01 | 0.01 | 0.01 | 0.01 | 0.01 | 0.01 | 0.01 |
| Al | 0.41 | 0.46 | 0.46 | 0.31 | 0.45 | 0.47 | 0.47 | 0.20 | 0.15 | 0.22 | 0.45 | 0.49 | 0.49 | 0.41 | 0.26 | 0.26 | 0.49 | 0.41 |
| Cr | 1.50 | 1.46 | 1.47 | 1.63 | 1.49 | 1.47 | 1.47 | 1.76 | 1.84 | 1.78 | 1.40 | 1.38 | 1.37 | 1.43 | 1.54 | 1.54 | 1.39 | 1.43 |
| V | 0.00 | 0.00 | 0.00 | 0.00 | 0.00 | 0.00 | 0.00 | 0.00 | 0.00 | 0.00 | 0.00 | 0.00 | 0.00 | 0.01 | 0.01 | 0.01 | 0.00 | 0.00 |
| $Fe^{3+}$ | 0.07 | 0.06 | 0.06 | 0.05 | 0.06 | 0.05 | 0.05 | 0.03 | 0.00 | 0.00 | 0.13 | 0.10 | 0.11 | 0.13 | 0.17 | 0.17 | 0.10 | 0.12 |
| $Fe^{2+}$ | 0.61 | 0.60 | 0.59 | 0.64 | 0.60 | 0.58 | 0.59 | 0.67 | 0.67 | 0.65 | 0.73 | 0.71 | 0.71 | 0.74 | 0.78 | 0.78 | 0.71 | 0.74 |
| Mn | 0.00 | 0.00 | 0.01 | 0.01 | 0.01 | 0.00 | 0.00 | 0.01 | 0.00 | 0.00 | 0.01 | 0.01 | 0.01 | 0.01 | 0.01 | 0.01 | 0.01 | 0.01 |
| Mg | 0.39 | 0.40 | 0.41 | 0.35 | 0.40 | 0.42 | 0.42 | 0.32 | 0.32 | 0.34 | 0.27 | 0.29 | 0.29 | 0.26 | 0.22 | 0.22 | 0.29 | 0.26 |
| Ni | 0.00 | 0.00 | 0.00 | 0.00 | 0.00 | 0.00 | 0.00 | 0.00 | 0.00 | 0.00 | 0.00 | 0.00 | 0.00 | 0.00 | 0.00 | 0.00 | 0.00 | 0.00 |
| Zn | 0.00 | 0.00 | 0.00 | 0.00 | 0.00 | 0.00 | 0.00 | 0.00 | 0.00 | 0.00 | 0.00 | 0.00 | 0.00 | 0.00 | 0.00 | 0.00 | 0.00 | 0.00 |

| wt% | GOM2B-16 core | GOM2B-17 core | GOM2B-18 core | GOM2B-19 core | GOM2B-20 core | GOM2B-10 rim | GOM2B-11 rim | GOM2B-12 rim | GOM2B-21 rim | GOM2B-23 rim | GOM2C-3 core | GOM2C-4 core | GOM2C-5 core | GOM2C-6 core | GOM2C-9 core | GOM2C-10 core | GOM2C-11 core | GOM2C-12 core |
|---|---|---|---|---|---|---|---|---|---|---|---|---|---|---|---|---|---|---|
| $TiO_2$ | 0.55 | 0.51 | 0.58 | 0.54 | 0.50 | 0.34 | 0.36 | 0.35 | 0.52 | 0.40 | 0.32 | 0.31 | 0.28 | 0.25 | 0.19 | 0.25 | 0.35 | 0.27 |
| $Al_2O_3$ | 10.04 | 10.64 | 10.25 | 8.96 | 6.44 | 3.15 | 1.69 | 1.99 | 5.06 | 2.69 | 12.07 | 12.09 | 11.98 | 8.57 | 7.68 | 10.91 | 11.64 | 6.62 |
| $Cr_2O_3$ | 52.93 | 52.98 | 53.06 | 52.98 | 55.24 | 61.40 | 61.66 | 60.76 | 57.12 | 61.63 | 55.54 | 55.25 | 55.17 | 58.57 | 58.04 | 54.96 | 55.24 | 60.82 |
| $V_2O_3$ | 0.18 | 0.18 | 0.16 | 0.22 | 0.18 | 0.14 | 0.17 | 0.15 | 0.22 | 0.20 | 0.12 | 0.10 | 0.11 | 0.09 | 0.12 | 0.18 | 0.12 | 0.12 |
| $Fe_2O_3$ | 4.72 | 4.56 | 4.54 | 6.32 | 6.72 | 5.02 | 6.57 | 6.38 | 6.50 | 4.80 | 0.88 | 1.42 | 1.51 | 2.23 | 3.36 | 2.41 | 1.55 | 1.71 |
| FeO | 25.56 | 25.69 | 25.87 | 26.31 | 26.71 | 27.93 | 27.81 | 27.16 | 27.06 | 27.57 | 20.78 | 20.86 | 21.00 | 22.42 | 22.77 | 21.73 | 21.28 | 23.25 |
| MnO | 0.42 | 0.35 | 0.30 | 0.29 | 0.27 | 0.40 | 0.37 | 0.43 | 0.33 | 0.24 | 0.08 | 0.14 | 0.09 | 0.29 | 0.26 | 0.25 | 0.28 | 0.19 |
| MgO | 5.12 | 5.32 | 5.16 | 4.86 | 4.25 | 3.40 | 3.25 | 3.39 | 3.95 | 3.43 | 8.37 | 8.33 | 8.18 | 7.00 | 6.54 | 7.44 | 7.87 | 6.30 |
| NiO | 0.07 | 0.07 | 0.08 | 0.01 | 0.05 | 0.00 | 0.03 | 0.07 | 0.03 | 0.09 | 0.04 | 0.04 | 0.05 | 0.05 | 0.08 | 0.08 | 0.05 | 0.03 |
| ZnO | 0.13 | 0.01 | 0.02 | 0.01 | 0.07 | 0.00 | 0.05 | 0.00 | 0.07 | 0.03 | 0.04 | 0.01 | 0.06 | 0.00 | 0.00 | 0.00 | 0.08 | 0.02 |
| Total | 99.71 | 100.31 | 100.03 | 100.50 | 100.39 | 101.87 | 101.95 | 100.67 | 100.86 | 101.09 | 98.26 | 98.57 | 98.42 | 99.47 | 99.03 | 98.23 | 98.44 | 99.34 |
| Ti | 0.01 | 0.01 | 0.02 | 0.01 | 0.01 | 0.01 | 0.01 | 0.01 | 0.01 | 0.01 | 0.01 | 0.01 | 0.01 | 0.01 | 0.00 | 0.01 | 0.01 | 0.01 |
| Al | 0.41 | 0.43 | 0.41 | 0.36 | 0.27 | 0.13 | 0.07 | 0.08 | 0.21 | 0.11 | 0.48 | 0.48 | 0.48 | 0.35 | 0.31 | 0.44 | 0.46 | 0.27 |
| Cr | 1.44 | 1.43 | 1.44 | 1.44 | 1.53 | 1.71 | 1.73 | 1.72 | 1.59 | 1.73 | 1.48 | 1.47 | 1.47 | 1.58 | 1.59 | 1.48 | 1.48 | 1.67 |
| V | 0.00 | 0.00 | 0.00 | 0.01 | 0.00 | 0.00 | 0.00 | 0.00 | 0.01 | 0.01 | 0.00 | 0.00 | 0.00 | 0.00 | 0.00 | 0.00 | 0.00 | 0.00 |
| $Fe^{3+}$ | 0.12 | 0.12 | 0.12 | 0.16 | 0.18 | 0.13 | 0.18 | 0.17 | 0.17 | 0.13 | 0.02 | 0.04 | 0.04 | 0.06 | 0.09 | 0.06 | 0.04 | 0.04 |
| $Fe^{2+}$ | 0.73 | 0.73 | 0.74 | 0.76 | 0.78 | 0.82 | 0.83 | 0.81 | 0.79 | 0.82 | 0.58 | 0.59 | 0.59 | 0.64 | 0.66 | 0.62 | 0.60 | 0.67 |
| Mn | 0.01 | 0.01 | 0.01 | 0.01 | 0.01 | 0.01 | 0.01 | 0.01 | 0.01 | 0.01 | 0.00 | 0.00 | 0.00 | 0.01 | 0.01 | 0.01 | 0.01 | 0.01 |
| Mg | 0.26 | 0.27 | 0.26 | 0.25 | 0.22 | 0.18 | 0.17 | 0.18 | 0.21 | 0.18 | 0.42 | 0.42 | 0.41 | 0.36 | 0.34 | 0.38 | 0.40 | 0.33 |
| Ni | 0.00 | 0.00 | 0.00 | 0.00 | 0.00 | 0.00 | 0.00 | 0.00 | 0.00 | 0.00 | 0.00 | 0.00 | 0.00 | 0.00 | 0.00 | 0.00 | 0.00 | 0.00 |
| Zn | 0.00 | 0.00 | 0.00 | 0.00 | 0.00 | 0.00 | 0.00 | 0.00 | 0.00 | 0.00 | 0.00 | 0.00 | 0.00 | 0.00 | 0.00 | 0.00 | 0.00 | 0.00 |

| wt% | GOM2C-13 core | GOM2C-14 core | GOM2C-15 core | GOM2C-16 core | GOM2C-17 core | GOM2C-18 core | GOM2C-19 core | GOM2C-21 core | GOM2C-22 core | GOM2C-23 core | GOM2C-25 core | GOM2C-26 core | GOM2C-27 core | GOM2C-28 core | GOM2C-29 core | GOM2C-30 core | GOM2C-31 core | GOM2C-32 core |
|---|---|---|---|---|---|---|---|---|---|---|---|---|---|---|---|---|---|---|
| $TiO_2$ | 0.28 | 0.26 | 0.34 | 0.35 | 0.33 | 0.33 | 0.32 | 0.33 | 0.18 | 0.16 | 0.32 | 0.35 | 0.38 | 0.29 | 0.36 | 0.29 | 0.31 | 0.38 |
| $Al_2O_3$ | 12.12 | 11.86 | 11.75 | 11.63 | 11.48 | 11.22 | 9.00 | 10.49 | 8.00 | 10.41 | 11.89 | 11.97 | 12.11 | 11.99 | 11.93 | 9.94 | 9.99 | 12.16 |
| $Cr_2O_3$ | 55.24 | 54.78 | 54.93 | 55.11 | 55.39 | 55.03 | 54.82 | 55.79 | 59.58 | 57.87 | 54.41 | 55.20 | 54.86 | 54.80 | 55.11 | 55.87 | 57.15 | 55.11 |
| $V_2O_3$ | 0.12 | 0.10 | 0.14 | 0.13 | 0.13 | 0.12 | 0.12 | 0.14 | 0.16 | 0.13 | 0.10 | 0.12 | 0.12 | 0.15 | 0.11 | 0.13 | 0.14 | 0.15 |
| $Fe_2O_3$ | 0.43 | 1.73 | 1.74 | 1.28 | 1.24 | 1.65 | 3.11 | 1.83 | 1.84 | 0.95 | 2.11 | 1.57 | 1.57 | 1.61 | 1.60 | 2.35 | 1.77 | 1.42 |
| FeO | 20.80 | 19.71 | 19.91 | 20.16 | 20.47 | 21.26 | 21.81 | 21.55 | 21.98 | 21.81 | 20.04 | 20.11 | 19.78 | 19.70 | 20.30 | 21.59 | 21.65 | 21.12 |
| MnO | 0.18 | 0.11 | 0.16 | 0.15 | 0.20 | 0.11 | 0.33 | 0.15 | 0.13 | 0.10 | 0.12 | 0.14 | 0.21 | 0.22 | 0.08 | 0.25 | 0.19 | 0.18 |
| MgO | 8.12 | 8.76 | 8.74 | 8.46 | 8.24 | 7.80 | 6.80 | 7.57 | 7.25 | 7.67 | 8.71 | 8.74 | 8.86 | 8.81 | 8.68 | 7.37 | 7.65 | 8.30 |
| NiO | 0.03 | 0.08 | 0.14 | 0.07 | 0.06 | 0.04 | 0.08 | 0.04 | 0.00 | 0.00 | 0.00 | 0.04 | 0.10 | 0.03 | 0.02 | 0.09 | 0.00 | 0.03 |
| ZnO | 0.00 | 0.05 | 0.00 | 0.04 | 0.08 | 0.03 | 0.00 | 0.00 | 0.02 | 0.00 | 0.00 | 0.06 | 0.07 | 0.02 | 0.00 | 0.07 | 0.00 | 0.00 |
| Total | 97.37 | 97.44 | 97.87 | 97.39 | 97.59 | 97.60 | 96.41 | 97.90 | 99.16 | 99.15 | 97.69 | 98.30 | 98.06 | 97.60 | 98.19 | 97.99 | 98.84 | 98.91 |
| Ti | 0.01 | 0.01 | 0.01 | 0.01 | 0.01 | 0.01 | 0.01 | 0.01 | 0.00 | 0.00 | 0.01 | 0.01 | 0.01 | 0.01 | 0.01 | 0.01 | 0.01 | 0.01 |
| Al | 0.49 | 0.47 | 0.47 | 0.47 | 0.46 | 0.45 | 0.37 | 0.42 | 0.32 | 0.41 | 0.47 | 0.47 | 0.48 | 0.48 | 0.47 | 0.40 | 0.40 | 0.48 |
| Cr | 1.48 | 1.47 | 1.47 | 1.48 | 1.49 | 1.49 | 1.52 | 1.51 | 1.61 | 1.55 | 1.45 | 1.47 | 1.46 | 1.46 | 1.47 | 1.52 | 1.54 | 1.46 |
| V | 0.00 | 0.00 | 0.00 | 0.00 | 0.00 | 0.00 | 0.00 | 0.00 | 0.00 | 0.00 | 0.00 | 0.00 | 0.00 | 0.00 | 0.00 | 0.00 | 0.00 | 0.00 |
| $Fe^{3+}$ | 0.01 | 0.04 | 0.04 | 0.03 | 0.03 | 0.04 | 0.08 | 0.05 | 0.05 | 0.02 | 0.05 | 0.04 | 0.04 | 0.04 | 0.04 | 0.06 | 0.05 | 0.04 |
| $Fe^{2+}$ | 0.59 | 0.56 | 0.56 | 0.57 | 0.58 | 0.61 | 0.64 | 0.62 | 0.63 | 0.62 | 0.57 | 0.56 | 0.56 | 0.56 | 0.57 | 0.62 | 0.62 | 0.59 |
| Mn | 0.01 | 0.00 | 0.00 | 0.00 | 0.01 | 0.00 | 0.01 | 0.00 | 0.00 | 0.00 | 0.00 | 0.00 | 0.01 | 0.01 | 0.00 | 0.01 | 0.01 | 0.00 |
| Mg | 0.41 | 0.44 | 0.44 | 0.43 | 0.42 | 0.40 | 0.36 | 0.39 | 0.37 | 0.39 | 0.44 | 0.44 | 0.44 | 0.44 | 0.44 | 0.38 | 0.39 | 0.41 |
| Ni | 0.00 | 0.00 | 0.00 | 0.00 | 0.00 | 0.00 | 0.00 | 0.00 | 0.00 | 0.00 | 0.00 | 0.00 | 0.00 | 0.00 | 0.00 | 0.00 | 0.00 | 0.00 |
| Zn | 0.00 | 0.00 | 0.00 | 0.00 | 0.00 | 0.00 | 0.00 | 0.00 | 0.00 | 0.00 | 0.00 | 0.00 | 0.00 | 0.00 | 0.00 | 0.00 | 0.00 | 0.00 |

| wt% | GOM2C-33 core | GOM2C-2 rim | GOM2C-7 rim | GOM2C-8 rim | GOM2C-24 rim | GR54A-1 core | GR54A-2 core | GR54A-3 core | GR54A-4 core | GR54A-5 core | GR54A-6 core | GR54A-7 core | GR54A-8 core | GR54A-9 core | GR54A-10 core | GR54A-11 core | GR54A-12 core | GR54A-13 core |
|---|---|---|---|---|---|---|---|---|---|---|---|---|---|---|---|---|---|---|
| $TiO_2$ | 0.34 | 0.13 | 0.26 | 0.37 | 0.43 | 0.30 | 0.30 | 0.30 | 0.31 | 0.30 | 0.33 | 0.33 | 0.30 | 0.33 | 0.30 | 0.31 | 0.25 | 0.34 |
| $Al_2O_3$ | 11.97 | 0.68 | 4.85 | 2.82 | 3.38 | 12.00 | 11.75 | 11.76 | 11.93 | 11.83 | 11.62 | 8.36 | 12.35 | 12.13 | 11.58 | 11.67 | 6.08 | 11.43 |
| $Cr_2O_3$ | 53.86 | 67.87 | 59.91 | 60.04 | 60.83 | 54.48 | 54.87 | 53.65 | 54.68 | 55.34 | 54.31 | 57.17 | 54.53 | 54.81 | 54.41 | 55.04 | 60.05 | 54.30 |
| $V_2O_3$ | 0.14 | 0.07 | 0.12 | 0.19 | 0.13 | 0.12 | 0.13 | 0.16 | 0.15 | 0.12 | 0.15 | 0.14 | 0.11 | 0.11 | 0.13 | 0.13 | 0.10 | 0.14 |
| $Fe_2O_3$ | 1.84 | 2.28 | 4.51 | 6.42 | 5.34 | 1.93 | 2.07 | 2.24 | 1.89 | 1.63 | 2.24 | 3.07 | 0.96 | 0.81 | 1.77 | 1.11 | 1.99 | 3.21 |
| FeO | 20.42 | 25.01 | 23.74 | 24.54 | 24.37 | 20.88 | 20.68 | 20.54 | 20.80 | 21.43 | 20.97 | 22.81 | 21.99 | 21.75 | 21.41 | 21.38 | 23.36 | 20.42 |
| MnO | 0.11 | 0.31 | 0.21 | 0.29 | 0.31 | 0.16 | 0.20 | 0.12 | 0.07 | 0.12 | 0.25 | 0.25 | 0.19 | 0.21 | 0.13 | 0.18 | 0.18 | 0.22 |
| MgO | 8.34 | 4.75 | 5.83 | 5.15 | 5.46 | 8.16 | 8.29 | 8.18 | 8.35 | 8.01 | 8.08 | 6.65 | 7.49 | 7.57 | 7.66 | 7.72 | 5.94 | 8.49 |
| NiO | 0.03 | 0.14 | 0.01 | 0.00 | 0.00 | 0.13 | 0.06 | 0.05 | 0.01 | 0.02 | 0.04 | 0.02 | 0.06 | 0.00 | 0.10 | 0.05 | 0.01 | 0.06 |
| ZnO | 0.06 | 0.00 | 0.01 | 0.04 | 0.00 | 0.00 | 0.05 | 0.00 | 0.07 | 0.02 | 0.05 | 0.02 | 0.03 | 0.00 | 0.05 | 0.00 | 0.05 | 0.03 |
| Total | 97.12 | 101.25 | 99.48 | 99.85 | 100.25 | 98.17 | 98.40 | 97.02 | 98.29 | 98.82 | 98.11 | 98.82 | 98.04 | 97.71 | 97.55 | 97.59 | 98.07 | 98.63 |
| Ti | 0.01 | 0.00 | 0.01 | 0.01 | 0.01 | 0.01 | 0.01 | 0.01 | 0.01 | 0.01 | 0.01 | 0.01 | 0.01 | 0.01 | 0.01 | 0.01 | 0.01 | 0.01 |
| Al | 0.48 | 0.03 | 0.20 | 0.12 | 0.14 | 0.48 | 0.47 | 0.47 | 0.47 | 0.47 | 0.46 | 0.34 | 0.49 | 0.49 | 0.47 | 0.47 | 0.25 | 0.45 |
| Cr | 1.45 | 1.90 | 1.66 | 1.68 | 1.69 | 1.45 | 1.46 | 1.45 | 1.46 | 1.47 | 1.45 | 1.56 | 1.46 | 1.47 | 1.47 | 1.48 | 1.67 | 1.44 |
| V | 0.00 | 0.00 | 0.00 | 0.01 | 0.00 | 0.00 | 0.00 | 0.00 | 0.00 | 0.00 | 0.00 | 0.00 | 0.00 | 0.00 | 0.00 | 0.00 | 0.00 | 0.00 |
| $Fe^{3+}$ | 0.05 | 0.06 | 0.12 | 0.17 | 0.14 | 0.05 | 0.05 | 0.06 | 0.05 | 0.04 | 0.06 | 0.08 | 0.02 | 0.02 | 0.05 | 0.03 | 0.05 | 0.08 |
| $Fe^{2+}$ | 0.58 | 0.74 | 0.70 | 0.73 | 0.72 | 0.59 | 0.58 | 0.59 | 0.59 | 0.60 | 0.59 | 0.66 | 0.62 | 0.62 | 0.61 | 0.61 | 0.69 | 0.57 |
| Mn | 0.00 | 0.01 | 0.01 | 0.01 | 0.01 | 0.00 | 0.01 | 0.00 | 0.00 | 0.00 | 0.01 | 0.01 | 0.01 | 0.01 | 0.00 | 0.01 | 0.01 | 0.01 |
| Mg | 0.42 | 0.25 | 0.30 | 0.27 | 0.29 | 0.41 | 0.42 | 0.42 | 0.42 | 0.40 | 0.41 | 0.34 | 0.38 | 0.38 | 0.39 | 0.39 | 0.31 | 0.43 |
| Ni | 0.00 | 0.00 | 0.00 | 0.00 | 0.00 | 0.00 | 0.00 | 0.00 | 0.00 | 0.00 | 0.00 | 0.00 | 0.00 | 0.00 | 0.00 | 0.00 | 0.00 | 0.00 |
| Zn | 0.00 | 0.00 | 0.00 | 0.00 | 0.00 | 0.00 | 0.00 | 0.00 | 0.00 | 0.00 | 0.00 | 0.00 | 0.00 | 0.00 | 0.00 | 0.00 | 0.00 | 0.00 |

| wt% | GR54A-14 core | GR54A-15 core | GR54A-16 core | GR54A-18 core | GR54A-19 core | GR54A-20 core | GR54A-21 core | GR54A-22 rim | GR54C-5 core | GR54C-6 core | GR54C-7 core | GR54C-13 core | GR54C-14 core | GR54C-15 core | GR54C-17 core | GR54C-18 core | GR54C-19 core | GR54C-22 core |
|---|---|---|---|---|---|---|---|---|---|---|---|---|---|---|---|---|---|---|
| $TiO_2$ | 0.37 | 0.36 | 0.32 | 0.34 | 0.38 | 0.15 | 0.32 | 0.57 | 0.22 | 0.32 | 0.30 | 0.24 | 0.26 | 0.27 | 0.26 | 0.31 | 0.33 | 0.26 |

| | | | | | | | | | | | | | | | | | | |
|---|---|---|---|---|---|---|---|---|---|---|---|---|---|---|---|---|---|---|
| $Al_2O_3$ | 11.53 | 11.52 | 9.29 | 11.57 | 12.44 | 6.21 | 7.07 | 2.79 | 11.61 | 11.59 | 11.26 | 12.20 | 12.29 | 12.09 | 11.85 | 11.82 | 11.23 | 11.18 |
| $Cr_2O_3$ | 54.40 | 53.70 | 55.14 | 53.82 | 53.69 | 59.76 | 57.56 | 57.16 | 55.72 | 56.13 | 55.99 | 55.98 | 56.32 | 55.34 | 55.42 | 55.16 | 54.82 | 55.88 |
| $V_2O_3$ | 0.14 | 0.13 | 0.17 | 0.19 | 0.16 | 0.13 | 0.15 | 0.15 | 0.09 | 0.17 | 0.14 | 0.15 | 0.11 | 0.11 | 0.11 | 0.12 | 0.14 | 0.11 |
| $Fe_2O_3$ | 2.89 | 3.15 | 3.77 | 2.37 | 2.40 | 3.06 | 4.57 | 7.58 | 2.14 | 1.91 | 2.39 | 1.67 | 1.88 | 2.50 | 2.50 | 2.78 | 3.94 | 2.48 |
| FeO | 20.84 | 20.72 | 22.91 | 21.91 | 21.22 | 23.12 | 23.58 | 24.87 | 21.75 | 22.21 | 22.40 | 21.87 | 21.73 | 22.32 | 22.21 | 22.37 | 22.46 | 22.43 |
| MnO | 0.12 | 0.07 | 0.17 | 0.03 | 0.15 | 0.31 | 0.20 | 0.14 | 0.16 | 0.13 | 0.11 | 0.05 | 0.25 | 0.09 | 0.19 | 0.28 | 0.28 | 0.15 |
| MgO | 8.40 | 8.29 | 6.71 | 7.48 | 8.18 | 6.10 | 6.22 | 4.85 | 7.82 | 7.74 | 7.59 | 8.04 | 8.16 | 7.75 | 7.69 | 7.60 | 7.54 | 7.43 |
| NiO | 0.05 | 0.04 | 0.00 | 0.07 | 0.00 | 0.06 | 0.07 | 0.04 | 0.06 | 0.07 | 0.03 | 0.00 | 0.05 | 0.06 | 0.04 | 0.07 | 0.05 | 0.05 |
| ZnO | 0.01 | 0.03 | 0.06 | 0.02 | 0.08 | 0.00 | 0.00 | 0.00 | 0.02 | 0.01 | 0.01 | 0.07 | 0.06 | 0.07 | 0.06 | 0.00 | 0.02 | 0.08 |
| Total | 98.82 | 98.01 | 98.59 | 97.80 | 98.69 | 98.92 | 99.77 | 98.24 | 99.57 | 100.28 | 100.22 | 100.24 | 101.11 | 100.59 | 100.32 | 100.51 | 100.80 | 100.05 |
| Ti | 0.01 | 0.01 | 0.01 | 0.01 | 0.01 | 0.00 | 0.01 | 0.02 | 0.01 | 0.01 | 0.01 | 0.01 | 0.01 | 0.01 | 0.01 | 0.01 | 0.01 | 0.01 |
| Al | 0.46 | 0.46 | 0.38 | 0.47 | 0.49 | 0.26 | 0.29 | 0.12 | 0.46 | 0.45 | 0.44 | 0.48 | 0.48 | 0.47 | 0.46 | 0.46 | 0.44 | 0.44 |
| Cr | 1.44 | 1.44 | 1.50 | 1.45 | 1.42 | 1.65 | 1.57 | 1.63 | 1.47 | 1.48 | 1.48 | 1.47 | 1.46 | 1.45 | 1.46 | 1.45 | 1.44 | 1.48 |
| V | 0.00 | 0.00 | 0.00 | 0.01 | 0.00 | 0.00 | 0.00 | 0.00 | 0.00 | 0.00 | 0.00 | 0.00 | 0.00 | 0.00 | 0.00 | 0.00 | 0.00 | 0.00 |
| $Fe^{3+}$ | 0.07 | 0.08 | 0.10 | 0.06 | 0.06 | 0.08 | 0.12 | 0.21 | 0.05 | 0.05 | 0.06 | 0.04 | 0.05 | 0.06 | 0.06 | 0.07 | 0.10 | 0.06 |
| $Fe^{2+}$ | 0.59 | 0.59 | 0.66 | 0.62 | 0.60 | 0.68 | 0.68 | 0.75 | 0.61 | 0.62 | 0.63 | 0.61 | 0.60 | 0.62 | 0.62 | 0.62 | 0.62 | 0.63 |
| Mn | 0.00 | 0.00 | 0.00 | 0.00 | 0.00 | 0.01 | 0.01 | 0.00 | 0.00 | 0.00 | 0.00 | 0.00 | 0.01 | 0.00 | 0.01 | 0.01 | 0.01 | 0.00 |
| Mg | 0.42 | 0.42 | 0.34 | 0.38 | 0.41 | 0.32 | 0.32 | 0.26 | 0.39 | 0.38 | 0.38 | 0.40 | 0.40 | 0.38 | 0.38 | 0.38 | 0.37 | 0.37 |
| Ni | 0.00 | 0.00 | 0.00 | 0.00 | 0.00 | 0.00 | 0.00 | 0.00 | 0.00 | 0.00 | 0.00 | 0.00 | 0.00 | 0.00 | 0.00 | 0.00 | 0.00 | 0.00 |
| Zn | 0.00 | 0.00 | 0.00 | 0.00 | 0.00 | 0.00 | 0.00 | 0.00 | 0.00 | 0.00 | 0.00 | 0.00 | 0.00 | 0.00 | 0.00 | 0.00 | 0.00 | 0.00 |

| wt% | GR54C-25 core | GR54C-26 core | GR54C-28 core | GR54C-29 core | GR54C-30 core | GR54C-35 core | GR54C-36 core | GR54C-37 core | GR54C-8 rim | GR54C-9 rim | GR54C-10 rim | GR54C-11 rim | GR54C-20 rim | GR54C-23 rim | GR54C-24 rim | GR54D-1 core | GR54D-2 core | GR54D-3 core |
|---|---|---|---|---|---|---|---|---|---|---|---|---|---|---|---|---|---|---|
| $TiO_2$ | 0.24 | 0.24 | 0.25 | 0.30 | 0.42 | 0.35 | 0.36 | 0.45 | 0.35 | 0.34 | 0.23 | 0.35 | 0.33 | 0.29 | 0.31 | 0.30 | 0.28 | 0.29 |
| $Al_2O_3$ | 10.96 | 6.41 | 11.16 | 11.13 | 10.35 | 11.14 | 10.95 | 8.50 | 1.72 | 1.55 | 3.10 | 2.59 | 6.00 | 1.73 | 3.75 | 11.08 | 10.99 | 11.02 |
| $Cr_2O_3$ | 56.12 | 62.88 | 55.72 | 55.39 | 55.26 | 56.11 | 55.93 | 57.12 | 64.97 | 65.20 | 65.29 | 64.76 | 59.54 | 64.30 | 62.55 | 56.24 | 56.80 | 56.05 |
| $V_2O_3$ | 0.11 | 0.20 | 0.14 | 0.11 | 0.10 | 0.10 | 0.14 | 0.17 | 0.18 | 0.18 | 0.11 | 0.13 | 0.15 | 0.15 | 0.14 | 0.08 | 0.11 | 0.10 |
| $Fe_2O_3$ | 2.86 | 1.06 | 3.03 | 3.14 | 4.04 | 2.69 | 3.18 | 4.55 | 3.80 | 4.17 | 2.88 | 3.80 | 4.55 | 4.88 | 3.69 | 1.24 | 1.14 | 1.52 |
| FeO | 22.36 | 23.61 | 22.52 | 22.50 | 23.25 | 22.95 | 22.67 | 23.47 | 24.91 | 24.85 | 24.45 | 24.85 | 23.78 | 25.15 | 24.44 | 20.38 | 20.13 | 20.57 |
| MnO | 0.21 | 0.12 | 0.23 | 0.18 | 0.15 | 0.02 | 0.24 | 0.15 | 0.22 | 0.15 | 0.24 | 0.16 | 0.26 | 0.11 | 0.08 | 0.22 | 0.22 | 0.10 |
| MgO | 7.49 | 6.40 | 7.44 | 7.45 | 7.00 | 7.44 | 7.47 | 6.88 | 5.12 | 5.26 | 5.64 | 5.50 | 6.13 | 5.12 | 5.56 | 8.35 | 8.57 | 8.31 |
| NiO | 0.00 | 0.09 | 0.00 | 0.00 | 0.12 | 0.02 | 0.04 | 0.04 | 0.03 | 0.09 | 0.07 | 0.01 | 0.08 | 0.00 | 0.03 | 0.05 | 0.03 | 0.09 |
| ZnO | 0.11 | 0.03 | 0.08 | 0.08 | 0.03 | 0.02 | 0.04 | 0.00 | 0.05 | 0.00 | 0.00 | 0.00 | 0.04 | 0.02 | 0.04 | 0.05 | 0.01 | 0.03 |
| Total | 100.45 | 101.03 | 100.56 | 100.28 | 100.73 | 100.84 | 101.03 | 101.33 | 101.36 | 101.78 | 101.99 | 102.15 | 100.87 | 101.76 | 100.59 | 98.00 | 98.27 | 98.10 |
| Ti | 0.01 | 0.01 | 0.01 | 0.01 | 0.01 | 0.01 | 0.01 | 0.01 | 0.01 | 0.01 | 0.01 | 0.01 | 0.01 | 0.01 | 0.01 | 0.01 | 0.01 | 0.01 |
| Al | 0.43 | 0.26 | 0.44 | 0.44 | 0.41 | 0.44 | 0.43 | 0.34 | 0.07 | 0.06 | 0.13 | 0.11 | 0.24 | 0.07 | 0.15 | 0.44 | 0.44 | 0.44 |
| Cr | 1.48 | 1.70 | 1.47 | 1.46 | 1.47 | 1.48 | 1.47 | 1.52 | 1.80 | 1.80 | 1.78 | 1.77 | 1.62 | 1.78 | 1.73 | 1.51 | 1.52 | 1.50 |
| V | 0.00 | 0.01 | 0.00 | 0.00 | 0.00 | 0.00 | 0.00 | 0.00 | 0.01 | 0.00 | 0.00 | 0.00 | 0.00 | 0.00 | 0.00 | 0.00 | 0.00 | 0.00 |
| $Fe^{3+}$ | 0.07 | 0.03 | 0.08 | 0.08 | 0.10 | 0.07 | 0.08 | 0.12 | 0.10 | 0.11 | 0.07 | 0.10 | 0.12 | 0.13 | 0.10 | 0.03 | 0.03 | 0.04 |
| $Fe^{2+}$ | 0.62 | 0.67 | 0.63 | 0.63 | 0.65 | 0.64 | 0.63 | 0.66 | 0.73 | 0.73 | 0.71 | 0.72 | 0.68 | 0.74 | 0.71 | 0.58 | 0.57 | 0.58 |
| Mn | 0.01 | 0.00 | 0.01 | 0.01 | 0.00 | 0.00 | 0.01 | 0.00 | 0.01 | 0.00 | 0.01 | 0.00 | 0.01 | 0.00 | 0.00 | 0.01 | 0.01 | 0.00 |
| Mg | 0.37 | 0.33 | 0.37 | 0.37 | 0.35 | 0.37 | 0.37 | 0.35 | 0.27 | 0.27 | 0.29 | 0.28 | 0.31 | 0.27 | 0.29 | 0.42 | 0.43 | 0.42 |
| Ni | 0.00 | 0.00 | 0.00 | 0.00 | 0.00 | 0.00 | 0.00 | 0.00 | 0.00 | 0.00 | 0.00 | 0.00 | 0.00 | 0.00 | 0.00 | 0.00 | 0.00 | 0.00 |
| Zn | 0.00 | 0.00 | 0.00 | 0.00 | 0.00 | 0.00 | 0.00 | 0.00 | 0.00 | 0.00 | 0.00 | 0.00 | 0.00 | 0.00 | 0.00 | 0.00 | 0.00 | 0.00 |

| wt% | GR54D-4 core | GR54D-5 core | GR54D-6 core | GR54D-7 core | GR54D-9 core | GR54D-11 core | GR54D-12 core | GR54D-13 core | GR54D-14 core | GR54D-15 core | GR54D-16 core | GR54D-17 core | GR54D-18 core | GR54D-21 core | GR54D-22 core | GR54D-25 core | GR54D-27 core | GR54D-20 rim |
|---|---|---|---|---|---|---|---|---|---|---|---|---|---|---|---|---|---|---|
| $TiO_2$ | 0.16 | 0.24 | 0.27 | 0.32 | 0.28 | 0.31 | 0.26 | 0.25 | 0.26 | 0.23 | 0.20 | 0.25 | 0.21 | 0.27 | 0.19 | 0.24 | 0.23 | 0.29 |
| $Al_2O_3$ | 7.12 | 10.65 | 10.79 | 11.00 | 8.46 | 6.21 | 11.64 | 10.65 | 10.68 | 10.58 | 10.53 | 10.67 | 7.25 | 7.05 | 7.74 | 9.10 | 10.33 | 3.18 |
| $Cr_2O_3$ | 59.44 | 57.24 | 56.06 | 56.14 | 58.96 | 59.50 | 55.00 | 56.29 | 56.92 | 56.35 | 56.36 | 56.90 | 61.34 | 59.28 | 59.65 | 58.86 | 56.79 | 61.42 |
| $V_2O_3$ | 0.10 | 0.09 | 0.11 | 0.14 | 0.11 | 0.11 | 0.14 | 0.12 | 0.13 | 0.12 | 0.12 | 0.11 | 0.06 | 0.09 | 0.10 | 0.13 | 0.15 | 0.13 |
| $Fe_2O_3$ | 2.80 | 1.45 | 1.87 | 1.45 | 2.26 | 3.97 | 0.00 | 1.99 | 2.01 | 2.14 | 1.93 | 1.92 | 1.65 | 3.05 | 2.05 | 1.97 | 1.82 | 4.51 |

| | | | | | | | | | | | | | | | | | | |
|---|---|---|---|---|---|---|---|---|---|---|---|---|---|---|---|---|---|---|
| FeO | 23.56 | 20.16 | 20.03 | 20.62 | 21.82 | 22.51 | 20.34 | 19.74 | 20.10 | 19.69 | 19.45 | 19.79 | 21.45 | 21.73 | 21.41 | 20.78 | 19.67 | 23.07 |
| MnO | 0.30 | 0.18 | 0.07 | 0.25 | 0.17 | 0.08 | 0.12 | 0.18 | 0.07 | 0.09 | 0.08 | 0.09 | 0.15 | 0.11 | 0.18 | 0.15 | 0.09 | 0.17 |
| MgO | 6.11 | 8.56 | 8.57 | 8.33 | 7.46 | 6.81 | 7.85 | 8.72 | 8.80 | 8.84 | 8.83 | 8.85 | 7.67 | 7.30 | 7.50 | 8.18 | 8.76 | 6.10 |
| NiO | 0.00 | 0.06 | 0.08 | 0.00 | 0.12 | 0.14 | 0.00 | 0.03 | 0.00 | 0.00 | 0.06 | 0.01 | 0.02 | 0.03 | 0.00 | 0.10 | 0.05 | 0.00 |
| ZnO | 0.04 | 0.04 | 0.03 | 0.00 | 0.07 | 0.03 | 0.00 | 0.00 | 0.00 | 0.00 | 0.04 | 0.12 | 0.00 | 0.00 | 0.05 | 0.01 | 0.04 | 0.00 |
| Total | 99.67 | 98.66 | 97.88 | 98.32 | 99.73 | 99.67 | 95.36 | 97.97 | 98.96 | 98.03 | 97.59 | 98.71 | 99.81 | 98.91 | 98.89 | 99.52 | 97.95 | 98.96 |
| Ti | 0.00 | 0.01 | 0.01 | 0.01 | 0.01 | 0.01 | 0.01 | 0.01 | 0.01 | 0.01 | 0.01 | 0.01 | 0.01 | 0.01 | 0.00 | 0.01 | 0.01 | 0.01 |
| Al | 0.29 | 0.42 | 0.43 | 0.44 | 0.34 | 0.25 | 0.48 | 0.43 | 0.42 | 0.42 | 0.42 | 0.42 | 0.29 | 0.29 | 0.31 | 0.36 | 0.41 | 0.13 |
| Cr | 1.62 | 1.53 | 1.50 | 1.50 | 1.58 | 1.63 | 1.51 | 1.51 | 1.51 | 1.51 | 1.51 | 1.51 | 1.65 | 1.62 | 1.62 | 1.57 | 1.52 | 1.72 |
| V | 0.00 | 0.00 | 0.00 | 0.00 | 0.00 | 0.00 | 0.00 | 0.00 | 0.00 | 0.00 | 0.00 | 0.00 | 0.00 | 0.00 | 0.00 | 0.00 | 0.00 | 0.00 |
| $Fe^{3+}$ | 0.07 | 0.04 | 0.05 | 0.04 | 0.06 | 0.10 | 0.00 | 0.05 | 0.05 | 0.05 | 0.05 | 0.05 | 0.04 | 0.08 | 0.05 | 0.05 | 0.05 | 0.12 |
| $Fe^{2+}$ | 0.68 | 0.57 | 0.57 | 0.58 | 0.62 | 0.65 | 0.59 | 0.56 | 0.56 | 0.56 | 0.55 | 0.56 | 0.61 | 0.63 | 0.61 | 0.59 | 0.56 | 0.68 |
| Mn | 0.01 | 0.01 | 0.00 | 0.01 | 0.00 | 0.00 | 0.00 | 0.01 | 0.00 | 0.00 | 0.00 | 0.00 | 0.00 | 0.00 | 0.01 | 0.00 | 0.00 | 0.01 |
| Mg | 0.31 | 0.43 | 0.43 | 0.42 | 0.38 | 0.35 | 0.41 | 0.44 | 0.44 | 0.45 | 0.45 | 0.44 | 0.39 | 0.38 | 0.38 | 0.41 | 0.44 | 0.32 |
| Ni | 0.00 | 0.00 | 0.00 | 0.00 | 0.00 | 0.00 | 0.00 | 0.00 | 0.00 | 0.00 | 0.00 | 0.00 | 0.00 | 0.00 | 0.00 | 0.00 | 0.00 | 0.00 |
| Zn | 0.00 | 0.00 | 0.00 | 0.00 | 0.00 | 0.00 | 0.00 | 0.00 | 0.00 | 0.00 | 0.00 | 0.00 | 0.00 | 0.00 | 0.00 | 0.00 | 0.00 | 0.00 |

| wt% | GR54D-23 rim | GR54D-24 rim | GR54D-26 rim | GR55-1 core | GR55-2 core | GR55-3 core | GR55-5 core | GR55-6 core | GR55-8 core | GR55-9 core | GR55-10 core | GR55-11 core | GR55-13 core | GR55-15 core | GR55-17 core | GR55-18 core | GR55-19 core | GR55-20 core |
|---|---|---|---|---|---|---|---|---|---|---|---|---|---|---|---|---|---|---|
| $TiO_2$ | 0.25 | 0.17 | 0.24 | 0.18 | 0.17 | 0.15 | 0.24 | 0.22 | 0.15 | 0.15 | 0.22 | 0.22 | 0.20 | 0.18 | 0.14 | 0.14 | 0.19 | 0.14 |
| $Al_2O_3$ | 4.21 | 5.63 | 4.58 | 9.50 | 9.43 | 9.83 | 11.15 | 11.20 | 10.63 | 11.11 | 10.98 | 10.62 | 10.67 | 10.79 | 10.68 | 11.36 | 10.98 | 11.15 |
| $Cr_2O_3$ | 61.12 | 61.95 | 63.70 | 65.54 | 57.92 | 61.45 | 61.04 | 61.12 | 60.88 | 60.18 | 61.67 | 61.02 | 60.68 | 60.87 | 60.41 | 60.62 | 61.16 | 59.88 |
| $V_2O_3$ | 0.12 | 0.08 | 0.13 | 0.17 | 0.16 | 0.18 | 0.19 | 0.18 | 0.18 | 0.16 | 0.20 | 0.24 | 0.18 | 0.22 | 0.13 | 0.17 | 0.15 | 0.22 |
| $Fe_2O_3$ | 3.69 | 3.16 | 2.29 | 0.00 | 0.00 | 0.00 | 0.00 | 0.00 | 0.00 | 0.00 | 0.00 | 0.00 | 0.00 | 0.00 | 0.00 | 0.00 | 0.00 | 0.00 |
| FeO | 22.73 | 22.06 | 23.70 | 14.03 | 18.42 | 16.24 | 17.31 | 16.98 | 18.18 | 17.44 | 16.43 | 16.61 | 16.75 | 16.57 | 18.35 | 17.29 | 17.86 | 17.93 |
| MnO | 0.21 | 0.40 | 0.28 | 0.05 | 0.18 | 0.04 | 0.13 | 0.25 | 0.16 | 0.10 | 0.11 | 0.05 | 0.12 | 0.07 | 0.01 | 0.13 | 0.11 | 0.07 |
| MgO | 6.27 | 7.04 | 6.11 | 9.60 | 9.74 | 9.33 | 9.51 | 9.68 | 9.07 | 9.38 | 9.24 | 9.33 | 9.85 | 9.19 | 8.99 | 9.42 | 9.61 | 9.51 |
| NiO | 0.01 | 0.00 | 0.01 | 0.05 | 0.09 | 0.08 | 0.07 | 0.04 | 0.06 | 0.03 | 0.10 | 0.04 | 0.10 | 0.09 | 0.01 | 0.00 | 0.05 | 0.10 |
| ZnO | 0.01 | 0.00 | 0.05 | 0.01 | 0.03 | 0.10 | 0.05 | 0.12 | 0.00 | 0.06 | 0.00 | 0.03 | 0.03 | 0.03 | 0.02 | 0.05 | 0.00 | 0.00 |
| Total | 98.66 | 100.50 | 101.13 | 99.16 | 96.86 | 97.56 | 99.74 | 99.81 | 99.30 | 98.60 | 98.95 | 98.15 | 98.77 | 98.01 | 98.74 | 99.19 | 100.15 | 99.01 |
| Ti | 0.01 | 0.00 | 0.01 | 0.00 | 0.00 | 0.00 | 0.01 | 0.01 | 0.00 | 0.00 | 0.01 | 0.01 | 0.00 | 0.00 | 0.00 | 0.00 | 0.00 | 0.00 |
| Al | 0.18 | 0.23 | 0.19 | 0.38 | 0.38 | 0.39 | 0.43 | 0.44 | 0.42 | 0.44 | 0.43 | 0.42 | 0.42 | 0.43 | 0.42 | 0.45 | 0.43 | 0.44 |
| Cr | 1.71 | 1.68 | 1.74 | 1.74 | 1.56 | 1.65 | 1.60 | 1.60 | 1.61 | 1.59 | 1.63 | 1.63 | 1.60 | 1.62 | 1.60 | 1.59 | 1.59 | 1.58 |
| V | 0.00 | 0.00 | 0.00 | 0.00 | 0.00 | 0.00 | 0.01 | 0.00 | 0.00 | 0.00 | 0.01 | 0.01 | 0.00 | 0.01 | 0.00 | 0.00 | 0.00 | 0.01 |
| $Fe^{3+}$ | 0.10 | 0.08 | 0.06 | 0.00 | 0.00 | 0.00 | 0.00 | 0.00 | 0.00 | 0.00 | 0.00 | 0.00 | 0.00 | 0.00 | 0.00 | 0.00 | 0.00 | 0.00 |
| $Fe^{2+}$ | 0.67 | 0.63 | 0.68 | 0.39 | 0.52 | 0.46 | 0.48 | 0.47 | 0.51 | 0.49 | 0.46 | 0.47 | 0.47 | 0.47 | 0.52 | 0.48 | 0.49 | 0.50 |
| Mn | 0.01 | 0.01 | 0.01 | 0.00 | 0.01 | 0.00 | 0.00 | 0.01 | 0.00 | 0.00 | 0.00 | 0.00 | 0.00 | 0.00 | 0.00 | 0.00 | 0.00 | 0.00 |
| Mg | 0.33 | 0.36 | 0.31 | 0.48 | 0.49 | 0.47 | 0.47 | 0.48 | 0.45 | 0.47 | 0.46 | 0.47 | 0.49 | 0.46 | 0.45 | 0.47 | 0.47 | 0.47 |
| Ni | 0.00 | 0.00 | 0.00 | 0.00 | 0.00 | 0.00 | 0.00 | 0.00 | 0.00 | 0.00 | 0.00 | 0.00 | 0.00 | 0.00 | 0.00 | 0.00 | 0.00 | 0.00 |
| Zn | 0.00 | 0.00 | 0.00 | 0.00 | 0.00 | 0.00 | 0.00 | 0.00 | 0.00 | 0.00 | 0.00 | 0.00 | 0.00 | 0.00 | 0.00 | 0.00 | 0.00 | 0.00 |

| wt% | GR55-21 core | GR55-22 core | GR55-23 core | GR55-24 core | GR55-25 core | GR55-26 core | GR55-27 core | GR55-28 core | GR55-29 core | GR55-30 core | GR55-7 rim | GR55-12 rim | GR55-16 rim |
|---|---|---|---|---|---|---|---|---|---|---|---|---|---|
| $TiO_2$ | 0.20 | 0.17 | 0.18 | 0.14 | 0.12 | 0.10 | 0.14 | 0.17 | 0.18 | 0.12 | 0.10 | 0.08 | 0.14 |
| $Al_2O_3$ | 10.81 | 11.17 | 11.27 | 11.10 | 11.66 | 11.01 | 11.60 | 11.33 | 11.27 | 11.52 | 5.29 | 5.26 | 5.39 |
| $Cr_2O_3$ | 60.40 | 60.97 | 60.05 | 59.43 | 59.32 | 59.68 | 60.06 | 59.14 | 60.55 | 60.54 | 69.01 | 66.69 | 67.10 |
| $V_2O_3$ | 0.21 | 0.26 | 0.16 | 0.17 | 0.17 | 0.23 | 0.17 | 0.18 | 0.16 | 0.18 | 0.16 | 0.14 | 0.15 |
| $Fe_2O_3$ | 0.00 | 0.00 | 0.00 | 0.00 | 0.00 | 0.00 | 0.00 | 0.00 | 0.00 | 0.00 | 0.00 | 0.00 | 0.00 |
| FeO | 17.14 | 16.03 | 17.45 | 17.25 | 16.14 | 16.10 | 16.26 | 17.58 | 17.86 | 17.96 | 16.19 | 18.30 | 16.68 |
| MnO | 0.04 | 0.01 | 0.16 | 0.12 | 0.23 | 0.13 | 0.09 | 0.13 | 0.14 | 0.19 | 0.27 | 0.28 | 0.13 |
| MgO | 9.71 | 9.65 | 8.96 | 9.07 | 9.27 | 9.17 | 8.86 | 8.57 | 9.00 | 8.94 | 9.20 | 8.40 | 8.92 |
| NiO | 0.13 | 0.13 | 0.06 | 0.02 | 0.00 | 0.11 | 0.03 | 0.03 | 0.07 | 0.08 | 0.04 | 0.02 | 0.00 |

| | | | | | | | | | | | | | |
|---|---|---|---|---|---|---|---|---|---|---|---|---|---|
| ZnO | 0.00 | 0.00 | 0.00 | 0.05 | 0.03 | 0.05 | 0.04 | 0.00 | 0.00 | 0.05 | 0.00 | 0.02 | 0.03 |
| Total | 98.65 | 98.39 | 98.33 | 97.37 | 96.94 | 96.71 | 97.25 | 97.11 | 99.23 | 99.63 | 100.27 | 99.18 | 98.61 |
| Ti | 0.01 | 0.00 | 0.00 | 0.00 | 0.00 | 0.00 | 0.00 | 0.00 | 0.00 | 0.00 | 0.00 | 0.00 | 0.00 |
| Al | 0.43 | 0.44 | 0.45 | 0.44 | 0.47 | 0.44 | 0.46 | 0.46 | 0.44 | 0.45 | 0.21 | 0.21 | 0.22 |
| Cr | 1.60 | 1.61 | 1.60 | 1.59 | 1.59 | 1.61 | 1.61 | 1.59 | 1.60 | 1.59 | 1.85 | 1.81 | 1.83 |
| V | 0.01 | 0.01 | 0.00 | 0.00 | 0.00 | 0.01 | 0.00 | 0.00 | 0.00 | 0.00 | 0.00 | 0.00 | 0.00 |
| $Fe^{3+}$ | 0.00 | 0.00 | 0.00 | 0.00 | 0.00 | 0.00 | 0.00 | 0.00 | 0.00 | 0.00 | 0.00 | 0.00 | 0.00 |
| $Fe^{2+}$ | 0.48 | 0.45 | 0.49 | 0.49 | 0.46 | 0.46 | 0.46 | 0.50 | 0.50 | 0.50 | 0.46 | 0.53 | 0.48 |
| Mn | 0.00 | 0.00 | 0.00 | 0.00 | 0.01 | 0.00 | 0.00 | 0.00 | 0.00 | 0.01 | 0.01 | 0.01 | 0.00 |
| Mg | 0.48 | 0.48 | 0.45 | 0.46 | 0.47 | 0.47 | 0.45 | 0.44 | 0.45 | 0.44 | 0.46 | 0.43 | 0.46 |
| Ni | 0.00 | 0.00 | 0.00 | 0.00 | 0.00 | 0.00 | 0.00 | 0.00 | 0.00 | 0.00 | 0.00 | 0.00 | 0.00 |
| Zn | 0.00 | 0.00 | 0.00 | 0.00 | 0.00 | 0.00 | 0.00 | 0.00 | 0.00 | 0.00 | 0.00 | 0.00 | 0.00 |

Tab. A4.3 Spinels microprobe analyses (core and rim) of Tripes and Limonadika (Gomati) massive chromitites.

| wt% | TRI10-3 | TRI10-9 | TRI10-14 | TRI10-18 | TRI10-1 | TRI10-2 | TRI10-7 | TRI10-8 | TRI10-12 | TRI10-13 | TRI10-16 | TRI10-17 | LIM3-8 | LIM3-13 | LIM3-14 | LIM3-15 | LIM3-7 | LIM3-12 |
|---|---|---|---|---|---|---|---|---|---|---|---|---|---|---|---|---|---|---|
| | core | core | core | core | rim | rim | rim | rim | rim | rim | rim | rim | core | core | core | core | rim | rim |
| $TiO_2$ | 0.25 | 0.31 | 0.31 | 0.26 | 0.60 | 0.01 | 0.90 | 0.17 | 0.09 | 0.26 | 0.17 | 0.22 | 0.16 | 0.16 | 0.07 | 0.11 | 0.08 | 0.14 |
| MnO | 0.69 | 0.55 | 0.22 | 0.25 | 1.08 | 0.76 | 0.95 | 0.56 | 0.39 | 0.27 | 0.28 | 0.29 | 0.33 | 0.38 | 0.37 | 0.36 | 0.30 | 0.40 |
| MgO | 8.37 | 8.63 | 11.88 | 11.92 | 2.91 | 7.33 | 3.90 | 7.98 | 9.48 | 11.07 | 11.01 | 9.99 | 7.59 | 10.49 | 7.26 | 7.19 | 6.66 | 7.30 |
| $Cr_2O_3$ | 43.54 | 43.73 | 44.74 | 45.22 | 44.63 | 50.64 | 40.80 | 50.93 | 56.94 | 50.24 | 51.73 | 51.88 | 63.83 | 57.69 | 68.18 | 68.38 | 66.78 | 66.51 |
| FeO | 25.29 | 25.18 | 20.33 | 20.63 | 35.52 | 24.57 | 36.41 | 24.09 | 20.99 | 20.85 | 20.01 | 21.04 | 23.04 | 19.30 | 22.64 | 22.54 | 23.55 | 22.72 |
| $Fe_2O_3$ | 3.25 | 3.15 | 3.15 | 3.26 | 7.99 | 1.84 | 9.42 | 1.77 | 1.71 | 2.71 | 2.04 | 1.85 | 1.45 | 1.40 | 1.10 | 0.95 | 1.54 | 1.34 |
| $Al_2O_3$ | 18.99 | 19.25 | 19.50 | 19.73 | 5.24 | 15.12 | 7.01 | 15.46 | 10.95 | 16.03 | 15.89 | 15.18 | 5.15 | 11.66 | 2.04 | 2.14 | 1.54 | 2.69 |
| NiO | 0.15 | 0.07 | 0.17 | 0.21 | 0.16 | 0.01 | 0.35 | 0.02 | 0.07 | 0.13 | 0.17 | 0.27 | 0.03 | 0.07 | 0.10 | 0.07 | 0.11 | 0.10 |
| Total | 100.60 | 100.92 | 100.37 | 101.54 | 98.28 | 100.38 | 99.88 | 101.02 | 100.70 | 101.59 | 101.35 | 100.77 | 101.62 | 101.23 | 101.85 | 101.86 | 100.64 | 101.26 |
| Ti | 0.01 | 0.01 | 0.01 | 0.01 | 0.02 | 0.00 | 0.02 | 0.00 | 0.00 | 0.01 | 0.00 | 0.01 | 0.00 | 0.00 | 0.00 | 0.00 | 0.00 | 0.00 |
| Mn | 0.02 | 0.01 | 0.01 | 0.01 | 0.03 | 0.02 | 0.03 | 0.02 | 0.01 | 0.01 | 0.01 | 0.01 | 0.01 | 0.01 | 0.01 | 0.01 | 0.01 | 0.01 |
| Mg | 0.40 | 0.41 | 0.55 | 0.55 | 0.16 | 0.36 | 0.20 | 0.39 | 0.46 | 0.52 | 0.52 | 0.48 | 0.38 | 0.50 | 0.37 | 0.37 | 0.35 | 0.37 |
| Cr | 1.10 | 1.10 | 1.10 | 1.10 | 1.26 | 1.31 | 1.12 | 1.30 | 1.47 | 1.25 | 1.29 | 1.31 | 1.70 | 1.47 | 1.85 | 1.85 | 1.84 | 1.81 |
| $Fe^{2+}$ | 0.67 | 0.67 | 0.53 | 0.53 | 1.06 | 0.67 | 1.06 | 0.65 | 0.58 | 0.55 | 0.53 | 0.56 | 0.65 | 0.52 | 0.65 | 0.65 | 0.69 | 0.65 |
| $Fe^{3+}$ | 0.09 | 0.08 | 0.08 | 0.08 | 0.24 | 0.05 | 0.27 | 0.05 | 0.05 | 0.07 | 0.05 | 0.05 | 0.04 | 0.04 | 0.03 | 0.03 | 0.04 | 0.04 |
| Al | 0.71 | 0.72 | 0.72 | 0.72 | 0.22 | 0.58 | 0.29 | 0.59 | 0.42 | 0.59 | 0.59 | 0.57 | 0.21 | 0.44 | 0.08 | 0.09 | 0.06 | 0.11 |
| Ni | 0.00 | 0.00 | 0.00 | 0.01 | 0.00 | 0.00 | 0.01 | 0.00 | 0.00 | 0.00 | 0.00 | 0.01 | 0.00 | 0.00 | 0.00 | 0.00 | 0.00 | 0.00 |

Tab. A4.4 Pyroxene microprobe analyses of Gomati chromitites and pyroxenites.

| wt% | GOM2B-1 | GOM2B-2 | GOM2B-3 | GOM2B-4 | GOM2B-5 | GOM2B-6 | GOM2B-7 | GOM2B-8 | GOM2B-9 | GOM2B-10 | GOM2B-11 | GOM2B-12 | GOM2B-13 | GOM2B-14 | GOM2B-15 | GOM2B-16 | GOM2B-17 |
|---|---|---|---|---|---|---|---|---|---|---|---|---|---|---|---|---|---|
| $SiO_2$ | 55.49 | 54.59 | 54.50 | 54.62 | 55.22 | 54.01 | 51.81 | 50.42 | 53.14 | 53.19 | 53.49 | 53.56 | 54.44 | 53.35 | 54.75 | 53.95 | 53.31 |
| $TiO_2$ | 0.07 | 0.01 | 0.01 | 0.05 | 0.07 | 0.00 | 0.03 | 0.00 | 0.06 | 0.04 | 0.04 | 0.03 | 0.03 | 0.00 | 0.10 | 0.03 | 0.04 |
| $Al_2O_3$ | 0.01 | 0.13 | 0.03 | 0.04 | 0.06 | 0.08 | 0.82 | 0.73 | 0.26 | 0.06 | 0.03 | 0.06 | 0.09 | 0.13 | 0.06 | 0.01 | 0.09 |
| $Cr_2O_3$ | 0.05 | 0.05 | 0.02 | 0.04 | 0.04 | 0.06 | 0.26 | 0.29 | 0.17 | 0.09 | 0.03 | 0.04 | 0.02 | 0.02 | 0.10 | 0.04 | 0.08 |
| $Fe_2O_3$ | 0.00 | 0.88 | 0.83 | 0.78 | 0.10 | 0.75 | 1.01 | 0.95 | 0.99 | 0.80 | 0.72 | 0.77 | 0.12 | 0.64 | 0.08 | 0.68 | 0.74 |
| FeO | 0.65 | 0.00 | 0.00 | 0.00 | 0.63 | 0.00 | 0.00 | 0.00 | 0.00 | 0.00 | 0.00 | 0.00 | 0.42 | 0.00 | 0.56 | 0.00 | 0.00 |
| MnO | 0.02 | 0.04 | 0.00 | 0.01 | 0.01 | 0.00 | 0.06 | 0.00 | 0.00 | 0.00 | 0.02 | 0.01 | 0.02 | 0.03 | 0.00 | 0.04 | 0.02 |
| NiO | 0.00 | 0.00 | 0.00 | 0.00 | 0.00 | 0.00 | 0.00 | 0.00 | 0.00 | 0.00 | 0.00 | 0.00 | 0.00 | 0.00 | 0.00 | 0.00 | 0.00 |
| ZnO | 0.00 | 0.00 | 0.00 | 0.02 | 0.04 | 0.00 | 0.00 | 0.00 | 0.00 | 0.00 | 0.00 | 0.01 | 0.01 | 0.02 | 0.05 | 0.01 | 0.00 |
| MgO | 18.00 | 18.46 | 18.44 | 18.29 | 19.00 | 18.61 | 22.43 | 23.30 | 21.14 | 18.57 | 17.88 | 18.59 | 18.27 | 18.65 | 18.47 | 18.25 | 18.64 |
| CaO | 25.78 | 25.20 | 25.95 | 25.45 | 24.48 | 24.55 | 20.71 | 20.22 | 21.57 | 24.83 | 25.82 | 24.61 | 24.83 | 23.72 | 24.89 | 24.65 | 24.13 |
| $Na_2O$ | 0.00 | 0.02 | 0.05 | 0.03 | 0.03 | 0.02 | 0.03 | 0.04 | 0.02 | 0.03 | 0.01 | 0.03 | 0.06 | 0.11 | 0.03 | 0.08 | 0.07 |
| Total | 100.08 | 99.36 | 99.84 | 99.32 | 99.70 | 98.09 | 97.17 | 95.96 | 97.35 | 97.60 | 98.05 | 97.71 | 98.32 | 96.70 | 99.11 | 97.74 | 97.13 |
| Si | 2.01 | 1.98 | 1.97 | 1.99 | 2.00 | 1.99 | 1.89 | 1.86 | 1.95 | 1.96 | 1.97 | 1.98 | 2.00 | 1.99 | 1.99 | 1.99 | 1.98 |

| | | | | | | | | | | | | | | | | | |
|---|---|---|---|---|---|---|---|---|---|---|---|---|---|---|---|---|---|
| Ti | 0.00 | 0.00 | 0.00 | 0.00 | 0.00 | 0.00 | 0.00 | 0.00 | 0.00 | 0.00 | 0.00 | 0.00 | 0.00 | 0.00 | 0.00 | 0.00 | 0.00 |
| Al | 0.00 | 0.01 | 0.00 | 0.00 | 0.00 | 0.00 | 0.04 | 0.03 | 0.01 | 0.00 | 0.00 | 0.00 | 0.00 | 0.01 | 0.00 | 0.00 | 0.00 |
| Cr | 0.00 | 0.00 | 0.00 | 0.00 | 0.00 | 0.00 | 0.01 | 0.01 | 0.01 | 0.00 | 0.00 | 0.00 | 0.00 | 0.00 | 0.00 | 0.00 | 0.00 |
| $Fe^{3+}$ | 0.00 | 0.02 | 0.02 | 0.02 | 0.00 | 0.02 | 0.03 | 0.03 | 0.03 | 0.02 | 0.02 | 0.02 | 0.00 | 0.02 | 0.00 | 0.02 | 0.02 |
| $Fe^{2+}$ | 0.02 | 0.00 | 0.00 | 0.00 | 0.02 | 0.00 | 0.00 | 0.00 | 0.00 | 0.00 | 0.00 | 0.00 | 0.01 | 0.00 | 0.02 | 0.00 | 0.00 |
| Mn | 0.00 | 0.00 | 0.00 | 0.00 | 0.00 | 0.00 | 0.00 | 0.00 | 0.00 | 0.00 | 0.00 | 0.00 | 0.00 | 0.00 | 0.00 | 0.00 | 0.00 |
| Ni | 0.00 | 0.00 | 0.00 | 0.00 | 0.00 | 0.00 | 0.00 | 0.00 | 0.00 | 0.00 | 0.00 | 0.00 | 0.00 | 0.00 | 0.00 | 0.00 | 0.00 |
| Zn | 0.00 | 0.00 | 0.00 | 0.00 | 0.00 | 0.00 | 0.00 | 0.00 | 0.00 | 0.00 | 0.00 | 0.00 | 0.00 | 0.00 | 0.00 | 0.00 | 0.00 |
| Mg | 0.97 | 1.00 | 0.99 | 0.99 | 1.02 | 1.02 | 1.22 | 1.28 | 1.16 | 1.02 | 0.98 | 1.02 | 1.00 | 1.03 | 1.00 | 1.00 | 1.03 |
| Ca | 1.00 | 0.98 | 1.01 | 0.99 | 0.95 | 0.97 | 0.81 | 0.80 | 0.85 | 0.98 | 1.02 | 0.97 | 0.98 | 0.95 | 0.97 | 0.98 | 0.96 |
| Na | 0.00 | 0.00 | 0.00 | 0.00 | 0.00 | 0.00 | 0.00 | 0.00 | 0.00 | 0.00 | 0.00 | 0.00 | 0.00 | 0.01 | 0.00 | 0.01 | 0.00 |

| wt% | GOM2B-18 | GOM2B-19 | GOM2B-20 | GOM2B-21 | GOM2B-22 | GOM2B-23 | GOM2B-24 | GOM2B-25 | GOM2B-26 | GOM2B-27 | GOM2B-28 | GOM2B-29 | GOM2B-30 | GOM2B-31 | GOM2B-32 | GOM2B-33 |
|---|---|---|---|---|---|---|---|---|---|---|---|---|---|---|---|---|
| $SiO_2$ | 54.00 | 53.79 | 52.77 | 52.82 | 53.23 | 53.86 | 53.95 | 53.89 | 52.93 | 53.89 | 51.81 | 53.11 | 54.28 | 54.49 | 54.45 | 53.85 |
| $TiO_2$ | 0.02 | 0.00 | 0.03 | 0.03 | 0.02 | 0.01 | 0.05 | 0.06 | 0.08 | 0.04 | 0.03 | 0.00 | 0.03 | 0.06 | 0.04 | 0.02 |
| $Al_2O_3$ | 0.09 | 0.01 | 0.02 | 0.11 | 0.12 | 0.04 | 0.18 | 0.06 | 0.05 | 0.06 | 0.08 | 0.23 | 0.04 | 0.14 | 0.02 | 0.04 |
| $Cr_2O_3$ | 0.13 | 0.32 | 0.22 | 0.49 | 0.16 | 0.05 | 0.04 | 0.06 | 0.14 | 0.05 | 0.11 | 0.25 | 0.03 | 0.09 | 0.03 | 0.06 |
| $Fe_2O_3$ | 0.34 | 0.78 | 0.73 | 0.80 | 0.75 | 0.81 | 0.62 | 0.69 | 0.70 | 0.69 | 0.61 | 0.71 | 0.00 | 0.00 | 0.34 | 0.20 |
| FeO | 0.22 | 0.00 | 0.00 | 0.00 | 0.00 | 0.00 | 0.10 | 0.00 | 0.00 | 0.00 | 0.00 | 0.00 | 0.62 | 0.69 | 0.41 | 0.51 |
| MnO | 0.00 | 0.02 | 0.00 | 0.02 | 0.00 | 0.01 | 0.00 | 0.00 | 0.03 | 0.04 | 0.01 | 0.00 | 0.02 | 0.01 | 0.01 | 0.01 |
| NiO | 0.00 | 0.00 | 0.00 | 0.00 | 0.00 | 0.00 | 0.00 | 0.00 | 0.00 | 0.00 | 0.00 | 0.00 | 0.00 | 0.00 | 0.00 | 0.00 |
| ZnO | 0.00 | 0.00 | 0.00 | 0.00 | 0.00 | 0.00 | 0.00 | 0.03 | 0.00 | 0.03 | 0.00 | 0.00 | 0.00 | 0.01 | 0.00 | 0.00 |
| MgO | 18.74 | 18.14 | 17.97 | 18.77 | 18.27 | 18.06 | 18.21 | 18.33 | 18.44 | 18.06 | 18.70 | 18.60 | 18.26 | 18.43 | 17.70 | 17.50 |
| CaO | 24.04 | 25.23 | 25.25 | 24.63 | 24.89 | 25.42 | 24.57 | 24.82 | 24.47 | 25.00 | 23.84 | 24.08 | 24.61 | 24.33 | 25.72 | 25.38 |
| $Na_2O$ | 0.04 | 0.00 | 0.00 | 0.04 | 0.06 | 0.02 | 0.11 | 0.06 | 0.06 | 0.06 | 0.08 | 0.12 | 0.01 | 0.06 | 0.05 | 0.04 |
| Total | 97.62 | 98.29 | 97.00 | 97.71 | 97.52 | 98.27 | 97.83 | 98.01 | 96.89 | 97.93 | 95.28 | 97.09 | 97.90 | 98.32 | 98.77 | 97.61 |
| Si | 1.99 | 1.98 | 1.97 | 1.95 | 1.97 | 1.98 | 1.99 | 1.98 | 1.97 | 1.99 | 1.95 | 1.97 | 2.00 | 2.00 | 2.00 | 2.00 |
| Ti | 0.00 | 0.00 | 0.00 | 0.00 | 0.00 | 0.00 | 0.00 | 0.00 | 0.00 | 0.00 | 0.00 | 0.00 | 0.00 | 0.00 | 0.00 | 0.00 |
| Al | 0.00 | 0.00 | 0.00 | 0.00 | 0.01 | 0.00 | 0.01 | 0.00 | 0.00 | 0.00 | 0.00 | 0.01 | 0.00 | 0.01 | 0.00 | 0.00 |
| Cr | 0.00 | 0.01 | 0.01 | 0.01 | 0.00 | 0.00 | 0.00 | 0.00 | 0.00 | 0.00 | 0.00 | 0.01 | 0.00 | 0.00 | 0.00 | 0.00 |
| $Fe^{3+}$ | 0.01 | 0.02 | 0.02 | 0.02 | 0.02 | 0.02 | 0.02 | 0.02 | 0.02 | 0.02 | 0.02 | 0.02 | 0.00 | 0.00 | 0.01 | 0.01 |
| $Fe^{2+}$ | 0.01 | 0.00 | 0.00 | 0.00 | 0.00 | 0.00 | 0.00 | 0.00 | 0.00 | 0.00 | 0.00 | 0.00 | 0.02 | 0.02 | 0.01 | 0.02 |
| Mn | 0.00 | 0.00 | 0.00 | 0.00 | 0.00 | 0.00 | 0.00 | 0.00 | 0.00 | 0.00 | 0.00 | 0.00 | 0.00 | 0.00 | 0.00 | 0.00 |
| Ni | 0.00 | 0.00 | 0.00 | 0.00 | 0.00 | 0.00 | 0.00 | 0.00 | 0.00 | 0.00 | 0.00 | 0.00 | 0.00 | 0.00 | 0.00 | 0.00 |
| Zn | 0.00 | 0.00 | 0.00 | 0.00 | 0.00 | 0.00 | 0.00 | 0.00 | 0.00 | 0.00 | 0.00 | 0.00 | 0.00 | 0.00 | 0.00 | 0.00 |
| Mg | 1.03 | 0.99 | 1.00 | 1.03 | 1.01 | 0.99 | 1.00 | 1.01 | 1.02 | 0.99 | 1.05 | 1.03 | 1.00 | 1.01 | 0.97 | 0.97 |
| Ca | 0.95 | 0.99 | 1.01 | 0.97 | 0.99 | 1.00 | 0.97 | 0.98 | 0.98 | 0.99 | 0.96 | 0.96 | 0.97 | 0.96 | 1.01 | 1.01 |
| Na | 0.00 | 0.00 | 0.00 | 0.00 | 0.00 | 0.00 | 0.01 | 0.00 | 0.00 | 0.00 | 0.01 | 0.01 | 0.00 | 0.00 | 0.00 | 0.00 |

| | GR54C-1 | GR54C-2 | GR54C-3 | GR54C-4 | GR54C-5 | GR54C-6 | GR54C-7 | GR54C-8 | GR54C-9 | GR54C-10 | GR54C-11 | GR54C-12 | GR54C-13 | GR54C-14 | GR54C-15 | GR54C-16 |
|---|---|---|---|---|---|---|---|---|---|---|---|---|---|---|---|---|
| $SiO_2$ | 55.57 | 55.99 | 53.99 | 54.11 | 53.01 | 54.59 | 55.29 | 54.26 | 55.89 | 55.57 | 55.62 | 53.71 | 55.07 | 52.64 | 54.78 | 55.07 |
| $TiO_2$ | 0.00 | 0.02 | 0.04 | 0.12 | 0.05 | 0.02 | 0.00 | 0.09 | 0.05 | 0.07 | 0.07 | 0.04 | 0.03 | 0.02 | 0.05 | 0.04 |
| $Al_2O_3$ | 0.19 | 0.37 | 0.28 | 0.16 | 0.25 | 0.13 | 0.32 | 0.13 | 0.08 | 0.09 | 0.11 | 0.13 | 0.11 | 0.22 | 0.09 | 0.33 |
| $Cr_2O_3$ | 0.00 | 0.03 | 0.05 | 0.08 | 0.04 | 0.02 | 0.02 | 0.03 | 0.03 | 0.04 | 0.04 | 0.04 | 0.05 | 0.09 | 0.04 | 0.08 |
| $Fe_2O_3$ | 0.00 | 0.00 | 0.39 | 0.45 | 0.46 | 0.44 | 0.10 | 0.57 | 0.00 | 0.00 | 0.39 | 0.56 | 0.00 | 0.00 | 0.48 | 0.09 |
| FeO | 0.33 | 0.35 | 0.00 | 0.00 | 0.00 | 0.00 | 0.33 | 0.00 | 0.40 | 0.39 | 0.00 | 0.00 | 0.64 | 0.48 | 0.00 | 0.37 |
| MnO | 0.03 | 0.00 | 0.02 | 0.02 | 0.00 | 0.01 | 0.00 | 0.02 | 0.01 | 0.00 | 0.00 | 0.02 | 0.00 | 0.01 | 0.03 | 0.05 |
| NiO | 0.00 | 0.00 | 0.00 | 0.00 | 0.00 | 0.00 | 0.00 | 0.00 | 0.00 | 0.00 | 0.00 | 0.00 | 0.00 | 0.00 | 0.00 | 0.00 |
| ZnO | 0.05 | 0.00 | 0.06 | 0.00 | 0.00 | 0.00 | 0.04 | 0.00 | 0.00 | 0.00 | 0.00 | 0.03 | 0.04 | 0.01 | 0.01 | 0.00 |
| MgO | 18.21 | 18.74 | 19.45 | 19.11 | 19.37 | 18.51 | 19.65 | 18.86 | 18.33 | 18.12 | 18.47 | 18.92 | 17.94 | 18.43 | 18.52 | 19.35 |
| CaO | 24.37 | 22.89 | 24.27 | 24.93 | 24.72 | 25.29 | 23.47 | 24.90 | 25.36 | 25.60 | 26.08 | 25.05 | 24.85 | 22.73 | 25.92 | 23.68 |
| $Na_2O$ | 0.12 | 0.23 | 0.16 | 0.13 | 0.14 | 0.06 | 0.12 | 0.05 | 0.05 | 0.04 | 0.06 | 0.04 | 0.05 | 0.04 | 0.00 | 0.12 |
| Total | 98.89 | 98.65 | 98.74 | 99.13 | 98.06 | 99.06 | 99.38 | 98.93 | 100.20 | 99.92 | 100.85 | 98.55 | 98.79 | 94.68 | 99.92 | 99.19 |

| | | | | | | | | | | | | | | | | |
|---|---|---|---|---|---|---|---|---|---|---|---|---|---|---|---|---|
| Si | 2.03 | 2.04 | 1.96 | 1.96 | 1.94 | 1.99 | 2.00 | 1.98 | 2.01 | 2.01 | 1.99 | 1.96 | 2.02 | 2.00 | 1.98 | 1.99 |
| Ti | 0.00 | 0.00 | 0.00 | 0.00 | 0.00 | 0.00 | 0.00 | 0.00 | 0.00 | 0.00 | 0.00 | 0.00 | 0.00 | 0.00 | 0.00 | 0.00 |
| Al | 0.01 | 0.02 | 0.01 | 0.01 | 0.01 | 0.01 | 0.01 | 0.01 | 0.00 | 0.00 | 0.00 | 0.01 | 0.00 | 0.01 | 0.00 | 0.01 |
| Cr | 0.00 | 0.00 | 0.00 | 0.00 | 0.00 | 0.00 | 0.00 | 0.00 | 0.00 | 0.00 | 0.00 | 0.00 | 0.00 | 0.00 | 0.00 | 0.00 |
| $Fe^{3+}$ | 0.00 | 0.00 | 0.01 | 0.01 | 0.01 | 0.01 | 0.00 | 0.02 | 0.00 | 0.00 | 0.01 | 0.02 | 0.00 | 0.00 | 0.01 | 0.00 |
| $Fe^{2+}$ | 0.01 | 0.01 | 0.00 | 0.00 | 0.00 | 0.00 | 0.01 | 0.00 | 0.01 | 0.01 | 0.00 | 0.00 | 0.02 | 0.02 | 0.00 | 0.01 |
| Mn | 0.00 | 0.00 | 0.00 | 0.00 | 0.00 | 0.00 | 0.00 | 0.00 | 0.00 | 0.00 | 0.00 | 0.00 | 0.00 | 0.00 | 0.00 | 0.00 |
| Ni | 0.00 | 0.00 | 0.00 | 0.00 | 0.00 | 0.00 | 0.00 | 0.00 | 0.00 | 0.00 | 0.00 | 0.00 | 0.00 | 0.00 | 0.00 | 0.00 |
| Zn | 0.00 | 0.00 | 0.00 | 0.00 | 0.00 | 0.00 | 0.00 | 0.00 | 0.00 | 0.00 | 0.00 | 0.00 | 0.00 | 0.00 | 0.00 | 0.00 |
| Mg | 0.99 | 1.02 | 1.05 | 1.03 | 1.06 | 1.00 | 1.06 | 1.02 | 0.98 | 0.98 | 0.99 | 1.03 | 0.98 | 1.04 | 1.00 | 1.04 |
| Ca | 0.95 | 0.89 | 0.95 | 0.97 | 0.97 | 0.99 | 0.91 | 0.97 | 0.98 | 0.99 | 1.00 | 0.98 | 0.97 | 0.92 | 1.00 | 0.92 |
| Na | 0.01 | 0.02 | 0.01 | 0.01 | 0.01 | 0.00 | 0.01 | 0.00 | 0.00 | 0.00 | 0.00 | 0.00 | 0.00 | 0.00 | 0.00 | 0.01 |

| | GR54C-17 | GR54C-18 | GR54C-19 | GR54C-20 | GR54C-21 | GR54C-22 | GR54C-23 | GR54C-24 | GR54C-25 | GR54C-26 | GR54C-27 | GR54C-28 | GR54C-29 | GR54C-30 | GR54C-31 |
|---|---|---|---|---|---|---|---|---|---|---|---|---|---|---|---|
| $SiO_2$ | 55.22 | 55.15 | 55.52 | 53.69 | 53.71 | 54.07 | 54.39 | 54.46 | 53.79 | 54.05 | 55.07 | 54.46 | 54.24 | 54.91 | 53.69 |
| $TiO_2$ | 0.04 | 0.04 | 0.03 | 0.04 | 0.02 | 0.03 | 0.03 | 0.05 | 0.04 | 0.05 | 0.08 | 0.03 | 0.07 | 0.07 | 0.00 |
| $Al_2O_3$ | 0.16 | 0.13 | 0.02 | 0.37 | 0.22 | 0.42 | 0.15 | 0.14 | 0.27 | 0.28 | 0.26 | 0.09 | 0.25 | 0.08 | 0.69 |
| $Cr_2O_3$ | 0.10 | 0.09 | 0.23 | 0.27 | 0.30 | 0.24 | 0.03 | 0.01 | 0.31 | 0.08 | 0.06 | 0.02 | 0.03 | 0.00 | 0.50 |
| $Fe_2O_3$ | 0.40 | 0.42 | 0.00 | 0.42 | 0.48 | 0.46 | 0.35 | 0.62 | 0.50 | 0.53 | 0.41 | 0.44 | 0.39 | 0.41 | 0.50 |
| FeO | 0.11 | 0.00 | 0.46 | 0.00 | 0.00 | 0.00 | 0.00 | 0.00 | 0.00 | 0.00 | 0.00 | 0.00 | 0.00 | 0.00 | 0.00 |
| MnO | 0.00 | 0.00 | 0.00 | 0.02 | 0.03 | 0.01 | 0.00 | 0.03 | 0.00 | 0.06 | 0.01 | 0.01 | 0.02 | 0.00 | 0.02 |
| NiO | 0.00 | 0.00 | 0.00 | 0.00 | 0.00 | 0.00 | 0.00 | 0.00 | 0.00 | 0.00 | 0.00 | 0.00 | 0.00 | 0.00 | 0.00 |
| ZnO | 0.01 | 0.00 | 0.00 | 0.01 | 0.02 | 0.05 | 0.00 | 0.00 | 0.04 | 0.00 | 0.00 | 0.00 | 0.00 | 0.02 | 0.00 |
| MgO | 19.22 | 18.82 | 18.33 | 19.77 | 18.74 | 18.62 | 18.71 | 18.64 | 18.54 | 18.67 | 18.86 | 18.76 | 19.20 | 18.39 | 19.20 |
| CaO | 24.39 | 25.11 | 25.67 | 24.31 | 24.39 | 24.72 | 25.38 | 25.48 | 25.35 | 25.05 | 25.49 | 25.38 | 24.63 | 25.81 | 23.91 |
| $Na_2O$ | 0.08 | 0.09 | 0.03 | 0.06 | 0.11 | 0.05 | 0.04 | 0.07 | 0.06 | 0.06 | 0.10 | 0.08 | 0.15 | 0.04 | 0.10 |
| Total | 99.75 | 99.85 | 100.30 | 98.95 | 98.03 | 98.69 | 99.09 | 99.51 | 98.90 | 98.84 | 100.35 | 99.28 | 98.98 | 99.74 | 98.60 |
| Si | 1.99 | 1.99 | 2.00 | 1.95 | 1.97 | 1.97 | 1.98 | 1.97 | 1.96 | 1.97 | 1.98 | 1.98 | 1.97 | 1.99 | 1.96 |
| Ti | 0.00 | 0.00 | 0.00 | 0.00 | 0.00 | 0.00 | 0.00 | 0.00 | 0.00 | 0.00 | 0.00 | 0.00 | 0.00 | 0.00 | 0.00 |
| Al | 0.01 | 0.01 | 0.00 | 0.02 | 0.01 | 0.02 | 0.01 | 0.01 | 0.01 | 0.01 | 0.01 | 0.00 | 0.01 | 0.00 | 0.03 |
| Cr | 0.00 | 0.00 | 0.01 | 0.01 | 0.01 | 0.01 | 0.00 | 0.00 | 0.01 | 0.00 | 0.00 | 0.00 | 0.00 | 0.00 | 0.01 |
| $Fe^{3+}$ | 0.01 | 0.01 | 0.00 | 0.01 | 0.01 | 0.01 | 0.01 | 0.02 | 0.01 | 0.01 | 0.01 | 0.01 | 0.01 | 0.01 | 0.01 |
| $Fe^{2+}$ | 0.00 | 0.00 | 0.01 | 0.00 | 0.00 | 0.00 | 0.00 | 0.00 | 0.00 | 0.00 | 0.00 | 0.00 | 0.00 | 0.00 | 0.00 |
| Mn | 0.00 | 0.00 | 0.00 | 0.00 | 0.00 | 0.00 | 0.00 | 0.00 | 0.00 | 0.00 | 0.00 | 0.00 | 0.00 | 0.00 | 0.00 |
| Ni | 0.00 | 0.00 | 0.00 | 0.00 | 0.00 | 0.00 | 0.00 | 0.00 | 0.00 | 0.00 | 0.00 | 0.00 | 0.00 | 0.00 | 0.00 |
| Zn | 0.00 | 0.00 | 0.00 | 0.00 | 0.00 | 0.00 | 0.00 | 0.00 | 0.00 | 0.00 | 0.00 | 0.00 | 0.00 | 0.00 | 0.00 |
| Mg | 1.03 | 1.01 | 0.98 | 1.07 | 1.03 | 1.01 | 1.01 | 1.01 | 1.01 | 1.01 | 1.01 | 1.01 | 1.04 | 0.99 | 1.04 |
| Ca | 0.94 | 0.97 | 0.99 | 0.94 | 0.96 | 0.97 | 0.99 | 0.99 | 0.99 | 0.98 | 0.98 | 0.99 | 0.96 | 1.00 | 0.93 |
| Na | 0.01 | 0.01 | 0.00 | 0.00 | 0.01 | 0.00 | 0.00 | 0.00 | 0.00 | 0.00 | 0.01 | 0.01 | 0.01 | 0.00 | 0.01 |

Tab. A4.5 Olivine microprobe analyses of Gomati chromitites and pyroxenites.

| wt% | GR54A-1 | GR54A-2 | GR54A-3 | GR54A-4 | GR54A-5 | GR54A-6 | GR54A-7 | GR54A-8 | GR54A-9 | GR54A-10 | GR54A-11 | GR54A-12 | GR54A-13 | GR54A-14 | GR54A-15 | GR54A-16 | GR54A-17 | GR54A-18 |
|---|---|---|---|---|---|---|---|---|---|---|---|---|---|---|---|---|---|---|
| $SiO_2$ | 40.90 | 40.38 | 41.22 | 40.77 | 40.52 | 41.74 | 40.52 | 41.25 | 41.47 | 40.69 | 41.68 | 41.59 | 41.80 | 41.58 | 41.40 | 41.13 | 41.12 | 41.12 |
| $TiO_2$ | 0.00 | 0.01 | 0.00 | 0.00 | 0.01 | 0.03 | 0.00 | 0.00 | 0.04 | 0.00 | 0.00 | 0.00 | 0.00 | 0.02 | 0.00 | 0.05 | 0.03 | 0.01 |
| $Al_2O_3$ | 0.00 | 0.00 | 0.01 | 0.00 | 0.00 | 0.00 | 0.01 | 0.01 | 0.02 | 0.01 | 0.01 | 0.00 | 0.00 | 0.00 | 0.00 | 0.00 | 0.00 | 0.00 |
| $Cr_2O_3$ | 0.00 | 0.00 | 0.02 | 0.06 | 0.01 | 0.03 | 0.00 | 0.02 | 0.02 | 0.00 | 0.01 | 0.01 | 0.00 | 0.00 | 0.00 | 0.02 | 0.03 | 0.02 |
| $Fe_2O_3$ | 0.00 | 0.00 | 0.00 | 0.00 | 0.00 | 0.00 | 0.00 | 0.00 | 0.00 | 0.00 | 0.00 | 0.00 | 0.00 | 0.00 | 0.00 | 0.00 | 0.00 | 0.00 |
| FeO | 6.61 | 6.41 | 6.62 | 6.87 | 6.79 | 6.18 | 6.47 | 6.55 | 6.71 | 6.90 | 7.11 | 6.99 | 7.08 | 6.78 | 6.53 | 6.57 | 6.62 | 6.25 |
| MnO | 0.09 | 0.07 | 0.04 | 0.09 | 0.12 | 0.08 | 0.11 | 0.13 | 0.09 | 0.09 | 0.10 | 0.06 | 0.10 | 0.06 | 0.06 | 0.09 | 0.06 | 0.05 |
| MgO | 52.37 | 53.03 | 52.19 | 52.68 | 52.47 | 52.04 | 52.72 | 51.98 | 52.85 | 53.50 | 52.68 | 52.76 | 52.42 | 53.28 | 53.74 | 53.64 | 53.57 | 53.64 |
| NiO | 0.00 | 0.00 | 0.00 | 0.00 | 0.00 | 0.00 | 0.00 | 0.00 | 0.00 | 0.00 | 0.00 | 0.00 | 0.00 | 0.00 | 0.00 | 0.00 | 0.00 | 0.00 |

| | | | | | | | | | | | | | | | | | | |
|---|---|---|---|---|---|---|---|---|---|---|---|---|---|---|---|---|---|---|
| CaO | 0.01 | 0.01 | 0.00 | 0.00 | 0.00 | 0.00 | 0.00 | 0.00 | 0.01 | 0.02 | 0.00 | 0.00 | 0.00 | 0.00 | 0.01 | 0.00 | 0.00 | 0.01 |
| TOT | 99.98 | 99.90 | 100.11 | 100.48 | 99.99 | 100.11 | 99.82 | 99.93 | 101.20 | 101.22 | 101.58 | 101.40 | 101.41 | 101.75 | 101.79 | 101.50 | 101.43 | 101.11 |
| Si | 0.98 | 0.97 | 0.99 | 0.98 | 0.98 | 1.00 | 0.98 | 1.00 | 0.99 | 0.97 | 0.99 | 0.99 | 1.00 | 0.98 | 0.98 | 0.97 | 0.97 | 0.98 |
| Ti | 0.00 | 0.00 | 0.00 | 0.00 | 0.00 | 0.00 | 0.00 | 0.00 | 0.00 | 0.00 | 0.00 | 0.00 | 0.00 | 0.00 | 0.00 | 0.00 | 0.00 | 0.00 |
| Al | 0.00 | 0.00 | 0.00 | 0.00 | 0.00 | 0.00 | 0.00 | 0.00 | 0.00 | 0.00 | 0.00 | 0.00 | 0.00 | 0.00 | 0.00 | 0.00 | 0.00 | 0.00 |
| Cr | 0.00 | 0.00 | 0.00 | 0.00 | 0.00 | 0.00 | 0.00 | 0.00 | 0.00 | 0.00 | 0.00 | 0.00 | 0.00 | 0.00 | 0.00 | 0.00 | 0.00 | 0.00 |
| $Fe^{3+}$ | 0.00 | 0.00 | 0.00 | 0.00 | 0.00 | 0.00 | 0.00 | 0.00 | 0.00 | 0.00 | 0.00 | 0.00 | 0.00 | 0.00 | 0.00 | 0.00 | 0.00 | 0.00 |
| $Fe^{2+}$ | 0.13 | 0.13 | 0.13 | 0.14 | 0.14 | 0.12 | 0.13 | 0.13 | 0.13 | 0.14 | 0.14 | 0.14 | 0.14 | 0.13 | 0.13 | 0.13 | 0.13 | 0.12 |
| Mn | 0.00 | 0.00 | 0.00 | 0.00 | 0.00 | 0.00 | 0.00 | 0.00 | 0.00 | 0.00 | 0.00 | 0.00 | 0.00 | 0.00 | 0.00 | 0.00 | 0.00 | 0.00 |
| Mg | 1.88 | 1.90 | 1.87 | 1.88 | 1.88 | 1.87 | 1.89 | 1.87 | 1.88 | 1.89 | 1.87 | 1.87 | 1.86 | 1.88 | 1.89 | 1.89 | 1.89 | 1.90 |
| Ni | 0.00 | 0.00 | 0.00 | 0.00 | 0.00 | 0.00 | 0.00 | 0.00 | 0.00 | 0.00 | 0.00 | 0.00 | 0.00 | 0.00 | 0.00 | 0.00 | 0.00 | 0.00 |
| Ca | 0.00 | 0.00 | 0.00 | 0.00 | 0.00 | 0.00 | 0.00 | 0.00 | 0.00 | 0.00 | 0.00 | 0.00 | 0.00 | 0.00 | 0.00 | 0.00 | 0.00 | 0.00 |

Tab. A4.6 Chlorite and serpentine microprobe analyses of Gomati chromitites and pyroxenites.

| wt% | GOM2A-2 | GOM2A-3 | GOM2A-4 | GOM2A-5 | GOM2A-6 | GOM2A-7 | GOM2A-8 | GOM2A-9 | GOM2A-10 | GOM2A-11 | GOM2A-12 | GOM2A-13 | GOM2A-14 | GOM2A-15 | GOM2A-16 | GOM2A-17 | GOM2A-18 | GOM2A-19 |
|---|---|---|---|---|---|---|---|---|---|---|---|---|---|---|---|---|---|---|
| min | chl | chl | chl | chl | chl | chl | chl | chl | chl | chl | chl | chl | chl | chl | chl | chl | chl | chl |
| MgO | 32.96 | 33.23 | 33.51 | 33.71 | 33.26 | 33.58 | 33.01 | 32.18 | 29.89 | 32.90 | 32.85 | 32.73 | 32.68 | 32.64 | 32.98 | 32.76 | 33.14 | 33.03 |
| $SiO_2$ | 31.27 | 31.69 | 31.90 | 31.92 | 31.46 | 31.32 | 31.97 | 31.59 | 28.96 | 31.03 | 31.24 | 30.69 | 31.06 | 31.44 | 31.54 | 31.66 | 31.67 | 31.86 |
| FeO | 1.50 | 1.48 | 1.44 | 1.57 | 1.60 | 1.70 | 1.59 | 1.57 | 3.18 | 1.34 | 1.14 | 1.39 | 1.55 | 1.41 | 1.48 | 1.43 | 1.50 | 1.57 |
| CaO | 0.00 | 0.00 | 0.02 | 0.00 | 0.00 | 0.00 | 0.00 | 0.02 | 0.02 | 0.01 | 0.00 | 0.02 | 0.00 | 0.00 | 0.00 | 0.00 | 0.01 | 0.02 |
| $Al_2O_3$ | 15.43 | 14.94 | 15.28 | 15.41 | 15.46 | 15.74 | 15.47 | 15.60 | 14.87 | 15.08 | 15.72 | 15.55 | 15.58 | 15.99 | 15.89 | 14.86 | 14.40 | 14.28 |
| $Cr_2O_3$ | 4.59 | 5.08 | 4.12 | 4.14 | 3.45 | 3.48 | 4.30 | 4.74 | 9.05 | 4.75 | 4.33 | 4.48 | 4.43 | 3.73 | 4.16 | 5.08 | 5.57 | 5.46 |
| NiO | 0.29 | 0.31 | 0.33 | 0.33 | 0.31 | 0.31 | 0.30 | 0.36 | 0.32 | 0.28 | 0.24 | 0.32 | 0.34 | 0.27 | 0.35 | 0.33 | 0.35 | 0.32 |
| Total | 86.09 | 86.79 | 86.63 | 87.14 | 85.54 | 86.14 | 86.68 | 86.11 | 86.34 | 85.45 | 85.57 | 85.30 | 85.77 | 85.49 | 86.41 | 86.19 | 86.66 | 86.57 |

| wt% | GOM2A-20 | GOM2A-21 | GOM2A-22 | GOM2A-23 | GOM2A-24 | GOM2A-25 | GOM2A-26 | GOM2A-27 | GOM2A-28 | GOM2A-29 | GOM2A-30 | GOM2A-31 | GOM2A-32 | GOM2A-33 | GOM2A-34 | GOM2A-35 | GOM2A-36 | GOM2B-1 |
|---|---|---|---|---|---|---|---|---|---|---|---|---|---|---|---|---|---|---|
| min | chl | chl | chl | chl | chl | chl | chl | chl | chl | chl | chl | chl | chl | chl | chl | chl | chl | chl |
| MgO | 33.79 | 32.82 | 32.70 | 32.50 | 32.56 | 33.62 | 32.10 | 32.06 | 33.16 | 33.26 | 32.49 | 32.58 | 33.85 | 33.69 | 33.67 | 33.74 | 33.13 | 34.40 |
| $SiO_2$ | 31.78 | 31.55 | 30.82 | 31.27 | 32.08 | 31.94 | 30.19 | 31.35 | 32.19 | 32.04 | 32.61 | 32.35 | 31.53 | 31.79 | 32.23 | 31.87 | 30.90 | 35.14 |
| FeO | 1.42 | 1.49 | 1.63 | 1.75 | 1.38 | 1.54 | 0.96 | 1.36 | 1.56 | 1.57 | 1.42 | 1.51 | 1.21 | 1.28 | 1.35 | 1.42 | 1.52 | 2.30 |
| CaO | 0.01 | 0.00 | 0.03 | 0.00 | 0.00 | 0.00 | 0.01 | 0.01 | 0.00 | 0.03 | 0.00 | 0.01 | 0.01 | 0.01 | 0.00 | 0.00 | 0.00 | 0.13 |
| $Al_2O_3$ | 15.31 | 15.52 | 15.73 | 16.12 | 15.59 | 15.30 | 18.18 | 16.46 | 14.99 | 13.44 | 14.72 | 14.98 | 14.99 | 14.95 | 15.05 | 15.19 | 15.94 | 10.23 |
| $Cr_2O_3$ | 4.31 | 4.39 | 3.56 | 3.53 | 3.94 | 3.56 | 2.93 | 3.10 | 3.72 | 4.37 | 4.83 | 4.82 | 4.80 | 4.36 | 3.87 | 3.87 | 3.59 | 2.30 |
| NiO | 0.28 | 0.33 | 0.26 | 0.33 | 0.32 | 0.27 | 0.19 | 0.30 | 0.38 | 0.30 | 0.27 | 0.24 | 0.30 | 0.32 | 0.35 | 0.30 | 0.34 | 0.00 |
| Total | 86.94 | 86.19 | 84.78 | 85.49 | 85.99 | 86.28 | 84.62 | 84.73 | 86.08 | 85.03 | 86.42 | 86.58 | 86.71 | 86.49 | 86.56 | 86.40 | 85.44 | 84.60 |

| wt% | GOM2B-2 | GOM2B-3 | GOM2B-4 | GOM2B-5 | GOM2B-6 | GOM2B-7 | GOM2B-8 | GOM2B-9 | GOM2B-10 | GOM2B-11 | GOM2B-12 | GOM2B-13 | GOM2B-14 | GOM2B-15 | GOM2B-16 | GOM2B-17 | GOM2B-18 | GOM2B-19 |
|---|---|---|---|---|---|---|---|---|---|---|---|---|---|---|---|---|---|---|
| min | chl | chl | chl | chl | chl | chl | chl | chl | chl | chl | chl | chl | chl | chl | chl | chl | chl | chl |
| MgO | 34.69 | 34.74 | 34.63 | 34.58 | 34.14 | 34.43 | 34.63 | 34.19 | 34.22 | 32.81 | 33.27 | 33.45 | 33.73 | 33.92 | 33.20 | 32.70 | 32.86 | 33.70 |
| $SiO_2$ | 33.85 | 32.99 | 32.81 | 33.27 | 33.19 | 33.56 | 33.73 | 33.20 | 33.47 | 31.07 | 31.67 | 31.48 | 32.20 | 30.67 | 30.66 | 31.75 | 30.94 | 31.88 |
| FeO | 2.20 | 2.02 | 2.21 | 2.17 | 2.41 | 2.16 | 2.22 | 2.42 | 2.39 | 2.67 | 2.40 | 2.47 | 2.23 | 2.52 | 2.33 | 2.04 | 2.60 | 2.29 |
| CaO | 0.11 | 0.07 | 0.06 | 0.03 | 0.04 | 0.06 | 0.24 | 0.01 | 0.02 | 0.06 | 0.03 | 0.01 | 0.00 | 0.02 | 0.02 | 0.03 | 0.02 | 0.00 |
| $Al_2O_3$ | 11.08 | 11.90 | 11.98 | 11.76 | 11.68 | 11.66 | 11.29 | 11.76 | 11.83 | 12.31 | 12.06 | 12.11 | 11.43 | 12.60 | 11.97 | 10.74 | 13.00 | 11.49 |
| $Cr_2O_3$ | 2.49 | 2.22 | 2.15 | 2.34 | 2.60 | 2.17 | 2.06 | 2.10 | 2.42 | 4.15 | 4.13 | 4.07 | 4.35 | 4.04 | 4.35 | 4.33 | 3.82 | 4.53 |
| NiO | 0.00 | 0.00 | 0.00 | 0.00 | 0.00 | 0.00 | 0.00 | 0.00 | 0.00 | 0.00 | 0.00 | 0.00 | 0.00 | 0.00 | 0.00 | 0.00 | 0.00 | 0.00 |
| Total | 84.46 | 84.02 | 83.88 | 84.20 | 84.11 | 84.08 | 84.22 | 83.71 | 84.37 | 83.12 | 83.60 | 83.64 | 83.97 | 83.81 | 82.56 | 81.63 | 83.27 | 83.94 |

| wt% | GOM2B-20 | GOM2B-21 | GOM2B-22 | GOM2B-23 | GOM2B-24 | GOM2B-25 | GOM2B-26 | GOM2B-27 | GOM2B-28 | GOM2B-29 | GOM2B-3 | GOM2B-10 | GOM2B-11 | GOM2B-12 | GOM2B-16 | GOM2B-17 | GOM2B-21 | GOM2B-24 |
|---|---|---|---|---|---|---|---|---|---|---|---|---|---|---|---|---|---|---|

# Appendix: Chapter 4

| min | chl | chl | serp | serp | chl | serp | chl | chl | chl | chl | chl | chl | serp | serp | chl | serp | chl | chl |
|---|---|---|---|---|---|---|---|---|---|---|---|---|---|---|---|---|---|---|
| MgO | 33.92 | 33.21 | 38.17 | 37.80 | 34.69 | 37.71 | 37.96 | 33.43 | 34.89 | 33.23 | 33.59 | 32.72 | 0.24 | 0.23 | 33.20 | 17.36 | 33.76 | 33.66 |
| $SiO_2$ | 32.18 | 30.94 | 40.77 | 41.14 | 34.10 | 40.15 | 41.50 | 35.39 | 36.84 | 33.09 | 33.39 | 33.22 | 31.90 | 31.31 | 32.82 | 54.06 | 33.19 | 32.71 |
| FeO | 1.81 | 2.30 | 1.87 | 1.98 | 2.12 | 1.98 | 2.06 | 1.95 | 1.95 | 2.10 | 1.79 | 1.76 | 10.92 | 11.01 | 2.51 | 0.59 | 2.14 | 2.30 |
| CaO | 0.03 | 0.02 | 0.14 | 0.03 | 0.01 | 0.02 | 0.04 | 0.10 | 0.26 | 0.05 | 0.01 | 0.03 | 34.24 | 34.11 | 0.00 | 25.70 | 0.00 | 0.05 |
| $Al_2O_3$ | 10.48 | 12.30 | 1.99 | 2.33 | 10.47 | 2.27 | 2.13 | 8.24 | 6.80 | 11.05 | 11.12 | 10.91 | 2.09 | 2.24 | 12.32 | 0.04 | 11.52 | 12.30 |
| $Cr_2O_3$ | 4.74 | 4.17 | 0.14 | 0.41 | 1.66 | 0.26 | 0.20 | 2.02 | 1.86 | 2.89 | 5.08 | 4.78 | 15.37 | 15.10 | 4.50 | 0.06 | 5.22 | 4.89 |
| NiO | 0.00 | 0.00 | 0.00 | 0.00 | 0.00 | 0.00 | 0.00 | 0.00 | 0.00 | 0.00 | 0.19 | 0.17 | 0.00 | 0.00 | 0.22 | 0.01 | 0.23 | 0.20 |
| Total | 83.23 | 82.99 | 83.16 | 83.76 | 83.09 | 82.46 | 83.91 | 81.15 | 82.64 | 82.45 | 85.29 | 83.68 | 95.07 | 94.22 | 85.63 | 97.98 | 86.12 | 86.17 |

| wt% | GOM2B-29 | GOM2C-1 | GOM2C-2 | GOM2C-3 | GOM2C-4 | GOM2C-5 | GOM2C-6 | GOM2C-7 | GOM2C-8 | GOM2C-9 | GOM2C-10 | GOM2C-11 | GOM2C-12 | GOM2C-13 | GOM2C-14 | GOM2C-15 | GOM2C-16 | GOM2C-17 |
|---|---|---|---|---|---|---|---|---|---|---|---|---|---|---|---|---|---|---|
| min | chl | chl | serp | chl | serp | chl | chl | chl | chl | serp | serp | serp | serp | serp | serp | serp | serp | chl |
| MgO | 34.06 | 33.99 | 40.90 | 33.31 | 37.18 | 34.02 | 33.53 | 34.16 | 33.47 | 37.18 | 39.81 | 40.29 | 40.82 | 37.46 | 38.61 | 40.08 | 38.01 | 33.28 |
| $SiO_2$ | 33.66 | 34.06 | 42.52 | 32.23 | 39.26 | 33.62 | 30.78 | 32.31 | 31.74 | 40.34 | 41.77 | 41.39 | 42.78 | 41.37 | 42.83 | 42.05 | 40.24 | 31.08 |
| FeO | 1.89 | 1.54 | 1.07 | 1.74 | 2.25 | 1.79 | 1.80 | 1.79 | 2.08 | 1.42 | 1.19 | 1.25 | 1.09 | 1.33 | 1.34 | 1.24 | 1.36 | 1.44 |
| CaO | 0.04 | 0.01 | 0.01 | 0.03 | 0.02 | 0.01 | 0.02 | 0.01 | 0.02 | 0.00 | 0.03 | 0.03 | 0.02 | 0.01 | 0.00 | 0.02 | 0.00 | 0.03 |
| $Al_2O_3$ | 11.77 | 10.77 | 0.09 | 13.32 | 3.35 | 11.26 | 14.65 | 13.45 | 14.96 | 2.98 | 0.21 | 0.08 | 0.16 | 3.06 | 1.68 | 0.31 | 3.06 | 13.83 |
| $Cr_2O_3$ | 2.67 | 5.38 | 0.37 | 3.99 | 4.00 | 4.50 | 3.64 | 3.40 | 3.53 | 2.70 | 0.36 | 0.17 | 0.24 | 2.50 | 0.75 | 0.25 | 2.88 | 3.85 |
| NiO | 0.26 | 0.18 | 0.24 | 0.21 | 0.15 | 0.14 | 0.21 | 0.10 | 0.19 | 0.14 | 0.20 | 0.25 | 0.20 | 0.09 | 0.08 | 0.23 | 0.09 | 0.26 |
| Total | 84.47 | 85.94 | 85.25 | 84.93 | 86.32 | 85.47 | 84.75 | 85.31 | 86.17 | 84.79 | 83.67 | 83.49 | 85.33 | 85.83 | 85.29 | 84.28 | 85.78 | 83.80 |

| wt% | GOM2C-18 | GOM2C-19 | GOM2C-20 | GOM2C-21 | GOM2C-22 | GOM2C-23 | GR54A-CHL-1 | GR54A-CHL-2 | GR54A-CHL-3 | GR54A-1 | GR54A-2 | GR54A-3 | GR54A-4 | GR54A-5 | GR54A-6 | GR54A-7 | GR54A-8 | GR54A-9 |
|---|---|---|---|---|---|---|---|---|---|---|---|---|---|---|---|---|---|---|
| min | serp | serp | serp | serp | chl | serp | chl | chl | serp | chl | chl | serp | chl | chl | chl | chl | serp | chl |
| MgO | 39.32 | 39.23 | 38.79 | 38.95 | 33.85 | 39.07 | 37.59 | 35.61 | 37.33 | 34.32 | 36.57 | 38.38 | 36.16 | 36.88 | 34.40 | 34.61 | 39.31 | 33.19 |
| $SiO_2$ | 41.21 | 41.64 | 43.50 | 41.77 | 32.16 | 42.84 | 38.02 | 35.85 | 39.79 | 32.91 | 35.36 | 40.61 | 36.15 | 37.99 | 32.85 | 32.38 | 42.30 | 32.29 |
| FeO | 1.01 | 0.98 | 1.58 | 1.07 | 1.53 | 1.44 | 1.48 | 1.49 | 1.31 | 1.63 | 1.36 | 1.06 | 1.28 | 1.25 | 1.72 | 1.66 | 1.10 | 1.79 |
| CaO | 0.01 | 0.03 | 0.00 | 0.02 | 0.01 | 0.00 | 0.00 | 0.02 | 0.02 | 0.03 | 0.02 | 0.01 | 0.00 | 0.00 | 0.00 | 0.01 | 0.03 | 0.02 |
| $Al_2O_3$ | 0.14 | 0.14 | 1.16 | 0.11 | 11.73 | 1.18 | 5.42 | 9.46 | 2.79 | 10.72 | 7.54 | 3.52 | 6.51 | 4.91 | 12.54 | 11.50 | 1.52 | 14.37 |
| $Cr_2O_3$ | 0.12 | 0.05 | 0.38 | 0.18 | 4.70 | 0.40 | 2.06 | 3.18 | 1.11 | 5.34 | 4.11 | 0.58 | 4.35 | 3.64 | 4.02 | 4.87 | 0.36 | 2.95 |
| NiO | 0.75 | 0.74 | 0.14 | 0.84 | 0.12 | 0.07 | 0.45 | 0.24 | 0.44 | 0.21 | 0.15 | 0.26 | 0.12 | 0.14 | 0.25 | 0.15 | 0.11 | 0.22 |
| Total | 82.60 | 82.83 | 85.56 | 83.06 | 84.22 | 85.01 | 85.11 | 85.87 | 82.90 | 85.24 | 85.21 | 84.51 | 84.70 | 84.85 | 85.90 | 85.25 | 84.75 | 84.88 |

| wt% | GR54A-10 | GR54A-11 | GR54A-12 | GR54A-13 | GR54A-14 | GR54A-15 | GR54A-16 | GR54A-17 | GR54A-18 | GR54A-19 | GR54A-20 | GR54A-21 | GR54C-CHL-1 | GR54C-1 | GR54C-2 | GR54C-3 | GR54C-4 | GR54C-5 |
|---|---|---|---|---|---|---|---|---|---|---|---|---|---|---|---|---|---|---|
| min | chl | chl | chl | chl | chl | chl | chl | chl | serp | chl | serp | serp | chl | chl | chl | chl | chl | chl |
| MgO | 33.79 | 33.36 | 32.89 | 33.47 | 33.27 | 33.24 | 32.79 | 35.72 | 42.78 | 36.83 | 38.97 | 39.59 | 34.22 | 33.29 | 33.14 | 33.05 | 33.54 | 33.58 |
| $SiO_2$ | 31.95 | 31.82 | 30.92 | 31.60 | 30.89 | 31.41 | 31.33 | 36.72 | 41.91 | 35.38 | 41.15 | 42.69 | 34.20 | 33.67 | 33.52 | 34.21 | 34.16 | 33.68 |
| FeO | 1.81 | 2.04 | 1.84 | 1.96 | 1.72 | 2.41 | 2.21 | 1.73 | 2.29 | 1.78 | 1.57 | 1.23 | 1.04 | 1.88 | 1.75 | 1.22 | 1.80 | 1.83 |
| CaO | 0.01 | 0.02 | 0.01 | 0.02 | 0.00 | 0.01 | 0.00 | 0.02 | 0.00 | 0.03 | 0.01 | 0.01 | 0.01 | 0.01 | 0.02 | 0.02 | 0.01 | 0.03 |
| $Al_2O_3$ | 12.48 | 14.58 | 15.32 | 14.28 | 13.48 | 14.23 | 14.73 | 5.84 | 0.66 | 7.26 | 1.98 | 0.24 | 10.67 | 13.54 | 13.48 | 11.23 | 13.36 | 13.11 |
| $Cr_2O_3$ | 4.23 | 3.31 | 3.34 | 3.59 | 3.85 | 3.26 | 3.25 | 4.38 | 0.86 | 5.12 | 2.39 | 0.37 | 5.37 | 4.02 | 4.03 | 5.14 | 4.03 | 4.21 |
| NiO | 0.20 | 0.19 | 0.29 | 0.24 | 0.13 | 0.20 | 0.25 | 0.05 | 0.14 | 0.13 | 0.14 | 0.27 | 0.21 | 0.20 | 0.20 | 0.18 | 0.22 | 0.15 |
| Total | 84.51 | 85.36 | 84.65 | 85.28 | 83.42 | 84.94 | 84.57 | 84.56 | 88.73 | 86.57 | 86.26 | 84.42 | 85.80 | 86.71 | 86.13 | 85.13 | 87.15 | 86.75 |

| wt% | GR54C-6 | GR54C-7 | GR54C-8 | GR54C-9 | GR54C-10 | GR54C-11 | GR54C-12 | GR54C-13 | GR54C-14 | GR54C-15 | GR54C-16 | GR54C-17 | GR54C-18 | GR54C-19 | GR54C-20 | GR54C-21 | GR54C-22 | GR54D-1 |
|---|---|---|---|---|---|---|---|---|---|---|---|---|---|---|---|---|---|---|
| min | chl | chl | chl | chl | chl | chl | chl | chl | chl | chl | chl | chl | chl | chl | chl | chl | chl | chl |
| MgO | 34.04 | 35.67 | 33.86 | 34.75 | 34.22 | 33.53 | 35.87 | 34.61 | 33.71 | 35.49 | 33.96 | 34.04 | 33.46 | 34.17 | 34.53 | 35.20 | 34.12 | 33.50 |
| $SiO_2$ | 33.93 | 35.39 | 34.11 | 34.86 | 35.08 | 33.69 | 37.80 | 35.10 | 33.71 | 35.29 | 33.17 | 33.57 | 33.09 | 33.54 | 34.88 | 34.76 | 34.40 | 33.12 |
| FeO | 1.64 | 1.18 | 1.90 | 1.20 | 1.39 | 1.67 | 1.24 | 1.30 | 1.68 | 1.10 | 1.59 | 1.29 | 2.00 | 1.63 | 0.93 | 1.05 | 1.29 | 1.67 |
| CaO | 0.01 | 0.05 | 0.02 | 0.02 | 0.00 | 0.00 | 0.01 | 0.01 | 0.04 | 0.00 | 0.00 | 0.01 | 0.01 | 0.04 | 0.01 | 0.02 | 0.07 | 0.02 |

| | | | | | | | | | | | | | | | | | | |
|---|---|---|---|---|---|---|---|---|---|---|---|---|---|---|---|---|---|---|
| $Al_2O_3$ | 11.61 | 11.30 | 12.40 | 10.38 | 11.44 | 13.84 | 9.15 | 12.70 | 13.16 | 9.96 | 12.95 | 11.54 | 13.34 | 12.05 | 11.36 | 10.87 | 11.27 | 14.07 |
| $Cr_2O_3$ | 4.58 | 4.03 | 4.60 | 5.09 | 4.78 | 3.81 | 3.03 | 2.48 | 4.17 | 5.64 | 4.22 | 4.49 | 4.03 | 4.48 | 3.80 | 3.85 | 4.62 | 4.00 |
| NiO | 0.21 | 0.18 | 0.19 | 0.19 | 0.23 | 0.28 | 0.15 | 0.18 | 0.15 | 0.19 | 0.19 | 0.21 | 0.23 | 0.20 | 0.20 | 0.23 | 0.19 | 0.20 |
| Total | 86.04 | 87.86 | 87.17 | 86.65 | 87.26 | 86.95 | 87.44 | 86.52 | 86.63 | 87.69 | 86.16 | 85.22 | 86.18 | 86.19 | 85.77 | 86.05 | 86.04 | 86.65 |

| wt% | GR54D-2 | GR54D-3 | GR54D-4 | GR54D-5 | GR54D-6 | GR54D-7 | GR54D-8 | GR54D-9 | GR54D-10 | GR54D-11 | GR54D-12 | GR54D-13 | GR54D-14 | GR54D-15 | GR54D-16 | GR54D-17 | GR54D-18 | GR54D-19 |
|---|---|---|---|---|---|---|---|---|---|---|---|---|---|---|---|---|---|---|
| min | chl | chl | chl | chl | chl | chl | chl | chl | chl | chl | chl | chl | chl | chl | chl | chl | chl | chl |
| MgO | 32.96 | 33.05 | 32.49 | 33.65 | 34.25 | 33.56 | 34.18 | 34.30 | 34.00 | 32.92 | 33.08 | 33.26 | 34.27 | 33.77 | 33.39 | 34.35 | 37.47 | 32.78 |
| $SiO_2$ | 32.12 | 31.31 | 32.07 | 32.65 | 33.47 | 31.98 | 32.45 | 33.00 | 33.05 | 32.22 | 32.65 | 31.98 | 33.37 | 32.51 | 32.24 | 32.72 | 38.01 | 31.71 |
| FeO | 1.68 | 1.72 | 1.44 | 1.54 | 1.62 | 1.85 | 1.52 | 1.40 | 1.16 | 2.01 | 1.73 | 1.60 | 1.11 | 1.52 | 1.67 | 1.23 | 1.27 | 1.46 |
| CaO | 0.03 | 0.01 | 0.03 | 0.01 | 0.00 | 0.00 | 0.00 | 0.02 | 0.00 | 0.00 | 0.00 | 0.02 | 0.01 | 0.02 | 0.01 | 0.02 | 0.00 | 0.04 |
| $Al_2O_3$ | 15.15 | 15.27 | 12.98 | 11.70 | 10.44 | 14.82 | 13.64 | 11.15 | 12.34 | 14.34 | 14.61 | 14.77 | 12.28 | 14.98 | 14.47 | 9.49 | 5.13 | 14.83 |
| $Cr_2O_3$ | 3.38 | 3.44 | 4.05 | 4.72 | 6.74 | 4.10 | 3.88 | 5.86 | 4.74 | 3.89 | 3.78 | 3.50 | 5.28 | 3.47 | 3.25 | 5.45 | 4.12 | 3.53 |
| NiO | 0.29 | 0.21 | 0.21 | 0.29 | 0.20 | 0.27 | 0.23 | 0.28 | 0.12 | 0.20 | 0.21 | 0.18 | 0.13 | 0.24 | 0.28 | 0.20 | 0.21 | 0.22 |
| Total | 85.69 | 85.10 | 83.33 | 84.59 | 86.75 | 86.66 | 85.94 | 86.05 | 85.44 | 85.72 | 86.08 | 85.41 | 86.45 | 86.55 | 85.41 | 83.52 | 86.25 | 84.62 |

| wt% | GR54D-20 | GR54D-21 | GR54D-22 | GR54D-23 | GR54D-24 | GR54D-25 | GR54D-26 | GR54D-27 | GR54D-28 | GR54D-29 | GR54D-30 | GR54D-31 | GR54D-32 | GR55-1 | GR55-2 | GR55-3 | GR55-4 | GR55-5 |
|---|---|---|---|---|---|---|---|---|---|---|---|---|---|---|---|---|---|---|
| min | chl | chl | chl | chl | chl | chl | chl | chl | chl | chl | chl | chl | chl | chl | chl | chl | chl | chl |
| MgO | 33.53 | 36.36 | 37.72 | 34.32 | 35.89 | 33.61 | 34.45 | 33.24 | 33.82 | 32.54 | 33.32 | 34.83 | 34.12 | 31.33 | 32.40 | 33.11 | 33.11 | 32.46 |
| $SiO_2$ | 32.11 | 36.77 | 40.14 | 33.17 | 36.03 | 32.25 | 33.78 | 31.96 | 33.33 | 32.10 | 32.19 | 33.45 | 33.60 | 31.23 | 32.31 | 32.22 | 31.97 | 31.45 |
| FeO | 1.73 | 1.42 | 1.50 | 1.37 | 1.59 | 1.51 | 1.67 | 1.46 | 1.34 | 1.68 | 1.53 | 1.25 | 1.53 | 1.30 | 1.02 | 1.09 | 1.23 | 1.19 |
| CaO | 0.00 | 0.03 | 0.00 | 0.01 | 0.01 | 0.02 | 0.01 | 0.01 | 0.02 | 0.01 | 0.02 | 0.03 | 0.01 | 0.04 | 0.08 | 0.00 | 0.03 | 0.05 |
| $Al_2O_3$ | 14.58 | 7.62 | 3.52 | 10.67 | 8.05 | 14.68 | 10.58 | 14.43 | 8.58 | 10.32 | 15.63 | 8.97 | 12.67 | 17.67 | 14.45 | 13.50 | 14.62 | 14.71 |
| $Cr_2O_3$ | 3.43 | 4.74 | 2.72 | 5.04 | 4.27 | 3.67 | 4.64 | 3.42 | 6.34 | 5.43 | 3.23 | 6.88 | 4.30 | 4.11 | 4.57 | 4.82 | 4.26 | 4.40 |
| NiO | 0.22 | 0.22 | 0.21 | 0.19 | 0.26 | 0.27 | 0.24 | 0.22 | 0.10 | 0.26 | 0.22 | 0.12 | 0.21 | 0.42 | 0.33 | 0.37 | 0.40 | 0.40 |
| Total | 85.68 | 87.20 | 85.83 | 84.82 | 86.16 | 86.02 | 85.41 | 84.77 | 83.55 | 82.35 | 86.18 | 85.59 | 86.59 | 86.45 | 85.26 | 85.24 | 85.66 | 84.72 |

| wt% | GR55-6 | GR55-7 | GR55-8 | GR55-9 | GR55-10 | GR55-11 | GR55-12 | GR55-13 | GR55-14 | GR55-15 | GR55-16 | GR55-17 | GR55-18 | GR55-19 | GR55-20 |
|---|---|---|---|---|---|---|---|---|---|---|---|---|---|---|---|
| min | chl | chl | chl | chl | chl | chl | chl | chl | chl | chl | chl | chl | chl | chl | chl |
| MgO | 31.68 | 32.93 | 33.11 | 32.90 | 33.01 | 32.71 | 32.96 | 33.28 | 32.76 | 33.36 | 33.18 | 32.94 | 32.68 | 32.65 | 32.98 |
| $SiO_2$ | 30.70 | 31.98 | 32.22 | 32.36 | 32.05 | 32.37 | 32.11 | 32.00 | 31.80 | 31.64 | 32.20 | 32.06 | 31.57 | 31.38 | 31.98 |
| FeO | 1.18 | 1.29 | 1.13 | 1.08 | 1.21 | 1.37 | 1.23 | 1.09 | 1.05 | 1.11 | 1.25 | 1.21 | 1.28 | 1.18 | 1.22 |
| CaO | 0.07 | 0.00 | 0.04 | 0.04 | 0.02 | 0.03 | 0.01 | 0.05 | 0.05 | 0.04 | 0.00 | 0.00 | 0.01 | 0.04 | 0.02 |
| $Al_2O_3$ | 15.14 | 14.43 | 14.18 | 14.10 | 14.39 | 14.40 | 14.79 | 14.53 | 14.50 | 14.61 | 14.43 | 14.70 | 14.48 | 14.77 | 14.63 |
| $Cr_2O_3$ | 4.44 | 4.27 | 4.66 | 4.95 | 4.50 | 4.36 | 4.14 | 4.29 | 4.93 | 4.20 | 4.34 | 4.17 | 4.03 | 3.24 | 4.43 |
| NiO | 0.41 | 0.39 | 0.36 | 0.33 | 0.46 | 0.40 | 0.43 | 0.37 | 0.35 | 0.37 | 0.42 | 0.42 | 0.39 | 0.35 | 0.43 |
| Total | 83.73 | 85.35 | 85.77 | 85.85 | 85.70 | 85.73 | 85.68 | 85.72 | 85.54 | 85.42 | 85.90 | 85.65 | 84.54 | 83.68 | 85.75 |

Tab. A4.7 Sulfides microprobe analyses of Gomati chromitites.

| wt% | S | Ir | Os | As | Rh | Pt | Ru | Pd | Fe | Ni | Cu | Totale |
|---|---|---|---|---|---|---|---|---|---|---|---|---|
| | | | | | | Heazlewoodite ($Ni_3S_2$) | | | | | | |
| GO2-2 | 27.80 | 0.00 | 0.01 | 0.22 | 0.00 | 0.64 | 0.00 | 0.00 | 2.08 | 70.42 | 0.00 | 101.17 |
| GO2-2b | 27.67 | 0.12 | 0.00 | 0.18 | 0.02 | 0.00 | 0.00 | 0.02 | 0.30 | 71.07 | 0.00 | 99.39 |
| GO2-3b | 27.01 | 0.15 | 0.02 | 0.06 | 0.00 | 0.00 | 0.00 | 0.00 | 0.36 | 73.46 | 0.00 | 101.07 |
| GO3-1 | 27.94 | 0.00 | 0.00 | 0.00 | 0.00 | 0.63 | 0.00 | 0.00 | 0.68 | 71.15 | 0.00 | 100.39 |
| GOM2B-SULF-19 | 28.12 | n.a. | n.a. | n.a. | n.a. | n.a. | n.a. | n.a. | 0.23 | 72.35 | 0.06 | 100.75 |
| GOM2BSULF65 | 26.51 | n.a. | n.a. | n.a. | n.a. | n.a. | n.a. | n.a. | 0.09 | 72.59 | 0.04 | 99.23 |
| GOM2BSULF59 | 27.00 | n.a. | n.a. | n.a. | n.a. | n.a. | n.a. | n.a. | 0.10 | 73.48 | 0.05 | 100.67 |
| GOM2B-SULF-2 | 26.32 | n.a. | n.a. | n.a. | n.a. | n.a. | n.a. | n.a. | 0.14 | 74.17 | 0.09 | 100.77 |

| | | | | | | | | | | | | |
|---|---|---|---|---|---|---|---|---|---|---|---|---|
| GOM2BSULF67 | 26.52 | n.a. | n.a. | n.a. | n.a. | n.a. | n.a. | n.a. | 0.09 | 73.07 | 0.06 | 99.73 |
| GOM2B-SULF-11 | 25.78 | n.a. | n.a. | n.a. | n.a. | n.a. | n.a. | n.a. | 0.34 | 73.24 | 0.00 | 99.36 |
| GOM2BSULF61 | 26.27 | n.a. | n.a. | n.a. | n.a. | n.a. | n.a. | n.a. | 0.07 | 73.59 | 0.06 | 99.99 |
| GOM2B-SULF-39 | 26.12 | n.a. | n.a. | n.a. | n.a. | n.a. | n.a. | n.a. | 0.18 | 73.60 | 0.06 | 99.96 |
| GOM2B-SULF-28 | 26.00 | n.a. | n.a. | n.a. | n.a. | n.a. | n.a. | n.a. | 0.12 | 73.70 | 0.12 | 99.94 |
| GOM2BSULF64 | 26.28 | n.a. | n.a. | n.a. | n.a. | n.a. | n.a. | n.a. | 0.17 | 73.95 | 0.06 | 100.47 |
| GOM2B-SULF-43 | 25.72 | n.a. | n.a. | n.a. | n.a. | n.a. | n.a. | n.a. | 0.14 | 73.98 | 0.10 | 99.94 |
| GOM2B-SULF-24 | 25.86 | n.a. | n.a. | n.a. | n.a. | n.a. | n.a. | n.a. | 0.13 | 74.41 | 0.04 | 100.46 |
| GOM2B-SULF-17 | 25.79 | n.a. | n.a. | n.a. | n.a. | n.a. | n.a. | n.a. | 0.14 | 74.55 | 0.05 | 100.53 |
| GOM2B-SULF-25 | 25.49 | n.a. | n.a. | n.a. | n.a. | n.a. | n.a. | n.a. | 0.12 | 74.99 | 0.01 | 100.61 |
| GOM2B-SULF-12 | 25.91 | n.a. | n.a. | n.a. | n.a. | n.a. | n.a. | n.a. | 0.19 | 75.11 | 0.00 | 101.22 |
| GOM2B-SULF-36 | 25.83 | n.a. | n.a. | n.a. | n.a. | n.a. | n.a. | n.a. | 0.19 | 75.12 | 0.07 | 101.21 |
| GOM2B-SULF-33 | 25.78 | n.a. | n.a. | n.a. | n.a. | n.a. | n.a. | n.a. | 0.17 | 75.49 | 0.00 | 101.44 |
| GOM2B-SULF-5 | 26.25 | n.a. | n.a. | n.a. | n.a. | n.a. | n.a. | n.a. | 0.19 | 73.43 | 0.06 | 99.93 |
| GOM2C-SULF-2 | 25.50 | n.a. | n.a. | 0.00 | n.a. | n.a. | n.a. | n.a. | 1.19 | 72.64 | 0.04 | 99.48 |
| GOM2C-SULF-6 | 25.44 | n.a. | n.a. | 0.00 | n.a. | n.a. | n.a. | n.a. | 1.08 | 72.54 | 0.04 | 99.10 |
| GOM2C-SULF-7 | 25.63 | n.a. | n.a. | 0.00 | n.a. | n.a. | n.a. | n.a. | 1.05 | 72.75 | 0.00 | 99.46 |
| GR54A-SULF-1 | 27.50 | n.a. | n.a. | 1.01 | n.a. | n.a. | n.a. | n.a. | 3.12 | 60.51 | 0.43 | 92.80 |
| GR54A-SULF-2 | 25.45 | n.a. | n.a. | 0.17 | n.a. | n.a. | n.a. | n.a. | 1.82 | 70.26 | 0.05 | 97.76 |
| GR54A-SULF-3 | 23.85 | n.a. | n.a. | 0.15 | n.a. | n.a. | n.a. | n.a. | 2.61 | 67.23 | 0.00 | 93.85 |
| GR54A-SULF-4 | 25.63 | n.a. | n.a. | 0.00 | n.a. | n.a. | n.a. | n.a. | 0.40 | 72.45 | 0.04 | 98.54 |
| GR54A-SULF-5 | 25.49 | n.a. | n.a. | 0.33 | n.a. | n.a. | n.a. | n.a. | 0.23 | 72.81 | 0.08 | 99.85 |
| GR54A-SULF-6 | 25.94 | n.a. | n.a. | 0.00 | n.a. | n.a. | n.a. | n.a. | 0.61 | 71.56 | 0.04 | 98.17 |
| GR54A-SULF-7 | 25.70 | n.a. | n.a. | 0.00 | n.a. | n.a. | n.a. | n.a. | 0.64 | 71.74 | 0.03 | 98.11 |
| GR54A-SULF-8 | 25.61 | n.a. | n.a. | 0.00 | n.a. | n.a. | n.a. | n.a. | 1.23 | 71.63 | 0.04 | 98.50 |
| GR54A-SULF-9 | 25.55 | n.a. | n.a. | 0.00 | n.a. | n.a. | n.a. | n.a. | 0.22 | 74.23 | 0.03 | 100.03 |
| GR54A-SULF-10 | 25.51 | n.a. | n.a. | 0.00 | n.a. | n.a. | n.a. | n.a. | 0.25 | 69.02 | 0.05 | 94.92 |
| GR54A-SULF-11 | 20.67 | n.a. | n.a. | 0.00 | n.a. | n.a. | n.a. | n.a. | 0.32 | 60.08 | 0.01 | 81.09 |
| GR54A-SULF-12 | 26.87 | n.a. | n.a. | 0.00 | n.a. | n.a. | n.a. | n.a. | 0.19 | 73.08 | 0.07 | 100.22 |
| GR54D-SULF-1 | 26.82 | n.a. | n.a. | 0.00 | n.a. | n.a. | n.a. | n.a. | 1.20 | 73.41 | 0.00 | 101.43 |
| GR54D-SULF-4 | 25.41 | n.a. | n.a. | 0.00 | n.a. | n.a. | n.a. | n.a. | 1.23 | 70.89 | 0.04 | 97.58 |
| GR54D-SULF-5 | 25.76 | n.a. | n.a. | 0.00 | n.a. | n.a. | n.a. | n.a. | 0.48 | 73.41 | 0.04 | 99.81 |
| GR54D-SULF-9 | 25.60 | n.a. | n.a. | 0.00 | n.a. | n.a. | n.a. | n.a. | 0.32 | 72.87 | 0.07 | 98.89 |
| GR54D-SULF-7 | 25.63 | n.a. | n.a. | 0.00 | n.a. | n.a. | n.a. | n.a. | 2.93 | 69.15 | 0.28 | 98.04 |
| | | | | | | Millerite (NiS) | | | | | | |
| NR09-16 | 36.03 | 0.00 | 0.01 | 0.27 | 0.00 | 0.00 | 0.00 | 0.00 | 1.01 | 63.04 | 0.00 | 100.37 |
| NR09-18 | 36.74 | 0.00 | 0.00 | 0.29 | 0.00 | 0.00 | 0.00 | 0.03 | 1.44 | 61.92 | 0.00 | 100.42 |
| LIM1-4 | 33.46 | 0.00 | 0.00 | 0.67 | 0.03 | 0.12 | 0.00 | 0.06 | 0.90 | 65.72 | 0.00 | 100.96 |
| LIM3-7 | 34.96 | 0.00 | 0.00 | 0.23 | 0.08 | 0.00 | 0.00 | 0.00 | 0.83 | 63.05 | 0.00 | 99.14 |
| TRI10-3 | 35.65 | 0.66 | 0.00 | 0.07 | 0.00 | 0.36 | 0.00 | 0.00 | 2.30 | 62.80 | 0.00 | 101.83 |
| TRI10A-29c | 35.04 | 0.25 | 0.02 | 0.00 | 0.00 | 0.62 | 0.00 | 0.03 | 2.18 | 62.55 | 0.00 | 100.68 |
| GOM2A-SULF-6 | 28.16 | n.a. | n.a. | 1.22 | n.a. | n.a. | n.a. | n.a. | 3.26 | 64.40 | 0.75 | 97.88 |
| GOM2A-SULF-7 | 31.76 | n.a. | n.a. | 3.06 | n.a. | n.a. | n.a. | n.a. | 3.07 | 62.51 | 0.02 | 100.51 |
| GOM2A-SULF-8 | 32.45 | n.a. | n.a. | 0.00 | n.a. | n.a. | n.a. | n.a. | 2.91 | 61.62 | 0.03 | 97.16 |
| GOM2A-SULF-10 | 34.11 | n.a. | n.a. | 0.00 | n.a. | n.a. | n.a. | n.a. | 1.74 | 63.18 | 0.17 | 99.28 |
| GOM2A-SULF-11 | 32.00 | n.a. | n.a. | 0.81 | n.a. | n.a. | n.a. | n.a. | 1.07 | 61.62 | 0.32 | 95.83 |
| GOM2A-SULF-12 | 33.83 | n.a. | n.a. | 0.00 | n.a. | n.a. | n.a. | n.a. | 1.34 | 62.58 | 0.01 | 97.76 |
| GOM2A-SULF-13 | 34.15 | n.a. | n.a. | 0.02 | n.a. | n.a. | n.a. | n.a. | 1.38 | 63.26 | 0.09 | 98.90 |
| GOM2A-SULF-16 | 29.69 | n.a. | n.a. | 0.94 | n.a. | n.a. | n.a. | n.a. | 1.75 | 63.26 | 0.07 | 95.83 |

| | | | | | | | | | | | | |
|---|---|---|---|---|---|---|---|---|---|---|---|---|
| GOM2B-SULF-7 | 33.73 | n.a. | n.a. | 0.00 | n.a. | n.a. | n.a. | n.a. | 2.23 | 63.90 | 0.44 | 100.38 |
| GOM2B-SULF-9 | 31.10 | n.a. | n.a. | 0.00 | n.a. | n.a. | n.a. | n.a. | 1.42 | 67.99 | 0.18 | 100.70 |
| GOM2C-SULF-4 | 31.47 | n.a. | n.a. | 0.00 | n.a. | n.a. | n.a. | n.a. | 1.18 | 64.82 | 0.00 | 97.55 |
| GOM2C-SULF-5 | 33.48 | n.a. | n.a. | 0.00 | n.a. | n.a. | n.a. | n.a. | 1.12 | 62.15 | 0.03 | 96.77 |
| GOM2C-SULF-8 | 31.58 | n.a. | n.a. | 0.00 | n.a. | n.a. | n.a. | n.a. | 1.37 | 69.32 | 0.05 | 102.33 |
| GOM2C-SULF-9 | 30.79 | n.a. | n.a. | 0.00 | n.a. | n.a. | n.a. | n.a. | 1.33 | 69.00 | 0.08 | 101.25 |
| GR54D-SULF-2 | 31.20 | n.a. | n.a. | 0.53 | n.a. | n.a. | n.a. | n.a. | 2.18 | 62.33 | 0.18 | 96.76 |
| GR54D-SULF-3 | 30.74 | n.a. | n.a. | 0.07 | n.a. | n.a. | n.a. | n.a. | 1.03 | 67.35 | 0.04 | 99.22 |
| GR54D-SULF-6 | 32.28 | n.a. | n.a. | 0.00 | n.a. | n.a. | n.a. | n.a. | 0.36 | 61.15 | 0.11 | 93.98 |
| GR54D-SULF-8 | 34.50 | n.a. | n.a. | 0.01 | n.a. | n.a. | n.a. | n.a. | 0.48 | 61.53 | 0.09 | 96.63 |
| GR55-SULF-2 | 34.30 | n.a. | n.a. | 0.35 | n.a. | n.a. | n.a. | n.a. | 1.19 | 60.60 | 1.15 | 97.65 |
| Pentlandite ($(Ni,Fe)_9S_8$) | | | | | | | | | | | | |
| GO3-3 | 33.08 | 0.00 | 0.00 | 0.13 | 0.04 | 0.48 | 0.00 | 0.00 | 22.78 | 41.45 | 0.48 | 98.44 |
| LIM1-8 | 33.19 | 0.14 | 0.11 | 0.03 | 0.00 | 0.19 | 0.00 | 0.00 | 23.91 | 39.50 | 0.00 | 97.08 |
| TRI10-2 | 37.47 | 0.00 | 0.00 | 0.05 | 0.00 | 0.00 | 0.00 | 0.00 | 14.66 | 48.17 | 0.00 | 100.35 |
| TRI10-5b | 33.22 | 0.48 | 0.00 | 0.01 | 1.10 | 0.31 | 0.00 | 0.02 | 22.52 | 42.17 | 0.02 | 99.85 |
| TRI10-10c | 34.51 | 0.19 | 0.04 | 0.00 | 0.08 | 0.00 | 0.00 | 0.06 | 22.67 | 42.23 | 0.00 | 99.77 |
| TRI10-12c | 33.91 | 0.47 | 0.00 | 0.00 | 0.79 | 0.14 | 0.00 | 0.00 | 22.26 | 41.55 | 0.01 | 99.13 |
| NR06-15 | 36.91 | 0.00 | 0.00 | 0.26 | 0.04 | 0.68 | 0.00 | 0.00 | 13.36 | 48.31 | 0.41 | 99.97 |
| TRI10A-19 | 32.26 | 0.24 | 0.00 | 0.06 | 0.01 | 0.00 | 0.00 | 0.00 | 27.81 | 38.25 | 0.00 | 98.63 |
| TRI10A-20 | 32.49 | 0.57 | 0.00 | 0.01 | 0.45 | 0.72 | 0.00 | 0.08 | 24.86 | 40.22 | 0.00 | 99.40 |
| TRI10A-22b | 32.02 | 0.04 | 0.06 | 0.00 | 0.45 | 0.05 | 0.00 | 0.02 | 21.31 | 43.54 | 0.00 | 97.49 |
| TRI10A-29d | 31.88 | 0.21 | 0.00 | 0.00 | 0.00 | 0.00 | 0.00 | 0.10 | 25.80 | 39.82 | 0.00 | 97.80 |
| GOM2A-SULF-9 | 31.93 | n.a. | n.a. | 0.00 | n.a. | n.a. | n.a. | n.a. | 22.16 | 43.61 | 0.00 | 98.02 |
| GOM2B-SULF-6 | 32.24 | n.a. | n.a. | 0.00 | n.a. | n.a. | n.a. | n.a. | 21.14 | 45.22 | 0.00 | 99.10 |
| Godlevskite ($(Ni,Fe)_9S_8$) | | | | | | | | | | | | |
| NR06-12 | 32.31 | 0.40 | 0.02 | 0.38 | 0.04 | 0.11 | 0.00 | 0.00 | 8.60 | 56.12 | 0.00 | 97.97 |
| Chalcocite ($Cu_2S$) | | | | | | | | | | | | |
| GO3-3b | 21.09 | 0.00 | 0.00 | 0.00 | 0.00 | 0.00 | 0.00 | 0.02 | 1.65 | 0.26 | 76.77 | 99.78 |
| GOM2A-SULF-14 | 21.41 | n.a. | n.a. | 0.00 | n.a. | n.a. | n.a. | n.a. | 1.20 | 1.88 | 72.03 | 96.52 |
| GOM2B-SULF-10 | 20.25 | n.a. | n.a. | 0.00 | n.a. | n.a. | n.a. | n.a. | 3.24 | 0.00 | 72.00 | 95.50 |
| GOM2B-SULF-2 | 21.05 | n.a. | n.a. | 0.00 | n.a. | n.a. | n.a. | n.a. | 1.27 | 0.00 | 69.63 | 91.94 |
| GOM2B-SULF-62 | 20.66 | n.a. | n.a. | 0.00 | n.a. | n.a. | n.a. | n.a. | 1.07 | 0.00 | 79.58 | 101.33 |
| GOM2B-SULF-63 | 23.69 | n.a. | n.a. | 0.00 | n.a. | n.a. | n.a. | n.a. | 1.13 | 0.00 | 77.08 | 101.91 |
| GOM2B-SULF-57 | 22.93 | n.a. | n.a. | 0.00 | n.a. | n.a. | n.a. | n.a. | 1.14 | 0.00 | 76.81 | 100.88 |
| Pyrite ($FeS_2$) | | | | | | | | | | | | |
| TRI10A-29b | 51.77 | 0.00 | 0.00 | 0.08 | 0.06 | 0.00 | 0.00 | 0.00 | 44.67 | 2.08 | 0.00 | 98.65 |
| unknown | | | | | | | | | | | | |
| LIM3-9 | 31.46 | 0.00 | 0.00 | 1.17 | 0.00 | 0.00 | 0.01 | 0.01 | 5.57 | 26.67 | 33.65 | 98.53 |
| GOM2C-SULF-1 | 32.74 | n.a. | n.a. | 0.00 | n.a. | n.a. | n.a. | n.a. | 4.23 | 33.95 | 23.73 | 95.14 |

Tab. A4.8 Arsenides microprobe analyses of Gomati chromitites.

| wt% | As | S | Ir | Pt | Ni | Fe | Cu | Sb | Total |
|---|---|---|---|---|---|---|---|---|---|
| Maucherite ($Ni_{11}As_8$) | | | | | | | | | |
| GOM2A-SULF-1 | 44.758 | 0.509 | na | na | 49.156 | 1.798 | 0.03 | 1.01 | 97.281 |
| GOM2C-SULF-10 | 46.238 | 0.141 | na | na | 51.284 | 1.329 | 0.06 | 1.562 | 100.614 |
| GR54C-SULF-2 | 45.535 | 0.15 | na | na | 54.387 | 0.286 | 0.048 | 2.719 | 103.207 |
| GR54C-SULF-3 | 45.848 | 0.19 | na | na | 52.535 | 0.171 | 0 | 2.544 | 101.338 |

| | | | | | | | | | |
|---|---|---|---|---|---|---|---|---|---|
| GR54C-SULF-6 | 45.609 | 0.209 | na | na | 52.522 | 0.158 | 0.055 | 2.578 | 101.196 |
| | | | | Nickeline (NiAs) | | | | | |
| GOM2A-SULF-4 | 50.603 | 0.405 | na | na | 41.557 | 1.894 | 0.007 | 3.161 | 97.636 |
| GOM2A-SULF-5 | 52.283 | 0.413 | na | na | 42.909 | 1.45 | 0 | 3.271 | 100.338 |
| GR55-SULF-1 | 54.569 | 0.16 | na | na | 41.303 | 1.09 | 0 | 0.297 | 97.419 |
| LIM1-9 | 55.03 | 0.7381 | 0 | 0.6935 | 42.26 | 1.35 | 0 | n.a. | 100.0716 |
| LIM3-6 | 55.67 | 0.0194 | 0.2487 | 0.2586 | 40.58 | 1.51 | 0 | n.a. | 98.2867 |
| TRI10-10d | 56.46 | 0.428 | 0.1377 | 0 | 42.34 | 1.22 | 0 | n.a. | 100.5857 |
| TRI10A-1 | 55.02 | 0 | 0 | 0 | 40.16 | 2.71 | 0 | n.a. | 97.89 |
| | | | | Dinerite* ($Ni_3(As,Sb)$) | | | | | |
| GOM2BSULF60 | 31.713 | 0 | na | na | 68.585 | 0.164 | 0.171 | 0.912 | 101.545 |
| GOM2B-SULF-32 | 32.09245 | 0 | na | na | 69.27934 | 0.1358 | 0.11058 | 1.17952 | 102.79769 |
| GOM2B-SULF-13 | 31.51724 | 0 | na | na | 67.4053 | 0.13095 | 0.09603 | 0.78182 | 99.93134 |
| GOM2B-SULF-10 | 31.90815 | 0.01746 | na | na | 67.69824 | 0.08536 | 0.16587 | 0.88367 | 100.75875 |
| GOM2B-SULF-42 | 32.10118 | 0.00388 | na | na | 68.07169 | 0.12707 | 0.12804 | 0.80122 | 101.23308 |
| GOM2B-SULF-9 | 31.46583 | 0 | na | na | 66.54103 | 0.0388 | 0.15326 | 0.86524 | 99.0661 |
| GOM2B-SULF-18 | 31.672 | 0.023 | na | na | 65.328 | 0.234 | 0.252 | 1.551 | 99.06 |
| GOM2BSULF68 | 32.18516 | 0 | na | na | 66.37932 | 0.13622 | 0.59584 | 0.75068 | 100.04722 |
| GOM2BSULF71 | 32.003 | 0 | na | na | 65.43 | 0.168 | 0.279 | 1.898 | 99.782 |
| GOM2BSULF66 | 32.05268 | 0.02328 | na | na | 65.99007 | 0.0582 | 0.14453 | 1.20086 | 99.46962 |
| | | | | $Ni_5(As,Sb)_2$ | | | | | |
| GOM2B-SULF-27 | 32.89852 | 0.01261 | na | na | 66.38098 | 0.09894 | 0.2231 | 1.1737 | 100.78785 |
| GOM2B-SULF-53 | 33.86228 | 0.02987 | na | na | 65.6419 | 0.12463 | 0.12463 | 0.68701 | 100.47032 |
| GOM2B-SULF-52 | 34.1857 | 0.00515 | na | na | 65.15059 | 0.10712 | 0.20291 | 0.70555 | 100.35702 |
| GOM2BSULF69 | 32.84925 | 0.03255 | na | na | 64.77345 | 0.1722 | 0.13965 | 1.7976 | 99.7794 |
| | | | | Orcelite ($Ni_{5-x}(As,Sb)_2$), x = 0.23 | | | | | |
| GOM2B-SULF-38 | 35.707 | 0.029 | na | na | 64.908 | 0.197 | 0.044 | 0.746 | 101.631 |
| GOM2B-SULF-45 | 34.6983 | 0.00735 | na | na | 64.71045 | 0.2331 | 0.13755 | 0.7077 | 100.49445 |
| GOM2B-SULF-41 | 35.214 | 0 | na | na | 64.549 | 0.252 | 0.147 | 0.651 | 100.817 |
| GOM2B-SULF-47 | 35.3262 | 0.04305 | na | na | 62.5233 | 0.20265 | 0.063 | 1.6443 | 99.8025 |
| GOM2B-SULF-49 | 34.60158 | 0.02756 | na | na | 65.04478 | 0.14946 | 0.1855 | 0.70596 | 100.71484 |
| GOM2B-SULF-54 | 34.3455 | 0.0105 | na | na | 62.8908 | 0.12705 | 0.3297 | 1.7682 | 99.47175 |
| GOM2B-SULF-58 | 35.80408 | 0.01768 | na | na | 63.36824 | 0.26208 | 0.06344 | 0.82368 | 100.3392 |
| GOM2A-SULF-2 | 34.516 | 0.018 | na | na | 62.249 | 1.358 | 0.955 | 1.187 | 100.283 |
| GOM2A-SULF-3 | 34.503 | 0 | na | na | 61.908 | 1.313 | 0.994 | 1.194 | 99.912 |
| GOM2B-SULF-55 | 32.978 | 0.02 | na | na | 57.71 | 0.266 | 0.079 | 1.12 | 92.182 |

Tab. A4.9 PGM microprobe analyses of Gomati chromitites.

| wt% | S | Ir | Os | As | Rh | Pt | Ru | Pd | Fe | Ni | Cu | Totale |
|---|---|---|---|---|---|---|---|---|---|---|---|---|
| | | | | | laurite ($RuS_2$) - erlichmanite ($OsS_2$) | | | | | | | |
| GO2-4 | 34.35 | 3.05 | 16.11 | 3.12 | 0 | 0 | 42.97 | 0 | 0.9504 | 0.2439 | 0 | 100.7943 |
| TRI10-4 | 34.73 | 3.49 | 21.23 | 0.7785 | 0 | 0 | 37.72 | 0 | 0.8562 | 0.1343 | 0 | 98.939 |
| TRI10-9 | 28.64 | 0 | 55.59 | 0.2712 | 0 | 0 | 11.43 | 0 | 1.07 | 0 | 0 | 97.0012 |
| TRI10-9b | 35.11 | 4.35 | 18.98 | 0.8813 | 0 | 0 | 38.42 | 0 | 1.57 | 0.097 | 0.0337 | 99.442 |
| TRI10-10 | 36.71 | 3.75 | 11.98 | 1.16 | 0 | 0 | 46.37 | 0 | 0.8777 | 0.2431 | 0.0488 | 101.1396 |
| TRI10-10b | 35.11 | 4.66 | 17.97 | 1.06 | 0 | 0 | 40.45 | 0 | 1.24 | 0.1757 | 0 | 100.6657 |
| TRI10-11b | 36.01 | 0.7379 | 17.28 | 1.02 | 0 | 0 | 43.6 | 0 | 1.13 | 0.1321 | 0.0181 | 99.9281 |
| TRI10-12b | 34 | 5.05 | 26.46 | 0.6291 | 0 | 0 | 32.24 | 0 | 1.21 | 0.1522 | 0.0243 | 99.7656 |

| | | | | | | | | | | | | |
|---|---|---|---|---|---|---|---|---|---|---|---|---|
| TRI10-13 | 34.59 | 3.27 | 17.98 | 2.75 | 0 | 0 | 41.73 | 0 | 0.4691 | 0 | 0 | 100.7891 |
| GOM2B2-11 | 32.17 | 2.88 | 19.87 | 3.37 | 0 | 0 | 40.47 | 0 | 0.7453 | 0.1095 | 0 | 99.6148 |
| TRI10A-2 | 31.22 | 3.72 | 33.15 | 0.9221 | 0 | 0 | 24.24 | 0 | 1.55 | 0.0687 | 0.0525 | 94.9233 |
| TRI10A-3 | 33.76 | 1.29 | 21.98 | 1.56 | 0 | 0 | 37.51 | 0 | 1.28 | 0.368 | 0 | 97.748 |
| TRI10A-14 | 33.49 | 4.25 | 22.3 | 1.28 | 0 | 0 | 35.9 | 0 | 0.8605 | 0.0775 | 0 | 98.158 |
| TRI10A-16 | 32.33 | 3.12 | 23.02 | 1.17 | 0 | 0 | 36.26 | 0 | 0.8557 | 0.1553 | 0 | 96.911 |
| TRI10A-31 | 33.5 | 3.87 | 19.77 | 1.35 | 0 | 0 | 39.37 | 0 | 0.8525 | 0.1433 | 0.0069 | 98.8627 |
| TRI10A-32 | 33.47 | 4.47 | 19.48 | 1.27 | 0 | 0 | 38.32 | 0 | 1.01 | 0.1297 | 0 | 98.1497 |
| GOM2A-PGM-1 | 33.67 | 6.03 | 11.6 | 1.48 | 0.4081 | 0 | 40.35 | 1.46 | n.a. | n.a. | n.a. | 94.9981 |
| GOM2A-PGM-2 | 33.8 | 5.91 | 11.66 | 1.36 | 0.589 | 0 | 40.62 | 1.53 | n.a. | n.a. | n.a. | 95.469 |
| GOM2A-PGM-3 | 34.08 | 8.41 | 20.26 | 1.18 | 1.5 | 0 | 34.82 | 1.39 | n.a. | n.a. | n.a. | 101.64 |
| GOM2A-PGM-4 | 33.99 | 8.12 | 20.3 | 1.21 | 1.37 | 0 | 34.73 | 1.28 | n.a. | n.a. | n.a. | 101 |
| GOM2A-PGM-5 | 33.9 | 8.46 | 20.15 | 1.16 | 1.56 | 0 | 34.77 | 1.24 | n.a. | n.a. | n.a. | 101.24 |
| GOM2A-PGM-6 | 33.98 | 2.17 | 23.9 | 1.2 | 0.8153 | 0 | 37.71 | 1.28 | n.a. | n.a. | n.a. | 101.0553 |
| GOM2A-PGM-7 | 33.94 | 2.15 | 23.88 | 1.24 | 0.7004 | 0 | 38.22 | 1.37 | n.a. | n.a. | n.a. | 101.5004 |
| GOM2A-PGM-8 | 32.77 | 3.14 | 18.23 | 3.79 | 0.702 | 0 | 41.55 | 1.47 | n.a. | n.a. | n.a. | 101.652 |
| GOM2A-PGM-9 | 33.36 | 3.46 | 18.64 | 3.44 | 0.7807 | 0 | 41.02 | 1.38 | n.a. | n.a. | n.a. | 102.0807 |
| GOM2A-PGM-10 | 31.8 | 7.67 | 15.25 | 1.45 | 1.67 | 0 | 35.15 | 1.27 | n.a. | n.a. | n.a. | 94.26 |
| GOM2A-PGM-11 | 32.04 | 7.57 | 15.06 | 1.52 | 1.99 | 0 | 36.3 | 1.32 | n.a. | n.a. | n.a. | 95.8 |
| GOM2A-PGM-14 | 32.65 | 7.07 | 22.09 | 1.47 | 1.25 | 0 | 32.34 | 1.11 | n.a. | n.a. | n.a. | 97.98 |
| GOM2A-PGM-15 | 31.88 | 7.01 | 22.38 | 1.31 | 1.08 | 0 | 32.96 | 1.09 | n.a. | n.a. | n.a. | 97.71 |
| GOM2A-PGM-16 | 34.36 | 4.1 | 21.87 | 1.35 | 1.16 | 0 | 35.91 | 1.33 | n.a. | n.a. | n.a. | 100.08 |
| GOM2A-PGM-17 | 34.51 | 4.44 | 21.43 | 1.37 | 0.8708 | 0 | 36.06 | 1.29 | n.a. | n.a. | n.a. | 99.9708 |
| CENTER1 GOM2B | 33.23 | 5.75 | 17.08 | 1.52 | 0.7462 | 0 | 33.08 | 1.21 | n.a. | n.a. | n.a. | 92.6162 |
| CENTER2 GOM2B | 33.59 | 5.76 | 17.9 | 1.51 | 0.7425 | 0 | 34.22 | 1.16 | n.a. | n.a. | n.a. | 94.8825 |
| CENTER3 GOM2B | 34.37 | 1.8 | 19.64 | 1.92 | 0.8943 | 0 | 40.19 | 1.25 | n.a. | n.a. | n.a. | 100.0643 |
| CENTER4 GOM2B | 32.53 | 1.29 | 20.3 | 1.45 | 1.04 | 0 | 37.35 | 1.27 | n.a. | n.a. | n.a. | 95.23 |
| GOM2C-PGM-1 | 33.21 | 6.14 | 23.91 | 1.12 | 1.13 | 0 | 34.14 | 1.31 | n.a. | n.a. | n.a. | 100.96 |
| GOM2C-PGM-2 | 33.75 | 5.72 | 23.96 | 1.08 | 1.04 | 0 | 34 | 1.02 | n.a. | n.a. | n.a. | 100.57 |
| GOM2C-PGM-3 | 33.87 | 7.59 | 17.76 | 1.32 | 1.35 | 0 | 38.16 | 1.36 | n.a. | n.a. | n.a. | 101.41 |
| GOM2C-PGM-4 | 34.12 | 7.72 | 17.99 | 1.33 | 1.21 | 0 | 37.81 | 1.27 | n.a. | n.a. | n.a. | 101.45 |
| GOM2C-PGM-5 | 32.3 | 7.43 | 26.79 | 1.18 | 0.982 | 0 | 31.77 | 1.09 | n.a. | n.a. | n.a. | 101.542 |
| GOM2C-PGM-6 | 32.6 | 7.03 | 26.32 | 1.06 | 0.9232 | 0 | 31.33 | 1.13 | n.a. | n.a. | n.a. | 100.3932 |
| GR54A-PGM-2 | 33.02 | 7.18 | 21.64 | 1.39 | 1.29 | 0 | 34.36 | 1.07 | n.a. | n.a. | n.a. | 99.95 |
| GR54A-PGM-3 | 32.25 | 7.19 | 20.54 | 1.09 | 1.11 | 0 | 33.42 | 1.21 | n.a. | n.a. | n.a. | 96.81 |
| GR54C-PGM-1 | 34.62 | 6.55 | 18.01 | 1.33 | 1.06 | 0 | 38.72 | 1.31 | n.a. | n.a. | n.a. | 101.6 |
| GR54C-PGM-2 | 34.91 | 6.64 | 17.72 | 1.3 | 1.09 | 0 | 37.77 | 1.52 | n.a. | n.a. | n.a. | 100.95 |
| GR54D-PGM-1 | 33.78 | 9.3 | 17.33 | 1.47 | 1.44 | 0 | 35.9 | 1.37 | n.a. | n.a. | n.a. | 100.59 |
| GR54D-PGM-2 | 33.99 | 9.26 | 17.41 | 1.48 | 1.4 | 0 | 36.32 | 1.43 | n.a. | n.a. | n.a. | 101.29 |
| GR54D-PGM-3 | 31.56 | 6.62 | 15.77 | 1.06 | 1.54 | 0 | 36.66 | 1.42 | n.a. | n.a. | n.a. | 94.63 |
| GR54D-PGM-4 | 32.32 | 6.82 | 15.61 | 1.04 | 1.79 | 0 | 35.48 | 1.3 | n.a. | n.a. | n.a. | 94.36 |
| GR54D-PGM-5 | 32.91 | 6.36 | 21.76 | 1.14 | 1.22 | 0 | 34.47 | 1.15 | n.a. | n.a. | n.a. | 99.01 |
| GR54D-PGM-6 | 32.94 | 6.31 | 22.05 | 1.25 | 1.29 | 0 | 34.89 | 1.23 | n.a. | n.a. | n.a. | 99.96 |
| GR54D-PGM-8 | 33.91 | 8.21 | 16.51 | 1.45 | 1.97 | 0 | 36.34 | 1.4 | n.a. | n.a. | n.a. | 99.79 |

| | | | | | | | | | | | | |
|---|---|---|---|---|---|---|---|---|---|---|---|---|
| GR54D-PGM-9 | 34.15 | 8.09 | 16.08 | 1.37 | 1.91 | 0 | 35.78 | 1.45 | n.a. | n.a. | n.a. | 98.83 |
| GR54D-PGM-10 | 32.79 | 9.74 | 19.27 | 1.06 | 1.23 | 0 | 33.46 | 1.08 | n.a. | n.a. | n.a. | 98.63 |
| | | | | | | unknown | | | | | | |
| TRI10-5 | 26.36 | 38.85 | 0 | 0 | 2.05 | 0.6872 | 0 | 0 | 7.98 | 17.41 | 6.12 | 99.4572 |
| TRI10-6b | 26.47 | 37.43 | 0 | 0 | 2.45 | 0.873 | 0 | 0 | 8.69 | 17.88 | 5.97 | 99.763 |
| TRI10-12 | 26.9 | 33.62 | 0 | 0 | 4.06 | 2.02 | 0 | 0.1099 | 8 | 18.13 | 6.26 | 99.0999 |
| TRI10A-22 | 24.88 | 33.94 | 0.0618 | 0 | 0.9348 | 8.11 | 0 | 0 | 7.92 | 16.11 | 5.88 | 97.8366 |
| | | | | | | Ru-iridsdite | | | | | | |
| TRI10A-29 | 35.93 | 22.09 | 4.55 | 1.07 | 0 | 0 | 29.09 | 0 | 4.66 | 3.33 | 1.48 | 102.2 |

Tab. A4.10 Spinels microprobe analyses of Skyros chromitites.

| wt% | SK3A-1 | SK3A-2 | SK3A-3 | SK3A-5 | SK3A-6 | SK3A-8 | SK3A-12 | SK3A-14 | SK3A-15 | SK3A-18 | SK3A-19 | SK3A-20 | SK3A-21 | SK3A-22 | SK3A-23 | SK3A-24 | SK3A-27 | SK3A-28 | SK3A-29 |
|---|---|---|---|---|---|---|---|---|---|---|---|---|---|---|---|---|---|---|---|
| $TiO_2$ | 0.27 | 0.21 | 0.23 | 0.22 | 0.22 | 0.25 | 0.22 | 0.24 | 0.27 | 0.26 | 0.22 | 0.26 | 0.28 | 0.23 | 0.24 | 0.24 | 0.32 | 0.30 | 0.23 |
| $Al_2O_3$ | 12.62 | 12.60 | 12.74 | 12.57 | 12.82 | 12.71 | 12.85 | 12.76 | 12.83 | 13.04 | 12.94 | 12.82 | 12.79 | 12.90 | 12.87 | 4.95 | 12.74 | 12.63 | 12.72 |
| $Cr_2O_3$ | 56.29 | 56.47 | 55.62 | 55.53 | 55.74 | 54.83 | 55.83 | 56.41 | 55.31 | 56.33 | 56.26 | 56.63 | 55.44 | 55.48 | 55.91 | 52.87 | 55.98 | 55.57 | 55.09 |
| $Fe_2O_3$ | 0.79 | 0.54 | 0.96 | 1.18 | 0.96 | 1.33 | 0.59 | 0.29 | 0.70 | 0.00 | 0.26 | 0.01 | 0.69 | 0.48 | 0.54 | 8.84 | 0.16 | 0.47 | 0.51 |
| FeO | 14.93 | 14.80 | 14.76 | 14.51 | 14.89 | 15.49 | 15.20 | 15.40 | 15.12 | 15.89 | 16.04 | 16.63 | 16.33 | 15.83 | 16.31 | 20.77 | 16.14 | 16.45 | 16.48 |
| MnO | 0.06 | 0.02 | 0.10 | 0.09 | 0.09 | 0.04 | 0.00 | 0.09 | 0.02 | 0.00 | 0.09 | 0.09 | 0.07 | 0.00 | 0.16 | 1.70 | 0.00 | 0.02 | 0.00 |
| MgO | 11.97 | 11.99 | 11.98 | 12.07 | 11.92 | 11.45 | 11.73 | 11.67 | 11.69 | 11.43 | 11.27 | 10.97 | 11.06 | 11.35 | 11.08 | 7.22 | 11.18 | 10.98 | 10.91 |
| Tot | 96.93 | 96.63 | 96.43 | 96.18 | 96.62 | 96.10 | 96.43 | 96.89 | 95.94 | 97.00 | 97.08 | 97.41 | 96.69 | 96.32 | 97.13 | 97.61 | 96.51 | 96.46 | 96.04 |
| Ti | 0.01 | 0.01 | 0.01 | 0.01 | 0.01 | 0.01 | 0.01 | 0.01 | 0.01 | 0.01 | 0.01 | 0.01 | 0.01 | 0.01 | 0.01 | 0.01 | 0.01 | 0.01 | 0.01 |
| Al | 0.49 | 0.49 | 0.50 | 0.49 | 0.50 | 0.50 | 0.50 | 0.50 | 0.51 | 0.51 | 0.51 | 0.50 | 0.50 | 0.51 | 0.50 | 0.21 | 0.50 | 0.50 | 0.50 |
| Cr | 1.47 | 1.48 | 1.46 | 1.46 | 1.46 | 1.45 | 1.47 | 1.48 | 1.46 | 1.48 | 1.48 | 1.49 | 1.46 | 1.47 | 1.47 | 1.47 | 1.48 | 1.47 | 1.46 |
| $Fe_{3+}$ | 0.02 | 0.01 | 0.02 | 0.03 | 0.02 | 0.03 | 0.01 | 0.01 | 0.02 | 0.00 | 0.01 | 0.00 | 0.02 | 0.01 | 0.01 | 0.23 | 0.00 | 0.01 | 0.01 |
| $Fe_{2+}$ | 0.41 | 0.41 | 0.41 | 0.40 | 0.41 | 0.43 | 0.42 | 0.43 | 0.42 | 0.44 | 0.45 | 0.46 | 0.46 | 0.44 | 0.45 | 0.61 | 0.45 | 0.46 | 0.46 |
| Mn | 0.00 | 0.00 | 0.00 | 0.00 | 0.00 | 0.00 | 0.00 | 0.00 | 0.00 | 0.00 | 0.00 | 0.00 | 0.00 | 0.00 | 0.00 | 0.05 | 0.00 | 0.00 | 0.00 |
| Mg | 0.59 | 0.59 | 0.59 | 0.60 | 0.59 | 0.57 | 0.58 | 0.58 | 0.58 | 0.57 | 0.56 | 0.54 | 0.55 | 0.57 | 0.55 | 0.38 | 0.56 | 0.55 | 0.55 |

| wt% | SK3A-31 | SK3A-32 | SK3A-34 | SK3A-36 | SK3A-38 | SK3A-39 | SK3A-40 | SK3A-41 | SK3A-42 | SK3A-43 | SK3E-1 | SK3E-2 | SK3E-3 | SK3E-4 | SK3E-5 | SK3E-12 | SK3E-16 | SK3E-20 | SK3H-2 |
|---|---|---|---|---|---|---|---|---|---|---|---|---|---|---|---|---|---|---|---|
| $TiO_2$ | 0.26 | 0.20 | 0.23 | 0.25 | 0.28 | 0.26 | 0.25 | 0.23 | 0.19 | 0.27 | 0.28 | 0.30 | 0.31 | 0.27 | 0.28 | 0.00 | 0.00 | 0.02 | 0.23 |
| $Al_2O_3$ | 12.68 | 12.91 | 12.33 | 13.09 | 11.99 | 12.36 | 12.17 | 12.65 | 12.75 | 12.40 | 18.19 | 18.24 | 17.95 | 18.07 | 18.10 | 0.00 | 0.00 | 0.05 | 13.80 |
| $Cr_2O_3$ | 54.97 | 55.13 | 54.70 | 55.30 | 55.21 | 55.79 | 55.08 | 55.36 | 55.81 | 55.98 | 46.66 | 46.64 | 46.74 | 46.50 | 46.24 | 0.07 | 0.22 | 0.72 | 55.50 |
| $Fe_2O_3$ | 0.59 | 0.62 | 1.82 | 0.31 | 0.00 | 0.00 | 1.03 | 0.50 | 0.74 | 0.44 | 2.62 | 2.54 | 2.38 | 2.69 | 3.00 | 73.21 | 73.40 | 74.06 | 0.00 |
| FeO | 16.20 | 16.21 | 16.67 | 16.39 | 17.08 | 16.52 | 16.63 | 16.08 | 16.23 | 16.16 | 20.92 | 21.10 | 20.76 | 20.84 | 21.33 | 32.73 | 32.73 | 33.54 | 16.27 |
| MnO | 0.10 | 0.05 | 0.46 | 0.00 | 0.17 | 0.18 | 0.03 | 0.08 | 0.19 | 0.07 | 0.18 | 0.09 | 0.10 | 0.19 | 0.23 | 0.13 | 0.21 | 0.10 | 0.08 |
| MgO | 11.12 | 10.98 | 10.57 | 10.98 | 10.68 | 10.65 | 10.69 | 11.00 | 11.01 | 11.02 | 8.73 | 8.64 | 8.72 | 8.62 | 8.44 | 0.11 | 0.12 | 0.10 | 10.77 |
| Tot | 96.11 | 96.13 | 96.87 | 96.32 | 95.99 | 96.43 | 95.95 | 95.92 | 96.92 | 96.34 | 97.62 | 97.56 | 96.96 | 97.19 | 97.69 | 106.28 | 106.70 | 108.63 | 96.64 |
| Ti | 0.01 | 0.00 | 0.01 | 0.01 | 0.01 | 0.01 | 0.01 | 0.01 | 0.00 | 0.01 | 0.01 | 0.01 | 0.01 | 0.01 | 0.01 | 0.00 | 0.00 | 0.00 | 0.01 |
| Al | 0.50 | 0.51 | 0.49 | 0.52 | 0.48 | 0.49 | 0.48 | 0.50 | 0.50 | 0.49 | 0.71 | 0.71 | 0.70 | 0.70 | 0.70 | 0.00 | 0.00 | 0.00 | 0.54 |
| Cr | 1.46 | 1.46 | 1.45 | 1.46 | 1.47 | 1.48 | 1.47 | 1.47 | 1.47 | 1.48 | 1.21 | 1.21 | 1.22 | 1.22 | 1.20 | 0.00 | 0.01 | 0.02 | 1.46 |
| $Fe_{3+}$ | 0.01 | 0.02 | 0.05 | 0.01 | 0.00 | 0.00 | 0.03 | 0.01 | 0.02 | 0.01 | 0.06 | 0.06 | 0.06 | 0.07 | 0.07 | 2.00 | 1.99 | 1.97 | 0.00 |
| $Fe_{2+}$ | 0.45 | 0.45 | 0.47 | 0.46 | 0.48 | 0.46 | 0.47 | 0.45 | 0.45 | 0.45 | 0.58 | 0.58 | 0.57 | 0.58 | 0.59 | 0.99 | 0.99 | 0.99 | 0.45 |
| Mn | 0.00 | 0.00 | 0.01 | 0.00 | 0.00 | 0.00 | 0.00 | 0.00 | 0.01 | 0.00 | 0.01 | 0.00 | 0.00 | 0.01 | 0.01 | 0.00 | 0.01 | 0.00 | 0.00 |
| Mg | 0.56 | 0.55 | 0.53 | 0.55 | 0.54 | 0.53 | 0.54 | 0.55 | 0.55 | 0.55 | 0.43 | 0.42 | 0.43 | 0.42 | 0.41 | 0.01 | 0.01 | 0.01 | 0.53 |

| wt% | SK3H-3 | SK3H-4 | SK3H-6 | SK3H-7 | SK3H-8 | SK3H-9 | SK3H-10 | SK3H-11 | SK3H-12 | SK3H-13 | SK3H-14 | SK3H-15 | SK3H-17 | SK3H-18 | SK3H-19 | SK3H-20 | SK3H-21 | SK3H-23 | SK3H-25 |
|---|---|---|---|---|---|---|---|---|---|---|---|---|---|---|---|---|---|---|---|
| $TiO_2$ | 0.24 | 0.22 | 0.23 | 0.18 | 0.18 | 0.19 | 0.25 | 0.16 | 0.21 | 0.29 | 0.21 | 0.25 | 0.28 | 0.24 | 0.27 | 0.27 | 0.20 | 0.24 | 0.19 |
| $Al_2O_3$ | 13.98 | 13.02 | 14.00 | 11.52 | 12.25 | 12.92 | 13.08 | 11.67 | 12.74 | 13.41 | 13.68 | 13.87 | 13.79 | 13.72 | 13.79 | 13.77 | 14.33 | 14.41 | 14.15 |
| $Cr_2O_3$ | 55.70 | 54.60 | 55.27 | 57.33 | 56.89 | 56.06 | 55.78 | 58.03 | 56.36 | 55.11 | 55.00 | 55.84 | 55.60 | 55.42 | 55.48 | 55.27 | 54.78 | 54.71 | 54.56 |
| $Fe_2O_3$ | 0.00 | 1.12 | 0.00 | 0.00 | 0.00 | 0.00 | 0.00 | 0.17 | 0.00 | 0.00 | 0.03 | 0.00 | 0.00 | 0.00 | 0.00 | 0.00 | 0.00 | 0.00 | 0.01 |
| FeO | 15.71 | 17.32 | 15.70 | 17.63 | 16.57 | 16.44 | 16.31 | 17.25 | 16.70 | 16.78 | 16.64 | 16.36 | 16.73 | 16.56 | 16.42 | 16.68 | 15.93 | 16.03 | 16.40 |
| MnO | 0.14 | 0.50 | 0.06 | 0.30 | 0.14 | 0.00 | 0.01 | 0.20 | 0.02 | 0.15 | 0.10 | 0.10 | 0.15 | 0.10 | 0.02 | 0.09 | 0.09 | 0.06 | 0.12 |
| MgO | 10.84 | 10.18 | 10.76 | 10.02 | 10.50 | 10.65 | 10.90 | 10.41 | 10.42 | 10.66 | 10.90 | 10.88 | 10.65 | 10.65 | 10.92 | 10.83 | 10.94 | 11.03 | 11.02 |
| Tot | 96.63 | 97.01 | 96.03 | 97.23 | 96.54 | 96.30 | 96.41 | 97.88 | 96.44 | 96.41 | 96.62 | 97.32 | 97.19 | 96.70 | 96.90 | 96.96 | 96.28 | 96.50 | 96.49 |
| Ti | 0.01 | 0.01 | 0.01 | 0.00 | 0.00 | 0.00 | 0.01 | 0.00 | 0.01 | 0.01 | 0.01 | 0.01 | 0.01 | 0.01 | 0.01 | 0.01 | 0.01 | 0.01 | 0.00 |
| Al | 0.55 | 0.51 | 0.55 | 0.46 | 0.49 | 0.51 | 0.52 | 0.46 | 0.50 | 0.53 | 0.54 | 0.54 | 0.54 | 0.54 | 0.54 | 0.54 | 0.56 | 0.56 | 0.55 |
| Cr | 1.47 | 1.44 | 1.46 | 1.52 | 1.51 | 1.49 | 1.48 | 1.53 | 1.50 | 1.46 | 1.45 | 1.46 | 1.46 | 1.46 | 1.46 | 1.45 | 1.44 | 1.44 | 1.43 |
| $Fe_{3+}$ | 0.00 | 0.03 | 0.00 | 0.00 | 0.00 | 0.00 | 0.00 | 0.00 | 0.00 | 0.00 | 0.00 | 0.00 | 0.00 | 0.00 | 0.00 | 0.00 | 0.00 | 0.00 | 0.00 |
| $Fe_{2+}$ | 0.44 | 0.48 | 0.44 | 0.50 | 0.47 | 0.46 | 0.46 | 0.48 | 0.47 | 0.47 | 0.46 | 0.45 | 0.46 | 0.46 | 0.46 | 0.46 | 0.44 | 0.45 | 0.46 |
| Mn | 0.00 | 0.01 | 0.00 | 0.01 | 0.00 | 0.00 | 0.00 | 0.01 | 0.00 | 0.00 | 0.00 | 0.00 | 0.00 | 0.00 | 0.00 | 0.00 | 0.00 | 0.00 | 0.00 |
| Mg | 0.54 | 0.51 | 0.54 | 0.50 | 0.53 | 0.53 | 0.54 | 0.52 | 0.52 | 0.53 | 0.54 | 0.54 | 0.53 | 0.53 | 0.54 | 0.54 | 0.54 | 0.55 | 0.55 |

| wt% | SK3H-26 | SK3H-27 | SK3H-29 | SK3H-30 | SK3H-31 | SK3H-32 | SK3H-33 | SK3H-34 | SK3H-35 | SK3H-37 | SK3H-38 | SK3H-39 | SK3H-40 | SK3I-1 | SK3I-2 | SK3I-3 | SK3I-4 | SK3I-5 | SK3I-6 |
|---|---|---|---|---|---|---|---|---|---|---|---|---|---|---|---|---|---|---|---|
| $TiO_2$ | 0.20 | 0.22 | 0.24 | 0.30 | 0.23 | 0.23 | 0.24 | 0.26 | 0.20 | 0.26 | 0.27 | 0.24 | 0.26 | 0.17 | 0.20 | 0.23 | 0.25 | 0.15 | 0.23 |
| $Al_2O_3$ | 14.26 | 14.38 | 14.31 | 14.41 | 14.31 | 14.40 | 14.31 | 14.42 | 14.32 | 14.47 | 14.35 | 14.14 | 14.11 | 11.46 | 11.99 | 12.04 | 12.17 | 12.19 | 12.14 |
| $Cr_2O_3$ | 54.82 | 54.84 | 54.55 | 54.95 | 54.68 | 55.28 | 54.66 | 55.22 | 55.09 | 54.69 | 55.51 | 54.78 | 54.14 | 56.00 | 56.27 | 56.62 | 55.05 | 55.22 | 55.87 |
| $Fe_2O_3$ | 0.00 | 0.00 | 0.00 | 0.00 | 0.00 | 0.00 | 0.00 | 0.00 | 0.00 | 0.00 | 0.00 | 0.00 | 0.00 | 1.89 | 1.15 | 1.14 | 1.58 | 1.45 | 1.32 |
| FeO | 16.04 | 16.20 | 16.33 | 15.98 | 16.11 | 16.06 | 15.85 | 15.88 | 15.96 | 16.17 | 16.06 | 15.98 | 16.79 | 18.69 | 18.78 | 18.73 | 18.46 | 18.23 | 18.23 |
| MnO | 0.00 | 0.09 | 0.16 | 0.02 | 0.18 | 0.12 | 0.14 | 0.05 | 0.24 | 0.07 | 0.00 | 0.00 | 0.00 | 0.05 | 0.16 | 0.08 | 0.19 | 0.11 | 0.23 |
| MgO | 11.01 | 10.78 | 10.93 | 11.01 | 10.81 | 10.84 | 10.89 | 10.92 | 11.01 | 10.73 | 10.82 | 10.85 | 10.75 | 9.56 | 9.57 | 9.82 | 9.64 | 9.80 | 9.92 |
| Tot | 96.35 | 96.52 | 96.59 | 96.68 | 96.32 | 96.93 | 96.12 | 96.75 | 96.83 | 96.37 | 97.00 | 96.25 | 96.04 | 97.86 | 98.14 | 98.70 | 97.38 | 97.23 | 98.01 |
| Ti | 0.00 | 0.01 | 0.01 | 0.01 | 0.01 | 0.01 | 0.01 | 0.01 | 0.00 | 0.01 | 0.01 | 0.01 | 0.01 | 0.00 | 0.01 | 0.01 | 0.01 | 0.00 | 0.01 |
| Al | 0.56 | 0.56 | 0.56 | 0.56 | 0.56 | 0.56 | 0.56 | 0.56 | 0.56 | 0.57 | 0.56 | 0.56 | 0.56 | 0.45 | 0.47 | 0.47 | 0.48 | 0.48 | 0.48 |
| Cr | 1.44 | 1.44 | 1.43 | 1.44 | 1.44 | 1.45 | 1.44 | 1.45 | 1.44 | 1.44 | 1.45 | 1.44 | 1.43 | 1.49 | 1.49 | 1.49 | 1.46 | 1.47 | 1.47 |
| $Fe_{3+}$ | 0.00 | 0.00 | 0.00 | 0.00 | 0.00 | 0.00 | 0.00 | 0.00 | 0.00 | 0.00 | 0.00 | 0.00 | 0.00 | 0.05 | 0.03 | 0.03 | 0.04 | 0.04 | 0.03 |
| $Fe_{2+}$ | 0.45 | 0.45 | 0.45 | 0.44 | 0.45 | 0.44 | 0.44 | 0.44 | 0.44 | 0.45 | 0.45 | 0.45 | 0.47 | 0.53 | 0.53 | 0.52 | 0.52 | 0.51 | 0.51 |
| Mn | 0.00 | 0.00 | 0.00 | 0.00 | 0.01 | 0.00 | 0.00 | 0.00 | 0.01 | 0.00 | 0.00 | 0.00 | 0.00 | 0.00 | 0.00 | 0.00 | 0.01 | 0.00 | 0.01 |
| Mg | 0.55 | 0.53 | 0.54 | 0.54 | 0.54 | 0.54 | 0.54 | 0.54 | 0.54 | 0.53 | 0.53 | 0.54 | 0.54 | 0.48 | 0.48 | 0.49 | 0.48 | 0.49 | 0.49 |

| wt% | SK3I-7 | SK3I-8 | SK3I-9 | SK3I-10 | SK3I-11 | SK3I-12 | SK3I-13 | SK3I-14 | SK3I-15 | SK3I-16 | SK3I-17 | SK3I-18 | SK3I-19 | SK3I-20 | SK3I-21 | SK3I-22 | SK3I-24 | SK3I-25 | SK3I-27 |
|---|---|---|---|---|---|---|---|---|---|---|---|---|---|---|---|---|---|---|---|
| $TiO_2$ | 0.20 | 0.22 | 0.22 | 0.19 | 0.22 | 0.19 | 0.20 | 0.18 | 0.20 | 0.24 | 0.22 | 0.23 | 0.21 | 0.17 | 0.21 | 0.22 | 0.24 | 0.20 | 0.22 |
| $Al_2O_3$ | 12.11 | 12.20 | 12.26 | 11.75 | 11.63 | 11.79 | 11.44 | 12.06 | 12.13 | 12.16 | 12.21 | 12.14 | 11.83 | 11.77 | 11.97 | 11.85 | 11.89 | 11.67 | 11.48 |
| $Cr_2O_3$ | 55.64 | 56.04 | 55.94 | 54.71 | 55.54 | 55.28 | 55.62 | 56.43 | 55.64 | 56.38 | 56.10 | 55.83 | 56.12 | 55.57 | 56.30 | 56.21 | 55.60 | 56.13 | 55.67 |
| $Fe_2O_3$ | 0.98 | 1.17 | 1.23 | 1.81 | 1.99 | 2.36 | 2.00 | 0.94 | 1.43 | 0.94 | 1.19 | 1.44 | 1.30 | 1.88 | 1.66 | 1.41 | 1.84 | 1.77 | 2.25 |
| FeO | 18.17 | 18.43 | 18.07 | 19.88 | 19.59 | 19.91 | 20.38 | 17.78 | 17.82 | 18.04 | 18.19 | 18.69 | 18.57 | 18.46 | 18.56 | 18.89 | 18.90 | 18.83 | 18.86 |
| MnO | 0.04 | 0.05 | 0.09 | 0.15 | 0.26 | 0.24 | 0.11 | 0.17 | 0.00 | 0.20 | 0.15 | 0.04 | 0.08 | 0.14 | 0.30 | 0.01 | 0.10 | 0.01 | 0.10 |
| MgO | 9.77 | 9.87 | 10.03 | 8.57 | 8.91 | 8.80 | 8.52 | 10.11 | 10.14 | 10.02 | 9.96 | 9.69 | 9.66 | 9.60 | 9.71 | 9.59 | 9.50 | 9.58 | 9.49 |
| Tot | 96.90 | 98.01 | 97.83 | 97.08 | 98.14 | 98.58 | 98.28 | 97.69 | 97.38 | 98.00 | 98.04 | 98.05 | 97.79 | 97.60 | 98.70 | 98.19 | 98.08 | 98.19 | 98.10 |
| Ti | 0.00 | 0.01 | 0.01 | 0.00 | 0.01 | 0.00 | 0.01 | 0.00 | 0.01 | 0.01 | 0.01 | 0.01 | 0.01 | 0.00 | 0.01 | 0.01 | 0.01 | 0.01 | 0.01 |
| Al | 0.48 | 0.48 | 0.48 | 0.47 | 0.46 | 0.47 | 0.45 | 0.47 | 0.48 | 0.48 | 0.48 | 0.48 | 0.47 | 0.47 | 0.47 | 0.47 | 0.47 | 0.46 | 0.45 |
| Cr | 1.48 | 1.48 | 1.48 | 1.47 | 1.48 | 1.47 | 1.48 | 1.49 | 1.47 | 1.49 | 1.48 | 1.47 | 1.49 | 1.48 | 1.48 | 1.49 | 1.47 | 1.49 | 1.48 |

| | | | | | | | | | | | | | | | | | | | |
|---|---|---|---|---|---|---|---|---|---|---|---|---|---|---|---|---|---|---|---|
| $Fe_{3+}$ | 0.02 | 0.03 | 0.03 | 0.05 | 0.05 | 0.06 | 0.05 | 0.02 | 0.04 | 0.02 | 0.03 | 0.04 | 0.03 | 0.05 | 0.04 | 0.04 | 0.05 | 0.04 | 0.06 |
| $Fe_{2+}$ | 0.51 | 0.51 | 0.50 | 0.57 | 0.55 | 0.56 | 0.57 | 0.50 | 0.50 | 0.50 | 0.51 | 0.52 | 0.52 | 0.52 | 0.52 | 0.53 | 0.53 | 0.53 | 0.53 |
| Mn | 0.00 | 0.00 | 0.00 | 0.00 | 0.01 | 0.01 | 0.00 | 0.00 | 0.00 | 0.01 | 0.00 | 0.00 | 0.00 | 0.00 | 0.01 | 0.00 | 0.00 | 0.00 | 0.00 |
| Mg | 0.49 | 0.49 | 0.50 | 0.43 | 0.45 | 0.44 | 0.43 | 0.50 | 0.51 | 0.50 | 0.49 | 0.48 | 0.48 | 0.48 | 0.48 | 0.48 | 0.47 | 0.48 | 0.47 |

| wt% | SK3I-28 | Sky8a | Sky8a | Sky8a | Sky8a | Sky8a | Sky8a | Sky8a | Sky8a | Sky8a | Sky8a | Sky8a | Sky8a | Sky8a | Sky8a | Sky8b | Sky8b | Sky8b | Sky8b |
|---|---|---|---|---|---|---|---|---|---|---|---|---|---|---|---|---|---|---|---|
| $TiO_2$ | 0.22 | 0.20 | 0.16 | 0.18 | 0.04 | 0.08 | 0.18 | 0.17 | 0.22 | 0.20 | 0.01 | 0.03 | 0.18 | 0.21 | 0.25 | 0.18 | 0.22 | 0.18 | 0.27 |
| $Al_2O_3$ | 11.37 | 17.47 | 17.44 | 0.70 | 0.54 | 0.33 | 17.48 | 17.74 | 17.73 | 17.62 | 0.23 | 0.51 | 17.47 | 17.65 | 17.56 | 16.93 | 17.00 | 16.18 | 16.83 |
| $Cr_2O_3$ | 55.95 | 53.49 | 53.82 | 47.58 | 30.00 | 27.87 | 54.35 | 53.58 | 53.78 | 54.14 | 11.28 | 32.82 | 53.50 | 54.25 | 54.16 | 53.12 | 53.59 | 54.57 | 54.06 |
| $Fe_2O_3$ | 2.19 | 2.99 | 2.29 | 18.46 | 33.60 | 39.30 | 2.32 | 2.26 | 2.22 | 2.03 | 59.00 | 34.97 | 2.72 | 2.22 | 2.37 | 2.31 | 2.40 | 2.02 | 2.02 |
| FeO | 18.75 | 13.06 | 13.41 | 26.44 | 26.49 | 26.30 | 13.30 | 13.48 | 13.78 | 14.15 | 30.50 | 24.79 | 12.83 | 13.32 | 13.08 | 11.81 | 12.48 | 12.83 | 12.68 |
| MnO | 0.16 | 0.10 | 0.07 | 3.99 | 5.12 | 4.23 | 0.01 | 0.05 | 0.12 | 0.05 | 0.85 | 5.55 | 0.06 | 0.11 | 0.10 | 0.03 | 0.02 | 0.06 | 0.07 |
| MgO | 9.51 | 14.68 | 14.36 | 1.59 | 0.77 | 0.53 | 14.62 | 14.43 | 14.34 | 14.12 | 0.54 | 0.74 | 14.79 | 14.64 | 14.83 | 14.94 | 14.77 | 14.37 | 14.66 |
| Tot | 98.16 | 102.00 | 101.56 | 99.65 | 97.93 | 98.78 | 102.26 | 101.75 | 102.25 | 102.34 | 102.52 | 99.43 | 101.60 | 102.43 | 102.41 | 99.36 | 100.50 | 100.25 | 100.62 |
| Ti | 0.01 | 0.00 | 0.00 | 0.01 | 0.00 | 0.00 | 0.00 | 0.00 | 0.01 | 0.00 | 0.00 | 0.00 | 0.00 | 0.00 | 0.01 | 0.00 | 0.01 | 0.00 | 0.01 |
| Al | 0.45 | 0.63 | 0.63 | 0.03 | 0.02 | 0.01 | 0.63 | 0.64 | 0.64 | 0.63 | 0.01 | 0.02 | 0.63 | 0.63 | 0.63 | 0.62 | 0.62 | 0.60 | 0.61 |
| Cr | 1.48 | 1.29 | 1.31 | 1.39 | 0.90 | 0.84 | 1.31 | 1.30 | 1.30 | 1.31 | 0.33 | 0.98 | 1.30 | 1.30 | 1.30 | 1.31 | 1.31 | 1.35 | 1.32 |
| $Fe_{3+}$ | 0.06 | 0.07 | 0.05 | 0.51 | 0.96 | 1.13 | 0.05 | 0.05 | 0.05 | 0.05 | 1.65 | 0.99 | 0.06 | 0.05 | 0.05 | 0.05 | 0.06 | 0.05 | 0.05 |
| $Fe_{2+}$ | 0.53 | 0.33 | 0.34 | 0.82 | 0.84 | 0.84 | 0.34 | 0.35 | 0.35 | 0.36 | 0.95 | 0.78 | 0.33 | 0.34 | 0.33 | 0.31 | 0.32 | 0.33 | 0.33 |
| Mn | 0.00 | 0.00 | 0.00 | 0.13 | 0.17 | 0.14 | 0.00 | 0.00 | 0.00 | 0.00 | 0.03 | 0.18 | 0.00 | 0.00 | 0.00 | 0.00 | 0.00 | 0.00 | 0.00 |
| Mg | 0.48 | 0.67 | 0.66 | 0.09 | 0.04 | 0.03 | 0.66 | 0.66 | 0.65 | 0.64 | 0.03 | 0.04 | 0.68 | 0.66 | 0.67 | 0.70 | 0.68 | 0.67 | 0.68 |

| wt% | Sky8b | Sky8b | Sky8b | Sky8b | Sky8b | Sky8b | Sky8b | Sky8b | Sky8b | Sky8b | Sky8b | Sky8b | Sky8b | Sky8b | Sky8b | Sky8b | Sky8b | Sky10 | Sky10 |
|---|---|---|---|---|---|---|---|---|---|---|---|---|---|---|---|---|---|---|---|
| $TiO_2$ | 0.21 | 0.23 | 0.19 | 0.27 | 0.23 | 0.22 | 0.25 | 0.20 | 0.28 | 0.22 | 0.26 | 0.16 | 0.21 | 0.22 | 0.24 | 0.21 | 0.20 | 0.32 | 0.30 |
| $Al_2O_3$ | 16.89 | 16.77 | 17.23 | 16.90 | 16.81 | 16.89 | 16.59 | 16.57 | 1.79 | 1.76 | 1.66 | 1.51 | 1.85 | 1.51 | 1.28 | 2.29 | 2.47 | 1.89 | 2.03 |
| $Cr_2O_3$ | 54.02 | 53.70 | 53.84 | 53.99 | 53.58 | 54.02 | 53.84 | 54.47 | 56.88 | 54.38 | 52.48 | 48.82 | 51.48 | 52.78 | 51.24 | 56.29 | 56.89 | 63.52 | 62.08 |
| $Fe_2O_3$ | 1.79 | 2.42 | 1.99 | 1.88 | 2.67 | 1.98 | 2.32 | 1.71 | 9.03 | 11.99 | 13.49 | 16.97 | 14.91 | 13.70 | 14.47 | 9.28 | 8.56 | 2.02 | 1.26 |
| FeO | 12.52 | 12.22 | 12.55 | 12.32 | 12.06 | 12.17 | 12.00 | 12.62 | 17.81 | 17.45 | 17.47 | 17.12 | 17.03 | 17.17 | 17.22 | 17.45 | 16.94 | 25.70 | 25.68 |
| MnO | 0.07 | 0.06 | 0.01 | 0.03 | 0.10 | 0.07 | 0.08 | 0.05 | 9.01 | 9.36 | 10.57 | 10.65 | 10.70 | 10.11 | 10.33 | 9.02 | 8.82 | 0.68 | 0.65 |
| MgO | 14.63 | 14.85 | 14.77 | 14.82 | 15.00 | 14.88 | 14.96 | 14.54 | 3.43 | 3.49 | 2.55 | 2.42 | 2.81 | 2.90 | 3.02 | 3.55 | 4.04 | 4.85 | 4.77 |
| Tot | 100.15 | 100.27 | 100.60 | 100.22 | 100.49 | 100.24 | 100.08 | 100.17 | 98.36 | 98.82 | 98.57 | 97.72 | 99.06 | 98.39 | 98.22 | 98.15 | 98.01 | 99.90 | 98.00 |
| Ti | 0.00 | 0.01 | 0.00 | 0.01 | 0.01 | 0.01 | 0.01 | 0.00 | 0.01 | 0.01 | 0.01 | 0.00 | 0.01 | 0.01 | 0.01 | 0.01 | 0.01 | 0.01 | 0.01 |
| Al | 0.62 | 0.61 | 0.63 | 0.62 | 0.61 | 0.62 | 0.61 | 0.61 | 0.08 | 0.08 | 0.07 | 0.07 | 0.08 | 0.07 | 0.06 | 0.10 | 0.11 | 0.08 | 0.09 |
| Cr | 1.33 | 1.32 | 1.32 | 1.32 | 1.31 | 1.33 | 1.32 | 1.34 | 1.65 | 1.57 | 1.53 | 1.44 | 1.49 | 1.54 | 1.50 | 1.63 | 1.64 | 1.78 | 1.77 |
| $Fe_{3+}$ | 0.04 | 0.06 | 0.05 | 0.04 | 0.06 | 0.05 | 0.05 | 0.04 | 0.25 | 0.33 | 0.37 | 0.48 | 0.41 | 0.38 | 0.40 | 0.26 | 0.23 | 0.05 | 0.03 |
| $Fe_{2+}$ | 0.33 | 0.32 | 0.32 | 0.32 | 0.31 | 0.32 | 0.31 | 0.33 | 0.55 | 0.53 | 0.54 | 0.54 | 0.52 | 0.53 | 0.53 | 0.53 | 0.52 | 0.76 | 0.78 |
| Mn | 0.00 | 0.00 | 0.00 | 0.00 | 0.00 | 0.00 | 0.00 | 0.00 | 0.28 | 0.29 | 0.33 | 0.34 | 0.33 | 0.32 | 0.32 | 0.28 | 0.27 | 0.02 | 0.02 |
| Mg | 0.68 | 0.69 | 0.68 | 0.69 | 0.69 | 0.69 | 0.69 | 0.68 | 0.19 | 0.19 | 0.14 | 0.13 | 0.15 | 0.16 | 0.17 | 0.19 | 0.22 | 0.26 | 0.26 |

| wt% | Sky10 | Sky10 | Sky10 | Sky10 | Sky10 | Sky10 | Sky10 | Sky10 | Sky10 | Sky10 | Sky10 | Sky10 | Sky10 | Sky10 | Sky10 | Sky10 | Sky10 | Sky10 | Sky10 |
|---|---|---|---|---|---|---|---|---|---|---|---|---|---|---|---|---|---|---|---|
| $TiO_2$ | 0.38 | 0.22 | 0.20 | 0.36 | 0.17 | 0.22 | 0.38 | 0.26 | 0.29 | 0.24 | 0.25 | 0.32 | 0.25 | 0.26 | 0.29 | 0.27 | 0.34 | 0.24 | 0.28 |
| $Al_2O_3$ | 7.63 | 7.43 | 5.25 | 7.07 | 19.63 | 19.54 | 3.13 | 6.26 | 5.19 | 19.65 | 19.27 | 2.23 | 2.24 | 3.21 | 9.16 | 6.67 | 6.53 | 18.19 | 18.65 |
| $Cr_2O_3$ | 60.74 | 56.07 | 48.42 | 63.07 | 52.24 | 51.82 | 65.12 | 48.45 | 63.95 | 52.24 | 52.28 | 64.68 | 56.43 | 60.46 | 60.43 | 60.22 | 59.87 | 52.75 | 51.67 |
| $Fe_2O_3$ | 3.03 | 0.00 | 0.00 | 1.75 | 2.72 | 2.93 | 3.22 | 1.61 | 1.29 | 2.33 | 2.77 | 1.38 | 5.85 | 0.00 | 0.00 | 0.00 | 0.00 | 2.18 | 3.29 |
| FeO | 19.09 | 21.35 | 23.19 | 16.99 | 11.87 | 12.12 | 21.39 | 19.98 | 21.02 | 12.06 | 12.60 | 23.05 | 19.83 | 22.32 | 17.08 | 17.95 | 19.01 | 13.03 | 12.42 |
| MnO | 0.34 | 0.52 | 0.48 | 0.52 | 0.05 | 0.15 | 0.36 | 0.55 | 0.48 | 0.10 | 0.00 | 0.46 | 0.49 | 0.30 | 0.17 | 0.21 | 0.32 | 0.04 | 0.07 |
| MgO | 9.45 | 9.74 | 7.89 | 11.59 | 15.81 | 15.56 | 7.64 | 14.18 | 7.89 | 15.63 | 15.42 | 6.61 | 6.99 | 7.69 | 12.03 | 11.38 | 10.75 | 14.74 | 15.23 |
| Tot | 100.73 | 100.02 | 97.46 | 102.17 | 102.51 | 102.36 | 101.34 | 98.53 | 100.35 | 102.26 | 102.64 | 99.55 | 92.68 | 96.40 | 100.50 | 98.85 | 99.28 | 101.25 | 101.64 |

| | | | | | | | | | | | | | | | | | | | |
|---|---|---|---|---|---|---|---|---|---|---|---|---|---|---|---|---|---|---|---|
| Ti | 0.01 | 0.01 | 0.01 | 0.01 | 0.00 | 0.01 | 0.01 | 0.01 | 0.01 | 0.01 | 0.01 | 0.01 | 0.01 | 0.01 | 0.01 | 0.01 | 0.01 | 0.01 | 0.01 |
| Al | 0.30 | 0.29 | 0.21 | 0.27 | 0.69 | 0.69 | 0.13 | 0.24 | 0.21 | 0.70 | 0.68 | 0.09 | 0.10 | 0.13 | 0.35 | 0.26 | 0.26 | 0.66 | 0.67 |
| Cr | 1.60 | 1.47 | 1.30 | 1.62 | 1.24 | 1.23 | 1.76 | 1.24 | 1.73 | 1.24 | 1.24 | 1.80 | 1.68 | 1.70 | 1.55 | 1.59 | 1.58 | 1.28 | 1.24 |
| $Fe_{3+}$ | 0.08 | 0.00 | 0.00 | 0.04 | 0.06 | 0.07 | 0.08 | 0.04 | 0.03 | 0.05 | 0.06 | 0.04 | 0.17 | 0.00 | 0.00 | 0.00 | 0.00 | 0.05 | 0.08 |
| $Fe_{2+}$ | 0.53 | 0.59 | 0.66 | 0.46 | 0.30 | 0.30 | 0.61 | 0.54 | 0.60 | 0.30 | 0.32 | 0.68 | 0.62 | 0.66 | 0.46 | 0.50 | 0.53 | 0.33 | 0.32 |
| Mn | 0.01 | 0.01 | 0.01 | 0.01 | 0.00 | 0.00 | 0.01 | 0.02 | 0.01 | 0.00 | 0.00 | 0.01 | 0.02 | 0.01 | 0.00 | 0.01 | 0.01 | 0.00 | 0.00 |
| Mg | 0.47 | 0.48 | 0.40 | 0.56 | 0.71 | 0.70 | 0.39 | 0.68 | 0.40 | 0.70 | 0.69 | 0.35 | 0.39 | 0.41 | 0.58 | 0.57 | 0.53 | 0.67 | 0.69 |

Tab. 4.11 Spinel microprobe analyses of Abdasht-Soghan chromitites.

| Wt% | IRAB-A01-C1 | IRAB-A01-C2 | IRAB-A01-C5 | IRAB-A01-C6 | IRAB-A01-C7 | IRAB-A01-C9 | IRAB-B01-C1 | IRAB-B01-C2 | IRAB-B01-C3 | IRAB-B01-C4 | IRAB-B01-C5 | IRAB-B01-C6 | IRAB-B01-C7 | IRSO-A02-C1 | IRSO-A02-C2 | IRSO-A02-C3 | IRSO-A02-C4 | IRSO-A02-C5 |
|---|---|---|---|---|---|---|---|---|---|---|---|---|---|---|---|---|---|---|
| $TiO_2$ | 0.15 | 0.20 | 0.19 | 0.16 | 0.07 | 0.13 | 0.20 | 0.18 | 0.20 | 0.12 | 0.14 | 0.19 | 0.10 | 0.09 | 0.11 | 0.13 | 0.07 | 0.11 |
| $Al_2O_3$ | 10.26 | 10.73 | 10.36 | 10.08 | 10.22 | 9.77 | 10.72 | 10.95 | 11.57 | 11.73 | 11.70 | 11.94 | 9.53 | 10.26 | 9.70 | 10.73 | 10.87 | 8.63 |
| $Cr_2O_3$ | 59.87 | 60.37 | 60.44 | 60.35 | 59.72 | 60.16 | 60.86 | 60.51 | 59.91 | 58.61 | 59.52 | 59.22 | 62.15 | 60.67 | 60.95 | 60.07 | 59.73 | 61.76 |
| $Fe_2O_3$ | 4.20 | 3.35 | 3.74 | 4.24 | 4.47 | 4.90 | 3.40 | 3.32 | 3.74 | 4.30 | 3.18 | 3.52 | 3.09 | 3.39 | 3.65 | 3.72 | 3.64 | 4.20 |
| FeO | 12.18 | 11.65 | 12.38 | 12.50 | 12.87 | 12.06 | 10.33 | 10.36 | 10.19 | 9.45 | 10.28 | 10.61 | 11.03 | 10.71 | 10.69 | 10.86 | 10.53 | 10.78 |
| MgO | 14.47 | 14.69 | 14.22 | 14.14 | 13.77 | 14.34 | 15.56 | 15.45 | 15.77 | 15.98 | 15.52 | 15.44 | 14.85 | 15.00 | 14.94 | 15.08 | 15.19 | 14.88 |
| NiO | 0.11 | 0.13 | 0.17 | 0.11 | 0.16 | 0.14 | 0.15 | 0.24 | 0.23 | 0.19 | 0.11 | 0.22 | 0.18 | 0.16 | 0.17 | 0.12 | 0.06 | 0.07 |
| Total | 100.63 | 100.84 | 101.12 | 101.22 | 100.85 | 101.05 | 100.88 | 100.71 | 101.27 | 100.01 | 100.19 | 100.78 | 100.72 | 100.00 | 99.85 | 100.36 | 99.77 | 100.01 |
| Ti | 0.00 | 0.00 | 0.00 | 0.00 | 0.00 | 0.00 | 0.00 | 0.00 | 0.00 | 0.00 | 0.00 | 0.00 | 0.00 | 0.00 | 0.00 | 0.00 | 0.00 | 0.00 |
| Al | 0.39 | 0.40 | 0.39 | 0.38 | 0.38 | 0.37 | 0.40 | 0.41 | 0.43 | 0.43 | 0.43 | 0.44 | 0.36 | 0.39 | 0.37 | 0.40 | 0.41 | 0.33 |
| Cr | 1.51 | 1.51 | 1.51 | 1.51 | 1.51 | 1.51 | 1.51 | 1.51 | 1.48 | 1.46 | 1.48 | 1.47 | 1.56 | 1.53 | 1.54 | 1.50 | 1.50 | 1.57 |
| $Fe^{3+}$ | 0.10 | 0.08 | 0.09 | 0.10 | 0.11 | 0.12 | 0.08 | 0.08 | 0.09 | 0.10 | 0.08 | 0.08 | 0.07 | 0.08 | 0.09 | 0.09 | 0.09 | 0.10 |
| $Fe^{2+}$ | 0.31 | 0.31 | 0.33 | 0.33 | 0.34 | 0.32 | 0.27 | 0.27 | 0.27 | 0.25 | 0.27 | 0.28 | 0.29 | 0.29 | 0.29 | 0.29 | 0.28 | 0.29 |
| Mg | 0.69 | 0.69 | 0.67 | 0.67 | 0.65 | 0.68 | 0.73 | 0.73 | 0.73 | 0.75 | 0.73 | 0.72 | 0.70 | 0.71 | 0.71 | 0.71 | 0.72 | 0.71 |
| Ni | 0.00 | 0.00 | 0.00 | 0.00 | 0.00 | 0.00 | 0.00 | 0.01 | 0.01 | 0.00 | 0.00 | 0.01 | 0.00 | 0.00 | 0.00 | 0.00 | 0.00 | 0.00 |

| Wt% | IRSO-A02-C6 | IRSO-A02-C7 | IRSO-A09-C1 | IRSO-A09-C2 | IRSO-A09-C3 | IRSO-A09-C4 | IRSO-A09-C5 | IRSO-CO1-C1 | IRSO-CO1-C2 | IRSO-CO1-C3 | IRSO-CO1-C4 | IRSO-CO1-C5 | IRSO-CO1-C6 | IRSO-CO1-C7 | IRSO-D03-C3 | IRSO-D03-C4 | IRSO-D03-C5 | IRSO-D03-C6 |
|---|---|---|---|---|---|---|---|---|---|---|---|---|---|---|---|---|---|---|
| $TiO_2$ | 0.18 | 0.18 | 0.10 | 0.18 | 0.15 | 0.07 | 0.08 | 0.16 | 0.14 | 0.19 | 0.17 | 0.18 | 0.14 | 0.19 | 0.15 | 0.22 | 0.17 | 0.18 |
| $Al_2O_3$ | 10.78 | 10.48 | 8.92 | 9.42 | 9.23 | 9.14 | 9.03 | 10.93 | 10.86 | 11.18 | 10.43 | 11.13 | 10.96 | 10.88 | 17.22 | 17.13 | 17.02 | 16.91 |
| $Cr_2O_3$ | 60.05 | 59.94 | 62.02 | 62.71 | 62.58 | 62.79 | 62.64 | 59.70 | 61.39 | 60.53 | 60.90 | 60.22 | 60.62 | 60.95 | 53.78 | 52.90 | 52.98 | 53.12 |
| $Fe_2O_3$ | 3.48 | 3.46 | 2.22 | 1.97 | 1.86 | 2.12 | 1.75 | 2.40 | 0.00 | 1.28 | 1.98 | 1.47 | 0.90 | 0.00 | 2.86 | 3.38 | 3.36 | 2.72 |
| FeO | 10.99 | 10.98 | 12.04 | 12.20 | 12.62 | 12.05 | 11.69 | 12.58 | 14.02 | 13.25 | 12.53 | 13.03 | 13.61 | 14.29 | 13.13 | 12.92 | 13.78 | 13.26 |
| MgO | 14.96 | 14.85 | 13.87 | 14.19 | 13.78 | 14.11 | 14.15 | 13.80 | 12.54 | 13.52 | 13.85 | 13.57 | 13.06 | 12.48 | 14.50 | 14.53 | 14.01 | 14.18 |
| NiO | 0.23 | 0.16 | - | - | - | - | - | 0.12 | 0.10 | 0.06 | 0.12 | 0.07 | 0.14 | 0.11 | 0.13 | 0.18 | 0.11 | 0.04 |
| Total | 100.34 | 99.82 | 98.95 | 100.46 | 100.02 | 100.06 | 99.17 | 99.45 | 99.05 | 99.94 | 99.84 | 99.56 | 99.39 | 98.90 | 101.53 | 100.92 | 101.15 | 100.14 |
| Ti | 0.00 | 0.00 | 0.00 | 0.00 | 0.00 | 0.00 | 0.00 | 0.00 | 0.00 | 0.00 | 0.00 | 0.00 | 0.00 | 0.00 | 0.00 | 0.01 | 0.00 | 0.00 |
| Al | 0.40 | 0.39 | 0.34 | 0.36 | 0.35 | 0.35 | 0.35 | 0.41 | 0.42 | 0.42 | 0.40 | 0.42 | 0.42 | 0.42 | 0.62 | 0.62 | 0.62 | 0.62 |
| Cr | 1.51 | 1.51 | 1.60 | 1.59 | 1.60 | 1.60 | 1.61 | 1.52 | 1.58 | 1.54 | 1.55 | 1.53 | 1.55 | 1.57 | 1.30 | 1.29 | 1.29 | 1.31 |
| $Fe^{3+}$ | 0.08 | 0.08 | 0.05 | 0.05 | 0.05 | 0.05 | 0.04 | 0.06 | 0.00 | 0.03 | 0.05 | 0.04 | 0.02 | 0.00 | 0.07 | 0.08 | 0.08 | 0.06 |
| $Fe^{2+}$ | 0.29 | 0.29 | 0.33 | 0.33 | 0.34 | 0.32 | 0.32 | 0.34 | 0.38 | 0.36 | 0.34 | 0.35 | 0.37 | 0.39 | 0.34 | 0.33 | 0.36 | 0.35 |
| Mg | 0.71 | 0.71 | 0.67 | 0.68 | 0.66 | 0.68 | 0.68 | 0.66 | 0.61 | 0.65 | 0.66 | 0.65 | 0.63 | 0.61 | 0.66 | 0.67 | 0.65 | 0.66 |
| Ni | 0.01 | 0.00 | - | - | - | - | - | 0.00 | 0.00 | 0.00 | 0.00 | 0.00 | 0.00 | 0.00 | 0.00 | 0.00 | 0.00 | 0.00 |

| Wt% | IRSO- | IRSO- | IRSO- | IRSO- | IRSO- | IRSO- | IRSO- | IRSO- | IRSO- | IRSO- | IRAB- | IRAB- | IRAB- | IRAB- | IRAB- | IRAB- | IRSO- | IRAB- |
|---|---|---|---|---|---|---|---|---|---|---|---|---|---|---|---|---|---|---|

| | D03-C7 | D03-C8 | D03-C9 | B03-C1 | B03-C2 | B03-C4 | B03-C5 | B03-C6 | B03-C7 | B03-C8 | A03-C6 | A03-C7 | A03-C8 | A03-C9 | A03-C1 | A03-C2 | B03-C3 | BO3-C1 |
|---|---|---|---|---|---|---|---|---|---|---|---|---|---|---|---|---|---|---|
| $TiO_2$ | 0.13 | 0.10 | 0.16 | 0.07 | 0.03 | 0.10 | 0.03 | 0.07 | 0.11 | 0.07 | 0.10 | 0.12 | 0.12 | 0.08 | 0.11 | 0.11 | 0.14 | 0.08 |
| $Al_2O_3$ | 16.88 | 16.30 | 16.15 | 19.17 | 18.52 | 19.24 | 19.24 | 19.45 | 19.34 | 19.31 | 6.56 | 6.93 | 6.72 | 6.08 | 6.42 | 5.96 | 4.84 | 11.59 |
| $Cr_2O_3$ | 52.52 | 52.46 | 52.42 | 50.30 | 50.66 | 49.66 | 50.36 | 49.82 | 50.13 | 49.54 | 58.46 | 57.77 | 58.35 | 58.19 | 58.81 | 59.27 | 44.05 | 58.08 |
| $Fe_2O_3$ | 3.36 | 3.01 | 3.09 | 2.05 | 2.34 | 2.50 | 2.31 | 2.22 | 2.21 | 2.85 | 6.33 | 6.46 | 6.47 | 6.30 | 6.36 | 5.95 | 17.98 | 3.83 |
| FeO | 13.16 | 13.44 | 13.38 | 17.94 | 17.14 | 17.19 | 16.97 | 17.50 | 17.28 | 17.64 | 22.11 | 23.64 | 20.52 | 23.87 | 21.83 | 22.40 | 30.19 | 13.06 |
| MgO | 14.16 | 13.62 | 13.69 | 11.44 | 11.72 | 11.82 | 12.04 | 11.72 | 11.89 | 11.65 | 7.39 | 6.52 | 8.37 | 6.09 | 7.58 | 7.07 | 1.32 | 13.63 |
| NiO | 0.07 | 0.10 | 0.05 | 0.01 | 0.07 | 0.09 | 0.03 | 0.00 | 0.05 | 0.03 | 0.00 | 0.06 | 0.01 | 0.05 | 0.05 | 0.10 | 0.03 | 0.14 |
| Total | 100.01 | 98.78 | 98.63 | 100.78 | 100.24 | 100.43 | 100.75 | 100.58 | 100.81 | 100.85 | 100.44 | 100.98 | 99.91 | 100.05 | 100.62 | 100.27 | 96.76 | 100.04 |
| Ti | 0.00 | 0.00 | 0.00 | 0.00 | 0.00 | 0.00 | 0.00 | 0.00 | 0.00 | 0.00 | 0.00 | 0.00 | 0.00 | 0.00 | 0.00 | 0.00 | 0.00 | 0.00 |
| Al | 0.62 | 0.61 | 0.60 | 0.71 | 0.69 | 0.71 | 0.71 | 0.72 | 0.71 | 0.71 | 0.26 | 0.28 | 0.27 | 0.25 | 0.26 | 0.24 | 0.21 | 0.44 |
| Cr | 1.29 | 1.31 | 1.31 | 1.24 | 1.26 | 1.23 | 1.24 | 1.23 | 1.23 | 1.22 | 1.57 | 1.55 | 1.56 | 1.59 | 1.58 | 1.60 | 1.28 | 1.47 |
| $Fe^{3+}$ | 0.08 | 0.07 | 0.07 | 0.05 | 0.06 | 0.06 | 0.05 | 0.05 | 0.05 | 0.07 | 0.16 | 0.17 | 0.16 | 0.16 | 0.16 | 0.15 | 0.50 | 0.09 |
| $Fe^{2+}$ | 0.34 | 0.36 | 0.36 | 0.47 | 0.45 | 0.45 | 0.44 | 0.46 | 0.45 | 0.46 | 0.63 | 0.67 | 0.58 | 0.69 | 0.62 | 0.64 | 0.93 | 0.35 |
| Mg | 0.66 | 0.64 | 0.65 | 0.53 | 0.55 | 0.55 | 0.56 | 0.55 | 0.55 | 0.54 | 0.37 | 0.33 | 0.42 | 0.31 | 0.38 | 0.36 | 0.07 | 0.65 |
| Ni | 0.00 | 0.00 | 0.00 | 0.00 | 0.00 | 0.00 | 0.00 | 0.00 | 0.00 | 0.00 | 0.00 | 0.00 | 0.00 | 0.00 | 0.00 | 0.00 | 0.00 | 0.00 |

| Wt% | IRAB-BO3-C2 | IRAB-BO3-C3 | IRAB-BO3-C4 | IRAB-BO3-C5 | IRAB-BO3-C6 | IRAB-BO3-C7 | IRAB-BO4-C1 | IRAB-BO4-C2 | IRAB-BO4-C3 | IRAB-BO4-C4 | IRAB-BO4-C5 | IRAB-BO4-C6 | IRAB-BO4-C7 | IRAB-BO5-C2 | IRAB-BO5-C3 | IRAB-BO5-C4 | IRAB-BO5-C5 | IRAB-BO5-C6 |
|---|---|---|---|---|---|---|---|---|---|---|---|---|---|---|---|---|---|---|
| $TiO_2$ | 0.12 | 0.09 | 0.14 | 0.09 | 0.11 | 0.08 | 0.18 | 0.10 | 0.15 | 0.13 | 0.18 | 0.14 | 0.18 | 0.12 | 0.17 | 0.12 | 0.21 | 0.17 |
| $Al_2O_3$ | 11.43 | 11.40 | 11.49 | 11.31 | 11.51 | 11.42 | 9.80 | 10.00 | 10.08 | 9.79 | 10.24 | 10.05 | 10.08 | 10.52 | 10.65 | 10.56 | 10.30 | 10.60 |
| $Cr_2O_3$ | 57.71 | 58.38 | 57.54 | 58.28 | 58.01 | 57.88 | 60.49 | 60.24 | 59.77 | 60.18 | 59.50 | 60.02 | 60.10 | 58.67 | 58.48 | 59.11 | 58.41 | 58.51 |
| $Fe_2O_3$ | 3.77 | 4.24 | 3.92 | 4.23 | 3.67 | 4.46 | 3.37 | 4.04 | 4.62 | 4.01 | 4.36 | 4.26 | 3.75 | 3.60 | 3.71 | 3.00 | 3.47 | 3.51 |
| FeO | 13.60 | 13.50 | 13.04 | 12.01 | 13.43 | 13.35 | 11.89 | 11.14 | 10.61 | 11.17 | 11.02 | 10.78 | 11.14 | 14.68 | 14.32 | 14.80 | 14.55 | 15.41 |
| MgO | 13.22 | 13.52 | 13.58 | 14.29 | 13.43 | 13.53 | 14.23 | 14.74 | 15.14 | 14.66 | 14.87 | 14.93 | 14.66 | 12.47 | 12.78 | 12.41 | 12.43 | 12.08 |
| NiO | 0.09 | 0.09 | 0.06 | 0.10 | 0.02 | 0.09 | 0.08 | 0.12 | 0.11 | 0.08 | 0.10 | 0.23 | 0.26 | 0.09 | 0.03 | 0.03 | 0.10 | 0.08 |
| Total | 99.56 | 100.82 | 99.41 | 100.00 | 99.81 | 100.50 | 99.70 | 100.02 | 100.00 | 99.66 | 99.85 | 100.01 | 99.83 | 99.84 | 99.77 | 99.80 | 99.19 | 100.02 |
| Ti | 0.00 | 0.00 | 0.00 | 0.00 | 0.00 | 0.00 | 0.00 | 0.00 | 0.00 | 0.00 | 0.00 | 0.00 | 0.00 | 0.00 | 0.00 | 0.00 | 0.01 | 0.00 |
| Al | 0.43 | 0.43 | 0.44 | 0.43 | 0.44 | 0.43 | 0.37 | 0.38 | 0.38 | 0.37 | 0.39 | 0.38 | 0.38 | 0.40 | 0.41 | 0.40 | 0.40 | 0.41 |
| Cr | 1.47 | 1.47 | 1.46 | 1.47 | 1.47 | 1.46 | 1.54 | 1.52 | 1.50 | 1.53 | 1.50 | 1.51 | 1.52 | 1.50 | 1.50 | 1.52 | 1.51 | 1.50 |
| $Fe^{3+}$ | 0.09 | 0.10 | 0.09 | 0.10 | 0.09 | 0.11 | 0.08 | 0.10 | 0.11 | 0.10 | 0.10 | 0.10 | 0.09 | 0.09 | 0.09 | 0.07 | 0.09 | 0.09 |
| $Fe^{2+}$ | 0.37 | 0.36 | 0.35 | 0.32 | 0.36 | 0.36 | 0.32 | 0.30 | 0.28 | 0.30 | 0.29 | 0.29 | 0.30 | 0.40 | 0.39 | 0.40 | 0.40 | 0.42 |
| Mg | 0.63 | 0.64 | 0.65 | 0.68 | 0.64 | 0.64 | 0.68 | 0.70 | 0.72 | 0.70 | 0.71 | 0.71 | 0.70 | 0.60 | 0.62 | 0.60 | 0.61 | 0.58 |
| Ni | 0.00 | 0.00 | 0.00 | 0.00 | 0.00 | 0.00 | 0.00 | 0.00 | 0.00 | 0.00 | 0.00 | 0.01 | 0.01 | 0.00 | 0.00 | 0.00 | 0.00 | 0.00 |

| Wt% | IRAB-BO5-C7 | IRSO-A03-C1 | IRSO-A03-C2 | IRSO-A03-C3 | IRSO-A03-C4 | IRSO-A03-C5 | IRSO-A03-C6 | IRSO-A03-C7 | IRSO-A04-C1 | IRSO-A04-C2 | IRSO-A04-C3 | IRSO-A04-C4 | IRSO-A04-C5 | IRSO-A04-C6 | IRSO-A04-C7 | IRSO-A04-C8 | IRSO-A08-C1 | IRSO-A08-C2 |
|---|---|---|---|---|---|---|---|---|---|---|---|---|---|---|---|---|---|---|
| $TiO_2$ | 0.22 | 0.14 | 0.12 | 0.17 | 0.14 | 0.15 | 0.21 | 0.15 | 0.11 | 0.17 | 0.15 | 0.12 | 0.14 | 0.18 | 0.18 | 0.19 | 0.21 | 0.14 |
| $Al_2O_3$ | 10.96 | 10.59 | 9.88 | 10.50 | 10.51 | 10.41 | 10.10 | 10.00 | 9.99 | 9.87 | 9.74 | 9.64 | 9.74 | 9.87 | 9.81 | 10.16 | 8.80 | 9.13 |
| $Cr_2O_3$ | 58.73 | 60.16 | 60.61 | 60.32 | 60.41 | 60.23 | 59.76 | 59.45 | 60.79 | 60.30 | 59.58 | 60.73 | 61.09 | 60.81 | 61.26 | 60.60 | 62.39 | 62.22 |
| $Fe_2O_3$ | 2.67 | 3.55 | 3.66 | 3.53 | 3.62 | 3.71 | 3.54 | 4.05 | 3.65 | 3.75 | 4.17 | 3.85 | 4.47 | 4.33 | 3.93 | 4.35 | 1.75 | 2.52 |
| FeO | 15.13 | 12.28 | 12.38 | 12.03 | 12.09 | 11.83 | 15.33 | 15.67 | 11.22 | 11.01 | 14.01 | 11.14 | 10.66 | 10.47 | 11.00 | 10.58 | 13.10 | 12.40 |
| MgO | 12.26 | 14.27 | 14.07 | 14.43 | 14.39 | 14.46 | 12.26 | 12.08 | 14.79 | 14.76 | 12.92 | 14.71 | 15.29 | 15.33 | 15.08 | 15.31 | 13.32 | 13.93 |
| NiO | 0.10 | 0.04 | 0.01 | 0.06 | 0.11 | 0.14 | 0.15 | 0.04 | 0.04 | 0.13 | 0.14 | 0.09 | 0.09 | 0.18 | 0.09 | 0.25 | - | - |
| Total | 99.83 | 100.72 | 100.54 | 100.67 | 100.91 | 100.54 | 101.01 | 101.04 | 100.27 | 99.71 | 100.32 | 99.90 | 101.03 | 100.80 | 101.02 | 101.09 | 99.39 | 100.10 |
| Ti | 0.01 | 0.00 | 0.00 | 0.00 | 0.00 | 0.00 | 0.01 | 0.00 | 0.00 | 0.00 | 0.00 | 0.00 | 0.00 | 0.00 | 0.00 | 0.00 | 0.01 | 0.00 |
| Al | 0.42 | 0.40 | 0.37 | 0.39 | 0.39 | 0.39 | 0.38 | 0.38 | 0.38 | 0.37 | 0.37 | 0.36 | 0.36 | 0.37 | 0.37 | 0.38 | 0.34 | 0.35 |
| Cr | 1.51 | 1.51 | 1.53 | 1.51 | 1.51 | 1.51 | 1.52 | 1.51 | 1.53 | 1.53 | 1.52 | 1.54 | 1.52 | 1.52 | 1.53 | 1.51 | 1.61 | 1.59 |
| $Fe^{3+}$ | 0.07 | 0.08 | 0.09 | 0.08 | 0.09 | 0.09 | 0.09 | 0.10 | 0.09 | 0.09 | 0.10 | 0.09 | 0.11 | 0.10 | 0.09 | 0.10 | 0.04 | 0.06 |

| | | | | | | | | | | | | | | | | | | |
|---|---|---|---|---|---|---|---|---|---|---|---|---|---|---|---|---|---|---|
| $Fe^{2+}$ | 0.41 | 0.33 | 0.33 | 0.32 | 0.32 | 0.31 | 0.41 | 0.42 | 0.30 | 0.30 | 0.38 | 0.30 | 0.28 | 0.28 | 0.29 | 0.28 | 0.36 | 0.33 |
| Mg | 0.59 | 0.68 | 0.67 | 0.68 | 0.68 | 0.69 | 0.59 | 0.58 | 0.70 | 0.71 | 0.62 | 0.70 | 0.72 | 0.72 | 0.71 | 0.72 | 0.65 | 0.67 |
| Ni | 0.00 | 0.00 | 0.00 | 0.00 | 0.00 | 0.00 | 0.00 | 0.00 | 0.00 | 0.00 | 0.00 | 0.00 | 0.00 | 0.00 | 0.00 | 0.01 | - | - |

| Wt% | IRSO-A08-C3 | IRSO-A08-C4 | IRAB-B06-C1 | IRAB-B06-C2 | IRAB-B06-C3 | IRAB-B06-C4 | IRAB-B06-C5 | IRSO-B01-C1 | IRSO-B01-C2 | IRSO-B01-C3 | IRSO-B01-C4 | IRSO-B01-C5 | IRSO-B01-C6 | IRSO-B01-C7 |
|---|---|---|---|---|---|---|---|---|---|---|---|---|---|---|
| $TiO_2$ | 0.08 | 0.08 | 0.13 | 0.05 | 0.21 | 0.14 | 0.20 | 0.06 | 0.15 | 0.20 | 0.15 | 0.19 | 0.21 | 0.20 |
| $Al_2O_3$ | 8.79 | 8.98 | 13.56 | 13.74 | 13.80 | 14.10 | 13.98 | 10.82 | 10.55 | 10.43 | 10.48 | 10.63 | 10.58 | 10.30 |
| $Cr_2O_3$ | 62.70 | 62.70 | 56.81 | 56.78 | 56.75 | 56.45 | 57.71 | 59.70 | 60.21 | 60.10 | 59.81 | 59.77 | 59.98 | 60.22 |
| $Fe_2O_3$ | 3.03 | 2.64 | 2.01 | 2.56 | 1.02 | 2.12 | 1.36 | 3.61 | 3.62 | 3.73 | 4.45 | 3.63 | 4.26 | 4.15 |
| FeO | 12.36 | 12.59 | 12.82 | 12.60 | 13.42 | 13.00 | 14.08 | 11.25 | 11.12 | 11.62 | 10.30 | 11.17 | 10.95 | 11.05 |
| MgO | 14.02 | 13.86 | 13.87 | 14.12 | 13.44 | 13.93 | 13.47 | 14.72 | 14.88 | 14.63 | 15.45 | 14.84 | 15.15 | 14.98 |
| NiO | - | - | 0.00 | 0.00 | 0.00 | 0.00 | 0.00 | 0.09 | 0.15 | 0.09 | 0.09 | 0.10 | 0.15 | 0.20 |
| Total | 100.69 | 100.59 | 99.00 | 99.58 | 98.54 | 99.52 | 100.66 | 99.89 | 100.33 | 100.44 | 100.30 | 100.00 | 100.97 | 100.71 |
| Ti | 0.00 | 0.00 | 0.00 | 0.00 | 0.00 | 0.00 | 0.00 | 0.00 | 0.00 | 0.00 | 0.00 | 0.00 | 0.00 | 0.00 |
| Al | 0.33 | 0.34 | 0.51 | 0.51 | 0.52 | 0.53 | 0.52 | 0.41 | 0.39 | 0.39 | 0.39 | 0.40 | 0.39 | 0.38 |
| Cr | 1.59 | 1.59 | 1.43 | 1.42 | 1.44 | 1.42 | 1.44 | 1.50 | 1.51 | 1.51 | 1.50 | 1.50 | 1.50 | 1.51 |
| $Fe^{3+}$ | 0.07 | 0.06 | 0.05 | 0.06 | 0.02 | 0.05 | 0.03 | 0.09 | 0.09 | 0.09 | 0.11 | 0.09 | 0.10 | 0.10 |
| $Fe^{2+}$ | 0.33 | 0.34 | 0.34 | 0.33 | 0.36 | 0.34 | 0.37 | 0.30 | 0.30 | 0.31 | 0.27 | 0.30 | 0.29 | 0.29 |
| Mg | 0.67 | 0.66 | 0.66 | 0.67 | 0.64 | 0.66 | 0.63 | 0.70 | 0.70 | 0.69 | 0.73 | 0.70 | 0.71 | 0.71 |
| Ni | - | - | 0.00 | 0.00 | 0.00 | 0.00 | 0.00 | 0.00 | 0.00 | 0.00 | 0.00 | 0.00 | 0.00 | 0.01 |

Tab. A4.12 Serpentine microprobe analyses of Skyros chromitites and serpentinites.

| wt% | SK3A-2 serp | SK3A-3 serp | SK3A-7 serp | SK3A-8 serp | SK3I-1 serp | SK3I-2 serp | SK3I-3 serp | SKY8A serp | SKY8A serp | SKY8A serp | SKY8A serp | SKY8A serp | SKY8A serp | SKY8A serp | SKY8A serp | SK3H-1 serp | SK3H-2 serp | SK3H-3 serp | SK3H-4 serp |
|---|---|---|---|---|---|---|---|---|---|---|---|---|---|---|---|---|---|---|---|
| $SiO_2$ | 41.23 | 38.76 | 36.92 | 38.60 | 41.77 | 41.98 | 42.10 | 42.73 | 42.06 | 43.08 | 43.24 | 42.95 | 43.38 | 42.41 | 42.54 | 39.00 | 38.93 | 40.87 | 40.10 |
| $TiO_2$ | 0.03 | 0.00 | 0.00 | 0.00 | 0.02 | 0.00 | 0.00 | 0.03 | 0.01 | 0.02 | 0.09 | 0.03 | 0.00 | 0.02 | 0.00 | 0.02 | 0.05 | 0.00 | 0.01 |
| $Al_2O_3$ | 0.57 | 0.46 | 0.37 | 0.33 | 0.44 | 0.44 | 0.45 | 0.65 | 0.79 | 0.66 | 0.71 | 0.92 | 0.72 | 1.01 | 0.86 | 3.07 | 2.54 | 0.83 | 2.33 |
| FeO | 2.69 | 1.66 | 2.17 | 2.25 | 2.28 | 2.07 | 2.01 | 2.58 | 2.15 | 2.28 | 1.93 | 1.68 | 1.97 | 3.18 | 2.38 | 1.83 | 1.78 | 1.59 | 1.82 |
| MnO | 0.02 | 0.05 | 0.08 | 0.01 | 0.00 | 0.03 | 0.00 | 0.05 | 0.07 | 0.09 | 0.05 | 0.07 | 0.04 | 0.05 | 0.06 | 0.00 | 0.03 | 0.01 | 0.00 |
| MgO | 35.25 | 37.16 | 40.14 | 39.36 | 36.37 | 38.68 | 35.65 | 38.51 | 38.98 | 39.02 | 38.84 | 39.21 | 38.83 | 37.27 | 38.82 | 39.48 | 39.45 | 40.12 | 38.72 |
| CaO | 0.06 | 0.06 | 0.10 | 0.05 | 0.09 | 0.10 | 0.13 | 0.11 | 0.04 | 0.10 | 0.07 | 0.04 | 0.05 | 0.15 | 0.08 | 0.05 | 0.03 | 0.06 | 0.03 |
| $Cr_2O_3$ | 0.54 | 0.82 | 0.65 | 0.42 | 0.65 | 0.64 | 0.62 | 1.00 | 1.00 | 0.05 | 1.00 | 1.00 | 1.00 | 1.80 | 1.20 | 1.52 | 1.29 | 0.90 | 1.42 |
| TOTAL | 80.38 | 78.97 | 80.42 | 81.02 | 81.61 | 83.95 | 80.96 | 85.66 | 85.11 | 85.30 | 85.92 | 85.89 | 85.98 | 85.89 | 85.93 | 84.98 | 84.10 | 84.39 | 84.44 |

Tab. A4.13 Chlorite microprobe analyses of Skyros chromitites.

| | SK3H-5 | SK3H-6 | SK3H-16 | SK3H-17 | SK3H-18 | SK3H-19 | SK3H-20 | SK3H-21 | SK3H-22 | Sky8b | Sky8b | Sky8b | Sky8b | Sky10 | Sky10 | Sky10 | Sky10 | Sky10 | Sky10 | Sky10 | Sky10 |
|---|---|---|---|---|---|---|---|---|---|---|---|---|---|---|---|---|---|---|---|---|---|
| $SiO_2$ | 34.13 | 35.47 | 32.98 | 32.59 | 33.17 | 33.27 | 33.16 | 33.69 | 33.06 | 33.57 | 33.91 | 33.78 | 32.06 | 28.60 | 29.26 | 30.36 | 31.05 | 30.08 | 30.26 | 29.16 | 29.04 |
| $TiO_2$ | 0.01 | 0.06 | 0.02 | 0.03 | 0.06 | 0.07 | 0.04 | 0.07 | 0.06 | 0.00 | 0.00 | 0.00 | 0.00 | 0.01 | 0.03 | 0.00 | 0.00 | 0.00 | 0.00 | 0.00 | 0.00 |
| $Al_2O_3$ | 11.75 | 11.11 | 10.83 | 13.67 | 10.14 | 10.62 | 10.60 | 10.96 | 10.52 | 15.26 | 13.62 | 14.90 | 14.44 | 17.79 | 17.61 | 12.96 | 17.49 | 17.49 | 17.94 | 17.60 | 17.42 |
| FeO | 0.89 | 1.23 | 0.91 | 0.72 | 0.95 | 0.83 | 0.79 | 0.86 | 1.01 | 0.69 | 0.75 | 0.58 | 0.52 | 0.70 | 0.57 | 0.90 | 0.43 | 0.74 | 0.50 | 0.56 | 0.63 |
| MnO | 0.01 | 0.04 | 0.02 | 0.01 | 0.06 | 0.00 | 0.00 | 0.04 | 0.00 | 0.00 | 0.04 | 0.06 | 0.03 | 0.00 | 0.01 | 0.00 | 0.00 | 0.00 | 0.00 | 0.00 | 0.01 |
| MgO | 35.08 | 36.15 | 34.58 | 33.57 | 34.91 | 34.51 | 34.94 | 35.27 | 35.22 | 34.60 | 35.09 | 34.71 | 33.35 | 33.34 | 33.33 | 35.19 | 33.75 | 33.39 | 33.48 | 33.40 | 33.21 |
| CaO | 0.01 | 0.04 | 0.03 | 0.00 | 0.03 | 0.00 | 0.00 | 0.00 | 0.05 | 0.01 | 0.01 | 0.03 | 0.00 | 0.02 | 0.01 | 0.02 | 0.01 | 0.01 | 0.05 | 0.02 | 0.00 |
| $Cr_2O_3$ | 2.40 | 2.73 | 4.63 | 3.04 | 4.12 | 4.49 | 4.47 | 3.30 | 4.10 | 0.73 | 0.75 | 0.56 | 4.23 | 5.04 | 4.45 | 4.70 | 2.80 | 5.00 | 2.20 | 4.90 | 4.00 |

| | | | | | | | | | | | | | | | | | | | | |
|---|---|---|---|---|---|---|---|---|---|---|---|---|---|---|---|---|---|---|---|---|
| TOTAL | 84.27 | 86.82 | 84.01 | 83.63 | 83.44 | 83.80 | 83.99 | 84.20 | 84.01 | 84.86 | 84.17 | 84.62 | 84.63 | 85.51 | 85.27 | 84.13 | 85.53 | 86.71 | 84.43 | 85.64 | 84.31 |

Tab. A4.14 Garnet microprobe analyses of Skyros chromitites.

| | SK3A-1 | SK3A-2 | SK3A-3 | SK3A-4 | SK3A-5 | SK3A-6 | SK3A-7 | SK3A-8 | SK3A-9 | SK3A-10 | SK3A-11 | SK3A-12 | SK3A-14 | SK3A-16 | SK3A-17 | SK3A-18 | SK3A-19 | SK3A-20 | SK3A-21 | SK3A-22 |
|---|---|---|---|---|---|---|---|---|---|---|---|---|---|---|---|---|---|---|---|---|
| $SiO_2$ | 31.78 | 31.98 | 32.47 | 33.53 | 30.42 | 34.40 | 34.30 | 34.34 | 34.72 | 34.01 | 34.76 | 34.33 | 34.61 | 33.80 | 34.61 | 34.47 | 33.97 | 34.54 | 34.45 | 34.10 |
| $TiO_2$ | 0.29 | 0.19 | 0.31 | 0.09 | 0.12 | 0.06 | 0.14 | 0.15 | 0.18 | 0.06 | 0.04 | 0.03 | 0.05 | 0.02 | 0.10 | 0.05 | 0.03 | 0.02 | 0.07 | 0.08 |
| $Al_2O_3$ | 0.59 | 0.53 | 0.38 | 0.33 | 1.21 | 0.12 | 0.11 | 0.09 | 0.17 | 0.23 | 0.07 | 0.12 | 0.10 | 0.06 | 0.06 | 0.08 | 0.10 | 0.10 | 0.10 | 0.11 |
| $Cr_2O_3$ | 20.83 | 19.03 | 19.96 | 14.64 | 19.82 | 14.63 | 14.23 | 12.96 | 15.85 | 13.42 | 12.91 | 12.82 | 13.14 | 12.53 | 12.66 | 12.59 | 12.05 | 11.36 | 12.63 | 12.39 |
| $Fe_2O_3$ | 15.98 | 17.39 | 14.57 | 21.21 | 22.53 | 19.54 | 19.19 | 21.52 | 17.30 | 22.34 | 20.59 | 21.11 | 20.89 | 21.87 | 21.38 | 21.81 | 22.78 | 22.99 | 21.87 | 22.26 |
| FeO | 0.00 | 0.00 | 0.00 | 0.00 | 0.00 | 0.00 | 0.00 | 0.00 | 0.00 | 0.00 | 0.00 | 0.00 | 0.00 | 0.00 | 0.00 | 0.00 | 0.00 | 0.00 | 0.00 | 0.00 |
| MnO | 0.00 | 0.02 | 0.04 | 0.16 | 0.22 | 0.00 | 0.00 | 0.08 | 0.10 | 0.18 | 0.04 | 0.00 | 0.03 | 0.00 | 0.06 | 0.05 | 0.00 | 0.05 | 0.00 | 0.04 |
| MgO | 0.48 | 0.29 | 0.16 | 0.35 | 1.15 | 0.06 | 0.01 | 0.09 | 0.30 | 0.15 | 0.04 | 0.05 | 0.06 | 0.07 | 0.05 | 0.11 | 0.06 | 0.16 | 0.12 | 0.08 |
| CaO | 30.43 | 29.83 | 30.84 | 29.70 | 26.69 | 31.00 | 30.98 | 31.40 | 31.18 | 30.87 | 31.10 | 31.01 | 31.59 | 30.96 | 31.23 | 31.42 | 31.19 | 31.05 | 31.29 | 31.13 |
| total | 100.38 | 99.26 | 98.73 | 100.00 | 102.14 | 99.79 | 98.95 | 100.62 | 99.80 | 101.25 | 99.55 | 99.47 | 100.46 | 99.29 | 100.15 | 100.58 | 100.17 | 100.27 | 100.53 | 100.19 |

| | SK3A-23 | SK3A-24 | SK3A-25 | SK3A-26 | SK3A-27 | SK3A-28 | SK3A-29 | SK3A-30 | SK3A-33 | SK3A-35 | SK3A-36 | SK3A-38 | SK3A-39 | SK3A-40 | SK3A-43 | SK3A-44 | SK3A-45 | SK3H-2 | SK3H-3 | SK3H-5 |
|---|---|---|---|---|---|---|---|---|---|---|---|---|---|---|---|---|---|---|---|---|
| $SiO_2$ | 34.32 | 35.08 | 34.96 | 34.89 | 33.98 | 34.99 | 35.26 | 35.05 | 34.19 | 33.84 | 34.93 | 34.65 | 34.32 | 34.50 | 34.93 | 34.81 | 34.42 | 35.11 | 35.01 | 34.84 |
| $TiO_2$ | 0.09 | 0.09 | 0.03 | 0.10 | 0.11 | 0.02 | 0.06 | 0.10 | 0.07 | 0.08 | 0.09 | 0.10 | 0.05 | 0.06 | 0.07 | 0.05 | 0.09 | 0.13 | 0.11 | 0.10 |
| $Al_2O_3$ | 0.10 | 0.13 | 0.14 | 0.08 | 0.11 | 0.08 | 0.09 | 0.10 | 0.11 | 0.15 | 0.11 | 0.12 | 0.13 | 0.08 | 0.11 | 0.11 | 0.08 | 0.11 | 0.11 | 0.04 |
| $Cr_2O_3$ | 11.70 | 12.04 | 12.35 | 11.76 | 13.23 | 13.11 | 12.84 | 12.22 | 14.35 | 13.33 | 12.64 | 12.62 | 12.62 | 12.64 | 12.25 | 12.25 | 12.22 | 12.78 | 12.37 | 12.46 |
| $Fe_2O_3$ | 23.26 | 21.85 | 21.65 | 22.01 | 22.08 | 20.48 | 20.58 | 20.72 | 20.54 | 21.91 | 21.25 | 21.54 | 22.06 | 22.06 | 21.56 | 21.33 | 22.83 | 20.03 | 20.78 | 21.57 |
| FeO | 0.00 | 0.00 | 0.00 | 0.00 | 0.00 | 0.00 | 0.00 | 0.00 | 0.00 | 0.00 | 0.00 | 0.00 | 0.00 | 0.00 | 0.00 | 0.00 | 0.00 | 1.97 | 1.99 | 1.38 |
| MnO | 0.02 | 0.07 | 0.01 | 0.05 | 0.00 | 0.00 | 0.01 | 0.00 | 0.06 | 0.00 | 0.00 | 0.00 | 0.00 | 0.01 | 0.04 | 0.00 | 0.05 | 0.03 | 0.06 | 0.03 |
| MgO | 0.17 | 0.09 | 0.07 | 0.10 | 0.06 | 0.05 | 0.04 | 0.04 | 0.05 | 0.04 | 0.12 | 0.05 | 0.07 | 0.04 | 0.08 | 0.04 | 0.07 | 0.06 | 0.05 | 0.18 |
| CaO | 31.27 | 31.59 | 31.39 | 31.09 | 31.34 | 31.61 | 31.43 | 31.19 | 31.18 | 31.18 | 31.19 | 31.50 | 31.54 | 31.69 | 31.53 | 31.15 | 31.13 | 31.21 | 31.09 | 31.24 |
| total | 100.93 | 100.93 | 100.60 | 100.08 | 100.91 | 100.34 | 100.30 | 99.41 | 100.56 | 100.53 | 100.33 | 100.57 | 100.78 | 101.07 | 100.56 | 99.73 | 100.89 | 101.43 | 101.56 | 101.84 |

| | SK3H-6 | SK3H-8 | SK3H-9 | SK3H-10 | SK3H-12 | SK3H-13 | SK3H-14 | SK3H-16 | SK3H-17 | SK3H-19 | SK3H-20 | SK3H-21 | SK3H-25 | SK3H-27 | SK3H-28 | SK3H-29 | SK3H-30 | SK3H-31 | SK3I-1 | SK3I-4 |
|---|---|---|---|---|---|---|---|---|---|---|---|---|---|---|---|---|---|---|---|---|
| $SiO_2$ | 35.16 | 34.66 | 34.81 | 34.89 | 33.79 | 33.02 | 33.73 | 33.19 | 34.20 | 33.16 | 33.44 | 33.20 | 35.09 | 34.20 | 33.72 | 34.38 | 32.52 | 34.03 | 36.16 | 35.98 |
| $TiO_2$ | 0.16 | 0.12 | 0.08 | 0.09 | 0.08 | 0.13 | 0.12 | 0.05 | 0.06 | 0.11 | 0.12 | 0.15 | 0.07 | 0.10 | 0.12 | 0.08 | 0.10 | 0.07 | 0.08 | 0.09 |
| $Al_2O_3$ | 0.09 | 0.11 | 0.10 | 0.07 | 0.06 | 0.21 | 0.12 | 0.20 | 0.13 | 0.13 | 0.20 | 0.18 | 0.10 | 0.09 | 0.06 | 0.05 | 0.10 | 0.05 | 0.05 | 0.07 |
| $Cr_2O_3$ | 12.46 | 12.82 | 12.50 | 12.86 | 13.00 | 17.16 | 14.52 | 17.46 | 13.12 | 14.93 | 17.87 | 16.53 | 13.63 | 13.00 | 13.02 | 13.57 | 13.17 | 13.90 | 11.25 | 11.69 |
| $Fe_2O_3$ | 19.97 | 20.69 | 21.45 | 20.90 | 23.48 | 18.72 | 20.80 | 17.14 | 21.25 | 20.09 | 17.30 | 18.50 | 19.86 | 22.13 | 22.23 | 20.46 | 24.06 | 21.14 | 20.26 | 20.50 |
| FeO | 2.26 | 1.49 | 1.27 | 1.41 | 0.00 | 0.00 | 0.01 | 0.00 | 0.88 | 0.00 | 0.00 | 0.00 | 2.10 | 0.49 | 0.00 | 0.98 | 0.00 | 0.70 | 3.22 | 3.21 |
| MnO | 0.04 | 0.09 | 0.00 | 0.08 | 0.11 | 0.00 | 0.03 | 0.07 | 0.05 | 0.00 | 0.11 | 0.01 | 0.00 | 0.00 | 0.02 | 0.00 | 0.06 | 0.08 | 0.05 | 0.08 |
| MgO | 0.16 | 0.05 | 0.05 | 0.01 | 0.06 | 0.11 | 0.09 | 0.10 | 0.08 | 0.12 | 0.12 | 0.12 | 0.06 | 0.08 | 0.07 | 0.05 | 0.38 | 0.04 | 0.04 | 0.04 |
| CaO | 30.90 | 31.13 | 31.48 | 31.45 | 32.09 | 31.70 | 31.40 | 31.52 | 31.12 | 31.26 | 31.42 | 31.36 | 31.08 | 31.49 | 31.52 | 31.31 | 31.16 | 31.15 | 31.19 | 31.02 |
| total | 101.20 | 101.14 | 101.75 | 101.77 | 101.83 | 99.83 | 100.82 | 98.81 | 100.88 | 99.27 | 100.09 | 99.49 | 101.98 | 101.57 | 100.65 | 100.88 | 99.85 | 101.16 | 102.29 | 102.70 |

| | SK3I-7 | SK3I-8 | SK3I-9 | SK3I-12 | SK3I-16 | SK3I-17 | SK3I-18 | SK3I-19 | SK3I-20 | SK3I-21 | SK3I-22 | SK3I-23 | SK3I-24 | SK3I-25 | SK3I-26 | SK3I-27 | SK3I-28 | SK3I-29 | SK3I-31 | SK3I-34 |
|---|---|---|---|---|---|---|---|---|---|---|---|---|---|---|---|---|---|---|---|---|
| $SiO_2$ | 35.00 | 35.43 | 35.50 | 35.27 | 35.36 | 35.01 | 35.33 | 35.44 | 34.00 | 35.34 | 36.32 | 35.15 | 31.72 | 35.11 | 35.45 | 35.09 | 34.57 | 34.90 | 35.28 | 34.51 |
| $TiO_2$ | 0.07 | 0.06 | 0.02 | 0.10 | 0.04 | 0.04 | 0.04 | 0.06 | 0.03 | 0.04 | 0.04 | 0.07 | 0.05 | 0.04 | 0.03 | 0.06 | 0.05 | 0.04 | 0.03 | 0.04 |
| $Al_2O_3$ | 0.05 | 0.10 | 0.08 | 0.05 | 0.09 | 0.05 | 0.07 | 0.08 | 0.12 | 0.05 | 0.09 | 0.11 | 1.24 | 0.08 | 0.08 | 0.10 | 0.05 | 0.08 | 0.12 | 0.09 |
| $Cr_2O_3$ | 11.89 | 12.29 | 12.05 | 11.85 | 12.73 | 12.03 | 11.77 | 12.25 | 12.78 | 12.74 | 9.99 | 12.61 | 16.39 | 13.19 | 12.47 | 13.12 | 12.83 | 13.96 | 12.02 | 11.64 |

| | | | | | | | | | | | | | | | | | | | | |
|---|---|---|---|---|---|---|---|---|---|---|---|---|---|---|---|---|---|---|---|---|
| $Fe_2O_3$ | 21.71 | 21.50 | 21.82 | 21.65 | 21.24 | 21.54 | 21.59 | 21.00 | 23.23 | 20.68 | 24.54 | 21.20 | 23.49 | 19.43 | 20.28 | 20.26 | 21.01 | 19.44 | 20.93 | 23.10 |
| FeO | 1.56 | 1.91 | 1.91 | 1.65 | 1.98 | 1.91 | 2.10 | 2.20 | 1.45 | 2.30 | 0.00 | 2.14 | 0.35 | 2.27 | 2.16 | 1.91 | 1.54 | 2.23 | 2.10 | 0.98 |
| MnO | 0.00 | 0.05 | 0.02 | 0.12 | 0.00 | 0.10 | 0.00 | 0.00 | 0.06 | 0.01 | 0.00 | 0.03 | 0.06 | 0.00 | 0.00 | 0.04 | 0.11 | 0.04 | 0.05 | 0.02 |
| MgO | 0.39 | 0.05 | 0.24 | 0.03 | 0.04 | 0.06 | 0.16 | 0.05 | 0.11 | 0.04 | 8.35 | 0.07 | 1.06 | 0.06 | 0.39 | 0.02 | 0.04 | 0.33 | 0.05 | 0.07 |
| CaO | 30.95 | 31.51 | 31.31 | 31.57 | 31.43 | 31.06 | 31.14 | 31.33 | 30.42 | 31.16 | 25.46 | 31.07 | 27.85 | 30.94 | 30.88 | 31.24 | 30.95 | 30.38 | 31.20 | 31.37 |
| total | 101.62 | 102.89 | 102.95 | 102.28 | 102.90 | 101.80 | 102.21 | 102.40 | 102.19 | 102.35 | 100.77 | 102.44 | 102.19 | 101.11 | 101.75 | 101.83 | 101.15 | 101.39 | 101.77 | 101.83 |

| | SK3I-35 | SK3I-36 | SK3I-37 | SK3I-38 | SK3I-39 | SK3I-40 | SK3I-41 | SK3I-42 | SK3I-43 | SK3I-44 | SK3I-45 | SK3I-46 | Sky8a | Sky8a | Sky8a | Sky8a | Sky8a | Sky8a | Sky8a | Sky8a |
|---|---|---|---|---|---|---|---|---|---|---|---|---|---|---|---|---|---|---|---|---|
| $SiO_2$ | 34.39 | 33.98 | 33.87 | 34.10 | 33.70 | 34.22 | 35.29 | 34.05 | 34.31 | 33.99 | 33.92 | 34.00 | 36.25 | 36.17 | 36.25 | 35.94 | 38.85 | 36.02 | 36.32 | 36.31 |
| $TiO_2$ | 0.05 | 0.19 | 0.14 | 0.04 | 0.11 | 0.06 | 0.08 | 0.13 | 0.06 | 0.08 | 0.11 | 0.08 | 0.09 | 0.13 | 0.09 | 0.10 | 0.14 | 0.02 | 0.06 | 0.04 |
| $Al_2O_3$ | 0.07 | 0.09 | 0.07 | 0.06 | 0.11 | 0.07 | 0.09 | 0.08 | 0.04 | 0.06 | 0.06 | 0.10 | 0.26 | 0.24 | 0.26 | 0.18 | 0.18 | 0.21 | 0.20 | 0.18 |
| $Cr_2O_3$ | 12.57 | 12.30 | 12.44 | 12.36 | 11.81 | 12.79 | 11.27 | 11.83 | 12.84 | 11.59 | 12.58 | 12.36 | 12.33 | 12.95 | 12.33 | 12.90 | 12.62 | 12.04 | 12.86 | 12.34 |
| $Fe_2O_3$ | 21.58 | 23.45 | 24.39 | 23.09 | 24.45 | 22.68 | 22.71 | 24.05 | 21.50 | 24.57 | 23.47 | 22.23 | 20.08 | 19.38 | 17.04 | 19.88 | 15.87 | 21.14 | 19.38 | 19.87 |
| FeO | 1.22 | 0.30 | 0.06 | 0.68 | -0.05 | 0.89 | 1.80 | 0.63 | 0.92 | 0.00 | 0.29 | 0.83 | 0.00 | 0.00 | 0.00 | 0.00 | 0.00 | 0.00 | 0.00 | 0.00 |
| MnO | 0.16 | 0.02 | 0.01 | 0.00 | 0.00 | 0.00 | 0.00 | 0.01 | 0.00 | 0.02 | 0.04 | 0.01 | 0.00 | 0.01 | 0.02 | 0.04 | 0.00 | 0.00 | 0.02 | 0.00 |
| MgO | 0.01 | 0.09 | 0.09 | 0.05 | 0.10 | 0.07 | 0.05 | 0.11 | 0.05 | 0.43 | 0.04 | 0.08 | 0.05 | 0.06 | 0.05 | 0.11 | 0.10 | 0.04 | 0.03 | 0.03 |
| CaO | 31.03 | 31.48 | 31.54 | 31.25 | 31.44 | 31.19 | 31.52 | 31.22 | 31.27 | 31.25 | 31.42 | 31.02 | 34.63 | 34.59 | 34.58 | 34.62 | 34.30 | 34.60 | 34.67 | 34.70 |
| total | 101.08 | 101.89 | 102.60 | 101.63 | 101.66 | 101.95 | 102.80 | 102.11 | 101.01 | 101.86 | 101.92 | 100.73 | 103.69 | 103.52 | 100.62 | 103.77 | 102.06 | 104.07 | 103.54 | 103.47 |

Tab. A4.15 BMM analyses of Skyros chromitites.

| wt% | As | S | Ni | Fe | Cu | Sb | Ir | Co | Pt | Pd | Rh | Total |
|---|---|---|---|---|---|---|---|---|---|---|---|---|
| | | | | | | Alloys | | | | | | |
| SK3H-SULF-5 | 0.00 | 0.00 | 76.23 | 22.96 | 0.80 | 0.00 | 0.00 | 1.41 | 0.00 | 0.00 | 0.00 | 101.40 |
| SK3H-SULF-14 | 0.00 | 0.02 | 78.72 | 23.18 | 0.71 | 0.02 | 0.00 | 1.27 | 0.00 | 0.00 | 0.00 | 103.92 |
| SK3I-SULF-6 | 0.00 | 2.30 | 73.98 | 19.82 | 0.56 | 0.00 | 0.00 | 0.56 | 0.00 | 0.00 | 0.00 | 97.22 |
| SKY14A-G3 | 0.01 | 0.02 | 7.76 | 63.12 | 3.02 | 0.00 | 0.00 | 0.00 | 0.00 | 0.02 | 0.00 | 73.99 |
| SKY14BA-H1 | 0.03 | 2.02 | 83.12 | 5.25 | 3.68 | 0.00 | 0.00 | 0.00 | 0.46 | 0.01 | 0.01 | 94.63 |
| | | | | | | Pentlandite | | | | | | |
| SK3A-SULF-1 | 0.00 | 31.21 | 37.71 | 26.67 | 0.00 | 0.00 | 0.12 | 0.99 | 0.00 | 0.00 | 0.00 | 96.70 |
| SK3A-SULF-4 | 0.00 | 31.05 | 39.85 | 24.83 | 0.00 | 0.02 | 0.04 | 1.33 | 0.00 | 0.00 | 0.00 | 97.11 |
| SK3A-SULF-6 | 0.00 | 31.88 | 41.14 | 24.26 | 0.05 | 0.00 | 0.00 | 0.71 | 0.00 | 0.00 | 0.00 | 98.03 |
| SKY8B-D9 | 0.00 | 33.86 | 42.33 | 22.44 | 0.00 | 0.00 | 0.00 | 0.00 | 0.00 | 0.03 | 0.02 | 98.68 |
| SKY8B-D1 | 0.03 | 33.42 | 43.18 | 22.61 | 0.00 | 0.00 | 0.00 | 0.00 | 0.05 | 0.00 | 0.04 | 99.35 |
| SKY8B-D6 | 0.02 | 33.58 | 42.11 | 22.58 | 0.00 | 0.00 | 0.00 | 0.00 | 0.00 | 0.00 | 0.03 | 98.36 |
| | | | | | | Millerite | | | | | | |
| SK3H-SULF-6 | 0.00 | 31.22 | 65.78 | 0.37 | 0.02 | 0.00 | 0.05 | 0.63 | 0.00 | na | 0.00 | 98.07 |
| SK3H-SULF-10 | 0.00 | 32.94 | 66.75 | 0.09 | 0.07 | 0.00 | 0.14 | 0.00 | 0.00 | na | 0.00 | 100.00 |
| SK3H-SULF-12 | 0.00 | 32.54 | 66.40 | 0.41 | 0.00 | 0.00 | 0.03 | 0.19 | 0.00 | na | 0.00 | 99.57 |
| SK3H-SULF-13 | 0.00 | 33.04 | 66.65 | 0.14 | 0.03 | 0.00 | 0.00 | 0.00 | 0.00 | na | 0.00 | 99.86 |
| SK3H-SULF-1 | 0.00 | 29.49 | 72.60 | 0.09 | 0.02 | 0.00 | 0.00 | 0.25 | 0.00 | na | 0.00 | 102.44 |
| SK3A-SULF-2 | 0.00 | 31.48 | 68.88 | 1.52 | 0.05 | 0.00 | 0.00 | 0.00 | 0.00 | na | 0.00 | 101.93 |
| SK3A-SULF-5 | 0.11 | 32.22 | 65.81 | 1.04 | 0.07 | 0.00 | 0.00 | 0.02 | 0.00 | na | 0.00 | 99.26 |
| SK3A-SULF- | 0.00 | 32.78 | 65.22 | 0.22 | 0.08 | 0.00 | 0.14 | 0.03 | 0.00 | na | 0.00 | 98.48 |

| | | | | | | | | | | | | |
|---|---|---|---|---|---|---|---|---|---|---|---|---|
| 12 | | | | | | | | | | | | |
| SK3A-SULF-13 | 0.00 | 32.16 | 65.38 | 0.78 | 0.05 | 0.00 | 0.01 | 0.00 | 0.00 | na | 0.00 | 98.38 |
| SKY8B-D8 | 0.00 | 35.78 | 63.39 | 0.82 | 0.00 | 0.00 | 0.05 | 0.00 | 0.54 | na | 0.05 | 100.74 |
| SKY10-I11b | 0.00 | 26.68 | 69.87 | 0.75 | 0.02 | 0.00 | 0.00 | 0.00 | 0.00 | na | 0.00 | 97.32 |
| | | | | | | Heazlewoodite | | | | | | |
| SK3I-SULF-4 | 0.00 | 25.35 | 72.52 | 2.00 | 0.01 | 0.00 | 0.00 | 0.18 | 0.00 | 0.00 | 0.00 | 100.07 |
| SK3I-SULF-5 | 0.00 | 26.21 | 71.78 | 1.40 | 0.03 | 0.00 | 0.00 | 0.27 | 0.00 | 0.00 | 0.00 | 99.69 |
| SK3I-SULF-7 | 0.00 | 27.21 | 72.64 | 1.43 | 0.02 | 0.00 | 0.00 | 0.12 | 0.00 | 0.00 | 0.00 | 101.41 |
| SK3I-SULF-8 | 0.00 | 26.06 | 73.24 | 1.36 | 0.06 | 0.00 | 0.00 | 0.10 | 0.00 | 0.00 | 0.00 | 100.83 |
| SK3I-SULF-9 | 0.00 | 26.23 | 73.12 | 1.47 | 0.06 | 0.00 | 0.00 | 0.09 | 0.00 | 0.00 | 0.00 | 100.97 |
| SKY14B-F3 | 0.01 | 24.99 | 70.18 | 1.69 | 0.09 | 0.00 | 0.00 | 0.00 | 0.16 | 0.00 | 0.00 | 97.12 |
| SKY14B-F2 | 0.01 | 27.18 | 70.39 | 1.52 | 0.00 | 0.00 | 0.00 | 0.00 | 0.14 | 0.06 | 0.00 | 99.30 |
| SKY14B-F5 | 0.01 | 27.43 | 70.40 | 1.45 | 0.00 | 0.00 | 0.00 | 0.36 | 0.00 | 0.69 | 0.04 | 0.00 | 100.38 |
| SKY14BA-H11 | 0.00 | 27.46 | 72.62 | 0.64 | 0.00 | 0.00 | 0.00 | 0.29 | 0.00 | 0.00 | 0.03 | 0.00 | 101.03 |
| SKY10-I2 | 0.02 | 26.28 | 71.19 | 0.27 | 0.00 | 0.00 | 0.00 | 0.60 | 0.00 | 0.35 | 0.00 | 0.00 | 98.72 |
| SKY10-I12 | 0.02 | 27.04 | 71.70 | 1.65 | 0.00 | 0.00 | 0.00 | 0.13 | 0.00 | 0.09 | 0.00 | 0.06 | 100.69 |
| SKY10-I5 | 0.00 | 27.38 | 73.25 | 0.13 | 0.00 | 0.00 | 0.00 | 0.00 | 0.00 | 0.37 | 0.00 | 0.00 | 101.22 |
| SKY4A-E2 | 0.00 | 26.81 | 70.45 | 0.13 | 0.00 | 0.00 | 0.00 | 0.00 | 0.00 | 0.00 | 0.00 | 0.02 | 97.41 |
| SKY4A-E1 | 0.09 | 27.48 | 72.13 | 0.23 | 0.00 | 0.00 | 0.00 | 0.00 | 0.00 | 0.00 | 0.01 | 0.00 | 99.95 |
| SKY8A-L1 | 0.03 | 27.47 | 70.82 | 1.08 | 0.00 | 0.00 | 0.36 | 0.00 | 0.24 | 0.06 | 0.00 | 100.18 |
| SKY8A-L2 | 0.00 | 27.14 | 70.29 | 1.36 | 0.00 | 0.00 | 0.46 | 0.00 | 0.55 | 0.00 | 0.00 | 99.80 |
| SKY8A-L5 | 0.00 | 27.39 | 72.15 | 1.15 | 0.00 | 0.00 | 0.14 | 0.00 | 0.00 | 0.00 | 0.03 | 100.86 |
| | | | | | | Copper Sulfides | | | | | | |
| SK3H-SULF-15 | 0.01 | 0.03 | 15.62 | 1.89 | 84.83 | 0.00 | 0.00 | 0.08 | na | na | na | 102.46 |
| SKY14A-G2 | 0.00 | 0.03 | 0.11 | 0.98 | 56.25 | 0.00 | 0.00 | 0.00 | na | na | na | 57.38 |
| | | | | | | Arsenides | | | | | | |
| SK3A-SULF-9 | 33.51 | 0.00 | 70.26 | 0.41 | 0.04 | 0.73 | 0.00 | 0.00 | na | na | na | 104.95 |
| SK3A-SULF-10 | 36.00 | 0.01 | 67.33 | 0.33 | 0.05 | 0.95 | 0.00 | 0.00 | na | na | na | 104.66 |

Tab. A4.16 BMM microprobe analyses of Abdasht-Soghan chromitites.

| wt% | As | Os | Fe | Ir | S | Ni | Pt | Ru | Cu | Rh | Pd | Total |
|---|---|---|---|---|---|---|---|---|---|---|---|---|
| | | | | | | Awaruite and alloys | | | | | | |
| IRSO-A1-C1-AWA1 | 0.05 | 0.00 | 24.22 | 0.57 | 0.00 | 74.55 | 0.00 | 0.01 | 0.00 | 0.00 | 0.01 | 99.41 |
| IRSO-A2-C1-AWA1 | 0.06 | 0.07 | 21.95 | 0.01 | 0.03 | 76.29 | 0.00 | 0.04 | 0.96 | 0.00 | 0.00 | 99.41 |
| IRSO-A2-C4-AWA2 | 1.98 | 0.00 | 10.32 | 0.18 | 0.02 | 83.28 | 0.28 | 0.07 | 3.28 | 0.00 | 0.00 | 99.41 |
| IRSO-A04-C3-AWA1 | 0.07 | 0.00 | 20.55 | 0.00 | 0.00 | 80.46 | 0.10 | 0.00 | 0.93 | 0.02 | 0.08 | 102.20 |
| IRSO-A04-C7-AWA2 | 0.07 | 0.00 | 22.95 | 0.14 | 0.00 | 78.21 | 0.21 | 0.00 | 0.52 | 0.00 | 0.00 | 102.09 |
| IRSO-A06-C1-1 | 0.00 | 0.00 | 24.65 | 0.00 | 0.00 | 71.41 | 0.10 | 0.01 | 0.00 | 0.00 | 0.10 | 96.26 |
| IRSO-A06-C2-1 | 0.30 | 0.00 | 14.67 | 0.00 | 0.00 | 81.51 | 0.00 | 0.00 | 3.51 | 0.00 | 0.01 | 100.00 |
| IRSO-B01-C5-AWA2 | 0.10 | 0.00 | 24.72 | 0.00 | 0.01 | 74.92 | 0.00 | 0.00 | 0.58 | 0.00 | 0.04 | 100.36 |
| IRSO-C02-C3-1 | 0.00 | 0.06 | 22.21 | 0.28 | 0.00 | 79.57 | 0.36 | 0.00 | 1.03 | 0.00 | 0.00 | 103.54 |
| IRSO-C02-C3-2 | 0.00 | 0.09 | 61.22 | 0.00 | 0.00 | 38.49 | 0.13 | 0.00 | 0.00 | 0.00 | 0.00 | 100.00 |
| IRSO-D03-C2-1 | 0.04 | 0.00 | 25.51 | 0.00 | 4.06 | 70.20 | 0.15 | 0.02 | 0.00 | 0.00 | 0.01 | 100.00 |
| IRSO-D03-C5-1 | 0.00 | 0.00 | 24.66 | 0.17 | 0.00 | 75.93 | 0.19 | 0.00 | 0.09 | 0.01 | 0.00 | 101.07 |
| IRAB-B01(2)-C3-AWA1 | 0.14 | 0.10 | 23.64 | 0.00 | 0.00 | 75.68 | 0.26 | 0.02 | 0.60 | 0.00 | 0.10 | 100.53 |

| | | | | | | | | | | | | |
|---|---|---|---|---|---|---|---|---|---|---|---|---|
| IRAB-B01(2)-C4-AWA2 | 0.06 | 0.00 | 24.18 | 0.45 | 0.00 | 75.27 | 0.23 | 0.00 | 0.23 | 0.00 | 0.00 | 100.41 |
| IRAB-B04-C3-AWA-4 | 0.00 | 0.19 | 21.61 | 0.00 | 0.00 | 74.76 | 0.00 | 0.03 | 2.83 | 0.05 | 0.01 | 99.48 |
| IRAB-B04-C6-AWA-5 | 0.00 | 0.04 | 24.08 | 0.00 | 0.01 | 75.00 | 0.09 | 0.00 | 0.18 | 0.00 | 0.00 | 99.41 |
| IRAB-B04-C1-AWA1 | 0.04 | 0.25 | 20.82 | 0.00 | 0.01 | 77.13 | 0.00 | 0.00 | 1.83 | 0.10 | 0.05 | 100.23 |
| Heazlewoodite | | | | | | | | | | | | |
| IRSO-A03-C3-SOLF1 | 0.04 | 0.12 | 0.66 | 0.21 | 26.96 | 71.37 | 0.00 | 0.00 | 0.00 | 0.00 | 0.05 | 99.41 |
| IRSO-A04-C3-SOLF1 | 0.00 | 0.08 | 3.25 | 0.00 | 26.59 | 73.89 | 0.00 | 0.00 | 0.00 | 0.10 | 0.00 | 103.92 |
| IRSO-A04-C7-SOLF2 | 0.00 | 0.13 | 2.32 | 0.00 | 26.50 | 74.06 | 0.00 | 0.00 | 0.00 | 0.00 | 0.00 | 103.01 |
| IRSO-D03-C3-1 | 0.00 | 0.10 | 1.90 | 0.20 | 28.01 | 71.74 | 0.34 | 0.00 | 0.00 | 0.02 | 0.00 | 102.30 |
| IRSO-D03-C4-1 | 0.00 | 0.00 | 0.93 | 0.31 | 28.06 | 74.03 | 0.47 | 0.00 | 0.00 | 0.00 | 0.00 | 103.80 |
| IRSO-D03-C4-2 | 0.00 | 0.21 | 1.43 | 0.38 | 27.95 | 73.19 | 0.00 | 0.00 | 0.00 | 0.04 | 0.03 | 103.23 |
| IRAB-A01-C1-SOLF1 | 0.01 | 0.00 | 0.35 | 0.12 | 27.50 | 73.28 | 0.00 | 0.00 | 0.00 | 0.00 | 0.00 | 101.26 |
| IRAB-A03-C1-SOLF1 | 0.03 | 0.00 | 0.22 | 0.38 | 27.33 | 73.86 | 0.00 | 0.00 | 0.00 | 0.00 | 0.01 | 101.82 |
| IRAB-A03-C1-SOLF2 | 0.07 | 0.11 | 0.21 | 0.76 | 27.25 | 73.87 | 0.00 | 0.00 | 0.00 | 0.00 | 0.00 | 102.27 |
| IRAB-B01-C1-PT4 | 0.06 | 0.05 | 0.70 | 0.16 | 26.86 | 72.25 | 0.06 | 0.00 | 0.00 | 0.01 | 0.00 | 100.14 |
| IRAB-B01-C1-1 | 0.07 | 0.30 | 0.45 | 0.00 | 27.80 | 75.05 | 0.00 | 0.00 | 0.00 | 0.11 | 0.03 | 103.81 |
| IRAB-B01-C1-2 | 0.10 | 0.20 | 0.75 | 0.00 | 28.69 | 72.79 | 0.86 | 0.00 | 0.00 | 0.09 | 0.02 | 103.50 |
| IRAB-B01-C2-1 | 0.00 | 0.00 | 0.00 | 0.00 | 27.37 | 75.81 | 0.16 | 0.00 | 0.00 | 0.01 | 0.00 | 103.35 |
| IRAB-B01-C4-1 | 0.00 | 0.02 | 0.47 | 0.00 | 28.15 | 74.29 | 0.00 | 0.00 | 0.00 | 0.02 | 0.00 | 102.95 |
| IRAB-B01-C4-2 | 0.21 | 0.00 | 0.12 | 0.08 | 27.67 | 75.66 | 0.00 | 0.00 | 0.00 | 0.00 | 0.02 | 103.77 |
| IRAB-B03-C1-SOLF1-1 | 0.02 | 0.00 | 0.09 | 0.08 | 26.62 | 73.84 | 0.00 | 0.00 | 0.00 | 0.03 | 0.00 | 100.68 |
| IRAB-B03-C3-SOLF-2 | 0.06 | 0.00 | 0.57 | 0.00 | 26.84 | 72.96 | 0.22 | 0.00 | 0.00 | 0.09 | 0.00 | 100.75 |
| IRAB-B03-C4-SOLF-3 | 0.00 | 0.08 | 0.20 | 0.00 | 26.65 | 73.80 | 0.00 | 0.00 | 0.00 | 0.02 | 0.00 | 100.75 |
| IRAB-B05-C5-SOLF2 | 0.13 | 0.00 | 0.54 | 0.32 | 28.29 | 70.81 | 0.05 | 0.00 | 0.00 | 0.00 | 0.04 | 100.18 |
| IRAB-B05-C5-SOLF3 | 0.08 | 0.00 | 0.46 | 0.00 | 26.82 | 72.55 | 0.65 | 0.00 | 0.00 | 0.05 | 0.01 | 100.63 |
| IRAB-B05-C7-solf4 | 0.15 | 0.00 | 0.95 | 0.21 | 27.24 | 71.12 | 0.40 | 0.00 | 0.00 | 0.00 | 0.00 | 100.07 |
| Pentlandite | | | | | | | | | | | | |
| IRSO-B03-C1-SOLF1 | 0.01 | 0.00 | 31.21 | 0.34 | 34.39 | 34.38 | 0.00 | 0.00 | 0.37 | 0.00 | 0.00 | 100.69 |
| IRAB-B05-2 | 0.26 | 0.00 | 26.00 | 0.00 | 35.83 | 37.81 | 0.00 | 0.00 | 0.00 | 0.10 | 0.00 | 100.00 |
| IRAB-B05-C3-SOLF1 | 0.00 | 0.06 | 21.05 | 0.29 | 33.65 | 44.01 | 0.00 | 0.13 | 0.16 | 0.03 | 0.02 | 99.41 |
| Millerite | | | | | | | | | | | | |
| IRAB-A01-C2-SOLF2 | 0.12 | 0.00 | 0.30 | 0.00 | 34.93 | 65.03 | 0.00 | 0.00 | 0.95 | 0.03 | 0.00 | 101.36 |
| IRAB-B01-C2-2 | 0.00 | 0.00 | 0.00 | 0.05 | 33.01 | 68.37 | 0.45 | 0.00 | 0.03 | 0.05 | 0.03 | 102.00 |
| IRAB-B04-C2-SOLF-2 | 0.00 | 0.00 | 0.87 | 0.26 | 32.73 | 65.96 | 0.36 | 0.00 | 0.00 | 0.00 | 0.00 | 100.18 |
| IRAB-A02-C4-2 | 0.02 | 0.00 | 0.46 | 0.25 | 36.32 | 64.46 | 0.10 | 0.00 | 0.00 | 0.00 | 0.04 | 101.65 |
| IRAB-A01-C5-SOLF3 | 0.10 | 0.00 | 0.07 | 0.04 | 35.67 | 65.58 | 0.10 | 0.00 | 0.16 | 0.03 | 0.01 | 101.76 |
| Ni arsenides | | | | | | | | | | | | |
| IRAB-A01-C1-NIC1 | 48.58 | 0.00 | 0.36 | 0.00 | 0.04 | 51.52 | 0.71 | 0.00 | 0.00 | 0.00 | 0.00 | 101.20 |
| IRAB-A01-C1-NIC2 | 48.27 | 0.03 | 0.87 | 0.12 | 0.00 | 51.33 | 0.21 | 0.00 | 0.00 | 0.00 | 0.00 | 100.83 |
| IRAB-A01-C1-NIC3 | 49.09 | 0.00 | 0.64 | 0.00 | 0.04 | 51.81 | 0.08 | 0.00 | 0.00 | 0.00 | 0.01 | 101.67 |
| IRAB-A01-C2-NICCO4 | 46.90 | 0.13 | 0.52 | 0.00 | 1.00 | 52.41 | 0.00 | 0.00 | 0.00 | 0.02 | 0.00 | 100.98 |
| IRAB-A02-C4-1 | 48.74 | 0.07 | 0.28 | 0.00 | 0.02 | 53.82 | 0.20 | 0.02 | 0.00 | 0.00 | 0.04 | 103.19 |
| IRAB-A02-C5-1 | 48.35 | 0.00 | 0.11 | 0.12 | 0.02 | 53.32 | 0.00 | 0.05 | 0.00 | 0.03 | 0.00 | 102.00 |
| IRAB-B05-C7-Ni1 | 45.67 | 0.12 | 1.03 | 0.45 | 0.00 | 53.46 | 0.23 | 0.10 | 0.00 | 0.00 | 0.00 | 101.06 |
| Bornite | | | | | | | | | | | | |
| IRSO-B03-C1-SOLF2 | 0.07 | 0.04 | 11.26 | 0.00 | 26.57 | 0.18 | 0.00 | 0.01 | 61.99 | 0.02 | 0.01 | 100.16 |

Tab. A4.17 PGM microprobe analyses of Abdasht-Soghan chromitites.

Appendix: Chapter 4

| wt% | As | Os | Fe | Ir | S | Ni | Pt | Ru | Cu | Rh | Pd | tot |
|---|---|---|---|---|---|---|---|---|---|---|---|---|
| IRAB-B01-C3-1 | 2.04 | 13.77 | 0.00 | 6.67 | 35.76 | 0.01 | 0.00 | 40.21 | 0.15 | 3.38 | 0.02 | 102.01 |
| IRAB-B01-C3-2 | 1.00 | 44.08 | 0.00 | 25.34 | 0.00 | 0.19 | 0.00 | 26.93 | 2.41 | 2.24 | 0.00 | 102.19 |
| IRAB-B01-C3-3 | 2.30 | 3.30 | 0.00 | 0.51 | 38.74 | 0.02 | 0.00 | 55.14 | 0.08 | 1.93 | 0.24 | 102.26 |
| IRAB-B01-C1-PT1 | 0.04 | 51.10 | 2.04 | 40.06 | 0.00 | 1.32 | 0.00 | 2.12 | 0.12 | 1.12 | 0.00 | 97.91 |
| IRAB-B01-C1-PT2 | 2.47 | 24.44 | 0.42 | 8.99 | 0.00 | 1.68 | 0.00 | 63.08 | 0.01 | 0.51 | 0.12 | 101.71 |
| IRAB-B01-C1-PT3 | 0.42 | 0.77 | 2.14 | 7.58 | 0.00 | 81.42 | 0.19 | 2.18 | 3.85 | 1.70 | 0.00 | 100.24 |
| IRAB-B03-C2-PT-2 | 2.28 | 11.49 | 0.00 | 6.88 | 34.40 | 0.05 | 0.00 | 40.70 | 0.10 | 2.56 | 0.14 | 98.61 |
| IRAB-B04-1 | 1.87 | 20.15 | 0.00 | 8.00 | 34.44 | 0.02 | 0.00 | 37.00 | 0.01 | 0.00 | 0.00 | 101.49 |
| IRAB-B04-2 | 2.53 | 21.47 | 7.16 | 9.99 | 0.04 | 0.78 | 0.00 | 57.21 | 0.00 | 0.82 | 0.00 | 100.00 |
| IRAB-B04-C2-PT-3 | 1.98 | 6.25 | 0.00 | 5.47 | 36.09 | 0.00 | 0.00 | 49.20 | 0.00 | 0.35 | 0.40 | 99.73 |
| IRAB-B05-1 | 3.45 | 19.70 | 0.00 | 13.06 | 31.89 | 0.00 | 0.00 | 30.49 | 0.10 | 2.18 | 0.00 | 100.87 |
| IRAB-B05-3 | 2.32 | 11.53 | 0.00 | 7.75 | 34.66 | 0.05 | 0.00 | 42.38 | 0.00 | 1.43 | 0.00 | 100.12 |
| IRAB-B05(2)-C1-PT1 | 2.58 | 5.89 | 0.00 | 3.27 | 37.40 | 0.47 | 0.00 | 49.15 | 0.02 | 1.91 | 0.38 | 101.06 |
| IRAB-B05(2)-C2-PT2 | 1.33 | 12.85 | 0.00 | 9.07 | 34.65 | 0.00 | 0.00 | 39.97 | 0.09 | 1.23 | 0.52 | 99.72 |
| IRAB-B05(2)-C2-PT3 | 0.03 | 0.00 | 3.27 | 45.87 | 25.20 | 0.00 | 0.00 | 0.05 | 8.78 | 13.80 | 0.00 | 97.00 |
| IRAB-B05(2)-C4-PT3 | 0.02 | 0.00 | 7.28 | 87.49 | 0.00 | 0.17 | 4.10 | 0.00 | 0.83 | 0.07 | 0.06 | 100.00 |
| IRAB-B05(2)-C4-PT4 | 1.33 | 51.21 | 0.00 | 8.66 | 27.90 | 0.00 | 0.00 | 10.15 | 0.00 | 0.13 | 0.04 | 99.41 |
| IRSO-A01-C2-1 | 2.37 | 11.70 | 9.65 | 4.74 | 0.26 | 35.28 | 0.00 | 34.57 | 0.47 | 0.38 | 0.01 | 99.41 |
| IRSO-A03-C1-PT2 | 0.00 | 17.12 | 0.00 | 78.56 | 0.00 | 0.21 | 0.00 | 0.67 | 0.59 | 0.97 | 0.01 | 98.13 |
| IRSO-A03-C1-PT1 | 1.46 | 17.09 | 0.00 | 9.73 | 33.79 | 0.00 | 0.00 | 36.27 | 0.19 | 0.43 | 0.37 | 99.33 |
| IRSO-B01-C4-PT1 | 0.06 | 66.25 | 0.68 | 31.28 | 0.01 | 0.00 | 0.00 | 0.74 | 0.07 | 0.31 | 0.00 | 99.41 |
| IRSO-C01-C3-1 | 2.35 | 8.26 | 0.00 | 9.19 | 34.38 | 0.00 | 0.00 | 42.64 | 0.07 | 1.53 | 0.48 | 98.89 |
| IRSO-C02-C1-1 | 1.66 | 19.82 | 0.00 | 8.07 | 34.67 | 0.00 | 0.00 | 36.22 | 0.00 | 0.90 | 0.22 | 101.56 |